Provenance studies of British prehistoric greenstone implements using non-destructive analytical methods

Thesis

Provenance studies of British prehistoric greenstone implements using non-destructive analytical methods

Michael Markham

November 2000

This thesis is submitted to the Open University for the degree of PhD

TEXT BOUND INTO THE SPINE

THESIS CONTAINS CD/DVD

THE OPEN UNIVERSITY

RESEARCH SCHOOL

Library Authorisation Form

Please return this form to the Research School with the two bound copies of your thesis to be deposited with the University Library. All candidates should complete parts one and two of the form. Part three only applies to PhD candidates.

Part One: Candidates Details

Name: M MARKHAM PI: M1GG8446

Degree: PhD

Thesis title: PROVENANCE STUDIES OF BRITISH PREHISTORIC GREENSTONE IMPLEMENTS USING NON-DESTRUCTIVE ANALYTICAL METHODS

Part Two: Open University Library Authorisation

I confirm that I am willing for my thesis to be made available to readers by the Open University Library, and that it may be photocopied, subject to the discretion of the Librarian.

Signed: ..... Date: 5 May 2001

Part Three: British Library Authorisation [PhD candidates only]

If you want a copy of your PhD thesis to be available on loan to the British Library Thesis Service as and when it is requested, you must sign a British Library Doctoral Thesis Agreement Form. Please return it to the Research School with this form. The British Library will publicise the details of your thesis and may request a copy on loan from the University Library. Information on the presentation of the thesis is given in the Agreement Form.

Please note the British Library have requested that theses should be printed on one side only to enable them to produce a clear microfilm. The Open University Library sends the fully bound copy of theses to the British Library.

The University has agreed that your participation in the British Library Thesis Service should be voluntary. Please tick either (a) or (b) to indicate your intentions.

☑ I am willing for the Open University to loan the British Library a copy of my thesis.
A signed Agreement Form is attached

☐ I do not wish the Open University to loan the British Library a copy of my thesis.

Signed: ..... Date: 5 May 2001

Declaration

This thesis has not been submitted to any other University

Except where identified all work has been undertaken by the Author

Michael Markham

November 2000

Abstract

Geochemical data obtained using field-portable non-destructive X-ray fluorescence instrumentation (PXRF), supported by magnetic susceptibility (MS) measurements, is able to narrow the provenance of IPC Group I prehistoric greenstone axes to two locations in West Cornwall: St Ives and Mullion Island. It also supports the provenance of IPC Group III axes to a greenstone quarry near Perranuthnoe, Cornwall and supports the Cornish origin of seven Irish gabbroic and doleritic axes. Provenancing methodology involved the examination of 149 axe and 73 greenstone thin sections, followed by comparison of 272 axe and over 100 exposure geochemical and magnetic analyses using Simple Component Analysis (SCA), element discrimination diagrams, Discriminant Analysis (DA) and comparative statistics (MANOVA, t-test). Accuracy, precision and detection limits of the PXRF are determined using international reference samples, greenstone samples and greenstone axes. PXRF instrumentation is generally linearly calibrated with zero offset, and with a compensatable bias for K, Ca, Ti, Mn, Fe, Rb, Sr, Y, Zr, Nb, Ba, Ce and Pb. Precision in measuring greenstone rock composition is 5.3% relative standard deviation of the mean based on two PXRF measurements and from elements with concentrations ten-times the PXRF detection limit (generally less than 900ppm for major elements and less than 30ppm for trace elements). Empirical studies using newly manufactured greenstone axes show that no adjustments to PXRF measurements are required when measuring polished curved axe surfaces, and that Ti, Y, Zr and Nb PXRF measurements made on weathered surfaces are statistically indistinguishable from those measured on fresh, flat surfaces of the same composition. KT5 magnetic susceptibility meter precision is 1.5% relative when measuring typical greenstone rock with MS of 0.6×10^{-3} SI. A robust correction procedure based on estimates of axe curvature, surface relief and dimensions is shown to correct the measured MS to that of the true rock value.

Acknowledgements

I would like to acknowledge my supervisors; Drs Olwen Williams-Thorpe, Peter Webb and Vin Davis for their enthusiasm, encouragement and direction. Our discussions have been fruitful and educational, for which I am greatly indebted.

The Open University has provided constant support throughout this project and I would like to particularly thank Brian Ellis, John Holbrook and John Watson for their assistance with production and preparation of rock samples for analysis.

It is always a great pleasure to discuss greenstone geology with Dr Peter Floyd, so sincerest thanks to Peter for his time and making his data available for this research. Many thanks also go to Mr Dave Weddle and his sons, David and Jimmy, for manufacturing the proto-axes used in this work and for providing practical insights on greenstone axe manufacture. I also thank Miss Amy Davis for her ICP-AES analyses of Carrock Fell samples and Dr Steve Mandal for his organisation and assistance with the examination of Irish axes.

I am greatly humbled by the support provided by many Museums and Organisation in making facilities and their axes available for research. I would particularly like to than (in no particular order) Anna Tyacke (Truro Museum), Peter Berridge (Colchester City Museum), Geoff Walford (Cornish Archaeologist), Julie Johns (Callington Museum Trust), John Allen (Exeter City Museum), David Dawson and Steve Minnit (Taunton Castle Museum), Elizabeth Walker (National Museum of Wales and Lithic Studies Society), Gail Boyle (Bristol City Museum), Paul Robinson (Devises Museum), Peter Woodward (Dorchester County Museum), Clare Connybear (Alexander Keiller Museum), Peter Saunders (Salisbury and South Wilts Museum), Kay Ainsworth (Hampshire County Museums Service), Alison Roberts (Ashmolean), Bill Milligan (Norwich Castle Museum), Jill Varndell (British Museum), Jon Cotton (Museum of London), Yvonne Boutwood (Archaeologist), Gail Foremand and Rose Nicholson (Hull City Museum), Karin Green (Down Farm Museum) and Fiona McAllister (Bristol City Museum). I apologise to those unsung heroes whose names I have forgotten.

I owe a great deal of indebtedness to my fieldwork assistants Dr Denise Lambkin and Mrs Alison Cann, whose help resulted in over 1,200 geochemical analyses and 2,500 measurements of magnetic susceptibility. I hope the beer and tour of England was worth it!

Finally, I would like to offer my profuse and sincere thanks for the Herculean amount of tolerance and support I received from my wife, (and fieldwork assistant!), Shirley. I wait to discover if there is life outside the study...

Contents

List of Figures

List of Tables

Appendixes

1 Provenancing of stone implements – application of non-destructive techniques

1.1 Background

Stone implements from the Neolithic period are visible and measurable records that provide insight into the socio-political and technological culture at that time. The Neolithic period in Britain began in the early fourth millennium BC (Kinnes 1988) when prehistoric society gradually changed from a hunter-gathering culture to a more sedentary, farming culture (Bradley & Edmonds 1993). This change is evidenced by the development of burial rituals (Bradley 1984), clearance of land for planting of cereals (Bradley 1978, Simmons & Tooley 1981) and the production of large stone and wooden monuments, such as henges, circles, cairns and tombs, e.g. Balfour 1992, Manley 1989, Bewley 1994. Social agglomeration is seen through the development of hill forts (e.g. Carn Brea (Bewley 1994)) and industrialisation (e.g. Langdale axe factory (Bradley & Edmonds 1993)). An aspect of this cultural transformation was the technological development of stone tools, especially axes, manufactured from rock types other than flint (Smith 1979, Edmonds 1995). This latter point acknowledges that flint is both a rock and stone, but for the purposes of this thesis the terms rock and stone are deemed to exclude references to flint.

Smith (1979) indicates that stone axe production in the British Isles started approximately 3250 BC and had ceased by approximately 1250 BC, with this latter date being taken as the beginning of the Bronze Age in Britain (Pearson 1993). These stone tools, or implements, were manufactured from many different types of rock, for example: sandstone, dolerite, basalt, silicified tuff, baked shale and greenstone (Keiller et al. 1941, Clough & Cummins 1979). The shape, size and material of these implements provide an insight as to the available technology in Neolithic times (Edmonds 1995), whereas their source (provenance) and place of discovery (find location) *can lead to inferences* on the socio-political aspects of life in the Neolithic (Bradley & Edmonds 1993, Cummins 1979).

It is known that people extensively used flint in prehistoric times. Flint is relatively simple to work using various forms of flaking techniques and can produce a very sharp-edged tool for various domestic uses (e.g. butchering). Flint is also widely available, especially in the chalk-rich areas in the east of England and as residual material found on beaches. It is postulated (based on Pearce 1981, Schick & Toth 1993, Edmonds 1995 amongst others) that the change from flint to other types of stone for the manufacture of tools at the beginning of the Neolithic occurred for several reasons. Flint tools are quick and simple to

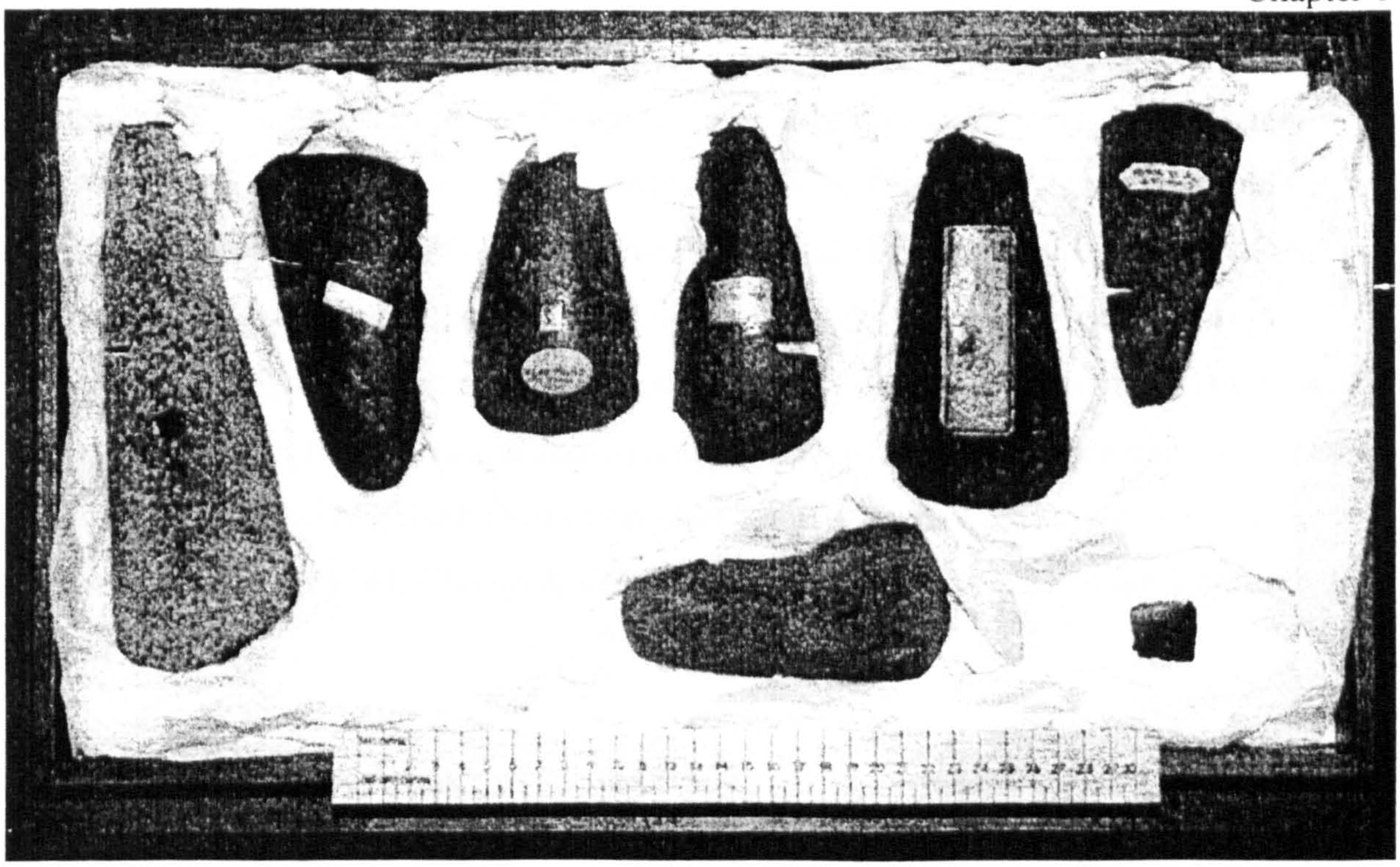

Figure 1 Selection of IPC Group I greenstone axes held by the British Museum. Note the variable morphology, colour and texture of these axes that have all been assigned to IPC Group I

make, taking a few minutes to produce a respectable knife or scraper, whereas a ground greenstone axe can take up to 100 working hours (Weddle pers. com.). Hence the effort and time needed to produce stone tools whilst hunter-gathering was probably not available, therefore, stone tool technology did not advance from the established and practised flint based technology. However, the need for resilient and sharp tools probably increased as forested land was cleared for primitive agriculture. Flint, being brittle, is not suited for repeated use as an axe, whereas certain stone, especially greenstone, is ideally suited for chopping down trees as it is both hard and *resilient* (Weddle pers. com.). Co-incidentally, it is proposed that there may have been more 'spare' time available in a primitive agrarian culture than a hunter-gathering culture so the ability to experiment with *new materials* aided the development of stone tools. Therefore the combination of the need for increased amounts of farmland and the availability of the human resource probably resulted in the impetus for the development of stone tool technology.

One simplistic but significant difference between stone monuments and stone implements is that the former are geographically fixed whilst the latter (especially stone axes) are portable. The geographical location of similar styles of henge and burial monuments indicates a movement, or migration, of concepts and skills (e.g. Bradley 1984, Simmons & Tooley 1981). The spatial and chronological advance of culture markers, such as grooved ware pottery, further illustrates this movement of concepts and skills (Renfrew 1973).

Thus culture markers can be taken to show the geographical advance of the associated culture, but only in terms of the migration or dispersal of ideas, concepts and practices. However, large, fixed, culture markers cannot clearly be used to infer trade between geographical locations. But, the geographically separated find location for many stone axes can indicate transportation, either incidental through migration of people or deliberately through transport of axes as goods for trade or barter. Recognition of axes of similar, but unique, rock types and subsequent location of the source rock exposure provide a sound basis on which to develop ideas on exchange (trade) systems in prehistoric Britain (Keiller et al. 1941, Clough & Cummins 1979, Edmonds & Sheridan 1993, Edmonds 1995).

The first recognised provenance of axe material to a source exposure was made in 1919 when a group of augite-granophyre implements was provenanced to exposures of the same rock at Craig Lwyd, North Wales and subsequently led to the discovery of the first axe factory in Britain (Warren 1919). Systematic identification of implement stone type was infrequent and de-centralised until 1937 when Alexander Keiller was instrumental in setting up "A Sub-Committee of the South Western Group of Museums and Art Galleries on the Petrological Identification of Stone Axes" (Keiller 1937a, 1937b). This committee concentrated on cataloguing stone implements found in the museums of Southwest England and in private collections, and identified a number of 'groups' to which implements were assigned on the basis of their petrology. In 1945 the Council for British Archaeology set up the Implement Petrology Committee (IPC) to extend the work carried out by the South Western Group of Museums and Art Galleries to cover all stone implements found in Britain (Grimes 1979). To date the IPC recognises 39 different petrological groups of implements and has identified axe factories for 7 of the groups (Clough & Cummings 1988), with probable outcrop locations for the remaining 32 groups. The first petrological group to be listed, IPC Group I, is a uralitised gabbro, or greenstone, that was believed to have originated from the Mount's Bay area of Cornwall based on petrological similarities between implements and greenstone rocks collected from Cornwall. This thesis aims to re-examine this belief using new techniques to identify and locate the actual greenstone exposure(s) that provided the raw material used in the manufacture of these implements and thus establish a provenance for them. A positive provenance for the axes will provide a sound basis to further infer the state of the Neolithic socio-political and technological cultures in prehistoric Britain.

1.2 Terminology

Throughout this work it will be necessary to discuss *groups* of implements, locations, rock types, etc., therefore the phrase IPC Group N (where N is in Roman Numerals) will be used when referring to the existing IPC petrological groups as defined in Clough & Cummins (1988). Additional terminology related to sub-groups of implements will be introduced in Chapter 4.

The majority of stone implements attributed to the Neolithic are described as axes (or fragments/part thereof) (e.g. Clough & Cummins 1988). As this work is predominantly concerned with axes, axe hammers, perforated axes, pebble hammers and maceheads the term 'axe' will normally be used in preference to 'implement' (as in many books & papers on the subject (e.g. Clough & Cummins 1979 & 1988 (Stone *Axe* Studies Vol. (I) & Vol. (II))). The use of the term 'implement' in the title of this work identifies that the technique for provenancing is not dependent on the *type* of stone object being investigated (providing it is large enough to be analysed c.f. Chapter 5 & 6).

In keeping with existing practice, dates suffixed 'BC' will refer to calendar years, whilst 'bc' will refer to radiocarbon years (both counted backward from Year 1AD).

1.3 Petrological analysis of British stone implements

By 1988 the IPC had assigned 53.5% of the 7625 recorded stone implements to the 39 petrological (axe) groups (Clough & Cummings 1988). The most common method of allocating implements to IPC Groups is carried out through examination of macro and microscopic mineralogical and textural characteristics of the implement. The difficulty in accurately determining subtle differences in mineralogy through macro examination caused by surface finish and weathering often results in the need for a petrological thin section to be taken from the implement and examined before the implement can be assigned to an IPC Group (Davis 1985). Although the method of extracting thin sections from implements has improved from simply slicing the implement in half (North (1942) describes this practice) to extracting a small core of material (Fenton & Travis 1988) it still destroys part of the axe forever. By personal experience it is found that the desire for a museum or collector to keep a valuable Neolithic implement intact is often greater than their need to know the provenance of the implement. This is probably one reason why many British stone implements have yet to be assigned to petrological groups and clearly illustrates the need for totally non-destructive provenancing.

In some cases, petrological examination alone cannot provenance an axe. For example IPC Group IX axes are manufactured from porcellanite and this relatively rare rock type is found in two geographically separate locations in Ireland, Tievebulliagh and Rathlin Island, and examination of thin sections alone cannot be used to discriminate between these two locales. In this case a different technique is needed in order to provenance porcellanite implements to one of the two possible sources. Mandal et al. (1997) showed that both exposures were geochemically distinguishable as they have different Sr and Y concentrations. Hence, by geochemically analysing samples taken from porcellanite implements using x-ray fluorescence (XRF) it became possible to assign individual implements to one of the two exposures (Mandal 1996, Mandal et al. 1997). However, as for petrological thin sections, part of the implement is destroyed in order to carry out conventional XRF. This incurs the same problem about balancing the desire to maintain an unblemished implement against the need to know where it originated and has so far resulted in keeping, for example, the valuable Malone Hoard of porcellanite axes intact.

Reflected light microscopy (ore mineral identification), electron microprobe (mineral analysis) and x-ray diffraction (mineral identification) are examples of other petrological and geochemical analytical methods available for characterisation of samples (Davis 1985). However as before, all of these require a sample of part of the implement and are partially destructive in nature. It is worth pointing out that it may be possible to carry out reflected light microscopy and electron microprobe analysis on existing thin sections if these sections could be re-polished. But, their original preparation and the fact that glass or resin is seen to cover all but the most recent axe (post 1998) thin sections examined as part of this work probably renders them useless for these types of investigation.

Excluding geochemical analysis techniques, the accuracy of assigning implements to IPC groups is often dependent on the experience of the petrologist examining the implement and thin section. With some rocks, especially greenstones, there may be subtle differences between the sample being examined and the reference specimen that are not seen by the examining petrologist. This gives rise to doubts about the petrological homogeneity of the IPC groups (Davis 1985).

To overcome the problems described above a non-destructive, analytical technique is required. This thesis involves the use of two such techniques, portable x-ray fluorescent

spectroscopy and magnetic susceptibility, both pioneered by The Open University (Williams-Thorpe & Thorpe 1993a, Williams-Thorpe et al. (1996), Potts et al. (1997a & b), Williams-Thorpe et al. (1999a & b, 2000)) in the investigation of the hypothesis that IPC Groups I, Ia, I/Ia, I(near) and III originate within the greenstones found in the Mount's Bay area of Cornwall. The next section introduces the two non-destructive analytical techniques used by The Open University that are used and further developed in this thesis.

1.4 Non-destructive analytical techniques

1.4.1 Portable x-ray fluorescent spectroscopy (PXRF)

Technological advances in portable geochemical analysis equipment have resulted in the production of field–portable x-ray fluorescent spectrometers (PXRF). These devices are able to measure elemental compositions of samples without the need for sample preparation (other than cleaning the surface to be measured) and therefore obtain geochemical analyses in a totally non-destructive manner (Williams-Thorpe et al. 1999a). A recent case study has clearly illustrated the potential of using PXRF analyses to provenance axes by measuring a number of IPC Group XIII axes using the PXRF and comparing the data with compositions of possible source exposures (Williams-Thorpe et al. op cit.).

This work follows the procedure identified by Williams-Thorpe et al. (op. cit.) but applied to a large number of greenstone axes identified in Section 1.5 below (and detailed in Chapter 2) and greenstone exposures found in SW England (c.f. Chapter 3). It is noted that PXRF analysis of greenstone axes has not been previously carried out and no PXRF analyses have been made on Cornish greenstones. In addition, the scale of the current investigation is also larger than any of its type so far undertaken in Britain. Hence, prior to the comparison of axe and exposure geochemistry (c.f. Chapters 7 & 8), a full review of the analytical performance of the PXRF as applied to greenstone axes and exposures will be carried out (c.f. Chapter 6).

1.4.2 Magnetic Susceptibility

A second non-destructive analytical technique is carried out to complement the PXRF analysis. Many igneous rocks, especially basaltic ones, contain ferro-magnetic minerals, e.g. magnetite, ilmenite, etc., and their presence determines the ease and extent (susceptibility) to which a rock can be magnetised (Sharma 1976). Measurement of magnetic susceptibility is rapid, simple and totally non-destructive (Williams-Thorpe &

Thorpe 1993a) and potentially provides an additional discriminant that can be used to provenance axes to exposures. Although the use of magnetic susceptibility to assist with provenancing is not new (Williams-Thorpe & Thorpe op. cit.) it is the first time a large number (over 225) of British axes have been measured.

Magnetic susceptibility measurements of greenstone axe and exposure will be made using an Exploranium KT5 magnetic susceptibility meter. Since this technique has not been used on greenstone axes on this scale before and it is a significant part of this work, a review of the analytical performance of the meter on axes is carried out prior to stating and discussing the results obtained (c.f. Chapter 5).

1.5 Axes to be investigated

The largest group of axes recognised by the IPC is IPC Group VI with 1612 members representing approximately 40% of the total allocated to groups (Clough & Cummings 1988). These axes have been provenanced to rock exposures in Great Langdale (Bunch & Fell 1949) and probably manufactured in an axe factory at the foot of Pike o'Stickle (Bradley & Edmonds 1993). The second largest group is IPC Group I with 384 members, representing approximately 10% of the axes assigned to IPC petrological groups by 1988 (Clough & Cummins 1988). Keiller et al. (1941) provenanced IPC Group I to the Mount's Bay area of Cornwall on the basis of sharing similar mineralogy and texture with (unidentified) greenstone rocks found between Penzance and Mousehole (c.f. Figure 2, Section 2.3). The difficulty in petrographically matching thin sections not only between axe and exposure, but also between axes, has resulted in the IPC introducing a further three greenstone groups IPC Group Ia, I/Ia and I(near) (although only IPC Group Ia is defined – the others are identified in the IPC catalogue only c.f. Chapter 2 for details). This work investigates the petrographic, magnetic and geochemical similarity between and homogeneity within these 4 groups and examines the hypothesis that these axes originate from a greenstone exposure on the west-side of Mount's Bay, between Penzance and Mousehole as proposed by Keiller et al. (1941).

IPC Group III has 20 members and has been provenanced by Keiller et al. (1941) to a single exposure on the east side of Mount's Bay near Perranuthnoe on the basis of a petrographical match between an axe thin section and one from the exposure. The exact location of the exposure is not given by Keiller et al. (op. cit.) and this thesis aims to

rectify this omission and will compare geochemical results from axes and exposure alike in order to test the hypothesis regarding IPC Group III's provenance.

Whenever possible and available IPC ungrouped and non-IPC (i.e. not registered by the IPC) greenstone axes are analysed using the non-destructive techniques described in Section 1.4. Results will be used to assign axes to IPC groups on the basis of non-destructive analyses alone. Similarly, a number of Irish gabbroic and doleritic axes are analysed for comparison with Cornish greenstone axes and exposures. In this latter case a positive match would support transportation of axes across the Irish Sea as hypothesised by Mandal (1996).

1.6 Examination of existing axe thin sections

Existing axe thin sections belonging to IPC Group I, Ia III & IIIa are examined to investigate the extent of mineralogical and textural differences seen within these IPC groups. This examination will form a foundation on which to develop the subsequent non-destructive investigations, as confirmation of any mineralogical and textural differences found within the collection of thin sections will be looked for in the PXRF and magnetic susceptibility data sets.

Comparison between existing axe and new greenstone exposure thin sections, collected as part of this thesis, is not expected to result in the identification of the source of the axes since the exact provenance has eluded a number of workers over the past 60 years. However, the converse is probable, new comparisons will assist with eliminating exposures as potential sources for the IPC greenstone axe groups being investigated. This latter exercise will provide new information since 'negative' (i.e. exposures that are not petrographically similar to axes) results have not been published by previous workers.

1.7 Introduction to Cornish greenstone

During the Devonian and Carboniferous geological eras the south-west of Britain was located within the Variscan Orogeny. This large scale tectonic event produced an amount of basaltic igneous activity associated with incipient oceanic spreading, continental rifting and back arc spreading (see Hutton & Sanderson 1984, Holder & Leveridge 1986, Floyd 1995). This basaltic activity gave rise to the emplacement of localised sub-aerial and submarine basalt (pillow) lavas, shallow and deeper level dolerite dykes and sills and larger intrusive masses of gabbro (Floyd et al. 1993). Subsequently, these basaltic rocks

were affected by pumpellyite-prehnite facies regional metamorphism caused by the emplacement of the Cornubian batholith and continued Variscan deformation (Warr et al. 1991), and by contact metamorphism through emplacement of localised granitic masses (e.g. Land's End granite) (Goode & Taylor 1988, Selwood et al. 1998). In many cases, the effect of the metamorphism caused the growth of secondary minerals within the basalt such as epidote, chlorite and amphibole. It is the presence of these minerals within the meta-basalt, meta-dolerite and meta-gabbro that give the rock a greenish tinge and led to 'greenstone' becoming the common name for this group of rocks.

The often-localised nature of the original basaltic igneous activity, the number of exposures and the varying degrees of alteration mineralogy has resulted in the failure to find an exact match between IPC Group I greenstone axes and greenstone exposures in Cornwall using macro and micro examination techniques (Keiller et al. 1941). However, different types of tecto-magmatic activity give rise to rocks of different composition that can be recognised through geochemical analysis (Rollinson 1993). As most magmatic activity in West Cornwall (known as the 'Penwith Peninsula') is not co-magmatic (i.e. does not originate from the same magmatic source) (Floyd 1984) it becomes possible to use these geochemical differences in order to narrow down, and possibly locate, the greenstone exposure that provided material for the manufacture of certain Neolithic greenstone axes.

1.8 Structure of thesis

Volume I of this thesis contains the narrative supported by key tables, figures, maps and charts and is divided into 10 chapters, plus bibliography. Chapter 1 introduces the thesis, Chapters 2 & 3, respectively, discuss the archaeological and geological background to the work. Chapter 4 examines the petrography of existing axe thin sections and greenstone exposures and introduces new axe sub-groups based on petrographic similarities (these sub-groups are used extensively in Chapters 7 & 8). Chapter 5 describes the analytical procedures for determining magnetic susceptibility and discusses the performance of the Exploranium KT5 meter prior to examining the results on axes and exposures. Chapter 6 describes the analytical performance of the PXRF for measuring greenstone rocks and axes, resulting in a series of correction factors for quantitative PXRF data. Chapter 7 examines axe PXRF data (*en masse*) and using information from Chapter 4 & 5 examines typical compositional ranges and the geochemical relationship between and within IPC axe groups. Chapter 8 uses the information from Chapters 3 to 7 and presents new PXRF

greenstone exposure data in order to provenance axes to exposures using various statistical procedures. Chapter 9 discusses the outcomes of the research and identifies future research possibilities, whilst Chapter 10 lists the thesis conclusions.

Volume 2 of the thesis contains a series of 31 Appendixes that contain primary, processed and other supporting data in the form of tables, charts, maps etc. Appendixes are numbered sequentially as they may support one or more chapters. The size of this volume (>400 pages) reflects the significant amount of data collected, summarised and evaluated as part of the research.

In addition to the two thesis volumes there are 5 Photo CD-ROMs containing approximately 500 digital petrographic and photographic images taken as part of the research. The contents of the 5 CDs are listed in Volume 2, Appendix 6.

1.9 Summary

Understanding the indelible record of pre-history provided by stone implements leads to a wider appreciation of the culture and environment inhabited during the Neolithic. Rarity of these implements and use of partially destructive provenancing techniques has resulted in a partial vision of the past from which to infer ideas concerning Neolithic trade and communication. The aim of this thesis is to increase this partial vision through the use of totally non-destructive analysis techniques that maintain the integrity of the record whilst simultaneously providing increased knowledge regarding the provenance of such implements.

The main objective of this work is to investigate the hypothesised provenance of IPC Group I greenstone axes to a source greenstone exposure in Mount's Bay, Cornwall, using new non-destructive PXRF geochemical analysis supported by established magnetic susceptibility techniques. Secondary objectives investigate the petrographical and geochemical similarities between and within IPC Groups Ia, I/Ia, I(near) III & IIIa as well as their provenance. Such investigations have not been carried out on the scale proposed or on this type of stone axe before so the performance of the PXRF and magnetic susceptibility equipment will be established as a precursor to the provenancing exercise. Provenancing will be primarily based on matching geochemical aspects of axe and exposure, and supported by magnetic susceptibility data. Examination of existing petrological thin sections is carried out to re-assess the petrological homogeneity of IPC

Group I, Ia III & IIIa and to form an initial basis from which to work. Using the processes developed in provenancing IPC Group I, the potential to assign ungrouped axes to established IPC groups and to investigate the origins of selected Irish doleritic and gabbroic axes using totally non-destructive analysis techniques is assessed.

Provenancing of axes to exposures has been carried out by the IPC for over 60 years. The methodology used, petrographic comparison, is well tried and trusted, but is partially destructive and has yet to definitively provenance IPC Group I axes to a particular greenstone exposure. Non-destructive techniques have the potential to refine and focus the provenancing of Neolithic stone tools, complementing and expanding the knowledge base established by the IPC.

2 Implement petrology and IPC axe groups

2.1 Introduction

Implement petrology involves the study of mineralogical, textural and more recently the geochemical and magnetic properties of prehistoric stone axes and hence of the stone used to manufacture them. Geographical (find location) and chronological (archaeological context) information of axes coupled with petrological data provides a sound basis from which knowledge of the Neolithic period, of social environment, the use and importance of mass production centres (axe factories), the economic value of artefacts (trade) and the development of stone technology in time and space can be inferred. These aspects are briefly reviewed below, forming the archaeological context to this research, prior to describing the relevant Cornish IPC axe groups.

Southwest England, and Cornwall in particular, has a rich Neolithic history that is seen in the numerous quoits (tombs), henges and settlements found in the region (see Balfour 1992, Manley 1989, Pearce 1981). Neolithic culture in this region is believed to have used and traded local greenstone to areas as far away as Yorkshire and possibly overseas to Ireland (Pearce op. cit., Clough & Cummins 1988, Mandal 1996). This new study of supposedly Cornish greenstone implements uses totally non-destructive analytical techniques and will allow a greater insight to aspects of the Neolithic highlighted above and will aid investigations of the distribution of axes throughout England and as far as Ireland.

2.2 Archaeological value of implement petrology

Tilley (1994) considers that stone implements provide an indelible record of prehistory, but goes on to indicate that these implements are only one aspect of the 'social space' inhabited by our ancestors. Tilley discusses that a holistic approach through the synthesis of archaeology, geology, human geography and anthropology is needed to understand the social, physical, economic and political environments inhabited during prehistoric times and that this holistic approach leads to a clearer understanding of how people treated, worked and ritualised the landscape (ibid.).

Models of Neolithic environments can be generated from observing modern equivalents such as the Australian Aborigines (Tilley 1994, Gron 1991). The term 'model' is appropriate here since parallels drawn between 'modern' Stone Age society and a

prehistoric Stone Age society, through homology, are 4000 years apart and the suggestion that modern stone age societies have not *evolved* is difficult to comprehend. However, these models do provide a framework from which to develop an understanding of how the scant records from prehistoric times, such as pottery, stone implements, monuments and graves can be related to provide insight to the 'social space' occupied in prehistoric times. Models that aim to develop an understanding of prehistoric social space need firm foundations on which to build, or 'to infer' from, or else they will fail, as new knowledge becomes available.

The further away inferences are extrapolated from factual basis the larger the potential error in interpretation becomes. Hawkes (1954) described this as a 'hierarchy of inference' which he illustrates through levels of difficulty:

1. To infer what techniques were used to create 'archaeological phenomena' is *relatively easy*
2. To infer the subsistence-economics of human groups from 'archaeological phenomena is *fairly easy*
3. To infer the socio-political relationships between prehistoric groups is *considerably hard*
4. To infer the religious and spiritual beliefs of prehistoric communities is the *hardest of all*

The combination of Stone Age models and a greater understanding of 'archaeological phenomena' and knowledge of the restrictions placed on inference can lead to a greater clarity in understanding the social space present during the Neolithic in Britain. Accurate provenance of stone tools provides a firm basis to commence and build inference on the social space occupied in the Neolithic. Thus, factual knowledge about this type of 'archaeological phenomena' (greenstone axe provenance) can lead to inferences on various technological, social, economic and political aspects of the Neolithic.

Specifically, Neolithic stone implements found in various remote locations, away from their source region will create a basis to make inferences on social interaction through trade or exchange between geographically separated populations (Keiller et al. 1941). Similarly, economic factors can be inferred through estimating the perceived *value* of implements as gauged by the distance they have been transported and the state of the implement (partly or completely finished) (Bradley 1984, Hodder & Lane 1982)). The

total population and geographical extent of petrologically similar stone implements can be used to infer the level of social and political importance placed on the rock source. The presence of recognisable manufacturing sites ('axe factories') can lead to inference on the social and economic importance of individual rock exposures as well as giving insight to stone technology (e.g. the Langdale axe factory (Bradley & Edmonds 1993)). The level of physical difficulty in accessing the source rock exposure may give additional insight as to the ritual or religious significance of the site (e.g. Tievebulliagh (Cooney & Mandal 1998) and Langdale (Bradley & Edmonds op. cit.)).

This thesis aims to provide new and sound knowledge on the provenance of Neolithic IPC Group I greenstone axes believed by Keiller et al (1941) to have originated within Southwest England. An accurate provenance for these greenstone axes will expand and enhance the base of substantiated facts available (e.g. Clough & Cummins 1988) for future research aimed at understanding the social space occupied during the Neolithic and Early Bronze Ages in Britain.

2.3 Review of Implement Petrology in Britain

It is not clear when the study of implement petrology began, although it probably developed in line with the advances in geological understanding in the early 19th Century. Evans (1872), whose work is almost certainly based on work by colleagues earlier in the century, discusses the identification of implement rock types and their possible sources. Individual collectors, societies and museums appear to have kept separate records until the formation of the Council for British Archaeology (CBA) in 1945. At this time, the CBA appointed a sub-committee to obtain and collate artefact data, including petrology (Grimes 1979). The Implement Petrology Committee (IPC) as it became known had already been in existence since 1937 as a sub-committee of the South Western Group of Museums and Art Galleries (Keiller et al. 1941). The synopsis, below, is largely based upon the history of the IPC as presented and discussed by Grimes (1979) and Davis (1997). Note that in this work 'IPC' and 'sub-committee of the South Western Group of Museums and Art Galleries' are used synonymously.

The IPC and colleagues have systematically catalogued the dispersed collection of British stone implements. In its original guise as a sub-committee of the 'South Western Group of Museums and Art Galleries' the IPC concentrated on the recording of stone implements, mainly axes, of the Neolithic and Early Bronze Ages with the purpose that "an exact

determination of the rock material and its original provenance, together with a knowledge of the locality at which the tool was found, would lead to far wider and more exact information concerning early trade routes and other factors of economic and social importance in Neolithic and Early Bronze Age times" (Keiller et al. 1941: p50). The IPC was formally established as a national body by the CBA in 1945 and became a standing committee in 1952, in order to continue and expand on the work of the original South Western Group on a national basis (Grimes 1979). As at 1988, over 7,600 stone axes had been recorded from museum and private collections, with just over 50% assigned to the 39 petrological 'groups' (Clough &Cummins 1988). These petrological 'groups' were defined through the examination of petrological thin sections of axes. Axes with similar characteristics were 'grouped' together and given titles such as 'Group XVII'. In seven cases the rock outcrop providing the axe material was readily located, either through prior archaeological knowledge of the site of manufacture (e.g. IPC Group VII from Graig Lwyd (Warren 1919 & 1922)), or by its unique petrology/mineralogy only occurring in restricted areas. For the remaining 32 petrological groups the axe material could only be provenanced to an area where the rock was found at outcrop and not to a single rock exposure.

The IPC provided a great impetus to the understanding of social interaction in the Neolithic and Early Bronze Ages by mapping the find location of axe groups and identifying actual or probable source exposures. Resultant distribution patterns were seen as indicating the existence of trade routes, or at least the transportation of the axes away from the source. In two cases, IPC Group I and IPC Group VI, the distribution pattern is extensive, suggesting that the manufacture and trade of the Neolithic axes was deliberate and possibly organised (Keiller et al. 1941, Edmonds 1995, Cummins 1979). The origin of the tuff used to manufacture IPC Group VI was found to be an exposure on Langdale Pike (Bunch & Fell 1949). This origin, combined with the location of a significant axe factory, just below Langdale Pike (ibid.) has allowed the subsequent distribution of Langdale axes to be inferred (Bradley & Edmonds 1993). However, the precise origin of IPC Group I remains a mystery and has been 'within the Mount's Bay area of Cornwall' since the first published report of the IPC (Keiller et al. 1941). In this case the lack of a precise source raises some doubt as to the validity of trade-related arguments based on the dispersion of IPC Group I from Cornwall.

Macroscopic examination of axes are often insufficient to determine the petrology/mineralogy of axes and other methods need to be employed (Grimes 1979, Mandal 1996). To date, the most common method used to determine axe rock type is by examination of petrological thin sections (hereafter referred to as 'thin sections'). This, partly destructive process, was used as early as 1914 and early attempts at sectioning resulted in some axes being sawn in half (North 1942). This partial and sometimes irrecoverable defacement of valuable implements is seen to have caused reluctance by collectors and museum curators in releasing their collections for petrological provenancing. However, the reluctance seems to have been largely overcome by adopting a less drastic sampling methodology (e.g. taking small slices of material, not cutting the axe in half). In an unpublished letter to The Museums Journal in 1942, North states "... and the method adopted in making thin sections is such that from the museum stand point the appearance and shape of the specimen is exactly as it was before slicing: this should remove the last shred of reluctance on the part of the archaeologist to allow their material to be prepared for the only form of examination that can be expected to yield conclusive results." (North 1942). Further improvements in extracting material for sectioning using a coring drill were developed in the 1980s (Fenton & Travis 1988). This process involves removing a core of material as opposed to a slice of material, with part of the core being used as a plug to fit back into the hole, and has improved the visual presentation of axes post sampling.

Although the use of thin sections to identify rock type is well understood (see Deer et al. 1992, Kerr 1942) it is often the case that a particular rock type may come from several rock exposures. This uncertainty in the ability to accurately provenance thin sections to a single exposure has given rise to doubts about the origins and homogeneity of some axe groups (Davis 1985). Further discriminants, used to reduce the number of probable source exposures and increase the confidence of grouping like implements, can be provided through instrumental analysis using X-ray fluorescence or microprobe techniques. These techniques provide information on elemental and mineralogical characteristics of rocks and can be used in order to increase the probability of provenancing the sample to a rock exposure. However, these methods are generally more expensive than thin sectioning and require an extensive database of potential sources to allow accurate provenancing (Davis 1985). In addition they are also partially destructive, as they require some of the sample to be ground to a powder, or otherwise processed prior to analysis. As stated in Chapter 1, newer, non-destructive methods for obtaining geochemical and magnetic susceptibility

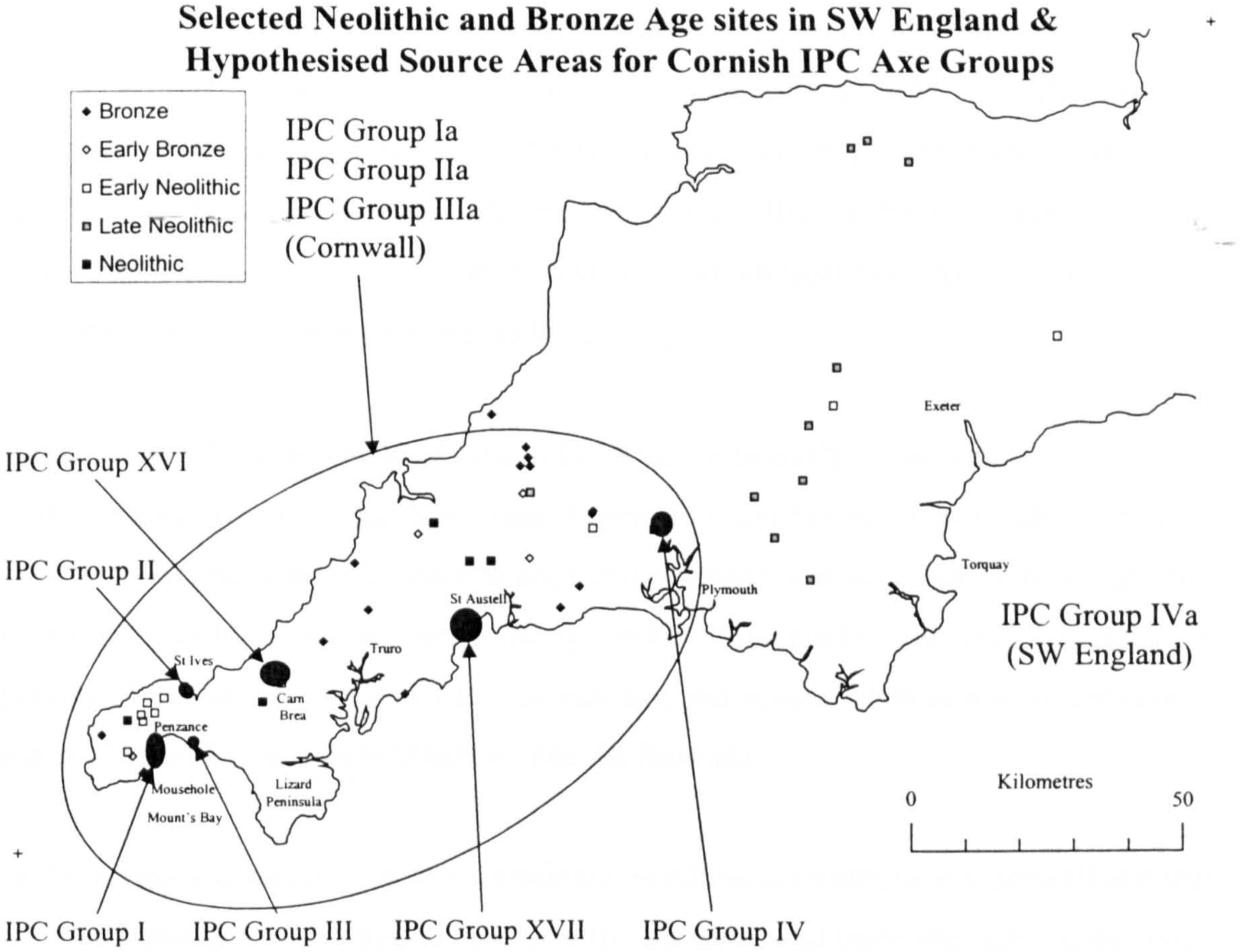

Figure 2 Map of SW England with selected Neolithic & Bronze Age sites and source of Cornish IPC axe groups (after Pearce 1981 & Clough & Cummins 1988). Sites are dated as reported in the literature references and generally represent the first occupation or use of the site. Site details are listed in Appendix 1. (Note Cornish IPC Group XIX is a greywacke and not included here)

data are being pioneered at The Open University and these methods provide great potential in the provenancing of stone tools (Williams-Thorpe et al. 1999a, b; Potts et al. 1995).

2.4 Occupation of Cornwall during the Neolithic and Early Bronze Age

The geographical focus of this research is based on the Keiller et al. (1941) belief that IPC Group I originated from the Mount's Bay area of Cornwall. This section briefly reviews the occupation of Cornwall in the Neolithic and Early Bronze Age using the location and type of settlements and monuments found. A more comprehensive summary of the archaeology of SW England has been produced by Pearce (1981) and of Cornwall by Barnatt (1982). A discussion on the evolution of social structure and associated development of cultural artefacts (e.g. henges, hill forts etc.) can be found in Bradley (1984).

The largest Neolithic occupation in Cornwall is found at Carn Brea, near Camborne. This hill fort/causewayed enclosure was occupied during the middle to late Neolithic based on evidence from two radiocarbon samples (BM-825 giving 3049bc ± 64 & BM-824 giving

2742bc ± 60) (Smith 1979). The human population within the 18ha site has been given as 100 to150 (Bewley 1994) and 200 (Balfour 1992). Evidence of artefact manufacture is through flint debitage, with transport of the flint and associated pottery from Dorset suggesting a trade link of some sort (Pearce 1981). Carn Brea is 20km from the hypothesised origin of IPC Group I axes, several of which have been found in unstratified (i.e. not datable) locations within the enclosure.

A number of Neolithic tombs are found in Cornwall, especially on the Penwith Peninsula. The presence of 'quoits' (= capstone) (see Appendix 1 and Figure 2), associated with late Neolithic burial practices indicates that population density was sufficient to plan and move dolmens of up to 30 tonnes (e.g. see Bradley 1984). Stone circles and other megaliths are indicative of the late Neolithic to Early Bronze age and several of these monuments are found in Cornwall (e.g. Merry Maidens, near St Buryan).

It can be concluded that there was a significant Neolithic community in Cornwall and that these people had the technology to manufacture, transport and trade artefacts. Indications from burnt remains and a significant number of arrowheads found at Carn Brea also indicated that towards the end of the Neolithic social interactions were occasionally hostile suggesting artefacts could be pillaged as well as traded. One hypothesis is, therefore, that the people at Carn Brea may have 'owned' something of sufficient *value* that others wanted to the point of doing violence?

2.5 Summary of IPC Axe Groups identified as originating within Cornwall: rock type and hypothesised origin

The IPC recognises a number of petrological axe groups that have been provenanced to rock types found in Cornwall. In some situations an exact provenance for the IPC group has been ascertained by petrographic matching of axe thin sections with exposures having the same mineralogy and texture. In other situations an exact provenance has eluded the IPC who are only able to hypothesise a Cornish origin for the axes through petrological & mineralogical similarity with rocks found in Cornwall, or because the highest density of axe finds is in Cornwall. This section identifies those IPC axe groups provenanced to Cornwall and gives details of group petrology and current hypothesised provenance.

Note that the number of members shown for each IPC group below is taken from Clough & Cummins (1988) and that all Cornish greenstone groups are listed. Section 2.8 details

the actual IPC groups selected for investigation. Although this work focuses on IPC Groups I and III (and related minor IPC groups, e.g. IPC Group Ia), as IPC Group I is the largest Cornish greenstone axe group and IPC Group III is provenanced to an outcrop on the east side of Mount's Bay, much of the material introduced in this thesis will be relevant to other Cornish axe groups, hence all Cornish greenstone groups are, at least, reviewed.

2.5.1 IPC Group I (384 members)

The 1st Report of the IPC (Keiller et al. 1941) identified the IPC Group I rock type as a uralitised (= blue-green amphibole, an alteration product) gabbro, or epidiorite, or greenstone; all three descriptions indicating an altered basic igneous rock. The axes were characterised as medium grained, dark green or greenish-grey, weathering to a rough surface. IPC petrographic examination of axe thin sections identified partial to total alteration of primary, sometimes ophitic, augite (a clinopyroxene) to fibrous blue-green amphibole (i.e. uralite). Primary feldspars, presumed albite, were 'much' altered and contained actinolite (an amphibole). Lastly, ilmenite was found to be the most common accessory mineral, often altered to leucoxene (Keiller et al. op. cit.). Subsequent IPC reports do not add to this description of the IPC Group I rock type, other than to comment on the small, but distinct, variability of group petrology (Evens et al. 1972).

Keiller et al. (1941) identified the probable source of IPC Group I as Cornwall or Devon based on the petrological examination of 'several hundred thin sections of greenstone from various igneous areas in the British Isles'. At this time (1941) it was concluded that the probable source was 'small' on account of the fact that the 20 axes allocated were all very similar to each other. The 3rd IPC Report (Stone & Wallis 1951) identified that 'very close' matches had been found between greenstones 'lying between Penzance and Mousehole' and IPC Group I, however no exact match had been found. That report goes on to speculate that a 5 to 10m sea level change may have occurred since the Neolithic and the source may therefore, be underwater. Subsequently two specimens from Gear Rock, a partly submerged exposure of greenstone approximately 1km south of Penzance harbour (Grid ref. SW479293) were examined and found to be 'near to Group I' but not an exact match (Evens et al. 1972). The current published source for IPC Group I is ' Mount's Bay area, near Penzance, Cornwall' (Clough & Cummins 1988).

2.5.2 IPC Group Ia (29 members)

IPC Group Ia is first described in the 3rd Report (Stone & Wallis 1951) as similar to IPC Group I, but with its more heterogeneous members having a smoother weathered surface and less altered augite and feldspar. Additionally, the bladed hornblende found in thin sections of this group are 'somewhat parallel' (Stone & Wallis op. cit.). Further IPC reports do not add anything to the original description.

At the time of description (1951) the hypothesised origin for IPC Group Ia was given as 'Cornwall' on the basis of petrological similarity between axe material and Cornish greenstones (Stone & Wallis 1951). Clough & Cummins (1988) summarise the source of IPC Group Ia as SW England.

2.5.3 IPC Group I(near) (22 members)

IPC Group I(near) is not defined in any of the IPC reports and only appears in the axe catalogues (Clough & Cummins 1979 & 1988). It is therefore assumed that axes have been assigned to this group as they share similar, but not exactly the same characteristics as IPC Group I.

2.5.4 IPC Group I/Ia (8 members)

IPC Group I/Ia contains a number of axes found in and around London. As for IPC Group I(near) it is assumed (because no references to the origin of the group have been found) that these axes are similar to both IPC Group I and Ia, but the petrologist carrying out the assignment could not decide which IPC group to place the axes in. A review of IPC minutes and letters may reveal the true reasons for this situation.

2.5.5 IPC Group II (3 members)

IPC Group II is described as similar to IPC Group I greenstone, but with no augite, amphibole as the only ferro-magnesium mineral present, a little biotite and overall finer grained than IPC Group I (Keiller et al. 1941).

The first (of only 3) members of this group was provenanced to a spot between Lay Point and St Ives by matching one axe thin section with an exposure thin section held in the Geological Survey collection (no 921). Lay Point is identified as a 'promontory 100 yards west of Porthminster Point' (Grid ref. SW524399) (Keiller et al. 1941).

2.5.6 IPC Group IIa (8 members)

IPC Group IIa is described as an epidiorite or greenstone, similar to IPC Group II but finer grained and with apatite as well as hornblende ('a felted mat of needles'), biotite and lack of augite (Stone & Wallis 1951).

An origin within Cornwall was hypothesised on the basis of the distribution patterns of IPC Group IIa axes that had been catalogued by 1951

2.5.7 IPC Group III (20 members)

Keiller et al. (1941) states that the petrographic appearance of IPC Group III axes is similar to IPC Group I but that IPC Group III consists largely of hornblende, present as 'large plates of parallel needles' and feldspar. The opaque mineral, ilmenite, is present as scattered grains that are 'largely decomposed to leucoxene' and a 'few stout needles of apatite' complete the mineralogy (Keiller et al. op. cit.). Subsequent IPC reports do not add further to this description.

Through a match between one axe in the group (Wi4/4) and an exposure thin section held by the British Museum (BM No 74141), IPC Group III is provenanced to Trenow Cove (Keiller et al. 1941). Based on the description in the 1st IPC Report, the quarry supplying the thin section is located between Perranuthnoe and Marazion and from the photograph in the report (Plate 1 lower) and the 1:10 000 Ordnance Survey (OS) maps of the district around Perranuthnoe, the most probable location of the quarry is at Grid ref. SW534297. The quarry marked on the OS map at this point is about half way between Trenow Cove and Perranuthnoe church and the quarry floor is on the 30m contour. Seawards of the quarry, there is a marine platform approximately 200m across lying on the 10-15m contour lines. It is therefore believed that the location identified by Clough & Cummins (1988) as 'nr. Marazion' is a little misleading as Marazion lies 1km north-west of Trenow Cove (although Marazion is the largest settlement within 5 km of Trenow Cove).

2.5.8 IPC Group IIIa (7 members)

IPC Group IIIa is macroscopically different to IPC Group III in that the former has distinct 'black spots' covering its greenish-grey exterior (Stone & Wallis 1951). However, microscopically, IPC Group IIIa has accessory brown mica (biotite?) and epidote in addition to secondary hornblende, ilmenite and a lack of augite (Stone & Wallis op. cit.). Overall, the axe rock type is still classified as greenstone.

Stone & Wallis (1951) conclude that IPC Group IIIa originates from Cornwall on the basis of 'petrological evidence' and this remains the accepted hypothesis.

2.5.9 IPC Group IV (38 members)

Keiller et al. (1941) state that macroscopically IPC Group IV and IPC Groups I & II are indistinguishable. Microscopically, IPC Group IV is described by Keiller et al. (1941) as a 'sheared tremolite rock with chlorite and ilmenite' where all the primary augite has been altered to secondary amphibole (i.e. tremolite) in such a way as to suggest the rock has been sheared. The rock is re-examined by Evens et al. (1962) who concluded that it is a picrite on the basis that the matrix was 'pale, almost isotropic chlorite' with abundant pale amphibole embedded within the chlorite. Irregular patches of greyish olivine are full of cracks but not serpentenised and no feldspar is found allowing the conclusion that the rock was originally a picrite or peridotite.

Stone & Wallis (1951) provenance IPC Group IV to Balstone Down near Callington in Cornwall, giving no supporting reasons or evidence. Evens et al. (1962) support this hypothesis, but again, do not say why. A small outcrop of peridotite is shown at grid reference SX370699 on BGS Sheet 337 (1994) and it must be assumed that the proximity of finds to this outcrop prompted the provenance.

2.5.10 IPC Group IVa (15 members)

IPC Group IVa was first introduced by Stone & Wallis (1951) and described as similar to IPC Group IV, but with 'differentiated hornblende needles' (as opposed to bunched) and the presence of epidote. Evens et al. (1962) refined this observation identifying that the rock had a chloritic matrix with embedded, irregularly orientated blades and needles of actinolite. Large 'plates of colourless, fibrous amphibole' that occasionally appeared to show relicts of an ophitic structure and fine grains of a brown mineral are also identified. Evens et al. (op. cit.) also noted the presence of 'grains and streaks of magnetite' which is different to the ilmenite contained in the other greenstones described so far. The rock was a named as a sheared greenstone.

Neither Stone & Wallis (1951) nor Evens et al. (1962) identified a potential source area for the rock. It is therefore assumed that Clough & Cummins (1988) identified 'SW England'

as the source on the basis of the finds being concentrated in Devon, Dorset & Somerset (after Davis et al. 1988).

2.5.11 IPC Group XVI (78 members)

Evens et al. (1962) introduce IPC Group XVI in the 4th report of the IPC. No macro description of the rock is given, other than it is a greenstone. Microscopically, the rock is identified as being dominantly hornblende, occurring as acicular patches and roughly aligned and most feldspar present have been altered to an almost isotropic mass. Pale brown mica (secondary biotite?), epidote and small, and occasionally 'skeletonised', grains of black iron ore are noted as accessory minerals. Subsequent IPC reports do not add to this description.

According to Evens et al. (op. cit.) the axe rock was matched with a greenstone from the Camborne area, although no details are given. The 5th report of the IPC supports the Camborne area origin by noting that '50% of the axes are from the Camborne area' and that nine were recovered from Carn Brea.

2.5.12 IPC Group XVII (17 members)

IPC Group XVII is introduced in the 4th report of the IPC (Evens et al. 1962) and is described as a greenstone 'consisting of parallel folia of clear crystallised feldspar' and intergranular green, fibrous hornblende occasionally forming 'knots' around which feldspar are found 'bent' producing an augen structure. Additionally, 'considerable magnetite' was noted in the IPC Group XVII thin sections (Evens et al. 1962). Nothing extra has been added to this description by subsequent IPC reports.

Evens et al. (1962) identified that similar rock types to that described for IPC Group XVII had been found near Kenidjack and at Terras Mill, near St Austell (note the sites are approximately 100km apart) but did not conclude on a provenance for the group. The reported source 'near St Austell' (Clough & Cummins 1988) suggests that either further information has been found, or that the possible Kenidjack origin has been forgotten.

2.5.13 Summary of findings on IPC axe groups of hypothesised Cornish origin.

The following points have arisen out of the review of Cornish IPC axe groups:

1. Twelve Cornish IPC axe groups are identified by the IPC, with many of the groups having similar petrography (c.f. Figure 2).

2. Only IPC Group II & III have each been provenanced to a single rock exposure on the basis of matching one axe and one exposure thin section, but no map references for the exposures providing material for IPC Groups II & III have been published.
3. The term 'greenstone' is used to cover a number of different mineralogies.
4. Re-evaluation (and subsequent re-categorisation) of axes has taken place as different workers review the data.
5 Some of the identified axe rock sources identified by Clough & Cummins (1988) are slightly conservative (i.e. non-specific such as SW England as opposed to Cornwall).

This position has been reached after nearly 60 years of research (1941 to 2000) and strongly suggests that a new approach to the provenancing of axes is required. The comparison of petrographic thin sections has resulted in the match between only two axes and two exposures, even though 'hundreds' of axe and exposure thin sections have been examined by various petrologists (unpublished IPC archives). It is possible that the failure to petrographically provenance more than two axe groups is due to two reasons: the body of source data (i.e. axe and exposure thin sections) is not comprehensive enough and matching thins sections by eye is subjective and requires both a reference collection and considerable petrographic expertise that are not always available. Hence, additional methods, such as geochemical profiling, which is able to characterise whole outcrops or regions, are needed to improve the chances of locating axe provenances.

2.6 Axe factories

2.6.1 Importance of locating axe production sites (Axe Factories)

Throughout reading the six IPC reports and the two volumes of Stone Axe Studies (Clough & Cummins 1978, 1988) it can be seen that there is a strong desire to locate archaeological sites that produced quantities of axes. This is exemplified by Stone & Wallis (1952) who state " Such a system (of petrologically grouping stone axes) is of value only if it leads to the discovery of factory sites which can be studied by exploration". This desire is probably driven by the expectation that excavation of axe factories will greatly enhance knowledge about stone-age technology and social interaction as well as providing the point of dispersion for axes. The excavations of the IPC Group VI axe factory at Langdale Pike, Cumbria (see Bradley & Edmonds 1993), revealed a great deal about the axe manufacturing process: extraction – roughing out – finishing that all took place on the slopes of Pike o'Stickle. The exact provenance, established technology and observed

distribution of IPC Group VI gave evidence from which to derive ideas of the social activity in Neolithic times. As IPC Group I is the next largest axe group after IPC Group VI, it follows an exact provenance of IPC Group I would be extremely useful for Neolithic studies.

With reference to Cornwall, Stone & Wallis (1952) state "The importance of Cornwall (as a source for IPC Groups I to IVa inc.) is therefore obvious ... it (Cornwall) contributed not only a great variety of rocks but also a great variety of different types of implement to the economy of the Southern Counties during the whole of the Neolithic period". Hence, it is clear that there was a significant drive to locate Cornish axe factories by the IPC members at that time.

2.6.2 Location of known axe factories

Table 1, below, lists the eight currently identified axe factories relating to established IPC petrological axe Groups.

IPC Group	Rock Type	Axe Factory Location
Group VI	Epidotised Tuff	Langdale, Cumbria (Bunch & Fell 1949)
Group VII	Augite granophyre	Craig Lwyd (plus others in Penmaenmawr area) North Wales (Warren 1922)
Group IX	Porcellanite	Tievebulliagh, Ireland (Jope 1952, Sheridan 1986) Rathlin Island, Ireland (Knowles 1906, Williams 1990)
Group X	Epidiorised dolerite	Seledin, near Plussulien, Brittany (Le Roux 1971)
Group XXI	Baked Shale	Mynydd Rhiw, Wales (Houlder 1961)
Group XXII	Riebeckite felsite	Northmaven District, Shetland (Richie & Scott 1988)
Group XXIV	Calc-silicate hornfels	Creag na Caillich, Near Killin, Scotland (Ritchie 1968, Edmonds & Sheridan 1993)

Table 1 List of known axe factories

A feature for many of these sites is that a considerable amount of waste material (debitage) and unfinished axes were found (e.g. Knowles 1906, Bradley & Edmonds 1993). The amount of the material relates to two things: the amount of production and the way in which the axes were manufactured. This latter point is directly linked to the way the stone material reacted to the manufacturing process. Many of the rock types identified in Table 1, especially epidotised tuff and porcellanite, are very fine grained and axe manufacture is carried out by 'flaking' pieces off an axe blank to form a rough out, prior to polishing. Although, subsequently the finished axe may have been removed from the site, the large number of flakes remained providing clues as to the presence of an axe factory. Hence, for similar rock types finding the source rock and the exposure could lead to finding the axe factory and vice versa: finding the axe factory would almost certainly lead to finding the source rock exposure. However, this method of production and the character of an axe

factory may not be the same for all rock type: the physical properties of the rock may not leave much evidence of manufacture. This point is discussed below.

2.6.3 Potential for existence of greenstone axe factories

Coope (1979), Fenton's results with production of battle-axes and axe hammers (Fenton 1984), discussions with an amateur historian and axe-maker (Weddle pers. com.) and personal experience has established the following:

1. Greenstone does not flake into small pieces, possibly due to its hardness, resilience and grain size.
2. Greenstone axes were manufactured by 'pecking' to a rough shape, followed by grinding and polishing to the desired shape and thus debitage would be in form of small grains and dust.
3. Greenstone axes have a relatively wide range of morphologies, possibly reflecting origin as beach pebbles, cobbles or boulders.
4. Greenstones are widely exposed along the coastline of Cornwall, but rarely crop out inland.

These facts lead to the conclusion that greenstone axe factories, if they existed, would be very difficult to find. The method of manufacture leaves only dust and small particles that are easily incorporated into soil and eroded, especially if the site was close to the sea (prevailing south-westerly gales being a considerable erosive force). Secondly there is a readily available and plentiful amount of greenstone beach cobbles suitable for axe manufacture. This would reduce or possibly remove the need to quarry for axe material and the witnessed varied morphology of greenstone axes could be the result of using stone provided and partly shaped by nature (c.f. Figure 1).

Therefore, it is unlikely that greenstone axe factories can be found. This means that the only reasonable way of confirming Cornish origins of possible Neolithic trade routes is to locate the source greenstone exposure or its eroded products (e.g. beach cobbles) that provided the raw axe material. Even if the axes were manufactured from beach cobbles it is thought probable that the source of the cobbles would not be far away. Note that if Cornish axes were manufactured from beach cobbles then it is anticipated that the axes would have varied geochemical compositions, reflecting the large number of coastal greenstone exposures (c.f. Chapter 3).

2.7 Morphology of axes

Study of the morphology of stone axes has revealed aspects about the evolution of stone axe manufacturing technology and has allowed development of ideas on the actual use of the tool. For example, Roe (1969) showed that the style of perforated tools related to time and identified three progressive classes of battle axe. No detailed morphological study is made on the greenstone axes investigated in this work. However, certain morphological characteristics were noted during fieldwork:

1. Overall, the greenstone axes seen had varied morphology, generally less than 20cm long
2. More pecked 'rough outs' were found in Cornish collections than from any other location, suggesting the source rock is within Cornwall
3. Many broken axes were observed to have fractured parallel to the blade edge (shown by Weddle to be a normal use-related failure of stone axes (Weddle pers. com.))
5. Many IPC Group I axes analysed in Yorkshire were curved along the long axis (i.e. 'banana' shaped and thus, were probably adzes)
6. Several perforated greenstone axes were encountered

An investigation between axe geochemical characteristics and axe morphology may produce interesting results and will be considered as a possible future study, once this work has been completed.

2.8 IPC axe groups selected for study

2.8.1 List of IPC axe groups studied

The table below lists the IPC axe groups chosen for study within this thesis and shows the numbers analysed by PXRF, measured for magnetic susceptibility and how many thin sections are examined. Further axe details can be found in Appendix 2.

IPC Group	No in Group (members)	No analysed by PXRF	Magnetic Susceptibility	No of Thin Sections reviewed	Appendix
Group I	384	149	127	119	Appendix 2.2
Group Ia	29	4	5	17	Appendix 2.3
Group I/Ia	8	6	6	0	Appendix 2.4
Group I (near)	22	6	7	0	Appendix 2.5
Group III	20	11	7	11	Appendix 2.6
Group IIIa	7	1	1	2	Appendix 2.6
Ungrouped	414+	72	76	0	Appendix 2.7
Irish	72	23	23	0	Appendix 2.8
Totals	956+	272	252	149	

Table 2 Summary of IPC and other axes investigated in this research. Group size based on data in Clough & Cummins (1988). See Chapters 4 (thin sections), 5 (Magnetic Susceptibility) and 7 (axe PXRF) for explanations on numbers analysed/examined.

2.8.2 Reasoning behind axe group selection for analytical work

IPC Group I is the largest population of axes awaiting accurate provenancing and is the second largest group of axes recognised by the IPC. Geochemical and magnetic susceptibility analysis of this IPC group will provide insight as to whether the group is petrologically homogeneous and provide a magnetic and geochemical data set for subsequent statistical analysis. Provenancing this group will provide additional insight to the social environments present during the Neolithic as it is the most widely dispersed of all IPC groups provenanced to localities within the British Isles, with only exotic axes (jade) known to have travelled further from their (Continental) source.

IPC Groups Ia, I/Ia & I(near) are all described as being, or assumed to be, similar to IPC Group I. Comparison of petrographic, magnetic and geochemical properties of these groups with similar data from IPC Group I will be used to examine the relationship of these three groups with IPC Group I. The outcome of the examination will establish if these groups are petrographically, magnetically and geochemically similar to IPC Group I, thus indicating that they have the same provenance as IPC Group I, or not.

IPC Group III is the largest greenstone group that has been provenanced to a single exposure. Comparison of geochemical and magnetic data gathered from the group and the hypothesised Trenow Cove site of origin will be used to investigate the validity of the provenance and give insight as to the performance of the non-destructive methodology.

Comparison between IPC Group III and IPC Group IIIa geochemical and magnetic data will test the relationship of the reported visual similarities between the two groups seen in thin section.

Approximately half (3,546) of the axes listed in the IPC catalogue (7,625) have not been assigned to groups, but have been thin sectioned. This suggests that petrographic examination of thin sections has been inconclusive in every other petrographic comparison. The reasons for this level of achievement are not fully understood, but obviously must relate to the difficulty of recognising petrographic characteristics. By statistically comparing geochemical and magnetic data gathered from ungrouped and grouped axes it may become possible to confidently assign ungrouped axes to one of the established groups without the need for petrographic examination, thus removing the perceived difficulty of recognising petrographic characteristics. If this method of provenancing is

shown to be successful then it may remove the need for thin sectioning, keeping the axe unblemished, whilst at the same time allowing it to be provenanced. It is likely that such a totally non-destructive method of provenancing would meet with approval from axe custodians.

Mandal (1996) indicated that some Irish gabbroic and doleritic axes shared similar characteristics to Cornish axes. Non-destructive analysis of these axes will investigate this hypothesis and could potentially strengthen ideas of trade across the Irish Sea.

The remaining Cornish greenstone groups identified in Section 2.5 (IPC Group II, IIa, IV, IVa, XVI and XVII) will not be investigated at this time as this work concentrates on the largest unprovenanced greenstone group (IPC Group I), the largest provenanced greenstone group (IPC Group III). But, as much of the work in this thesis forms a basis for further research, the inclusion of these groups in this chapter is considered as preparation for future research.

2.8.3 Priority and selection of axes for analysis

The main analysis equipment, a portable x-ray fluorescence spectrometer (c.f. Chapter 6) was only available for limited periods, which resulted in the need to carefully plan access to the axes in order to maximise use of the equipment. Inspection of the axe catalogue (Clough & Cummins 1988) revealed that axes within the target groups were widely dispersed amongst museums and private collectors. The combination of these two factors resulted in the following order of priority being set for axes to be analysed:

1. IPC Group I
2. IPC Group III
3. IPC Group Ia, I/Ia, I(near)
4. IPC Group IIIa
5. Irish gabbroic, doleritic axes
6. Ungrouped greenstone axes
7. Any other axes not included in the above

Institutions with significant collections of IPC Group I axes were approached first. On confirmation that access to the required axes was allowed, other Institutions with smaller collections of the target groups were invited to send/bring their axes to the main Institution

for analysis. The overwhelming support this approach received resulted in the PXRF analysis of over 272 axes in 4 working weeks.

Geochemical analysis of axes was given priority over measurement of magnetic susceptibility. However, since the latter procedure took a few minutes compared with tens of minutes for the former, the vast majority of axes were also measured for magnetic susceptibility (Chapter 5).

2.8.4 Availability of existing petrological thin sections

A legacy of the IPC and its association with the South Western Group of Museums and Art Galleries is that all thin sections taken from axes found in the southwest are centrally located at Taunton Museum. IPC Group I, Ia and III thin sections within this collection were made available for this work by the South Western Group of Museums and Art Galleries and subsequently provided a framework on which base the investigation of geochemical and magnetic properties of axes (c.f. Chapter 4).

2.9 Distribution of Group I and III axes

2.9.1 Human or natural transportation?

All six IPC reports discuss the pattern of distribution that is evolving as the number of Neolithic axe finds increases. Axe distribution is frequently taken as evidence for some form of trade between Neolithic communities, which in turn enables inferences to be made on the socio-economic environment in prehistory (e.g. Cummins 1979, Bradley & Edmonds 1993). This implies that it has been assumed that (for IPC Groups I, III, & VI especially) the only way of creating the distribution pattern is by human intervention and not through the more widespread availability of stone transported from outcrop by glacial activity (i.e. glacial erratics). Briggs (1976) disagrees with this position, proposing that selective use of glacial erratics was the root cause behind the observed distribution patterns. Whilst Briggs' ideas reflect the observed north to south movement of the glacial ice sheet (Harmer 1928) and thus southward movement of material, he does not explain the south to north movement of material from Cornwall to Yorkshire. Although a south to north carriage of material is theoretically possible through ice rafting, the author has found no evidence of this in the literature. A southwards carriage of rock by the ice sheet and the use of these erratics as axe material is supported by the geochemical provenancing of glacial erratics found in central England that have originated from the Scottish Midland Valley and from the Whin Sill (Williams-Thorpe et al. 1999b). Thus, ideas concerning

human transport, whether through trade or migration will be strengthened if it is shown that IPC Group I axes found in N Yorkshire actually do originate from Cornwall. Confirmation of the Cornish provenance, although not definitive proof of human intervention, would help to reduce the possibility that the greenstone used to manufacture Yorkshire IPC Group I axes had originated from Scandinavia and had been transported by advancing ice sheets.

2.9.2 Disparity in distribution

Cummins (1979) suggested that a two stage trade in IPC Group I axes existed and based his arguments on the density of finds in Essex as indicating a secondary dispersal point in the distribution of axes from Cornwall. Since 1979 more axes have been allocated to IPC Group I and the high relative density of finds in Essex is no longer substantiated. This point illustrates the evolving picture of axe distribution and highlights the need to consider axe clusters in associated discussions. Axe clusters may be present through several factors:

1. The concentration of finds at excavated Neolithic sites; possibly the reason for high concentrations in Wiltshire owing to extended excavations and archaeological investigations on Salisbury Plain.
2. The concentration of finds as a by product of gravel extraction for industrial use; possibly the reason for a high concentration of finds along the Thames, where gravel has been extracted for building projects such as the M4 motorway.
3. Concentration of finds through the activity of local collectors – possibly the reason for high concentrations of finds in Cornwall and Wiltshire.
4. Depletion of finds through prior 'robbery'; it is possible that a large number of Cornish Neolithic graves have been destroyed in the (misguided) search for treasure, with axes being thrown away because at that time they held no commercial value
5. Under-representation of finds in rural areas; it is probable that axes have an increased chance of being found in urban areas than rural areas.
6. Poorly located finds; many finds by local collectors, general public, etc., are not accurately located which leads to problems with relative density calculations.

(Mainly after Smith 1979.)

In addition to Cummin's work, Hodder & Lane (1982) concluded that the size of IPC Group I axes diminished relative to the increasing distance from Mount's Bay, Cornwall and used this to support ideas of *social ablation* – continued reworking of axes as the

distance from the source prevented acquisition of new material. Although not specifically measured, field notes do support this observation with IPC Group I axes in Yorkshire generally being smaller than those observed in Cornwall. (Field notes also report that many of the axes in Yorkshire are adze shaped (e.g. curved along the long axis, similar in profile to a banana.) Thus, both Cummins and Hodder & Lane conclude that there is a deliberate transport of IPC Group I axes from a Cornish point of origin.

2.9.3 Overview of distribution maps

Figures 3 to 9 are based on the data contained in Clough & Cummins (1988). Unlike the distribution maps in Cummins (1979) no factors relating to the possible over-representation of axes by axe fragments/flakes have been taken into account. Each entry in Clough and Cummins (1988) for the IPC groups in question has been faithfully plotted. The reasoning behind this is that during the fieldwork phases of this research it became apparent that all axe fragments/flakes seen were from separate axes. Thus, the distribution maps in this work are believed to represent a more complete representation of the distribution of axes than that achieved by Cummins.

2.9.4 Generation of distribution maps

Ordnance Survey (OS) grid references given in Clough & Cummins (1988) were converted to latitude and longitude using formulae given in OS Paper 2/1998, based on the National Projection (Ordnance Survey 1998). Six figure OS grid references were converted to latitude and longitude without any alteration. Latitude and longitudes for axes that had find locations given to the nearest 1km square (e.g. SU4258) are based on the centre of that square (e.g. in this example the latitude and longitude is calculated for SU42558). This was done to increase the probability that the find location was within a radius of approximately 700m of the plotted co-ordinate, and not approximately 1,400m if the corner of the grid-square was used. This assumes the normal convention of giving OS grid references had been followed, that is it is always the south-western point of the grid square that is referenced (see instruction of how to write grid references on any 1:50 000 OS map). Axe find locations that have been questioned (e.g. indicated in Clough & Cummins (1988) as SU4258?) have been treated as 4-figure grid references and adjusted to represent the centre of the 1km square, as described above. Finally, all axe find locations that have only been given to the nearest 10km (e.g. SU45) have been ignored. Carrying out the same procedure as above would result in the error of uncertainty being 7km, which is believed to be too large.

2.9.5 Distribution maps

The following six distribution maps illustrate the find locations for all IPC Group I, Ia, I/Ia, I(near), III, IIIa and ungrouped greenstones identified by Clough & Cummins (1988). IPC Group I and IPC ungrouped greenstones the axes that have been geochemically analysed are plotted separately from the remaining (unanalysed) axes. Hence both maps together show the full distribution of axes in these two groups.

Figures 3 and 4 show that IPC Group I axes are distributed throughout England and Wales, with the highest density of finds being in Cornwall. It is observed that five (Cornwall, Central-Southern England, London, Anglia and Northeast England) of the six (as before plus Midlands) relatively high-density clusters of axes have been sampled as part of this work, thus providing a generally geographically unbiased set of samples. Figure 5 shows IPC Group Ia and I(near) have a similar, but less dense, distribution pattern to IPC Group I. In this case, there is some geographical bias in axes analysed, with IPC Group Ia and I(near) axes only represented from Cornwall (2), Yorkshire (2), Essex (3), Somerset (1) and Lincolnshire (1). The distribution of IPC Group III in Figure 6 axes appears to be centralised around Central-Southern England, and not near Mount's Bay, the hypothesised provenance for the group. The axes analysed are representative of the whole geographical extent of the group. The overall distribution of IPC ungrouped axes illustrated in Figures 8 and 9 (note Figure 7 is not used) is similar to IPC Group I, with relatively dense clusters in Cornwall, Central-Southern England, Anglia and Yorkshire. In general, only IPC ungrouped axes from Cornwall, Yorkshire and Norfolk have been examined as part of this work.

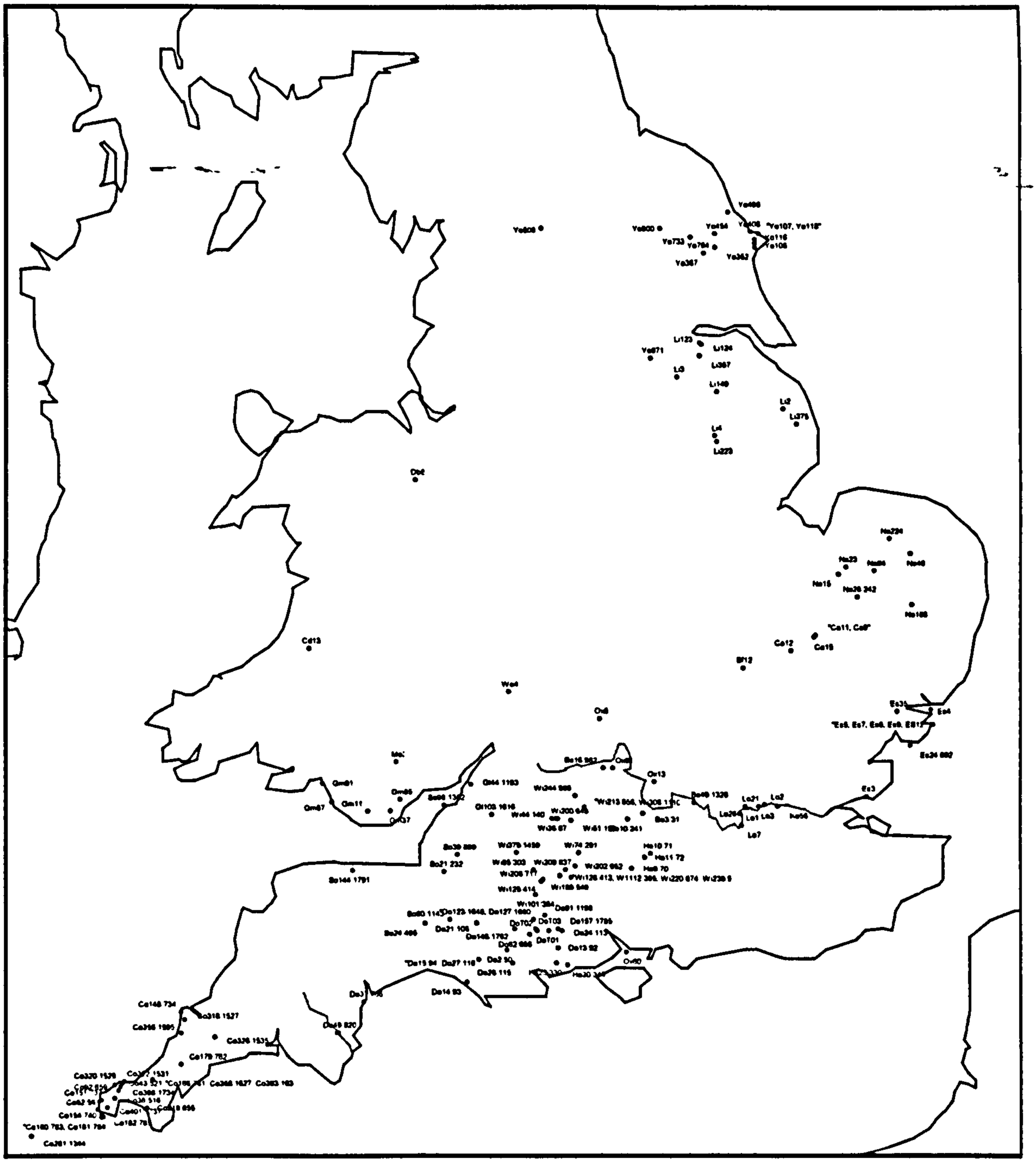

*Figure 3 Distribution of **IPC Group I** axes that have been geochemically **analysed** by PXRF. The clustering of axes is caused by the locations visited: Colchester, Truro, Dorchester, Salisbury, Winchester, London and Hull (The Norfolk axes were loaned to Hull Museum). The selection of IPC Group I axes is therefore not a random selection of the population, but includes axes from the (supposed) source area and four geographically separated areas (Central-Southern England, London, Anglia and North East England.*

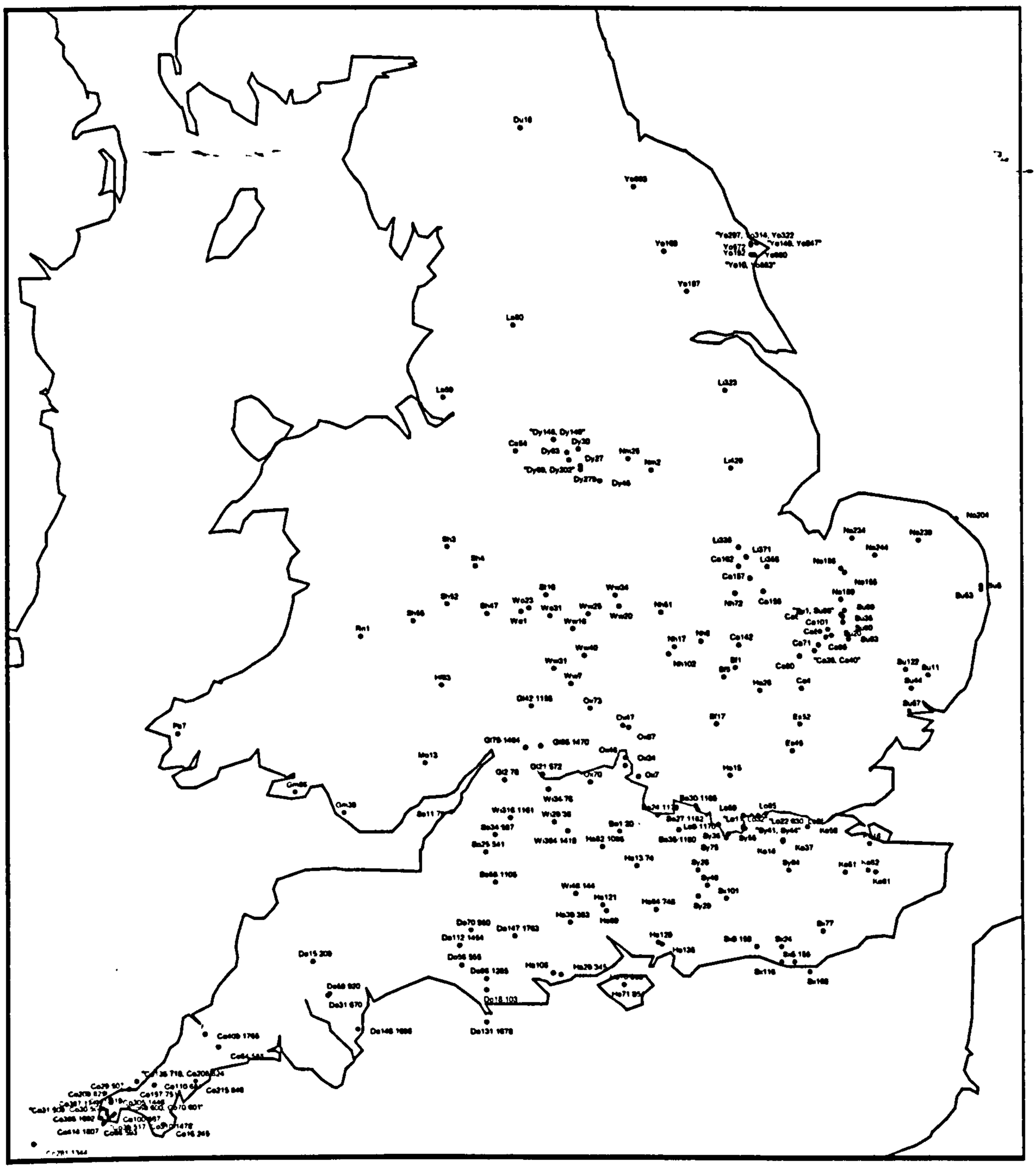

*Figure 4 Distribution of **IPC Group I** axes that were **not geochemically analysed** by PXRF. The clustering of axes seen is similar to Figure 3 since there were a large number of axes held in private collections in Cornwall, Wiltshire & Yorkshire that were not available for analysis. Note that the only area not represented in this work is the Midlands. The combination of Figures 3 and 4 reflects the whole distribution of IPC Group I*

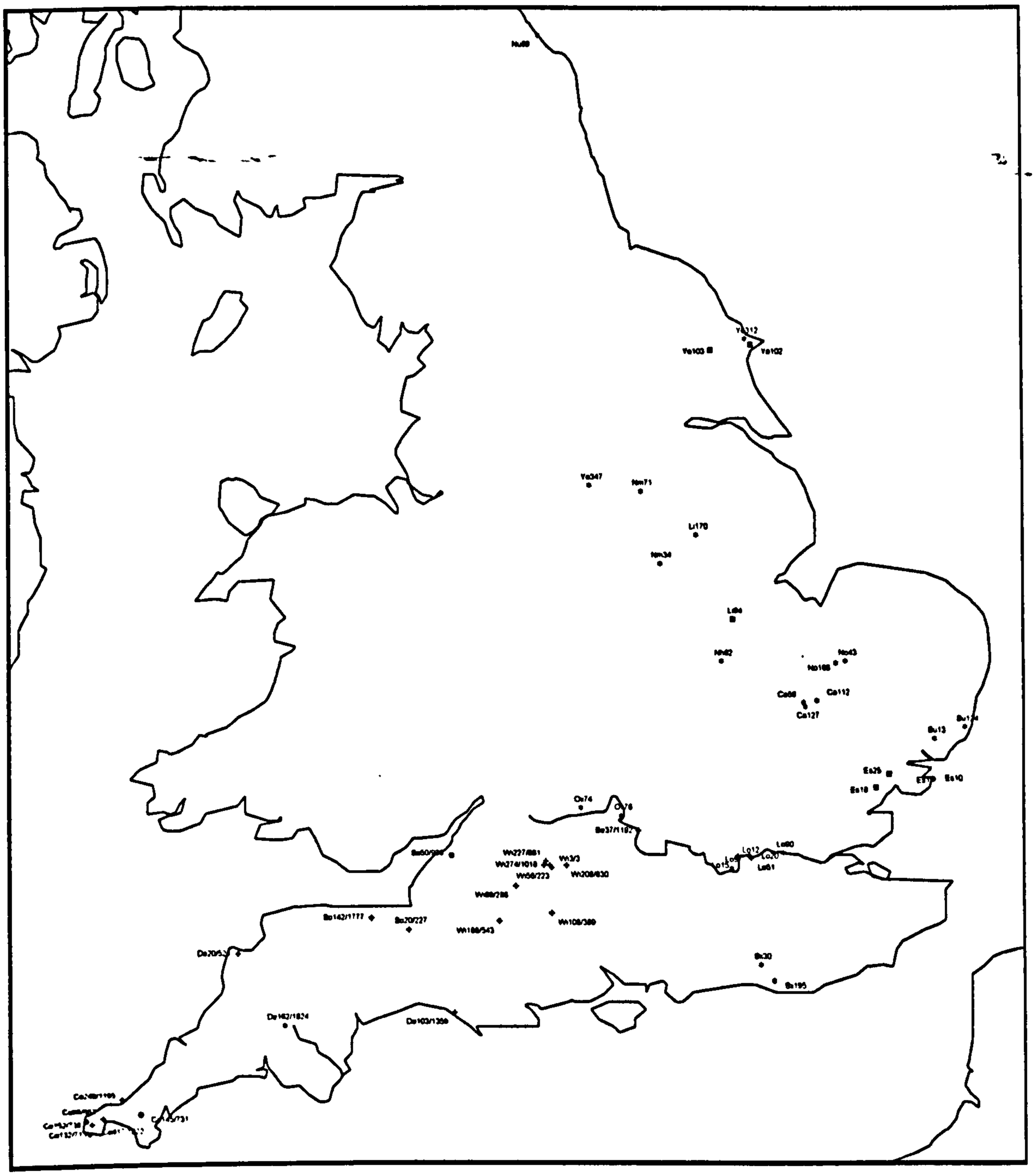

Figure 5 *Distribution of **IPC Group Ia** (black dot) and **IPC Group I(near)** (black square) axes that have been geochemically analysed and distribution of IPC Group Ia (+) and IPC Group I(near) (*) that have not been geochemically analysed. IPC Group I/Ia is not included as all these axes were found in and around London. It is seen that the overall distribution pattern is similar to IPC Group I with clusters in Cornwall, Wiltshire, London and Yorkshire.*

*Figure 6 Distribution of **IPC Group III** axes geochemically analysed as part of this work (black dots), IPC Group III axes not analysed as part of this work (black diamond). The grey star represents the hypothesised origin of IPC Group III. The distribution of IPC Group III is clearly concentrated in Central-Southern England (Wiltshire).*

*Figure 8 Distribution of **IPC ungrouped** axes that have been **geochemically analysed** by PXRF. The distribution represents the spare time at Truro and Hull that was available after all IPC Group I axes available had been analysed*

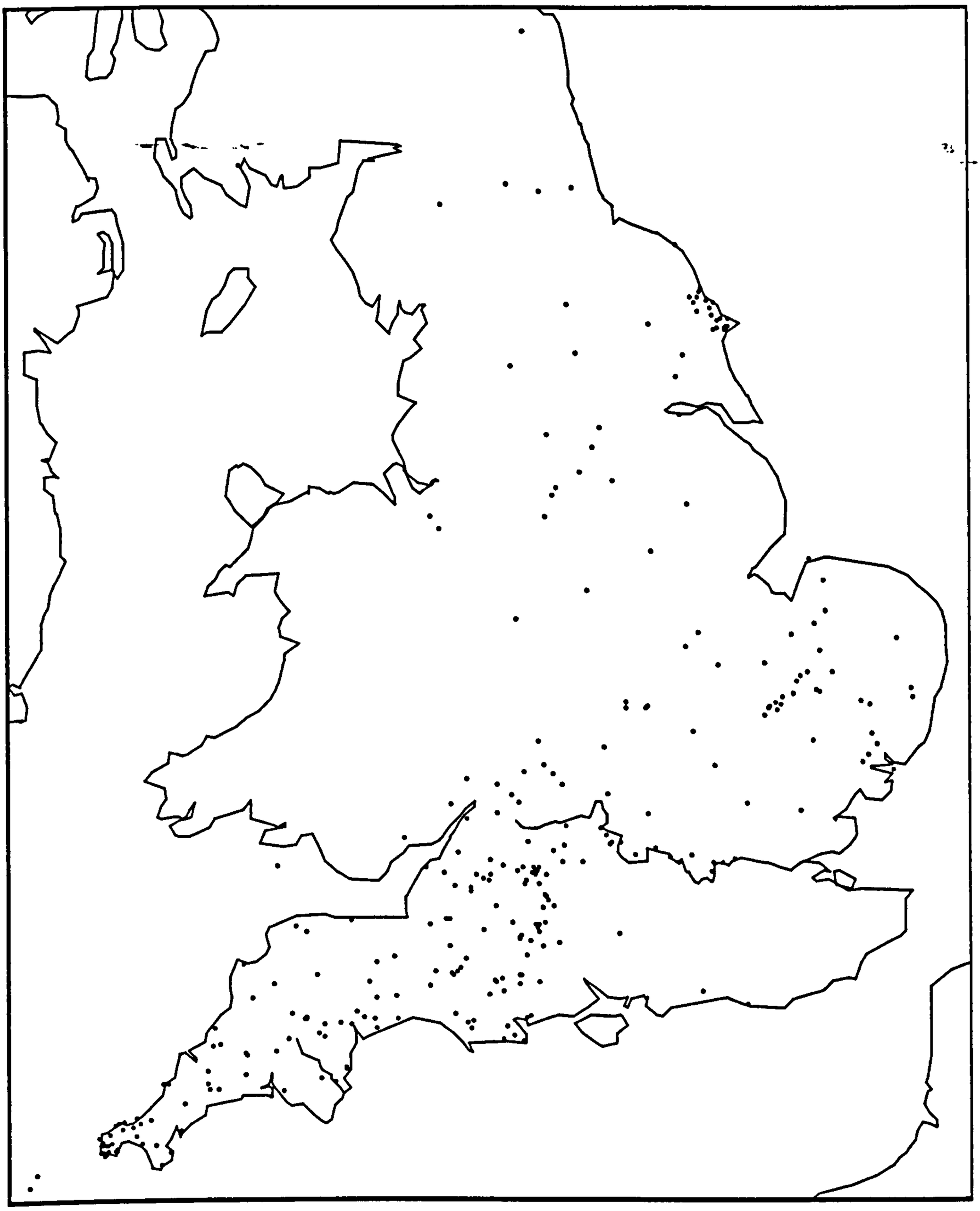

Figure 9 *Distribution of **IPC ungrouped** greenstones **not geochemically analysed**. The distribution pattern is similar to that of IPC Group I, hence suggesting potentially similar origins and controls of distribution. (The density of points on the map precludes adding any axe identification as the required font size is far too small.)*

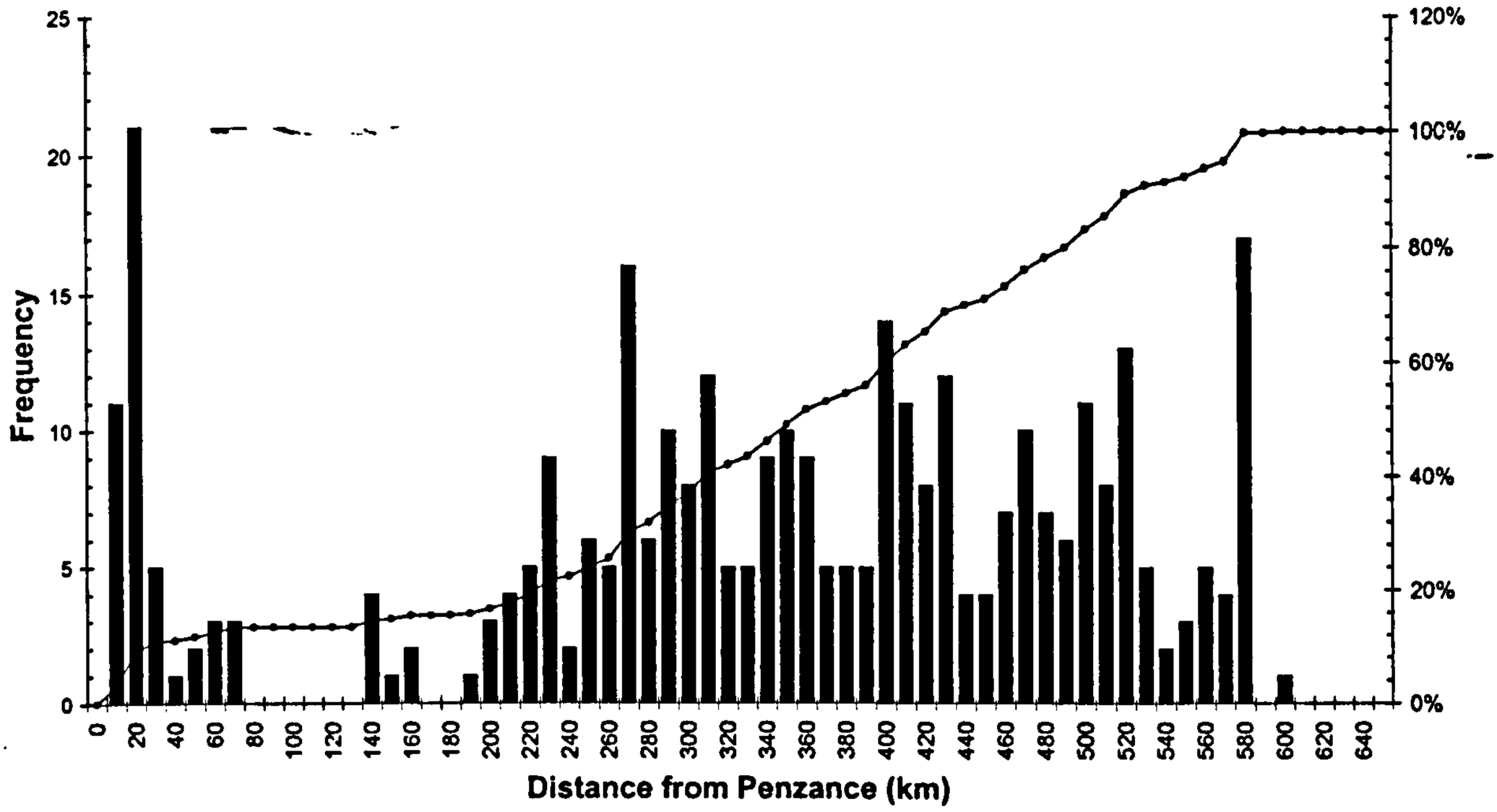

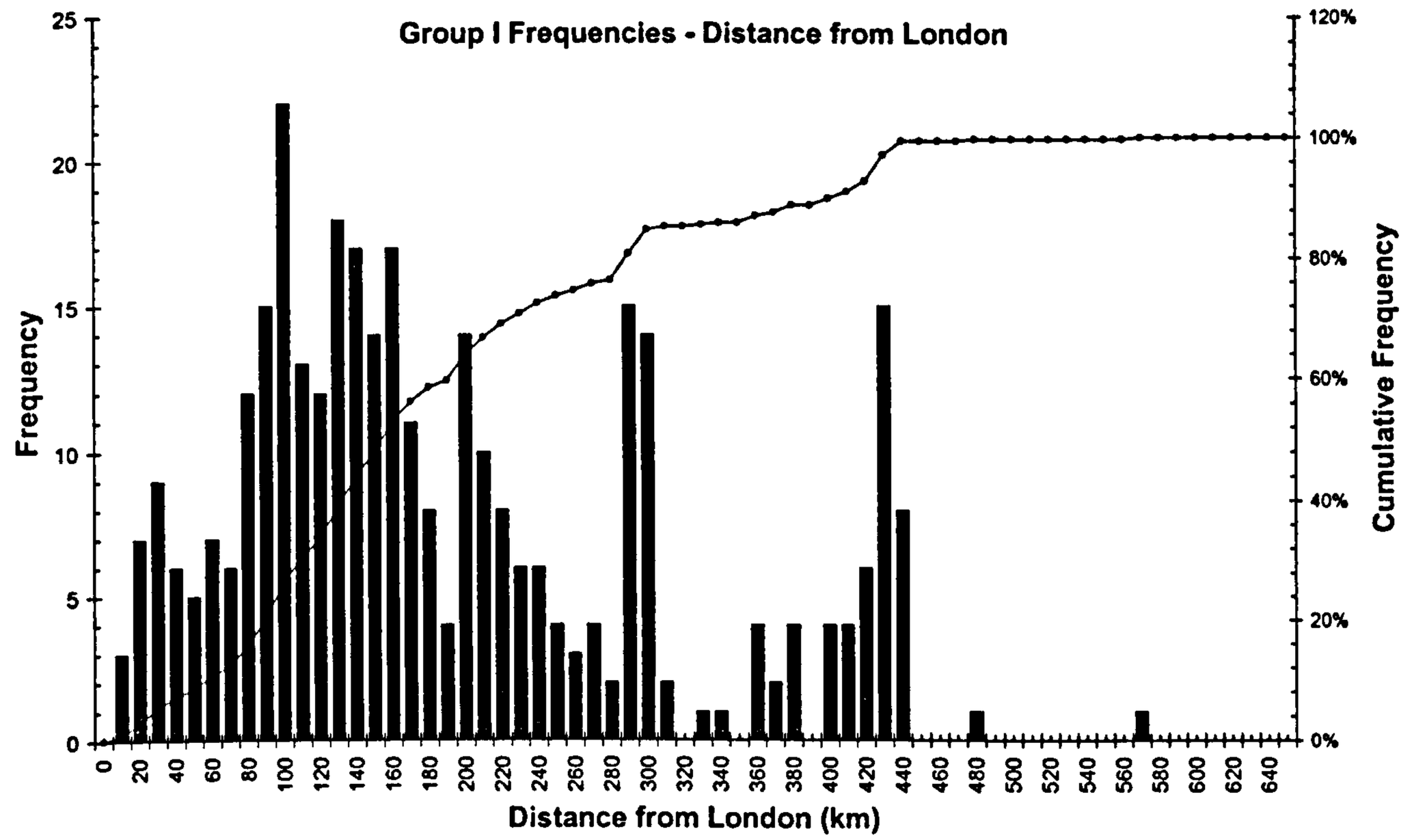

Figure 10 Upper - Chart of frequency of IPC Group I finds and their distance from the Penzance. Lower - Chart of frequency of IPC Group I finds and their distance from the centre of London. The data is not normally or exponentially distributed indicating a non-random (i.e. deliberate) dispersion of axes. The two-stage distribution reported by Cummins (1979) is not seen. Instead it appears there may be several smaller distribution centres at 20, 220, 270, 300 420 and 580 km from Penzance (upper chart).

2.9.6 Cumulative frequency-distance charts for IPC Group I

The distribution maps in Figures 3 to 9 do not clearly illustrate the fact that several axes may have been found at a single location (e.g. Carn Brea). Although it is possible to represent distribution & population by using different sized map symbols proportional to the number of axes recorded from locations (e.g. Cummins 1979) this was not done because the emphasis of the maps is to illustrate the find locations only. Instead, the relationship between distance from source and associated population is more clearly seen through the use of cumulative frequency distance charts.

Figure 10 shows the frequency of axes found at linear distances calculated from Penzance and Central London, both as a bar chart and a superimposed cumulative frequency chart. The chart is based on 10km intervals and the whole population of IPC Group I axes (including parts & fragments thereof) and are similar to those produced by Cummins (1979).

It is assumed that a chart representing a *randomly sampled* and *random dispersion* of axes from a *localised* source, with the origin of the chart (0 distance) representing the source location (i.e. Penzance) would show an exponentially decreasing frequency at increasing distances from the source. A similar distribution plotted on a frequency chart with the origin of the chart set at a distance from the actual source (i.e. Central London) would show a normal distribution of frequencies, with the frequency distribution centred at the distance from the real origin. It can be seen that the chart with a Penzance origin is neither exponentially or normally distributed and, likewise, the chart with London as the origin does not show a normal distribution. This indicates that either the sampling is not random, that the distribution is not random or a combination of both of these factors. It is probable for reasons already stated that there is some non-representative sampling and this is seen through the number of peaks seen in the bar chart. Visual inspection of the Penzance chart does suggest that there are several distances around which the frequency appears to be normally distributed (e.g. at 360 km and 480 km) and similar patterns can be seen in the London based chart (e.g. at 100km and 210 km). This is interpreted as indicating the possibility of localised axe distribution centres and strongly indicates the deliberate transport of axes.

Thus, the cumulative frequency charts indicate a distribution pattern that could be achieved through a deliberate transport of axes to various secondary centres from which further

random distribution occurred. The data does not indicate the presence of a single secondary IPC Group I axe distribution centre as proposed by Cummins (1979).

2.9.7 Restrictions in interpretations regarding axe distribution

It is emphasised that the illustrations and discussions in this section assume that each IPC group is homogenous and originates from within the site/area indicated in the six IPC reports.

Figure 10 reflects a single dimensional view (distance) of a two dimensional distribution (area). By moving the origin of the chart (i.e. from Penzance to Central London) the *area* represented by the 10km distance bands increases and thus the frequency of axe finds in that enlarged band most likely increases. A more rigorous mathematical investigation into the expected and achieved distribution patterns is needed to support this hypothesis, but is beyond the scope of this thesis. However, it is the shape of the chart that is important in this case, not the total population, hence the conclusions drawn in Section 2.9.6: that the distribution of IPC Group I axes is probably not random.

2.10 Archaeological age of IPC Axe Groups studied

A review of the earlier IPC reports, culminating in the 4th Report (Evens et al. 1962) associates IPC Group I, Ia, III, & IIIa with distribution of axes outside Cornwall occurring in the Mid-Late Neolithic. Piggott (in Evens et al. op. cit.) divides the Neolithic into four phases and, with the (then) innovation of radiocarbon dating techniques, assigns axe distribution episodes to these four phases. This is illustrated in Figure 11, below. The earliest IPC Group I axes are assigned to Piggott's Phase II, the middle to end of the 3rd Millennium BC around 2500 bc. (Note the radiocarbon dates quoted here and given by Piggott are not recalibrated to chronological dates). Distribution of IPC Group I was joined by IPC Groups Ia & III by the 3rd Phase, approximately 2000 bc, which was also given as the time of migration of the Beaker People. The 4th Stage was dated at approximately 1500 to 1400 bc and coincided with the development of Wessex I & II cultures and saw the decline in axe distribution.

Smith (1979) supports the observation that the production and distribution of IPC Group I axes occurred during the first quarter of the 3rd Millennium BC, i.e. late Neolithic. Likewise, and through associations with morphology of the finds (Roe 1966), Smith (op. cit.) associates two IPC Group III Stage III battle axes with the late 3rd / early 2nd

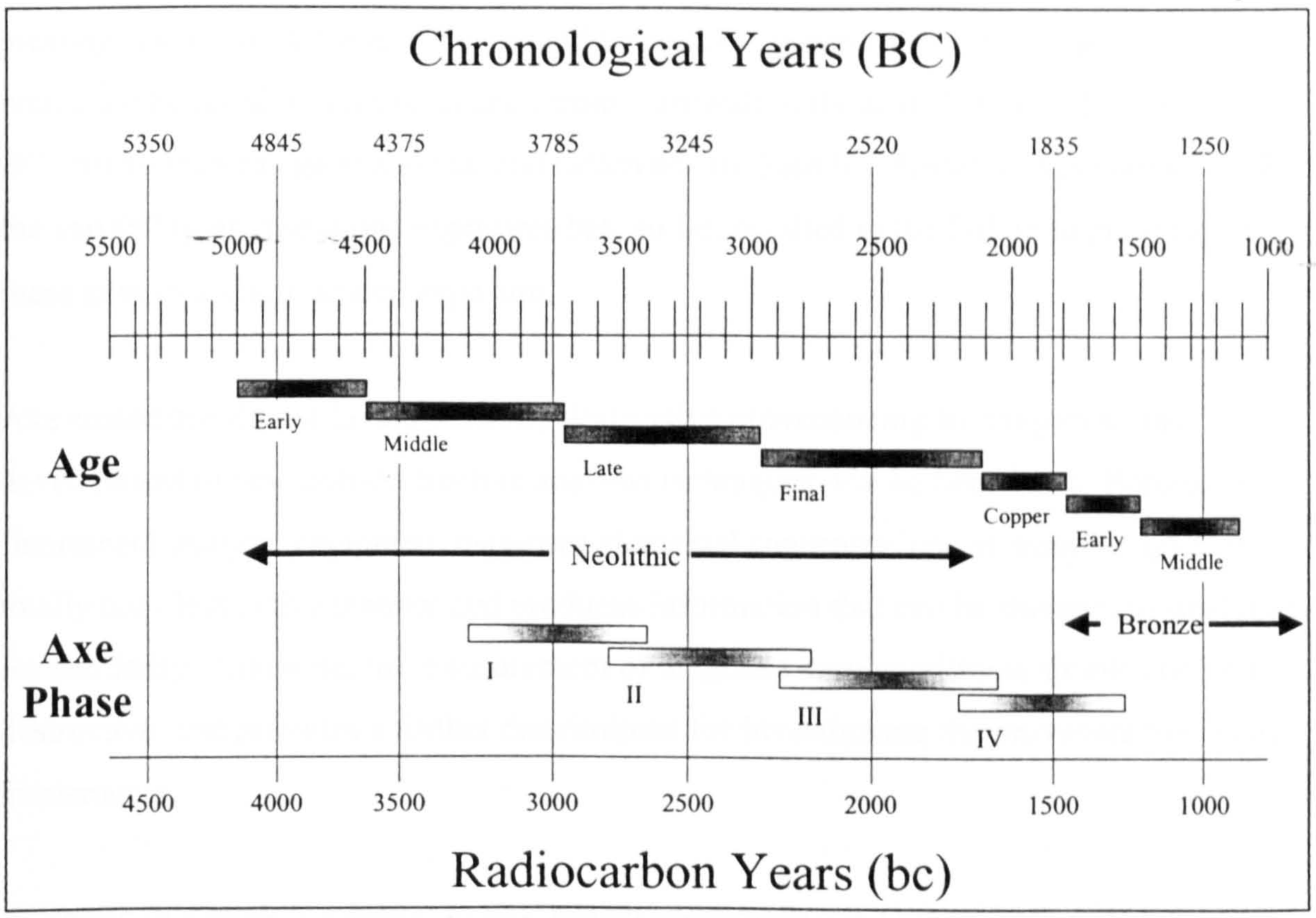

Figure 11 Comparison of chronological time and radiocarbon time for ages of the pre-historic and phases of axe manufacture (after Bradley 1984 (based originally on Clarke 1975), Piggott 1962, & Evens 1972.)

Millennium BC. Since both IPC Group I & III contain Stage III battle-axes it is seen that production of axes continued well into the 2nd Millennium BC (Roe 1966). It is not clear when production of IPC Groups I & III actually ceased and continued use (or the first example of a private collection) is possibly indicated by So25/541 being found within a 3rd Century Roman House (Stone & Wallis 1951).

The above, brief, review of the chronology of IPC Groups I & III is aimed at providing background to this research only as this work is concentrated on provenancing axes using non-destructive geochemical techniques. Work to correlate axe find locations with calibrated radiocarbon dates may reveal beneficial information on the timing of the distribution of axes. However, until it is known that grouped axes actually belong to the same source region, any such work could be flawed. Therefore, this work concentrates on accurately provenancing axes, which will provide the basis for future research on chronological aspects of axe distribution.

2.11 Summary

Implement petrology has so far identified that many Neolithic and Early Bronze Age stone implements can be assigned to 39 petrological groups and associated sub-groups. Petrological investigations have revealed potential sources of most axe groups and aided in

locating seven axe factories. The second largest IPC group consists of greenstone axes, which are believed to have originated from Cornwall in the mid 3rd to late 2nd Millennia BC. Small mineralogical and textural difference in these IPC Group I axes coupled with the variability of greenstone exposures has, so far, resulted in the failure to provenance these axes to a single source exposure.

Axe custodians do not favour partially destructive provenancing techniques so the development of new non-destructive analysis techniques will be beneficial. Portable x-ray fluorescent analysis equipment measures elemental concentrations of stone samples in a totally non-destructive manner and produces information that can be statistically analysed for similarity. Likewise, the measurement of magnetic susceptibility is simple and non-destructive, and provides a further discriminant for investigating the provenance of stone implements.

Although this work is relevant to all Cornish greenstone axe groups, both of these analytical techniques, plus an examination of existing thin sections, will be used only to characterise IPC Group I, Ia, I/Ia, I(near), III, IIIa and ungrouped greenstone axes, as well as selected Irish gabbroic & doleritic axes in order to ascertain group homogeneity, similarity and provenance. This thesis will provide a basis for future research into the remaining Cornish greenstone axe groups.

It is unlikely that successful provenancing of any IPC greenstone axe group will lead to the location of a greenstone axe factory as the method of manufacture for this type of axe does not leave significant permanent debitage. Distribution of IPC Group I axes is not random, with distribution maps showing regional clusters in Cornwall, Central-Southern England (mainly Wiltshire), London, Anglia (mainly Norfolk) and Northeast England (mainly Yorkshire). A linear representation of the two-dimensional distribution supports the non-random distribution, but concludes that a unique secondary distribution centre proposed in Cummins (1979) is unlikely. Few axes have been found in a datable context, hence there is little information on the archaeological age of axe production, other than mid-late Neolithic for IPC Group I.

The positive provenance of the selected Cornish IPC axe groups to a single (or several?) greenstone exposure in Cornwall will increase the level of knowledge for the Neolithic culture in Britain and, through the various levels of inference, will enhance the understanding of the social space occupied in the 2nd and 3rd Millennia BC.

3 Potential sources of greenstone in SW England

3.1 Introduction

There are over one hundred known meta-basic rock outcrops and associated exposures in SW England (Appendix 3). These outcrops are reported to have a relatively small range of mineralogical compositions and textural features (Keiller et al. 1941) which is probably one of the main reasons why the source exposure providing material for IPC Group I axes has not yet been positively identified using petrographic analysis (c.f. Chapter 2). (Note the term 'outcrop' will be used to define the geographical extent of a rock type concealed only by drift deposits and the term 'exposure' will be used for outcropping rock) The failure by skilled petrologists to find an exact petrographic match between IPC Group I axes and a greenstone exposure, especially considering the large number of axe and exposure thin sections examined (unpublished IPC archive data), suggests it is highly improbable that one will be found using thin sections alone. Therefore a non-petrographical technique, for example geochemical fingerprinting, must be used to locate the provenance of IPC Group I axes.

Geochemical analysis of rocks through determination of major and trace element compositions using x-ray fluorescence spectroscopy can reveal much about the origin, evolution (i.e. petrogenesis) of the rock (Rollinson 1993: table 1.2 & 1.3). The abundance and ratios of certain elements within igneous rocks can be used to differentiate between the tectonic regimes in which they originated (c.f. Figure 12 and Appendix 30, also see Rollinson 1993) and even for geographically close outcrops, and especially between igneous rocks in SW England (Floyd 1984). Therefore, the use of major and trace element signatures can provide a potential diagnostic tool to discriminate between petrographically similar outcrops. Figure 12 illustrates the potential to use trace elements to assess the genesis of rocks in Devon and Cornwall, matching these rocks with one of five tectonic regimes:

Constructive plate margins (i.e. extensional tectonics) produce **N-MORB** (Normal- mid ocean ridge basalt) or **E-MORB** (Evolved-MORB (or T-MORB) are usually associated with plume activity coinciding with a spreading ridge)).

Mantle plume or hot-spots generally result in the production of **within-plate alkali basalts** (from deep mantle melting) or **within-plate tholeiitic basalts** (indicating shallow melting, just beneath thinned continental crust), both usually away from continental margins (i.e. within plate).

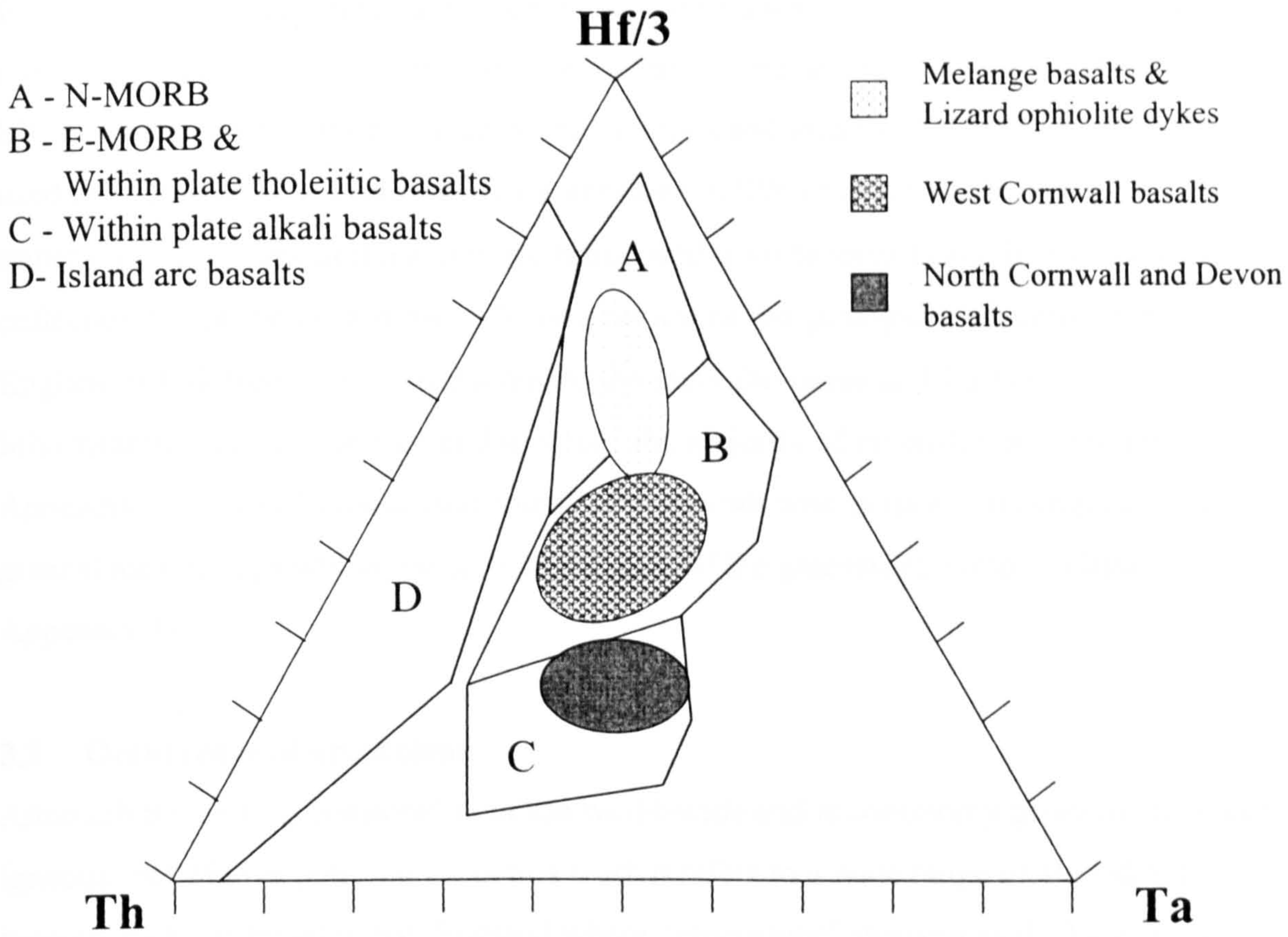

Figure 12 Th-Hf-Ta ternary discrimination diagram from Floyd et al. (1993: figure 4.3) showing that igneous rocks in SW England can be assigned to one of five igneous tectonic regimes and illustrating the potential level of discrimination between them. In this example it is observed that basaltic rocks in SW England are generally related to extensional tectonics or within-plate mantle plumes and not destructive margins.

Destructive tectonic plate margins (ocean-ocean in this case) produce **island arc basalts**, which generated from an arc of active volcanic islands above the descending oceanic crust. (From OU S267 Blocks 2, 3 & 4.)

Figure 12, taken from Floyd et al. (1993), indicates that igneous rocks in SW England are generally related to extensional tectonics or within-plate mantle plumes and not to destructive margins.

Thus, geochemical analysis of igneous rocks on a regional scale has the potential to delineate the geographical extent of a particular tectonic regime and has the further potential to discriminate between individual igneous events within that regime. This is especially true for the igneous rocks found in SW England where, based on Floyd (1984 and pers. com.) there exists the potential to geochemically characterise (or fingerprint) many of the one hundred meta-basic outcrops found in Cornwall and Devon. Hence there is the potential to be able to geochemically provenance an unknown igneous rock sample (i.e. a Neolithic greenstone axe) to an individual exposure.

In preparation for geochemical provenancing (in Chapters 6, 7 & 8), this chapter (3) provides the geological background to this thesis, summarising the geological evolution of SW England, identification of greenstone outcrops and locations of greenstone samples used in this work. The occurrence of greenstone in SW England and its main mineralogical and textural features are introduced prior to identifying the rationale for collection of greenstone samples. A short review of the geological evolution of SW England is followed by an introduction to the main Devonian and Early Carboniferous litho-tectonic units in SW England in which the majority of greenstones are found (c.f. Appendix 3). These litho-tectonic units are then dealt with in turn, with emphasis on the greenstone outcrops within the units and details of the greenstone samples obtained (c.f. Appendix 4).

3.2 Occurrence of greenstone

Although the term 'greenstone' is in use world-wide and is commonly given to any green igneous rock (Floyd pers. com.), in this work it refers to a wide range of altered basic igneous rocks as found in SW England where "greenstone" is given as the local name. These dark green/greyish rocks are exposed at numerous locations in the SW peninsula and are best seen along the Cornish coastline since inland outcrops have little relief and are often covered with drift deposits (author's observation, Flett 1946). Greenstones are the product of metamorphic alteration of basic, intrusive and extrusive igneous bodies primarily through regional and contact metamorphism. Although greenstones are predominantly medium grained, the term is also used for the finer basic (usually submarine) lavas (spilites), which are often associated with the intrusive igneous bodies. Greenstone outcrops in Devon and Cornwall are usually small, less than 1 km^2 in extent, and often found emplaced within Devonian and Carboniferous sediments at shallow levels as sill like bodies, or penecontemporaneous pillow lavas (Goode & Taylor 1988). Deeper level intrusive basic igneous rocks are known (e.g. at Cudden Point) and these have also been altered to greenstone.

Greenstone bodies are often referred to as metadolerite, metagabbros, metabasic volcanics or undifferentiated metabasic rocks on geological maps. These bodies are best seen exposed along coastal sections where differential erosion has resulted in the harder greenstone forming a resistant headland and raised cliff lines (and possibly submarine cliff lines). Numerous quarries are identified on OS maps of Cornwall and Devon with many of the coastal quarries easily visible to anyone walking along the long distance Cornish Coastal Footpath. Many of these quarries extract(ed) greenstone for use as roadstone (e.g.

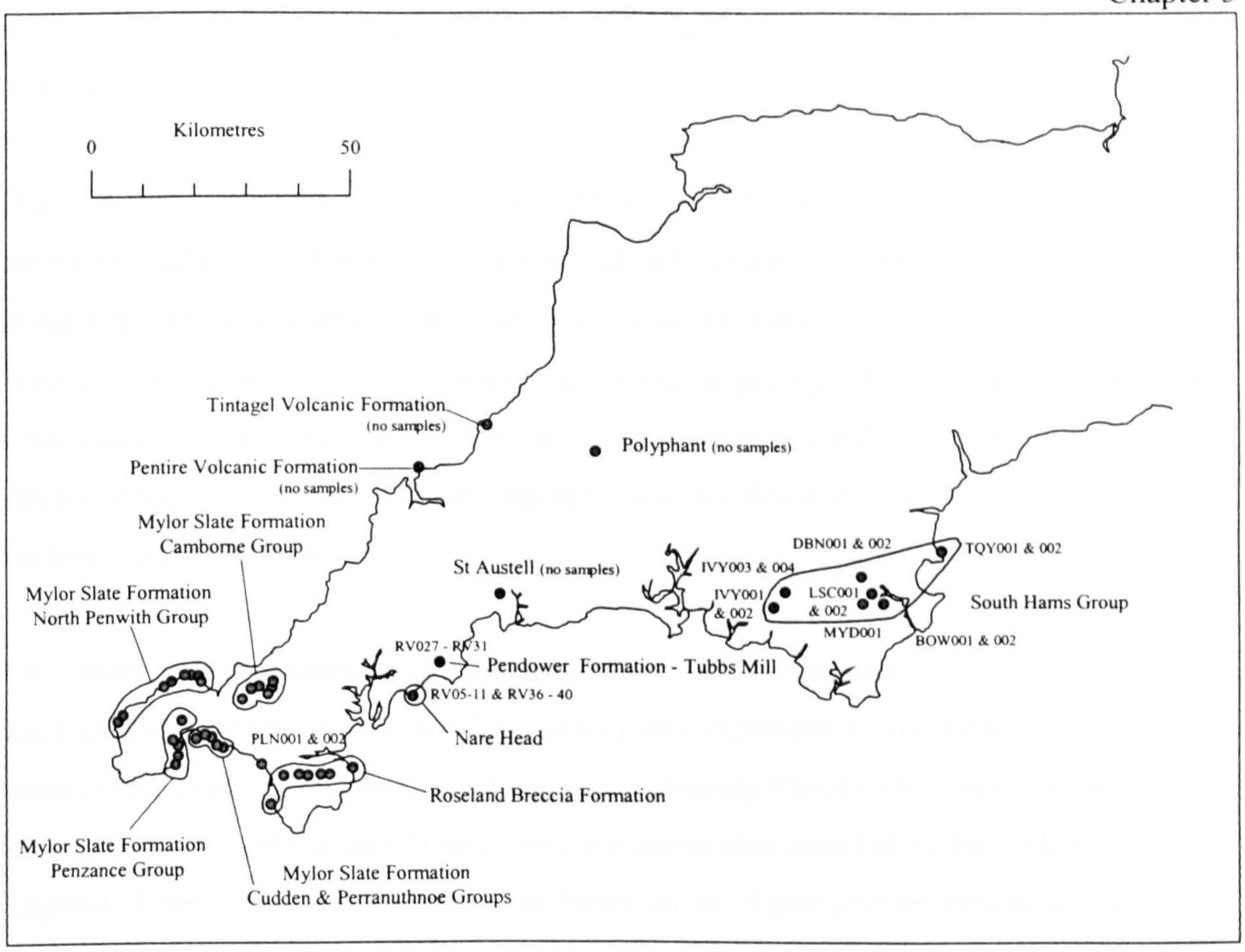

Figure 13 Map of SW England showing the location of greenstone exposures sampled as part of this work and other selected meta-basic rock exposures. Samples are identified on this map if other maps in this Chapter do not cover them.

Carn Gwavas, Penlee, and Perranuthnoe). One aspect that makes greenstone useful as roadstone, and especially for axes, is its toughness and resilience to wear, impact, etc. This is derived from the alteration of the primary rock mineralogy (pyroxene + (originally calcic) plagioclase + titaniferous opaque (± olivine, ± biotite)) to a secondary mineralogy dominated by amphibole, usually actinolite or tremolite-actinolite (and albite + altered titaniferous opaques (leucoxene or sphene) + chlorite (± epidote, ± biotite ± sericite)). This alteration occurred at prehnite-pumpellyite, and occasionally lower greenschist, grade regional metamorphism (Floyd et al. 1993). The pervasive amphibole effectively 'knits' the rock together, similar to steel re-enforcing rods within pre-stressed concrete and results in the altered rock being resilient as well as tough. It is this resilience to repeated percussion and the toughness that make this an ideal rock for making axes (Markham 1997).

The presence and amount of secondary biotite and the hornfels texture seen in some greenstone rocks indicates alteration through contact metamorphism. As contact metamorphic aureoles are seen to extend up to 1km away from granite emplacements (see BGS Sheets 349 Ivybridge and 351/358 Penzance) it is probable that any greenstone with

abundant secondary biotite and hornfels texture originates within 1km of a granite batholith.

Figure 13 shows the general location of greenstone outcrops in Devon and Cornwall that are considered as part of this thesis. Details of each location can be found in Appendix 3, along with (where available) a description of the outcrop and the associated rock found at exposure. Information about the outcrop and rock, its geological period/age and host litho-stratigraphic unit has been taken from various references as cited in Appendix 3. Details of samples obtained from each litho-stratigraphic unit are detailed in Sections 3.6 and 3.7, and are listed in Appendix 4.

3.3 Rationale and method of collection of greenstone samples

Rock samples have been collected from twenty-one exposures by the author and from twenty-three exposures by other workers, predominantly Floyd (pers. com.) and Al Samman (1980) (with seven of these latter exposures also sampled by the author) in SW England. Precise sample collection sites, based on six-figure grid references, are shown in Figures 17 to 23 below. Identification of samples collected from the 21 exposures visited as part of this work is in the form of 'AAA111' (e.g. CUD010 being the 10th sample collected from the CUDden area). The only exceptions to this are samples with prefix 'MM' where these samples have been provided by other collectors (e.g. MM3 was collected as a loose boulder by Mr D Weddle and came from a pipe trench away from known greenstone exposures).

The rationales behind the choice of greenstone exposures to be sampled are:

1. Proximity of the exposure to the hypothesised source of IPC Group I (i.e. exposures at and around Penzance, Penlee and Mousehole)
2. Proximity of the exposure to the hypothesised source of IPC Group III (i.e. exposures near Perranuthnoe, Cudden Point and Trenow Cove)
3. Greenstone exposures within areas having an established geochemical similarity (Floyd et al. 1993, Floyd pers. com.) with ones around Mount's Bay (i.e. Zennor Point and Gurnard's Head)
4. Greenstone exposures in Devon (South Hams Group) believed to be geochemically dissimilar to the Cornish greenstones, used to assess the ability of the geochemical analytical technique to differentiate between tectonic environments.

Wherever practical, samples were extracted from the exposure using a sledgehammer. Where approaching the exposure was dangerous (e.g. unstable quarry face) or the outcrop

was obscured (e.g. no exposures) the most likely samples (e.g. large cobbles/boulders close to the exposure) were collected from the immediate vicinity. Sufficiently large samples were collected to be thick enough to provide an 'infinite thickness' when measured by the PXRF (c.f. Chapter 6) and of sufficient quantity for independent WDXRF analysis. In practice this meant that each sample collected by the author weighed over 1kg and had a volume of at least 64cm^3 (i.e. 4 x 4 x 4cm in size).

It was discovered that the audible 'ring' of the sledgehammer blow on the rock exposure related to the resilience of the rock. A bell-like ring indicated that the greenstone was tough and resilient, whereas a dull ring, or thud, indicated the rock had weathered or was less competent. It is speculated that this property could form the basis of a simple test to assess the suitability of greenstone rocks for axe manufacture.

A large amount of petrological information has been published on the meta-basic rocks of SW England (see Floyd & Al Samman 1980, Floyd 1984, Floyd et al. 1993). These data have been used extensively along with previously unpublished geochemical data kindly made available by Dr P. A. Floyd for inclusion in this thesis. Such samples used for geochemical analysis are listed in Appendix 4, with their origin shown in Figures 13 and 17 to 23, and can be identified by their "AA11" style of reference (e.g. CG1) and their named source (other than the author).

3.4 Short review of the geological evolution of SW England

This section reviews the origin of the greenstones found in Devon and Cornwall and identifies the tectonic regimes at the time of their formation. In addition, this section provides the context for the discussion on the major Devonian and Carboniferous litho-tectonic units and associated structures contained in the next section.

Nearly all the sedimentary, igneous and metamorphic rocks in Cornwall as well as the majority in Devon were formed in the Palaeozoic. Extensional rifting in the Precambrian crystalline basement, in the region now occupied by Northern Europe, SW England and Southern Ireland, during the Silurian led to the formation of the predominantly east to west Rhenohercynian Ocean into which detrital material from the Old Red Continent (Laurasia) to the north and Normannia (part of Gondwanaland) to the south, was deposited as Lower Devonian shales and grits (Holder & Leveridge 1986, Selwood et al. 1998).

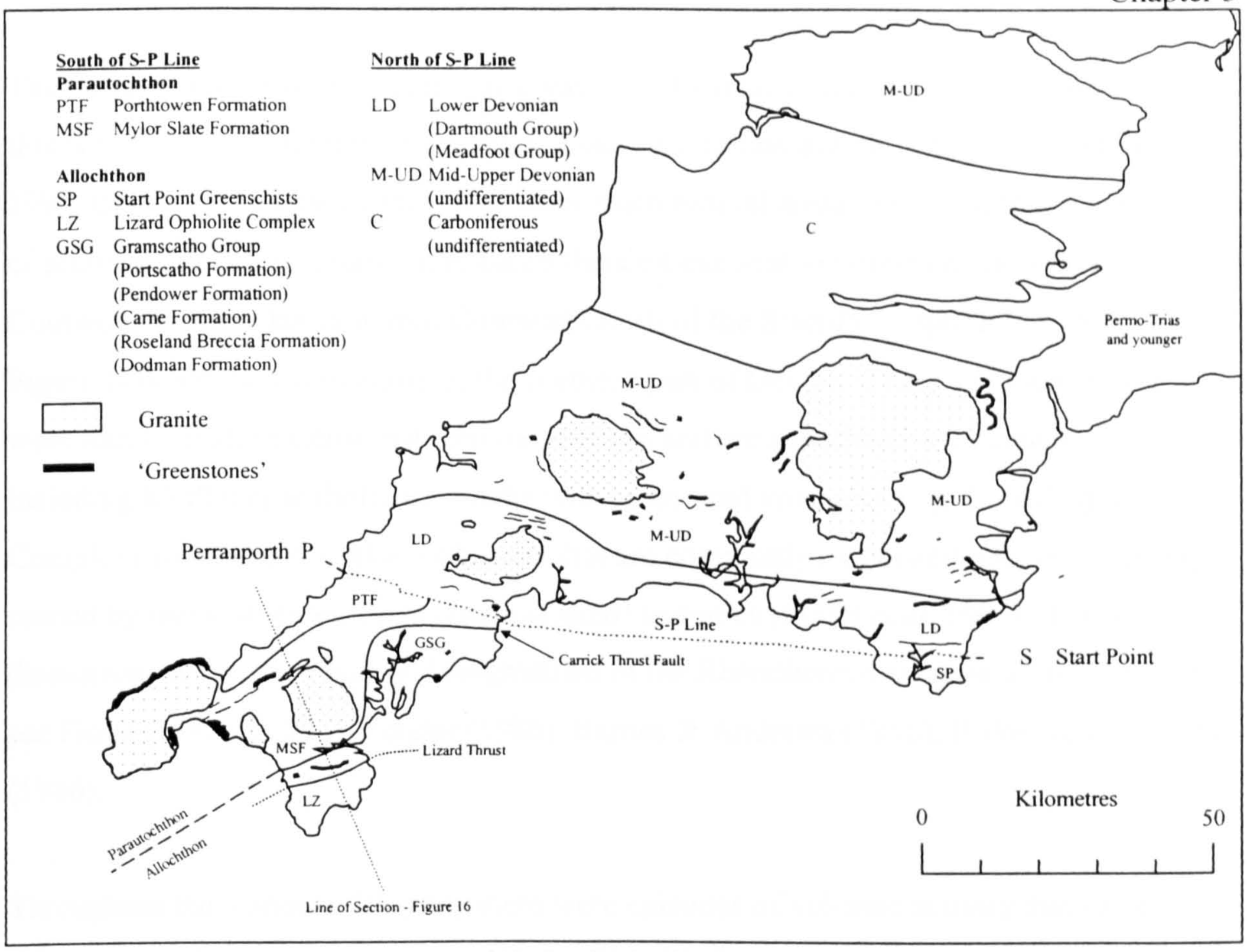

Figure 14 Simplified geological map of SW England (after Holder & Leveridge 1986, Bristow 1996, Selwood et al. 1998)

It is not known precisely when the extensional regime ended, but a compressional regime known as the Variscan Orogeny commenced in the Mid-Devonian (approximately 380Ma) and continued for nearly 80Ma, concluding in mid Carboniferous times. The oblique collision of Laurasia and Gondwanaland during the Variscan Orogeny helped to form the single continent Pangaea through the closure of the Rhenohercynian Ocean. SW England falls into the Rhenohercynian Zone of the Variscan deformation and shares structural and sedimentological similarities with counterparts in Northern Europe (Floyd 1995).

The oblique, dextral collision of Laurasia and Gondwanaland that resulted in the closure of the Rhenohercynian Ocean gave rise to a complicated series of sedimentary basins and structures. As Rhenohercynian oceanic crust was subducted southwards, beneath the northward advancing Normannia, a series of low angle, southward dipping, thrust planes developed that allowed stacking of partly consolidated flysch sedimentation and emplacement of the allochthon (moved block) over the parautochthon (little moved) and the autochthon (stable foreland) (see Figures 15 & 16). This stacking had many effects, including the emplacement of exotic terranes such as the Lizard Complex, and raising the temperature at the base of the stacked pile so increasing the metamorphic grade (Weber 1984).

The oblique compressional regime also gave rise to areas of transtensional tectonics and this is evidenced through the formation of back arc basins and pull-apart basins (Floyd 1995, Barnes & Andrews 1986). The three main basinal areas, distinguished by the depth of sedimentation, are: Gramscatho Basin (hence Gramscatho Group) in the west of Cornwall, Trevone Basin in mid Cornwall (north of the Start-Perranporth line (S-P Line on Figure 14)) and the Culm Basin in the northern part of Devon. These sedimentary basins were formed under extensional tectonic regimes and are associated with magmatism including MORB type tholeiitic basalts with associated volcanics (e.g. Lizard Ophiolite Complex) and intraplate alkaline basalts that are commonly associated with initial rifting caused by incipient extensional (basin-related) tectonics (Floyd et al. 1993). For further discussions on the tectonics and magmatism of the Rhenohercynian zone of the Variscan see Floyd (1982 & 1995), Zeigler (1986), Barnes & Andrews (1986), Holder & Leveridge (1986).

Throughout the Variscan Orogeny there were episodes of volcanic activity that can be associated with two tectonic regimes (after Floyd 1984, 1995, Floyd et al. 1993, Floyd pers. com.).

1) The oblique plate collision during the Variscan Orogeny, similar to the current situation between the Australian and Asian tectonic plates, caused back arc spreading, an extensional regime, which is typified by Mid Ocean Ridge (MOR)-tholeiitic basalts that form at incipient spreading ridges. In SW England this type of magmatism is found within the sedimentary basins.
2) Initial crustal extension is often associated with crustal weakening caused by mantle plumes (e.g. North Sea Basin). Intraplate alkali igneous activity is usually associated with these hot spots, where the rising mantle plume increases the ductility of the lower crust allowing initial rifting of the continental crust (providing an extensional regime is present). In SW England this type of magmatism is found on the margins of the sedimentary basins.

It can be reasonably expected that the subduction and resultant closure of the Rhenohercynian Ocean during the Variscan would have produced Island Arc related magmatism. Magmatism at these destructive plate margins is, early in their formation, dominated by tholeiitic magmas formed by water induced melting (de-watering of the descending oceanic slab providing the fluid) of the mantle wedge beneath the subduction

zone. As the volcanic pile increases the magmas become more intermediate (silicic) in composition through partial melting of the thickened crust or/and fractional crystallisation. However, this type of island arc magmatic activity has yet to be clearly recognised in the Variscan of SW England (Floyd 1995).

In SW England extension related magmatic regimes have been identified by using major and trace element geochemistry (see Rollinson 1993 for details on geochemical discrimination of magmatic regimes and Appendix 30 for a summary of the discrimination diagrams used in this thesis). Figure 12 (Section 3.1) shows that Devonian basic igneous rocks in the west of Cornwall are generally MORB and within-plate related tholeiites, whilst those to the north and east of Cornwall and west and south of Devon (including the Early Carboniferous) are intraplate alkali basalts (Floyd et al. 1993).

At the end of the Variscan Orogeny, approximately 300 Ma ago, the mountain range created by the continental collision began to collapse through gravity sliding along planes of weakness, with the thrust planes that carried the allochthon being reactivated as normal fault planes (Bristow 1996). This is why many of the outcrop features of the 'thrust planes' such as the Lizard boundary fault were originally, incorrectly, diagnosed as normal faults (Bristow 1996). Slightly later (approx. 270 to 290 Ma), the Cornubian batholith was emplaced (Selwood et al. 1998). The magmatic heat of this peraluminous, predominantly S-type granite batholith (Goode & Taylor 1988; p16) generated a 1km wide contact metamorphic aureole. The diachronous emplacement of the six main granite plutons (Dartmoor, Bodmin Moor, St Austell, Carnmenellis, Lands End and Scilly Isles) between 275Ma (Lands End) and 293Ma (Carnmenellis) has been documented by U-Pb and ^{40}Ar-^{39}Ar isotope methods (Chen et al. 1993, Chesley et al. 1993). The primary heat and secondary heat, through radioactive decay, initiated convection cells of magmatic and meteoric fluids that resulted in hydrothermal activity and the creation of Sn, Zn, Cu lodes which have been extensively mined in Cornwall (e.g. Selwood et al. 1998). The episodic basaltic magmatism in evidence during the Variscan appears to have been completed prior to the emplacement of the granites. It is probable that metamorphism of the existing igneous rock, producing greenstone, occurred slightly prior to and during the emplacement of the Cornubian batholith, that is prior to 293Ma.

The continued gravity collapse and erosion of the granite-buoyed upland eventually exposed the Cornubian batholith during the Triassic (240 Ma). Triassic and younger rocks mostly outcrop in the east of Devon and beneath sea level in the Bristol Channel and

English Channel, having been eroded (or not deposited?) in Cornwall and west Devon. There are a few Quaternary exposures, e.g. St Erth beds near St Ives, and the Crousa Downs gravels on the Lizard peninsular. Igneous activity post emplacement of the granites is found only in the east of Devon. The Exeter Volcanic series are predominantly alkali basalts and are restricted to the Crediton Trough (Floyd et al. 1993). Rare rhyolites and a series of NE-SW trending lamprophyre dykes are thought to be related to the emplacement of the granite (Floyd op. cit.).

In summary, the greenstone rocks found in Devon and Cornwall were predominantly erupted/emplaced (c.f. next section) during the Variscan Orogeny and prior to the emplacement of the Cornubian granitic batholith. Regional metamorphism caused by the orogeny, and contact metamorphism as a result of the emplacement of the granites altered the originally mafic tholeiitic and alkali basalts to greenstone. Geochemical properties of the Devonian and Early Carboniferous igneous rocks support the presence of extensional tectonic regimes as evidenced by the various sedimentary basins.

3.5 Overview of major Devonian and Early Carboniferous stratigraphy, structure and igneous activity in Cornwall and Devon

The main litho-tectonic units and structures containing altered basic igneous rocks of interest, i.e. greenstone in Cornwall (especially around Mount's Bay) and Devon were formed in the earlier parts of the Variscan Orogeny (c.f. Section 3.4,above). This section provides an overview of the stratigraphy, structure and igneous activity in Cornwall and Devon during the Devonian and early Carboniferous in preparation for subsequent descriptions of lithology, igneous activity and details of samples taken. Tectonic environments after the Mid Carboniferous, involving thin skinned folding and nappe formation, have been deliberately ignored since the last igneous event of interest is the emplacement of the Tintagel Volcanic Formation during the Visean.

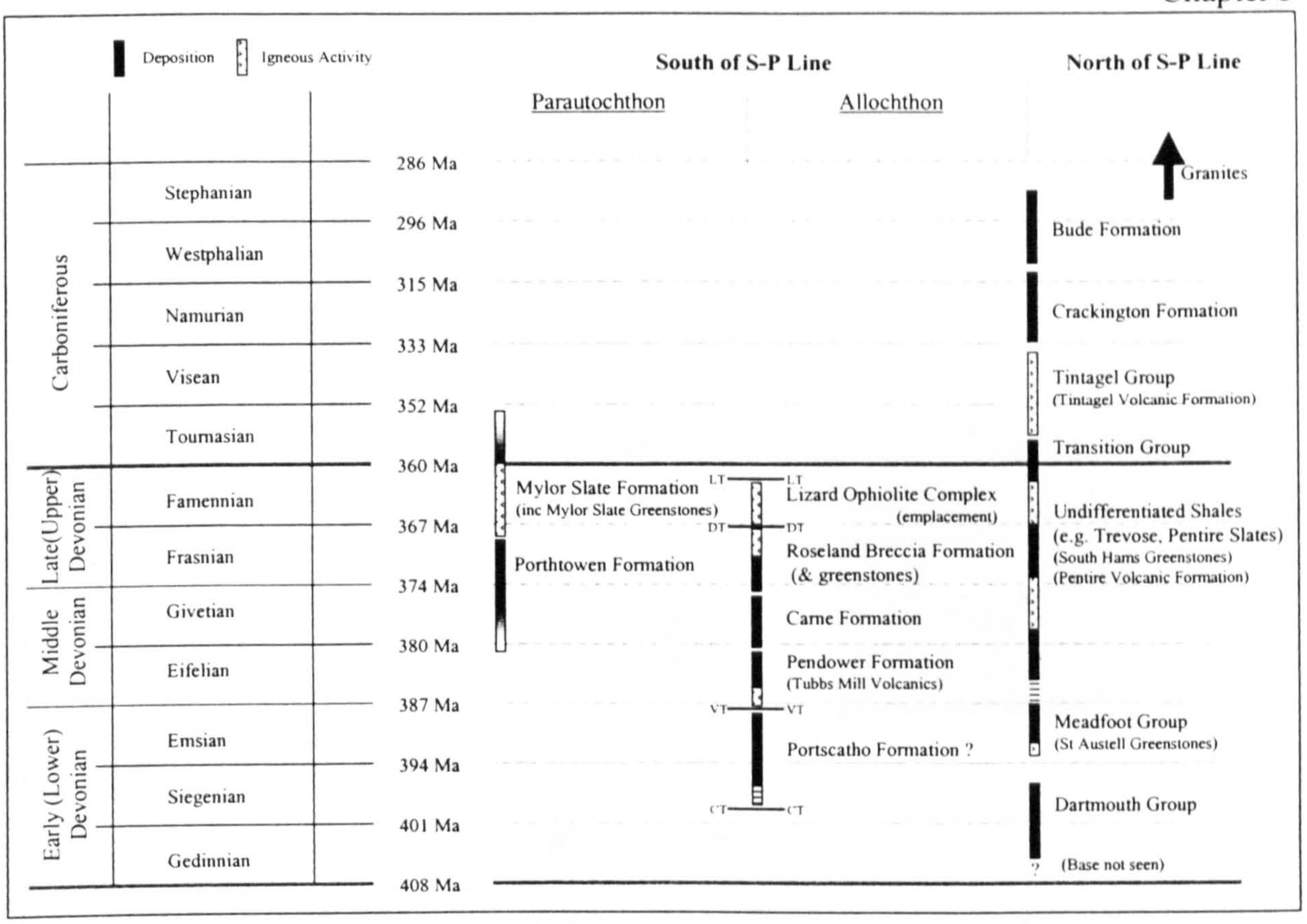

Figure 15 Simplified geological time scale of SW England showing timing of lithic units and associated mafic igneous activity during the Devonian and Carboniferous eras. CT – Carrick Thrust, VT – Veryan Thrust, DT – Dodman Thrust, LT – Lizard Thrust. (Time scale after Harland 1984, other details after Bristow 1996, Selwood et al. 1998, Edmonds et al. 1975). S-P Line – Start-Perranporth Line.

The formalisation of the stratigraphy of Devon and Cornwall is still developing as a greater understanding of the geology is achieved (e.g. compare the latest BGS Sheet 337 (Tavistock) with its predecessor). For the purpose of this work named Cornish stratigraphic units (after Holder & Leveridge 1986) prevail over locally named lithologies. Figure 15 illustrates the temporal relationship between major Cornish and Devonian litho-tectonic units and associated igneous rocks that are investigated as part of this work. These units have been divided into two zones: those north of the Start-Perranporth line (S-P Line) and those to the south, with the southern units being further divided into autochthonous and allochthonous litho-tectonic units. These divisions recognise the effect of the S-P Line and the thin-skinned thrust tectonics have on the structure and placement of the geology of SW England.

3.5.1 Start – Perranporth Line (S-P Line)

As stated above, geology in Cornwall can be divided by the 'Start – Perranporth' Line (S-P Line) (Holdsworth 1989, Figure 14). The S-P Line represents a zone of intensely sheared and deformed rocks that can be seen in exposures between Holywell Bay and Perran Bay on the north Cornish Coast, and Pentewan and Mevagissey on the south coast. The zone of deformation is believed to be along a reactivated basement (Precambrian) line of weakness

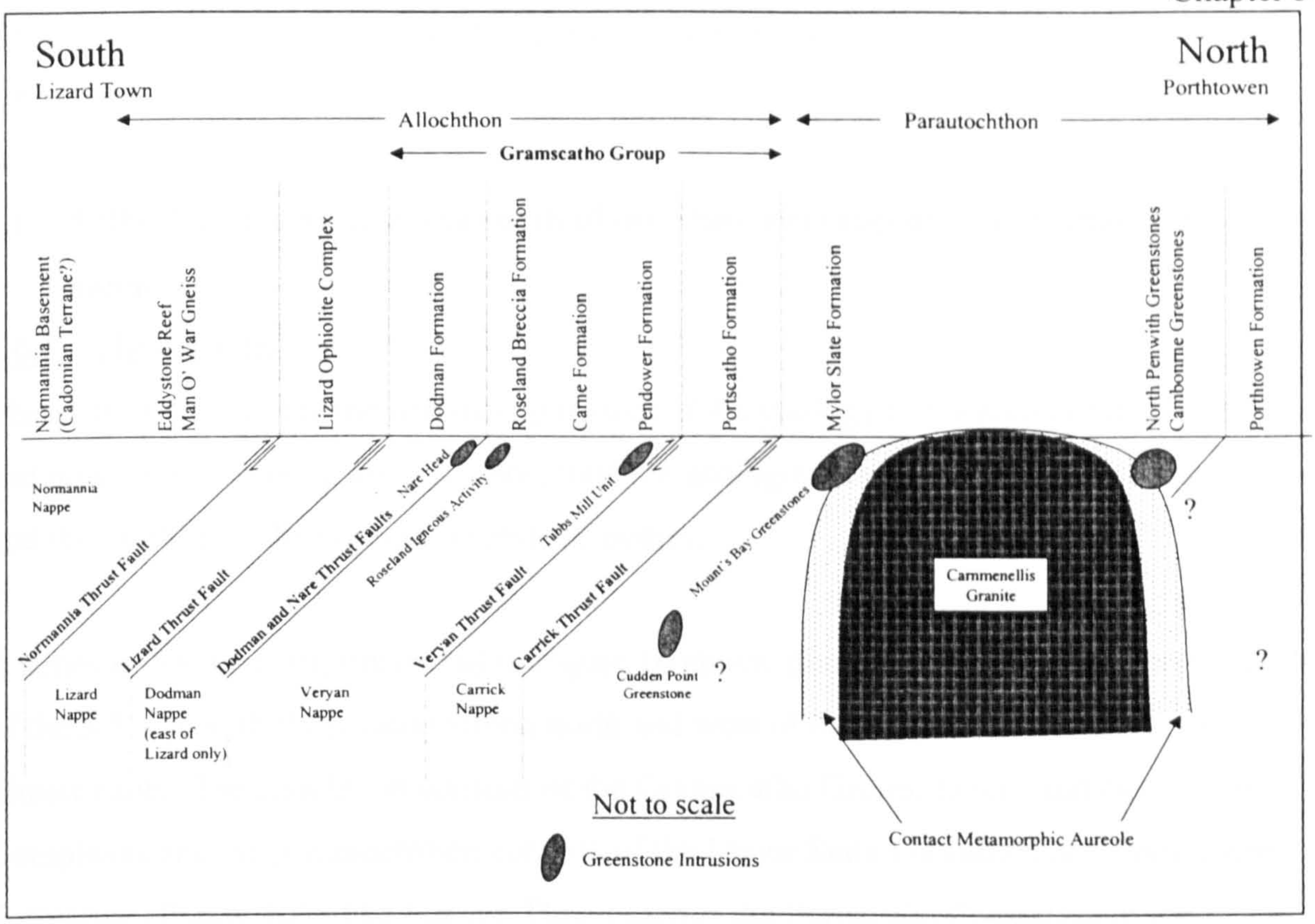

*Figure 16 Schematic cross section, **south of the S-P Line**, across Cornwall from Lizard Town to Porthtowen illustrating the stacking of the various thrust terranes (Line of section indicated on Figure 14) (After Bristow 1996 and Selwood et al. 1998)*

that, during the Variscan Orogeny, became a WNW to ESE dextral strike slip fault with a significant dip – slip movement. Rocks to the north of the S-P line are predominantly Lower Devonian and formed in shallow waters (see below), whereas to the south sediments were deposited in deeper waters and are Mid to Upper Devonian in age (ignoring the allochthonous slice of the older Gramscatho Group). This deeper, southern basin is called the Gramscatho Basin and is believed to have formed either as a transtensional (pull-apart) basin or a back arc basin (Floyd 1995, Bristow 1996). The Lizard Ophiolite is believed to be an obducted slice of the Gramscatho Basin floor, indicating that extensional tectonics had resulted in the formation of oceanic crust by approximately 370Ma ago (Davies 1984). Subsequent Transitional type MORB (T-MORB) to intermediate tholeiitic volcanism found in the Gramscatho Group and Mylor Slate Formation indicate that incipient extensional tectonics had never concluded with the production of true normal MORB (N-MORB) oceanic crust (Floyd 1984).

The next two sections, 3.6 & 3.7, deal with the lithologies to the south and north of the S-P Line and provide details on the character of the igneous activity and, more importantly, the locations of samples collected as part of this work and by other workers. In order to provide a complete picture (and for future reference) a review of the geological environment and sedimentation (where appropriate) of all the main lithostratigraphical

units illustrated in Figures 15 & 16 is given, including those that do not contain greenstones.

3.6 Litho-tectonic units to the south of the Start-Perranporth Line: character and sampling

3.6.1 Thrust faults

Thrust fault tectonics is the controlling feature of the geology to the south of the S-P line and must be reviewed in order to appreciate the geological environment of W Cornwall and the location of the various greenstone bodies.

A series of thrust faults, illustrated in Figure 16 above, divides the stratigraphy to the south of the S-P line with the parautochthon north and west of the basal allochthon Carrick Thrust Fault. The allochthon consists of the Gramscatho Group, Lizard and Normannia Complexes and the parautochthon consists of the Mylor Slate Formation and Porthtowen Formation (Figure 16). The Carrick Thrust carries the Portscatho Formation of the Gramscatho Group, and is at the base of the thrust pile, followed by the Veryan Thrust (Roseland Breccia Formation, Carne Formation, Pendower Formation of the Gramscatho Group), Dodman & Nare Thrust (lateral equivalents of Lizard), Lizard Thrust (Lizard Ophiolite) and Normannian Thrust (Precambrian crystalline basement (Cadomian Terrane?)) (Bristow 1997).

3.6.2 Allochthon

3.6.2.1 Normannia Basement (Cadomian Terrane?)

Normannia formed the northern part of Gondwanaland and was carried northwards on the Normannia Thrust Fault as the Variscan tectonic front moved northward. The presence of the Normannia High is confirmed by high-grade metamorphic material found in the Roseland Breccia Formation (Bristow 1997), a melange deposit at the foot of the prograding allochthonous stack of thrust sheets. Outcrops of the Normannian basement in SW England are the garnetiferous gneiss of the Eddystone Reef and the hornblende and chlorite rocks of the Man O' War gneiss (south of the Lizard peninsula). Sandeman et al. (1997) have indicated that the parental magmas of the Man O' War gneiss were formed approximately 500Ma, making them Ordovician. The Start Point greenschists are possibly related to the Precambrian Normannia Basement, however dating evidence has not been found and structural interpretation is as yet inconclusive. It has been proposed that the Start Point greenschists are part of an obducted piece of Variscan Ocean floor since they

have MORB type affinities (Floyd et al. 1993). (based on Selwood et al. 1998, Sadler 1974, Holder & Leveridge 1986, Bristow 1996, Flett 1946)

3.6.2.1.1 Igneous activity

Although the Start Point greenschists (*not* greenstones) have MORB affinities (Floyd 1995) they are heavily deformed and their original geological environment is poorly understood.

3.6.2.1.2 Samples

None, as there are no Neolithic axes manufactured from the relatively soft greenschist, and the greenschist is not a greenstone.

3.6.2.2 Lizard Ophiolite

Formation and obduction of the Lizard Ophiolite took place in a geologically short time. Formation of the Lizard gabbros has been dated at 375 ± 37Ma (Davies 1984) and the emplacement/formation age of the acidic material of the Kennack gneiss at 369 ± 12Ma (Styles & Rundle, 1984). Emplacement of the Lizard, on the Lizard basal thrust (see Figures 15 and 16) therefore occurred very quickly after formation as it was obducted by ?early Famennian (360 – 367 Ma).

3.6.2.2.1 Igneous activity

The Lizard Ophiolite is not a complete fragment of oceanic crust as the carapace of extrusive submarine volcanics and associated sedimentation normally associated with a complete ophiolite sequence is not present within the Lizard complex. Pillow lavas seen at Mullion Island and in other locations within Roseland Breccia Formation are not related to the Lizard magmatic suites (Floyd 1995). Medium to fine grained, often plagioclase porphyritic MORB related tholeiitic dykes are found at Porthoustock and Coverack and are believed to represent the dyke swarm that fed the (missing) pillow lavas. Further south, coarse-grained gabbro, frequently cut by darker, finer grained doleritic veins is seen between Coverack and Porthoustock and represents the feeder magma chamber that would have been beneath the spreading centre. The extensive Lizard serpentinite formed by hydration of the ultra-mafic peridotite mantle represents the bottom layer of the ophiolite sequence and is predominantly found in the west of the Lizard peninsula. The boundary between the peridotite and the gabbro, the petrological Moho, is seen on the beach at Coverack where the gabbro grades into peridotite over a distance of a few hundred metres. Finally, although extensive work has been carried out on the variety and geochemistry of

rocks found in the Lizard, a full explanation of the formation of the Landewednack and Traboe hornblende schists, Kennack Gneiss and localised felsic rocks south of Porthallow has yet to be provided. (after Flett 1946, Selwood et al. 1998)

3.6.2.2.2 Samples

Figure 17 shows the location where two samples of the greenstone dyke material exposed at Porthoustock were collected as large loose boulders on the shoreline at Manacle Point, close to the exposure of sheeted dykes (identified in Figure 17 as MM1 & 2). These samples are thought to represent the closest match to greenstone found within the Lizard Ophiolite Complex and their geochemical make up should support the documented difference between the Lizard and Roseland Breccia igneous rocks (Floyd et al. 1993, Floyd 1984, Barnes & Andrew 1986).

3.6.2.3 Gramscatho Group (Overview)

In this work the Gramscatho Group is limited to the allochthonous sediments of the Portscatho, Pendower, Carne, Roseland Breccia and Dodman Formations and does not include the parautochthonous Mylor Slate and Porthtowen Formations. Selwood et al. (1998) enlarge the Gramscatho Group to include all sediments that formed within the Gramscatho Basin including the Porthtowen Formation (see below).

The Gramscatho Group consists of basinal, flysch and olisthostrome deposits of the Portscatho, Pendower, Carne, Roseland Breccia and Dodman Formations that were deposited into the Gramscatho Basin during the Mid to Upper Devonian. These formations are part of the Cornish allochthon, transported by the Dodman, Veryan and Carrick Thrust faults (Holder & Leveridge, 1986). The Porthtowen Formation is also considered (basal) part of the Gramscatho Group, but forms part of the parautochthon and is dealt with below. The Gramscatho Group is Mid to Upper Devonian in age (Barnes 1984) although recent work suggest a slightly younger, Upper Devonian, age for Portscatho Formation (Selwood et al. 1998), hence suggesting the whole of the Gramscatho Group is younger than previously thought.

The tholeiitic basic rocks (now overprinted with pumpellyite grade metamorphism) of the Gramscatho Group are extensional, MORB, related. The earliest unit, at Tubbs Mill, could represent the initial stages of crustal extension, which then developed into an active extension zone producing the basaltic lavas found within the Roseland Breccia Formation but failing to produce true MORB oceanic floor basalts (Barnes & Andrews 1986). Floyd

et al. (1993) showed that the melange volcanics were distinctive from other SW igneous groups by virtue of high Zr/Nb ratios (>7). Barnes & Andrews (1986) similarly showed the melange basalts were different from those of the Lizard ophiolite.

3.6.2.4 Gramscatho Group: Portscatho Formation

The Portscatho Formation consists of 5,400m of submarine fan distal turbidites, comprising calcareous sandstones, silts and interbedded grey shales (Holder & Leveridge 1986) and has similarities with the Porthtowen Formation. This sedimentation formed in deep water from distal submarine fan deposits (Selwood et al. 1998, Holder & Leveridge 1984). It is the sole lithic unit within the Carrick Nappe and is bounded by the Carrick thrust fault below and the Veryan thrust fault above.

3.6.2.4.1 Igneous activity

None reported

3.6.2.4.2 Samples

None, as there are no igneous rocks found in the unit.

3.6.2.5 Gramscatho Group: Pendower Formation

The Pendower Formation comprises approximately 500m of sediments of approximately Mid-Eifelian age. Four rock types are seen: slumped silts and muds, thinly bedded but coarsely grained siliciclastic sands, thickly bedded calciclastic sandstone-mudstone couplets and biogenic cherts (Selwood et al. 1998). Holder & Leveridge (1986) suggest these sediments formed in a hemipelagic-shielded basin. This formation is the lowest within the Veryan Nappe and lies immediately above the Veryan thrust fault.

3.6.2.5.1 Igneous activity

The Tubbs Mill volcanic unit, towards the base of the Pendower Formation, comprises of MORB – Transitional tholeiitic pillow lavas that are unrelated to the Lizard Ophiolite (Floyd 1984, Barnes 1984). Floyd et al. (1993) indicates these pillow lavas may be subduction – back arc related although this is not certain.

3.6.2.5.2 Samples

Geochemical data from five samples collected from the quarried exposure of the Tubbs Mill pillow lavas are available and are geographically located in Figure 13 (Section 3.2, identified as RV27-RV31) (Floyd pers. com.).

3.6.2.6 Gramscatho Group: Carne Formation

This unit, to 250m thick, comprises medium to thickly bedded turbidite sandstone units deposited on basin slope and proximal submarine fans. Although no palaeontological information is available a Givetian age is probable, given the conformable contact with the Pendower Formation below and the Roseland Breccia Formation above (Holder & Leveridge 1986, Selwood et al. 1998).

3.6.2.6.1 Igneous activity

Outcrops of greenstone/dolerite at Cury shown on BGS Sheet 359: Lizard, indicate igneous activity within the Carne formation. Flett (1946) indicates these outcrops are 'small masses of irregular shaped and ill exposed' ophitic diabase, devoid of vesicles and that they have 'intrusive characteristics'. Flett goes on to indicate that these greenstones are less structurally altered than the nearby Porthleven greenstones. However later geological maps of the Lizard (see Kirby 1979) place these greenstones within the Roseland Breccia Formation, although this has yet to be confirmed by BGS.

3.6.2.6.2 Samples

Two samples were collected by field walking across the meta-basic outcrop at Cury (CUR001 & CUR002, see Figure 17, below), however as these samples were not collected from exposures subsequent analyses must be treated with caution.

3.6.2.7 Gramscatho Group: Roseland Breccia Formation

The Roseland Breccia Formation (formerly Meneague Breccia) represents the main part of the south Cornish melange. This formation represents the flysch (molasse) deposit laid down in front of the northwards moving Variscan front during the Middle to Upper Devonian. It includes 200m sized blocks of Ordovician Quartzite, (a similar rock type to 'Gres Amorcia' in northern France (Sadler 1974)) and Lower to Mid Devonian greywackes all set in a black mudstone matrix (Barnes & Andrews 1986). Two main outcrops of Roseland Breccia Formation are found; one north of the Lizard, south of the Helston river and the second, north of Dodman Point, east of Falmouth. The Roseland Breccia Formation is the uppermost unit within the Veryan Nappe and bounded above by the Dodman & Nare thrust fault.

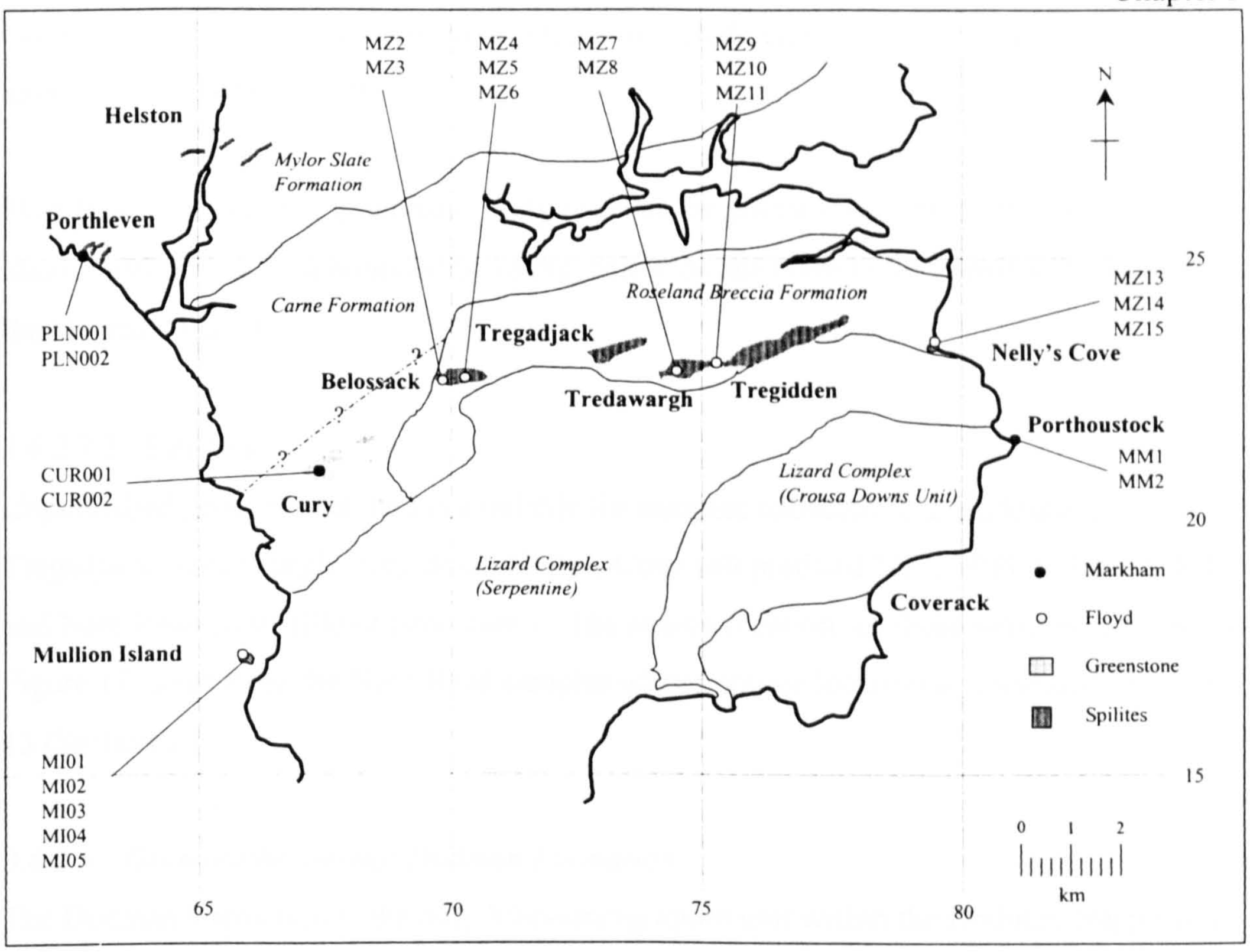

Figure 17 Lizard and Roseland Breccia Formation sample sites (map based on BGS Sheet 359 – Lizard, with additions)

3.6.2.7.1 Igneous activity

Considerable contemporaneous tholeiitic extrusive and high level intrusive igneous activity is recorded by large, kilometre-sized, blocks of igneous material, which have subsequently slid northwards, down the unstable advancing allochthon slope into the Gramscatho Basin (Holder & Leveridge 1986). Floyd (1984) and Barnes (1984) showed that the Roseland Breccia related basalts are broadly N-Type MORB but are dissimilar to those found in the Lizard ophiolite, and suggested that the N-MORB to E-MORB chemistry indicates that the extensional regime did not achieve the generation of true oceanic crust in this case.

Figures 13 and 17 illustrates that the allochthonous tholeiitic pillow lavas and hyaloclastics (e.g. spilites) of the melange can be seen at Mullion Island, Nelly's Cove, Gorran Haven, Nare Head and east of Great Perhaver Point where distinct incompatible element ratios and N-type to T-type MORB affinities support the idea of crustal extension. In addition these rocks have undergone low-grade regional pumpellyite facies metamorphism, with primary phases replaced by an epidote – plagioclase – hornblende assemblage (Floyd 1984).

Mullion Island pillow lavas, dated by condonants as Frasnian in age, is a mildly enriched aphyric tholeiite with zoned plagioclase, relict clinopyroxene and ilmenite which has been

altered by low grade regional metamorphism to include chlorite, pumpellyite and amphibole (Floyd et al.1993).

Nare Head consists of a greenstone body overlain by pillow lavas and is thought to be a major olistholith as it is bounded by faults, below by the Nare Head Thrust and above by the Dodman Thrust.

3.6.2.7.2 Samples

Unpublished geochemical data is available for samples collected from Belossack, Tregadjack, Tredawargh, Tregidden, Nelly's Cove (all prefixed MZ), Mullion Island (MI) and Nare Head (RV) (Floyd pers. com.). The source location for these samples is shown in Figure 17, apart from the Nare Head samples whose source location is illustrated in Figure 13 (Section 3.2)

3.6.2.8 Gramscatho Group: Dodman Formation

The Dodman Formation is the only litho-stratigraphic unit within the Dodman Nappe and comprises phyllitic mudstones and sandstones that have been thrust over the Roseland Breccia Formation. The Dodman Nappe is bounded by the Dodman thrust fault below and the Lizard thrust fault above.

3.6.2.8.1 Igneous activity

There is no igneous activity reported within the Dodman Formation, although the Nare Head Greenstone body is identified as being separate from the preceding Veryan Nappe complex (Selwood et al. 1998).

3.6.2.8.2 Samples

Nare Head is covered within the Roseland Breccia Formation section (Section 3.6.2.7) as its position within the Dodman Formation is not absolutely certain.

3.6.3 Parautochthon

3.6.3.1 Porthtowen Formation

The Porthtowen Formation consists of metre sized turbidite sequences of coarse, angular quartz, lithic fragments and occasional granophyric fragments to fine laminated grey to green shales (now slate) deposited into deep water (Wilson & Taylor 1976, Holder & Leveridge 1986). Chronologically it is the oldest member of the Gramscatho Group, below the Portscatho Formation and above the Meadfoot Group. Holder and Leveridge

(1986) suggest the Portscatho and Porthtowen Formations are actually the same sequence, with the Portscatho Formation above the basal Carrick Thrust, hence part of the allochthon, and Porthtowen below the Carrick Thrust as part of the parautochthon. Whatever the case there is no recorded volcanic activity within the Porthtowen Formation, and taken with the equivalent lack of volcanics in the Porthscatho Formation, suggests the initial infilling of the Gramscatho Basin was not accompanied by any volcanic activity.

3.6.3.1.1 Igneous activity

No igneous activity reported.

3.6.3.1.2 Samples

None, as no igneous rocks are present.

3.6.3.2 Mylor Slate Formation

The Mylor Slate Formation consists of variably coloured, grey-green, blue-grey or dark grey-black slates that represent deposition of fine silts and muds in a rise, slope and outer shelf environment (Holder & Leveridge 1984, Goode & Taylor 1988). Microfossils have allowed the dating of the Mylor Slate Formation as late Devonian to early Carboniferous (Famennian) (Turner et al. 1979) and not Frasnian to Famennian as generally accepted. The continued northward closure of the Gramscatho Basin during the Variscan is represented in the Mylor Slate parautochthon as complex folding and faulting.

3.6.3.2.1 Igneous activity

The Mylor Slate Formation is exposed around Penwith Peninsula, west of Porthleven to Mousehole and intermittently west of St Ives to Botallack Head (c.f. Figures 14 and 18 to 23). Intense volcanic activity is evident by the large number of pillow lavas and intrusive basic rocks within the formation. Many igneous sills are found along the southern coastline of the Penwith Peninsula, with exposures at Cudden Point, Trenow Cove, Marazion, Penzance, Mousehole and Tater Du being prime examples. The northern coast of the peninsula is dominated by pillow lavas and shallow level intrusives with exposures found at St Ives, Carrick Du, Clodgy Point, Zennor, Gurnards Head, Porthmeor, Pendeen and Botallack being noteworthy.

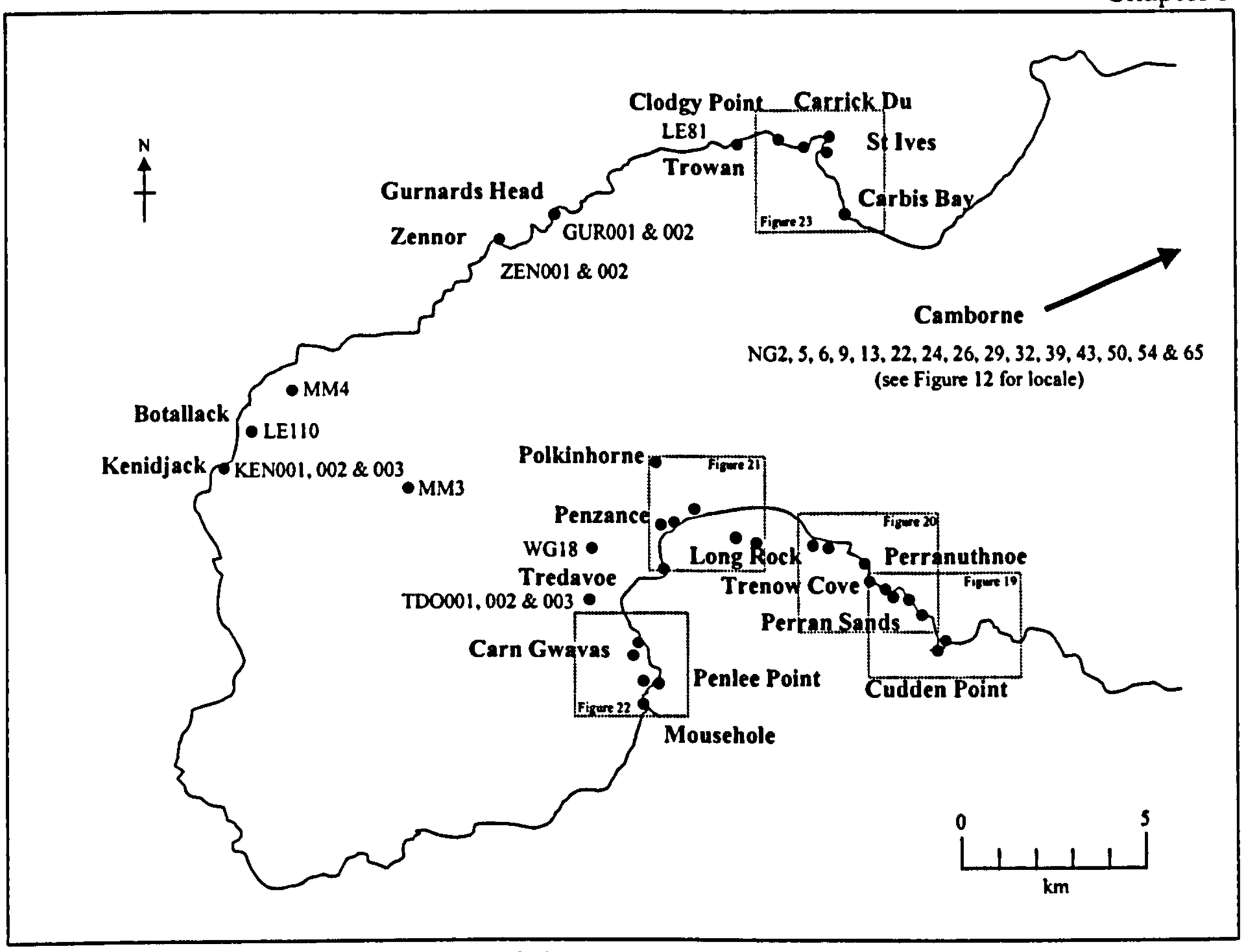

Figure 18 Map showing greenstone sample locations within the Mylor Slate Formation. Samples not covered in subsequent figures (identified and outlined) are shown in this Figure.

These tholeiitic basaltic rocks are intermediate between MORB and intraplate types with a range of basic rock types found, from the hydrous and primitive Cudden Point gabbro to the intermediate, dioritic, rock quarried at Carn Gwavas near Penzance (Floyd et al. 1993, Floyd & Al Samman 1980). Bristow (1996) suggested that the chemistry of the Mylor Slate igneous rocks was intermediate between those of the Pentire Point alkali complex and that of the Roseland Breccia basalts.

Floyd and Al Samman (1980) divided the igneous rocks contained in the Mylor Slate Formation into four geographically separate groups using immobile element geochemistry:

1. **Camborne Group**

   A co-magmatic series of extrusive pillow lavas and shallow intrusives that have anomalous high Y concentrations is found in the Camborne - Redruth area. These tholeiitic rocks form a co-magmatic spatially related series.

2. **Cudden – Perranuthnoe Group**

   A co-magmatic group of primitive tholeiites, with Cudden Point being the most primitive, and the only location along Mount's Bay where primary brown amphibole is found. In the area around Perranuthnoe the tholeiitic intrusive rocks are more evolved (c.f. Figures 19 and 20).

3. **Penzance Group**

A series of shallow level intrusives (towards the coast near Penzance – Mousehole) and extrusives inland north on Penzance itself. The large sill (or pipe?) at Carn Gwavas, near Newlyn, is distinct from other intrusives in the Penzance Group as it is dioritic and not doleritic. Invariably this group has been affected by the proximity of the Lands End Granite, with contact metamorphic minerals common. An exception to the overall tholeiitic type geochemistry is the pillow lava at Gulval, which is alkaline (c.f. Figures 21 and 22).

4. **North Penwith Group**

A series of pillow lavas and shallow level intrusive sills (emplaced into wet sediments) are found between St Ives and Kenidjack, and are partly within the Lands End Granite aureole. More exotic mineral assemblages are found towards Kenidjack where a higher degree of contact metamorphism is observed through the presence of cordierite crystals seen in hand specimen and thin sections.

The Cudden and Penzance groups plot within the tholeiitic 'intra plate basalt' tectonic environment as defined by the Pearce and Cann ternary Ti–Y–Zr discrimination diagram (Al Samman 1980). They can be discriminated using bivariate plots based on Zr & Nb, with Cudden having low Zr (<90ppm) and low Nb (<5ppm) and Penzance having high Zr (ca 300ppm), high Nb (ca 40ppm). The Camborne Group plots within the tholeiitic island arc setting in the same discrimination diagram, having different Y-Zr ratios than the other three groups (Al Samman 1980). The North Penwith Group is geochemically similar to the Penzance Group but can be distinguished by slightly different Zr-Y ratios (Floyd et al 1993 & Floyd pers. com.). Finally, Floyd et al. (1993) reported that Nb/Zr ratios can be used to differentiate igneous rocks from the Roseland Breccia Formation, the north Penwith Coast, Mount's Bay and north Cornish lower Carboniferous volcanics (c.f. Appendix 30.2 Part 2/6). The geographical extent of these all groups mentioned in this section and the location of samples collected is illustrated in Figure 18 and detailed in Figures 19 to 23.

In general, basic igneous rocks within the Mylor Slate Formation have undergone low-grade prehnite-pumpellyite facies regional metamorphism that has altered the primary plagioclase + pyroxene + ilmenite mineralogy to amphibole + chlorite + sphene/leucoxene ± epidote. Locally, contact metamorphism gives rise to hornfels and cordierite, especially around Kenidjack and Botallack Head (Floyd et al. 1993)

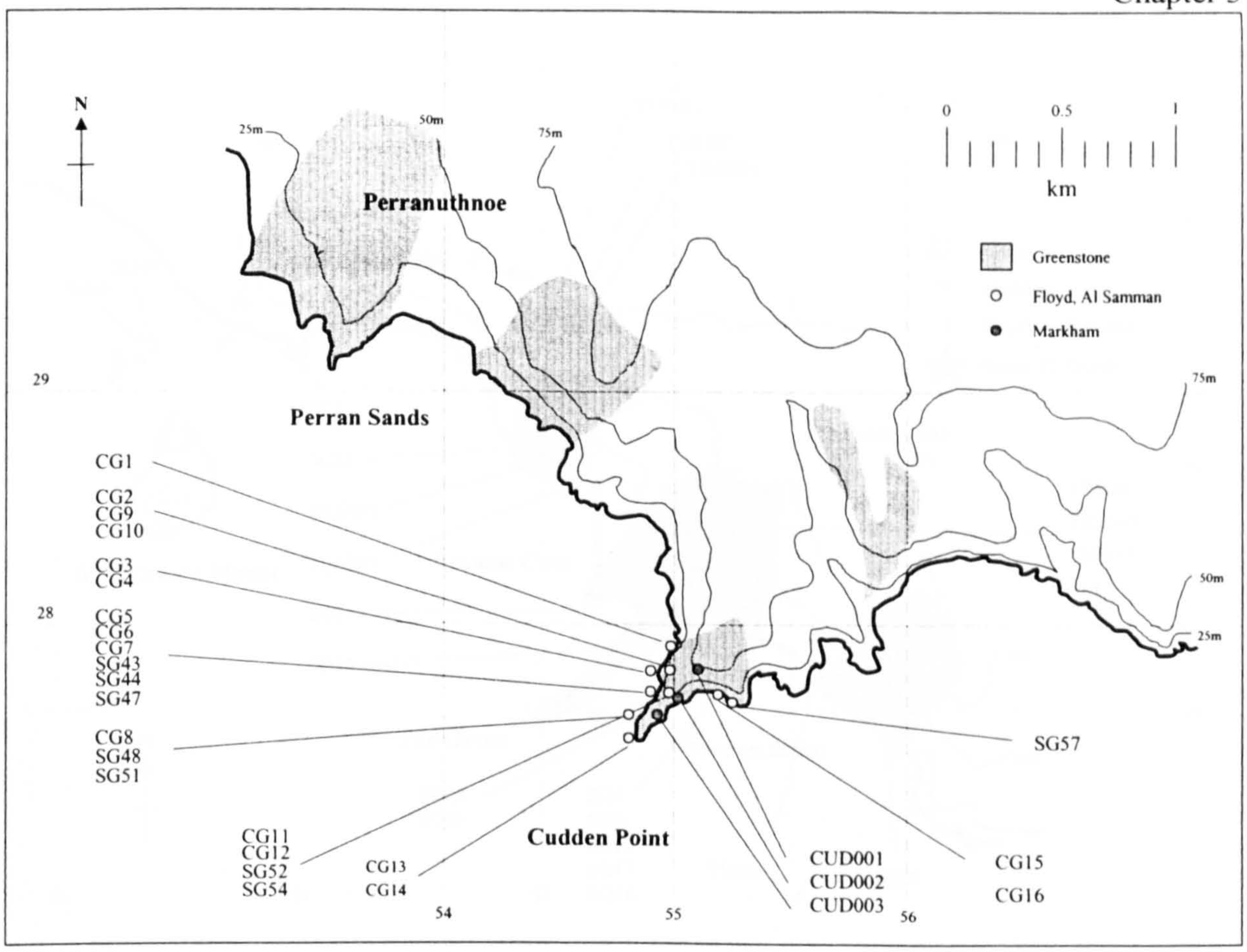

Figure 19 *Map showing the source location of the 'Cudden Point Group' of greenstone samples*

3.6.3.2.2 Samples

As the hypothesised origin of IPC Group I axes is within the 'Mounts Bay area (Keiller et al. 1941), over thirty samples were collected from greenstone exposures around Mount's Bay and along the North Penwith Coast. Geochemical data for samples collected from the same localities is also available as is additional geochemical data covering other greenstone exposures in the vicinity that have not been sampled as part of this work. In light of the four-fold division of igneous geochemistry the sample sites have been divided into five groups: Camborne, Cudden Point, Perranuthnoe, Penzance & Mousehole and North Penwith Coast (c.f. Figure 18).

Camborne Group

Geochemical data is available for 14 samples (prefixed NG) collected previously within the Camborne area (Floyd pers. com.). The source of these samples is geographically is illustrated in Figure 18

Cudden Group

Three samples were collected from locations on the east side of Cudden Point (CUD) and geochemical data is available for a further twenty-four samples (CG, SG) (Floyd pers. com.). The source of these samples is geographically is illustrated in Figure 19.

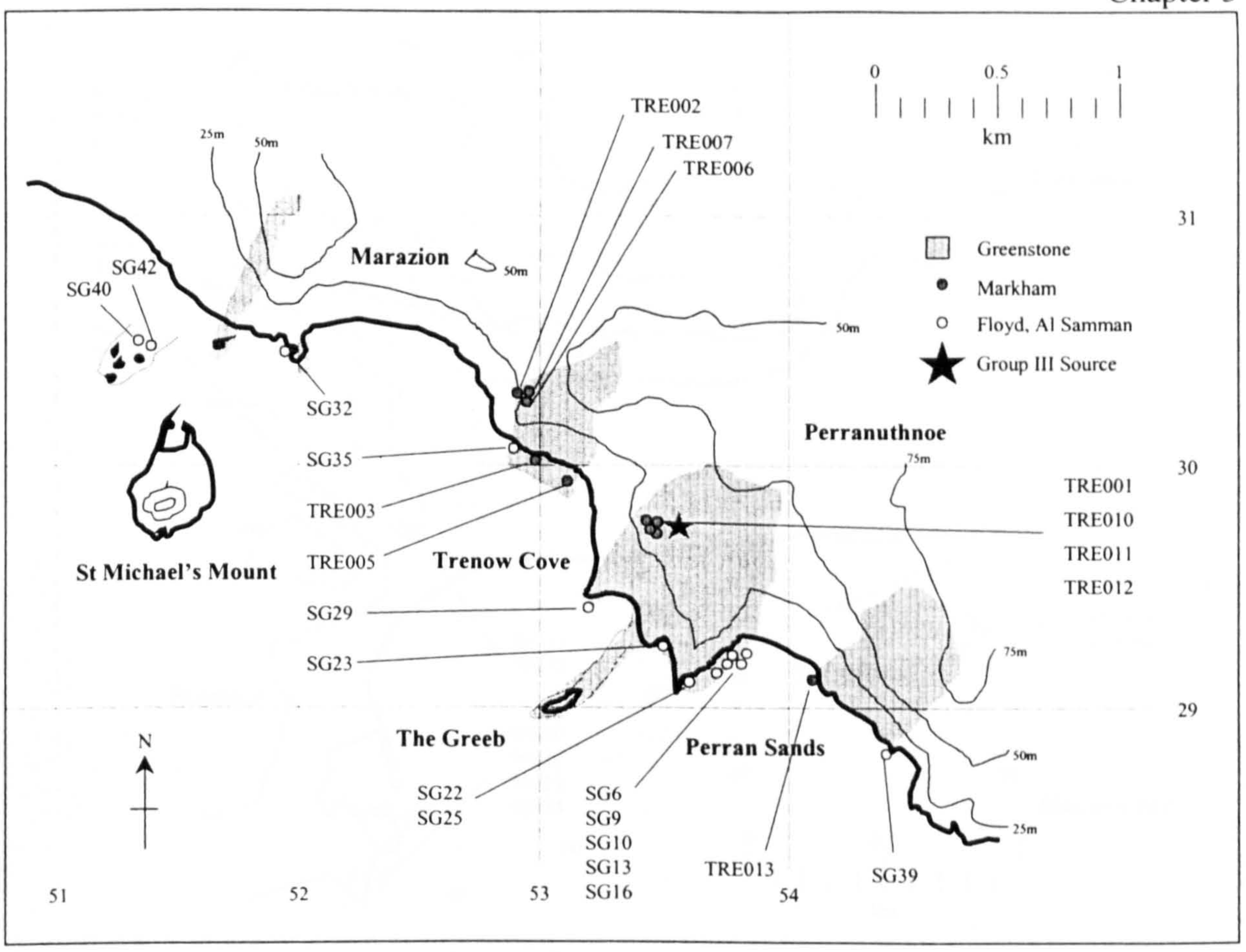

Figure 20 Map showing the source location for the 'Perranuthnoe Group' of greenstone samples

Perranuthnoe Group

Three exposures yielding ten samples were visited as part of this work. From visual clues in Keiller et al. (1941: lower plate 1, facing page 64) the quarry in the picture foreground was located and four samples taken (TRE001, 010, 011, 012, with the quarry identified as a black star in Figure 20). Since the quarry face was judged dangerous and the quarry had been extensively used as a dumping ground the last sample was collected as a loose boulder near the quarry entrance. The second exposure visited lies approximately 0.5km NW of the quarry and forms a resistant headland approximately 25m above sea level forming an ancient cliff-line and continues down to the current shoreline (TRE002, 003, 006, 007 with TRE005 collected as a large loose boulder within Trenow Cove). TRE013 was taken from the greenstone exposure SE of Perranuthnoe at Perran Sands. Floyd (pers. com.) and Al Samman (1980) supplied additional geochemical data for 14 other samples from the Perranuthnoe area. The source of all these samples is geographically is illustrated in Figure 20.

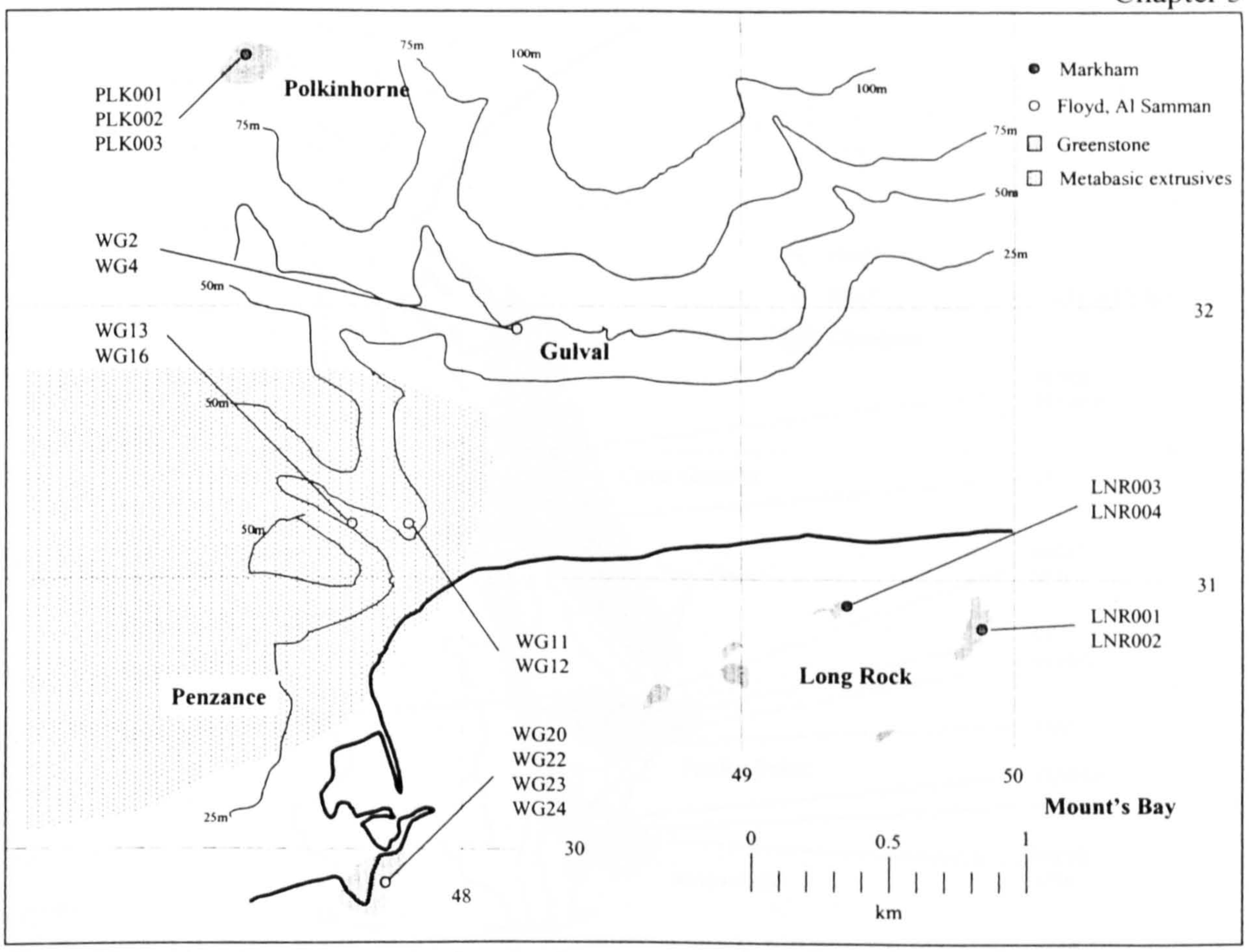

Figure 21 Map showing the source location for greenstone samples collected near Penzance and Long Rock

Penzance & Mousehole

Exposures along the coast at Carn Gwavas, Penlee Point, Mousehole and Long Rock were sampled (PEN & LNR). At two inland greenstone outcrops, Tredavoe and Polkinhorne, no fresh exposures could be found. At Tredavoe a sample was collected from the side of partly infilled quarry and a further two samples (TDO) from large boulders from a dismantled stone wall. Likewise at Polkinhorne, samples (PLK) were collected from an old field wall being demolished to form a new gateway. In both these cases data from these samples should be used with extreme caution. Geochemical data from a further 27 samples (prefixed LE, M, WG) collected in the Penzance area have been made available (Floyd pers. com.). The source of samples collected from Penzance and Mousehole is geographically illustrated in Figures 21 and 22.

North Penwith Coast

Exposures at Kenidjack, Gurnards Head and Zennor Point were visited and yielded 7 samples (KEN, GUR, ZEN). In addition geochemical data from 8 locations around St Ives and 1 from Botallack (prefixed LE) were made available (Floyd pers. com.). The source of samples collected from near St Ives is geographically is illustrated in Figure 23

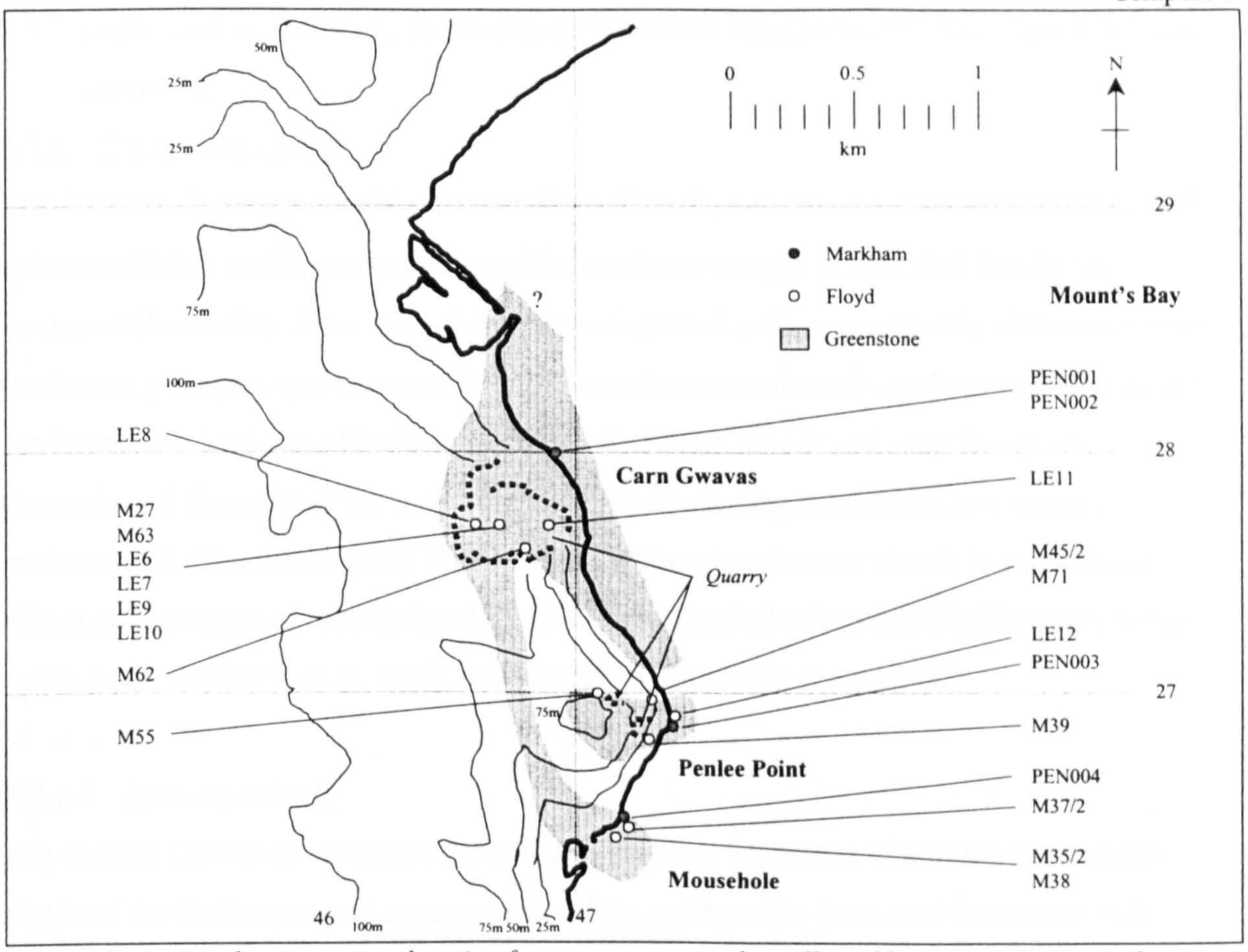

Figure 22 Map showing source location for greenstone samples collected between Penzance and Mousehole

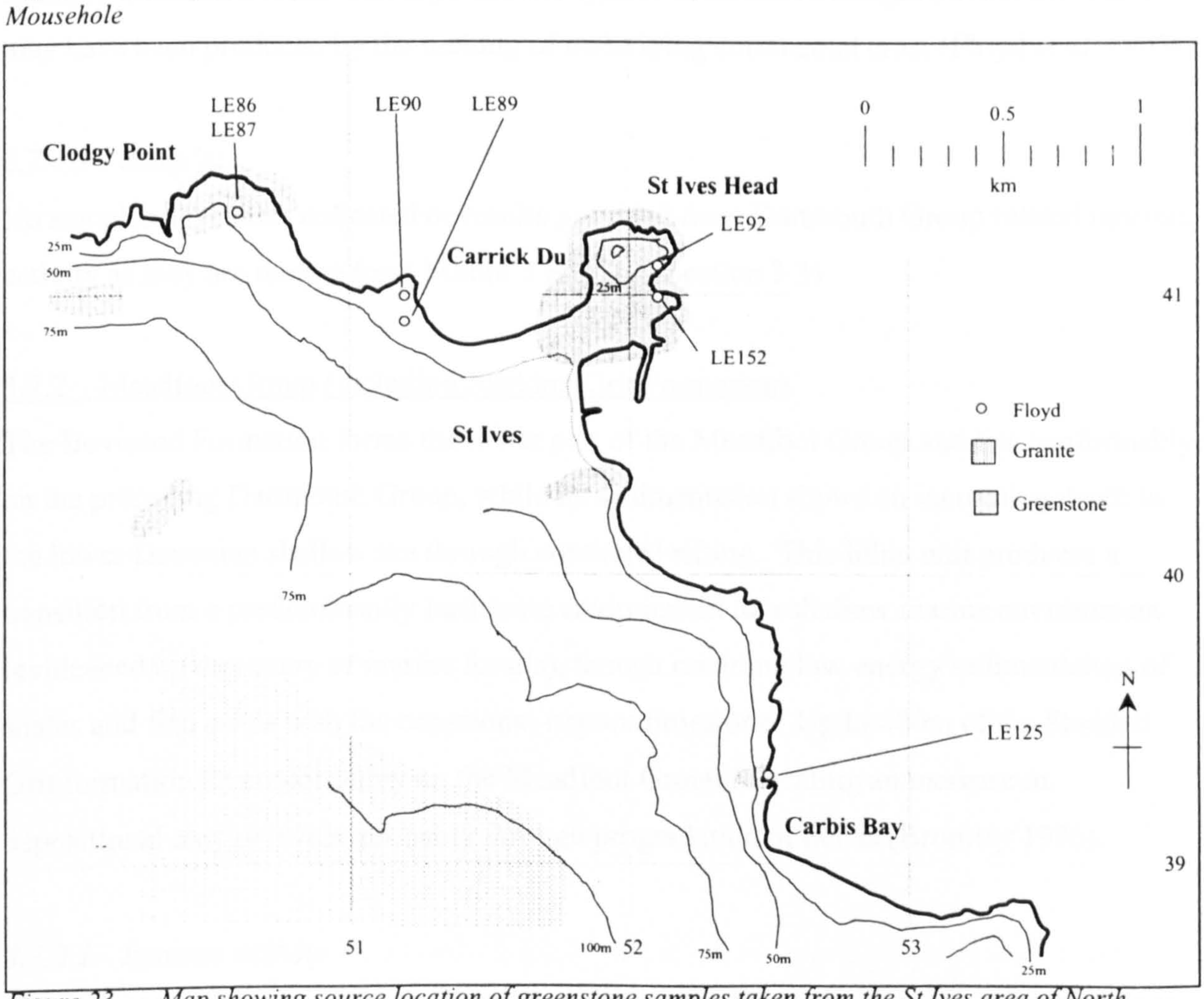

Figure 23 Map showing source location of greenstone samples taken from the St Ives area of North Penwith

3.7 Litho-tectonic units to the north of the Start-Perranporth Line: character and sampling

3.7.1 Dartmouth Group

The Dartmouth Group consists of over 4km of muds, silts and fine sandstones deposited in ephemeral lakes on the coastal plain of the southern margin of Old Red Sandstone continent (Laurasia). Five litho-facies are recognised: pale green muddy siltstone, purple mudstone, pale grey-green or mottled green and mauve siltstone , pale greenish–grey fine sandstone and lastly an off-white quartzite. Sediment colour and very fine pyrite disseminated throughout the rock both indicate a reducing, anaerobic, low energy environment. The thickness of the Dartmouth Group sediments attests to continental rifting environment accommodated by E-W trending faults forming a half-graben to the south. (after Selwood et al. 1998, Bristow 1996, Edmonds et al. 1975.)

3.7.1.1 Igneous activity

The earliest Devonian volcanics recorded in England are found within the Dartmouth Slates of the Gedinnian and consist of rhyolitic and basaltic lavas and intrusives with spatially associated tuffs. The rhyolites are typical of an active margin environment and may have been produced by the melting of underlying continental crust (Floyd et al. 1993).

3.7.1.2 Samples

No samples have been collected or results provided from Dartmouth Group related igneous activity as they are remote from Mount's Bay (c.f. Section 3.3)

3.7.2 Meadfoot Group (including Staddon Grit Formation)

The Bovisand Formation forms the lower part of the Meadfoot Group and lies conformably on the preceding Dartmouth Group, while its sedimentation shows an increasing depth to the lower Devonian shallow sea through continued rifting. This lithic unit produces a transition from a predominantly lacustrine environment to a shallow marine environment (evidenced by discovery of marine fossils), though retaining low energy sedimentation of shales and fine sands with the occasional impure limestone. Up to 400m of the Staddon Grit formation lie conformably on the Meadfoot Group indicating an increase in depositional energy levels, probably through progradation of deltas (Bromley 1996).

3.7.2.1 Igneous activity

A series of lower Devonian basic volcanics and intrusives are found around the St Austell area, where they intrude into the Meadfoot Group. Quarries exploiting the dolerite are

found near Carlyon Bay, Par, Trewoon, Black Head, Tregongeeves, Molingey and Duporth.

3.7.2.2 Samples

No samples have been collected or results provided from Meadfoot Group related igneous activity as they are geographically remote from Mount's Bay (c.f. Section 3.3).

3.7.3 Mid to Upper Devonian Slates

No single name is given to the series of monotonous slates of the mid to upper Devonian rocks of SW England that formed from the steady rain of marine muds and shales deposited down in the low energy environment of the developing Trevone (W Cornwall), and smaller South Devon, Basins. The Trevone succession includes the Trevose, Pentire, Polzeath, Haywood and Milepost Slate Formations. Towards the east, the South Devon Basin includes Plymouth, Torquay and Chudleigh Limestones towards the base of the succession and variably named slate formations (e.g. Ostracod, Whitchurch Slates). These basins are believed to have formed through re-activation of basement faults during the Mid-Devonian and eventually provided space for up to 6,000m of sediments. (Selwood et al. 1998)

3.7.3.1 Igneous activity

Igneous rocks of the Trevone Basin are enriched alkaline indicating an ensialic setting. Pentire Volcanic Formation consists of anhydrous alkalitic dolerites and comagmatic explosively formed extrusives including vesicular pillow lavas and tuffs. Medium-grained, patchily vesicular and altered doleritic intrusions are exposed at The Rumps, Com Head and Lundy Bay (Selwood et al. 1998).

Trevose Slate Formation includes two igneous suites. A Frasnian/Famennian group consisting of anhydrous tholeiitic dolerite sills intruded at shallow levels can be found at Dinas Head (Selwood et al. 1993) (Floyd et al. (1993) report this as alkali?) and Merope Rocks. The younger, Famennian, suite consists of shallow level hydrous alkali dolerites within the Polzeath and Haywood Slate Formations. This suite can be seen at Trevose Head, Cataclews Point, St Saviour's Point and Rock Quarry.

Extensive tuffs with associated basic igneous intrusives are found in the South Hams district of South Devon where they are penecontemporaneous with the mid-Givetian to Frasnian limestones.

3.7.3.2 Samples

Samples of basic igneous intrusive rocks were taken from disused greenstone at quarries at Maryland (House) (MYD), Bow Bridge (BOW)and Pople's Bridge (IVY). Two samples of greenstone were collected from the beach at Ansty Cove (TQY), near Torquay, and are believed to have originated from the large doleritic intrusion at Black Head, less than a hundred metres south of Ansty Cove. Samples of tuff were taken form a disused quarry at Dorsley Barton (DBN). All of these sites are within the South Hams area of Devon and are henceforth referred to as the South Hams Group. The source of these samples is geographically is illustrated in Figure 13 (Section 3.2).

No samples or data from rocks of the Pentire Slate Formation or igneous rocks within the Trevone Succession have been taken or used as these outcrops are geographically remote from Mount's Bay (c.f. Section 3.3).

3.7.4 Barras Nose, Tintagel Volcanic and Trambley Cove Formations

This group of formations follows on from the Devonian to Carboniferous Transition Group and forms part of the complex 'nappe of the Culm Basin terrane' (Selwood et al. 1998). The Culm Basin is extensive throughout Devon and east Cornwall and includes the Barras Nose, Tintagel Volcanic and Tramby Cove Slate Formations. Barras Nose Formation comprises of sequences of shales, siltstones and thin sandstones, with occasional ash/thin lavas deposited in a low energy, anoxic basin deposited across the Tournaisian to Visean boundary. After the igneous activity that formed the Tintagel Volcanic Formation low energy deposition of black shales returned, producing the Trambley Cove Slate Formation.

3.7.4.1 Igneous activity

Intraplate alkali basalts, seen in exposure at Brent Tor and around Launceston, as well as at Tintagel make up the Tintagel Volcanic Formation. These rocks have undergone the highest grade of regional metamorphism (lower greenschist) seen within Devon and Cornwall (Sexton 1987).

3.7.4.2.. Samples

Two samples from large loose boulders found on Hanger Down (IVY), near Ivybridge are believed to represent a contact metamorphosed dolerite outcropping within an outlier of Culm Measures found on the south side of Dartmoor. These are included within the 'South Hams Group' of samples.

3.8 Summary

Basic igneous rocks and greenstones in particular, found in SW England can be recognised in terms of tectonic origin, petrology, geochemistry and post-depositional alteration effects. The tectonic environment in the Devonian and Carboniferous periods gave rise to local and geologically short lived transtensional regimes that produced varying quantities of tholeiitic to alkali basalts. Apart from the obducted ophiolite of the Lizard, the basalts survive as pillow lavas, thin, metre-sized, sills and dykes emplaced at shallow depths and some more substantial sills (or bosses?) emplaced at greater depths. Though predominantly fine to medium grained, some occasionally coarsely gabbroic rocks can be observed (e.g. Cudden Point). Subsequent movement (e.g. Roseland Breccia) and compression (e.g. Mylor Slate Formation) have made it difficult to locate the place and time of the igneous events thus preventing a detailed reconstruction of the geological history.

The relationship between the basaltic igneous rock type and tectonic regime is reflected in their location, with predominantly tholeiitic rocks found in the south and west of Cornwall and alkaline rocks to the north of Cornwall and east of Devon. It is believed that the alkali rocks formed on the edges of the basins and are associated with basin margins, possibly representing the early stages of rifting. The tholeiitic rocks are found within the tectonic basins (e.g. Mylor Slate Formation within the Gramscatho Basin). It is possible to differentiate between these igneous rocks using geochemical discrimination diagrams and potentially to within a single lithological unit using selected geochemical fingerprints such as Nb & Zr concentrations.

The geochemistry of unknown greenstone samples (i.e. Neolithic axes) can indicate the petrogenesis of the source rock using established discrimination methods based on major and trace element concentrations and ratios. This information, coupled with knowledge of where these regional geochemical characteristics are found can narrow down the geographical range in the search for the provenance of an unknown sample. Previous work has shown that there is the potential to geochemically characterise individual magmatic episodes within Cornwall and Devon and therefore, it is thought possible to be able to geochemically provenance an unknown sample to a single outcrop or exposure.

The geographical range of the twenty-one sites sampled as part of this work should provide a reasonable coverage of the variable igneous geochemistry likely to be found in SW

England. This is further enhanced by the amount of data previously collected and provided (Floyd pers. com.), representing over one hundred samples from twenty-three locales. The coverage and number of samples provides a large geochemical database that can be used to investigate the origin of unknown greenstone samples.

4 Petrography of greenstone axes and comparison with greenstone exposures in SW England

4.1 Introduction

In order to provide a basis from which to develop the viability of the non-destructive techniques used to characterise axe populations (c.f. Chapter 5 & 6) it is necessary to review existing work so that a continuity is provided between the established petrographic methodology and the new non-destructive methodologies. To achieve this, one hundred and forty-nine existing axe thin sections, held by The South Western Federation of Museums and Art Galleries at Taunton Castle Museum, have been examined and compared with new thin sections obtained from greenstone exposures in Cornwall (c.f. Chapter 3, Appendix 4 & 5.4). In part, this methodology of comparing thin sections mimics the procedure used by the IPC and others to allocate axes to petrological groups and subsequently to provenance the groups to a particular rock outcrop. The basis from which to develop the new discriminatory techniques involves establishing the mineralogical and textural differences of IPC Group I, Ia, III and IIIa axes and investigating the hypothesis that the axe material is similar to greenstones found within Mount's Bay (c.f. Section 2.5). It is emphasised that no new axe thin sections were made for this work as the thin section production process is partly destructive and is therefore contrary to the aims of this thesis. The early parts of this chapter (4) examine the existing axe thin sections and the later parts use graphical and quantitative methods to compare them with exposure thin sections.

4.2 Problems associated with the use of petrological thin sections in provenancing axes

Examination of petrological thin sections is an established method for assessing the mineralogical and textural properties of rock and stone implements (Fenton & Travis 1988, Cooney & Mandal 1997, Kerr 1942, Deer et al. 1992). These properties provide a petrographic fingerprint that can help with classification of the rock and the grouping together of samples with similar features. In this way the IPC has recognised thirty-nine petrographically different groups of stone axes, with the ones studied in this thesis introduced in Chapters 1 & 2. By matching axe thin sections with ones taken from rock exposures it is further possible to provenance axes to exposures, a practice which is a founding tenet behind the formation of the IPC (Keiller et al. 1941).

Petrographic analysis of axe thin sections has two main drawbacks. The first is that rocks from different geographical locations can have very similar petrography, so petrological microscopy may not be able to distinguish between them. This is especially pertinent to greenstones found in Devon and Cornwall: they may share primary mineralogical characteristics, and having been partially re-crystallised through low-grade metamorphic events, samples from geographically separate exposures can be difficult to tell apart. This fact and the petrological variability of individual greenstone exposures (Keiller et al. 1942) means that two greenstone samples may have come from two locales metres apart on the same exposure, or from two different exposures that are many kilometres apart. The second drawback is that the method used to extract axe material for the manufacture of thin sections is partly destructive, with a slice, or core, of material being taken from the valuable axe (c.f. Section 1.3). High quality cosmetic 'repairs' can make the damage difficult to see, but the majority of axes observed during this work showed marked visible evidence of slices having been taken. This may be as a result of the handling and cleaning of axes eroding the water-based paint used to colour the inert filler. Cosmetic problems are partly overcome by the relatively new coring approach (Fenton & Travis 1988) that minimises visible damage since the plug of material extracted is placed back into the cored hole, leaving a smaller visual scar. But, as witnessed during fieldwork, many museum curators remain against any form of destructive analysis, no matter how small the potential scar.

4.3 Résumé on the current provenance of axes examined and notes on terminology

4.3.1 Current provenance of IPC Group I, Ia, III & IIIa

Chapter 2, Section 2.5, summarises the provenance of Cornish IPC axe groups:

IPC Group I is believed to originate from an outcrop(s) between Penzance and Mousehole (Section 2.5.1)

IPC Group Ia is described as originating from Cornwall (Section 2.5.2)

IPC Group III is provenanced to a quarry near Perranuthnoe (SW534297) (Section 2.5.7)

IPC Group IIIa is described as originating from Cornwall (Section 2.5.8)

(Note that thin sections for IPC Groups I/Ia and I(near) were not available.)

4.3.2 ¨Note on terminology used to describe groups of axes

Throughout the examination of axe thin sections it became apparent that it was possible to recognise sub-groups of thin sections within the defined IPC groups on the basis of

mineralogical and textural similarities. In order to reduce confusion between IPC groups and sub-groups developed in this chapter the following nomenclature will be followed:

1. All IPC groups will be stated in full, with group numbers in Roman numerals, suffixed accordingly (e.g. IPC Group I, IPC Group Ia, IPC Group III, etc.).
2. All subgroups introduced in this thesis will be uniquely identified by abbreviating the host IPC group name and adding a numeric character to the Roman numeral representing the IPC group (e.g. GpI-7, GpIa-3. GpIII-4).

4.4 Examination of existing IPC Group I and Group Ia petrological thin sections

4.4.1 IPC petrological description of IPC Group I

IPC Group I is described by the IPC as:-

"Uralitised gabbro, epidiorite or greenstone in which the augite, sometimes slightly ophitic, occurs in colourless to pale brown plates which show no crystal outlines and exhibit a variable amount of alteration to fibrous green hornblende along cleavage cracks and outer edges. Occasionally, alteration from pyroxene to hornblende is complete. Feldspar, presumed albite, much altered and riddled with small needles of actinolite. Main accessory mineral is ilmenite which is often altered to leucoxene" (Keiller et al. 1941, Section 2.5.1).

4.4.2 Development of new sub-groups within IPC Group I

Since all of the one hundred and nineteen IPC Group I thin sections obtained for this part of the research had been previously examined and placed in IPC Group I by experienced petrologists it was anticipated that there would be little mineralogical variation between them. However, examination using a monocular polarising petrological microscope showed that it was possible to differentiate between some thin sections and recognise sub-groups within the main IPC group.

The criteria for establishing a sub-group is based on the petrographic distinctiveness of thin section texture and mineralogy. Initially, one thin section was selected at random and used as a reference for other thin sections to be compared against. As this process progressed, it became possible to delineate several distinctive and individually recognisable sub-groups within IPC Group I that each shared similar characteristics. After comparing every thin section with the reference, the recognition of distinctive characteristics led to the establishment of thirteen sub-groups, each of the thin sections were once more examined to confirm that the members of each sub-group shared similar petrographic characteristics.

The petrographic characteristics of the largest sub-group, GpI-1, are described in detail below, but only the main differences to this description are noted for the remaining twelve sub-groups. Plain polarised (ppl) and cross-polarised (xpl) photomicrographs in Section 4.3.4 are used to illustrate the mineralogy and micro-texture of the IPC Group I sub-groups (and the assigned scores given during the quantitative analysis exercise (c.f. Section 4.8)). Petrological descriptions of all axe thin sections can be found in Appendix 5. All one hundred and nineteen IPC Group I thin sections have been photographed in ppl and xpl and the photomicrographs subsequently digitised. These are provided, in digital form, on the five CD-ROMS accompanying this work, and the content list of all photomicrographs is contained in Appendix 6.

4.4.3 Sub-groups within IPC Group I

4.4.3.1 Sub-group GpI-1 (59/119 IPC Group I thin sections examined)

Sub-group GpI-1 comprises plentiful altered euhedral, occasionally partly ophitic clinopyroxenes (cpx), probably augite, with very pale brown to clear colour in plain polarised light (ppl) and first to mid-second order birefringence (blue, red & purple are the most frequent interference colours encountered, with an occasional bright lime green colours suggesting augite/diopside). Basal cpx sections show clear, approximately 90° cleavage intersections and show grey to white colour in cross polarised light (xpl). Most cpx crystals are approximately 1mm long, although it is common to find some cpx crystals to 2mm. Varying degrees of secondary alteration are seen across the sub-group where cpx is found replaced by fibrous to tabular grains of amphibole, probably tremolite-actinolite and hornblende, the latter recognised by the middle second order birefringence. Some larger grains of amphibole display a diamond lattice created by two cleavages intersecting at approximately 60°.

Chlorite is not obvious in many thin sections as it is difficult to positively identify in a fine-grained groundmass, with only very small patches of the thin section showing the distinctive anomalous Berlin blue colour, indicative of chlorite.

In general the primary feldspar is almost totally altered to a fine mica, probably sericite, and plentiful fine-grained actinolite, both within pseudomorphs of feldspar. Secondary alteration makes it hard to clearly see any type of feldspar twinning, hence identification of the type of feldspar is difficult. However, it is most likely to be plagioclase recognised in

xpl by the lath to tabular outlines seen with indistinct lamellar twinning picked out from the variably altered grey-black groundmass of very fine-grained sericite.

Actinolite needles and prisms to 0.1mm in length are common within the groundmass, although they are not present in every GpI-1 thin section. Cloudy masses of very fine grains with high relief and indeterminate birefringence seen within the feldspar alteration are taken as some form of fine granular epidote. However, the presence of ilmenite, often close to the cloudy masses indicates that these fine-grained, high relief areas could also be granular sphene (note the term 'sphene' is used in preference to 'titanite' throughout this thesis). Obvious grains of epidote are very rare in GpI-1 thin sections. Apatite and biotite mica are not common in this subgroup.

Ilmenite is the most common opaque mineral, present as 0.5-2mm sized angular masses usually showing polygonal outlines with 60° internal angles between crystal faces and is also found as elongate grains, with several grains stacked to form a ladder-like appearance. Ilmenite grains usually appear corroded (i.e. have irregular sides, often bulbous with slightly transparent patches) and are often partially altered to sphene/epidote or leucoxene, with the latter more common than the former. (Note that axe thin sections are not polished so reflected light petrography could not be used to *positively* identify opaque grains, identification is primarily based on grain shape and it is noted that pyrite and magnetite can also appear as psuedohexagonal and triangular shaped grains.)

Be10/241	Co218/855	Co52/561	Do127/1660	Gl2/78	Wi112/395	Wi306/1110
Be8/223	Co29/507	Co66/593	Do18/103	Gl42/1156	Wi128/413	Wi316/1161
Co100/667	Co30/508	Co70/601	Do24/113	Gl44/1193	Wi129/414	Wi369/1434
Co148/734	Co310/1478	De15/209	Do26/115	Gl79/1464	Wi200/649	Wi379/1459
Co151/737	Co356/1595	De164/1860	Do27/116	So11/79	Wi206/717	Wi85/303
Co166/761	Co38/516	De31/670	Do56/555	So21/232	Wi213/856	
Co179/782	Co39/517	De37/766	Do70/950	So39/899	W220/874	
Co182/785	Co409/1765	Do112/1454	Do91/1198	So58/1105	Wi239/947	
Co208/824	Co41/519	Do123/1648	Do96/1285	So60/1143	Wi29/36	

Table 3 List of sub-group GpI-1 axes (59/119 IPC Group I thin sections examined)

Table 3, above, lists the fifty-nine axes assigned to sub-group GpI-1 on the basis that their thin sections all share similar petrography. Figure 24 shows ppl and xpl images of axe thin section Be10/241. This thin section illustrates the petrology and texture of a typical GpI-1 thin section described above.

4.4.3.2 Sub-group GpI-2 (13/119 IPC Group I thin sections examined)

Members of GpI-2 are **similar to GpI-1**, with the main difference that large, >2mm, partly ophitic cpx are present in addition to smaller non-ophitic cpx as seen in GpI-1. Secondary biotite is seen as small brown patches, with the quantity increasing in conjunction with the amount of alteration. Clear, small (<0.1mm) grains of epidote are seen in ppl. No acicular actinolite is found in GpI-2. Feldspar and pyroxene alteration is similar to that found in GpI-1, as is the lack of apatite and the rare presence of chlorite.

Co136/718	Co154/740	Co209/825	Co215/846	Co31/509	Co387/1712	Co401/1737
De166/1862	Do147/1763	Do2/50	Wi101/384	Wi34/76	Co398/1734	

Table 4 List of sub-group GpI-2 axes (13/119 IPC Group I thin sections examined)

Table 4 lists the thirteen axes assigned to GpI-2 and Figure 25 shows ppl and xpl images of GpI-2 axe thin section Co154/740. The images show a heavily altered, partly ophitic clinopyroxene grain >2mm long (top-centre of each image) illustrative of those commonly found in this sub-group.

4.4.3.3 Sub-group GpI-3 (6/119 IPC Group I thin sections examined)

GpI-3 is **similar to GpI-1**, but with larger opaque grains that are almost totally altered to a very fine-grained mineral, probably sphene. In two thin sections (Co69/600 & 69a/600) the alteration of the opaque grain has revealed distinct polygonal skeletons, with rhombic and triangular partings indicating the host grain was probably ilmenite. Pyroxenes are altered to a fibrous amphibole (uralite) around their rims.

Co69/600	Co281/1344	Co69a/600	De146/1698	De49/820	Do15/94

Table 5 List of sub-group GpI-3 axes (6/119 IPC Group I thin sections examined)

Table 5 lists the six axes assigned to GpI-3 and Figure 26 shows ppl and xpl images of GpI-3 axe thin section Co281/1344. The images illustrate the large opaque masses associated with this sub-group.

4.4.3.4 Sub-group GpI-4 (16/119 Group I thin sections examined)

The notable feature of GpI-4 is that the euhedral, 1mm sized, cpx grains have first to low second order birefringence, with extinction angles approximately 45° and 25°, suggesting it is probably low Ca augite and/or pigeonite. Secondary, amphibolitic alteration of the cpx is similarly pale coloured, suggesting tremolite and not ferroactinolite is present, although in a few GpI-4 thin sections second order birefringence is seen in some amphibole grains. In general there is more fibrous amphibole present in this sub-group

than GpI-1, suggesting a higher degree of alteration. The groundmass has many needles and small laths of actinolite and sericite patches with rare apatite. In all other respects this sub-group **is similar to GpI-1.**

Be16/962	Co180/783	Co325/1534	Do14/93	Wi202/652	Wi44/140
Be49/1328	Co181/784	Co326/1535	So34/587	Wi209/837	
Co16/245	Co322/1531	De59/920	So98/1362	Wi36/87	

Table 6 List of sub-group GpI-4 axes (16/119 IPC Group I thin sections examined)

Table 6 lists the sixteen axes assigned to GpI-4 and Figure 27 shows ppl and xpl images of GpI-4 axe thin section Be49/1328. The images illustrate the fibrous amphibolite fringes surrounding altered non-ophitic clinopyroxenes.

4.4.3.5 Sub-group GpI-5 (2/119 IPC Group I thin sections examined)

Wi434/1873 and Wi439/1878 appear **'fresher' than GpI-1** although with the same primary cpx-feldspar mineralogy. Plagioclase feldspar clearly shows lamellar twinning, which is only partly obscured by slight alteration. Partially altered cpx crystals are consistently >2mm, non-ophitic with embayed feldspar laths. Secondary amphibole is common, as replacement of the pyroxenes and as discrete acicular to bladed crystals growing across the feldspar. A small amount of apatite is clearly visible. Fine-grained brown, secondary, biotite is present along the edges of the feldspar.

Figure 28 shows ppl and xpl images of GpI-5 axe thin section Wi434/1873. The images reflect the less altered nature of both the axe thin sections forming this sub-group.

4.4.3.6 Sub-group GpI-6 (13/119 IPC Group I thin sections examined)

Distinct bright (in xpl) amphibole, possibly hornblende, has almost totally replaced the cpx in GpI-6 thin sections. Feldspar laths, up to 3mm long, are recognised in the groundmass, along with minor quantities of fine-grained quartz. Apatite is present in all GpI-6 thin sections. Generally GpI-6 appears to have undergone **a higher degree of metamorphic alteration than GpI-1,** but had the same original mineralogy.

Co110/681	Co305/1446	Co318/1527	Co386/1692	Co43/521	Do131/1678	Gl85/1470
So24/495	So25/541	Wi189/549	Wi49/172b	Wi74/291	Gl103/1610	

Table 7 List of sub-group GpI-6 axes (13/119 IPC Group I thin sections examined)

Table 7 lists the thirteen axes assigned to GpI-6 and Figure 29 shows ppl and xpl images of GpI-6 axe thin section Co110/681, where abundant amphibole is clearly seen.

4.4.3.7 Sub- group GpI-7 (3/119 IPC Group I thin sections examined)

The three members of this subgroup: Co64/588, Wi244/966 and Wi49/172A are markedly more cloudy in appearance than GpI-1 and lacking fine-grained acicular actinolite. Relict small non-ophitic and larger ophitic pyroxenes are visibly altered to a fine feathery almost granular secondary amphibole. Apatite is clearly present as are small amounts of secondary biotite. GpI-7 has a **similar primary mineralogy to GpI-1** but has undergone slightly different alteration.

Figure 30 shows ppl and xpl images of GpI-7 axe thin section Wi49/172A. The images illustrate the fine relict clinopyroxenes and general cloudy appearance of the sub-group thin sections.

4.4.3.8 Sub-group GpI-8 (2/119 IPC Group I thin sections examined)

Co358/1627 and Co363/1632 have bright amphibole pseudomorphs after cpx dominating the thin section. No feldspar is seen, either as discrete feldspar or lath-like shapes in the groundmass. Fibrous tremolite-actinolite has a distinct wavy appearance, and although there is no preferred alignment of grains, the fibrous grains pick out a possible shear fabric. Fine, irregular opaque grains are scattered throughout both thin sections. No biotite is seen and epidote is only present as cloudy masses of fine grains. These two thin sections contain more fibrous amphibole, with brighter birefringence than GpI-1, but probably had **similar original mineralogy to GpI-1.**

Figure 31 shows ppl and xpl images of GpI-8 axe thin section Co358/1627. The images illustrate the possibility of a shear fabric within the rock that is picked out by fibrous amphibole grains.

4.4.3.9 Sub-group GpI-9 (1/119 IPC Group I thin sections examined)

Thin section Co157/751 is different to GpI-1 in that the feldspar grains are less altered than the cpx grains and it has both ortho- and clinopyroxene present. In some places secondary, fibrous amphibole has completely replaced primary pyroxene. No twinning is seen in the feldspar. The range of pyroxene textures, from partly to totally replaced and the presence of both pyroxenes makes this thin section **different to any IPC Group I** thin section examined.

Figure 32 shows ppl and xpl images of the GpI-9 axe thin section Co157/751. A large orthopyroxene grain can be seen in the top-left quadrant of each images along with a large non-ophitic clinopyroxene grain in the bottom right quadrant.

4.4.3.10 Sub-group GpI-10 (1/119 IPC Group I thin sections examined)

Thin section Wi364/1418 is the sole member of this group and is **similar to GpI-1** in that it contains primary pyroxene and feldspar, the latter of which has been completely altered. It is unique in the collection, having small clusters of clinopyroxene grains in addition to larger, ophitic grains.

Figure 33 shows ppl and xpl images of the GpI-10 axe thin section Wi364/1418 which illustrate the small cluster of pyroxene grains that typifies this thin section.

4.4.3.11 Sub-group GpI-11 (1/119 IPC Group I thin sections examined)

Wi440/1879 has altered ophitic pyroxene up to 2mm across which is surrounded by altered, but recognisable feldspar and free quartz, the latter with rare granophyric texture. Brown, possibly primary, amphibole is seen. The secondary alteration of the cpx is predominantly to a very fine brown fibrous mineral (amphibole?), within the bounds of the original pyroxene grain. All feldspar present has been partly altered to sericite and epidote. Some chlorite can be seen as small Berlin blue patches within the feldspar alteration. The style of alteration of the pyroxenes, within and not across the crystal boundary **is unique and not seen in any other of the thin sections examined.**

Figure 34 shows ppl and xpl images of the GpI-11 axe thin section Wi440/1879. Distinct laths of feldspar and small quartz grains can be seen towards the centre of both images.

4.4.3.12 Sub-group GpI-12 (1/119 IPC Group I thin sections examined)

Thin section Do146/1762 is dominated by platy chlorite with deep brown/opaque birefringence not seen in any other of the IPC Group I thin sections. Plentiful small rhombs of actinolite penetrate the platy chlorite fabric. No pyroxene is visible and all feldspar is heavily altered but still recognisable. Small amounts of stressed quartz and apatite are present. It is **unlike any other IPC Group I** thin section examined.

Figure 35 shows ppl and xpl images of the GpI-12 axe thin section Do146/1762. The unique combination of actinolite rhombs and platy chlorite is clearly seen in the images.

4.4.3.13 Sub-group GpI-13 (1/119 IPC Group I thin sections examined)

Thin section CoGWA3 is petrographically distinct from all other thin sections assigned to IPC Group I by having large, 2mm, almost asbestiform aggregates of tremolite, probably after feldspar, often surrounding chlorite (penninite – Mg rich chlorite, typified by the anomalous Berlin blue colour in xpl). Patches of medium to high relief, brown granular grains (seen in ppl) are most probably biotite, whilst other, clearer high relief patches, show mid-second order interference colours of, probably, amphibole replacing pyroxene. In the latter case the amphibole is not fibrous/acicular, but granular. It is **unlike other IPC Group I** thin section examined.

Figure 36 shows ppl and xpl images of the GpI-13 axe thin section CoGWA3 where the atypical large asbestiform texture of tremolite-actinolite is clearly seen dominating the centre of both images.

4.4.4 IPC Group I sub-group microphotographs

The following 13 pages contain photomicrographs of typical (or the only) axe thin sections of the 13 IPC Group I sub-groups. These illustrations in ppl and xpl are taken from the CD-ROM store of digital images accompanying this work (Appendix 6 and associated CD-ROMs). The 'scores' noted at the bottom of each figure are part of the quantitative analysis procedure, which is explained and developed in Section 4.8.

Sub-group GpI-1
Be10/241

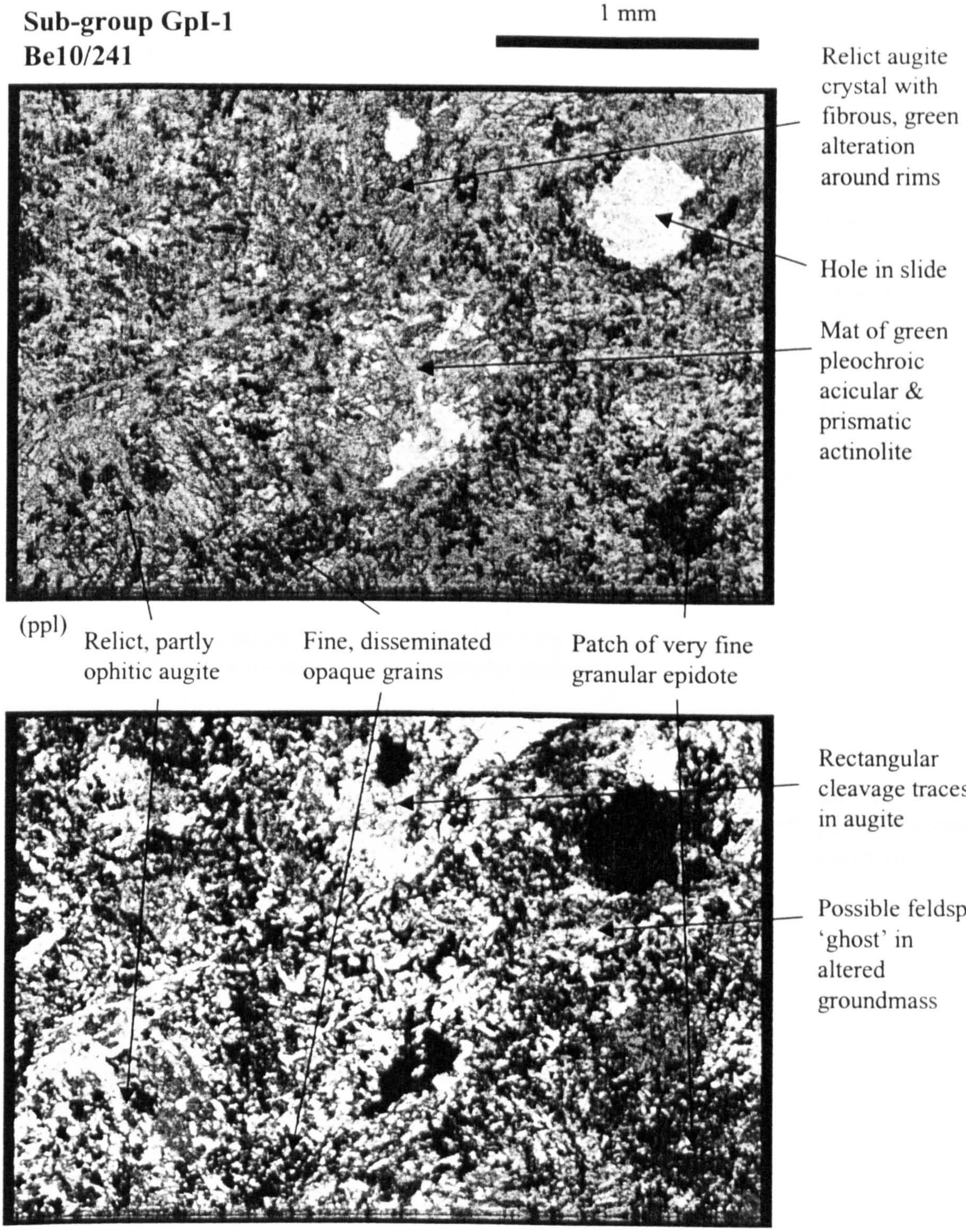

Score: Col:4, Size:7, Px:5, Fsp:8, Mica:2, Amp:2, Epi:1, Opa:7, Apa:0

Figure 24 Photomicrograph of IPC Group I – sub-group GpI-1 axe Be10/241

Sub-group GPI-2
Co154/740

1 mm

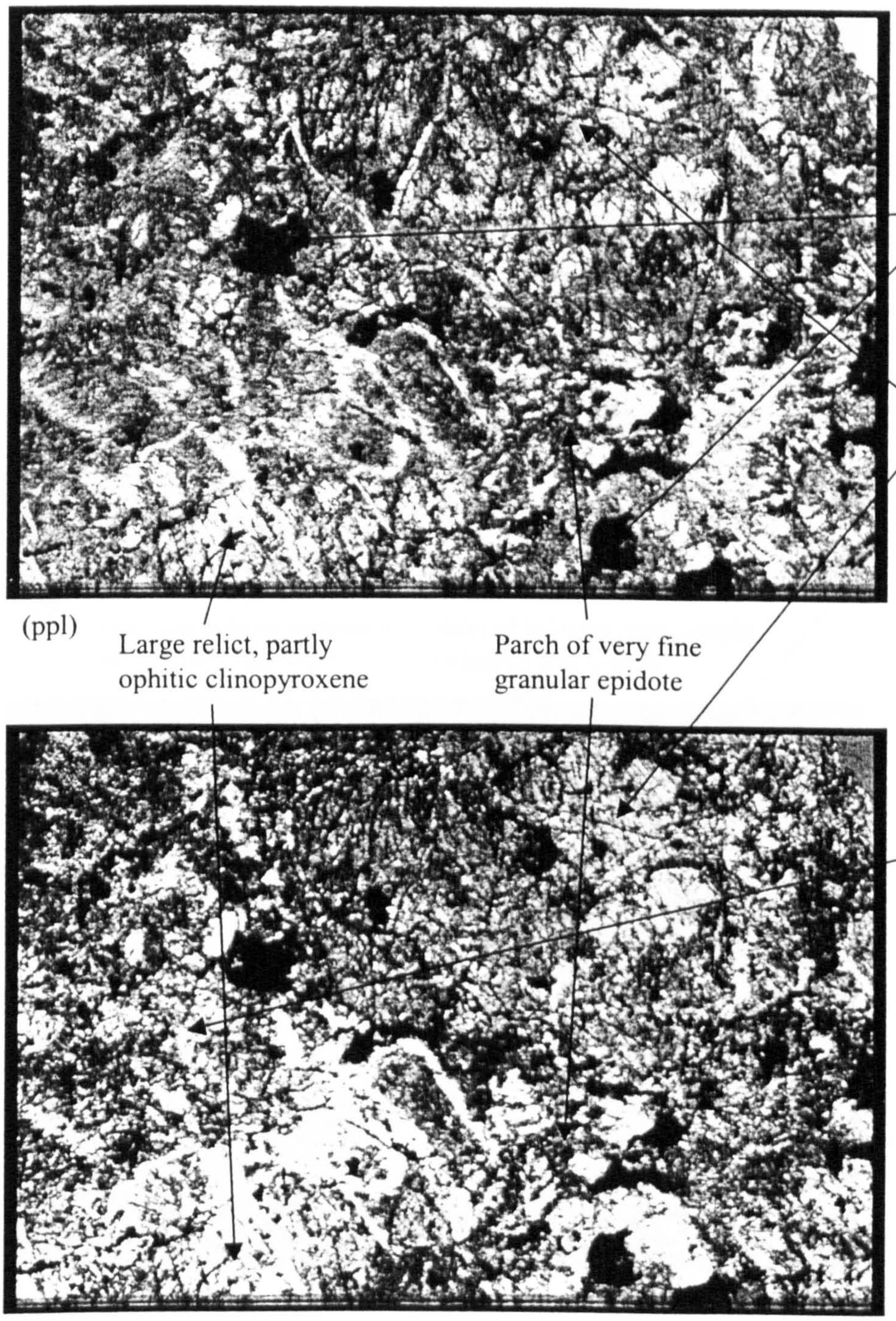

Score: Col:5, Size:7, Px:6, Fsp:9, Mica:2, Amp:2, Epi:1, Opa:7, Apa:0

Figure 25 Photomicrograph of IPC Group I – sub-group GpI-2 axe Co154/740

Sub-group GPI-3
Co281/1344

1 mm

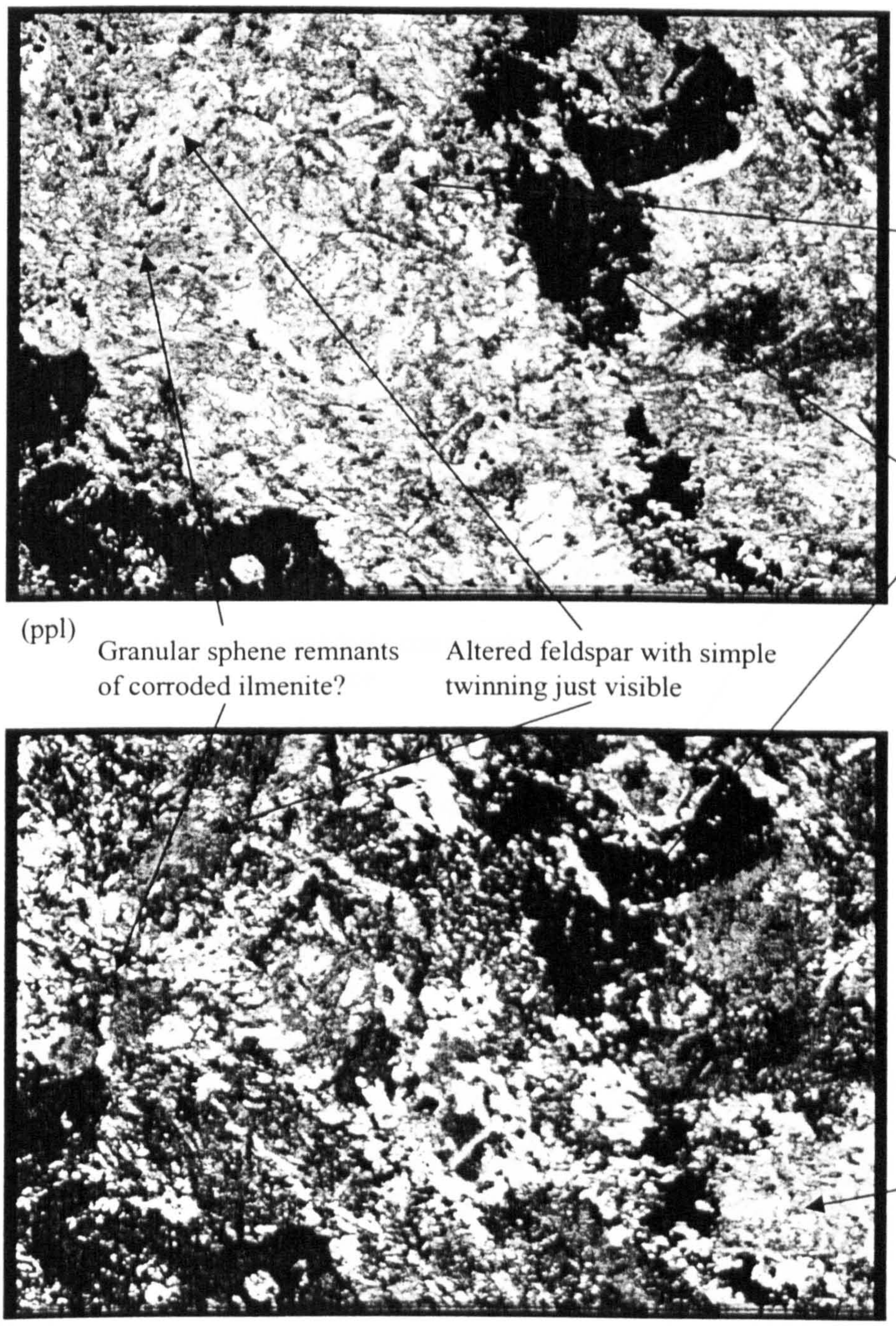

Score: Col:5, Size:7, Px:6, Fsp:7, Mica:2, Amp:2, Epi:1, Opa:2, Apa:0.

Figure 26 Photomicrograph of IPC Group I – sub-group GpI-3 axe Co281/1344

Sub-group GPI-4
Be49/1328

1 mm

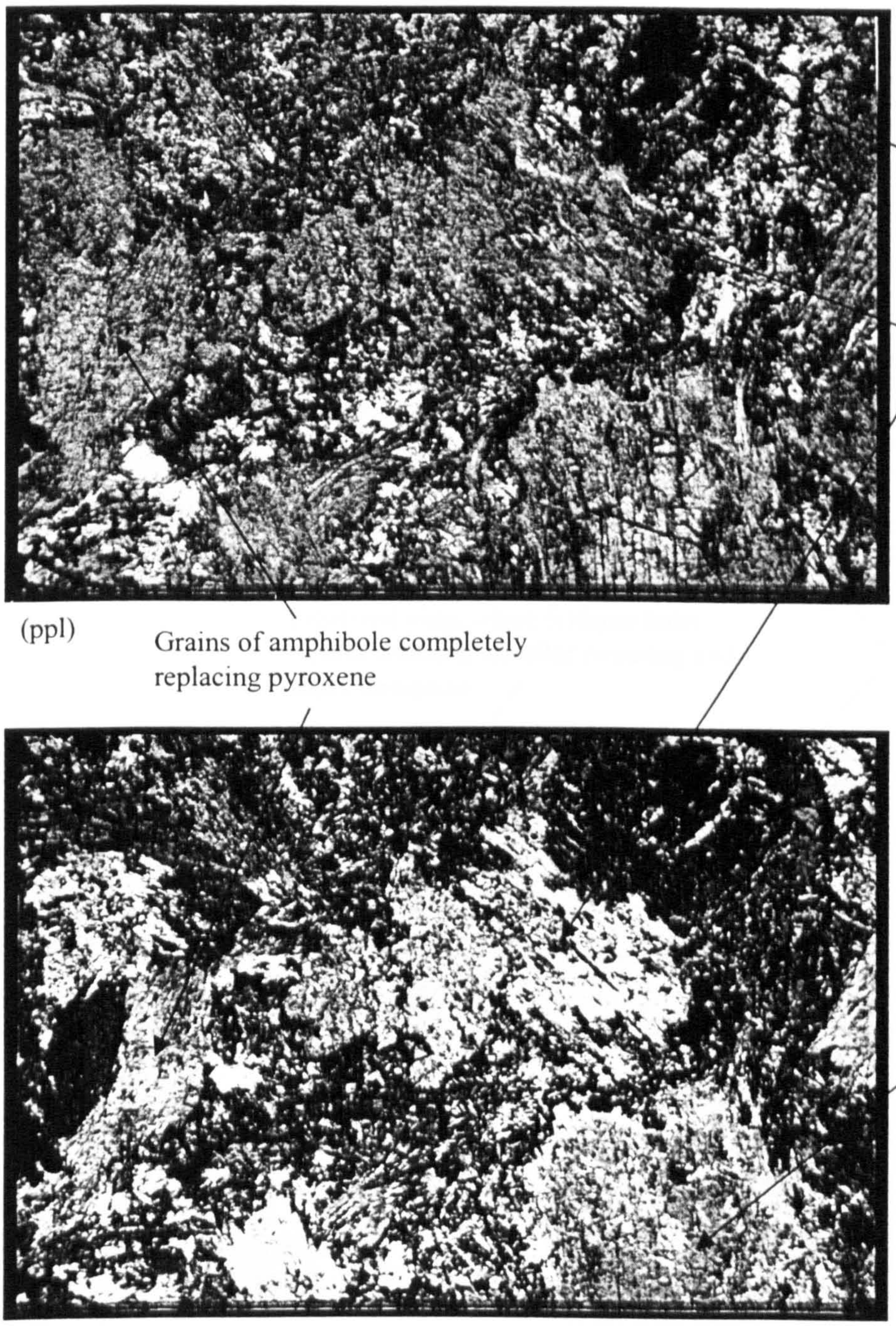

Score: Col:5, Size:7, Px:8, Fsp:7, Mica:2, Amp:2, Epi:1, Opa:7, Apa:0

Figure 27 Photomicrograph of IPC Group I – sub-group GpI-4 axe Be49/1328

Sub-group GPI-5
Wi434/1873

1 mm

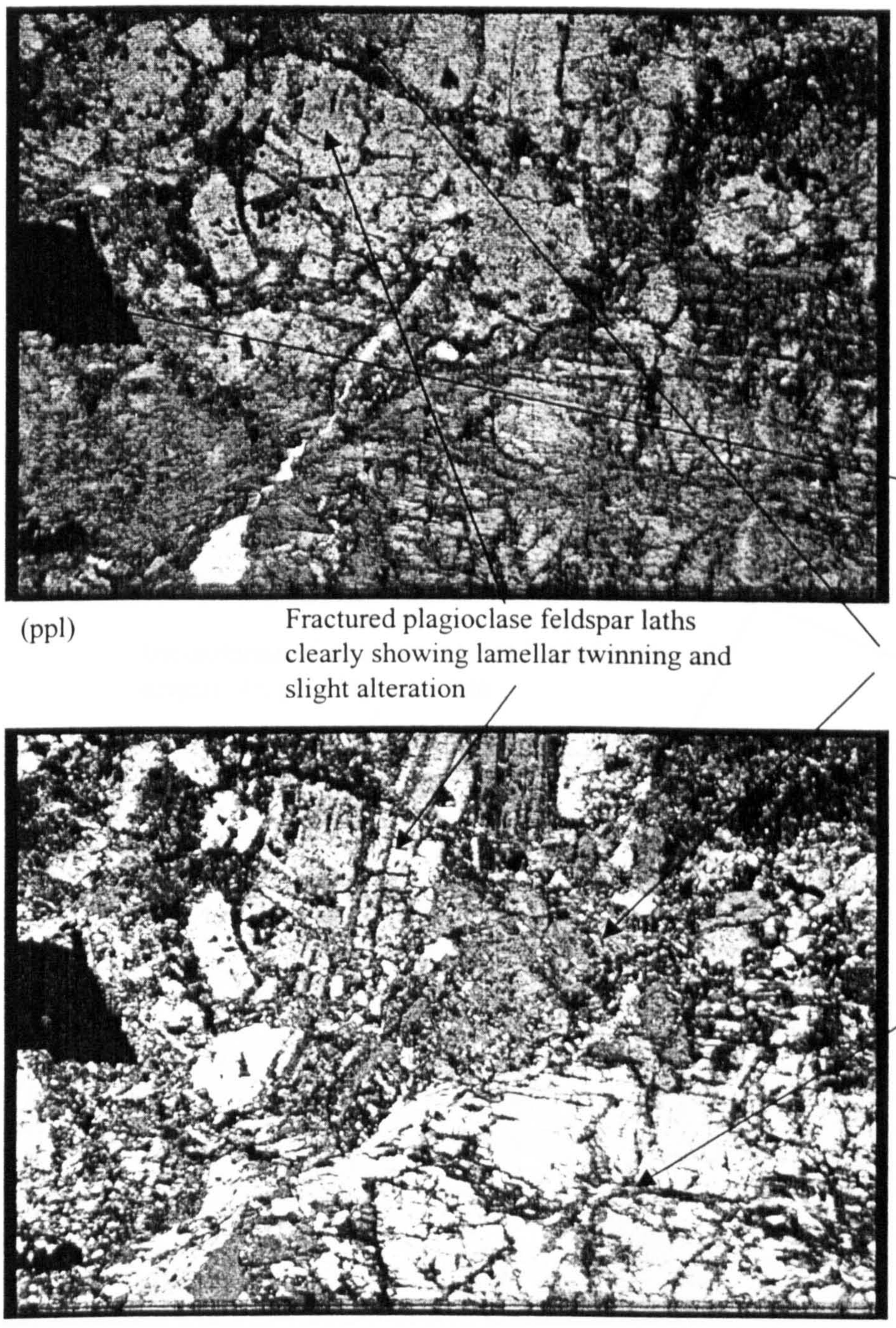

(ppl)

Typical angular opaque grain

Fine grained masses between plagioclase contain secondary biotite

Fractured plagioclase feldspar laths clearly showing lamellar twinning and slight alteration

Large, non-ophitic clinopyroxene, partially altered to amphibole

(xpl)

Score: Col:5, Size:8, Px:4, Fsp:5, Mica:2, Amp:2, Epi:1, Opa:5, Apa:1.

Figure 28 Photomicrograph of IPC Group I – sub-group GpI-5 axe Wi434/1873

Sub-group GPI-6
Co110/681

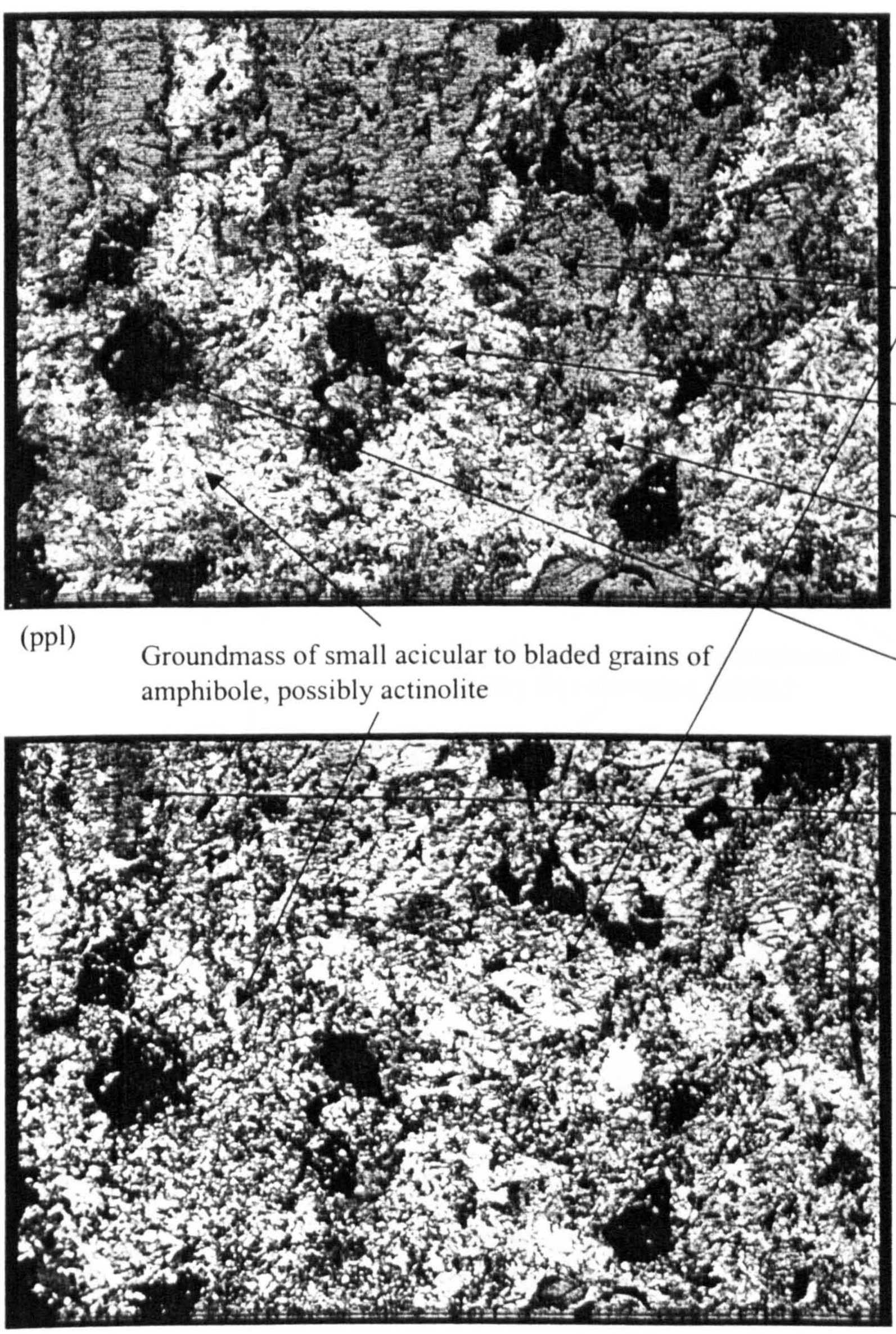

Score: Col:5, Size:6, Px:9, Fsp:10, Mica:2, Amp:2, Epi:2, Opa:8, Apa:1.

Figure 29 Photomicrograph of IPC Group 1 – sub-group Gpl-6 axe Co110/681

Sub-group GPI-7
Wi49/172A

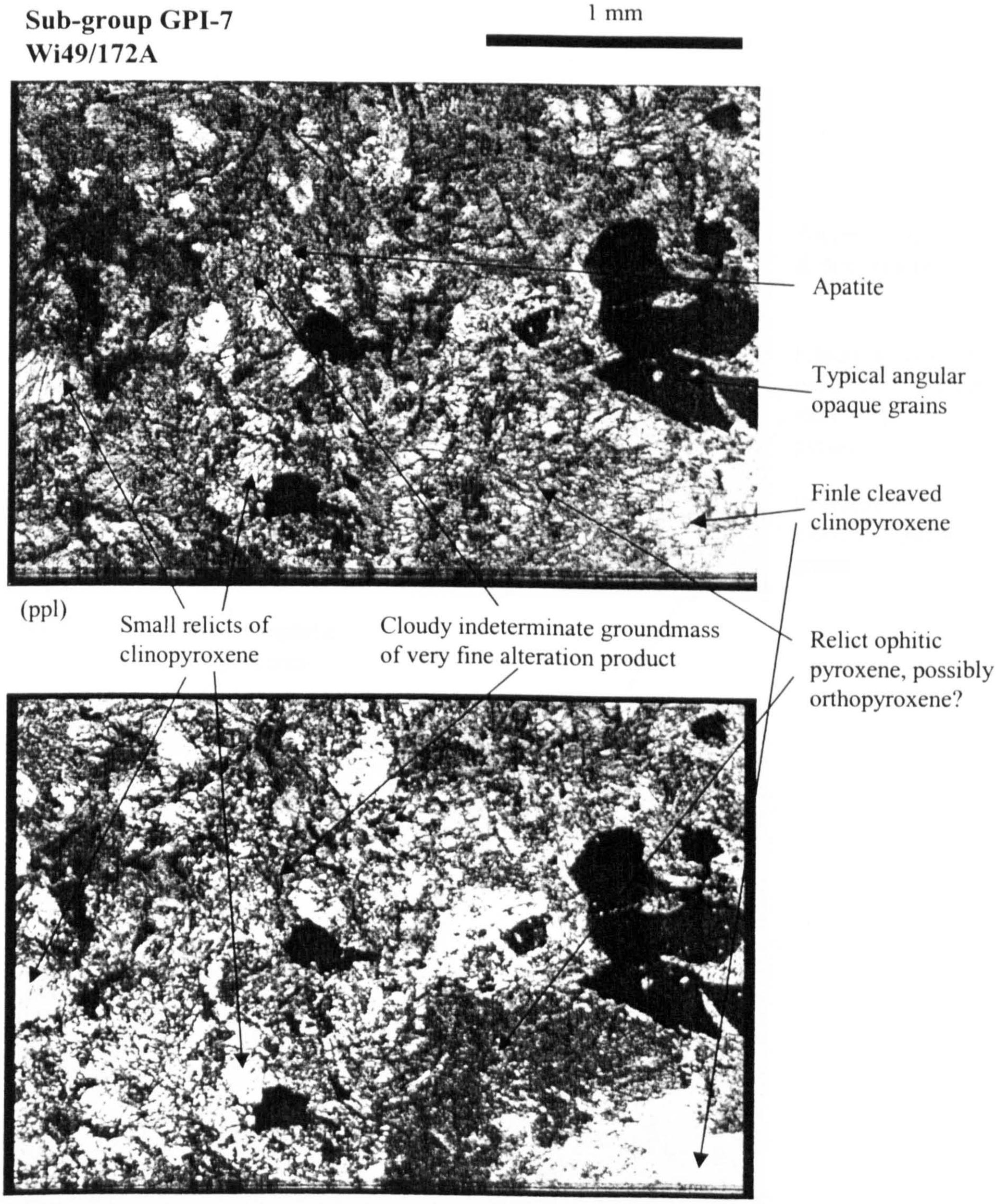

Score: Col:6, Size:4, Px:7, Fsp:9, Mica:2, Amp:2, Epi:1, Opa:4, Apa:1

Figure 30 Photomicrograph of IPC Group I – sub-group GpI-7 axe Wi49/172A

Sub-group GPI-8
Co358/1627

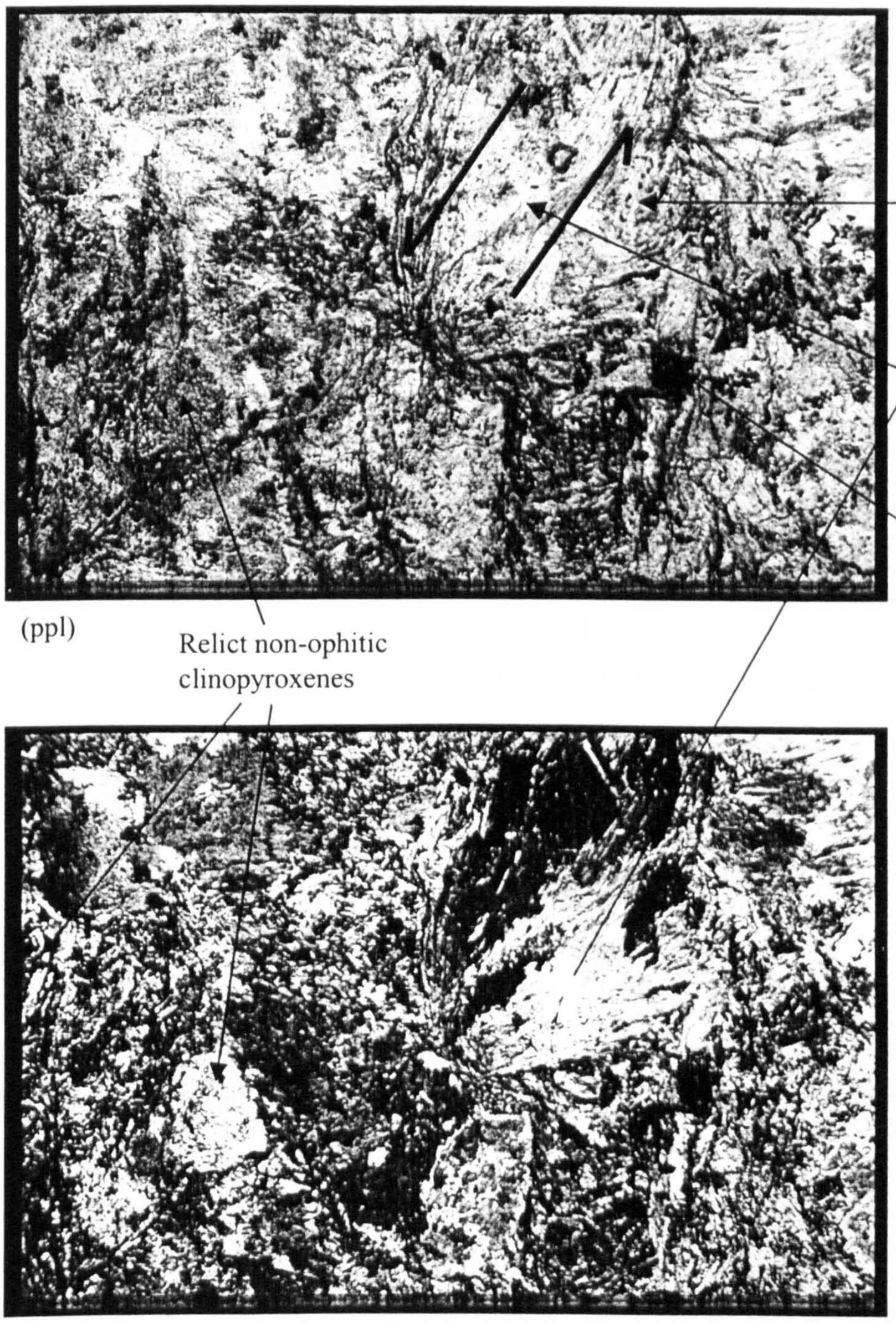

Score: Col:3, Size:7, Px:9, Fsp:10, Mica:2, Amp:2, Epi:1, Opa:8, Apa:0

Figure 31 Photomicrograph of IPC Group I – sub-group GpI-8 axe Co358/1627

Sub-group GPI-9
Co157/751

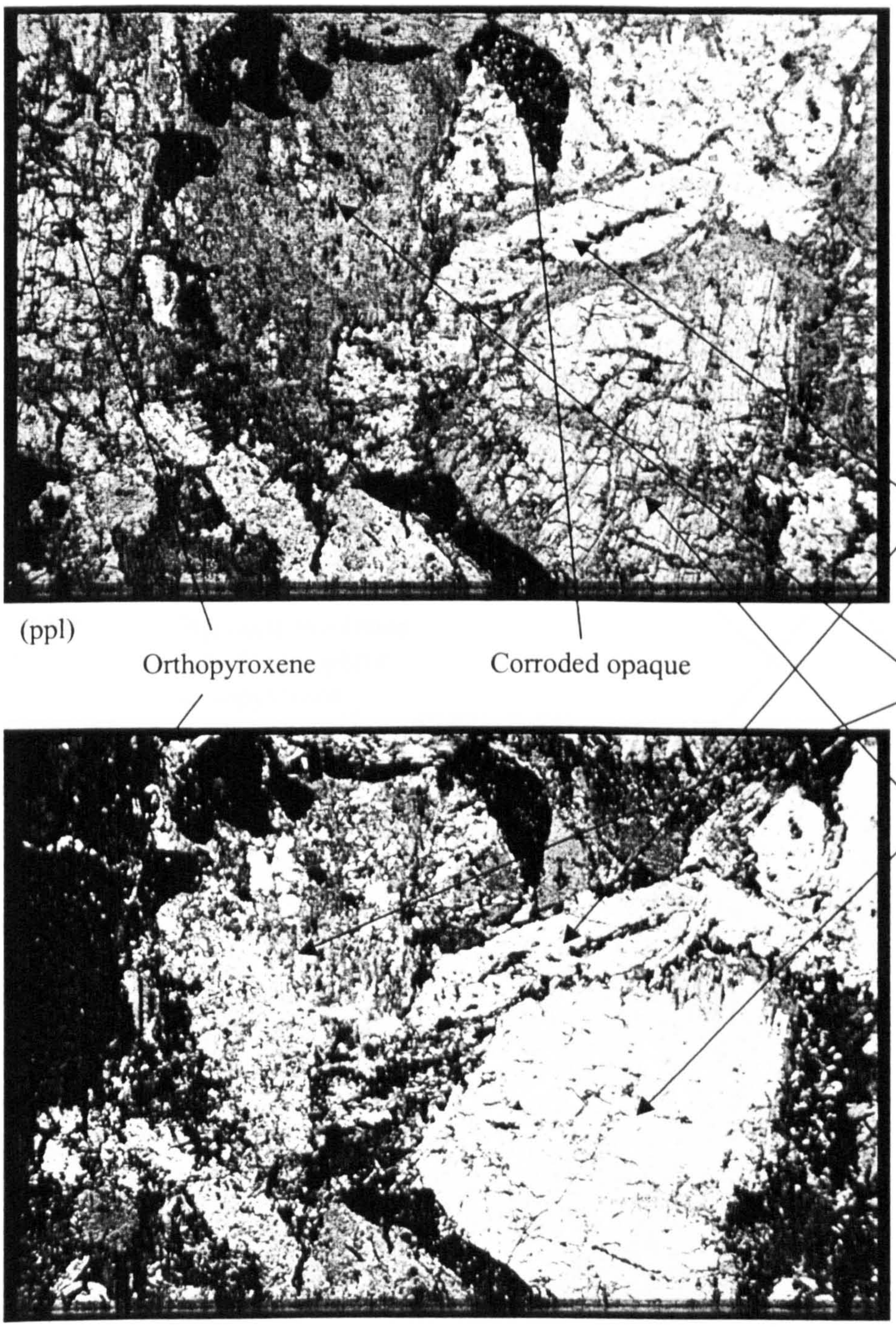

Score: Col:6, Size:8, Px:8, Fsp:5, Mica:2, Amp:2, Epi:2, Opa:3, Apa:0

Figure 32 Photomicrograph of IPC Group I – sub-group GpI-9 axe Co157/751

Sub-group GPI-10
Wi364/1418

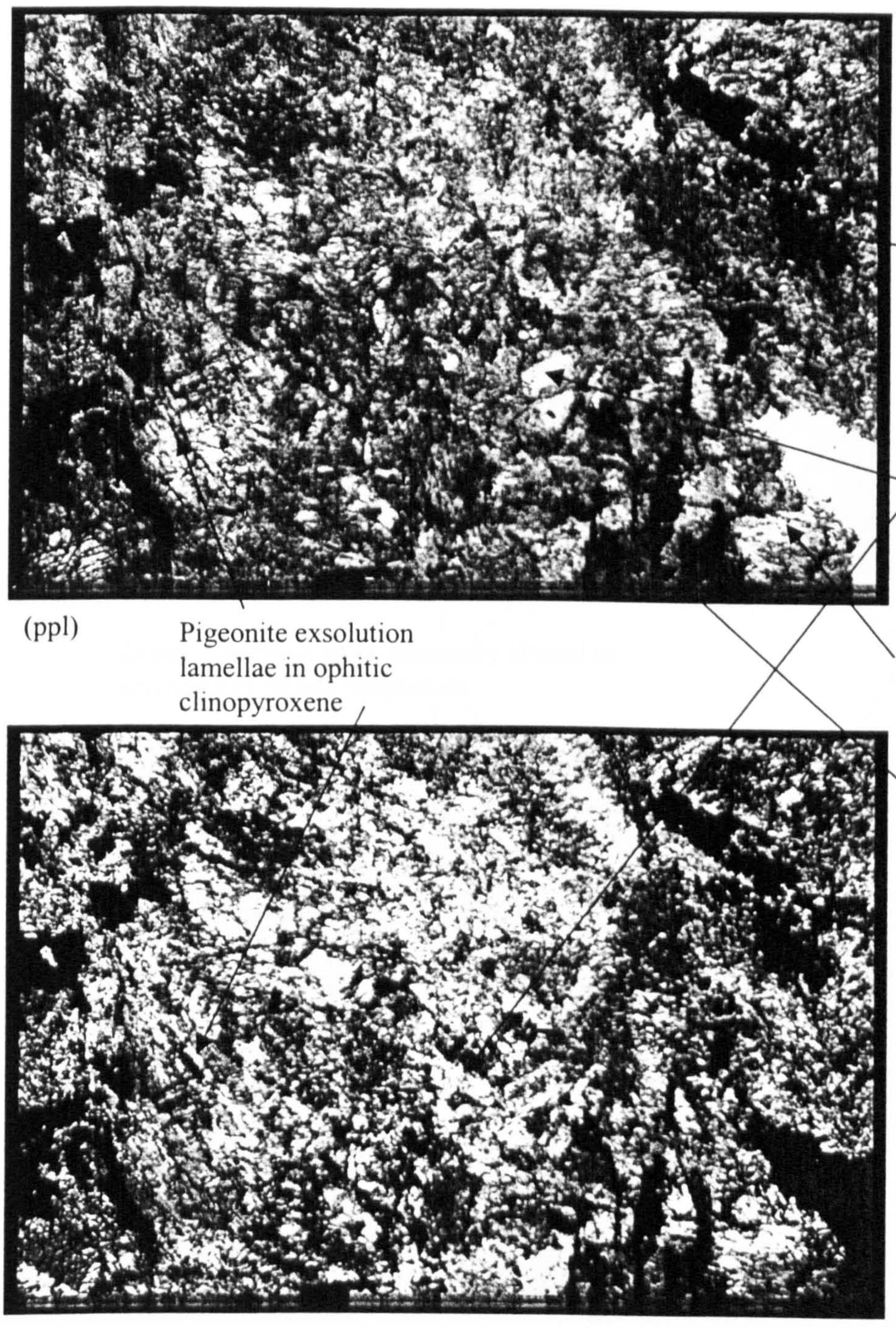

Score: Col:6, Size:4, Px:5, Fsp:10, Mica:2, Amp:2, Epi:1, Opa:8, Apa:0

Figure 33 Photomicrograph of IPC Group I – sub-group Gpl-10 axe Wi364/1418

Sub-group GPI-11
Wi440/1879

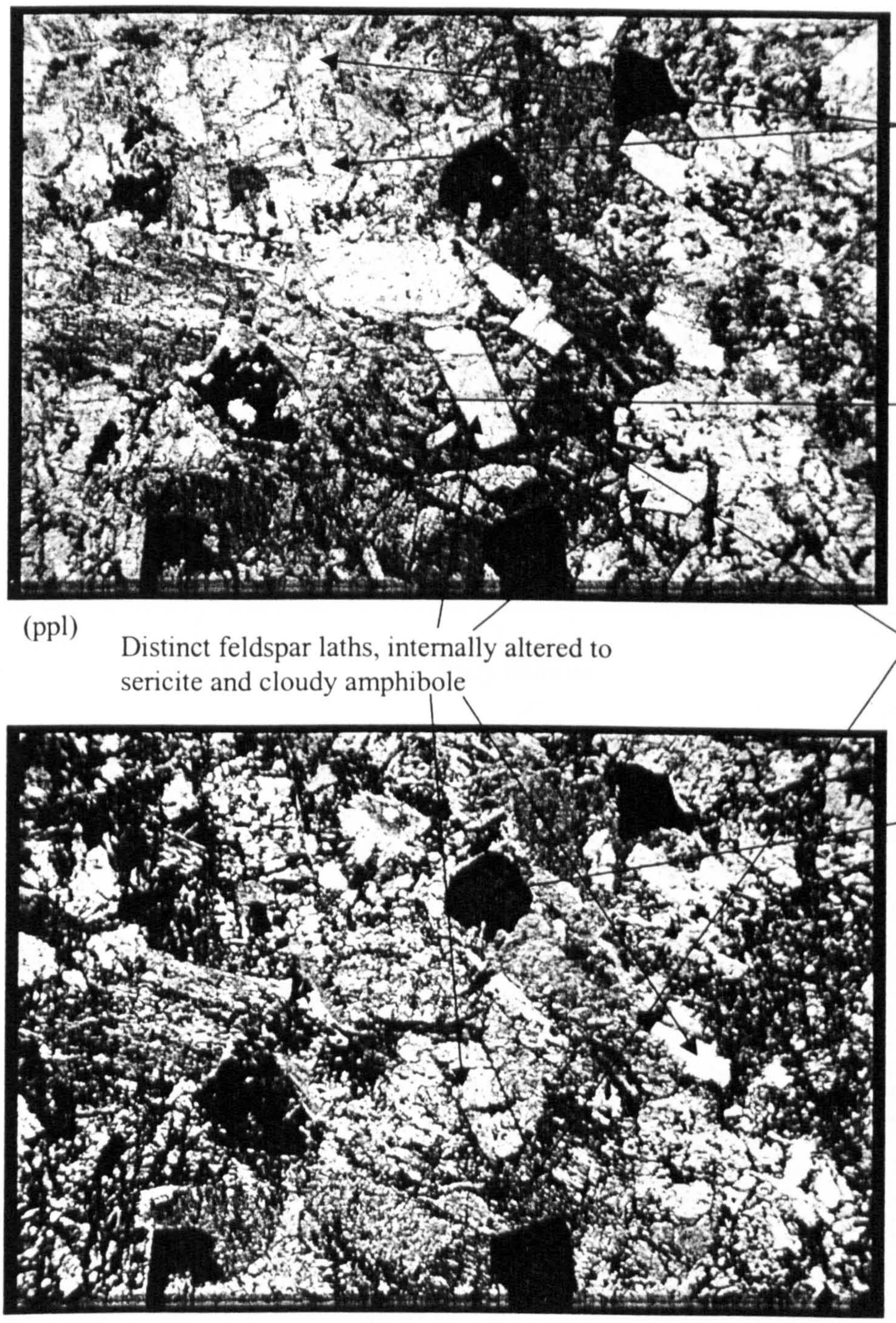

Score: Col:3, Size:5, Px:7, Fsp:6, Mica:2, Amp:2, Epi:2, Opa:4, Apa:0

Figure 34 Photomicrograph of IPC Group I – sub-group GpI-11 axe Wi440/1879

Sub-group GPI-12
Do146/1762

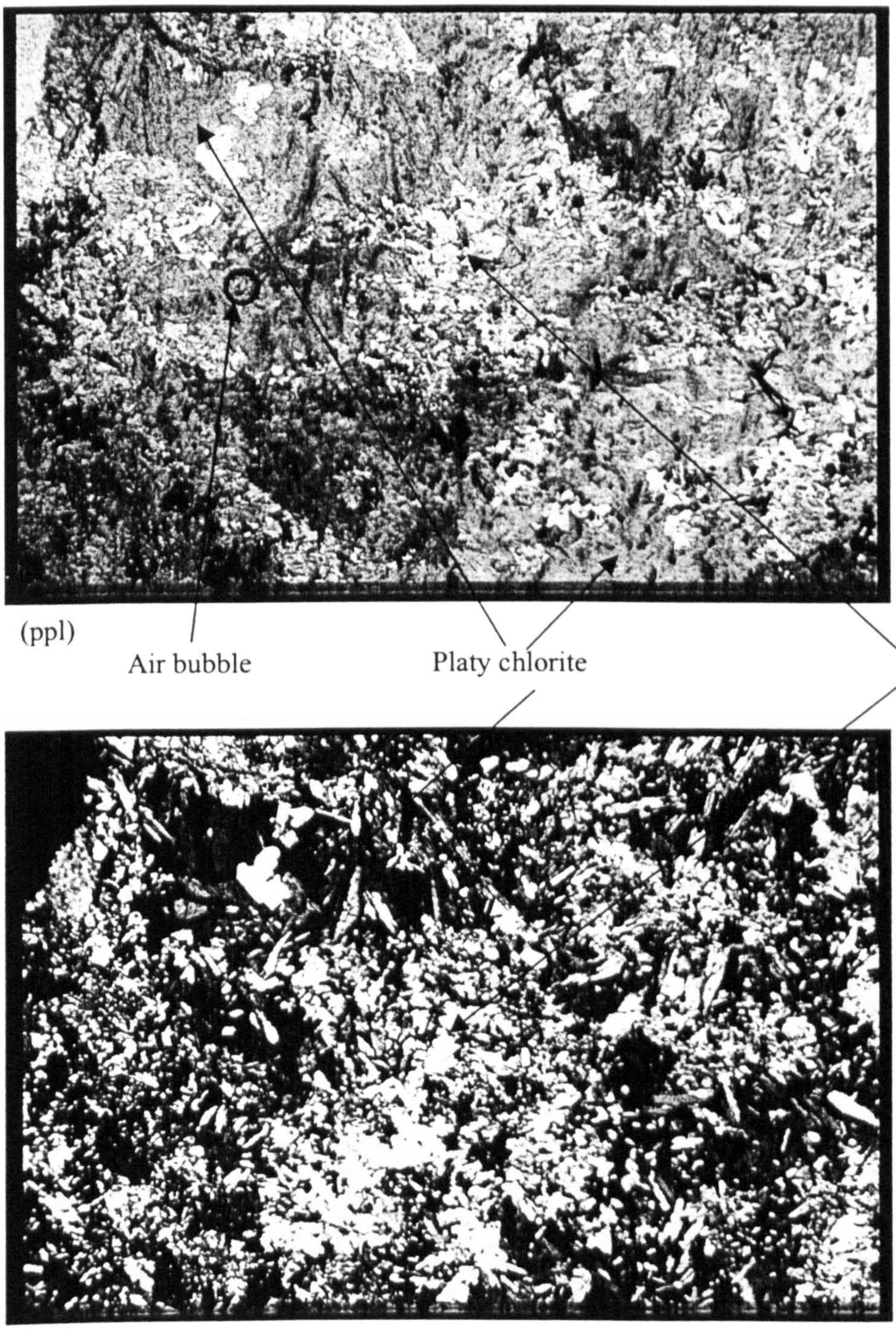

Score: Col:5, Size:4, Px:10, Fsp:7, Mica:2, Amp:2, Epi:2, Opa:8, Apa:1

Figure 35 Photomicrograph of IPC Group I – sub-group GpI-12 axe Do146/1762

Sub-group GpI-13
GWA3

(ppl)

(xpl)

Score: Col:3, Size:5, Px:9, Fsp:10, Mica:2, Amp:2, Epi:1, Opa:4, Apa:0.

Figure 36 Photomicrograph of IPC Group I – sub-group GpI-13 axe CoGWA3

4.4.5 IPC petrological description of IPC Group Ia

Stone & Wallis (1951) introduced Group Ia as:

"Microscopically, the augite is not quite completely altered to hornblende, and the feldspars are not so extensively riddled with small needles of hornblende. The hornblende often occurs in small blades showing somewhat parallel arrangement. In other respects sections are very similar in character to the well known Group I, though nothing like so homogeneous." (Stone & Wallis 1951, Section 2.5.2)

4.4.6 Sub-groups within IPC Group Ia

Seventeen Group Ia thin sections have been examined and, following the process described for the development of IPC Group I sub-groups, they have been divided into six petrographically recognisable sub-groups. Descriptions for all seventeen thin sections can be found in Appendix 5.2 and Appendix 6 identifies the location of associated digital photomicrograph images contained in the accompanying CD ROMs.

4.4.6.1 Sub-group GpIa-1 (5/17 IPC Group Ia thin sections examined)

These five IPC Group Ia thin sections form the first sub-group recognised and are therefore designated GpIa-1: Co145/731, Co152/738, Do103/1359, So142/1777and Wi188/543. In all respects **GpIa-1 thin sections are petrographically similar to GpI-1,** hence are unlike Stone & Wallis's description for IPC Group Ia (see above).

Figure 37 shows ppl and xpl images of the GpIa-1 axe thin section Co152/738. The texture is clearer than that seen in Figure 24 but contains the same, partially altered cpx and heavily altered plagioclase feldspar mineralogy typical of sub-group GpI-1.

4.4.6.2 Sub-group GpIa-2 (4/17 IPC Group Ia thin sections examined)

The four IPC Group Ia thin sections that make up GpIa-2 are: Co123/713, So20/227, Wi106/389 and Wi208/830. In all respects **GpIa-2 thin sections are similar to GpI-6,** having a higher degree of alteration than GpI-1.

4.4.6.3 Sub-group GpIa-3 (5/17 IPC Group Ia thin sections examined)

All five members of GpIa-3: Co249/1195, Co96/663, Wi3/3, Wi56/223 and Wi69/286 are **similar to GpI-7,** with the groundmass being cloudier and lacking the actinolite seen in GpI-1. It is suspected that Wi3/3 was the founding member of IPC Group Ia as it meets the description provided by Stone & Wallis (1962).

4.4.6.4 Sub-group GpIa-4 (1/17 IPC Group Ia thin section examined)

Thin section De20/528 is **similar to GpI-2** with the slight difference that the pyroxenes in De20/528 are more altered to amphibole.

4.4.6.5 Sub group GpIa-5 (1/17 IPC Group Ia thin sections examined)

The mm-sized non-ophitic pyroxenes in So50/939 all show first order birefringence, with oblique extinction angles typical of clinopyroxene. The alteration of the pyroxenes is probably chloritic as it has first order birefringence, with almost straight (± 5°) extinction. The groundmass is completely altered and there is no evidence of feldspar. The unique feature of this thin section is the alteration of the irregular to rounded, sub mm, opaques to sphene and granular biotite. The opaque alteration in axe thin section So50/939 is **unique** as it has **not been seen on any other IPC Group I or Ia** thin section.

4.4.6.6 Sub-group GpIa-6 (1/17 IPC Group Ia thin sections examined)

Thin section Wi274/1018 is similar to those in GpI-2, but the feldspars in this thin section are less altered and patches of a dark brown-red fine-grained mineral (?variety of epidote or sphene) surround distinct rhombs of amphibole. These features **are not found in any other IPC Group I or Ia** thin section examined.

4.4.7 Photomicrograph of sub-group GpIa-1

Figure 37 on the following page shows ppl & xpl images of Co152/738 which is a typical sub-group GpIa-1 thin section.

Sub-group GpIa-1
Co152/738

(xpl)

Score: Col:4, Size:6, Px:5 Fsp:6, Mica:2, Amp:2, Epi:1, Opa:7, Apa:0.

Figure 37 Photomicrograph of IPC Group Ia – sub-group GpIa-1 axe Co152/738

4.5 Examination of existing IPC Group III and IIIa petrological thin sections

4.5.1 IPC petrological description of IPC Group III and IIIa

Keiller et al. (1941) describe IPC Group III as:

"Hornblende, feldspar and decomposed ilmenite. Green hornblende forms large plates of needles roughly parallel to each other. Ilmenite as scattered grains, decomposed to leucoxene. Few stout needles of apatite are also present." (Keiller et al. 1941, Section 2.5.7). Stone & Wallis (1951) introduced IPC Group IIIa as having amounts of brown mica and epidote in addition to the mineralogy found in IPC Group III (Section 2.5.8)

4.5.2 Sub-groups within IPC Group III and IIIa

Thin sections from eleven of the twenty axes assigned to this group, plus two thin sections assigned to Group IIIa were examined as part of this work. As for Group I, petrographic differences were found in the thirteen thin sections allowing them to be sub-grouped. It is suspected from the work carried out by Keiller, Piggott and Wallis that Group III was founded on axe county reference Wiltshire 4 (Wi4/4) as this is the thin section they compare to a thin section from a quarry near Perranuthnoe (Keiller et al. 1941). This quarry is not precisely located in Keiller et al. (op. cit.), but suspected to be a disused quarry approximately 1km southeast of Perranuthnoe church. The resulting match between the two thin sections allowed Keiller et al. to deduce that this exposure was the source of IPC Group III (see Section 2.5.7 for additional details on the source of IPC Group III and Section 2.5.8 for IPC Group IIIa)

4.5.2.1 Sub-group GpIII-1 (2/13 IPC Group III & IIIa thin sections examined)

Wi4/4 (IPC Group III founding member) and Wi110/393 contain once partly ophitic pyroxenes to 2mm across that have been totally replaced by acicular and occasionally feathery aggregates of amphibole, with bright, second order birefringence which suggests tremolite-actinolite or hornblende. These mm-sized mats of amphibole are surrounded and penetrated by fine granular patches of a very fine-grained mineral, possibly a clay or more likely mica such as sericite, after feldspar. Clear, high relief grains of clinozoisite (iron-free epidote) are also associated with the feldspar alteration. Small (<0.1mm) apatite grains are readily visible in the groundmass. Irregular, eroded opaques are surrounded by fine granular sphene/leucoxene.

Figure 38 shows ppl and xpl images of axe thin section Wi4/4, believed to be the founding member of IPC Group III and one of the two axe thin sections assigned to GpIII-1.

4.5.2.2 Sub-group GpIII-2 (5/13 IPC Group III & IIIa thin sections examined)

Five Group III thin sections: Co53/562, Do156/1784, So22/267, Wi199/648 and Wi205/687 appear **petrographically similar to GpIII-1** with the addition of distinct pale green patches made up from a mat of very fine granular and slightly coarser grains. Both the fine and coarse grains have first order birefringence, and are thought to be a combination of chlorite and amphibole after pyroxene.

4.5.2.3 Sub-group GpIII-3 (4/13 IPC Group III &IIIa thin sections examined)

Thin sections: Do12/91, Do6/54, Wi42/137(IIIa) and 1993/81/A (no county number) are dominated by mats of fibrous to granular amphibole showing first order birefringence, with the occasional fibrous grains of tremolite-actinolite showing second order birefringence, probably after pyroxene. Rare feldspar and quartz is recognised in a fine-grained granular groundmass containing small amphibole and ?clay minerals. One of the sections, Dorset 12/91, shows alignment of grains. Apart from a slight difference in texture and the presence of quartz **GpIII-3 is similar to GpIII-1.**

4.5.2.4 Sub-group GpIII-4 (1/13 IPC Group III & IIIa thin sections examined)

Overall Co426/1884 is very fine grained with alignment of minerals and **is different to the other IPC Group I, Ia, III & IIIa** thin sections examined. The groundmass is chloritic, fine grained and very pale brown in ppl, turning to dark grey/black under xpl. Within the fine-grained groundmass, elongated grains of quartz and albite(?) are seen following the fabric of the section. Higher relief, granulated areas have bright second order birefringence and may be a combination of very fine granular biotite and muscovite mica, with the grain size making it difficult to confirm. There are relatively few opaques in the section, generally less than 0.5mm across.

4.5.2.5 Sub-group GpIII-5 (1/13 IPC Group III & IIIa thin sections examined)

In thin section Wi84/302 (IIIa) the relatively unaltered, sub mm, plagioclase feldspar contain small acicular actinolite and granular epidote. These features and the bright, mid second order birefringence, amphiboles, which have completely replaced the once non-ophitic sub mm euhedral pyroxenes, make this thin section **similar to Group I-6** and different to any other thin section assigned to Group III.

4.5.3 Photomicrograph of sub-group GpIII-1

Figure 38, on the following page shows ppl & xpl photomicrographs of the founding member of IPC Group III – Wi4/4.

Sub-group GPIII-1
Wi4/4

Score: Col:4, Size:1, Px:9, Fsp:10, Mica:2, Amp:2, Epi:2, Opa:7, Apa:1.

Figure 38 Photomicrograph of IPC Group III – sub-group GpIII-1 axe Wi4/4

4.6 Remarks on the examination of axe thin sections

4.6.1 Petrographic similarity of IPC axe groups

The examination of existing axe thin sections has shown that the primary mineralogy of IPC Groups I, Ia, III & IIIa is similar: clinopyroxene (plus rare orthopyroxene) + plagioclase feldspar + opaque (usually ilmenite), and that they all share similar, but varying degrees of, alteration to amphibole ± biotite ± epidote ± chlorite. The alteration seen in IPC Group III & IIIa is more complete than IPC Groups I & Ia, with very little primary mineralogy remaining. The original mineralogy of all four IPC groups appears to have been medium grained indicating an intrusive, as opposed to extrusive, igneous environment of crystallisation.

Although compositionally similar, there are recognisable mineralogical and textural differences that have resulted in the recognition of 24 sub-groups (IPC Group I – 13, IPC Group Ia – 6, IPC Groups III & IIIa – 5). Petrographic similarity within the sub-groups suggests the members may have originated from a single exposure. However, the differences between the sub-groups may indicate that the subgroups could have originated from a single exposure with distinguishable compositional variation *or* from several individual exposures.

If it can be assumed that the 119 IPC Group I thin sections examined is representative of the 384 axes in the whole Group, then GpI-1 can be considered to represent the most common petrography within IPC Group I. Using the same argument, GpIa-1 represents approximately just less than one-third of IPC Group Ia. Therefore, the observed petrographic similarity between GpI-1 and GpIa-1 suggests about one-third of IPC Group Ia could be assigned to IPC Group I. If GpIa-2 (similar to GpI-6) and GpIa-3 (similar to GpI-7) are also considered then it appears that the large majority of IPC Group Ia axes are potentially the same as those assigned to IPC Group I.

Sub-group GpIII-1 represents IPC Group III as it contains what is the author believes is the founding member of the group, axe Wi4/4. However, as the other 9 of the 11 axe thin sections examined are assigned to other sub-groups, the mineralogical and textural homogeneity of the IPC Group III is called into doubt. This observation, coupled with those made in the previous paragraph hint at the desirability of re-classifying the whole of IPC Groups I, Ia, III and IIIa.

During the petrographic examination it was noted that several thin sections were markedly different from the majority of thin sections examined, and especially different to GpI-1, GpIa-3 & GpIII-1 which are believed to represent the reported IPC group petrology. In these cases it must be questioned whether these axes (listed in Table 8, below) actually do belong to the IPC group they have been assigned to.

Sub-group	Axe reference	Main differences
GpI-9	Co157/751	Feldspar less altered than ortho & clino- pyroxenes
GpI-11	Wi440/1879	Free quartz & granophyric texture present
GpI-12	Do146/1762	Platy chlorite fabric & actinolite rhombs
GpI-13	CoGWA3	Asbestiform aggregates of tremolite & granular amphibole
GpIa-5	So50/939	Alteration of opaques to sphene & granular biotite
GpIa-6	Wi274/1018	Epidote? surrounding distinct rhombs of amphibole
GpIII-4	Co426/1884	Fine grained with obvious alignment of minerals
GpIII-5	Wi84/302	Closer to GpI-6 than GpIII-1

Table 8 Summary of thin sections probably incorrectly assigned to IPC groups on the basis of petrographical characteristics

In conclusion, it can be seen that individual IPC groups do not appear to be as petrographically homogenous as the IPC concept behind establishment of petrological groups suggests. Petrographical similarities between IPC groups indicate that there is potential to redefine membership of IPC groups, if not the individual IPC groups themselves. Further, it appears that a small number of axes are incorrectly categorised.

4.6.2 Petrogenesis of Group I, Ia, III & IIIa axe material

The primary mineralogy of the majority of the greenstone axe thin sections is predominantly medium grained with, occasionally ophitic, Ca poor clinopyroxenes (pigeonite and augite), plagioclase feldspar and titano-ferrous opaques. This, coupled with the rare presence of orthopyroxene and apatite and the lack of olivine and orthoclase feldspar, indicates a tholeiitic origin (Rollinson 1993, Mackenzie et al. 1982). Occasional diopside and higher Ca augite suggests a more evolved nature to the tholeiite in some cases. The lack of evidence for de-vitrified volcanic glass supports the observation that the medium grain size indicates an intrusive, possibly shallow level, emplacement of the original basic igneous rock. These observations suggest the greenstone may have been emplaced as sills or dykes within an N-MORB to E-MORB or within plate (extensional?) tectonic environment (Rollinson 1993, Appendix 30).

Subsequent alteration of the primary mineralogy resulted in the assemblage: amphibole (tremolite-actinolite, hornblende), chlorite, sericite, epidote, sphene and albite which corresponds to metamorphic alteration within the pumpellyite-prehnite to greenschist

facies (Floyd et al. 1993). Growth of subsequent biotite indicates the possible influence of K-rich fluids and could indicate proximity to or within a metamorphic aureole (Al Samman 1980).

N-MORB, E-MORB and within plate tholeiitic igneous activity is known to have occurred in Cornwall during the Devonian (Floyd et al. 1993, Chapter 3), along with low grade regional metamorphism associated with the Variscan Orogeny and contact metamorphic aureoles due to the emplacement of the Cornubian batholith (Section 3.4). As such, it appears entirely reasonable that IPC Group I, Ia, III and IIIa axe material originated within Cornwall.

4.7 Comparison between selected greenstone exposure samples and axe thin sections

4.7.1 Introduction to comparison exercise

Petrographic comparison between exposure and axe thin sections is a main feature of the work of the IPC and it is known from unpublished IPC archives that previous researchers have examined several hundred axe and greenstone exposure thin sections. Since the large number of comparisons has yet to yield an exact match between IPC Group I and Ia axes and a single greenstone exposure it would be remarkable if a match is found within the outcrop thin sections available in this work. However, the comparison will be carried out since it is probable that the converse can be established: that certain exposures could not have been the source of IPC Group I, Ia, III & IIIa axes. This information will be very useful when investigating the geochemical relationship between axe and exposure in Chapter 8.

Seventy-three new thin sections from greenstone samples collected as part of this work have been examined in order to investigate the petrographic similarity between greenstone exposures and axe thin sections. Exposure thin sections are listed in Appendix 5.4 and are identified in a similar manner to the corresponding rock sample (c.f. Section 3.3). The source of thin sections (using the sample identifier) is detailed in Appendix 4 and their distribution is illustrated in Figures 13 and 17-23 (in Chapter 3). Photomicrographs of all exposure thin sections are stored in digital form within the 5 CD-ROMS accompanying this thesis. The CD-ROM content lists are contained in Appendix 6.

Comparisons between exposure and axe sub-groups are introduced in the same order as the exposures are described in Chapter 3, Sections 3.6 and 3.7.

4.7.2 Lizard Dykes

Thin sections MM1 and MM2 (c.f. Section 3.6.2.2.2 and Figure 17) contain laths of plagioclase feldspar that are markedly less altered than the once ophitic, sub mm, pyroxenes. Amphibole, especially acicular actinolite, is present throughout. These two thin sections are *mineralogically similar to GpI-6 and GpIII-5*, but the texture found in MM1&2, dominated by the fine laths of plagioclase feldspar, is unique and not seen in any axe thin section examined.

4.7.3 Gramscatho Group (Carne Formation)

CUR001 and CUR002 were collected from field-walks around Cury (c.f. Section 3.6.2.6.2 and Figure 17). CUR002 is a fine-grained, quartz rich, sedimentary rock and therefore not related to igneous greenstone axes. CUR001 has abundant clinozoisite & epidote and a chloritised matrix and is unlike any axe thin section examined during this investigation.

4.7.4 Mylor Slate Formation: Cudden Point (inc. Porthleven)

CUD001, 2 & 2a-b (c.f. Section 3.6.3.2.2 and Figure 19) have plentiful clinozoisite and epidote, which sets them aside from all axe thin sections reviewed above. In addition and uniquely within the five Cudden Point thin sections, CUD003 contains primary magmatic, brown, amphibole which is not seen in any axe thin section that has been examined. CUD003 is coarse grained with some altered, partly ophitic pyroxenes up to 7mm long, again unlike any axe thin section examined.

The groundmass of PLN001 (c.f. Figure 13) has been completely altered to fine grained clays, micas and amphiboles, with albite (quartz?) as larger grains randomly intermixed. Bright red rutile grains are present in part of the thin section. In PLN002 2mm sized almost square, crystals of plagioclase show fine lamellar twinning. The rest of the thin section contains mats of fibrous radiating bundles of amphibole and mica. Neither of these textures have been seen in an axe thin section examined in this work.

4.7.5 Mylor Slate Formation: Perranuthnoe (inc. Trenow Cove)

Thirteen thin sections represent the Perranuthnoe Group (c.f. Section 3.6.3.2.2 and Figure 20). All pyroxene in TRE001 has been completely replaced by a granular to fibrous mat of

amphibole and chlorite. Feldspars are only suggested by virtue of polymorphs composed of sericite. Apatite is readily visible as fine acicular grains, with isotropic hexagonal basal sections. The alteration, especially the matted amphibole/chlorite, is not seen in any axe thin section.

TRE002, 3, 3A, 6 & 7 are dominated by 2 to 3mm sized plagioclase feldspar, sometimes showing alignment of grains and is reminiscent of thin sections from the dioritic exposure at Carn Gwavas (PEN001 & PEN002), suggesting this rock is more intermediate than basic. Coarse apatite grains are plentiful, a further feature not seen in axe thin sections.

TRE005 is similar to TRE001, however there is a range of clinozoisite – epidote and plentiful large apatite grains. Rare relicts of pyroxene and the shape of the fibrous mats of amphibole replacing pyroxene suggest a once ophitic nature. This texture, plus the abundant epidote, is not seen in any axe thin section so far reviewed.

The fibrous mats of amphibole and chlorite in TRE010 are similar to those in TRE010A, with the exception that in TRE010 the mats have an overall brown colouration, otherwise these two sections are similar and have a texture not seen in axe thin sections examined in this work.

TRE011A & B come from the same rock sample and demonstrate the variation in greenstone rocks over a few cm. TRE0011A is heavily chloritised with no pyroxene or feldspar visible, instead there is groundmass of fine fibrous amphibole and granular sericite, with apatite and epidote. TRE011B, on the other hand, has uralitised partly ophitic clinopyroxenes surrounded and penetrated by slightly altered mm-sized laths of lamellar twinned plagioclase feldspars, although the groundmass does contain similar proportion of apatite to TRE011A. This grain size and level of abundance of epidote is not seen in any axe thin section.

TRE012 is similar to TRE002, etc, with the exception the former has been heavily chloritised leaving smaller feldspars in the groundmass. This level of distinctive chloritisation has not been seen in any axe thin sections reviewed in this work.

Fibrous amphibole, probably after pyroxene and sericite after feldspar, dominate TRE013, with the latter as pseudomorphs of plagioclase (rare relicts of lamellar twinning is still

visible.) Veins filled with radiating, almost spherulitic, fine grained amphibole are seen across the section. Fine apatite is visible throughout along with a few small epidote grains. This texture has not been seen in any axe thin section.

In summary, none of the 13 TRE thin sections are similar to any IPC Group I, Ia, III & IIIa axe thin sections. This is surprising, since IPC Group III is provenanced to the same quarry that provided samples TRE001, 010, and 011A & B. It is concluded that the exposure must have variable texture and degree of alteration, as illustrated by sample TRE011A & B, it is possible that the actual source for Group III axes could have quarried away after the matching specimen was taken.

4.7.6 Mylor Slate Formation: Penzance and Mousehole

The source of samples from Penzance, Mousehole and surrounding areas used to make the 18 thin sections discussed below is shown in Figures 21 & 22 (c.f. Section 3.6.3.2.2).

Almost fresh, ophitic clinopyroxenes up to 4mm long are surrounded and penetrated by smaller plagioclase feldspar laths in Long Rock samples LNR001B & 4A. Granular chlorite/amphibole is seen replacing some clinopyroxene. The freshness of pyroxenes and feldspars is not seen in any axe thin section that has been reviewed. The pyroxenes in LNR004, once to 4mm and ophitic have been completely replaced by granular to fibrous mats of amphibole showing first order birefringence and oblique extinction. Feldspars are similarly as altered, but to sericite/amphibole . It is probable that all three thin sections are related, with LNR004 being an altered version of LNR001b & 4a. **The type of alteration, but not the coarse-grained mineralogy, seen in LNR001B, 4 & 4A is similar to some of the axe sub-groups described above – notably GpI-5 & GpI-11.**

The very fine-grained LNR002 & 3 are petrographically both similar. The total lack of opaque grains and any visible pseudomorphic grain structure makes them different to any axe thin section examined in this work.

PEN001, 2 & 2A-B thin sections are almost totally a mixture of plagioclase and orthoclase feldspar. Biotite mica is plentiful as granular patches surrounding the feldspar grains. Amphibole is seen within cracks in the feldspar. The texture and composition of these samples has not been seen in the axe thin sections.

Within PEN003, plentiful, acicular actinolite and bladed hornblende is scattered throughout the groundmass and large eroded opaque grains reveal a polygonal skeleton. Elongate, fine crystals of apatite are seen. The lack of pyroxene, presence of mats of fibrous to tabular amphibole and the other petrographic features seen **in PEN003 are similar to those found in GpI-6.**

Small, <0.25mm diameter, grains of bright (xpl) amphibole seen in PEN004, possibly hornblende, suggest the rock once contained non-ophitic fine euhedral pyroxenes. The groundmass is completely altered to clay and very fine acicular actinolite. Overall the texture seen in **PEN004 is similar to GpI-6 and MM4,** but with less of the secondary biotite.

Fine granular hornblende and quartz dominate PLK001 & 2, whereas PLK003 has equal quantities of coarse-grained biotite and quartz. None of these three thin sections resemble any axe thin section examined in this work.

The three TDO thin sections are all hornfelsed, with a fine granular matrix overprinting a once coarser grained texture. In TDO001 & 2 relict clinopyroxenes are readily visible, along with heavily altered feldspars. Large quantities of coarse apatite are also present, unlike TDO003 which has less apatite, and the pyroxenes are almost totally altered to a fine granular mass of chlorite and biotite. In all three thin sections ilmenite has been altered to leucoxene. The granular, hornfelsed texture has not been seen in any axe thin sections examined in this work.

The similarities between PEN003, 4, MM4 and axe Group I-6, and the textural similarities between LNR001a, 4 &4a and GpI-5 & GpI-11 are the closest seen between an exposure in Mount's Bay and axe thin sections. These findings, therefore, support the IPC observations that IPC Group I may have originated on the west side of Mount's Bay, however the similarities above are only seen in 17 of the 119+17 IPC Group I & Ia axe thin sections reviewed.

4.7.7 Mylor Slate Formation: North Penwith Coast

The location for Gurnard's Head, Zennor Point and Kenidjack samples is shown in Figure 18 (c.f. section 3.6.3.2.2)

Both **GUR001 & 2 share textural similarities with GpI-7 and GpIa-3**, however the exposure sections contain plentiful acicular plagioclase feldspar to 0.5mm, partly altered to granular amphibole, unlike the two axe sub-groups. GUR001 & 2 also contain heavily altered pyroxenes, replaced by bright (xpl) fibrous amphibole. Plentiful fine-grained biotite is present in both slides. Although there are some petrographic similarities between Gurnard's Head thin sections and the two sub-groups indicated, the match is less than conclusive and would need additional exposure thin sections to confirm/deny the relationship.

ZEN001, 1A, 1B are all laminated, very fine grained with mica (biotite & muscovite), quartz and probably albite in the groundmass. This, and the total lack of opaques makes them unlike any axe thin section examined in this work.

ZEN002, 2A, 2B are all heavily altered mafic rocks that have been extensively epidotised. Fine, fan-shaped agglomerates of acicular tremolite-actinolite are present along with finely disseminated opaque grains and heavily altered laths of plagioclase feldspar to 1mm long. The presence of biotite in ZEN002 indicates that this rock was metamorphosed on the edge of the Lands End granite contact aureole. The overall texture has not been seen in any axe thin section, the acicular to lath-shaped feldspars being distinctive.

Hornfelsic KEN001 has abundant granular biotite, very fine acicular to bladed amphibole and possible poikiloblasts of staurolite and larger andalusite. Mats of fibrous, first to low second order birefringent amphibole are intermixed with low relief patches of albite/quartz. KEN002 & 003 are similar, but with larger amphibolite grains. All three thin sections show schistosity and contain high temperature metamorphic minerals, and are unlike any axe thin section, except for KEN001, which shares some similarity to GpIII-3, but with plentiful granular biotite not seen in the axe thin sections.

4.7.8 South Devon: South Hams Group

The 13 thin sections taken from exposures in the South Hams are located in Figure 13 and introduced in Sections 3.7.3.2 & 3.7.4.2.

BOW001 & 2 are not similar to any axe thin section, containing no pyroxene or amphibole. Chloritic alteration of feldspars is distinctive, as are the plentiful, small (<0.25mm) granular, partly altered opaques.

DBN001 is characterised by finely disseminated, opaque grains and granular patches of very fine mica, probably biotite. DBN002 is almost completely made up of sub 0.5mm laths of plagioclase feldspar all partly altered to chlorite. High birefringent grains of epidote and red-brown, isotropic rutile complete the mineralogy of DBN002. DBN001 & 2 are not similar to any axe thin section detailed above.

IVY001 & 2 are dominated by large, to 2mm, ophitic clinopyroxenes with alteration to chlorite, and by plagioclase feldspar laths, also to 2mm, partly altered to chlorite. This texture, and the lack of amphibole, makes these thin sections different to any axe thin sections described above.

Abundant apatite, often associated with brown tabular biotite and chlorite dominate IVY003 & 4. IVY003 has plentiful plagioclase feldspar, whilst IVY004 contains quartz (or granular albite?) instead of feldspar. The abundance of apatite is distinctive for these two thin sections and this amount of apatite has not been seen in any axe thin section.

Ophitic, sub mm sized grains of matted amphibole after clinopyroxene stand out in a heavily altered groundmass containing abundant clinozoisite, epidote, quartz and clay minerals in LSC001. In addition LSC002 has 2mm sized phenocrysts of orthoclase feldspar. Neither of these textures is seen in the axe thin sections examined in this work.

Plentiful small grains of epidote in MYD001 stand out from a dark matted groundmass of amphibole and mica. The fine to very fined grained nature of this thin section is not seen in any axe section examined in this work.

TQY001 & 2 have classic ophitic doleritic texture, with occasional patches of chlorite and calcite(?). Chadacrysts of feldspar surround 4mm sized clinopyroxene oikocrysts. Plentiful apatite and mm-sized angular grains complete the mineralogy observed in the thin sections. The combination of almost fresh pyroxene and distinct chloritic patches has not been seen in any axe thin section examined in this work.

In summary, and as expected, the samples collected from South Devon have no petrographic similarities to any IPC Group I, Ia, III or IIIa axe thin sections examined in

this work, although some do contain similar mineralogy: pyroxene, plagioclase and opaques grains with varying degrees of alteration.

4.7.9 Greenstone samples unrelated to exposures

Mr D. Weddle discovered two large pieces of greenstone rock, MM3 (weighing 16kg) & MM4 (weighing over 100kg), well away from known greenstone exposures (Figure 18, Appendix 4) but relatively close to some Neolithic sites in NW Cornwall (Compare Figure 2 & 18). Macroscopic observation showed that these rocks appeared to have similar mineralogy and texture to greenstone axes, hence their inclusion in this thesis.

The thin section from **MM3 is very similar to GpI-1 and GpI-2** with partly altered partly ophitic clinopyroxenes and heavily altered feldspar. Abundant actinolite and cloudy epidote, coupled with patches of biotite makes up the groundmass of the rock thin section.

MM4A-D are very similar to GpI-6, with the addition of biotite and bright (xpl) amphibole totally replacing non-ophitic pyroxene seen in MM4A-D. The groundmass consists of altered feldspar, with acicular actinolite and plentiful patches of granular biotite. Apatite is readily visible in these 4 thin sections.

4.7.10 Remarks on the comparison between exposure and axe thin sections

As anticipated, no exact match between axe and exposure thin sections has been found. However, some greenstone rocks do contain similar mineralogies and textures to some of the axes, supporting the hypothesis that the IPC groups in question could and probably do originate from Cornwall. The best matches found (result summarised in Table 9 below) are between IPC Group I axes and rock from greenstone exposures at Penlee, Long Rock and Gurnard's Head. Both Penlee and Long Rock are on the west and north side respectively of Mount's Bay, whilst Gurnard's Head is on the North Penwith Peninsula. The closest petrographic match observed was between GpI-1 and MM3. But, since MM3 was not found in situ it cannot shed any light on the source exposure except that MM3 was a 16kg and greater than 30cm diameter boulder which may not have been transported far from its source, thus suggesting a North Penwith origin.

Exposure Group	Similar to axe sub-group -	Comment
Lizard Dykes	GpI-6, GpIII-5	Mineralogically similar, but distinct textural differences
Gramscatho Group- Carne Fm	None	
Cudden Point Group	None	
Perranuthnoe Group	None	
Penzance & Mousehole	GpI-6	Petrographically similar to PEN003 & 004 (Penlee)
Group	GpI-5, 11,	Style of alteration similar to LNR004 (Long Rock)
North Penwith Group	GpI-7, GpIa-3	Similar to GUR001, 2 apart from granular amphibole
South Hams Group	None	
MM3 & MM4	GpI-1, 2	Petrographically similar to MM3
	GpI-6	Petrographically similar to MM4

Table 9 Summary of comparisons between selected greenstone exposures and IPC Group I, Ia, III & IIIa axe thin sections

Several rock samples were taken from the same quarry that provided the thin section used to provenance IPC Group III. The failure to find any similarity between the rock and IPC Group III can be put down to one of three possibilities: the quarry is heterogeneous and the wrong area was sampled, the source rock has been quarried away, or that it is the wrong quarry. All of these possibilities are feasible, however the state of the quarry face suggests it has been idle for a very long time and the view from the quarry is almost exactly the one provided in Plate 1 (lower) of the 1st IPC report (Keiller et al. 1941). Thus the first of the three probabilities is thought most likely.

Petrographic comparison has found no convincing match between any axe sub-group and rocks collected from Cudden Point, Perranuthnoe or the South Hams and suggests the source for IPC Group I & Ia is not on the east side of Mount's Bay or in the South Hams area of Devon. The failure to find a match between the single sample representing the Gramscatho Group (Carne Formation only) must be treated with caution as it is a single sample that was collected by field walking and not from an in-situ exposure.

4.8 New quantitative petrographic analysis system used to examine thin sections

4.8.1 Scoring parameters for petrographic analysis

An initial review of twenty randomly selected IPC Group I axe thin sections revealed small differences in mineralogy that eventually led to the formation of the sub-groups described above. During the examination of these axe thin sections it was felt a more systematic and quantitative approach to gauging the slight differences seen in thin sections may prove beneficial, especially to less skilled petrologists. Therefore, an attempt to measure differences in thin sections using an empirically based quantitative 'scoring' system was devised. This system is based upon observations of thin section colour, grain size, degree

of alteration, size and shape of opaque minerals and the presence of a number of readily identifiable minerals, and is described in detail below.

4.8.1.1 Colour

All IPC Group I thin sections are various shades of green to the naked eye. The scores, 1 to 9 indicate the darkness of the thin section, with 1 representing a transparent, colourless thin section, and 9 representing a near opaque, very dark green thin section. A score of 10 indicates another predominant, non-green colour (encountered mainly in *rock* rather than axe thin sections). Initially, twenty IPC Group I axe thin sections were arranged in a row on a white background and divided into groups of visually equal colour, with the largest population frequency (mode) given a score of 5. All remaining thin sections were then assigned a colour score using the initial sorting of theses twenty thin sections as a colour template.

4.8.1.2 Grain size

Noting that the original mineralogy had been altered to some degree and that the original grains may be obscured or altered, a simple visual approach to assessing grain size was adopted. Using a grain size card (supplied by GEO Supplies Ltd, Chapeltown, Sheffield), each of the thin sections were viewed with a x10 hand lens and the best match between grain size displayed on the grain size card and the thin section established. This measurement was then complemented by re-estimating the grain size using the polarising microscope at x40 & x100 magnification (4.0mm & 1.6mm field of view (f.o.v.) respectively). In reality the average of the longest dimension of pyroxene grains, with their ubiquitous amphibolitic alteration, determined the thin section grain size recorded since these grains (pseudomorphs) were the most visible evidence of original rock texture. Table 10 details the scores assigned to the grain sizes displayed on the grain size chart values. In general, axe thin sections scored around 6, indicating an average grain size of 1mm.

Thin Section Score	Average Grain Size (mm)
1	<0.250 (or not measurable)
2	0.250
3	0.375
4	0.500
5	0.750
6	1.000
7	1.500
8	2.000
9	4.000
10	>4.000

Table 10 Grain size scores based on the GEO grains size chart (supplied by GEO Supplies Ltd, Chapeltown, Sheffield).

4.8.1.3 Pyroxene Alteration

A scoring system relating to the amount of alteration of the pyroxenes contained within the thin section is detailed in Table 11 below. The concept behind this subjective scoring is that pyroxene, altered to some amount, is very common in IPC Group I axe thin sections and in many greenstone rocks. The scoring is based on visually estimating the percentage of alteration of the pyroxene grains seen in the thin section and the number of grains altered. The type of alteration (usually to amphibole/chlorite) is not recorded, neither is the grain size or nature of the grains (e.g. ophitic) but, details of these aspects are contained within the individual descriptions in Appendix 5. The range of scores in Table 11 anticipates the potential use of this procedure on basic igneous rocks with little pyroxene alteration. Pyroxenes within most greenstone axe thin sections were altered to such an extent that the majority of the thin sections scored 6-7, indicating that less than 25% of the primary pyroxene remained unaltered.

Thin Section Score	Pyroxene scores, established by eye
1	All pyroxene grains visible in the thin section are unaltered
2	Less than 50% of pyroxene grains visible have <5% of the original grain altered.
3	A majority of pyroxene grains visible have <10% of the original grain altered.
4	All pyroxene grains visible have <25% of the original grain altered.
5	All pyroxene grains visible have between 25% - 75% of the original grain altered
6	All pyroxene grains visible have 75% - 95% of the original grain altered
7	Approximately 5% of the original pyroxene is still visible in the majority of altered grains.
8	Small amounts, <5% of the original pyroxene is visible in a few altered grains
9	Possible pyroxene pseudomorphs are seen in the thin section
10	No pyroxene or pyroxene pseudomorphs are visible

Table 11 Scores given for the alteration of pyroxene grains seen in thin sections

4.8.1.4 Feldspar Alteration

The scoring regime based on the progressive alteration of feldspar is detailed in Table 12 below. Feldspars found in IPC Group I and IPC Group III thin sections were usually heavily altered to a very fine grained mineral, probably sericite, and often had radiating bundles of bladed actinolite within the original crystal perimeter. The difficulties with identifying the alteration product(s) means that feldspar scores are related to the evidence for the original feldspar remaining and not the type of alteration. Further, it was often not possible to determine the actual variety of feldspar as the alteration clouded the assessment of twinning and other evidence (relief, twinning angles, etc.) so the table of scores relates to a visual estimate of the amount of unaltered feldspar found in the thin section. It should be noted that secondary albite may have been incorrectly diagnosed as primary feldspar. The considerable alteration to feldspars within axe thin sections means that the majority of the thin sections scored 7 to 9, indicating that there is little primary feldspar remaining.

Thin Section Score	Feldspar Alteration
1	Fresh unaltered feldspar with cleavage and twinning readily visible
2	Less than 5% alteration on less than half feldspar crystals, cleavage may be seen, twinning readily visible
3	All feldspar crystals up to 10% altered. Cleavage not seen, twinning readily visible.
4	All feldspar crystals between 10% - 50% altered. Cleavage not visible, twinning readily visible.
5	All feldspar crystals between 50% - 90% altered. Cleavage not visible, twinning readily seen.
6	Little unaltered feldspar visible, majority of crystals with no fresh feldspar remaining. No cleavage seen, twinning readily visible.
7	All feldspar completely altered, but with original shape and twinning clearly visible.
8	All feldspar completely altered, with original shape and suggested twinning visible throughout slide.
9	All feldspar completely altered, with original shape and suggested twinning visible in few areas of slide.
10	No feldspar, or lath pseudomorphs visible

Table 12 Scores for feldspar alteration seen in thin sections

4.8.1.5 Opaque Minerals

Accessory opaque minerals are present in every IPC Group I and III thin section. The scoring system, detailed in Table 13, is based upon the shape and size of the opaque grains and not the quantity or type. In practice the score was based on the larger grains seen under the microscope, as most thin sections contained fine, <<0.1mm, rounded grains associated with the alteration of pyroxene to chlorite/amphibole. The scores represent the wide range of opaque grain size and shape encountered. The most common scores for axe thin sections are 6 and 8, indicating that larger grains present in many thin sections are elongate/ladder-like in appearance, and that the majority of the remainder contain fine-medium grained opaque grains.

Thin Section Score	Opaque
1	Coarse, angular opaque grains, > 2 mm
2	Coarse opaque grains, with alteration and skeletal structure or elongate grains visible, >2 mm
3	Coarse angular opaque grains with clear polygonal skeletons, >2 mm
4	Medium, angular opaque grains, 0.5 mm to 2.0 mm, with no skeletal or ladder-like lattice seen
5	Medium, angular opaque grains, with distinctive polygonal skeleton(s) 0.5mm to 2.0 mm
6	Medium angular opaque grains, with elongate/ladder like grains 0.5mm to 2.0 mm
7	Medium angular opaque grains with eroded appearance and no skeleton visible 0.5mm to 2.0 mm
8	Fine opaque grains < 0.5 mm
9	Opaque grains not meeting any of the above descriptions
10	No opaque grains seen in thin section

Table 13 Scores based on the size and shape of the opaque grains seen in thin section.

4.8.1.6 Amphibole & Mica (chlorite & biotite)

The fine-grained nature of the alteration of the IPC Group I thin sections made it very difficult to determine what type of amphibole or mica was present. Hence the simple scoring system is based upon the presence of primary (Score 1) or secondary (Score 2) amphibole/mica. Lack of amphibole/mica was scored as 0. In practice only one thin section was found to contain primary magmatic amphibole (CUD003) and all thin sections contained some form of secondary mica (usually biotite) or chlorite, hence the value of this particular form of scoring in this situation is minimal. However, presence/absence of amphibole/mica is a good discriminatory factor and may prove useful in future research, hence its inclusion in the quantitative system.

4.8.1.7 Epidote

A simple scoring system, based on the lack, probable and certain evidence for epidote has been used. No epidote present in the thin section was scored as 0. Presence of very fine grained, high relief, cloudy masses seen within feldspar alteration were taken as probable evidence for the presence of epidote and scored 1. In some cases it is possible that sphene has been incorrectly identified as epidote (and vice versa), with the very fine grains making it difficult for positive identification. Distinct, often small (<0.2mm), grains clearly of epidote or clinozoisite scored 2 on the empirical 0, 1, 2 scale.

4.8.1.8 Apatite

Apatite is an easily recognised accessory mineral, with distinctive hexagonal basal sections often clearly visible when surrounded by alteration products. The lack of apatite in thin section was scored as 0, with the presence of small grains (<0.1mm) scoring 1 and larger grains (>0.1mm) scoring 2. Plentiful (visible throughout the thin section), but fine-grained apatite also scored 2 on the empirical 0, 1, 2 scale.

4.8.2 Analysis of quantitative (scoring) results

4.8.2.1 Estimation of error associated with scoring

Although the descriptions for the thin sections detailed in Appendix 5 were written over a long period of time, the scoring of all thin sections took place over a period of seven days. This was done to minimise human bias in assessing the scores for each thin section. The empirical quantitative system was developed on examination of twenty thin sections which had been examined approximately 18 months previously to the seven-day exercise, and the scores allocated to the thin sections at that time were deliberately re-estimated in order to

see if any human bias had developed in the intervening time. It was found that the majority of the 'new' and 'old' scores agreed within ±1 scoring unit (apart from opaques scores, which are not incremental) hence leading to the conclusion that the potential error on assigning scores is ±1 of the given score. The devised system was easy to use and, once practised, scores could be assigned within minutes.

4.8.2.2 Presentation of results

All thin section scores are contained in Appendixes 5.1 to 5.4. Scores given to typical axe sub-group members are illustrated in the photomicrographs contained earlier in this chapter. The quantitative results are examined in 3 ways:

1. Bivariate plots

   Pyroxene and feldspar are the most common minerals found in axe thin section and bivariate plots for the associated scores show the range and relationship of the alteration of these minerals found in thin sections. Bivariate plots comparing the range and relationship of all axe sub-groups are contained in Section 4.8.3 below

2. Multiple parameter (profile) plots

   Scoring profiles based on the average scores for 7 of the 9 categories provide a graphical indication of the similarity between groups of thin sections. Average scores for each axe and exposure sub-group were calculated in the normal manner (formula: (∑scores)/n), where ∑scores is the sum of individual scores and n is the number of axes/samples in the sub group*). Colour, grain size, pyroxene and feldspar* alteration are all incremental scores, hence the average gives a meaningful estimate for the overall group property. Similarly *epidote*, and *apatite* can also be considered incremental, with 0 representing no evidence of the mineral to 2 representing clear evidence. Calculated apatite and epidote averages have been increased by a factor of 5 to bring them in line with the 0 to 10 range as used for the remaining categories. However, *opaque* scores are not incremental, the score representing size and morphology, so opaque averages must be treated with caution. Scores for *amphibole and mica* are not included within the profiles as they do not vary and therefore do not provide any discrimination. Profiles are provided for all 24 axe sub-groups. Additionally, scoring profiles for axe sub-group and exposure thin sections that have petrographic similarities (see Section 4.7.10) are plotted on the same chart. The implication is that if the two profiles overlay each other then there is a marked petrographic similarity between the corresponding axe sub-group and exposure.

3. Quantitative arithmetical comparison

The degree of similarity between graphical profiles can be arithmetically measured by adding together the moduli of the differences between each average score from the two profiles being considered, ignoring the opaque scores for reasons discussed above and amphibole and mica scores as they are largely similar throughout. For example, say that there are two profiles consisting of average scores (colour, grain size, pyroxene, feldspar, epidote & apatite) 5, 7, 5, 8, 6 & 3 and 7, 3, 8, 6, 7 & 4 respectively. Then, the sum of the modulus of the difference is obtained by the expression (|5-7| + |7-3| + |5-8| + |8-6| +|6-7| + |3-4|), giving 13 as the sum of the moduli of the differences, called the residue. Therefore, a perfect match in profiles would result in a zero residue, whilst a low residue indicates a close match and a high residue indicates a poor match in at least one of the scoring categories. This method can be used to examine the degree of similarity within and between axe sub-groups and exposure sub-groups.

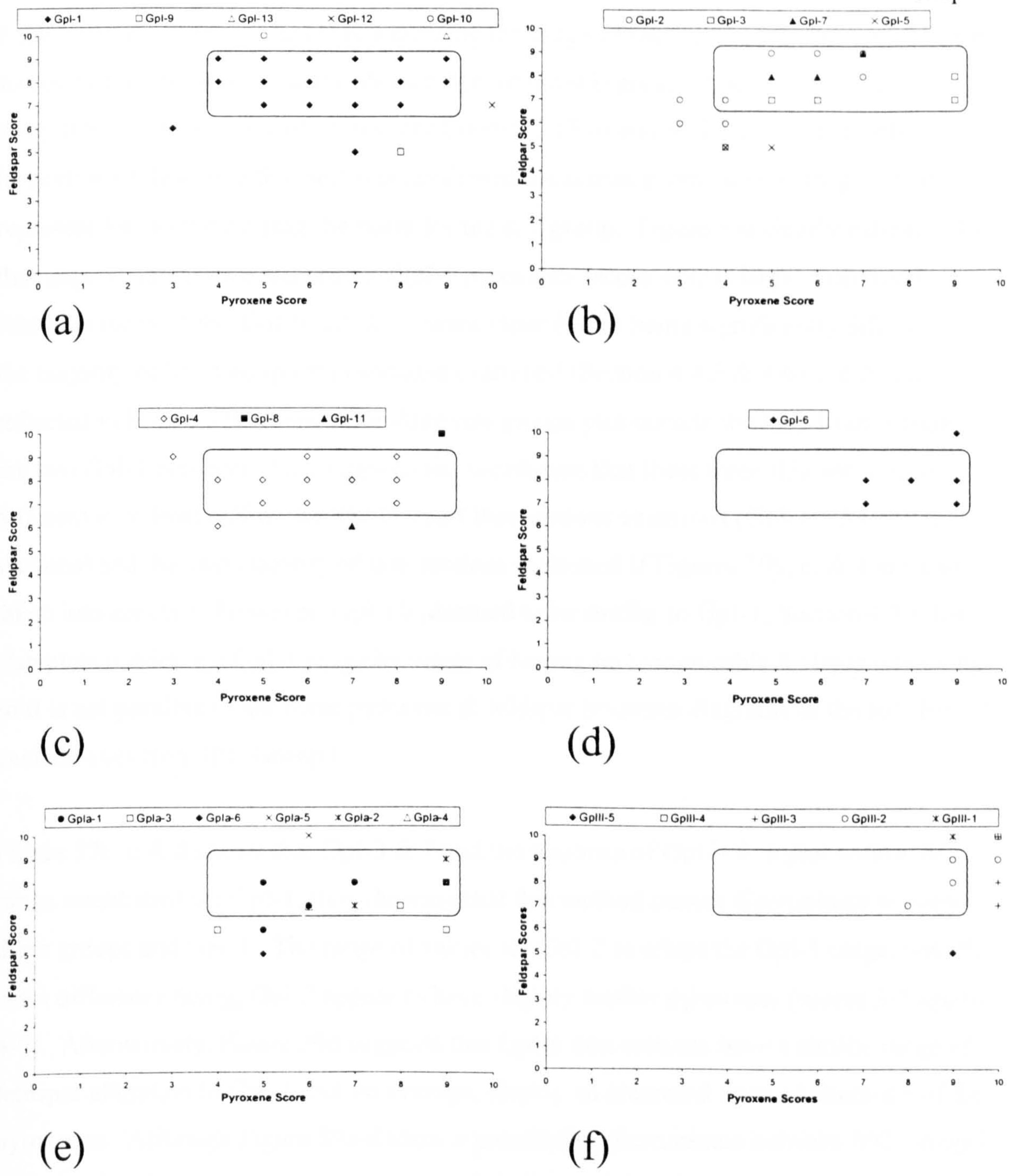

Figure 39 Bivariate plots based on pyroxene and feldspar scores for all 24 axe sub-groups. IPC Group I is contained in plots a-d, IPC Group Ia in plot e and IPC Group III (inc. IIIa) in plot f. The rectangle illustrates the range of the majority of GpI-1 scores and is plotted on all charts to provide a visual reference. (See Section 4.8.3.3 for remarks concerning limitations on interpretation of these bivariate plots.)

4.8.3 Results and remarks on the quantitative petrographic analysis of thin sections.

4.8.3.1 Bivariate plots of all axe sub-group pyroxene v feldspar scores

The six bivariate charts in Figure 39(a-f) compare pyroxene and feldspar scores for each of the 24 axe sub-groups, with the range of the majority of GpI-1 scores (Figure 39a) being represented on each chart to provide a visual reference. The variety of symbols and non-sequential sub-groups used in Figure 39a-d are chosen in order to maximise the observed separation between sub-groups.

Figure 39a shows the rectangle representing the range of the GpI-1 pyroxene and feldspar scores surrounds all but 2 of the 59 members of the sub-group. These two outliers (i.e. away from the main body of scores) are Co66/593 (3,6) and Wi29/36 (7,5). Further inspection of these two thin sections confirmed the scores given, acknowledging that they represent less alteration than the norm for the sub-group. Figure 39a clearly indicates that the range of alteration observed for GpI-1 pyroxenes (score 4-9) is larger than that for feldspars (score 7-9). GpI-9, 12, & 13 were identified as being significantly different to the majority of IPC Group I thin sections examined (Section 4.4.3 & 4.6) and this is reflected in Figure 39a where these three sub-groups plot outside the GpI-1 range (ignoring the two GpI-1 outliers). This supports the conclusion that these three thin sections are different to at least half of the IPC Group I thin sections examined (GpI-1 = 59/119 thin sections) and the vast majority of thin sections examined if Figures 39b, c, & d are also taken into account. However, GpI-10 (deemed to be similar to GpI-1, Section 4.4.3.10) also plots outside the GpI-1 range by virtue of having no recognisable feldspar remaining so it is not possible to use these pyroxene & feldspar bivariate diagrams as the sole basis to exclude axes from IPC Group I.

Figure 39b, c & d shows that GpI-3 & 7 and the majority of GpI-4 & 6 plot within the range established for GpI-1, thus showing that this method cannot discriminate between these groups and GpI-1. The range of values for GpI-2 overlaps the GpI-1 range, with the main difference being, GpI-2 appear to have slightly fresher pyroxenes (scores 3-7 against 4-9). Alternatively, Figure 39d suggests that GpI-6 thin sections have a similar range of feldspar alteration to GpI-1, but on average, display an increased level of alteration of the pyroxenes. Although Figure 39a-d show a potential to discriminate between IPC Group I sub-groups, if GpI-1 is ignored, it is noted that the small numbers within these sub-groups means that the data may not be representative of the true situation (which would require all axe thin sections to be examined).

In general, Figure 39e shows that IPC Group Ia thin sections appear to contain comparatively fresher feldspar, but similar degrees of pyroxene alteration to IPC Group I. The considerable overlap in plotted positions between GpI-1, 2 & 6 and GpIa-1, 2, 3, & 4 supports the observations (Section 4.5.6) that these 7 sub-groups are petrographically similar. GpIa-5 & 6 are noted as being petrographically different to other IPC Group Ia thin sections examined (Section 4.4.6.5 & 6) and Figure 39e reflects this situation, with the two sub-groups plotting above (GpIa-5) and below (GpIa-6) the other 4 sub-groups.

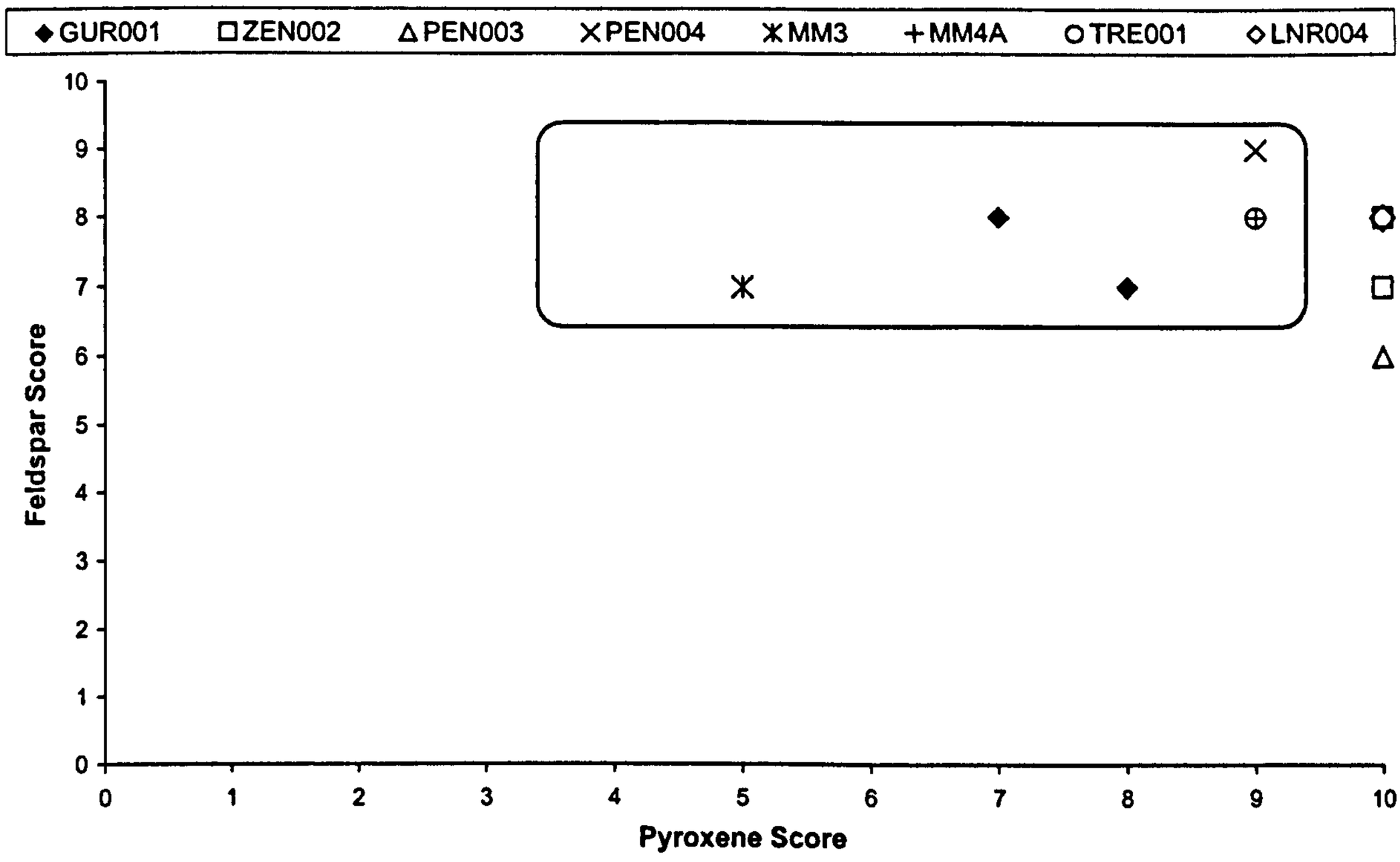

Figure 40 Bivariate plot based on pyroxene and feldspar scores for selected greenstone rock thin sections. Selection is based on the observed similarity between axe and rock thin sections reported in Section 4.7.10, plus TRE001 and ZEN002. The rectangle represents the range of GpI-1 scores (c.f. Figure 39a)

Figure 39f shows that, apart from GpIII-5 (which is an IPC Group IIIa thin section and unlike any other axe thin section examined (Section 4.5.2.5), all IPC Group III thin sections plot in the very top right of the chart indicating that little, if any pyroxene remains. Although there is some overlap with IPC Group I thin section scores (compare Figure 39e with Figure 39a-d) it is clear that there is potential to discriminate between IPC Group III & IIIa and IPC Group I & Ia thin sections.

4.8.3.2 Bivariate plots between selected axe sub-groups and exposure samples

Table 9 in Section 4.7.10 identifies 7 rock thin sections that have petrographic similarities with various axe sub-groups. The associated pyroxene and feldspar scores for six of these thin sections are shown in Figure 40, along with ZEN002 and TRE001. Comparison between Figure 39 and Figure 40 shows that the range of pyroxene and feldspar scores for sub-groups GpI-1, 3, 6, GpIa-3 and GpIII-2, 3 provide the greatest overlap with the rock thin sections. On a larger scale, the rock thin sections appear to have degrees of pyroxene alteration closer to those observed in IPC Group III thin sections than IPC Group I & Ia thin sections. TRE001 has been included in Figure 40 as the thin section originates from rock collected at the hypothesised source of IPC Group III. ZEN002 is included to illustrate where samples that have not been petrographically matched with axe sub-groups could plot.

It is not possible to provenance any sub-group to a single exposure with confidence since full range of pyroxene & feldspar alteration from an exposure cannot be ascertained from the few thin sections available. However, the proximity and degree of overlap observed between rock and axe thin sections does support the findings in Section 4.7.10 and therefore supports the usefulness of the pyroxene and feldspar bivariate plot as part of the quantitative analysis of thin sections (but see below).

4.8.3.3 Remarks on limitations of bivariate plots

Bivariate plots based on scores assigned to varying degrees of pyroxene and feldspar alteration are simple to produce and understand. However, their interpretation needs care as only the range of alteration is represented and not the disposition of the whole population (i.e. each point plotted on the variation diagram could represent one or many thin sections). The coarse nature of the quantitative scoring system means that overlaps are to be expected, thus reducing the ability to differentiate between sub-groups. Both these problems may be overcome by plotting average and associated standard deviation values for axe sub-groups. But, the often small sub-group size means that any such statistics would need to be treated carefully. It is believed that, with an increased number of petrographic observations of both axe and rock thin sections, it may become possible to associate unknown thin sections with an axe sub-group or exposure with some statistical significance, and thus potentially to identify a possible provenance for the axe.

4.8.3.4 Multiple parameter (profile) plots for axe sub-group thin sections

Figure 41a-d below, show the average score profiles (c.f. 4.8.2.2) for sub-groups, with the GpI-1 profile plotted on each of the charts a-d for reference. Figure 41a clearly shows that GpI-1, 2, 3 & 4 follow similar profiles indicating that they are petrographically similar. Figures 41b-d show an increasing level of variation when compared with the GpI-1 profile reflecting an increased petrographic difference. Profiles for GpI-9, 11,12 & 13 are clearly separated from GpI-1 therefore supporting the observation that these sub-groups may have been incorrectly categorised (Section 4.7).

Sub-groups GpIa-1, 2, 3 & 4 follow similar profiles in Figure 41e supporting the observations that these four sub-groups share similar petrographic features. The two anomalous sub-groups, GpIa-5 & GpIa-6 clearly deviate the most from GpIa-1 profile which supports the observations in Section 4.4.6 that these two axe thin sections are

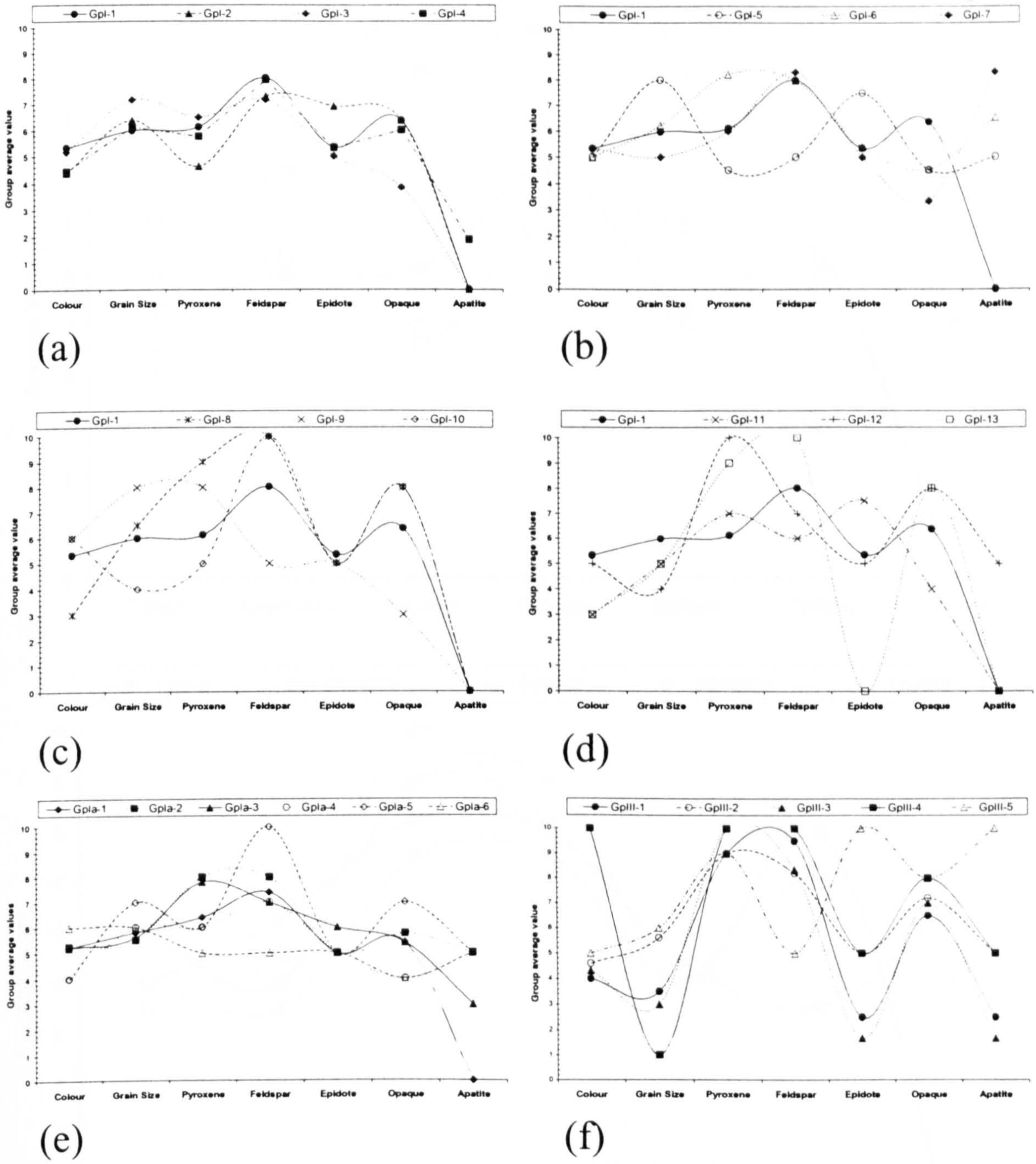

Figure 41 Multiple parameter plots comparing profiles between selected axe sub-groups. Axe sub-groups that share a similar profile are petrographically similar.

different to other IPC Group Ia thin sections. Comparison between Figure 41a and 41e indicates that GpIa-1, 2, 3, & 4 appear to have smaller grain size averages than GpI-1, 2, 3 & 4 suggesting that the IPC Group I a axes are finer grained than the majority of IPC Group I.

Figure 41f shows that IPC Group III (note IPC Group IIIa is included within the six IPC Group III sub-groups) profiles are more sinuous than IPC Group I & Ia sub-group profiles. This heightened sinuosity is due to the high (9-10) pyroxene and feldspar scores coupled with relatively fine grain sizes and range of apatite and epidote scores. Profiles indicate that GpIII-1 & GpIII-3 are petrographically similar. GpIII-2 follows a similar profile to

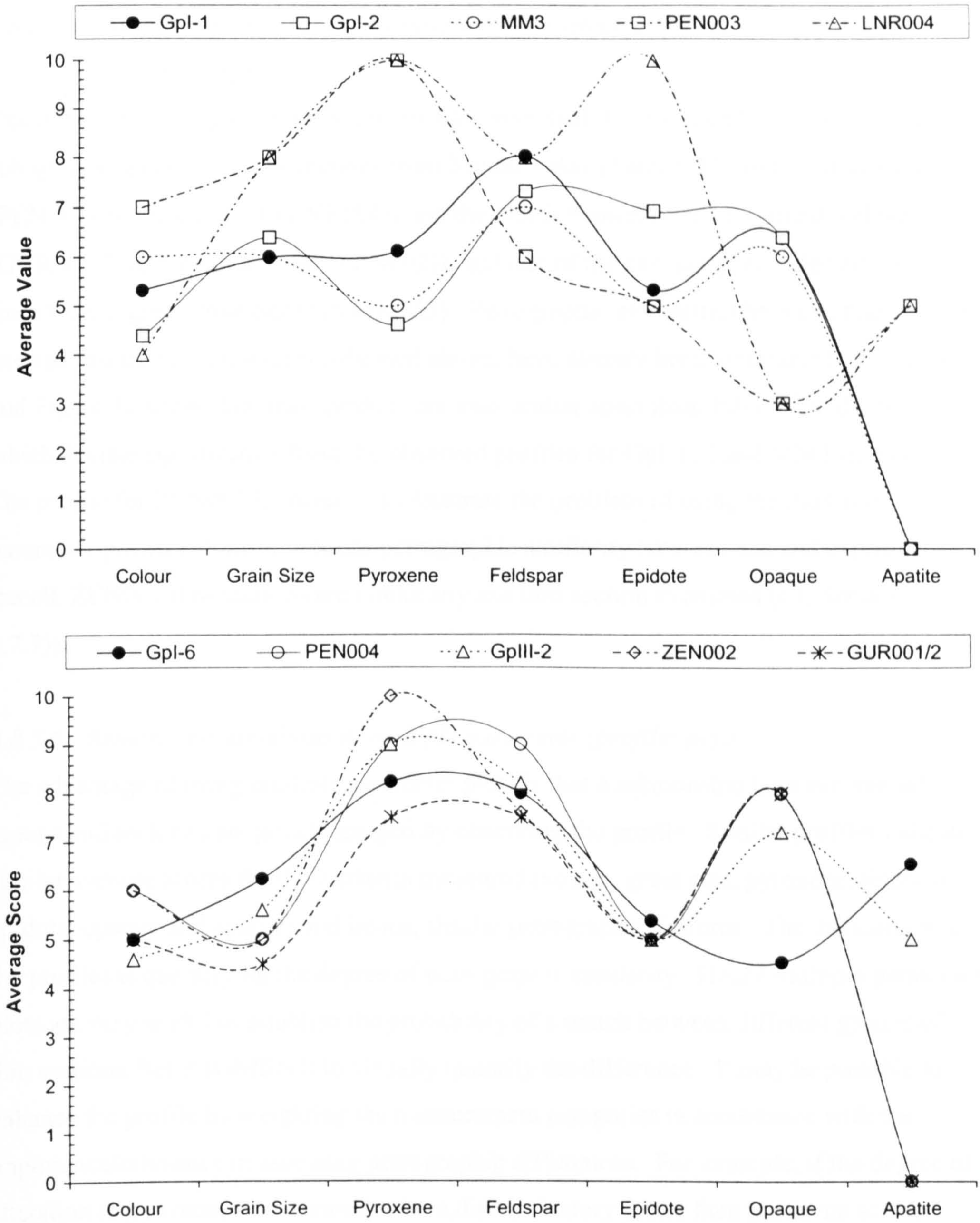

Figure 42 Multiple parameter plots comparing profiles between selected axe sub-groups and rock thin sections. Axe and rock samples that share a similar profile are considered to be petrographically similar.

GpI-1, but has a higher pyroxene score indicating the alteration of pyroxene in GpIII-2 is more extensive than GpI-1. Section 4.5.2.5. indicates that GpIII-5 is petrographically similar to GpI-6, but the profile (compare Figure 41b & f) indicates that GpIII-5 appears to contain fresher feldspar and more epidote and apatite than GpI-6.

4.8.3.5 Multiple parameter (profile) plots between selected axe sub-groups and selected exposure samples

The two charts in Fig 42 above show profiles from GpI-1, GpI-2, GpI-6 and GpIII-2 axe sub-groups, greenstone thin sections from Mount's Bay (Penlee (PEN003), Mousehole (PEN004) and Long Rock (LNR004)) and the North Penwith coast (Gurnard's Head (GUR001/2) and Zennor Point (ZEN002)), and one of the two samples collected away from known greenstone exposures (MM3). Petrographic similarities between many of the axe sub-groups and exposures indicated above, have already been ascertained (Section 4.7) and Figure 42 shows that their profiles are also similar apart from PEN003 and LNR004, which deviate significantly from the observed profiles for GpI-1, 2 and MM3 (top chart). The profile for ZEN002 is included to illustrate the problem of using the multiple parameter profiles alone to indicate petrographic similarity between axe and exposure (recall, ZEN002 thin sections are unlike any axe thin section examined (c.f. Section 4.7.7)).

4.8.3.6 Remarks on usefulness of multiple parameter (profile) plots

The advantage of using multiple parameter plots is that a relationship between axe sub-groups and rock can be quickly gauged by observing the profile. Similar profiles indicate similar average scores for the 7 criteria measured (colour, grain size, pyroxene, feldspar, epidote, opaque and apatite) and hence, similar petrographic features. The difficulty with the profiles is quantifying the degree of petrographic similarity. Hence multiple parameter plots are very useful to establish the probability of a match between different groups of thin sections, but it is difficult to visually quantify the difference. It may be possible to enhance the profile by weighting the measurement categories in accordance with their importance/relevance in assessing petrographic differences. For example, if the degree of alteration to pyroxene was deemed to be a discriminatory factor then pyroxene scores could be multiplied by a factor to increase the separation of the profiles. (Note: this was effectively done for epidote and apatite.) Using this style of presenting petrographic data it could become possible to recognise 'typical' IPC group profiles which could assist with the classification of axe thin sections as well as assisting provenancing studies.

4.8.3.7 Quantitative arithmetical comparison within and between axe sub-groups

Using the method described in Section 4.8.2.2 the residual scores for all 276 combinations of the 24 axe sub-groups ($^{24}C_2 = 276$) have been calculated and reported in Appendix 5.6. The theoretical maximum score (residue) is 56 (|10-1| for colour, grain size, pyroxene &

feldspar and |0-10| for epidote and apatite = ((9 x 4) + (10 x 2) = 56) and theoretical minimum score (residue) is 0 (i.e. both profiles are the same). The actual average and associated standard deviation of all 276 scores is 12.26 ± 5.15. The lowest 8 residues, all less than or equal to an arbitrary score of 4, are listed in Table 14 below. The highest recorded residue is 28.

Comparison between sub-group-	And sub-group-	Gives residual-
GpI-1	GpIa-1	1.54
GpI-3	GpIa-1	1.73
GpIa-2	GpIII-2	1.95
GpI-1	GpI-3	2.91
GpI-6	GpIa-2	3.13
GpI-1	GpI-4	3.38
GpI-6	GpIII-2	3.92
GpIa-4	GpIa-5	4.00

Table 14 Lowest 8 residuals calculated from comparisons between the 24 axe sub-groups. (Extracted from Appendix 5.6)

Comparison between Table 14 above and Sections 4.4.3, 4.4.6 and 4.5.2 shows the quantitative method clearly reflects the petrographic observations. The low residues between GpI-1, GpIa-1, GpI-3 and GpI-4 clearly indicate a marked similarity between these groups. Similarly, the comparison between GpI-6 and GpIa-2 returns a low residual supporting the observation in Section 4.4.6.2. A petrographic similarity between GpIa-2 and GpIII-2, and GpI-6 and GpIII-2 is not noted in the narrative indicating the usefulness of this procedure to identify possible matches.

4.8.3.8 Quantitative arithmetical comparison between selected axe sub-groups and exposures

Residues from comparisons between axe sub-group and selected (c.f. Section 4.7, Table 9) exposure thin section scores are reported in Table 15 (from data in Appendix 5.6). At this stage of the investigation it is not known what score constitutes a 'good' match, with more work being required to establish the relationship between the magnitude of the residue and the associated petrographic similarity. But, based on the assumption that a perfect match results in zero residue, then values close to zero must indicate a marked similarity in profile, (which is supported by findings discussed in Section 4.8.3.4 above) hence mineralogy & texture. Values extracted from Appendix 5.6 and reported in Table 15 below indicate that the lowest residuals (hence 'best' match) between axe sub-groups and greenstone *rocks* are between GpI-1 and GpIa, MM3, and GpI-6 and GpIII-2, MM4 (note that MM3 & 4 were not collected from actual greenstone exposures). The lowest residual between an axe sub-group and greenstone *exposure* is between GpIa and GUR001 & 2

(2.70) followed by GpIa-1 and ZEN002 (5.40) GpI-8 and PEN004 (5.40), GpIa-1 and PEN004 (5.80), and. GpI-1 and PEN004 (5.86) (Values from Appendix 5.6).

	GpI-1	GpI-6	GpIa-1	GpIII-2	MM4	PEN003	PEN004	ZEN002	GUR001, 2
MM3	**3.17**	12.38	**2.80**	12.00	11.25	14.00	7.00	6.60	5.50
MM4	10.18	**2.67**	10.45	**3.25**	-	7.25	8.25	8.65	10.75
PEN003	14.93	9.46	14.00	8.00		-	13.00	10.60	14.50
PEN004	5.86	10.92	5.80	7.80			-	**2.40**	4.50
ZEN002	6.30	11.32	5.40	8.60				-	4.10
GUR001/2	4.04	9.88	**2.70**	8.70					-

Table 15 Extract from Appendix 5.6 summarising residues of comparisons between selected axe sub-group and exposure thin sections. Residues less than 4.00, equivalent to the closest matches, are indicated in bold.

As stated above, by using this method it is found that the closest petrographic match between an axe sub-group and greenstone exposure is between GpIa-1 and the greenstone found at Gurnard's Head. However, any assumptions on provenance must be treated with caution as Section 4.7.7 indicates that the two Gurnard's Head thin sections shared petrographic similarities with GpI-7 and GpIa-3. Also, the Gurnard's Head samples contain secondary biotite, not often seen in axe thin sections and which is not covered in any of the calculations/categories above. Additional evidence for caution in interpreting the residues is given by one of the 'best' (i.e. the lowest residual) matches being between two exposure specimens PEN004 and ZEN002 (2.40), which are geographically separated by over 30km.

4.8.3.9 Remarks on the usefulness of quantitative arithmetical comparison

The most significant aspect of this method of comparison is that the single numerical value produced is related to the observed petrographic similarities, even after noting the difficulties discussed in the paragraph above. However, the relationship between the magnitude of the residual and the degree of petrographic similarity has not been ascertained, other than the lowest residuals represent the 'best' petrographic matches. This means that the magnitude of residues alone cannot be used to indicate petrographic matches with certainty, but does provide an indication of similarity. The addition of more scoring criteria, possibly related to the volume of minerals present, could improve the situation.

4.8.4 Final remarks on the new quantitative petrographic analysis system

The results of the petrographic examinations in Sections 4.4 to 4.7 are largely reproduced using the quantitative analysis system, not unsurprising since the same data source (petrographic observations) is used in both cases. However, the three analytical methods

of examining petrographic relationships within and between axe sub-groups and greenstone rocks using the quantitative data appears to have significant potential in discriminating between, and eventually recognising, different groups of thin sections. Eventually, it is anticipated that the relatively simple processes described above could assist with categorising and provenancing unknown basic igneous axe thin sections. This latter ambition relies on the development of an extensive database of quantitative exposure thin section data. The empirical basis of the quantitative system devised only relates to greenstone rocks so further investigation and analysis of other axe petrologies will be necessary in order to reveal the full potential of this system. However, it must be emphasised that the quantitative system requires the examination petrological thin sections and is therefore, still a partially destructive method of provenancing.

4.9 Summary and conclusions

It has been shown that IPC Group I, Ia, III & IIIa axe thin sections show sufficient petrographic variability within each IPC group to allow a total of 24 sub-groups to identified. The primary mineralogy of IPC Group I, Ia, III & IIIa axes of pyroxene + feldspar + opaque indicates an evolved (or evolving?) tholeiitic affinity. Subsequent low-grade regional and contact metamorphism has altered the primary mineralogy to some degree in all the axe thin sections reviewed in this work. Both these features (i.e. low-grade metamorphosed tholeiites) are found in the greenstone rocks of Cornwall, especially within the Mylor Slate Formation, which, in turn, includes a number of greenstone exposures around Mount's Bay.

No direct match between a single greenstone exposure and IPC Group I, Ia, III & IIIa axe thin sections has been achieved. However, similarities between some IPC Group I axes and greenstone rocks found on the west side of Mount's Bay at Penlee and Mousehole, the north part of Mount's Bay at Long Rock and the North Penwith coastline at Gurnard's Head and Zennor have been observed. This observation supports the Keiller et al. (1941) hypothesis that the source of IPC Group I is between Penzance and Mousehole, but adds the possibility of a provenance to outcrops found on the North Penwith coast. The closest mineralogical and textural match between axe and rock is between sub-group GpI-1 and MM3. Unfortunately, MM3 was not found in situ, but in close proximity to the North Penwith coast.

It has been possible to eliminate certain exposures as potential sources of IPC Group I & Ia, as greenstones found at Cudden Point, Trenow Cove and within the South Hams are distinctly different to IPC Group I axe thin sections. It has not been possible to match any IPC Group III thin sections with ones collected from the quarry at Perranuthnoe believed by the author to be the source of IPC Group III (Section 2.5.7). As stated earlier, there may be several reasons for this, but this failure does raise some question as to validity of the IPC provenance of this group.

A new petrographic analysis system based on empirical observations of thin section colour, grain size and presence/degree of alteration of pyroxene, feldspar, amphibole, chlorite, epidote, apatite and opaque minerals has allowed a quantitative assessment of the degree of petrographic similarity between individual and groups of thin sections. Bivariate and multiple parameter (profile) charts allowed the petrographic relationship within and between axe sub-groups, and between greenstone rock and axe sub-groups to be examined. Use of a simple arithmetical process allowed the magnitude of petrographic differences to be numerically established. In all, the results from using the quantitative analysis system have supported the qualitative observations of petrographic similarity between axe and exposure thin sections reported in Section 4.7. With a more extensive petrological database of axe and rock thin sections and development of more comprehensive scoring criteria it is believed that this system has the potential to discriminate between IPC axe groups, to assist with categorising axes and provide evidence for axe provenancing. However, it is based on a partially destructive process and this would limit its use to existing thin sections.

There are four main conclusions to be drawn from this chapter:

1. There is an observed level of petrographic difference within the IPC groups investigated, which calls into doubt the possibility of a single provenance for the whole group.

2. IPC Group I and Ia axe thin sections appear to have been drawn from the same population and, as many IPC Group Ia thin sections are similar to ones contained in IPC Group I, the need for IPC Group Ia is called into doubt.

3. Petrographic similarities exist between IPC Group I axe thin sections and rocks from exposures on the west side of Mount's Bay at Penlee, Mousehole and Long Rock, thus supporting the belief that IPC Group I is provenanced to this area. However, it is also seen that rocks from the North Penwith coastline at Zennor Point and Gurnard's Head are also similar to some IPC Group I thin sections.

4. The new empirically based quantitative analysis system can be used to observe and measure petrographic differences between groups of thin sections and has the potential, with a larger database and more comprehensive criteria, to be able to categorise and indicate a provenance for unknown thin sections.

5 Use of magnetic susceptibility in the non-destructive provenancing of British Neolithic greenstone axes

5.1 Introduction

Measurement of magnetic susceptibility (MS) has been shown to be a rapid and cost effective method of non-destructive characterisation of archaeological artefacts and has enabled the provenancing of Roman granitoid columns to sites *within* the originating quarry (Williams-Thorpe & Thorpe 1993, Williams-Thorpe et al. 1996). The ability to provenance archaeological artefacts to a geographical location using this non-destructive methodology is investigated for greenstone axes, with the investigation largely following the processes used by Williams-Thorpe & Thorpe in the provenancing of Roman granitoid columns (op. cit.). The performance of the magnetic susceptibility measuring device (KT5 meter) is examined in the first half of this chapter and includes a discussion of the performance of the KT5 in measuring stone axes. The second half of the chapter reports the results from measuring over 225 British Neolithic greenstone axes and from 5 greenstone exposures, and examines the potential to use MS to provenance axes to exposures.

5.2 Terminology

The KT5 meter is calibrated assuming that the area where the sample is measured is flat, and of 'infinite' surface dimension (i.e. a circle >100mm can be inscribed on the surface to be measured) and thickness (i.e. the sample is >60mm thick, beneath the measured surface) (Exploranium 1990, c.f. Section 5.5.1). KT5 measurements on samples that do not meet these criteria will need to be adjusted so that the correct MS value can be established. Therefore, to avoid confusion when discussing KT5 MS measurements the following terminology will be used: -

'reading' is defined as an individual value displayed by the KT5

'measurement' is defined as the average of several *readings*

'uncorrected' refers to the actual KT5 measurement or reading (e.g. an 'uncorrected measurement' is the average of a number of readings before any adjustment to the value are made)

'corrected' refers to *readings or measurements* that have been adjusted to take into account sample shape

'true rock' is used to indicate the MS value of a sample when no corrections were necessary.

Additional terminology relating to sample surface and shape will be introduced in Section 5.5.2.

5.3 Short review of magnetic susceptibility (MS)

Magnetic Susceptibility (MS) defined as a measure of a sample's susceptibility to magnetisation, with its value determined by measuring the effect of applying a known magnetic force to the sample. The induced magnetic intensity, J_i, is only present when the inducing magnetic field, H, is present and is therefore a temporary property of the sample. The constant of proportionality, *k*, that relates the strength of the magnetising force of an inducing field, H, with the intensity of induced magnetisation, J_I, is a measure of the MS. Hence, *k* can only be measured whilst the magnetising force is applied. Both H and Ji are measured in Amps/metre (Am^{-1}) and are related by the equation $J_i = kH$, where *k* is normally measured in non-dimensional SI units. MS should not be confused with thermo-remanent magnetism that is 'fixed' within a sample as it cools below the Curie Point and is related to the Earth's magnetic field at that time.

The magnitude of MS is almost totally dependent upon the presence, size and type of ferrimagnetic minerals within the sample being measured. Magnetite is the largest single mineralogical contributor to *k*, with a single crystal measuring as much as 150 SI (Sharma 1976). Ilmenite, which is a common accessory mineral within greenstones, has a much smaller magnetic susceptibility, between 0.01% and 20% of magnetite (c.f. Williams-Thorpe & Thorpe 1993). Low-grade metamorphism and surface weathering can affect the potential MS of rocks. During low-grade metamorphic events, minerals such as magnetite and ilmenite can often be partially or totally altered to secondary, non-magnetic minerals (e.g. ilmenite to leucoxene) thus reducing the potential MS. Weathering can oxidise ferric/ferrous minerals on the surface and within cracks in the rock and again can reduce the overall MS of the rock. These factors are probably two of the reasons why most greenstones encountered during this work have low magnetic susceptibility values, commonly less than 2×10^{-3} SI. However, the dominant factor for low MS values is almost certainly the scarcity of ferrimagnetic minerals in greenstones (c.f. Chapter 4).

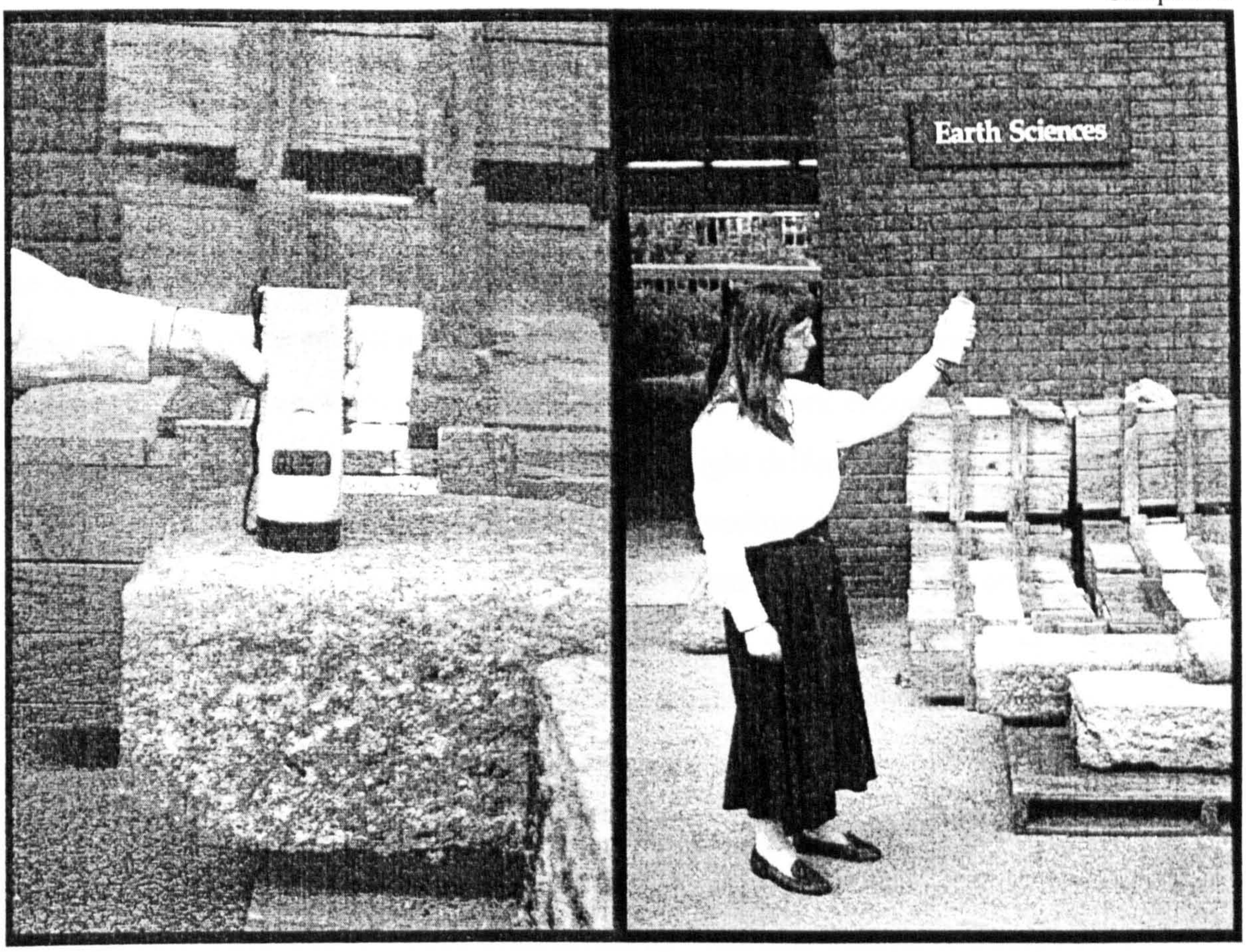

Figure 43 Exploranium KT5 magnetic susceptibility meter in use gently pressed against a sample (a) and being zeroed in air (b)

5.4 Exploranium KT5 Magnetic Susceptibility meter: description, operation, performance and precautions

5.4.1 Description of KT5 MS Meter

An Exploranium G. S. Ltd. KT5 magnetic susceptibility meter was used exclusively to obtain magnetic susceptibility measurements of implements and exposures alike (Figure 43). The KT5 measures in size 65 x 65 x 187mm, weighs 0.35kg and is powered by a single 9V alkaline battery. The meter is calibrated in SI units x 10^{-3} with a resolution of 0.01 x10^{-3} SI (for low values of MS) and it is operated through two push buttons, one to activate the measuring process and one to review the (up to 12) stored measurements.

5.4.2 Operation

The two-stage measurement process involves activating the KT5 in air at greater than 0.3m away from any magnetic material to give a 'background' reading which represents zero baseline (Figure 43b). The second stage involves gently placing the KT5 sensor head (Figure 43a) against the sample and re-activating the KT5. Magnetic susceptibility is determined by the KT5 microprocessor from the difference in induced frequency of the sensor head between the two operations (Exploranium 1990, c.f. Williams-Thorpe &

Thorpe 1993). The whole procedure takes approximately 5 seconds for each reading, and approximately 1-minute for a measurement consisting of 10 readings.

5.4.3 Performance

The KT5 measures 'apparent susceptibility' and not 'true magnetic susceptibility', and for values less than 100 x 10^{-3} SI units the difference between apparent and true susceptibility is less than 5% relative (Exploranium 1990). Since this work encountered MS magnitudes less than 10 x 10^{-3} SI in the majority of cases, the slight difference between apparent and true magnetic susceptibility is only noted and KT5 readings have not been adjusted for this factor. Therefore, all MS readings in this work are that of apparent MS only.

It is assumed that the KT5 calibration and accuracy has not altered throughout the measurement period (1996-1999). This assumption is based in part on the results obtained by Williams-Thorpe & Thorpe (1993) and Williams-Thorpe et al. (1996) and the consistency of the magnitude of greenstone rock/axe measurements (commonly <2 x 10^{-3} SI). Precision of the KT5 has been established by Williams-Thorpe & Thorpe (1993) at 5% relative (1 sigma) for a value of 0.2 x 10^{-3} SI and 0.2% relative (1 sigma) for a value of 7 x 10^{-3} SI. As part of this thesis, eleven fully replicate measurements of a 0.5cm thick slice of sample MM3 (a typical greenstone), measuring 10.0cm x 7.5cm were made. The average MS for this piece of MM3 was established at 0.61 x 10^{-3} SI with a (sample) standard deviation of 0.01 x 10^{-3} SI (Appendix 8.1, measurement MM3- 5). This gives a relative precision of 1.5% at a typical level of MS response for greenstones, complementary to that obtained by Williams-Thorpe & Thorpe and further suggests little, if no, movement in KT5 precision between 1993 and 1999 (the same KT5 meter was used in both projects).

5.4.4 Precautions taken when using KT5

The location of the KT5 placement can affect the value of the reading. Williams-Thorpe et al. (2000) showed that different 'background' materials affect the reading depending upon the sample thickness and the type of substrate. In their work Williams-Thorpe et al. (op. cit.) show that a sample thickness of 50mm is sufficient to mask 98% of the influence the background material may have (Williams-Thorpe et al. 2000: figure 2). Since all axes and rock samples in this work were measured in 'air' (see below for method of measuring axes) this effect was not encountered and, therefore, no adjustments to KT5 readings made.

Two other precautions involved avoiding heavily weathered areas of rock surfaces, as these measurements would not return a true rock value, and measuring representative areas of rock, away from mineral veins.

However, an observation made whilst measuring a sample indoors is worth a cautionary note. Greenstone rock sample MM3, weighing 16kg and greater than 30cm in diameter, was placed on the kitchen floor at the author's home, and measured using the KT5. The KT5 returned a reading of 0 (zero) SI and not the expected greenstone value of around 1 x 10^{-3} SI. Subsequent investigations used a 1kg jar of coarse iron filings with MS measured at approximately 600 x 10^{-3} SI using the KT5 meter. Repeated KT5 readings showed rapidly (probably exponential) diminishing values, starting at 600 x 10^{-3} SI 1.5m above the kitchen floor, reducing to 0 SI at floor level. The reason for this reduction in response is not understood, although it is suspected that the pre-stressed concrete floor beams may have contributed in developing a diamagnetically opposed induced field, thus swamping the paramagnetic effect induced in the sample. This effect was noted early on in the research, and subsequently all measurements taken within buildings were made with the sample elevated at least 1.5m above floor level.

5.5 Requirement and application of factors used to correct KT5 readings for small and irregular-sized samples (especially axes)

5.5.1 Overview of need for correction factors

The KT5 is calibrated assuming its sensor head is placed on an absolutely flat surface of a magnetically homogeneous sample that is at least 10cm in diameter and more than 6cm thick (Exploranium 1990: section 4). Any sample that does not meet these criteria would return KT5 MS readings lower than for a piece of the same sample meeting or exceeding the physical dimensions described above. Therefore, KT5 MS readings of non-ideal samples need to be adjusted using pre-determined factors that 'correct' the KT5 reading to give a 'true rock' value (Exploranium 1990). An added complication for stone axes is that not only do they have irregular surfaces and are often less than the prescribed dimensions, they also have curved surfaces and are often wedge-shaped. This results in the need for several corrections to the KT5 readings of typical stone axes before the equivalent 'true rock' MS can be established.

5.5.2 Additional terminology

The following terminology is used when discussing the various correction factors required to establish the true rock value of MS for a less than ideal sample:-

'peak to pit' is defined (by Exploranium) as the difference between the highest peak and deepest pit in the area to which the KT5 is applied whilst taking a reading (Exploration 1990, c.f. Figure 44).

'irregular surface', *'irregular surface relief'* or *'surface relief'* are used when describing a non-flat surface. The *value* given for *surface relief* is the average, or range of pit to peak differences (in mm) on the surface being measured.

'effective gap' is used to describe the gap that would appear between the KT5 sensor head and the sample if it were possible to flatten the irregular surface of the sample without moving both sample and KT5 (c.f. Figure 44 and 45).

5.5.3 Correction factors for irregular surface relief

The KT5 is calibrated assuming that its sensor head (i.e. measuring surface) is in full and even contact with the sample's flat surface: any gap between the two surfaces will reduce MS readings. The reduction in readings is quantified by Exploranium (1990), who indicate that there is a relative 50% decrease in the value of MS when there is a uniform 5mm gap between the KT5 sensor head and the flat surface of a sample. This relative decrease in readings increases to 90% with a 20mm gap, and 99% with a 60mm gap (Exploranium 1990: figure 16).

In practice a uniform (i.e. parallel) gap between the sample and the KT5 sensor head is not experienced, instead an *irregular surface* in normally encountered where the KT5 may only be in contact with the sample at points over the measuring surface (c.f. Figure 44c). In order to adjust the KT5 reading made on an irregular surface Exploranium provide a series of correction factors based on the 'peak to pit' distance of the irregular surface and these factors are repeated in Table 16 (and displayed graphically in Appendix 7.1). Additional factors representing 11mm & 12mm peak to pit differences (encountered on some axes –see Section 5.5.4 below) have been estimated by visually extrapolating the Exploranium data.

What is not defined, but can be deduced from Exploranium 1990: table 1 and figure 16, is that the assumption made by Exploranium is that their irregular surface is symmetrical. The 'peak to pit' distance quoted by Exploranium (1990: table 1) is equal to an *effective*

gap between the KT5 sensor head and the sample equal to half the peak to pit measurement (Exploranium 1990: figure 1). For example, a gap of 5mm reduces the value of MS by 50% (figure 16) hence requiring a correction factor of 2 to increase the observed MS value to the true rock value. Simultaneously, table 1 indicates that a 10mm irregular surface requires a correction factor of 1.96 (i.e. approximately 2). Hence it is assumed that a peak to pit difference of 10mm is the same as a gap of 5mm. (The slight difference between 2 and 1.96 is explained by the small scale of the graph in Exploranium' s figure 16, which prevents an estimate of the correction factor to more than two significant figures.)

Surface Relief (mm) (peak to pit difference)	Exploranium Correction Factor	Effective gap (mm)
1	1.07	0.5
2	1.15	1.0
3	1.23	1.5
4	1.32	2.0
5	1.41	2.5
6	1.51	3.0
7	1.61	3.5
8	1.72	4.0
9	1.84	4.5
10	1.96	5.0
11	2.08	5.5
12	2.21	6.0

Table 16 Irregular surface relief correction factors from Exploranium KT5 Manual, table 1, showing the correction (multiplication) factors for uneven surfaces, with added column indicating effective gap between a sample's flat surface and the KT5 sensor head. Factors for 11mm & 12 mm have been determined by graphically extrapolating the Exploranium data.

Observation of irregular surfaces on over 225 stone axes and several rock exposures revealed that it is not possible to determine whether the surface relief is symmetrical or not, thus calling into doubt the correction factor based on the maximum peak to pit difference (c.f. Figure 44). However, since it is almost impossible to estimate the effective gap of an irregular surface with any accuracy it was decided to base the correction for irregular surfaces on a visual estimation of the average peak to pit difference on the surface to be measured. In practice, the average peak to pit difference was estimated to the nearest mm, or to a range of values if the degree of surface irregularity differed over the sample. For example, a measurement of surface relief of 1mm indicates that the average peak to pit difference on the sample is visually estimated at 1 ± 0.5mm. A measurement of 0mm indicates the surface of the sample is smooth (not necessarily flat – see section 5.5.4 below) and a measurement of 2-3mm indicates the average peak to pit differences vary over different areas of the sample and that a single figure is difficult to determine. In this latter case, it is probable that the *average* peak to pit difference, hence surface relief, of the whole sample lies between 2 and 3mm.

Cartoon illustrating the measurement of 'surface relief' for a typical stone axe

Note that the terms - 'peak to pit' and 'surface relief' are used synonymously

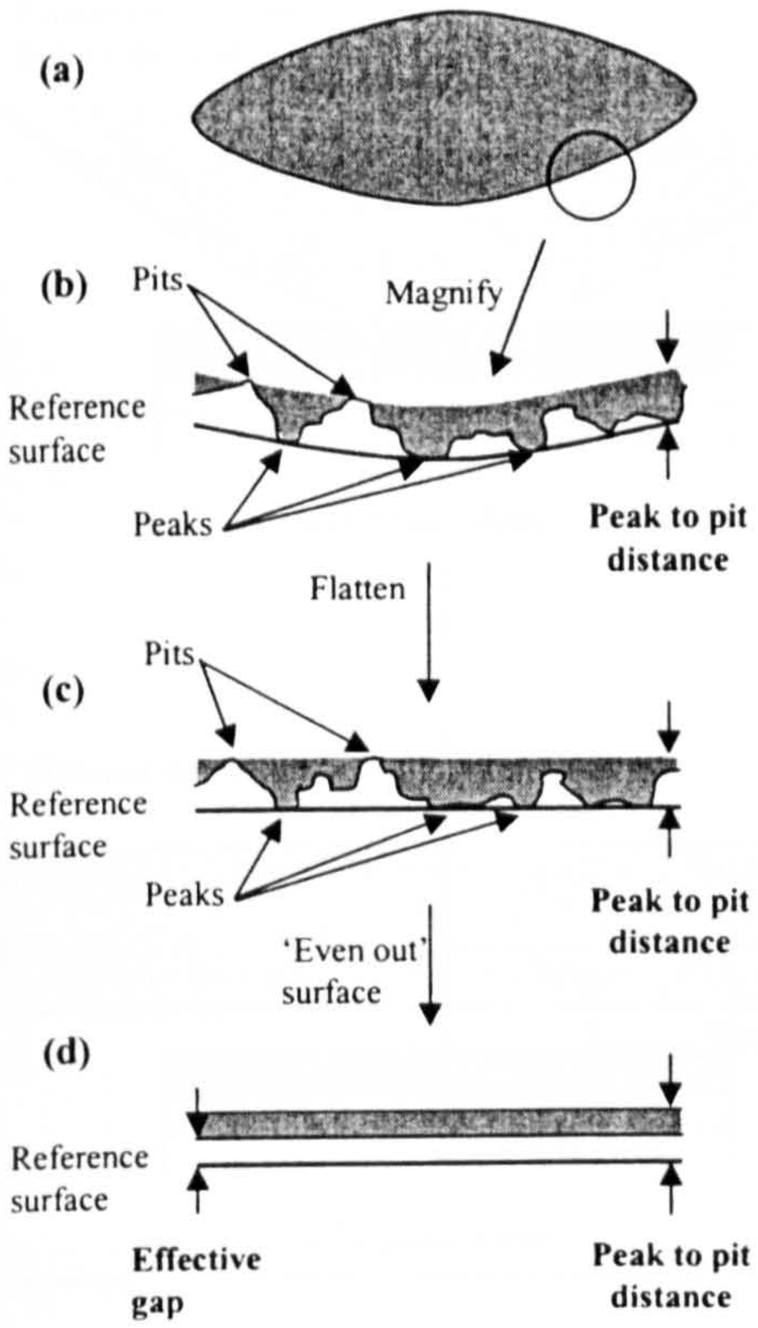

(a) Typical cross section of stone axe
(not to scale)

(b) Magnification of part of irregular surface of axe.
The 'surface relief' or 'irregularity' recorded for axes and rocks is the maximum 'peak to pit' difference, to the nearest mm, estimated by eye.

(c) 'Flattening out' the magnified curved surface has minimal effect on the estimate of the peak to pit difference and no adjustments to the estimation is made.

*Note: an adjustment for the potential air gap caused by the curvature of the axe surface **is** required (c.f. Section 5.5.4)*

(d) When the magnified irregular surface has been 'evened out', the resulting situation can be represented by a solid block of rock, plus an 'effective' air gap to the reference surface. The depth of the **effective gap** is less than the 'surface relief' measured. Thus the visual estimate of surface relief is equivalent to the maximum possible effective air gap.

For example: assume the maximum peak to pit distance estimated by eye is 1mm then the **effective gap** will be < 1mm. Assuming symmetry of surface relief (c.f. Section 5.5.3) the effective air gap would be measured at half the peak to pit difference; 0.5mm. However in practice surface relief is not always so symmetrical which means that the Exploranium assumption may not hold and the effective gap, and subsequently the correction factor for surface relief may cause an under or overestimate of the magnetic susceptibility.

Figure 44 Cartoon illustrating the measurements of surface relief for a typical axe and illustrating the relationship between the peak to pit difference and the effective gap

5.5.4 Corrections for surface curvature

Corrections must also be applied to KT5 readings when the instrument is used to measure a curved surface, because when measuring a curved surface the sensor head cannot be in full and even contact over the whole area to be measured. Exploranium provide a set of correction factors to use when measuring cylindrical surfaces of diameters 60 to 120mm (e.g. drill cores) (Exploranium 1990: table 3). Williams-Thorpe & Thorpe (1993) have determined factors for diameters between 30 and 130cm by establishing the size of the effective gap between the KT5 sensor head and the column. Using empirical methods Williams- Thorpe and Thorpe (op. cit.) showed the two dimensional ratio of gap to sample (equivalent to the ratio of areas a:b indicated in Figure 45) was 74:26, based on a 30cm column. Using table the Exploranium KT5 Manual: table 1, corrections for uneven surfaces, Williams-Thorpe & Thorpe then went on to establish the correction factor for columns of 30cm diameter as 1.13, reducing to 1.01 for columns of 100cm diameter. These empirically determined factors were subsequently tested on two granite columns with corrected KT5 measurements of curved surface being within 1% relative of the measurement made on the flat end of the same column (Williams-Thorpe & Thorpe 1993).

Determination of the effective gap between the KT5 sensor head and a typical axe.

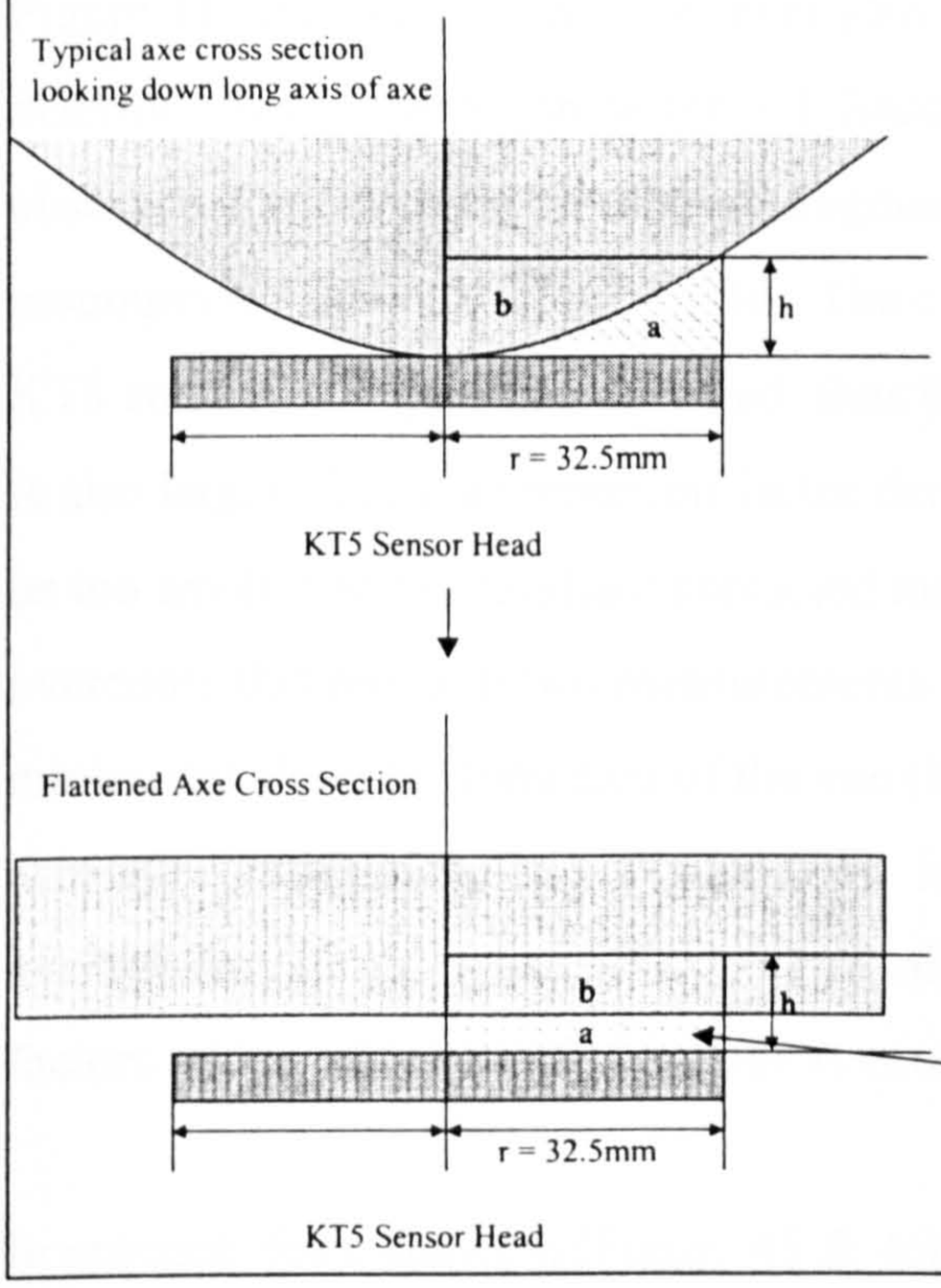

The aim is to establish the effective gap represented by the area 'a' in the diagrams.

In order to achieve this it is assumed that the curvature as viewed along one of the major *axes* of a typical greenstone axe is parabolic and can be represented by the simple quadratic equation:

$f(x) = mx^2$, where $m = h/(r)^2$ (r = 1/2 diameter of the KT5 sensor head)

Area 'a' is the area beneath the axe surface (represented by the given quadratic equation). This size of the area can be obtained by integrating f(x) between limits 0 and r.

Hence

$a = \int mx^2$

$a = [1/3mx^3]$

when $x = r$ and $m = h/r^2$ this gives

$a = 1/3rh$

and since the total area (a + b) = rh

The ratio a/(a+b) is 1/3

This means that the **effective gap** represented by the area 'a' beneath the axe is equivalent to 1/3h of the distance between the edge of the KT5 sensor head and the axe.

Figure 45 Cartoon illustrating the relationship between the curvature of a typical greenstone axe and the effective gap so that a correction factor for axe curvature can be determined (c.f. Section 5.5.4)

Typical axe surfaces are asymmetrical and curved in more than one plane as opposed to a single plane for drill cores and cylindrical columns. This means that the published correction factors for cores and columns are not totally suitable to correct measurements made on axes and therefore, a new method of determining the correction factor to adjust axe MS measurements is required.

The following method to establish curvature corrections for axe MS measurements is based on estimating the effective gap between the KT5 and axe (similar to that used by Williams-Thorpe & Thorpe 1993). The width of the effective gap is directly related to the surface relief correction factors (c.f. Section 5.5.3 - 3rd paragraph) and therefore, a curvature correction factor can be determined. Figure 45 illustrates that the effective gap between the KT5 sensor and a typical axe is equal to one-third the distance between the edge of the KT5 sensor head and the surface of the axe (h in Figure 45), assuming the following:

1. That the axe is symmetrical and the surface is parabolic, not circular.
2. The axe surface is smooth
3. Only curvature in one plane is considered

In practice, axe morphology is highly variable and these assumptions are based on the ideal situation. Observations of over 250 axes indicate that in most cases axe curvature is approximately parabolic (i.e. not circular) and symmetrical, thus assumption 1 above

generally holds true. Many axes were observed to have pitted and eroded surfaces (c.f. Figure 44) and thus, the surface relief also needs to be taken into account when determining the correction factor (c.f. Section 5.6). Almost every axe and part axe observed was curved in all three orthogonal axes (c.f. Figure 46) and this means that assumption 3, above, does not hold. The consequences of this are that the gap between the KT5 and axe is larger than assumed, thus the effective gap (represented by h in Figure 45) is also larger. Thus, a correction factor derived using the assumptions above in reality, will be too small, and the resultant corrected measurement of MS will be too low. To overcome this problem two measurements of axe curvature were made, one (usually the minimum) along the long axis of the axe (Figure 46b) and one (usually the maximum) across the width of the axe (Figure 46c). It is expected that these two values bracket the average curvatures, hence effective gap, of the axe and provide a range of correction factors within which the *correct* one is contained, but see discussion below.

In practice, the distance h (Figure 45 & 46b & c) was estimated by eye, to the nearest mm, with *half* (h/2) of this value being recorded as the axe curvature. The correction factor was then determined using h/2 and the surface relief correction table (Table 16, and Appendix 7.1). The distance h/2 is used in preference to the calculated distance, h/3, for two reasons. Firstly, as described above, the calculated effective gap (h/3) based on the assumptions above is too small and even using the two measurements of curvature, the range of corrections would probably be on the low side, thus potentially resulting in underestimation of MS. By using h/2 instead of h/3, the potential for underestimating the vale of MS is reduced (by h/6). Secondly, it was generally difficult to measure h with any degree of accuracy because of the varied axe morphology and it was simpler to record h/2 than h/3. The following example illustrates the effect of using h/2 as opposed to h/3. Assume h is measured as 6-8mm (a typically encountered axe curvature). Then using h/2, the range of correction factors is 1.23 (3mm) to 1.32 (4mm). Using h/3, the range of correction factors is 1.15 (2mm) to 1.20 (2.67mm). Thus, not only is the magnitude of correction factor increased, the range is also increased. The use of h/2 to generate a curvature correction factor is empirically examined in Section 5.7 below.

5.5.5 Corrections for sample surface dimensions (below 10cm in diameter)

The KT5 calibration assumes the object being measured covers the 6.5cm-diameter KT5 sensor head with at least a 1.75cm overlap either side (i.e. >10cm diameter object). The Exploranium KT5 manual provides correction factors for objects with inscribed diameters

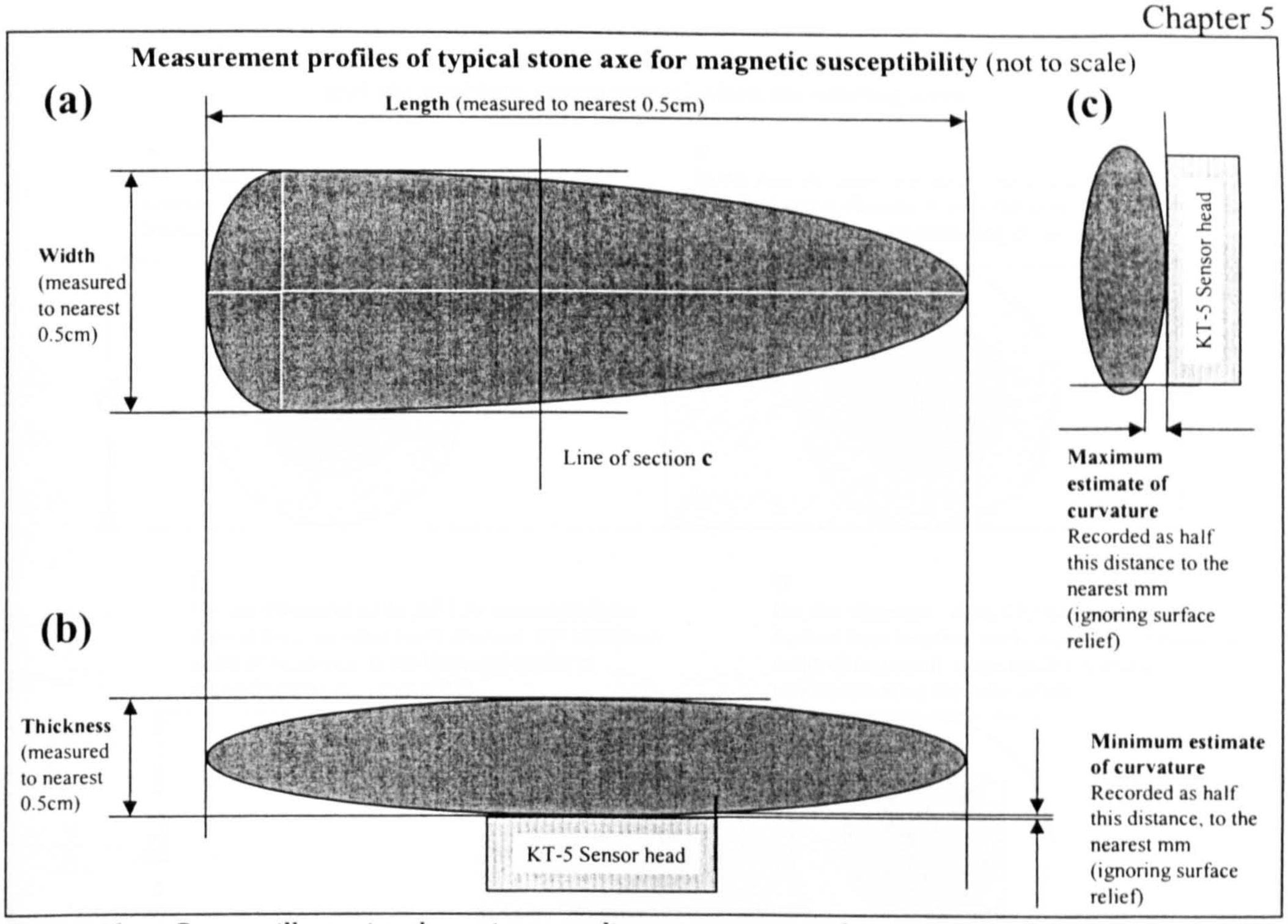

Figure 46 Cartoon illustrating the various axe dimensions measured to provide the basis for subsequent corrections to magnetic susceptibility measurements (c.f. Sections 5.5.4 to 5.5.6)

down to 6cm, i.e. just below the size of the sensor head. These correction factors are reproduced in Table 17 and graphically illustrated in Appendix 7.2 with additional factors for inscribed diameters of 40, 45, 50 and 55 mm obtained by extrapolating the Exploranium data using cubic regression analysis (cubic regression provided the best fit to the published data). Exploranium do warn that it is ineffective to measure on surfaces having less than 6cm inscribed diameter (Exploranium 1990), hence measurements of MS on axes less than 6cm in width/length should be treated with caution.

Diameter (mm)	Correction Factor
40	1.48
45	1.39
50	1.31
55	1.25
60	1.19
65	1.15
70	1.11
75	1.08
80	1.05
85	1.04
90	1.03
95	1.02
100	1.01

Table 17 Correction factors for sample diameter (width/length) with factors for 65, 75, 85 & 95 mm determined by interpolation and factors for 40, 45, 50 & 55 mm determined by extrapolation of the Exploranium data using cubic regression analysis (Exploranium KT5 Manual, table 2)

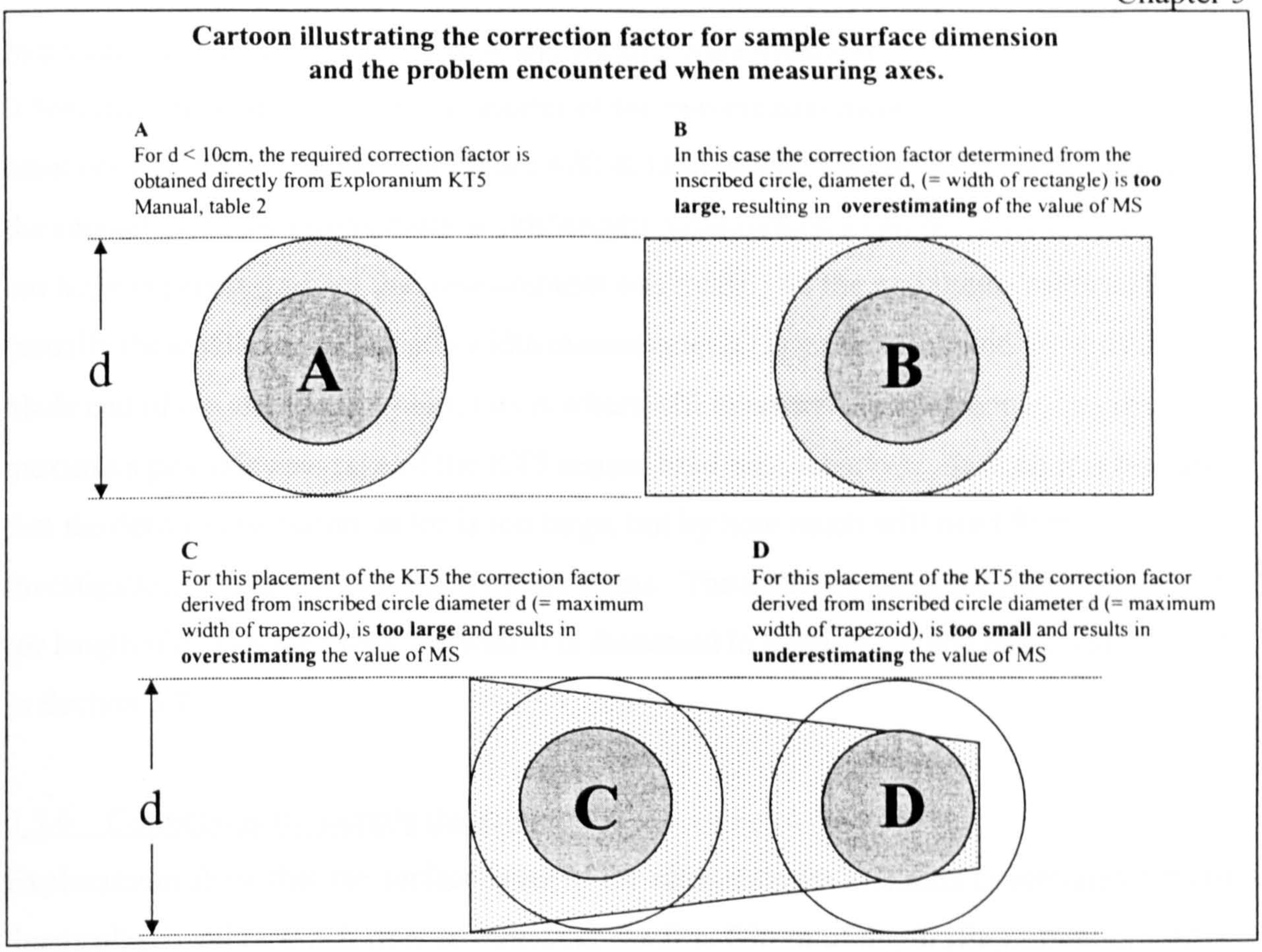

Figure 47 Cartoon illustrating the problem with estimating a correction factor for surface dimension. The smaller circles (dark stipple) represent the KT5 sensor head, the larger circles (lighter stipple) represent an inscribed circle of diameter 'd' (see Section 5.5.5 for discussion)

Figure 47 illustrates a problem associated with using this correction for axes. The correction factor assumes a circular cross-section (and is flat and 'infinitely' thick), as shown in Figure 47A. Figure 47B shows the situation where the surface is not circular. In this case the material outside the inscribed circle results in a higher MS reading, meaning that application of the correction factor, based on the diameter of the inscribed circle, results in an overestimating of the true value of MS, i.e. the correction factor is too large. Figure 47C & D illustrate a similar situation to that which is encountered when measuring axes. In Figure 47C the material outside the inscribed circle has greater effect on the value of MS than the material missing inside the inscribed circle. Hence, the correction factor based on the maximum width of the trapezoid (representing a stylised axe and equal to the diameter (d) of the inscribed circle in this case) is too large, resulting in an overestimation of the real MS value. The opposite occurs in Figure 47D, where the effect of the material 'missing' (effectively reducing the value of MS) inside the inscribed circle is greater than the material outside the inscribed circle. Hence, in this case the correction factor based on the maximum width is too small, resulting in an underestimation of the real value of MS.

In practice, the maximum axe widths and lengths were measured by eye to the nearest 0.5cm using a 30cm rule, with the shorter of the two measurements used to derive the associated correction factor. As Figure 47C & D illustrate, the correction factor based on the smaller of the two (maximum width/length) measurements can be either too small or too large depending where the measurement was made. As the maximum width of the axe (usually the smaller of the length-width measurements) is generally found towards the blade end of the axe (Figure 46a), this is where MS measurements were made so that maximum possible coverage of the KT5 sensor head was achieved. As such it is probable that the derived correction factor is too large, but by how much will need further investigation, above that presented in this thesis. The effect of using the maximum width (or length if it is smaller than the width) is discussed in Section 5.6 and empirically tested in Section 5.7.

5.5.6 Corrections for sample thickness

Exploranium show that the surface layer of the sample down to 20mm contributes 90% of the displayed value which rises to >99% for the first 60mm of depth (Exploranium 1990: page 14 and figure 16). Using a series of polished blocks of Whin Sill quartz dolerite, ranging in thickness from 3 to 48mm, thus allowing stacks of differing overall thickness to be made, Williams-Thorpe et al. (2000) investigated the effect of sample thickness on KT5 readings and determined correction factors for sample of thickness 3 to 102mm using curvilinear regression. These factors are reproduced in Table 18 (to 2 decimal places) and graphically illustrated in Appendix 7.3 for sample thickness between 5 and 60mm.

Mean Thickness (mm)	Correction Factor
5	1.88
10	1.35
15	1.18
20	1.11
25	1.06
30	1.04
35	1.02
40	1.01
45	1.01
50	1.01
55	1.00
60	1.00

Table 18 Correction factors for sample thickness (Taken from Williams-Thorpe et al. 2000; table 1, rounded to 2 decimal places)

Based on observations of over 250 axes it is seen that axes vary in thickness over the length of the axe, with maximum thickness usually found towards the blade end of the axe.

Therefore a correction factor based on the measured maximum thickness of the axe will result in an underestimation of the real value of MS. This underestimation is due to the gap between the KT5 and the axe and a similar *gap* on the other side of the axe between an imaginary plane touching the point (or area) of maximum thickness and parallel to the KT5 sensor head. The gap between the KT5 sensor and the axe has already been accounted for by deriving the curvature and irregular surface correction factors and (with the assumptions on compounding corrections discussed below) these corrections effectively make the axe surface *flat*. Thus, the underestimate of the value of MS is directly related to the *gap* on the side away from the KT5. Noting that 90% of the displayed MS originates from the first 20mm and that axes were observed to be generally greater than 20mm (and predominantly >30mm) thick at their thickest point, the magnitude of the underestimate is expected to be small. This expectation is empirically examined in Section 5.7.

5.5.7 Non-magnetically homogeneous and weathered samples

There are no correction factors to take account of a sample not being magnetically homogeneous. Likewise, there are no correction factors available to counter any effect the weathering of a sample may have on MS. The first of these two factors is witnessed through significant variations in MS readings over the surface of the sample; variations that cannot be associated with non-ideal dimensions. The second is more difficult to notice as the weathering may have formed a thin (1 to 5mm) crust over the sample where any magnetic minerals have been eroded or altered, thus resulting in a lower value of MS (the crust acting like and air gap, see Section 5.7 below). To overcome these two factors, fresh samples or exposure surfaces are used wherever possible, with MS measurements made away from obvious mineralogical differences in the sample (e.g. mineral veins). This is not always possible with axes, as apart from cleaning the axe, no other preparation of the axe surface is allowed. Hence, these factors are borne in mind when taking and examining axe MS measurements.

5.6 Derivation of a single correction factor for axes and rock samples

Most axes and some rock samples have dimensions (length, width, thickness, surface relief and flatness) that require corrections to the MS readings in order to determine the true rock value, which are necessary so that the MS of axe, rock and exposure can be directly compared. The relevant correction factor is used to multiply the KT5 reading in order to determine the true value of MS, and it is assumed that the three correction factors introduced in Section 5.5 (surface relief (including curvature), surface dimension and

thickness) can be compounded. That is, if more than two criteria do not meet, or exceed, the minimum requirement (e.g. the surface being measured is not flat) then the correction factor for each case can be multiplied together and used to adjust the KT5 reading towards the true value. Using this assumption it is possible to establish and an overall correction factor for the sample as described below

Since two estimations of curvature are commonly made (section 5.5.4 above) and surface relief is sometimes given as a range of values then it is possible to generate two overall correction factors. Following the discussion in Section 5.5, it is believed that the 'true' correction factor for curvature and surface relief will lie between these two estimates. The generation of the corresponding two overall sample correction factors is illustrated below:

Let S_{max} = overall sample correction factor – **max**imum (i.e. maximum correction factor: the 'true' correction factor is less than this value)
Let S_{min} = overall sample correction factor – **min**imum (i.e. minimum correction factor: the true correction factor is greater than the value)
and
Let CR_u = correction factor from Table 16 established by adding (h/2 derived from the larger of the two measurements of curvature) and (the larger of the two measurements estimating surface relief). This is representative of the maximum (theoretical) gap between the axe and KT5)
Let CR_l = correction factor from Table 16 established by adding (h/2 derived from the smaller of the two measurements of curvature) and (the smaller of the two measurements estimating surface relief). This is representative of the minimum (theoretical) gap between axe and KT5)
Let **T** = correction factor from Table 18 established from the measurement of maximum sample thickness
Let **W** = correction factor from Table 17 established from the smaller of the measurements of maximum length and maximum width of the sample.
(Note that CR CR_u and CR_l are expected to bracket the 'true' correction value for surface relief and that **T** is probably an underestimate, and **W** is probably an overestimate.)

Using the above definitions the whole sample correction factor **maximum value (upper limit)** is found by
$S_{max} = CR_u \times T \times W$

And the whole sample correction factor **minimum value (lower limit)** is found by

$$\mathbf{S_{min} = CR_l \times T \times W}$$

The generation of whole sample correction factors is illustrated using the following example. Consider a typical greenstone axe that is recorded as having 1-2mm surface relief, 4-6mm curvature (h/2) and is 15cm long, 5cm wide (at its widest point) and 3.5cm thick (at its thickest point). The overall factors are generated as shown in Table 19 below:

	Combined relief (CR) (Table 16)	Width (W) (Table 17)	Thickness (T) (Table 18)	Overall correction factor
Maximum Correction factor	2 + 6 = 8mm 1.72	5cm 1.31	3.5cm 1.02	**Upper Limit 2.29**
Minimum Correction factor	1 + 4 = 5mm 1.41	5cm 1.31	3.5cm 1.02	**Lower Limit 1.88**

Table 19 Illustration of the calculation of maximum (upper limit) and minimum (lower limit) overall correction factor limits for a typical greenstone axe. These factors are used to multiply the KT5 readings to obtain a maximum and minimum value for the true rock MS.

The expectation is that the true rock value of MS of the axe lies between the uncorrected KT5 measurement multiplied by 2.29 (the maximum (upper limit) overall sample correction factor) and 1.88 (minimum (lower limit) overall sample correction factor), based on the given measurements and assuming that:

1. the sample is magnetically homogeneous and not weathered
2. the underestimate of the correction factor obtained from measuring the maximum thickness is small
3. the overestimate of the correction factor obtained from the smaller of the maximum width/length measurements is small (and balances out the effect of the underestimate associated with the thickness correction)
4. the individual correction factors can be multiplied together to form an overall correction factor

5.7 Empirical investigation into compounded correction factors

5.7.1 Overview of experiment

In order to test the effectiveness of the overall correction factors, introduced above, the KT5 was used to measure a number of variably shaped and finished pieces of greenstone rock. These pieces were the by-products from two rock samples, MM3 and PTX002, used in the manufacture of axes (called proto-axes) to investigate the performance of the PXRF in measuring uneven and weathered surfaces (c.f. Chapter 6). As each of the pieces were

unique, with different dimensions, thickness' and variably curved surfaces, it was expected that the corrected (i.e. true) value of MS for each piece of the associated sample would be similar, thus providing a good test for the ideas introduced in Section 5.6.

Both MM3 and PTX002 were chosen as raw material for the manufacture of stone-axes as it was believed they represented 'typical' greenstone rock. As these samples were not directly extracted from a known greenstone exposure, MS measurements of the actual exposure are not available. However, the original size of MM3 (a boulder > 30cm diameter) meant that a MS measurement relating to 'infinite' size was possible. Unfortunately, PTX002 (a brick-shaped boulder measuring 220 x 120 x 80mm) was broken prior to any measurement, and thus a MS value relating to 'infinite' size is not available.

5.7.2 Procedure

All MS measurements were made sequentially, on the same day, using the Exploranium KT5 meter and the method identified in Section 5.4.2. In total, four pieces of PTX002 and five pieces of MM3 were measured, with at least 9 individual measurements made on all four pieces of PTX002 and four of the five pieces of MM3. The relatively small size of the pieces of rock compared with the KT5 sensor head meant that some of the readings were overlapping, i.e. the areas covered by the KT5 sensor head were partly overlapped. Results of the investigation are described below and are detailed in Appendix 8.1, which also includes the dimensions of the individual pieces of MM3 and PTX002. The results are graphically displayed in Appendix 8.2.

5.7.3 Results and discussion

5.7.3.1 MM3 results

Measurement reference MM3-1 consists of 11 readings made on a fractured but generally flat, fresh surface of a large, 6kg, piece of MM3, with its surface relief estimated at an average 2-3mm peak to pit (typical of those encountered at exposures). The 10 readings making up measurement MM3-2 were made on a weathered part of the same piece as for MM3-1. In this case a weathered crust was estimated at 1-2mm thick and visually pale brown/grey in colour, with the measured surface being uneven (<1mm pit-peak) and convex (h/2 = 3-5mm).

Another piece of the MM3 greenstone boulder with both a lapped flat, and a polished curved, surface provided the third and fourth sets of readings, referenced MM3-3 and MM3-4 respectively. The flat part of this piece, measuring 9 x 7cm, had been sawn and then lapped smooth resulting in a planar surface. A total of 10 KT5 readings, all partly overlapping each other, were made and referenced MM3-3. The curved surface of the same piece of MM3 was manufactured by initially pecking to a rough axe-like curved shape using a rock hammer and then hand ground to a smooth finish using quartz sand. Although the piece was not large enough to manufacture a whole axe the resulting curved surface is observed to be similar to that found on axes. The curved surface is 12 x 7cm and smooth with a curvature (h/2) of between 1 to 4mm and the 9 readings taken are referenced as MM3-4.

A 5mm thick slice of MM3 measuring 10 x 7.5cm, with parallel flat sides, provided the fifth MS measurements, which consists of 11 almost totally overlapping individual readings, referenced MM3-5.

A smaller piece of MM3, where the weathered surface had been removed by hand grinding using quartz sand as the abrasive was the fourth piece of MM3 to be measured. The resulting surface was smooth and has a curvature estimated at between 2 to 6mm (h/2) and was measured 10 times with the KT5 meter (reference MM3-6).

The final two sets of readings, MM3-7a & 7b, were taken on the largest piece of MM3 remaining. This piece was cut using a diamond saw to provide a flat surface >20cm in diameter and in such a way that the depth of rock below the flat surface was >10cm. Two sets of 6 KT5 readings were taken on the flat surface. Within each set the individual readings were all partly overlapping each other, whereas the two areas where the two sets of readings were taken did not overlap. The reason for taking two sets of readings was that it was noticed that the higher readings (see Appendix 8.1; MM3-7a) were associated with a fine crack in the rock sample that may have allowed the migration of pore fluids to slightly alter the existing mineralogy so that it was more susceptible to magnetisation. Time was not available to undertake a detailed mineralogical study of the two areas so the above comment cannot be substantiated at this time. However, it is noted that MS measurements of this piece of MM3 require no corrections and as such can be considered to represent the true rock value at this location on the sample. The uncorrected measurement for MM3-7b is $1.38 \pm 0.05 \times 10^{-3}$ SI, which is closer to the range of uncorrected measurements made on

the other pieces of MM3 (0.61 ± 0.01 to 1.23 ± 0.03 x 10^{-3} SI, see Table 20 below and Appendix 8). Since this measurement is made away from the crack it is assumed that it represents the true rock value of a magnetically homogeneous piece of MM3, of 'infinite' dimension.

Reference	Description of MM3 surface measured	Uncorrected, KT 5 average (x 10^{-3} SI ± 1sd)	Overall correction factor (CR x T x W) = S	Corrected KT5 average (x 10^{-3} SI)
MM3-1	fractured fresh but irregular surface	1.07±0.08	(1.15 x 1 x 1) =1.15 (1.23 x 1 x 1) = 1.23	1.22 (lower) 1.31 (upper)
MM3-2	convex, weathered	0.69±0.03	(1.32 x 1 x 1) =1.32 (1.61 x 1 x 1) = 1.61	0.92 (lower) 1.12 (upper)
MM3-3	Lapped flat surface	1.16±0.03	(1 x 1.11 x 1.01) =1.12	1.30
MM3-4	Polished and curved	1.23±0.03	(1.07 x 1.11 x 1.04) = 1.23 (1.32 x 1.11 x 1.04) = 1.52	1.51 (lower) 1.87 (upper)
MM3-5	Parallel slice	0.61±0.01	(1 x 1.08 x 1.88) = 2.03	1.23
MM3-6	Ground, natural surface	0.90±0.02	(1.15 x 1.19 x 1.04) = 1.42 (1.51 x 1.19 x 1.04) = 1.87	1.28 (lower) 1.68 (upper)
MM3-7a	Sawn surface, over crack	1.67±0.04	(1 x 1 x 1) = 1 i.e. no correction	1.67
MM3-7b	Sawn surface (away from crack)	1.38±0.05	(1 x 1 x 1) = 1 i.e. no correction	1.38

Table 20 Summary of KT5 measurements for pieces of rock sample MM3, associated overall corrections and corrected maximum and minimum values (extracted from Appendix 8). Individual factors for CR (combined surface relief), W (width) T (thickness) are shown along with S, the whole sample correction factor. Note MM3-2 is made on a weathered surface and is expected to have different MS than MM3-7a & 7b (see below).

5.7.3.2 MM3 Discussion

MS measurements on the largest piece of MM3, away from the crack (MM3-7b), probably represent a good approximation of the MS for the greenstone rock from which MM3 came. Thus the corrected KT5 readings of other pieces of MM3 are expected to bracket or be approximately 1.38 x 10^{-3} SI, assuming the rock is magnetically homogeneous.

Inspection of Table 20 and Appendix 8.1 and 8.2 shows that only one corrected measurement (MM3-6) brackets the expected value of 1.38 10^{-3} SI, with the lower corrected MS value (1.28 x 10^{-3} SI) being close to MM3-7b (1.38 x 10^{-3} SI). Three corrected measurements, MM3-1, 3 and 5, range from 0.07 x 10^{-3} to 0.27 x10^{-3} SI *below* the expected reading of 1.38 x10^{-3} SI (c.f. Appendix 8.2). One of the two remaining measurements, MM3-4, has an uncorrected average value of 1.23 x 10^{-3} SI and a lower corrected measurement of 1.51 x 10^{-3} SI, which together bracket the expected value of 1.38 x 10^{-3} SI. In this latter case, the corrected MS values for MM3-4 bracket the upper value obtained near the crack on the largest piece of MM3 (MM3-7b: 1.67 x 10^{-3} SI). It is

therefore possible that this, smaller, piece of MM3 may have physically originated from close to the cracked region seen in the larger piece.

The measurement with the largest difference between expected and corrected MS is MM3-2 (0.92 x 10^{-3} to 1.12 x 10^{-3} SI, i.e. greater than 0.26 x 10^{-3} SI below MM3-7b) and this is the only sample to be measured with its original weathered surface intact. (Hence cannot be used to assess the similarity between true and corrected values as it may be magnetically different to fresh rock.) It is therefore probable that the 1-2mm weathered crust is depleted in magnetic minerals in the rock and that the weathered crust has an effect on measurement similar to that produced by a gap of 1-2mm

On balance (excluding MM3-2) it appears that the overall correction factors for 'non-ideal' pieces of MM3 are slightly low as the corrected MS values are, generally, slightly below that expected from an 'infinite' and homogeneous piece of MM3 (MM3-7b). However, since MM3 has been found to be slightly heterogeneous it is possible that the half of MM3 used to manufacture the proto-axe had slightly lower MS than the piece remaining which was used to determine the true rock values.

5.7.3.3 PTX002 results

It became clear during the investigation that PTX002 was not magnetically homogeneous as a larger than expected range of MS readings was observed on the four pieces measured. Hence, one of the main assumptions used to derive the overall correction factor (that the sample is magnetically homogeneous) does not hold. This means that the results cannot be used to directly assess the effect of the overall correction factors and thus, negates the aim of the investigation. However, the experiment was completed as it was felt the results could provide insight to the level of heterogeneity that may be encountered when measuring axes. The results from PTX002 are summarised in Table 21 and detailed in Appendix 8.

The PTX002 proto-axe was measured twice, once on each side of the axe. The first set of readings (reference PTX002-1) consisted of 11 partly overlapping measurements on the wider, blade end, of the proto-axe where a prominent round white patch (of an unknown mineral) was observed. The second set of readings (PTX002-2), consisting of 10 partly overlapping measurements, was made on the other, more curved, side of the axe, again

towards the wider blade end of the proto-axe in order to maximise the coverage of the KT5 sensor head.

A third set of readings (PTX002-3) were obtained from a piece of debitage material (waste) from the manufacture of the proto-axe. This piece had a lapped flat (planar) surface on one side, a very irregular surface on the other and was at least 1.5cm thick, increasing to 3.5cm thick towards one end. A series of 11 partly overlapping KT5 readings were made on the flat side and towards the thicker (3.5cm) end of this piece.

A fourth series of measurements (PTX002-4) was made on a smaller piece of debitage that has a slightly irregular sawn surface (flat with <1mm surface relief).

Reference	Description of piece of PTX002	Uncorrected, KT 5 average (x 10^{-3} SI) and SD	Overall correction factor (maximum and minimum)	Corrected KT5 average (x 10^{-3} SI)
PTX002-1	Proto-axe	1.14±0.08	1.31	1.49 (lower)
			1.50	1.71 (upper)
PTX002-2	Proto-axe (other side)	0.66±0.05	1.50	0.99 (lower)
			1.72	1.14 (upper)
PTX002-3	Slab-like debitage	1.01±0.10	1.22	1.23
			1.22	1.23
PTX002-4	Smaller piece of debitage	1.85±0.11	1.32	2.43

Table 21 Summary of KT5 measurements for pieces of rock sample PTX002, associated overall corrections and corrected maximum and minimum values (extracted from Appendix 8)

5.7.3.4 PTX002 discussion

Prior to applying the overall sample correction factor Table 21 and Appendix 8 shows that there is a difference between the first two measurements (PTX002-1 & -2), with the first series of readings averaging 1.14 ± 0.08 x 10^{-3} SI and the second set averaging 0.66 ± 0.05 x 10^{-3} SI. Both series of measurements require the same correction factors for thickness and width, with PTX002-2 requiring a larger correction for its greater curvature. This results in the correction factors being separated by approximately 0.2 which is insufficient to bring the two MS measurements close together when the corrections are applied. This is could be due to the fact that PTX002 is not magnetically homogeneous or that the overall correction factor is not working as hoped. The two sets of readings were taken on different sides of the proto-axe with the only difference in morphology being the increased curvature encountered by the second set of readings. In order to get both corrected MS readings to be equal, the curvature correction for the second series of readings would need to be around 2, i.e. about twice the 3-5mm curvature actually estimated (10mm peak to pit correction = 2, Table 16). A check on the curvature of the sample confirmed that the

estimated curvatures were reasonable and it is therefore concluded that the sample is magnetically heterogeneous.

The uncorrected average MS value for the fourth piece of PTX002 (PTX002-4) is 1.85 ± 0.11 x 10^{-3} SI, which is higher than the corrected MS values for the other measurements. Since all pieces are from the same original greenstone rock this result supports the assumption that the original rock was magnetically heterogeneous.

Since homogeneity is a primary assumption within the development of the overall correction factor, the results from greenstone rock PTX002 cannot be used to support the applicability of the overall correction factor. However, the results clearly show that it is possible for uncorrected KT5 readings taken on a typical piece of greenstone to vary from 0.66 to 1.85 x 10^{-3} SI. This fact needs to be borne in mind when measuring real axes.

5.7.4 Summary of empirical investigation into overall correction factor

This, short, empirical experiment has shown that mineral heterogeneity within greenstone rocks can have a marked effect on MS measurements, and this should be borne in mind when comparing MS values from axes with rock and exposure MS measurements. However, if the greenstone rock sample and source exposure are considered to be homogeneous then correction factors derived from measurements of surface relief, curvature, thickness and width can result in corrected MS values being significantly closer to the true rock value than the uncorrected MS values. Based on the results from the greenstone rock MM3, it is probable that the overall correction factor is slightly low and that the corrected maximum value is probably closest to a whole rock value. Weathered surfaces encountered on typical greenstones (on the basis of one example) may affect the MS by reducing response.

It is concluded that more investigation is needed to confirm the behaviour of the overall correction factor, but using the overall corrections factor can bring MS values of undersized and variably curved samples (like axes) closer to the true rock value.

5.8 Magnetic Susceptibility of greenstone exposures

5.8.1 Overview

Magnetic susceptibility measurements were made at a number (3 to 5) sites within five greenstone exposures (also called locations) in Cornwall using the KT5 meter (c.f. Appendix 9 for details). The aim of these measurements was to establish the magnitude of MS of typical Cornish greenstones and to assess the amount of variability of MS within and between exposures. The five exposures, at Cudden Point, Trenow Cove, Penlee, Zennor and Gurnard's Head, are considered to be typical of the greenstones that outcrop around Mount's Bay and along the North Penwith coastline, and may be considered as a small sample of the numerous greenstone outcrops in Cornwall. If it was found that these five greenstone exposures had individually recognisable MS 'signatures' then it may become possible to use MS to provenance axes to a single greenstone exposure.

As identified in Chapter 4 and discussed above, there is little magnetite in the Cornish greenstone rocks from these five exposures, and the amount of ilmenite (the most magnetically responsive mineral encountered) varies, commonly being less than 1% by volume. Therefore, low values of MS are expected.

5.8.2 Methodology

Repeated, non-overlapping, readings using the KT5 were made on fresh and slightly weathered surfaces at locations within the greenstone exposures. Wherever possible measurements were made on freshly broken rock surfaces where the weathered crust had been removed. Slightly weathered surfaces (identified by eye) were measured when fresh surfaces were not available. Surfaces obviously covered in lichen or contaminated (e.g. oil) were avoided. Likewise, heavily pitted surfaces, caused through differential erosion of minerals, were avoided. At each location the surface relief was estimated by eye to the nearest mm.

At least one large sample was taken from each of the greenstone exposures and sawn to provide a flat surface. The size and subsequent flat surface of these rock samples is such that they require no corrections to the KT5 readings and therefore, represent the true rock MS value, based on an ideal sample.

5.8.3 Results of typical greenstone MS investigation

KT5 measurements and associated corrections are detailed in Appendix 9.1, summarised in Table 22 below and are shown in maps contained in Appendixes 9.3 to 9.5. Nineteen sites within a total of five greenstone exposures were measured.

Exposure and location reference.	Uncorrected average ($\times 10^{-3}$ SI ± 1sd)	Corrected measurement min to max ($\times 10^{-3}$ SI)	Sawn sample average ($\times 10^{-3}$ SI ± 1sd)
Trenow Cove			
T2 (n=5)	0.44 ± 0.09	0.44 to 0.47	
T2a (n=2)	0.50 ± 0.10	0.54 to 0.58	
T2b (n=2)	0.63 ± 0.05	0.72	0.75 ± 0.01 (n=11)
T3 (n=6)	0.61 ± 0.10	0.70 to 0.75	sample from location T2b
T3a (n=4)	0.47 ± 0.03	0.51 to 0.54	
Cudden Point			
C1 (n=6)	0.39 ± 0.04	0.45 to 0.45	0.57 ± 0.01 (n=12)
C1a (n=5)	0.33 ± 0.03	0.35	sample from location C1
C3 (n=8)	0.48 ± 0.06	0.51 to 0.55	
Penlee			
P2 (n=8)	0.66 ± 0.21	0.70 to 0.76	
P3 (n=9)	0.68 ± 0.10	0.73 to 0.78	0.69 ± 0.02 & 1.10 ± 0.03 (n=11)
P3a (n=4)	0.60 ± 0.10	0.60 to 0.64	2 samples from location P3
P4 (n=12)	0.31 ± 0.09	0.65 to 0.70	0.70 ± 0.07 (n=11)
			sample from location P4
Gurnards Head			
G1 (n=7)	0.61 ± 0.08	0.61 to 0.65	0.77 ± 0.01 & 0.82 ± 0.01
G1a (n=4)	0.53 ± 0.08	0.53 to 0.57	2 samples from location G1
G2 (n=10)	0.68 ± 0.07	0.73 to 0.78	(n=12 & 11 respectively)
Zennor Point			
Z2 (n=6)	0.54 ± 0.07	0.57 to 0.65	
Z2a (n=7)	0.47 ± 0.07	0.50 to 0.54	
Z2b (n=4)	0.62 ± 0.28	0.67 to 0.72	0.59 ± 0.01 (n=11)
Z2c (n=9)	0.50 ±0.03	0.50 to 0.53	sample from location Z2b

Table 22 Summary of greenstone MS measurements, averaged uncorrected and corrected readings for exposure sites and averaged readings for associated exposure samples (summarised from Appendix 9). Exposure locations are corrected for surface relief only as all other dimensions were 'infinite'. All samples had sawn flat surfaces and were of 'infinite' dimension and thickness, hence required no correction to the KT5 readings. (n = the number of readings taken at each location/ on each sample)

5.8.4 Discussion on magnetic susceptibility of greenstone exposures

It can be seen that all greenstone sites have corrected MS values below 0.78 x 10^{-3} SI, generally falling into the range 0.50 to 0.80 x 10^{-3} SI and probably reflects the low strength and quantity of ferrimagnetic minerals present in all five greenstone exposures (c.f. Chapter 4). The relative errors (calculated from sd/average given in Table 22) for MS readings at the sites within the greenstone exposures typically fall between 10 to 20%. Noting that the precision of the KT5 has been established at 5% relative for values around 0.2 x 10^{-3} SI (Williams-Thorpe & Thorpe, 1993) and 1.5% relative for a value of 0.61 x 10^{-3} SI (Section 5.4.3), this larger variance is probably related to rock heterogeneity, since site readings were all non-overlapping and subject to the similar surface conditions.

No corrections are required to KT5 readings of the greenstone *samples* because the measured (sawn) surfaces of each samples is 'flat' and the sample dimensions (thickness & width) can be considered 'infinite' (c.f. Section 5.4 above). Hence, the KT5 indicates the true rock value of the sample. Inspection of Table 22 above shows that samples T2, C1, P3 (2^{nd}), G1 (both) return higher average MS values than their associated source location. Sample P4 has an average the same as the maximum corrected P4 location and samples P3 (1 sample of 2) & Z2b have lower average MS readings than the minimum corrected value from the source location. In this latter case, samples P3 & Z2b MS averages are closer to the uncorrected location average.

Apart from the assumed heterogeneity of the rock there are three other possible explanations accounting for the difference between MS measurements at locations and samples from the locations. Firstly, the rock surfaces at field locations may have been slightly weathered to some extent. As seen in the experiment with sample MM3 (c.f. Section 5.7.3 & 4), weathering can cause a reduction in the measured magnetic susceptibility. Secondly, surface relief was estimated as the maximum difference between the KT5 sensor head and the greenstone rock surface. It is possible that the effective gap (Section 5.4) between KT5 and rock is non-symmetrical and was more than half this maximum peak to pit distance (as used to establish the correction factors), thus requiring a larger correction factor than the one used. Thirdly, it is possible that the peak to pit difference was underestimated, since an increase of each upper estimate of unevenness by 1 mm would expand the range of the corrected min-max readings to encompass the average rock sample values.

There is no conclusive evidence as to which of the four factors in the previous paragraph accounts for the difference between sample and associated original location (corrected) KT5 readings. Heterogeneity within a greenstone sample, as seen in Section 5.4 above, can result in a single piece of rock having different MS, depending on which side it is measured. Weathering and incorrect estimation of surface relief, or an irregular surface, can also cause a small difference in MS readings between samples of and exposures of greenstone rock. On balance, it is believed that underestimating surface relief at the point of measurement is probably the main factor why rock samples return higher MS values than their source exposure, directly as a result of the difficulty associated with accurately measuring the peak to pit distance.

Further inspection of Table 22 and the chart in Appendix 9.2 shows that it is impossible to provenance a greenstone rock to a single site within the five exposures examined on the basis of MS. For example, assume a greenstone rock returns a corrected value of 0.65 x 10^{-3} SI, then it is possible that, on the basis of MS alone, that this sample could have originated from P4, G1 or Z2 sites. However, it is possible to state whether an axe has an MS value similar to that found at typical Cornish greenstone exposures.

Finally, data in Appendix 9 shows that the relative error (1 sd/average) for KT5 readings on the greenstone rock samples (not exposure) is better than 3% for MS values between 0.50 to 0.80 x10^{-3} SI. This relative error is comparable to the 5% relative error for KT5 MS values around 0.2 x 10^{-3} SI established by Williams-Thorpe & Thorpe (1993) and the 1.5% relative error for a value of 0.61 x 10^{-3} SI established earlier (Section 5.4.3).

5.8.5 Summary and remarks concerning MS of greenstone exposures

The five greenstone exposures measured as part of this work returned corrected magnetic susceptibility values of 0.44 to 0.78 x 10^{-3} SI with a range of up to ± 0.20 x 10^{-3} SI (10 to 20% relative) at each site within the exposure, probably due to rock heterogeneity rather than the application of correction factors. The higher values of susceptibility measured on prepared samples taken from the exposure are probably due to the freshness of the sample's sawn surface or, believed more likely, an underestimate of the surface relief at the rock exposure.

The large overlap of MS values between and within Trenow, Penlee, Gurnards Head and Zennor Point means that no axe or specimen with an MS value between 0.50 and 0.80 x 10^{-3} SI could be provenanced to any one of these exposures on the basis of MS alone. If these exposures are representative of the 100+ known greenstone exposures (Chapter 2 & Appendix 3) then it must be concluded that it will be impossible to provenance axes to any single exposure with any degree of certainty using magnetic susceptibility alone. However it may be possible to achieve the converse, to show that axes did not originate from certain exposures. For example it is probable that axes with corrected magnetic susceptibility value greater than 0.8 x 10^{-3} SI do not originate from the Cudden Point greenstone and axes with values greater than 2 x 10^{-3} SI probably do not originate from greenstones around Mount's Bay or the North Penwith coastline.

5.9 Magnetic Susceptibility of British Neolithic greenstone axes

5.9.1 Introduction

Measurements of MS were made on over 225 axes using the Exploranium KT5 meter. The results of all measurements are contained in Appendix 11 along with dimension, surface relief and curvature of each axe, established using the methods described in Section 5.5 above.

The main aims of this part of the MS work were to :

1. investigate if axes could be sub-grouped using magnetic susceptibility alone
2. investigate if it is possible to assign axes to one or more of the exposures discussed above
3. to investigate the homogeneity of the IPC axe groups
4. to determine the usefulness of MS as a discriminating factor/variable in the non-destructive provenancing of Neolithic axes (complementing PXRF geochemistry)

5.9.2 Repeatability of estimations of axe curvature and surface relief

Throughout the investigative period of the research 21 axes were measured twice, approximately one year apart. The second series of measurements were carried out independently of the first, with all MS measurements, axe curvature and surface relief estimations carried out without recourse to those established for the first series of measurements. Results from these two series of measurements are detailed in Appendix 10.

Appendix 10.1 shows that 84% (53/63) measured dimensions of the axes are the same to within 5mm, with the remaining 16% (10/63) within 10mm. The estimates of surface relief and curvature are more varied with estimates of curvature having the greatest disparity(e.g. Co 207/823 with curvature first estimated as 7 to 8mm and secondly at 1 to 2mm). The same KT5 meter was used for both measurements, with 10 to 12 readings taken on each axe using the process described in section 5.3 above.

The differences in measurements of dimensions are put down to rounding errors, either rounding up or down to the nearest 0.5cm. The author carried out all estimations of curvature and surface relief so the difference in these estimates is put down to experience, gained as the research progressed, and/or recording h, not h/2 during the first set of

measurements. The first series of estimations was made at the beginning of the research period, with the second series made well into the research programme.

Apart from three axes (Co151/737, Co152/738 and Co318/1527) all uncorrected KT5 MS averages of each pair of measurements are within 1sd of each other. The slight variability between averages is greater than expected in some cases and this is probably due to the different placement of the KT5 on the variable surface of the axe. The range of corrected minimum to maximum measurements overlap in 13 of the 21 pairs of measurements, with a further 6 of the 21 sets separated by less than 0.10 $x10^{-3}$ SI. Of the two remaining pairs, with measurements separated by more than 0.10 x 10^{-3} SI, the difference for DB8 is predominantly due to the larger MS recorded for the first measurement and for Co207/823 the larger estimation of curvature recorded at the time of the first measurement (the estimate was probably recorded as h and not h/2).

Since the precision of the KT5 is not in doubt, it is concluded that there is slight human inconsistency in the measurement process, predominantly through increasing experience gained using the KT5 and difficulties in visually estimating axe curvature. However, in the main, the difference between uncorrected measurements is generally less than 1sd of the average of the readings and after correction the majority of corrected readings overlap, or are separated by a small amount (<0.10 x 10^{-3} SI). Since no realistic adjustment to the data is possible to take account of human inconsistency the potential variation in results must be borne in mind when examining measurements of axe magnetic susceptibility. However, based on the observations above the maximum error present in corrected MS measurements is likely to be less than 0.10 x 10^{-3} SI, which (by observation of Appendix 11.1) is smaller than typical min-max ranges on most axes.

5.9.3 Magnetic susceptibility of IPC grouped and ungrouped axes

5.9.3.1 IPC Group I axes

As discussed in Chapter 2 & 3, IPC Group I has been established on the basis of its axes sharing similar petrological characteristics, hence it may be expected that IPC Group I will also have similar MS characteristics. From inspection of Appendix 11.1 & 11.2 this appears to be broadly true as the majority of the 127 IPC Group I axes measured returned corrected MS values between 0.50 and 1.50 x 10^{-3} SI. However inspection of IPC Group I reveals axes reference Db8, Do91/1198, Gm37, Gm85, Ha23, Wi200/649, Yo800 and CoGWA3 have markedly different corrected and uncorrected MS values from the majority

of IPC Group I, differences that cannot be accounted for by whole sample correction factors or possible variability in estimating curvature and surface relief alone. Hence these are judged atypical of IPC Group I and should be considered for re-evaluation. KT5 readings and averages from these 8 axes are excluded from further statistical analysis and discussion of IPC Group I. Note that this includes CoGWA3, the sole member of GpI-13 and already identified as being petrographically different to the majority of IPC Group I axes.

Axe	Uncorrected measurements (x 10^{-3} SI)(±2sd where indicated)	Range of corrected measurements (x 10^{-3} SI) (±2sd where indicated)
IPC Group I*	0.65 ± 0.50*	Lower = 0.95 ± 0.72 Upper = 1.09 ± 0.80*
Db8	3.27	5.40 to 5.91
Do91/1198	1.13**	3.10 to 3.31
Gm37	2.61	1.70 to 4.04
Gm85	0.06	0.09
Ha23	5.47	7.41 to 7.95
Wi200/649	3.18	4.75 to 5.10
Yo800	47.82	68.06 to 78.12
CoGWA3	6.88	11.27 to 12.90

*Table 23 Summary of IPC Group I axes with uncorrected MS average outside ±2sd of the uncorrected IPC Group I mean (0.65 ± 0.50 x 10^{-3} SI) or corrected MS values outside ±2sd of the corrected IPC Group I average minimum to maximum range (0.23 to 1.89 x 10^{-3} SI). Note * - IPC Group I average and standard deviation calculated from all IPC Group I axe measurements, except those listed in this table. ** - Although the uncorrected measurement is just within 0.65 ± 0.50 x 10^{-3} SI, the corrected measurement is greater than 1.09±0.80 x 10^{-3} SI and as such this axe has been excluded from further analysis of IPC Group I.*

Figures 48a to c show histograms of IPC Group I uncorrected average and maximum and minimum corrected values, after the removal of the atypical axes listed above. The histogram showing the uncorrected axe averages (Figure 48a) has a slight, positively skewed distribution. The corrected reading histograms, Figure 48b (minimum) and 48c (maximum) are less positively skewed, with shorter tails, but introduces the possibility of a bimodal distribution caused by a second population. Acknowledging the potentially bimodal nature of Figure 48b and c, all three histograms have a positive skew and are a similar shape to those derived when analysing elemental concentrations of rocks from the same location (Swan & Sandilands 1995). Since it is assumed that MS and mineralogy are inter-linked it is therefore plausible that the IPC Group I axes measured originate from a single greenstone exposure. The **average maximum** MS value of 131 IPC Group I axe measurements, calculated as the average of all IPC Group I axe maximum MS measurements including duplicates but excluding the 8 axes identified in Table 23, is **1.09 ± 0.40 x 10^{-3} SI (1sd).** Similarly, the **average minimum** MS value is **0.95 ± 0.36 x10^{-3} SI (1sd).** Noting the assumption that the upper range of the corrected measurements is likely to be close to the actual rock value then this data suggests an outcrop value of approximately 1.1 x 10^{-3} SI. Further, if we assume the same symmetry of distribution then

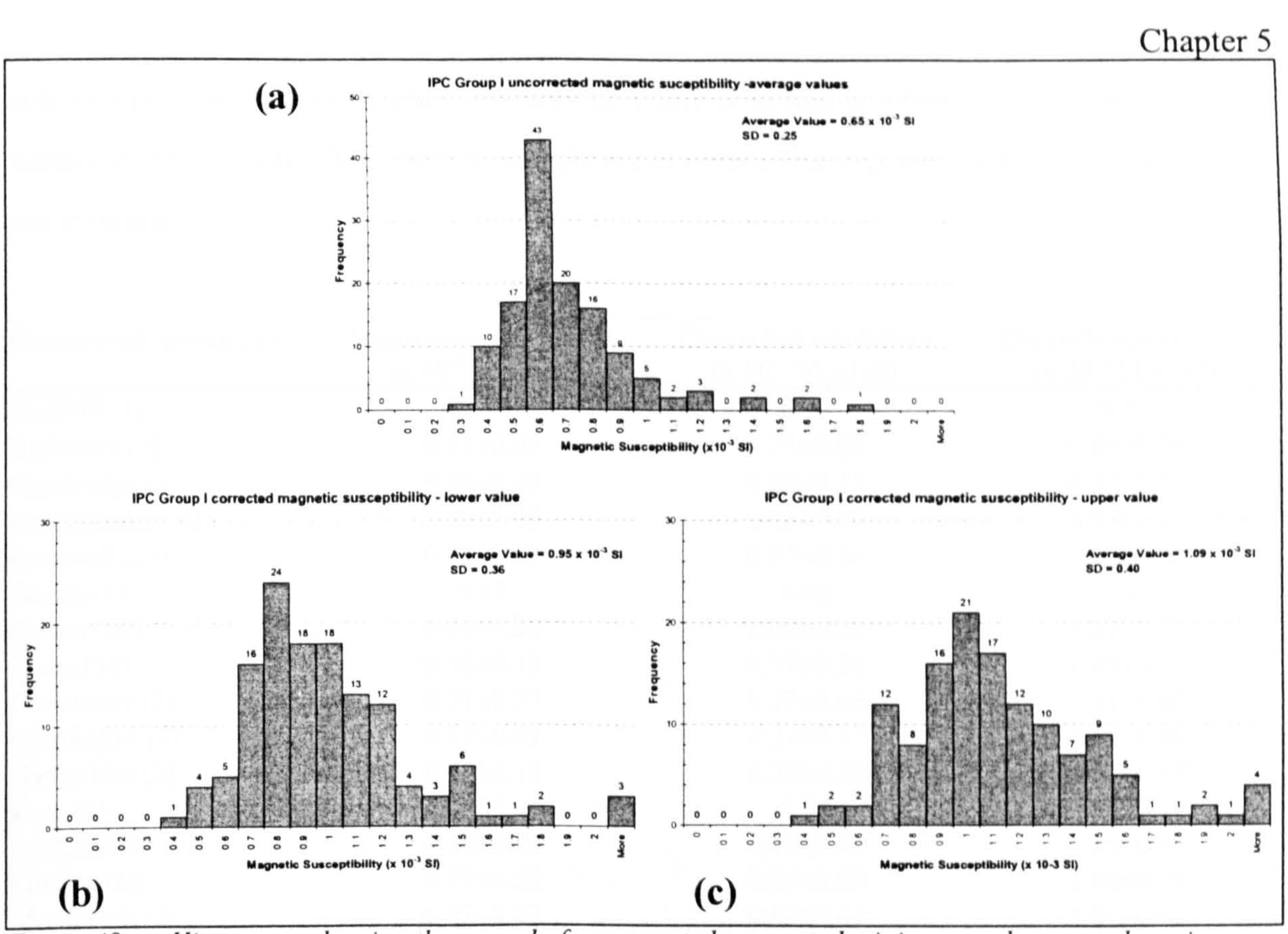

Figure 48 Histograms showing the spread of uncorrected, corrected minimum and corrected maximum MS values for IPC Group I axes, and associated average and sd.

the likely range around the mean of potential source exposures is $1.1 \pm 0.4 \times 10^{-3}$ SI. On the basis of overlapping ranges for corrected exposure measurements it is theoretically possible that all exposures discussed in this section could be the source of some, but not all, IPC Group I axes (based on ±2sd limits).

Uncorrected average, and corrected maximum & minimum MS values for axes by county and by petrological sub-group are detailed in Table 24 below. Table 24 shows that there is considerable overlap between county and axe sub-groups for both uncorrected and corrected MS values and that statistical analysis is not able to separate the groups with any certainty because of the proximity of means, magnitude of the standard deviations and the low sample numbers. For example, Student's two-tailed t-test for comparing Cornwall and Yorkshire axe uncorrected and corrected MS values indicates that the null hypothesis (that the means are 'equal') cannot be rejected at a 0.05 significance value. Two tailed probabilities are calculated as: 0.17 for comparing uncorrected values, 0.74 for corrected minimum and 0.56 for corrected maximum MS values. Hence, the axes found in Yorkshire and Cornwall could have come from the same parent population on the basis of this evidence. However, in some cases the differences between the MS values are worth noting. For example, the 6 axes from Norfolk appear to have lower corrected MS than all other counties apart from the single representative from Devon. Likewise the upper corrected MS value for GpI-8 is similar to the Norfolk axes and is the lowest found in the

sub-groups. This suggests that there may be some potential in using MS to differentiate certain *groups* of axes, but the low sample sizes means that rigorous statistical analysis is not possible.

County/sub-group (no)	Uncorrected Average ($x 10^{-3}$ SI ±1sd)	Corrected minimum ($x 10^{-3}$ SI ±1sd)	Corrected maximum ($x 10^{-3}$ SI ±1sd)
Bedford (1)	0.57	0.76	0.87
Berkshire (3)	0.51±0.07	0.74±0.04	0.80±0.09
Cambridge (5)	0.54±0.03	0.83±0.11	0.93±0.13
Cardiganshire (2)	0.60±0.00	0.85±0.09	0.97±0.11
Cornwall (27)	0.73±0.22	0.97±0.24	1.09±0.26
Devon (1)	0.47	0.62	0.66
Dorset (10)	0.63±0.20	1.06±0.21	1.22±0.23
Essex (10)	0.56±0.15	0.97±0.28	1.09±0.31
Gloucester (2)	0.71±0.33	1.17±0.66	1.41±0.85
Glamorgan (6)	0.51±0.21	0.77±0.37	0.84±0.40
Hampshire (3)	0.73±0.15	1.20±0.20	1.33±0.17
Kent (1)	0.92	1.55	1.65
Lincolnshire (9)	0.68±0.24	0.99±0.40	1.20±0.44
London (6)	0.69±0.22	0.86±0.23	1.00±0.26
Monmouth (2)	0.52±0.02	0.80±0.01	0.91±0.01
Norfolk (6)	0.42±0.12	0.60±0.09	0.70±0.10
Oxford (4)	0.67±0.16	1.04±0.08	1.15±0.05
Somerset (4)	0.78±0.51	1.02±0.51	1.14±0.52
Wiltshire (16)	0.75±0.35	1.13±0.60	1.23±0.67
Yorkshire (13)	0.61±0.29	0.92±0.42	1.15±0.56
GpI-1(23)	0.72±0.30	0.99±0.38	1.10±0.39
GpI-2 (4)	0.48±0.11	0.76±0.20	0.85±0.25
GpI-3 (1)	0.65	1.31	1.40
GpI-4 (14)	0.70±0.22	0.98±0.20	1.11±0.23
GpI-6 (6)	0.84±0.26	1.30±0.23	1.47±0.88
GpI-7 (1)	0.52	0.90	0.96
GpI-8 (2)	0.47±0.04	0.58±0.09	0.69±0.01

Table 24 Average uncorrected and average corrected maximum and minimum IPC Group I axe MS values sorted by county and petrographic sub-group. All values are x 10^{-3} SI, with ±1sd where shown. (n= the number of measurements in the group, excluding anomalous axes (Table 23) but including duplicate measurements)

5.9.3.2 IPC Group Ia, I/Ia and near I axes

Table 25 summarises Appendix 11.3 and 11.4, which report and display MS measurements made on the five IPC Group Ia, six I/Ia and seven I(near) axes examined. Evaluation of the MS data shows that all three groups have similar MS characteristics to IPC Group I and it is not possible to determine with any statistical significance that these axes are dissimilar to IPC Group I, with the exception of IPC Group I/Ia axe Lo114. This axe has comparatively low magnetic susceptibility (uncorrected average = 0.17 x 10^{-3} SI), atypical of IPC Group I and other axes assigned to IPC Group I/Ia. There is insufficient representation of subgroups to produce statistically meaningful conclusions as to whether MS can be used to discriminate between IPC Group Ia, I/Ia & I(near) axes.

IPC group/sub-group (n)	Uncorrected Average ($x 10^{-3}$ SI ±1sd)	Corrected minimum ($x 10^{-3}$ SI ±1sd)	Corrected maximum ($x 10^{-3}$ SI ±1sd)
IPC Group Ia (n=7)	0.63±0.24	0.97±0.31	1.10±0.40
GpIa-1 (n=4)	0.50±0.08	0.76±0.10	0.85±0.11
GpIa-5 (n=1)	0.84	1.39	1.70
IPC Group I/Ia (n=6)	0.58±0.31	0.85±0.42	1.03±0.53
IPC Group I/1a excluding Lo114	0.66±0.26	0.95±0.38	1.16±0.48
IPC Group I(near) (n=7)	0.57±0.19	0.83±0.27	0.99±0.31

Table 25 Summary of uncorrected and corrected MS measurements of IPC Groups Ia, I/Ia & I(near). (Note: n for IPC Group Ia includes 2 duplicate measurements)

5.9.3.3 IPC Group III and IIIa axes

Appendixes 11.5 and 11.7 contain details on the measurements of magnetic susceptibility made on seven IPC Group III and one IIIa axes that are summarised in Table 26. There is an overlap between the IPC Group IIIa axe, Wi119/402, and IPC Group III axe MS values, with all 8 measurements being similar. Their range is within that seen for IPC Group I hence it is not possible to separate IPC Group III and IPC Group I axes by magnetic susceptibility alone. It is worth noting that GpIII-1 (Wi199/648, petrographically similar to the founding member of IPC Group III) has the lowest MS when compared to other IPC Group III axes. But, it is the only member of the sub-group measured (Wi4/4 is too small to measure with any certainty) so it is not known whether its MS value is an anomaly or representative of systematic pattern.

IPC group/sub-group (n)	Uncorrected Average ($x 10^{-3}$ SI ±1sd)	Corrected minimum ($x 10^{-3}$ SI ±1sd)	Corrected maximum ($x 10^{-3}$ SI ±1sd)
IPC Group III (n=7)	0.59±0.13	0.89±0.28	0.98±0.39
GpIII-1 (n=1)	0.49	0.70	0.70
GpIII-2 (n=3)	0.53±0.13	0.79±0.27	0.81±0.30
IPC Group IIIa (n=1)	0.63	1.08	1.16

Table 26 Summary of uncorrected and corrected MS measurements of IPC Groups III & IIIa

5.9.3.4 Other IPC Grouped axes

Measurements made on one IPC Group II, one IPC Group IV and two IPC Group XVI axes are included here for reference, with details in Appendix 11.6 & 11.7 and summarised in Table 27. It is concluded that, on the basis of MS measurements alone, the IPC Group II axe and two IPC Groups XVI axes could not be distinguished from IPC Group I or III. However, the single IPC Group IV axe (De25/576) is distinctly different all the other IPC groups reported here by having a true rock value between 34.3 to 36.7 x 10^{-3} SI. If this axe is representative of its IPC group then MS may assist in confirming membership to IPC Group IV, providing no other IPC greenstone group has similar MS values.

IPC group (n)	Uncorrected Average (x 10^{-3} SI ±1sd)	Corrected minimum (x 10^{-3} SI ±1sd)	Corrected maximum (x 10^{-3} SI ±1sd)
IPC Group II (n=1)	0.46	0.66	0.71
IPC Group IV (n=1)	26.6	34.3	36.7
IPC Group XVI (n=2)	0.70	0.94	1.06

Table 27 Summary of uncorrected and corrected MS measurements of IPC Groups II & IV and XVI.

5.9.3.5 Ungrouped greenstone axes

As stated above, it is not possible to provenance an axe to a single greenstone exposure using measurements of magnetic susceptibility alone, and neither is it possible to definitively provenance an axe to any of the IPC groups discussed above, except possibly IPC Group IV. However it is possible to state that an axe is not likely to belong to a certain group. From inspection of Appendix 11.8 and 11.9 it can be seen the following 13 of the 76 axes measured are unlikely to be mineralogically similar to IPC Group I or III based on the fact that their corrected MS values are outside corrected IPC Group I, Ia, I/Ia, I(near) and III MS averages ±2sd (taken as having a minimum corrected MS below 0.23 x 10^{-3} SI and a maximum corrected MS above 1.89 x 10^{-3} SI).

Axe	Uncorrected average KT5 readings (x 10^{-3} SI)	Corrected KT5 minimum (x 10^{-3} SI)	Corrected KT5 maximum (x 10^{-3} SI)
Ha108	84.32	109.61	109.61
Wi345/1348	73.71	87.33	93.40
CoADZE	29.08	32.92	37.86
Co185/788	13.10	23.15	32.65
Es20	8.46	13.00	13.99
Co323/1532	5.50	11.30	11.30
Yo662	5.46	6.43	7.40
HaT01	2.62	3.92	4.49
Co12/184	1.54	1.80	2.07
Yo127	1.52	1.85	2.44
Co320/1529	1.28	2.90	3.30
De96/1295	1.07	1.35	2.69
MED	0.13	0.21	0.24

Table 28 IPC ungrouped and non-IPC greenstone axes unlikely to be associated with IPC Groups I, Ia, I/Ia, I(near), III, IIIa, on the basis of their corrected minimum or maximum MS measurement is outside the range of IPC Group I average values ± 2sd.

As anticipated the IPC ungrouped and non-IPC axes have a greater variation in MS values because it is assumed that if they have been assessed by petrologists then they did not match one of the IPC petrologies or that they have yet to be examined (or thin sectioned). Using the average corrected maximum MS value of IPC Group I as reference; 40 of 76 (52%) ungrouped axes are within ±1sd (0.69 to 1.49 x 10^{-3}SI), and 63 of 76 (83%) are within ±2sd (0.29 to 1.89 x 10^{-3}SI). This suggests the majority of IPC ungrouped and non-

IPC greenstone axes examined share similar MS values to at least one of those obtained for IPC Group I, Ia, I/Ia, III & IIIa and hence could be related to these IPC groups. Therefore, with the data sets available at this time it is not possible to assign ungrouped axes to a single IPC group using MS alone, but it is possible to conclude that some axes are unlikely to be related to IPC Group I, (and possibly IPC Groups Ia, I/Ia, I(near), III or IIIa).

5.10 Summary and conclusions

Measurement of magnetic susceptibility using an Exploranium KT5 meter is found to be both quick and simple and has been shown to produce useful information that may be used to assist with provenancing archaeological artefacts.

By combining manufacturer and other published correction factor data an overall sample correction factor was determined for use on samples whose dimensions do not meet, or do not exceed, minimum requirements, such as axes and small rock samples. Experiments using pieces of sample MM3 showed the maximum correction factor produces results closer to the true rock value than the minimum correction factor, but in both cases these correction factors increased the KT5 readings towards the true rock value. Two independent series of measurements of a number of axes revealed that the human component in assessing curvature and surface relief of axes usually has a small effect, measured at less than 0.1×10^{-3} SI on the resulting maximum and minimum estimates of rock/axe MS.

Measurements of five greenstone exposures produce typical corrected MS values between 0.5 and 0.8×10^{-3} SI, along the lines expected noting ilmenite is the dominant ferrimagnetic mineral present in greenstones. MS measurement at sites within the greenstone exposures revealed a 10 to 20% relative error, believed to be caused by the heterogeneity of the greenstone since results had shown that the precision of the KT5 for the range 0.5 to 0.8×10^{-3} SI is better than 3% relative. The most notable factors affecting the correct determination of exposure MS include weathering and the estimation of surface relief. The considerable overlap of exposure magnetic susceptibility values for the five exposures measured indicates the difficulties in provenancing a greenstone rock sample or axe to a single exposure, although the converse appears possible, identifying axes that did not come from these exposures.

Analysis of KT5 measurements of over 225 greenstone axes led to the conclusion that it is not possible to assign axes to specific IPC groups or greenstone exposures on the basis of magnetic susceptibility alone, but that it was possible to identify atypical axes that in all probability do not belong to certain IPC groups. This resulted in the identification of 8 axes previously assigned to IPC Group I which have anomalous MS and are therefore atypical of IPC Group I. Approximately 80% of IPC ungrouped and non-IPC greenstone axes examined share similar MS values to those established for IPC Groups I, Ia, I/Ia, I(near), III and IIIa, but cannot be assigned to any one of these six IPC groups with any degree of confidence.

IPC Groups I, Ia, I/Ia, I(near), III & IIIa, greenstone axes have corrected maximum MS values between 0.98 x 10^{-3} SI (IPC Group III) to 1.16 x 10^{-3} SI (IPC Group I/Ia). With the findings of the proto-axe experiment that the maximum corrected value for typical axes is just below the whole rock MS, then the source greenstone exposure(s) would be expected to have similar, but slightly higher MS values. The greenstone exposures at Trenow Cove (near Perranuthnoe), Penzance & Mousehole, Gurnard's Head and Zennor Point all have corrected maximum MS values (less than 0.78 x 10^{-3} SI), thus generally lower than comparative axe measurements.

It is therefore concluded that MS measurements of greenstone alone cannot be used to provenance greenstone artefacts to a single greenstone exposure (or site within an exposure) or to IPC Groups I, Ia, I/Ia, I(near), III & IIIa. However, it is possible to state whether an axe or artefact probably does not originate from a particular greenstone exposure (or site) or is atypical to those found within IPC Groups I, Ia, I/Ia, I(near), III & IIIa.

6 Portable X-ray Fluorescence Spectrometry: principles, procedures and performance

6.1 Introduction

Geochemical data obtained non-destructively using a portable x-ray fluorescence spectrometer (PXRF) has been shown to assist with the provenancing of stone implements (Williams-Thorpe et al. 1999a). This investigation uses and expands on this new analytical method as applied to provenancing British Neolithic greenstone axes. This chapter introduces the PXRF equipment and establishes the accuracy, precision and detection limits when measuring greenstone rocks and axes-shaped samples, prior to examining the axe and exposure PXRF data in Chapters 7 & 8. A description and the operation of the PXRF equipment follows a short overview of x-ray fluorescence spectroscopy, with the remainder of the chapter devoted to establishing the analytical performance of the method.

6.2 Terminology

Terminology used in this chapter is that summarised by Potts (1997) (denoted IR (International Reference)) with the following emphasis and additions (author's definitions denoted AD):

'True value' (IR) is a value that would be obtained by a perfect measuring device: in this work it refers to the *actual* elemental concentration within a sample

'Conventional true value' (IR) is used to denote the published elemental concentrations of the international reference samples that are used to assess accuracy of the experimental procedure.

'Surrogate true values' (AD) are those values obtained from the surrogate datum.

'Measurement datum' or 'datum' (AD) is used when referring to the conventional true values (i.e. published values) of the international reference samples. The datum forms the basis from which error (q.v.) is calculated.

'Surrogate datum' (AD) is used to indicate the measurements obtained by the OU WDXRF equipment (after establishing the relation between the conventional true values and the values obtained by the OU WDXRF from the reference samples (q.v.)). The surrogate datum provides the surrogate true values (q.v.) for greenstone samples that are, in turn, used to establish the accuracy of the PXRF when measuring greenstone samples.

'Error' (IR) is the difference between the conventional true value and that measured.

'Bias' (IR) is the systematic deviation of the actual PXRF measurement from the conventional true value or the surrogate true value assuming no precision errors.

'PXRF SD' (AD) (a measure of *'instrument precision'*) refers to the number automatically produced by the PXRF that is largely dictated by the statistics of x-ray counting and is taken to represent 1sd of the PXRF measurement of element concentration (Potts et al. 1997: p39).

'Sampling precision' (AD) refers to the precision in measurement obtained from replicate (i.e. non-overlapping measurements on the same sample) PXRF measurements and relates also to the variations of mineralogy within the excited volume (Potts et al. 1997).

'Reference pellets' (AD) are the thirteen pressed powder pellets made from geochemical reference materials, whose elemental concentrations are accurately known and published, for example in Potts et al. 1992 and Govindaraju et al. 1994.

'Control pellets' (AD) are the two reference pellets, ACE and WSE, used on a daily basis to check the long term accuracy and precision of the PXRF

'Exposure samples' (AD) are those samples collected from rock (usually greenstone) exposures that, unless otherwise stated, have been sawn to provide a flat (<<1mm relief) surface on which PXRF measurements are made.

'Exposure pellets' (AD) are those pressed powder pellets made from certain exposure samples (q.v.) using the process described in Watson (1996).

'Proto-axe(s)' (AD) is a term used to describe the two greenstone samples (MM3 & PTX002) that have been processed to represent the various stages of axe manufacture and are used to investigate the performance of the PXRF when measuring variable, non-flat surfaces.

6.3 X-ray fluorescence spectroscopy

X-ray fluorescence spectroscopy (XRF) is a widely-used technique that is capable of determining the concentrations of major and trace elements in prepared rock samples to a high precision (Potts & Webb 1992). XRF involves fluorescing a sample with x-ray radiation (called *primary* radiation) and measuring the intensity of the emitted x-rays (*secondary* or *fluorescent* radiation). The intensity of the characteristic (elemental) lines of secondary radiation is proportional to concentrations of elements within the sample, thus making it possible to determine the elemental composition of samples.

In standard, laboratory-based, XRF equipment primary x-rays are generated using an x-ray tube. Such tubes produce x-ray wavelengths of 0.003nm to 3nm generated by electrons leaving a heated tungsten filament and driven by a high electric potential (typically 40kV to 100kV) towards a metallic anode. On collision with the anode, specific x-ray lines, particular to the type of anode, and a continuum of x-ray energies are produced. These x-

rays are then used to fluoresce the sample being analysed. This, primary, ionising radiation is designed to be of greater energy than the binding energies of K & L shell electrons of elements to be analysed, and hence are able to dislodge inner shell (i.e. K & L shell) electrons of these elements.

Once an inner shell electron has been ejected, another electron from an outer shell fills the vacant position and in doing so emits an x-ray equivalent to the difference in energy between the originating electron shell and the resting shell. The resulting spectrum of secondary x-rays (characteristic lines) is unique to any element and the intensity of characteristic lines is proportional to the concentration of that element in the sample. In practice only K and L shell electrons are aimed at, thus giving rise to secondary radiation, including Kα, Kβ, Lα and Lβ lines.

Fluorescent x-rays need to escape the sample without being absorbed ("Auger" effect) and travel to the detector unimpeded so that the intensity of the secondary emitted x-ray spectrum is maximised. In laboratory-based XRF equipment the potential loss of x-rays is minimised by placing the sample in a vacuum and minimising the sample-detector distance. Absorption (also see below) of x-rays within a sample is dependent upon sample compositional characteristics and since absorption effects are most significant for low energy x-rays (i.e. light elements), this reduces the effectiveness of XRF analysis of elements lighter than fluorine. Thus, samples with significant light element concentrations may give imprecise and spurious results for those elements.

In laboratory based WDXRF equipment, fluorescent x-rays are collimated and reflected off a diffracting crystal before being measured by a detector, usually a flow counter or a scintillation detector that, using associated electronics, translates the energy spectra into elemental intensities. These intensities are then quantified through prior calibration, established using reference materials, in order to ascertain the concentrations of elements present in unknown samples (after Fitton 1997, Potts & Webb 1992).

6.3.1 Potential errors and restrictions inherent in the use of XRF equipment

There are three significant sources of systematic error inherent in XRF equipment that need to be accounted for in the quantitative analysis of fluorescent x-rays: detector dead time, line overlap and absorption & enhancement.

Detector dead time refers to the fact that at high count rates the instrument may not have time to process all the incoming x-rays, resulting in a reduced concentration being reported. This error is minimised by applying a correction factor that takes into account the dead time or by extending the actual count time (Potts & Webb 1992: p262).
Line overlap is a problem where characteristic lines are close and the equipment is unable to identify to which element the line(s) relate. The effect of line overlap can be reduced in two ways: increasing the resolution of the detector or by calculating overlap factors often by using synthetic samples containing the interfering elements (Fitton 1997).

X-rays are attenuated within a sample: primary x-rays can be *absorbed* to produce fluorescent x-rays or scattered, through elastic (Rayleigh scattering) or inelastic collisions (Compton scattering). Fluorescent x-rays, themselves, can be re-absorbed producing tertiary x-rays (*enhancement* effect) or further scattered before detection by the XRF detector (Fitton 1997, Potts & Webb 1992). The amount of attenuation of x-rays is related to the wavelength of the x-rays and the bulk composition of the sample, its thickness and density. Shorter wavelengths are less strongly absorbed than longer wavelengths. The effect of attenuation caused by the sample can be estimated from its composition, the primary x-ray spectrum and system geometry. Potts et al. (1997a: table 2) report that the depth (or thickness) of a basalt sample, BCR-1 (see Table 30) that returns 99% of the fluorescent x-rays compared to that of an infinitely thick sample (i.e. the critical penetration depth) is less than 5mm for elements between K and Nb. This is based on a standard 35mm diameter XRF pressed powder pellet with density 2.8g cm^{-3}. Providing samples exceed critical penetration depths comparability is maintained in their response (Potts et al. 1997a, Webb pers. com.).

Probably the most important random error is that the precision of the XRF measurement of element concentration is directly related to the number of fluorescent x-ray emissions counted, for which the random error measurement is related to $\pm\sqrt{n}$, where n is the total number of 'counts' received. Hence precision can be improved by extending the count time.

With reference to restrictions inherent in the use of XRF equipment, Wavelength dispersive (WDXRF) and energy dispersive (EDXRF) are the two common types of XRF equipment in use within laboratories. Generally, WDXRF is capable of a high throughput of uniform samples (pressed powder pellet or glass disc) with a high precision, whereas EDXRF is able to accommodate larger samples at a lower rate and with a lower level of

precision. Both WD & EDXRF are capable of detecting and measuring elements ranging between F and U in the Periodic Table, with the WDXRF having lower detection limits (Potts & Webb 1992). One drawback with WDXRF when it is used to analyse prehistoric artefacts is that it requires part of the artefact to be ground to a fine powder for the manufacture of pressed powder pellets and glass discs (i.e. is partially destructive). A second drawback is that both the WD and EDXRF are conventionally laboratory-based and non-portable which means that the artefact being examined will need to leave the (museum) collection in order for it to be measured. Portable XRF equipment has the potential to overcome both of these 'limitations' that are a disadvantage when analysing prehistoric stone artefacts.

6.4 Portable X-Ray Fluorescence Spectrometer (PXRF)

A portable x-ray fluorescence spectrometer (PXRF) uses similar principles as standard, laboratory based, XRF equipment, that is irradiation of a sample with primary x-rays and detection and analysis of the emitted fluorescent x-rays. However, in the PXRF the primary x-rays are generated by decay of radioactive isotopes and detection is by a solid state, Hg_2I_2 detector. Also, the PXRF equipment is compact, powered by rechargeable batteries and requires little maintenance. These features are incorporated within the Spectrace 'TN9000' PXRF, which is marketed by Thermo FI, Sussex Manor Park, Gatwick Road, Crawley, Sussex RH10 2QQ, and is the PXRF used in this work.

6.4.1 PXRF primary radiation - sources and generation

The TN9000 PXRF has three isotopes that are used in turn to provide the primary radiation: ^{55}Fe, ^{109}Cd and ^{241}Am. The ^{55} **Fe** isotope has a maximum activity of 1.85 GBq (50mCi) through proton decay to a neutron and electron (electron capture: $^{55}Fe \rightarrow {}^{55}Mn + e^-$) with a half-life of 2.7 years. This results the production of Mn Kα x-rays at 5.9keV and Mn Kβ x-rays at 6.5 keV that are used to excite K, Ca, Ti K-lines. Lighter elements (low energy x-rays) than these suffer too much absorption in the PXRF window and in air, and cannot be successfully detected. The ^{109}**Cd** isotope has a maximum activity of 185 MBq (5mCi) through proton decay to a neutron and electron (electron capture: $^{109}Cd \rightarrow {}^{109}Ag + e^-$) with a half-life of 1.24 years. This results in the production of Ag Kα x-rays at 22.1 keV and Ag Kβ x-rays at 24.9 keV that are used to excite Mn, Fe, Rb, Sr, Y, Zr, Nb K-lines and Pb L-line. The third source, ^{241}**Am** has a maximum activity of 185 MBq (5mCi) through the emission of an alpha particle and subsequent reduction in daughter atom (^{241}Np) state by release of gamma radiation ($241Am \rightarrow 241Np + \alpha + \gamma$) and has a half

life of 458 years. This decay results in the production of 59.9 keV of γ radiation which is used to excite Ba, La and Ce K-lines. Note that the PXRF isotopes are able to excite a wider range of K & L lines than discussed above, only the ones pertinent to this work have been identified. For prior reviews of the PXRF performance and applications see Potts et al. 1995, 1997a, 1997b; Williams-Thorpe et al. 1999a.

6.4.2 PXRF detection of fluorescent x-rays

The non-externally-cooled solid state mercury iodide (Hg_2I_2) detector in the Spectrace TN9000 PXRF gives 260eV FWHM (full width half maximum) resolution for Mn Kα using the ^{55}Fe source and compares well to laboratory based silicon detectors (Si(Li)) which can give 150eV resolution with liquid N_2 cooling, or 180 to 200 eV with Peltier cooling. WDXRF has a resolution of 1 to 3eV (both for Mn Kα) in comparison (Spectrace 1994).

6.4.3 PXRF data processing, reported precision and detection limits

The electrical signals created by the PXRF detector are processed through a 2048 multi-channel analyser to produce x-ray energy spectra. The manufacturer's quantitative software package calculates the elemental concentration from the energy spectra plus an associated *fitting error*, a value that indicates the precision of the measurement based on uncertainties associated with counting and spectrum analysis. Software, incorporating a 'Fundamental Parameter Program', is used to calibrate and provide measurement corrections for absorption, etc., for the PXRF. Reported precision and detection limits for the Spectrace TN9000 PXRF are reproduced in Table 29 below.

Source	Element	Detection Limit* (Thermo FI) ('siliceous matrix' 200 s count time per source)	Detection Limit ** ('silicate rock' 200 s count time per source)	Relative Precision** (200 s count time per source – based on Whin Sill sample)	Detection Limit*** (Achievable by WDXRF)
^{55}Fe	K	150 ppm	360 ppm	1.6% (8 302ppm)	5 – 10 ppm
^{55}Fe	Ca	70 ppm	225 ppm	0.45% (64 540ppm)	5 – 10 ppm
^{55}Fe	Ti	55 ppm	120 ppm	1.8% (14 560ppm)	1 – 5 ppm
^{109}Cd	Mn	200 ppm	354 ppm	13.5%(1 320ppm)	5 – 10 ppm
^{109}Cd	Fe	110 ppm	424 ppm	1.5% (93 380ppm)	5 – 10 ppm
^{109}Cd	Rb	5 ppm	13 ppm	9.5% (27ppm)	0.1 – 1 ppm
^{109}Cd	Sr	4 ppm	14 ppm	2.2% (442ppm)	0.1 – 1 ppm
^{109}Cd	Y	4 ppm	9 ppm	14.0% (34ppm)	0.1 – 1 ppm
^{109}Cd	Zr	3 ppm	9 ppm	3.2% (206ppm)	0.1 – 1 ppm
^{109}Cd	Nb	4 ppm	6 ppm	29.4% (18ppm)	0.1 – 1 ppm
^{241}Am	Ba	9 ppm	21 ppm	2.0% (350ppm)	5 – 10 ppm
^{241}Am	Ce	7 ppm	14 ppm		0.1 – 1 ppm
^{109}Cd	Pb	15 ppm	39 ppm		1 – 5 ppm

*Table 29 Reported Spectrace TN9000 PXRF detection limits & relative precision and typical WDXRF detection limits. The associated Whin Sill elemental concentrations are given in brackets after the relative precision. (*Manufacturers data, ** Potts et al. 1995: table 1 & 2, *** Fitton 1997: figure 6.1)*

6.4.4 Factors that may affect PXRF performance

6.4.4.1 Detector dead time, line overlap, absorption & enhancement

As introduced in Section 6.3.1 there are three main systematic errors that relate to XRF equipment: detector dead time, line overlap and absorption & enhancement. The problem with detector dead time is overcome within the PXRF processing program and the effect of line overlap is countered by spectrum fitting/deconvolution within the PXRF software.

Unlike laboratory based XRF equipment the PXRF x-ray sources, Hg_2I_2 detector and the sample are not contained within a vacuum. This means that primary and secondary x-rays may be scattered and absorbed in the air gaps and the window between the sources/detector and the sample. Since the geometry of the source-sample detector is fixed and providing the sample to be measured is flat, fully covers the PXRF window and is positioned in the plane of analysis, allowances are automatically made for the potential reduction in fluorescent x-rays reaching the detector. The effect that uneven samples have on PXRF measurements is investigated in Section 6.13.

Absorption & enhancement effects within the sample are related to the composition of the sample (i.e. the matrix). By calculating a bulk mass attenuation of a basaltic rock sample (BCR-1, c.f. Appendix 12 for its composition) and assuming a density of 2.8 g cm^{-3}, Potts et al. (1997a) determined the thickness of the sample of which various percentages of the fluorescent signal originated when compared to a infinitely thick sample. This information is reproduced and expanded to cover 12 of the 13 elements commonly measured as part of this thesis.

	K	Ca	Ti	Mn	Fe	Rb	Sr	Y	Zr	Nb	Ba	Ce	Pb
99%	0.03	0.04	0.05	0.12	0.16	0.63	0.69	0.77	0.91	0.95	6.8	7.7	-
90%	0.02	0.02	0.02	0.08	0.07	0.30	0.34	0.39	0.45	0.48	3.4	3.9	-
80%	0.01	0.01	0.02	0.04	0.05	0.22	0.24	0.27	0.32	0.33	2.4	2.7	-
50%	0.01	0.01	0.01	0.01	0.02	0.09	0.10	0.12	0.14	0.14	1.0	1.2	-

Table 30 Thickness (mm) from which 99%, 90%, 80% and 50% of the fluorescent x-rays observed from an 'infinitely' thick sample of basaltic composition (BCR-1) originates, assuming a density of 2.8g cm^{-3} and based on K-line photon energies (Webb pers. com., after Potts et al. 1997)

It is noted that the elemental composition of the basalt BCR-1 is similar to that obtained for greenstones. Providing that exposure pellets have a similar density and pellet thickness exceed 1mm there is no need to adjust PXRF measurements for sample thickness for elements K to Nb, inclusive. However, PXRF measurements of Ba and Ce from exposure pellets may be slightly lower than expected. This possibility is examined in Section 6.10.

Note that all axe and actual rock samples are greater than 10mm thick so PXRF measurements of these samples will not need to be adjusted for absorption/enhancement effects.

6.4.4.2 Age of radioactive sources

The relatively short half-lives (<3 years) of ^{55}Fe and ^{109}Cd, result in the need to replace these isotope sources every 3 to 5 years in order to maintain satisfactory primary x-ray intensities. Between replacements the PXRF equipment is date sensitive and automatically takes into account the reduction of excitation intensity when calculating elemental concentrations. To allow levels of detection and instrument precision to be optimised sample exposure (count) times can be increased to a maximum of 200 seconds per isotope, the extended count time counteracting the lower count rate, hence lower n (counts) caused as a result of reduced x-ray intensities.

6.4.4.3 Sample precision in relation to grain size

As part of the overall PXRF precision, sampling precision is related to sample mineralogy and numbers of measurements made. Sampling precision is unaffected by the count time as it is a property of variations in the mineral assemblage of the sample (assuming the sample is flat, 'infinitely thick' etc.) (Potts et al. 1997: p39). Potts et al (op. cit.: table 8) have shown that approximately 2 PXRF measurements of the medium grained Whin Sill dolerite (grain size approximately 1mm, with occasional grains to 2mm) are required to achieve a precision of 5% standard deviation of the mean, for values greater than 10 times the PXRF SD. As greenstones have similar grain size to the Whin Sill dolerite (c.f. Chapter 4) it follows that 2 PXRF measurements should produce a similar sample precision. The sample precision achieved by the PXRF is examined in Section 6.13.

6.5 Description of the PXRF and ancillary equipment used in the field

The PXRF consists of a spectrometer unit (referred to as the 'probe') and a control unit with associated cables, test samples and stand packed in a single, portable container. The two main units, probe and control unit, are described below.

6.5.1 PXRF spectrometer unit (probe)

The PXRF probe (Figure 49a) houses the ^{109}Cd, ^{55}Fe, ^{241}Am isotopes and the mercury iodide detector in a robust, all-weather case complete with carrying handle and measures 127mm x 76mm x 216mm, weighing 1.9kg. The primary and fluorescent x-ray radiation is

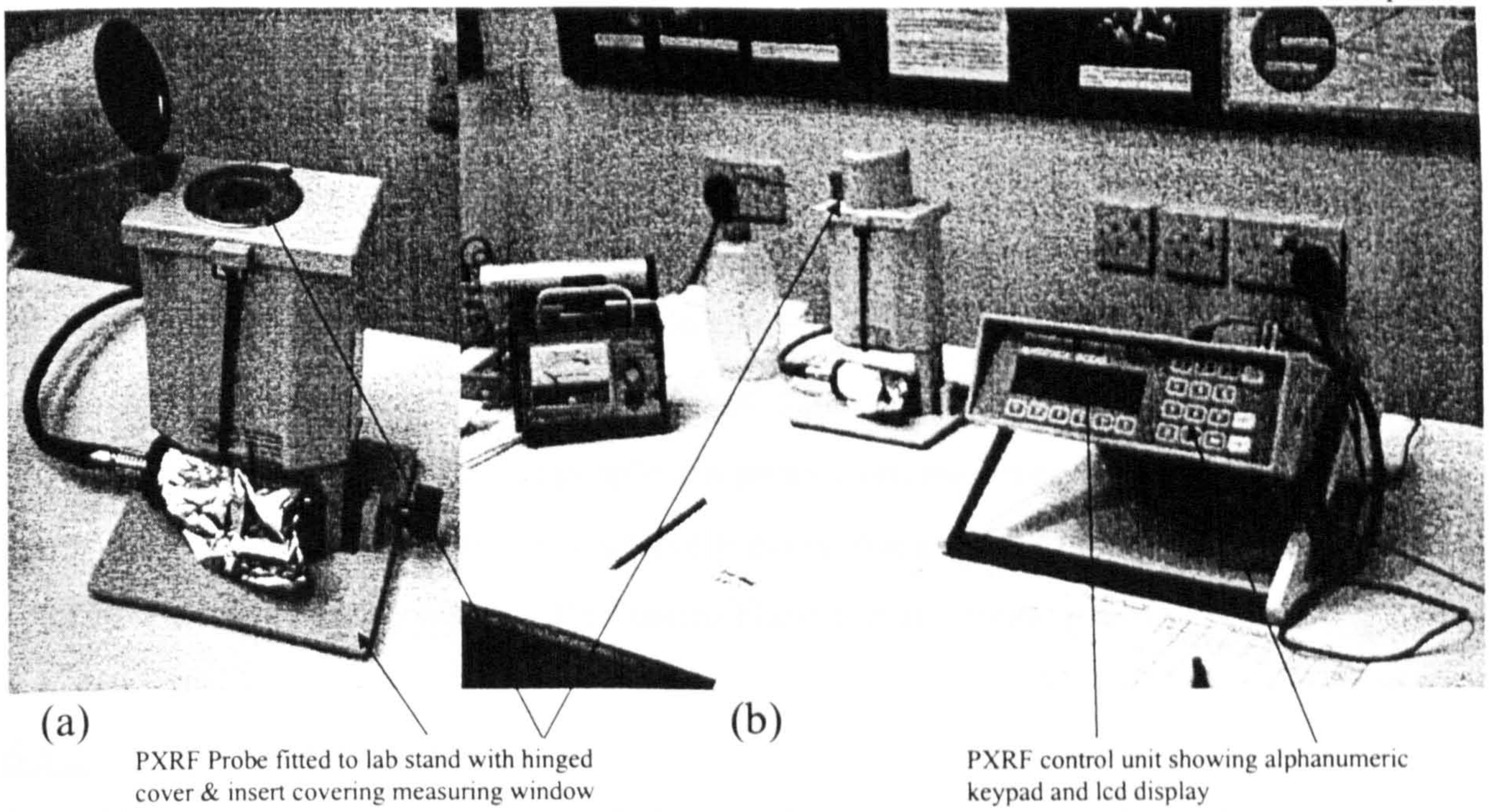

Spectrace TN900 Portable XRF Equipment

Figure 49 Spectrace TN9000 Portable XRF equipment

emitted and detected through a 25mm diameter window covered by a polypropylene membrane (25 μm thick) to prevent dust ingress into the active surfaces within the probe. All three radioactive sources are contained within a shielded section of the probe and are, in turn, exposed to fluoresce the sample being measured for a predetermined *count time*. Two protective probe covers are provided to cover the probe window when the equipment is not in use or is undergoing energy calibration. Both covers include a safety interlock to prevent the accidental exposure of the radioactive sources, and provide a radiation safety shield should the exposed isotope not retract into the shielded section of the PXRF probe. One of these covers is always fitted when the PXRF is in transit or not in use. The two covers differ in function as one is also used for energy calibration of the PXRF energy spectra. The probe handle contains an activation button that allows the user to activate (and deactivate) the probe in hand held operation. A red flashing LED indicates when the radioactive isotopes are exposed. Ancillary PXRF equipment includes a stand for the probe, which holds the instrument with the window uppermost and gives a platform on which samples can be placed for analysis (see Figures 49a & 50a).

Samples (up to approximately 1kg) are normally rested on the probe, over the window, with the probe fixed to its lab stand. The probe is placed against larger or in-situ samples (Figure 50b). For smaller samples, especially the 35mm diameter pressed powder pellets, a hinged, cup-like cover is fitted to the PXRF probe, under which the sample is placed for

analysis (Figure 49a). This cover further reduces the possibility of radiation leakage that may occur if a sample does not cover the probe window.

In terms of radiation safety, the maximum radioactive dose rate measured at 100mm from the window is 267 μGy hr^{-1} when the ^{109}Cd source is exposed and there is no sample covering the window (i.e. the 'most dangerous' situation). This reduces to 0.7 μGy hr^{-1} at 2m from the probe indicating that people 2m away from the probe are unlikely to receive a significant radiation dose in the very unlikely event that a source is exposed with no cover or sample over the probe window (Williams-Thorpe et al. 1999a: p 216).

6.5.2 PXRF Control Unit

The PXRF control unit is a 320mm x 300mm x 100mm weatherproof unit that collects and analyses data from the probe through on-board, customisable software, and is able to transmit data through a RS232 link to other electronic devices (Figure 49b & 50). Operator interaction is through a sealed keypad with audible tones generated on keystroke and start up. A 240 x 60 LCD (30 column x 8 alphanumeric) display with graphics capability displays a menu driven set of operating instructions and analysis results. The unit is capable of storing 300 sets of analyses and 40 sets of energy spectra. Each record can have up to an 11 character alphanumeric label (or automatically generated label) attached. Data is stored in the processor unit memory until deliberately deleted, or until memory is full when the earliest analysis will be automatically deleted in favour of the latest (after the operator has been warned). An integral and rechargeable NiCad battery pack is able to power the PXRF for up to 5 hours.

6.5.3 Ancillary equipment

Additional PXRF equipment includes a robust transportation case, suitable for air travel, various ready use spares (e.g. spare window membrane) and carrying satchels for portable use.

A portable (laptop) computer, containing the manufacturer's support software can be connected to the processor unit via an RS422 link to extract and display analysis data and spectra. This support software allows users to customise the PXRF control unit software: to select elements for measurement, to indicate expected compositional ranges, to set the units of measurement etc.

Figure 50 Spectrace TN9000 PXRF: typical operational environments

6.6 PXRF Experimental procedure

Most of the work undertaken in this research was carried out in university laboratories and museums during 3 fieldwork periods known as *Week 1*, *Week 2&3*, and *Week 4*. Wherever possible, the PXRF was set up with the probe as remote as possible from the main operating area containing the control unit for safety purposes (see Figure 50a). Setting up the PXRF normally took about 10 minutes and involved initial operational checks. These consisted of ensuring the correct date and time was entered in the control unit and that the correct calibration programme was current (called 'Rocks 2OU style'). Once the equipment was physically set and powered up a period of time, up to 30 minutes, was allowed for the PXRF to equilibrate at ambient temperature before any measurements were made. An energy calibration was then carried out before the equipment was used to measure samples. This 600-second calibration procedure checked that the energy spectra of the isotopes were as expected and automatically made any necessary adjustments to the PXRF calibration data used in spectrum processing.

After the energy calibration, the count times (isotope exposure) were set. For Week 1 and the first half of Week 2 & 3 the count times were 100s (^{109}Cd), 50s (^{55}Fe) and 40s (^{241}Am), as recommended by previous workers (Williams-Thorpe pers. com.). These times were increased to 110s, 60s, 50s, respectively, for the remainder of Week 2&3 (from date letter V, see Table 31 below) and for Week 4, as it was found that the PXRF SD had increased slightly when measuring the control pellets (see below). The increase in count time was aimed at returning instrument precision to previous levels.

Each analysis was given a unique filename in the form AXYZ123#2. The first letter represents the date of measurement, the second group (XYX123 in this case) was the (usually abbreviated) sample name and #2 indicates that this was the 2nd reading for this sample on that date. The fieldwork period, associated dates, letter of the day and locations are summarised in Table 31. In total over 1,300 individual measurements were made during the three fieldwork periods (totalling 28 days) the PXRF was used.

At least once during each fieldwork period a set of thirteen reference samples was measured to establish PXRF bias (see below). At the beginning and end of each working day, and usually once in the middle of the day, two of these thirteen (ACE and WSE) were measured in order to monitor the performance of the PXRF and confirm that the responses remained within acceptable limits (see Section 6.16 below).

Providing the axe or rock sample was not too heavy, the PXRF probe was mounted in its stand and the sample, after washing with (preferably) de-ionised or fresh tap water, thoroughly drying and dusting (where necessary), was placed over the probe window and measured. Pressed powder pellets were usually measured once on each side, medium grained greenstone implements and rocks were normally measured twice (to achieve a sample precision of better than 5% standard deviation of the mean (c.f. Section 6.4.4.3). For rock samples and axes, a third reading was taken if the two previous ones were observed to be significantly different (usually if any two consecutive major element concentrations differed by several thousand ppm).

A log of results was maintained along with a record of measurements for ^{55}Fe, ^{109}Cd and ^{241}Am backscatter peak intensities (since this backscatter data was not automatically saved in the associated PXRF electronic data file). These backscatter measurements record the intensity of the Rayleigh and Compton scattering encountered during the measurement.

Period	Date	Letter of the day	Cd count time (s)	Fe count time (s)	Am Count time (s)	Location
Week 1	23 May 1997	I	100	50	40	Open University
Week 1	24 May 1997	J	100	50	40	Open University
Week 1	26 May 1997	K	100	50	40	Open University
Week 1	27 May 1997	L	100	50	40	Colchester Castle Museum
Week 1	28 May 1997	M	100	50	40	Dorchester Museum
Week 1	29 May 1997	N	100	50	40	Truro Museum
Week 1	30 May 1997	O	100	50	40	Truro Museum
Week 2&3	22 May 1998	P	100	50	40	Open University
Week 2&3	23 May 1998	Q	100	50	40	Ivybridge
Week 2&3	24 May 1998	R	100	50	40	Ivybridge
Week 2&3	25 May 1998	S	100	50	40	Taunton Museum
Week 2&3	26 May 1998	T	100	50	40	Salisbury Museum
Week 2&3	27 May 1998	U	100	50	40	Winchester Museum
Week 2&3	28 May 1998	V	110	60	50	Ashmolean, Oxford
Week 2&3	29 May 1998	W	110	60	50	British Museum
Week 2&3	30 May 1998	X	110	60	50	Ivybridge
Week 2&3	1 June 1998	Y	110	60	50	Hull Museum
Week 2&3	2 June 1998	Z	110	60	50	Hull Museum
Week 2&3	3 June 1998	A	110	60	50	Hull Museum
Week 2&3	4 June 1998	B	110	60	50	Hull Museum
Week 2&3	5 June 1998	C	110	60	50	Open University
Week 4	8 January 1999	D	110	60	50	Open University
Week 4	9 January 1999	E	110	60	50	Open University
Week 4	10 January 1999	F	110	60	50	Open University
Week 4	11 January 1998	G	110	60	50	National Museum of Ireland, Dublin
Week 4	12 January 1999	H	110	60	50	National Museum of Ireland, Dublin
Week 4	13 January 1999	AI	**200**	60	50	University College, Dublin
Week 4	15 January 1999	AJ	110	60	50	Open University

Table 31 Summary of analysis period, date, letter of the day, count times and location of PXRF activities (Note: 200s Cd count time set during week 4 was used to analyse porcellanite axes only)

6.7 Investigation in to the quantitative accuracy, precision, and detection limits of the PXRF

6.7.1 Introduction

The performance of the PXRF in terms of accuracy, precision, and detection limits of the TN9000 PXRF has been reported by the manufacturer and other workers (see Spectrace 1994, Potts et al. 1995, and Williams-Thorpe et al. 1999a for reviews and Table 29 for summary). However, notwithstanding the published performance standards of the PXRF it is essential to confirm/establish that the performance standards of the PXRF are applicable to the measurement of greenstone rocks and axes. As such, this work in part repeats but also expands work undertaken by Williams-Thorpe et al. (1999a) and Potts et al. (1997a, 1997b,..1995) in order to establish PXRF accuracy, precision and detection limits.

Relationships between measurements and data for different materials

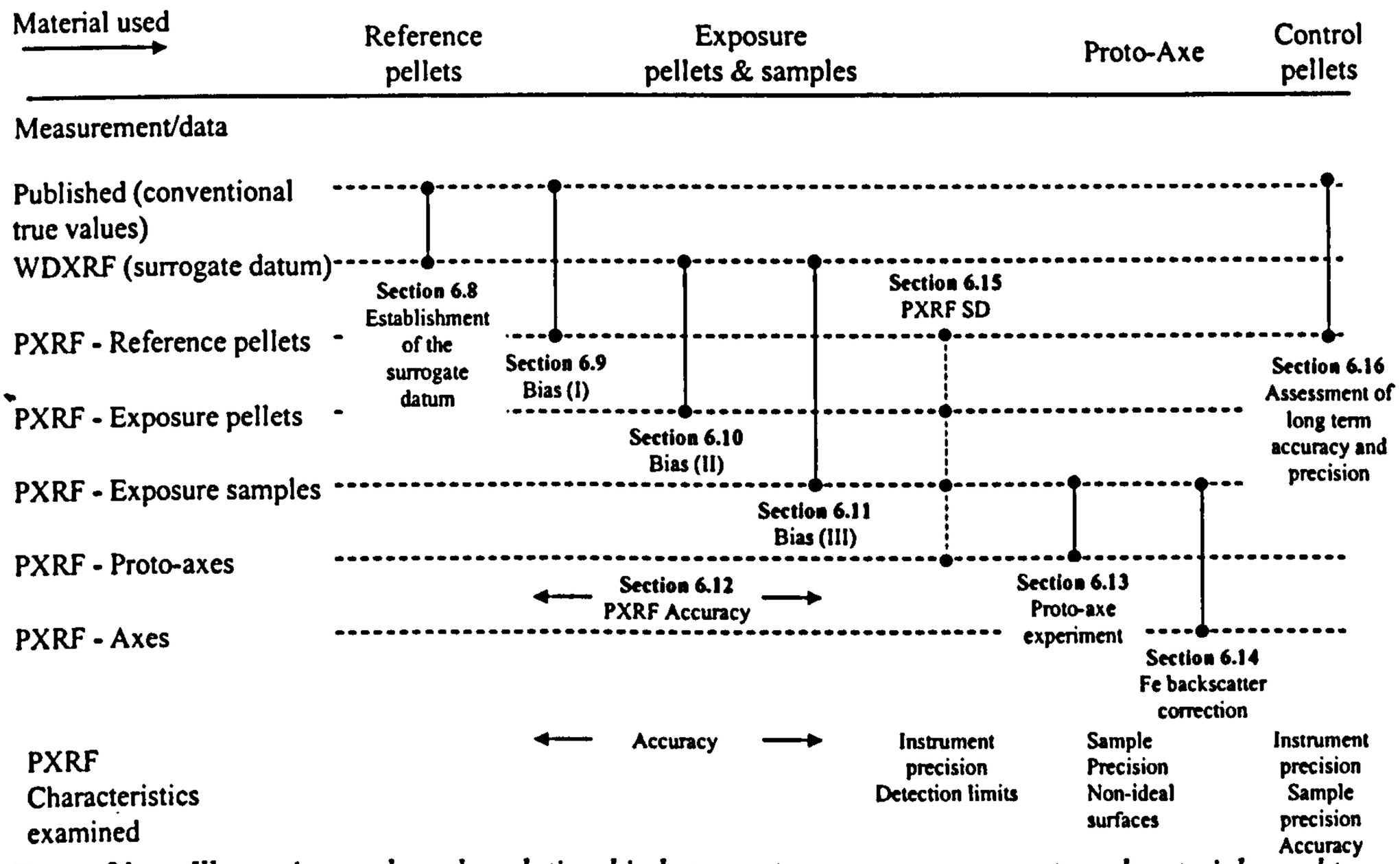

Figure 51 Illustration to show the relationship between types on measurements and materials used to examine the performance of the PXRF

In general, the accuracy of the PXRF is assessed by comparing conventional true values with PXRF and WDXRF measurements made on the international reference samples and exposure pellets, and PXRF measurements of greenstone exposure samples (with flat surfaces). Specifically, the difference between the *reference and surrogate datum* (i.e. conventional true values and surrogate true values) and the PXRF measured values is used to determine the achieved PXRF accuracy and establish the magnitude of any bias corrections (c.f. Sections 6.8 to 6.11). Long term precision and accuracy of the PXRF when measuring pressed powder pellets is established through repeatedly measuring the control pellets (c.f. Section 6.16). Sample precision, appropriate to the PXRF measurement of greenstone axe and exposure samples, is empirically established from measurements of a proto-axe (c.f. Section 6.13). The effect of curved, irregular and weathered sample surfaces on PXRF measurements is examined for a proto-axe in section 6.13 and in relation to Fe backscatter in Section 6.14. Analysis of PXRF SD values is used to examine instrument precision over the range of elemental concentrations encountered in this work and to estimate the detection limits of the PXRF (c.f. section 6.15). These activities are expanded below.

6.7.2 Overview of process to quantify PXRF measurements

Figure 51 illustrates the relationship between measurements/data and the material used in the eight activities described below.

1. Establishment of the surrogate datum

   The accuracy of the surrogate datum is established by comparing the conventional true values and the surrogate true values for the reference pellets (i.e. the published and WDXRF measured values of the reference pellets). Fundamentally, this comparison investigates whether the WDXRF is accurately calibrated and whether it can be used to determine the surrogate true values of the exposure pellets.
   (Results in Section 6.8)

2. PXRF Bias (I): Determination of the PXRF accuracy by measurement of reference pellets

   The accuracy of the PXRF in measuring reference pellets is determined by comparing conventional true values and PXRF measurements of the reference pellets using linear regression. The results of the regression analysis are used to establish the magnitude of PXRF bias for each element during each of the 3 fieldwork periods.
   (Results in Section 6.9)

3. PXRF Bias (II): Determination of the PXRF accuracy by measurement of exposure pellets

   This comparison is similar to PXRF Bias (I) above but uses surrogate true values of greenstone exposure pellets instead of the reference pellets to examine the accuracy of the PXRF. The surrogate true values of the exposure pellets are compared with PXRF measurements of the same exposure pellets using linear regression. This comparison establishes the PXRF bias in measuring pelletised samples of greenstone rock during the second fieldwork period (Week 2&3 – the only time the exposure pellets were measured by the PXRF). A comparison between Bias (I) (Week 2&3) and Bias (II) data is used to examine whether there are any differences in PXRF accuracy when measuring reference or exposure pellets.
   (Results in Section 6.10)

4. PXRF Bias (III): Evaluation of the PXRF accuracy by measurement of exposure rock samples

This comparison establishes the accuracy of the PXRF when measuring actual exposure samples. As above, linear regression is used to compare the surrogate true value of the exposure sample and PXRF measurements of the actual exposure rock sample. PXRF measurements of the flat and 'infinitely thick' exposure samples were made during the first fieldwork period (Week 1). Hence the results of the regression analysis to determine Bias (III) values are compared with Bias (I) (Week 1) to examine any differences in PXRF accuracy when measuring exposure pellets and exposure samples. Note that this investigation deals with PXRF measurements of *exposure samples* and not *homogenised* pellets, hence variations of the mineral assemblage within the excited volume may result in distinct differences between replicate measurements.

(Results in Section 6.11)

5. PXRF Proto Axe: Examining the effect of non-ideal surfaces on PXRF measurements

The PXRF is used to measure non-ideal surfaces of axes (i.e. axes, which are non-flat and may not fully cover the PXRF window, etc.) and this activity examines the effect of similar non-ideal surfaces on the accuracy of PXRF measurements. Two exposure samples, MM3 & PTX002, were used to manufacture 'proto-axes' which resulted in pieces of MM3 & PTX002 with varied surfaces, comparable to those encountered on greenstone axes, as well as an ideal (i.e. flat and of infinite thickness) piece of each sample. PXRF measurements made on the ideal sample surface are statistically compared with those made on non-ideal surfaces to establish if there is any difference in PXRF accuracy. In addition, the sample precision achieved from replicate measurements of actual greenstone rock is also examined.

(Results in Section 6.13)

6. PXRF Fe backscatter correction: Potential to adjust measurements of non-ideal surfaces

Potts et al (1997b) proposed a normalisation procedure that would compensate PXRF measurements to take into account gaps of up to 3mm between the PXRF window and the sample being measured. The value of the Fe backscatter is

automatically produced by the PXRF from the measurement of intensities of ^{55}Fe Mn Kα & Kβ Rayleigh and Compton scatter seen when measuring a sample. The normalisation procedure involves using the ratio of PXRF Fe backscatter recorded for an ideal surface to that of a non-ideal surface, of similar composition, to normalise the PXRF measurement made on the non-ideal surface. Although Potts et al. used uniform air gaps between the PXRF window and the sample being measured, the proposed normalisation procedure is applied here to PXRF proto-axe data (see 5 above) to examine whether the accuracy of PXRF measurements made on non-ideal surfaces can be improved.
(Results in Section 6.14)

7. PXRF SD: Examination of instrument precision and elemental detection limits.
The PXRF automatically produces an estimate of instrument precision based largely on the statistics associated with the total number of x-ray counts that contribute to a measurement (Potts et al. 1997b: p39). The variation of the reported instrument precision, which is believed to represent 1sd of the associated measurement, with elemental concentration is graphically and statistically examined in order to determine the relationship between elemental concentration and instrument precision. It is proposed that the value of the given instrument precision at zero concentration is directly related to the detection limit for the element in question. Hence, using graphical examination coupled with regression analysis, PXRF detection limits for all 13 elements routinely measured in this thesis are established.
(Results in Section 6.15)

8. PXRF Repeatability: Assessment of long term accuracy and precision
Control pellets were measured by the PXRF at least twice every day that the equipment was used, providing a large data set of containing over 80 individual measurements of each pellet. This data set is used to examine the day to day and week to week accuracy of the PXRF, and to examine the precision obtained through repeated measurements of the same pellets.
(Results in Section 6.16)

6.8 Establishment of the surrogate datum

The thirteen international reference samples used in this work are listed in Table 32 and are a sub-set of those used previously in establishing the analytical performance of the PXRF (Potts et al. 1995). The rock samples were processed into pressed powder pellets at the Open University using the method described in Watson (1996) and were analysed specifically for this work by the OU WDXRF in January 1998 (approximately mid-way through the research).

Reference Name	Rock Type	Source & (Issuing Organisation)
ACE (or AC-E)	Microgranite	Ailsa Craig (GIT –IWG)
AGV-1	Andesite	(USGS)
BCR-1	Basalt	(USGS)
BHVO-1	Basalt	(USGS)
G2	Granite	(USGS)
GH	Granite	(GIT-IWG)
GSP-1	Granodiorite	(USGS)
MICAFE	Biotite	(GIT-IWG)
PMS	Microgabbro	Pitscurrie (GIT-IWG)
QLO-1	Quartz Latite	(USGS)
RGM-1	Rhyolite	(USGS)
STM-1	Syenite	(USGS)
WSE (or WS-E)	Quartz Dolerite	Whin Sill (GIT-IWG)

Table 32 List of the 13 international reference samples used within this research. All listed in (apart from PMS and WSE) Potts et al. 1992, PMS and WSE from Govindaraju et al. 1994. (USGS: United States Geological Survey, GIT- IWG: Group Internationale de Travail: International Working Group.)

Published conventional true values (Potts et al. 1992, Govindaraju et al. 1994) and OU WDXRF measurements of the reference samples are detailed in Appendix 12. Data in Potts et al. (1992) is given confidence intervals of less than 10% relative (2 sigma) for most elements and Govindaraju (1994) quotes similar intervals for samples WSE and PMS.

OU WDXRF results are available for pressed powder pellets only, since glass disks used when measuring major oxides were not available, as such major elements K, Ca, and Mn are not contained in the summary table below. Indicative concentrations for Ti and Fe are provided by the WDXRF when measuring powder pellets and have been reported for *illustrative* purposes only. Major element data in Appendix 12 (Part 1 of 2) is presented as both '% oxide by weight' and ppm, with all trace elements reported in ppm only. Conversion from oxides to ppm is carried out using stoichiometric conversion factors published by Potts et al. (1992).

Sample	Ti	Fe	Rb	Sr	Y	Zr	Nb	Ba	Pb
ACE	*60ppm*	*6.7%*	-0.8%	0.7ppm	-4.6%	-4.5%	-1.7%	4.5%	3.5ppm
AGV-1	-4.2%	6.7%	-3.4%	2.2%	1.3ppm	-3.1%	1.3%	1.9%	2.5ppm
BCR-1	*-5.4%*	0.4%	-3ppm	-1.5%	-1.6%	0%	0.7%	**-7.5%**	1.6ppm
BHVO	0%	-0.7%	-1.1ppm	1.7%	-0.7%	2.2%	-0.3%	**-6.8%**	-0.4ppm
G-2	*6.1%*	*13.1%*	1.5%	**5.1%**	1.8ppm	1.3%	1.8ppm	4.7%	4ppm
GH	*30ppm*	-4.5%	2.6%	0.8ppm	-4.2%	4.3%	1.4%	-2.5%	4ppm
GSP-1	1.5%	*17.4%*	1.2%	2.8%	3ppm	**7.7%**	2.7%	4.4%	4ppm
MICAFE	-2.6%	*-12.5%*	-2.2%	-1.3ppm	**9.2%**	**-7.8%**	**-11.9%**	**11%**	0%
PMS	1.7%	2.7%	-0.7ppm	1.7%	-3.3%	1.4%	-0.5ppm	**-6.6%**	N/A
QLO-1	-4.2%	*8.7%*	-.0.3%	2.8%	-0.8%	-0.5%	-0.8ppm	-1.7%	3.4ppm
RGM-1	-4.8%	2.1%	-0.1%	**6.6%**	1.5ppm	-3.7%	-0.5ppm	3.2%	2.5ppm
STM-1	0%	*8.7%*	-1.4%	1.5%	-3.6ppm	-4.9%	**6.3%**	-5.0%	2.5ppm
WSE	-2.8%	0.2%	1.3%	1.5%	1.9%	1.5%	-0.9ppm	-4.1%	0.8ppm

Table 33 Differences between conventional true values and surrogate true values for the 13 reference samples/pellets. All trace element differences are <5% relative or <4ppm, unless highlighted in bold. WDXRF measurements for Ti & Fe are illustrative only. Relative difference = (Published value – WDXRF value)/(published Value) expressed as a percentage. Where the relative difference is >5% the actual difference (in ppm) is shown if the actual difference is <4ppm. (Extracted from Appendix 12 part 2 of 2, based on data in Appendix 12 part 1 of 2)

Table 33 summarises the differences between the conventional true values and the surrogate true values (i.e. OU WDXRF measured values for the reference samples/pellets). The differences are normally reported as relative to the conventional true value. If the relative difference is greater than 5% but within ±4ppm of the conventional true value then the actual difference is reported. This is done to remove possible spurious relative percentages obtained at low concentrations. For example, the conventional true value for Nb in PMS is 3ppm and the average (n=2) OU WDXRF measured concentration is 3.5ppm, giving a relative difference of 16.7%; it is felt that a difference of 0.5ppm is more indicative of the accuracy of the OU WDXRF in this case.

Inspection of Table 33 reveals that there are only 11 cases where the difference between the conventional true and measured trace element values is >5% relative or >4ppm. MICAFE accounts for 4 of these cases (Y, Zr, Nb, Ba) and this observation is discussed in more detail in Section 6.9.3.1, below. In two cases (GSP-1 & STM-1) the difference exceeds 5% relative at high values of Zr (530ppm) and Nb (268ppm) respectively, and values like these are unlikely to be encountered in greenstones. The remaining 5 cases are divided between Ba (BCR-1, BHVO-1 & PMS) and Sr (G-2 & RGM-1) and in all these cases the relative error is less than 7.5%. It is re-iterated that Ti & Fe are only provided as illustrative values by the WDXRF, hence the differences cannot be used to assess WDXRF accuracy.

It can be concluded that the accuracy of the OU WDXRF better than 5% relative or 4ppm for Rb, Y, Zr, Nb, Pb, (except high values of Zr & Nb) and 7.5% relative for Sr & Ba

(noting MICAFE discussion in Section 6.9.3.1) when compared with conventional true values. It is therefore assumed that OU WDXRF measurements of (greenstone) exposure pellets will be as accurate and that these measurements can be considered as surrogate true values of the associated greenstone samples. (Note that the OU WDXRF did not measure Ce and it is assumed that the OU WXDRF is correctly calibrated for K, Ca, Ti, Mn & Fe.)

6.9 PXRF Bias (I): Determination of the PXRF accuracy by measurement of reference pellets

6.9.1 PXRF Bias (I): data

Conventional true values for the 13 reference samples are detailed in Appendix 12. Actual PXRF measurements of the associated reference pellets are listed in Appendix 13. During the first fieldwork period (Week 1) the reference pellets were measured twice, once on each side. During the second fieldwork period (Weeks 2&3) the reference pellets were measured on both sides at the beginning of the period and on one side at the end of the period, giving a total of three sets of data. During the third fieldwork period (Week 4) the reference pellets were measured twice, on both sides each time, giving four sets of data.

6.9.2 PXRF Bias (I): results

Figure 52 shows bivariate charts for Ti, Y, Zr & Nb, just a selection of the 13 full-page charts contained Appendix 14.2. These charts plot the conventional true value (reference value: independent variable) against the PXRF measured value (dependent variable) for each reference sample/pellet. PXRF data for the second and third fieldwork periods has been averaged prior to being plotted on the charts (note: only one set of measurements was made in Week 1). Error bars, calculated as twice the PXRF SD (instrument precision) at the mid-range of the spread of reference sample values, are also plotted on each chart.

Table 34 summarises the results of linear regression analysis between the two data sets, with the conventional true value as the independent variable and the PXRF measurement as the dependent variable (the full set of results is contained in Appendix 14.1). Linear regression analysis is carried out twice for each of the three fieldwork periods (using averaged values for the second and third fieldwork periods) in order to determine the accuracy of the PXRF during each period. For each fieldwork period the regression is first constrained through the chart origin (0,0) and then unconstrained (i.e. the regression is not constrained through (0,0)). The reason for this was to examine the difference in the degree

of linearity, reported by the R^2 statistic, between the each pair of regressions and to examine the possibility of there being a static offset within the PXRF calibration.

Element & Fieldwork period		Regression constrained through (0,0)		Regression unconstrained		
		Coefficient of regression	R^2	Coefficient of regression	R^2	Offset (ppm)
K	Week 1	**0.997**	0.998	**1.014**	0.999	-863
	Week 2&3	**0.983**	0.996	**1.005**	0.998	-1 428
	Week 4	1.036	0.996	1.081	0.999	-1 537
Ca	Week 1	0.930	1.000	0.928	1.000	**115**
	Week 2&3	0.915	1.000	0.910	1.000	**296**
	Week 4	0.978	0.999	0.961	1.000	1 001
Ti	Week 1	1.200	0.996	1.220	0.997	**-237**
	Week 2&3	1.254	0.996	1.271	0.996	**-190**
	Week 4	1.276	0.996	1.301	0.996	**-288**
Mn	Week 1	1.224	0.861	1.395	0.886	**-195**
	Week 2&3	1.094	0.912	**1.157**	0.917	**-70**
	Week 4	1.180	0.847	1.263	0.853	**-92**
Fe	Week 1	1.016	0.999	1.034	0.999	-1 500
	Week 2&3	**0.991**	0.998	**1.006**	0.999	**-1 035**
	Week 4	**0.997**	0.999	**1.013**	0.999	-1 097
Rb	Week 1	1.095	0.990	1.124	0.991	**6.2**
	Week 2&3	1.071	0.972	**1.095**	0.973	**-4.9**
	Week 4	**1.031**	0.990	**1.023**	0.990	**-1.0**
Sr	Week 1	1.150	0.998	1.160	0.998	**-4.6**
	Week 2&3	1.102	0.999	1.101	0.999	**-0.5**
	Week 4	1.102	0.995	1.113	0.995	**-5.3**
Y	Week 1	**1.017**	0.990	1.055	0.993	-4.4
	Week 2&3	0.937	0.987	**0.958**	0.988	**-2.3**
	Week 4	0.943	0.991	**0.971**	0.993	**-3.1**
Zr	Week 1	1.142	0.998	1.148	0.998	**-4.0**
	Week 2&3	1.116	0.997	1.133	0.997	**-11.2**
	Week 4	1.125	0.997	1.141	0.997	**-10.4**
Nb	Week 1	**1.019**	0.993	1.045	0.995	-4.1
	Week 2&3	**0.997**	0.994	**1.002**	0.994	**-0.8**
	Week 4	**1.019**	0.996	**1.027**	0.996	**-1.2**
Ba	Week 1	0.820	0.992	0.804	0.993	**17.8**
	Week 2&3	0.833	0.984	0.816	0.985	**19.5**
	Week 4	0.812	0.983	0.791	0.984	**23.5**
Ce	Week 1	0.667	0.759	0.821	0.976	-45.5
	Week 2&3	0.656	0.810	0.799	0.988	-40.8
	Week 4	0.644	0.853	0.774	0.989	-35.4
Pb	Week 1	1.350	0.008	2.421	0.638	-38.3
	Week 2&3	1.510	-0.487	3.304	0.416	-44.8
	Week 4	1.516	-0.337	2.462	0.661	-40.2

Table 34 Summary of regression analysis data for Bias (I). Data presented here is extracted from Appendix 14.1. Values in bold indicate that the range of 95% confidence limits straddles 1 (for regression coefficients) or 0 (for offset)

6.9.3 PXRF Bias (I): discussion

6.9.3.1 Bivariate charts

Visual inspection of the charts in Figure 52 and Appendix 14.2 clearly indicates that there is a linear relationship, close to 1:1, between the conventional true values and those obtained by the PXRF for each element except for Ti, Ba, Ce and Pb. PXRF Ti measurements exceed the conventional true values, with a difference greater than twice the instrument precision for values above 10,000ppm. PXRF measurements of Ba and Ce are

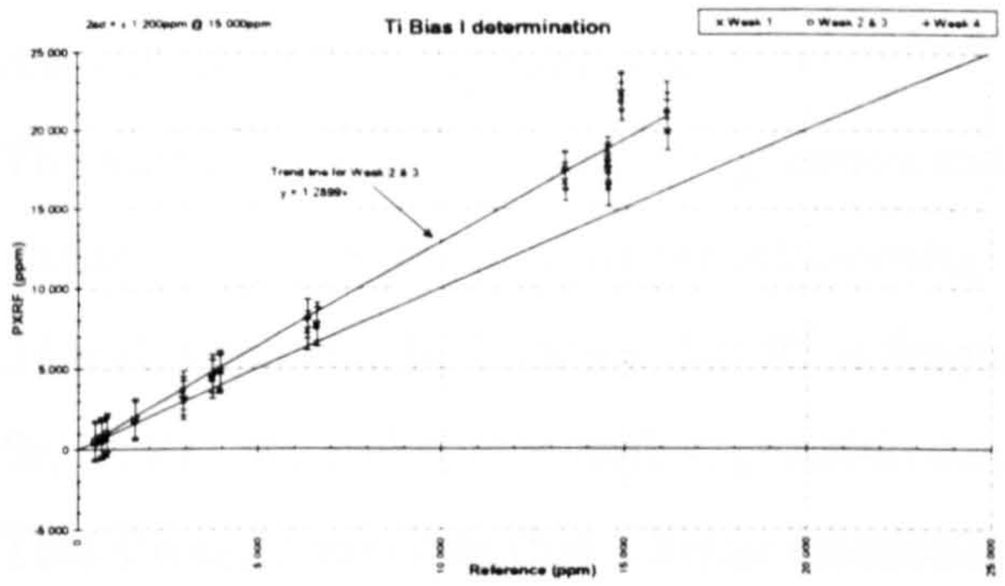

(a)

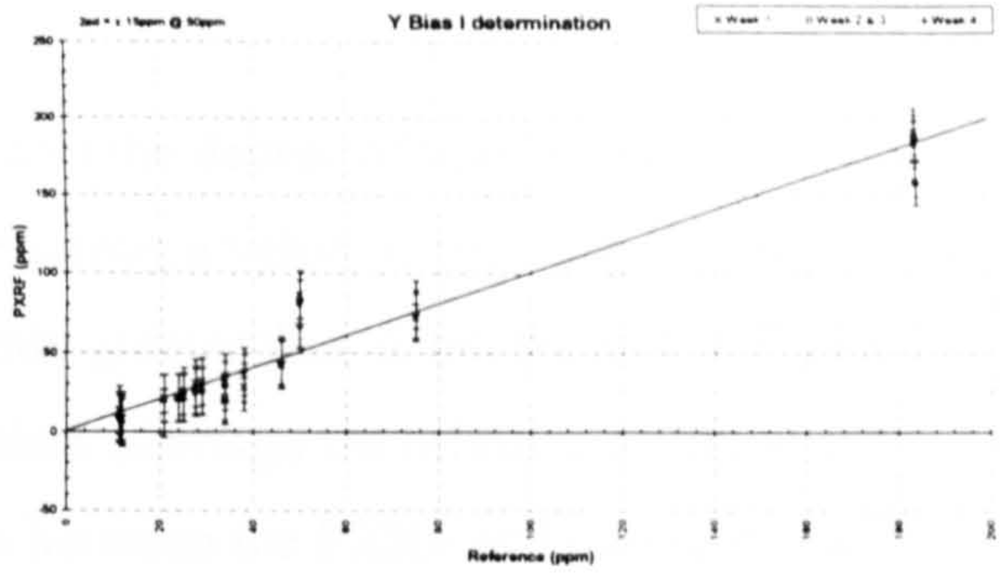

(b)

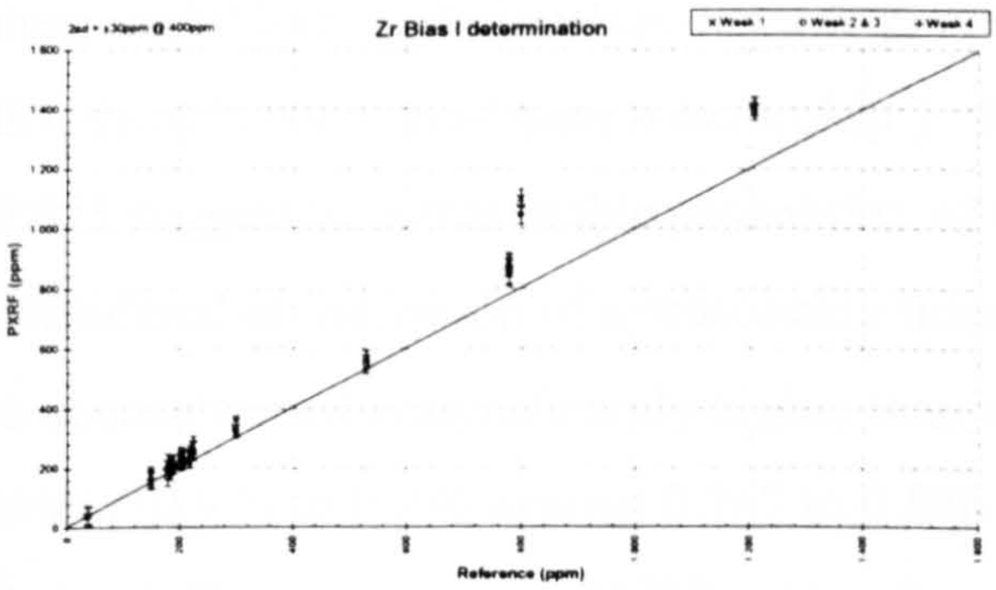

(c)

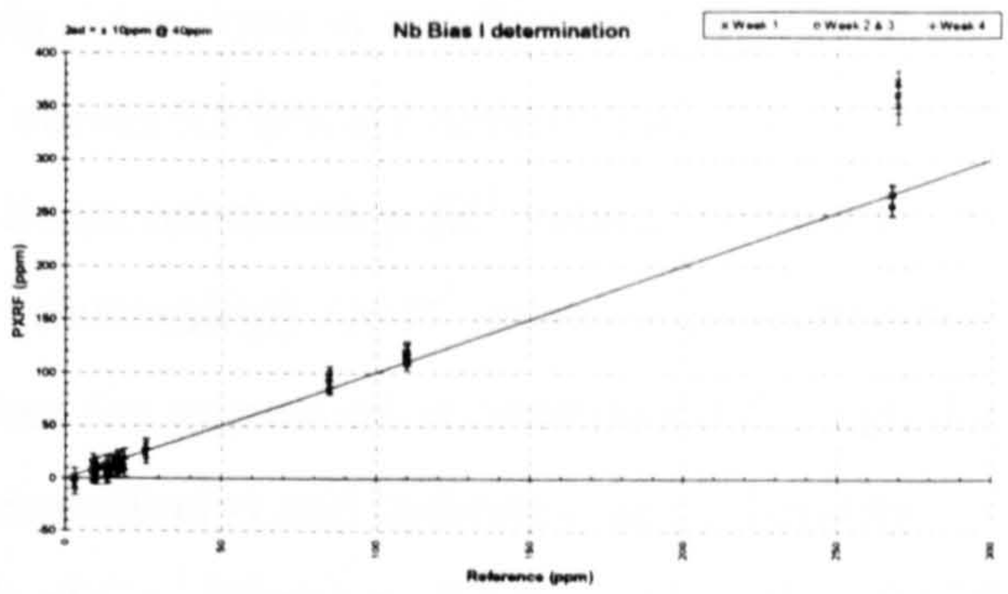

(d)

Figure 52 Examples of Bias (I) bivariate charts taken from Appendix 14.2. In each case the independent variable (x-axis) is the conventional true value of the reference material and the dependent variable (y-axis) is the PXRF measurement of the reference pellet

lower than the conventional true values with Ce appearing to have a static offset of approximately -40ppm. The low concentrations, generally less than 60ppm, and relatively low instrument precision, ±30ppm, for Pb makes it difficult to determine whether there is any relationship between the conventional true value and the PXRF measured value for concentrations of less than 60ppm.

MICAFE Anomaly

Visual inspection of the bivariate charts and as already noted in Table 33, data reveal that PXRF measured MICAFE concentrations are significantly different to those published. MICAFE (biotite mica) is known to contain many 'exotic' elements at unusually high concentrations that can and do affect the ability of XRF equipment to correctly determine element concentrations (Webb pers. com.). Additionally, the plate-like grains of mica may be preferentially aligned as a result of compression of the powder pellets during their manufacture and this non-random distribution of grains may also result in analytical bias (Potts & Webb 1992). These two factors are thought to be reasons for the significant differences in MICAFE measurements, and as biotite mica is not a major constituent of greenstone rocks (c.f. Chapter 4), it was decided not to use any MICAFE measurements in the statistical analysis associated with the accuracy of the PXRF.

6.9.3.2 R^2 statistic of regression

The value of the R^2 statistic of regression indicates the degree of linearity between two variables, with a 'perfect' linear relationship returning a value of one. Inspection of Table 34 and Appendix 14.1 shows that R^2 is frequently greater than 0.990 for K, Ca, Ti, Fe, Rb, Sr, Y, Zr, Nb, and Ba for both regression exercises (through the origin and otherwise). This strongly suggests that a linear relationship between the PXRF and published data exists for these elements (any R^2 value >0.950 is considered to have a statistically meaningful linear relationship, or more precisely, 'that there is insufficient reason to doubt that there is not a non-linear relationship'). R^2 values for Mn are approximately 0.875 ± 0.025 suggesting a reasonable probability of a linear relationship (R^2 values > 0.80 are considered as indication of a reasonably linear relationship). Ce R^2 value when regression is unconstrained is significantly higher than when the regression is constrained through the origin (0.976 to 0.986 against 0.767 to 0.846 respectively) and indicates the probability that an offset is present in PXRF measurements of Ce. R^2 values for Pb are less than 0.638 in all cases and indicate the improbability of a linear relationship between the conventional true value and PXRF measured values at concentrations less than 60ppm.

6.9.3.3 Offset when regression analysis is unconstrained

The offset (i.e. the value 'b_0' in the standard straight-line equation $y = b_1x + b_0$) (see Table 34), plus upper and lower 95% confidence intervals of the offset are given in Appendix 14.1 along with the associated standard error. It is proposed that if the upper and lower 95% confidence limits for the offset straddle zero, then there is no reason to reject the hypothesis that the regression passes through the origin of the chart (0,0). It can be seen in Table 34 that offset values for Ca (apart from Week 4), Ti, Mn, Rb, Sr, Zr and Ba straddle zero (indicated in bold), hence there is no reason to suspect the PXRF is offset for these elements. Y and Nb each contain one offset that does not straddle 0, hence indicating that there may be a PXRF offset of -1 to -2ppm when compared with the conventional true values. Noting the Y & Nb standard error (1.7 & 1.6 respectively) and the fact the remaining two regression for each element do straddle zero, it can be concluded that the size of the offset is insignificant and that regression through the origin could be assumed. Ce and Pb intercepts are distinctly negative, strongly suggesting that PXRF measurements of these two elements contain an offset. In the case of Ce, the associated R^2 value when the regression is unconstrained complements the probability of an offset, whilst the Pb results are inconclusive. Hence for Ce & Pb the relationship between the PXRF and published values cannot be considered to pass through (0,0) based upon measuring pressed

powder pellets. Inspection of the Fe chart and associated offset values indicate the possibility of a PXRF offset of approximately -1,000ppm in measuring Fe concentrations, which is about twice the calculated standard error for the intercept (c.f. Appendix 14.1). This potential offset will be taken into account when discussing accuracy below. The intercept values for the three regression calculations and their associated 95% confidence limits for the element K also suggests an offset. However, inspection of the associated chart (Appendix 14.2 Part1/13) reveals that there is a marked deviation from the (visually estimated) best-fit straight line through the data points for values less than 10,000ppm. This is possibly due to the PXRF reaching its detection limit for this relatively light element (with low sensitivity) and will need to be taken into account when discussing accuracy below. However, for values greater than 10,000ppm the visually estimated best fit straight line passes close to the origin of the chart, supporting the suggestion that that the offset may only be significant at low K concentrations (<10,000ppm or approx. 1.5% wt. K_2O).

6.9.3.4 Coefficient of regression

The coefficient of regression ('b_1' in $y = b_1x + b_0$) in the regression analyses is a measure of the accuracy of the PXRF with reference to the conventional true values, when measuring pressed powder pellets. A coefficient of one would indicate that the two variables in the regression have a 1:1 relationship and, would mean that there is no PXRF bias over the range of concentrations encountered (although there may still be an offset). Thus, a constrained regression which results in a b_1 coefficient and a R^2 value both greater than 0.950 indicate that the PXRF is linearly calibrated, through the origin (using a 0.05 significance value). A coefficient of regression different to unity would indicate the PXRF overestimates (coefficient >1) or underestimates (coefficient <1) elemental concentrations (providing R^2 remains >0.950 and the data has been constrained). Hence, as R^2 calculated from PXRF and conventional true values is greater than 0.950 for all elements except Mn, Ce & Pb, it is assumed that the calculated regression coefficient b_1 is a measure of the proportional bias of the PXRF when measuring that element.

Figure 53 illustrates the regression coefficient (bias) and associated upper and lower 95% confidence limits for each element based on constrained regression for each fieldwork period (data in Appendix 14.1). Table 34, above, lists the coefficients of regression. If the interval range of the upper and lower 95% confidence limits straddles one (indicated in bold in Table 34) then the null hypothesis: 'that there is no bias between PXRF and the

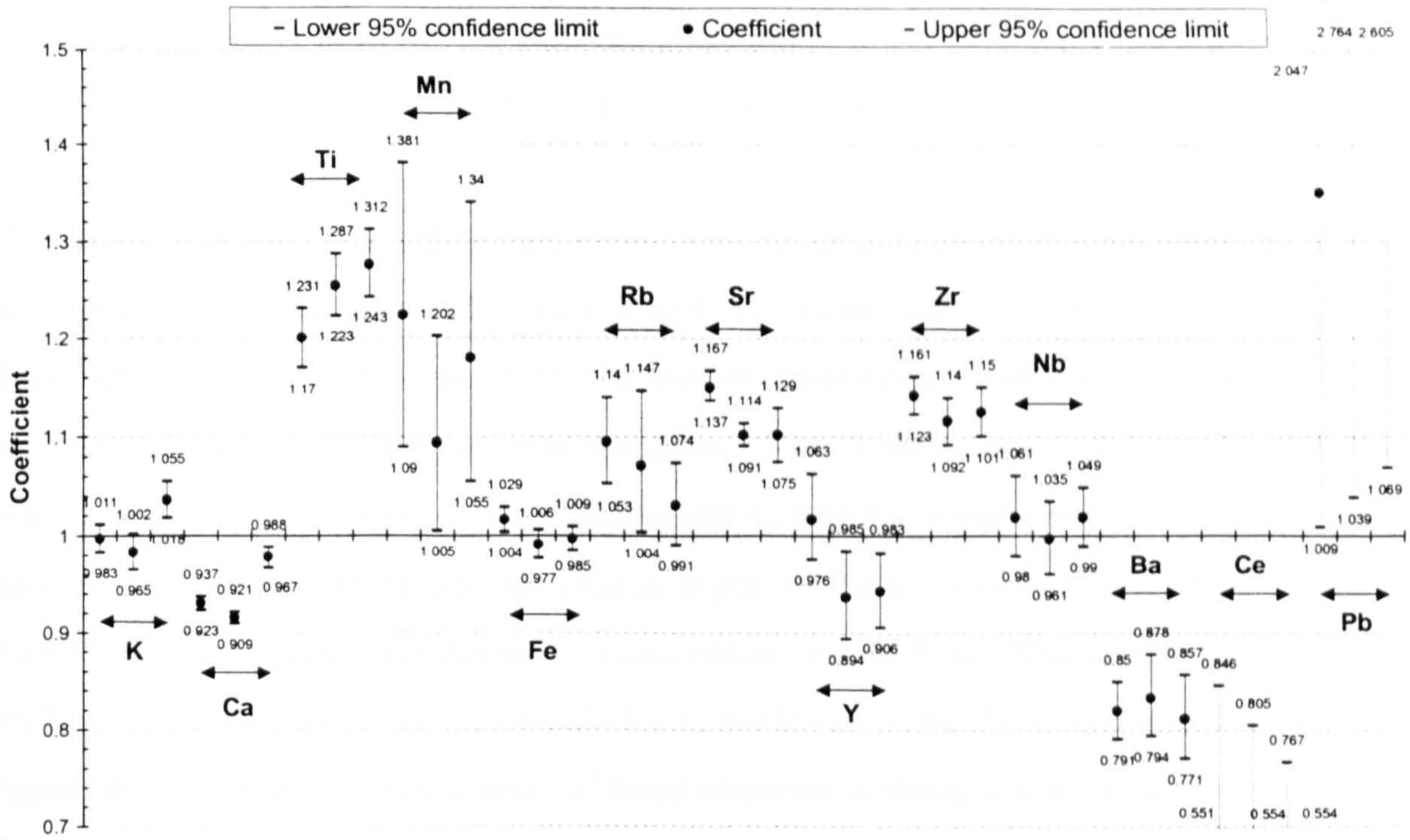

Figure 53 Chart illustrating the 95% upper and lower confidence range of Bias (I) coefficients of regression (b_1) for each element analysed when regression is constrained through (0,0) for each of the three field work periods: Week 1 left, Week 2&3 centre and Week 4 right hand of each set of coefficients. (Data from Appendix 14.1)

conventional true values, cannot be rejected 0.05 significance value). Inspection of Table 34 and Figure 53 shows that the null hypothesis cannot be rejected for Nb and in part to K, Fe, Rb & Y. Confidence limits for all Ca, Ti, Sr, Zr, Ba, Ce and Pb regressions and certain K, Fe, Rb & Y regressions indicate that a bias in PXRF measurement is probable. Further inspection of Figure 53 and Appendix 14.1 show a slightly different bias for each element between each of the fieldwork periods but that the range of confidence limits overlap to some degree. The reason for this slight variation are not understood and it is possible that these differences (apart from K & Ca, see below) are random and related to the operational characteristics of the PXRF (or that insufficient analyses have been made). Thus, generally speaking, each element's regression coefficient can be considered as being similar for all three fieldwork periods and usually within 5% relative to the average of the associated three coefficients.

The first two coefficients (Week 1 and Week 2&3) for K and Ca are similar, with the third coefficient (Week 4) being noticeably higher for both elements. This is put down to the fact that the PXRF probe window cover was changed after the second fieldwork period (Weeks 2&3) and before the third fieldwork period (and Week 4) to a thinner, polypropylene membrane. This is assumed to have reduced the absorption of x-rays for these two lighter elements compared to the previous window, thus increasing the intensity

of fluorescent x-rays detected and the PXRF reporting higher than actual concentrations of K and Ca (noting the bias for Ca remains less than one for all fieldwork periods).

Considering the elements individually, the PXRF is considered to have underestimated Ca concentrations by approximately 3 to 8%, and Ba concentrations by 16 to 19% during the three analysis periods. The reason for the former is not understood and is probably a calibration bias in the PXRF (and the change in PXRF window membranes). However the reason that Ba concentrations were underestimated may be in part due to the pressed powder pellet being thinner than the critical depth for Ba Kα x-rays (Section 6.4.4). The PXRF appears to have overestimated Ti concentrations by 20 to 28%, Mn by 10 to 23%, Rb by 3 to 10%, Sr by 10 to 15% and Zr by 12 to15% over the three fieldwork periods. Again, the reason for overestimation of these elements is thought to be a calibration bias in the instrument. The PXRF measures Nb concentrations to ±2% and Y concentrations to +2 to -6%, indicating that these variations may just be random bias around an accurate (1:1) calibration.

As remarked above, the PXRF measurement of K concentrations below 10,000ppm seems to be consistently lower than expected and this is reflected in the consistently negative *y-axis* intercept values. This also explains why the constrained regression coefficients detailed in Table 34 above, for Weeks 1 and 2&3 are just below unity. At this stage of the discussion it is concluded that the PXRF underestimates K concentrations by up to 1,000ppm for measured values less than 10,000ppm and correctly reports concentrations above 10,000ppm. This will be discussed further in Bias (II) & (III) below.

Fe regression coefficients suggest very little bias (<±2%) with the PXRF possibly underestimating concentrations by approximately 1,000ppm. As for K, above, this issue is discussed further below, however, at this stage of the investigation it is concluded that the PXRF accurately reports Fe concentrations to ±2% relative.

Finally, results of Ce and Pb regression analysis are inconclusive with the data available. Visual examination of the associated charts reveals a possible relationship between PXRF and published values for Ce, with the PXRF constantly underestimating actual concentrations by 30 to 50ppm and this is partly borne out by regression analysis. The reasons for the poor relationship may, in part, be due to pellet thickness being less than the critical depth for Ce (Pb measured using L lines). Whatever the reason, it is concluded that

PXRF Ce and Pb concentrations cannot be corrected for bias or offset and that they should only be used for indicative purposes.

6.9.4 Summary of Bias (I) investigation

Inspection of bivariate charts and regression analysis has shown that there is a significant linear relationship between conventional true and PXRF measured values of the reference samples/pellets (except MICAFE) for 11 of the 13 elements analysed. Pb and Ce are the only two elements where the null hypothesis (that there is a significant linear relationship) can be rejected (at a 5% significance value). Examination of regression coefficients and *y-axis* intercepts show that PXRF measurements are not generally offset, only in the cases of K (only below 10,000ppm), Ce and Pb. The confidence intervals (95%) for the regression coefficient only straddles unity in 9 of the 39 cases, indicating that the PXRF has a proportional bias in 30 cases that will need to be corrected for before the PXRF measurements can be directly compared with measurements from other sources.

6.10 PXRF Bias (II) – Determination of the PXRF accuracy by measurement of exposure pellets

6.10.1 PXRF Bias (II): data

The reference samples used in the Bias (I) investigation (Section 6.9) had been chosen to give a wide range of elemental concentrations in order to review the performance of the PXRF over a significant range of silicate rock compositions. However the main rock type encountered in this work is greenstone, which is not represented within the reference samples. In order to investigate the accuracy of the PXRF when measuring greenstone a selection of greenstone rocks was obtained from exposures in Cornwall and prepared for analysis in the form of pressed powder pellets and glass discs. OU WDXRF analyses of the powder and glass discs (i.e. the surrogate true value for the associated rock sample) are detailed in Appendix 15. At least two PXRF analyses of the exposure pellets (one on each side) were made during the second fieldwork period (Week 2&3). Results from these analyses are detailed in Appendixes 15.3 and 15.4. Appendix 15.1 summarises the data provided in Appendixes 15.2 to 15.4 by sample to allow comparison of WDXRF, pellet and rock values from the same sample.

6.10.2 Processing of exposure samples (for Bias (II) & (III))

Greenstone rock samples were split using a hydraulic rock splitter in order to remove weathered surfaces and reduce the sample for crushing to sub 4mm size using a Fritsch jaw crusher. Samples were subsequently ground to a fine powder (90% <65μm) using an agate crusher (tema). The resulting powder was used to prepare pressed powder pellets in the manner described by Watson (1996) and into glass discs using the process described in Ramsay et al. (1995). Larger pieces of each exposure sample were sawn to provide a flat surface of sufficient size to totally cover the PXRF probe window and to be of 'infinite' thickness with regards to x-ray absorption (i.e. > 2cm thick).

6.10.3 PXRF Bias (II): results

Figure 54 shows bivariate charts for Ti, Y, Zr & Nb, a selection of the 13 full-page charts contained in Appendix 16.2. These charts plot the surrogate true value (WDXRF measurement of the greenstone pellet: independent variable) against the average PXRF measured value of the exposure pellet (dependant variable). (Note these charts are also used to illustrate the Bias (III) investigation.) Error bars, with the same values as used in Figure 52 and Appendix 14.2, ±2 PXRF SD are based on the value at the mid-range of the spread of reference sample values.

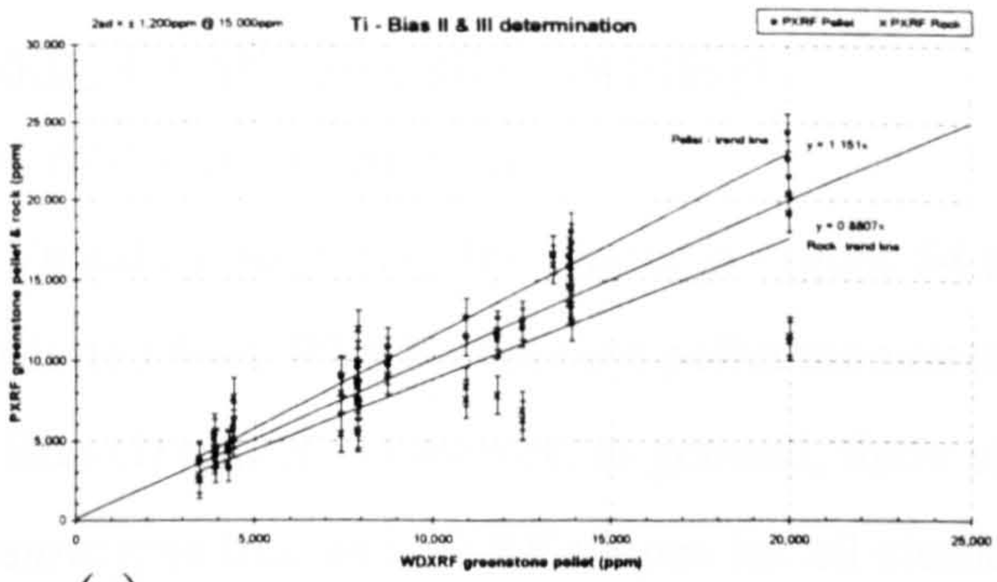

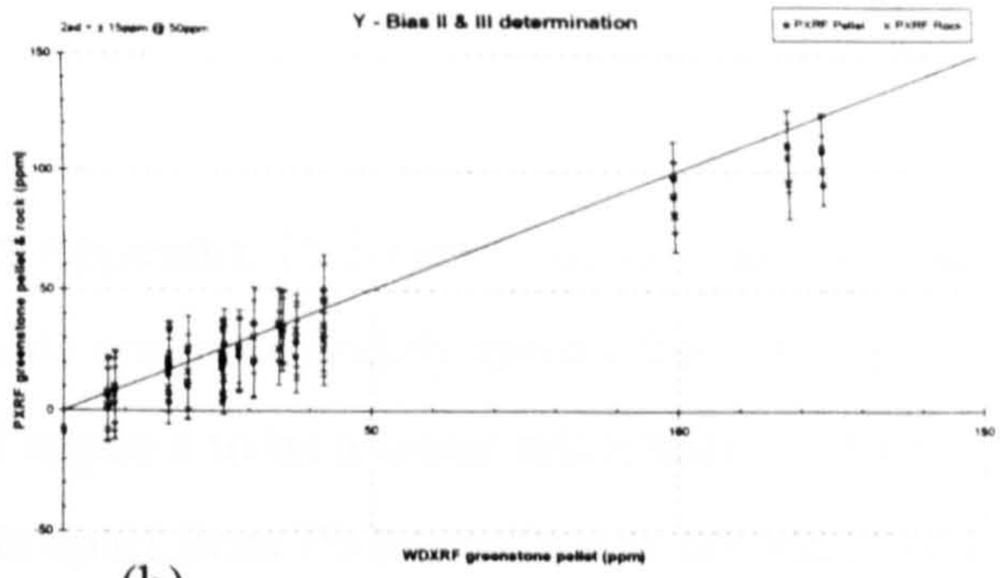

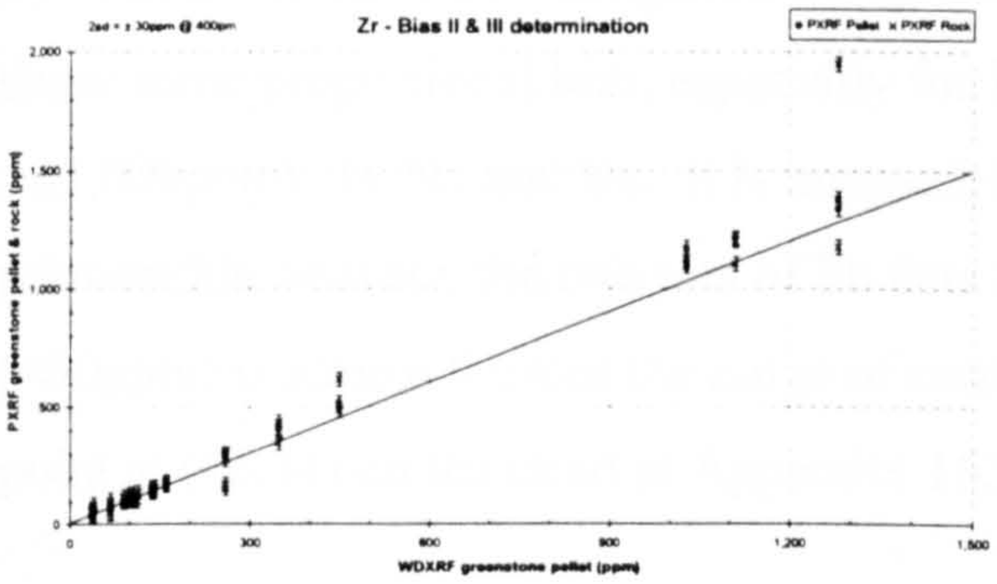

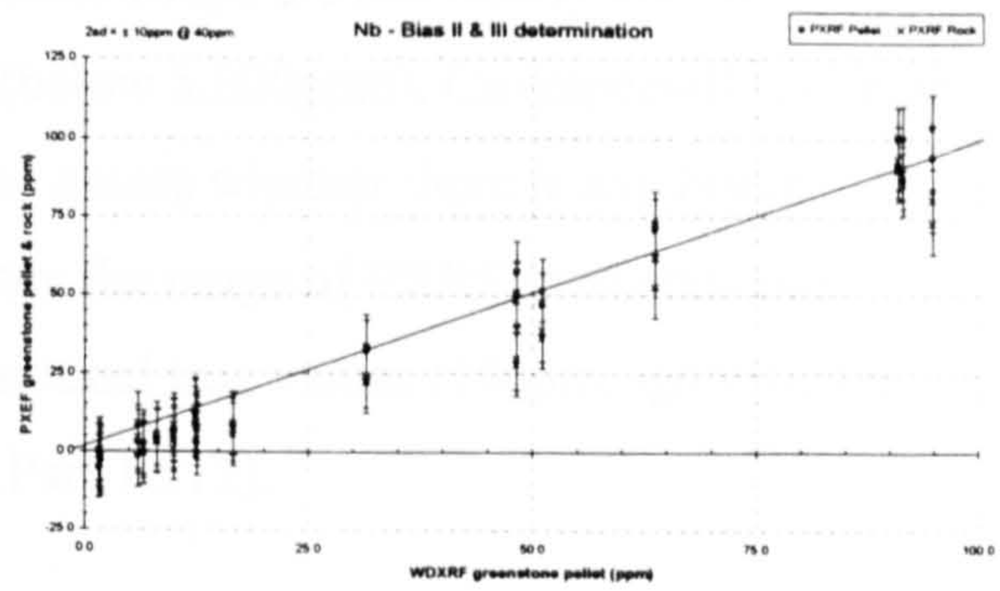

Figure 54 Examples of Bias (II) and Bias (III) bivariate charts taken from Appendix 16.2. In each case the independent variable (x-axis) is the surrogate true value of the exposure sample and the dependent variable (y-axis) is the PXRF measurement of the exposure pellet and exposure rock sample.

Table 35 summarises the results of linear regression analysis between the two data sets with WDXRF measurements as the independent variable and PXRF measurements as the dependant variable (the full set of results is contained in Appendix 16.1). As for Bias (I), linear regression analysis is carried out twice with the same data, constrained (0,0) and unconstrained.

Element & Fieldwork period		**Regression constrained through (0,0)**		**Regression unconstrained**		
		Coefficient of regression	R^2	Coefficient of regression	R^2	Offset (ppm)
K	Week 2&3	0.939	0.984	**1.057**	0.978	-1 312
Ca	Week 2&3	0.922	0.999	0.927	0.997	**-315**
Ti	Week 2&3	1.151	0.992	1.165	0.963	**-159**
Mn	Week 2&3	1.141	0.985	1.218	0.938	**-157**
Fe	Week 2&3	1.027	0.999	**1.021**	0.990	**427**
Rb	Week 2&3	**1.058**	0.971	**1.058**	0.940	**0.1**
Sr	Week 2&3	1.157	0.998	1.168	0.994	**-5.7**
Y	Week 2&3	0.921	0.990	0.922	0.976	**0.0**
Zr	Week 2&3	1.091	0.999	1.084	0.998	**5.4**
Nb	Week 2&3	**1.040**	0.989	1.115	0.988	-5.0
Ba	Week 2&3	0.821	0.979	0.919	0.951	-15.7
Ce	Week 2&3	not measured		not measured		
Pb	Week 2&3	**0.870**	0.124	**1.089**	0.139	**-5.1**

Table 35 Summary of regression analysis data for Bias (II). Data presented here is from Appendix 16.1. Values in bold indicate that the range of 95% confidence limits straddles unity (for regression coefficients) or 0 (for offset). In some cases unconstrained R^2 is surprisingly larger than the equivalent constrained R^2 value. The reasons for this are not understood and are probably related to the software (SPSS) used.

6.10.4 PXRF Bias (II): discussion

6.10.4.1 Bivariate charts

Visual inspection of the charts in Figure 54 and Appendix 16.2 clearly shows that the data plotted from PXRF exposure pellet measurements are more widely spread than seen in Bias (I) charts. However, in general, there still appears to be a linear relationship between surrogate true and PXRF values for all elements apart from Pb (note Ce was not measured by WDXRF). In this investigation the linear relationships are not clearly 1:1, but often show some proportional bias, especially for K (below 5,000ppm), Ca (especially at values >25,000ppm), Ti, Sr, and Ba. It is impossible to assess whether there is any linear relationship between the two sets of Pb data since the range of PXRF measurements (<90ppm) is almost 9 times the range of conventional true values (10ppm, ignoring the point at (46,34) on the chart at Appendix 16.2, Part 12/12).

6.10.4.2 R^2 statistic of regression

Table 35 shows that values of the R^2 statistic are >0.971 for all elements measured (when regression is constrained), apart from Pb (Ce is not measured). These values, being greater than 0.95, suggest that there is a significant linear relationship between PXRF and WDXRF measurements. Inspection of the equivalent R^2 statistic when regression is unconstrained reveals that there remains a significant linear relationship between PXRF and WDXRF measurements apart from for Mn & Rb and Pb. Overall, Bias (II) R^2 values appear numerically slightly less than the equivalent Bias (I) R^2 values (compare Table 34 and 35), but still show there is a significant linear relationship between PXRF and WD XRF for most measurements.

6.10.4.3 Offset when regression analysis is unconstrained

Table 35 shows that range of upper and lower 95% confidence limits for the *y-axis* intercept straddles zero for all elements apart from K, Nb and Ba (indicated in bold in Table 35, and numerically in Appendix 16.1). The K offset (-1,312ppm) is similar to that found in Bias I, i.e. an offset of up to -1,000ppm for concentrations less than 10,000ppm. Nb is offset by -5ppm, with upper and lower limits -2.8 to -7.1ppm respectively, similar to that found during Week I of the Bias (I) regression (offset -4.1ppm, range -0.7 to -7.8ppm). Inspection of the Nb chart (Figure 54d & Appendix 16.2 Part 10/12) does show that PXRF Nb values are lower than the associated WDXRF values for Nb concentrations less than 20ppm and are the reason for the slight negative offset. The Ba offset is negative (-15.7ppm) and possibly related to pellet thickness being below critical penetration depth

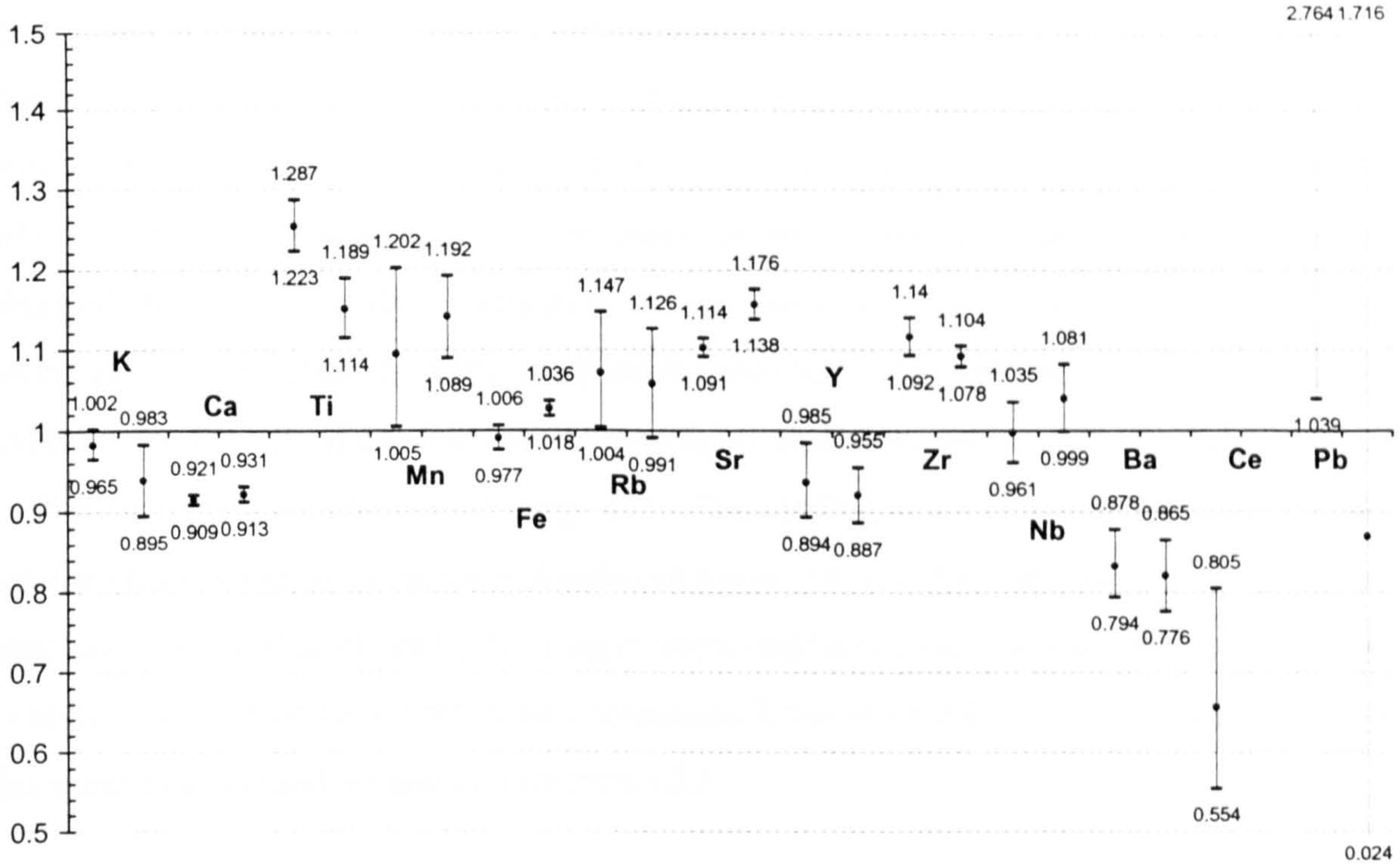

Figure 55 Chart illustrating the 95% upper and lower confidence range of Bias (I) Week 2&3 and Bias (II) coefficients of regression (b_1) when regression is constrained through (0,0). The left hand of each pair is Bias (I) and the right hand is Bias (II). (Data from Appendix 14.1 and 16.1)

(c.f. Table 30), resulting in lower PXRF values. Apart from these three elements, it is concluded that there is insufficient evidence to reject the null hypothesis: that the regression does not pass through the origin (0,0), at a 0.05 significance value. Handling of the three elements, K, Nb, Ba that appear to have significant offsets is discussed in Section 6.12, after examining the results of Bias (III).

6.10.4.4 Coefficients of regression

Regression coefficients and their associated ranges, at 95% confidence limits, are detailed in Appendix 16.1 and summarised in Table 35, with those b_1 coefficients where the 95% confidence range straddles unity shown in bold. Figure 55 compares the Bias (I) and (II) regression coefficients and associated 95% confidence limits (the left hand of each pair of data being Bias(I) Week 2&3). Examination of Bias (II) data in Table 35, Appendix 16.1 and Figure 55 indicates that it is probable that there is a bias between the PXRF and WDXRF for all elements apart from Rb and Nb. Comparing Bias (I) and (II) regression coefficients (Figure 55) it is seen that the lower and upper 95% confidence limit ranges overlap for K, Ca, Mn, Rb, Y, Zr, Nb, Ba and Pb. This indicates that it is probable (at a 95% confidence level) that the coefficients obtained in Bias (I) and Bias (II) for these elements are not different. The ranges of Bias (I) and (II) upper and lower confidence limits for Fe are separated by 0.012 for the second fieldwork period (Week 2 & 3) (c.f. Figure 55), but do overlap if Week 1 Fe Bias (I) coefficients were used in stead of Week 2

& 3. Likewise, the upper and lower 95% coefficient limit range for Sr Bias (I) and (II) for Week 2&3 are separated by 0.024, but if Bias (I) Week 1 regression values are used instead of Week 2&3 then Sr Bias (I) & (II) coefficient ranges almost totally overlap each other. In these latter two cases it is not unreasonable to conclude that the coefficients obtained from the Bias (II) investigation are similar to those obtained in the Bias (I) investigation. The Bias (II) 95% confidence range for Ti is separated by 0.034 (c.f. Figure 55) from the Bias (I) Week 2&3 coefficient range and only just (0.019) overlaps the Week 1 (Bias (I) regression coefficient range and. The small overlap and the difference (0.034) between data obtained in the same fieldwork period (Week 2&3) means it is not possible to conclude that the Bias (I) and (II) Ti regression coefficients are similar. This raises doubt as to the accuracy of the PXRF when measuring Ti concentrations in greenstone rocks and this point is discussed further in section 6.12.2.

6.10.5 Summary of Bias (II) investigation

This investigation has shown that there is a significant linear relationship between PXRF and WDXRF measurements of exposure pellets for all elements, apart from Pb and that regression probably passes through (0,0) for all elements, apart from K, Nb and Ba. Bias (II) also establishes the probability of a bias in the PXRF when measuring K, Ca, Ti, Mn, Fe, Sr, Y, Zr and Ba. It has not been possible to determine PXRF accuracy in measuring Pb.

Comparison between Bias (I) and Bias (II) using the range of upper and lower 95% confidence limits reveals that the two sets of regression coefficient values are within the 95% confidence limits for most elements, apart from Fe, Sr and Ti. However, the Fe and Sr Bias (II) regression coefficient values are similar to those obtained during the first fieldwork period and the differences in coefficients observed in the second fieldwork period (Week 2&3) do not warrant further investigation. The difference in Ti regression coefficients is considered to be significant and will require further examination (c.f. Section 6.12.4).

It can therefore be reasonably assumed that the accuracy of the PXRF in measuring reference pellets is largely the same for greenstone exposure pellets for all but three elements: Ti accuracy appears to be significantly different, Pb accuracy cannot be measured and Ce accuracy cannot be confirmed as it was not measured as part of the Bias (II) examination.

6.11 PXRF Bias (III): Evaluation of the PXRF accuracy by measurement of exposure rock samples

6.11.1 PXRF Bias (III): data

As Figure 54 illustrates, Bias (III) examines the relationship between PXRF measurements of exposure rock samples and their associated surrogate true values. The surrogate true values (i.e. obtained using the OU WDXRF) for the exposure samples are detailed in Appendix 15.2. PXRF measurements of exposure samples are detailed in Appendix 28.3, and summarised in Appendix 15.1. At least two PXRF measurements were made on sawn flat, fresh surfaces of each exposure sample, with each PXRF measurement made on non-overlapping areas of the sample, during Week 1.

6.11.2 PXRF Bias (III): results

Figure 54 shows bivariate charts plotting surrogate true values against PXRF measurements of associated rock samples for Ti, Y, Zr and Nb, a selection of the 12 full-page charts contained in Appendix 16.2 (c.f. 6.10.3 for a description of the charts).

Table 36 summarises the results of linear regression analysis between the conventional true values and the average PXRF measurement of the exposure sample. As before, linear regression has been carried out twice for each set of variables: constrained through (0,0) and unconstrained. Full details of both regression analyses are contained in Appendix 17.1.

Element & Fieldwork period		Regression constrained		Regression unconstrained		
		Coefficient of regression	R^2	Coefficient of regression	R^2	Offset (ppm)
K	Week 1	0.731	0.819	0.757	0.626	**-289**
Ca	Week 1	0.892	0.978	**0.966**	0.915	**-5 011**
Ti	Week 1	0.881	0.927	0.750	0.678	**1 598**
Mn	Week 1	**1.043**	0.954	**0.931**	0.737	**221**
Fe	Week 1	**1.068**	0.944	**1.295**	0.577	**-17 343**
Rb	Week 1	**1.057**	0.834	**1.086**	0.721	**-4.0**
Sr	Week 1	**1.035**	0.815	**1.033**	0.550	**0.8**
Y	Week 1	0.846	0.990	0.857	0.978	**-0.7**
Zr	Week 1	1.122	0.965	1.135	0.943	**-10.0**
Nb	Week 1	0.884	0.973	**0.952**	0.963	**-4.4**
Ba	Week 1	0.849	0.847	**0.981**	0.676	**-20.6**
Ce	Week 1	Not	measured	Not	measured	
Pb	Week 1	**0.998**	0.327	**0.690**	0.158	**6.7**

Table 36 Summary of regression analysis data for Bias (III). Data presented here is from Appendix 17.1. Values in bold indicate that the range of 95% confidence limits straddles unity (for regression coefficients) or 0 (for offset). As indicated in Table 35, and clearly shown here, in some cases unconstrained R^2 is larger than the equivalent constrained R^2 value. The reasons for this are not understood and are probably related to the software (SPSS) used

6.11.3 PXRF Bias (III): discussion

6.11.3.1 Bivariate charts

Inspection of Figure 54 and Appendix 16.2 clearly shows that the PXRF measurements of the exposure samples have a greater spread of values in comparison to those for the equivalent exposure pellets. This is almost certainly related to variation in mineral assemblage within the excited volume when non-overlapping PXRF measurements are made on the same sample. For example, in the five replicate PXRF measurements made on exposure sample CUD003, Fe concentrations ranged from 109,000ppm to 167,000ppm (Appendix 16.2 Part 5/12 and Appendix 16.1).

Examination of each chart in Appendix 16.2 reveals that PXRF measurements of exposure samples are broadly linear with respect to the surrogate true values apart from Pb. The elements with the greatest difference observed between exposure pellet and exposure sample values are K, Ca, Ti (concentrations >10 000ppm) and Sr (concentrations >400ppm). Just as for Bias (I) & (II), the PXRF measurements of Pb are too widely spread, preventing any realistic estimation of the relationship between the two data sets.

6.11.3.2 R^2 statistic of regression

Table 36 shows the value of the R^2 statistic in both regression analyses (fixed and free) are lower than those obtained for Bias (I) & (II), suggesting that there is less of a linear relationship between PXRF measurements of the exposure samples and the associated conventional true (WDXRF) values. In some cases (notably K, Rb, Sr and Ba) the R^2 value is less than 0.95 indicating that there is sufficient reason to reject the null hypothesis: that there is linear relationship between PXRF and WD XRF measurements. Since the major difference between Bias (I) & (II) and Bias (III) is that the PXRF is measuring different parts of a fine to medium grained mineral assemblage and not opposite sides of a homogenised powder pellets it is presumed that more PXRF measurements of each exposure rock sample would be necessary to fully determine the degree of linearity between the two data sets.

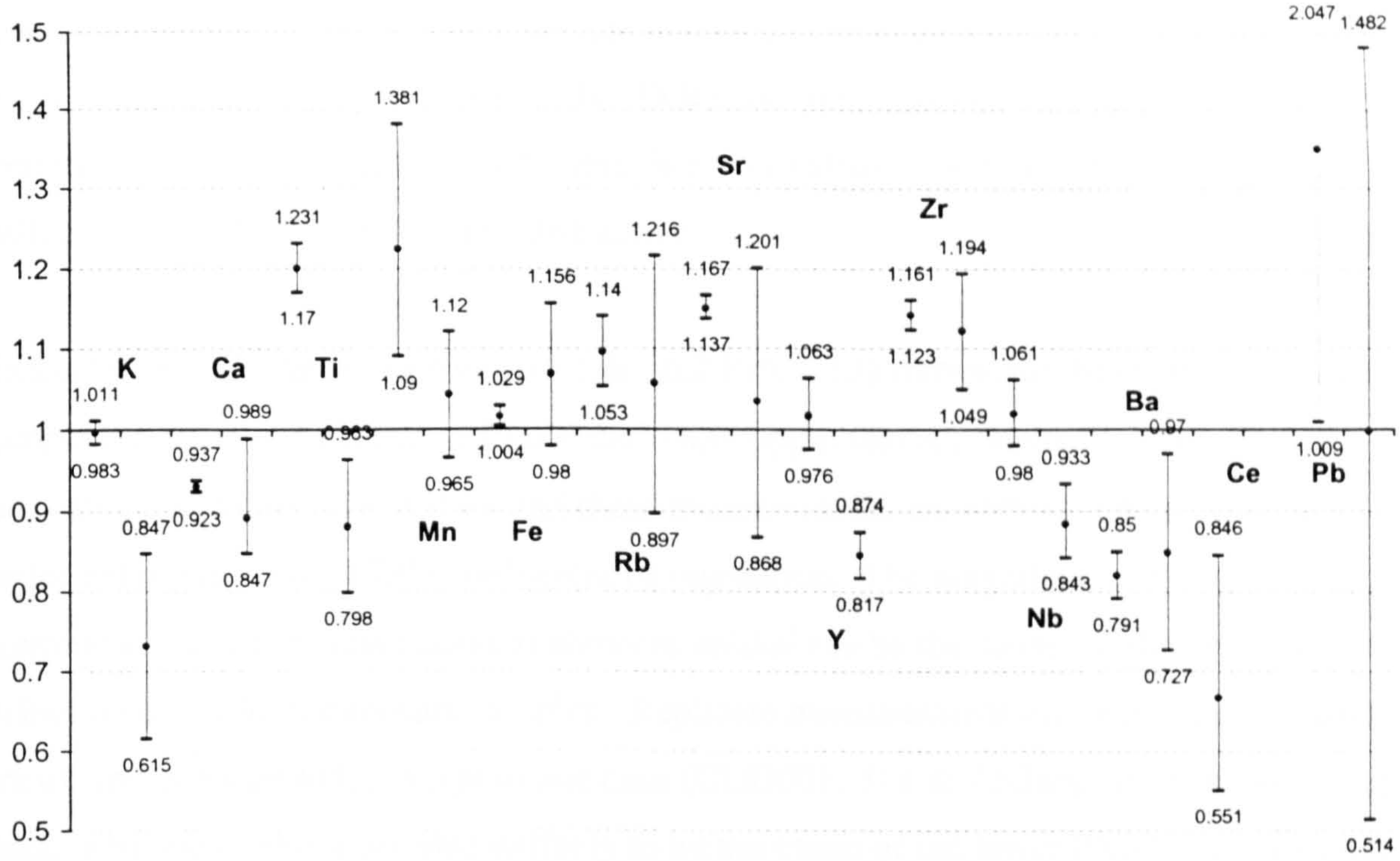

Figure 56 Chart illustrating the 95% upper and lower confidence range of Bias (I) Week 1 and Bias (III) coefficients of regression (b_1) when regression is constrained through (0,0). The left hand of each pair is Bias (I) and the right hand is Bias (III). (Data from Appendix 14.1 and 17.1)

6.11.3.3 Offset when regression is unconstrained

Table 36 indicates that the 95% upper and lower confidence interval for the *y-axis* intercept straddles zero for all elements measured, apart from Nb. Hence, the null hypothesis: the regression passes through the origin (0,0), cannot be rejected at a 0.05 significance value, except for Nb. The offset for Nb (-4.4ppm, with range -1.4 to -7.3ppm) is similar to that observed for Bias (II) and during Week 1 in Bias (I) and suggests that there may be a systematic offset of approximately -4ppm in PXRF Nb measurements, especially during the first fieldwork period.

6.11.3.4 Regression Coefficients

Figure 56 compares the regression coefficients and associated upper and lower 95% confidence limits of Bias (III) (right hand of each pair) and Bias (I) Week 1 (left hand of each pair). It is seen in Figure 56 that the range of 95% confidence limits obtained for Ca, Mn, Fe, Rb, Sr, Zr, Ba and Pb in the Bias (III) investigation all overlap the equivalent Bias(I) ranges (obtained in Week 1). Hence, it is probable that the Bias (III) coefficients could be the same as the Bias (I) coefficients for these elements. PXRF measurements of K from a rock sample are (approximately 15%) lower than those obtained by WDXRF and 5 to 10% lower than using equivalent rock powder pellets. This understatement could be due to any one or a combination of reasons such as; a) that the PXRF is reaching the K detection limit, b) that K is concentrated in localised areas within the rock, c) there are

insufficient analyses for each rock sample or d) the exposure pellet is not representative of the whole rock geochemistry. Similarly, PXRF measurements of Y & Nb in exposure samples are both approximately 10% less than equivalent measurements made on exposure pellets for any of the reasons indicated above.

Examination of K data (Appendix 16.1 & 16.2 Part 1/12) shows that there are 6 exposure sample measurements between 10,000 and 16,000ppm that are distinctly lower than the equivalent exposure pellet values and these measurements are almost certainly the major factor behind the low (0.731) coefficient of regression. The magnitude of these concentrations means that reason a) above is unlikely to be the cause for the lower K values obtained from exposure samples. Replicate measurements on each exposure sample are of similar magnitude, except in one case (CUD001: 511 & 7,956ppm), thus indicating reasons b) and c) above are also unlikely to be the cause of the lower PXRF measurement. This leaves option d): that the exposure glass disc is not representative of the K concentration found within the actual rock. As it will only be possible to confirm d) if more exposure discs are produced (a future research option) it can only be noted that PXRF K rock measurements may be up to 15% lower than the surrogate true value in some cases.

Inspection of Y data (Figure 54b, Appendix 16.2 Part 8/13) shows that PXRF measurements of exposure and pellet samples are similar, and are often within ±2 PXRF SD of each other (indicated by the overlapping error bars) and can thus be considered to be equivalent when the instrument precision is taken into account. Thus none of the four reasons given above are likely to apply to Zr and it is therefore presumed the difference between regression coefficients is related to the instrument precision only. Similarly, inspection of Nb data (Figure 54d, Appendix 16.1 and 2 Part 10/12) shows that Nb values from exposure and pellet samples distinctly overlap below 25ppm, but that exposure values appear consistently lower than pellet samples for higher (>25ppm) concentrations. Therefore, the smaller regression coefficient could also be related to instrument precision

It is noted that the Ti coefficient of regression has reduced during each Bias investigation: from 1.200 to 1.276 (Bias (I)); to 1.151 (Bias (II)) and finally to 0.881 (Bias (III)). Examination of the results (Figure 54a, Appendix 16.2 Part 3/12) show that the range of measurements across the samples and the similarity of replicate analyses on each rock/pellet samples allows that reasons a), b) & c) above can be rejected. This leaves d)

that the exposure pellet is somehow not representative of the whole rock Ti content. As Ti is an important element in geochemical analysis techniques the relationship between PXRF measurement of rock and powder pellets is examined further in Section 6.12.4 below.

6.11.4 Summary of Bias III

In summary, linear regression analysis between PXRF measurements of exposure rock samples and their surrogate true values reveals a reduced degree of linearity between the two variables, compared to Bias (I) and (II) regression results. This is almost certainly due to variable mineral abundance within the excited volume, giving rise to different PXRF measurements of the sample. Regression coefficients do suggest that the regression goes through, or close to, the origin (0,0) and that some PXRF proportional bias is likely for K, Ca, Ti, Y, Zr, Nb and Ba. Elements Ca, Mn, Fe, Rb, Sr, Zr, Ba and Pb have regression coefficients, hence bias, that are statistically similar to Bias (I) coefficients determined during the same fieldwork period. Y & Nb have reduced coefficient values compared with exposure pellets, but the level of difference amounts only to a few ppm and is possibly related to instrument precision. K & Ti concentrations are markedly lower in exposure samples than equivalent pellets. This could be related to the matrix/mineralogical differences between finely ground rock powder and actual rock and is investigated further (Ti only) below.

6.12 Accuracy of PXRF measurements based on Bias (I), (II) & (III) results

6.12.1 Comparison of all three bias investigations

It was anticipated that there would be no significant difference between the Bias (I) and (II) investigation and that there might be some difference between the Bias (I) & (II) and the Bias (III) investigation. The first two investigations used pressed powder pellets, measured by the same equipment with the only difference between the two investigations being that of material composition. The third investigation introduced further factors including variable mineralogy within exposure rock samples. In addition, Bias (I) also examined if there were any changes in PXRF bias between the three fieldwork periods.

(The following discussion uses data from Tables 34, 35, 36, Figures 53, 55, 56 and the associated Appendixes.)

6.12.2 PXRF offset in calibration and linearity in response

Bias (I) and (II) R^2 statistic values when regression is constrained through (0,0) are all greater than 0.950, apart from Mn (>0.80), Ce and Pb (both <0.80). This indicates that there is a marked linearity between the conventional true value and the PXRF values for reference and exposure pellets for K, Ca, Ti, Fe, Rb, Sr, Y, Zr, Nb and Ba. Bias (III) R^2 values for Ca, Mn, Y, Zr and Nb are all greater than 0.950, and K, Ti, Fe, Rb, Sr and Ba are all greater than 0.80 and therefore, support the linear relationship observed in Bias (I) & (II).

The range of 95% confidence limits for the *y-axis* intercept indicates a possible offset for K (approximately 1,000 to 1,300ppm (Bias (I) & (II)), Fe (approximately 1,100ppm (Bias (I)), Nb (approximately -4ppm (Bias (II) & (III)), Ce (approximately -40ppm (Bias (I)) and Pb (approximately -40ppm (Bias (I)).

Combining the two observations above, for R^2 and offset, it is probable that the PXRF is linearly calibrated over the range of concentrations encountered and that the calibration passes through zero (i.e. there is no offset) for Ca, Ti, Rb, Sr, Y, Zr and Ba. For the remaining 6 elements:

1. Inspection of K data strongly suggests a linear calibration but that at concentrations below 5,000ppm the PXRF reports values up to approximately 1,300ppm lower than actual when measuring greenstones and up to 1,000ppm when measuring reference samples.

2. The relatively large value of instrument precision (±800ppm) and the low range of concentrations (generally < 2,000ppm) are probably the reason for Mn R^2 values (Bias (I) only) to be <0.950. As Bias (II) and (III) R^2 values are >0.950 over a larger range of compositions (<4,000ppm) it is reasonable to assume that the PXRF Mn is linearly calibrated with no offset.
3. Inspection of Fe offsets suggests that the PXRF reports values up to approximately 1,100ppm lower than actual. This is equivalent to 0.16% by weight of Fe_2O_3 and is also less than the instrument precision at 90,000ppm (±1,250ppm). As this represents approximately 1 to 2% of the measured concentrations normally encountered in this work it will be assumed that PXRF is linearly calibrated with no appreciable offset.
4. Inspection of Nb data indicates that the PXRF reports concentrations approximately 1 to 4ppm below actual depending on the concentration. Noting the instrument precision below 10ppm is ±2 to 4ppm it can be reasonably assumed that PXRF Nb is linearly calibrated with no appreciable offset, but that reported values *may* be slightly lower than actual by a few ppm (less than 4ppm) when measuring greenstones (Bias (II)).
5. Regression analysis of Ce data (Bias (I) only) reveals that there is almost certainly an offset of 35 to 40ppm, with PXRF Ce values consistently lower than conventional true values. The value of the R^2 statistic is approximately 0.8 when regression is unconstrained indicating there is evidence for a linear relationship between measured and conventional true values. Hence the PXRF Ce may be linearly calibrated, but there is an obvious (static) error in calibration.
6. The small range (usually < 50ppm) of PXRF Pb values and associated poor instrument precision means that PXRF Pb calibration cannot be measured with any certainty. Hence all Pb data should be treated with caution.

6.12.3 PXRF proportional bias

Having shown above that PXRF calibration K (concentrations > 5 000ppm only), Ca, Ti, Mn, Fe, Rb, Sr, Y, Zr Nb and Ba is linear and passes through zero it follows that the reported regression coefficients reflect the bias (hence accuracy) of the PXRF. Table 37 below summarises the PXRF accuracy in terms of relative percentage using the formula: ((|measured value- true value|)/ true value) x 100%. For example the regression coefficient for Y for Bias (I): Week 1 is 1.017 (c.f. Table 34). This means that when the true value is

100ppm the PXRF measured value is 101.7ppm (ignoring sample and instrument precision, etc.) and the accuracy is 2%, to the nearest whole percentage value.

Period	Bias (I) Week1	Bias (I) Week 2	Bias (I) Week 4	Bias (II) Week 2&3	Bias (III) Week 1
K	0%	-2%	-4%	-6%	-27%
Ca	-7%	-8%	-2%	-8%	-11%
Ti	20%	25%	28%	15%	-12%
Mn	22%	9%	18%	14%	4%
Fe	2%	-1%	0%	3%	7%
Rb	10%	7%	3%	6%	6%
Sr	15%	10%	10%	16%	4%
Y	2%	-6%	-6%	-8%	-15%
Zr	14%	12%	13%	9%	12%
Nb	2%	0%	2%	4%	-12%
Ba	-18%	-17%	-19%	-18%	-15%

Table 37 PXRF accuracy expressed as relative percentage (i.e. proportional bias). Zero values indicate that there is no bias, a negative value indicates the PXRF underestimates the true value. Bias (I) and (II) represent measurements made on powder pellets, Bias (III) represents measurements made on actual rock samples (see text for discussion)

Table 37 shows that Bias (I) values are generally similar across the three fieldwork periods. Bias (II) values for Ca, Mn, Fe, Rb, Sr, and Ba are similar to Bias (I). There is a slight decrease in proportional bias during Weeks 2 & 3 for Zr and a slight increase in proportional bias for K, Y and Nb, compared to Week (I). Values for Bias (III) show the largest difference with Bias (I) and (II), which is in part due to the rock heterogeneity. The proportional bias values for Ti shows the greatest variation, from 28% to -12% and is discussed below.

(Note: Values used to correct PXRF measurements for accuracy are discussed in Section 6.17)

6.12.4 Ti anomaly

The Ti regression coefficients range from 1.28 to 1.20 for Bias (I) to 1.15 for Bias (II) and 0.88 for Bias (III), as illustrated in Figure 57. The only difference between Bias (I) and (II) investigations is that the latter used greenstone pressed powder pellets against international reference materials used in the former. Since the expected range of compositions are similar (1,000 to 25,000ppm) it was expected that the coefficients would be similar. But, Bias (III) produced a Ti coefficient below unity, at 0.88 suggesting the PXRF was now underestimating Ti concentrations. It is assumed that the Ti values of the international reference samples are correctly reported (c.f. Section 6.8), hence there is strong evidence for PXRF bias when measuring Ti on pelletised samples. This is partly borne out, but to a lesser degree, when measuring exposure pellets. The only difference between the two sets

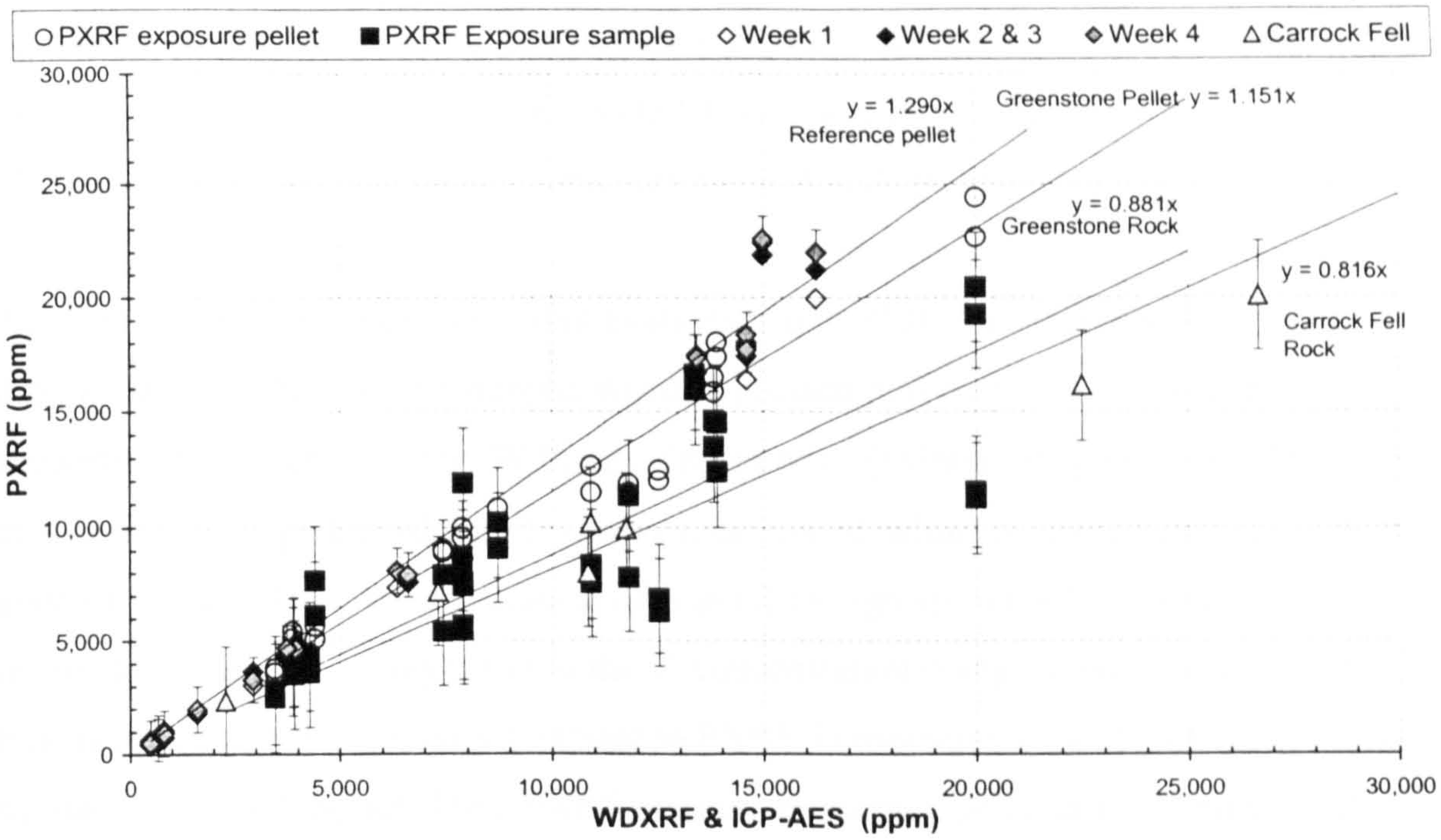

Figure 57 Chart illustrating the relationship between conventional & surrogate true values and ICP values (established by publication, WDXRF or ICP-AES) and PXRF measured values for reference pellets (averages of Week 1, Week 2&3, and Week 4 are shown (including MICAFE)), exposure rock pellets and exposure samples of both greenstone and Carrock Fell rock

of pellets is that they were manufactured at different times by different people, but using the same procedure. The difference between pelletised and equivalent rock measurements (Bias (III)) cannot be accounted for by heterogeneity alone as it is seen that replicate measurements on rock samples are in relatively close agreement (c.f. Appendix 16.2 Part 3/13). If heterogeneity was significant then it is expected that more of the Ti measurements would be higher than the equivalent pellet concentration (only 3/32 Ti rock measurements > equivalent Ti pellet measurement). This calls into doubt the accuracy of the PXRF when measuring Ti in greenstone rock samples.

The problem with the accuracy of PXRF Ti data has also been noted by William-Thorpe et al (1999a). In their paper, Williams-Thorpe et al suggest the problem arises from the preferential absorption of Ti Kα x-rays by the Fe-Ti oxide grains commonly present in basaltic and intermediate rocks.

A further investigation into PXRF Ti bias was carried out as part of this work and involved using gabbroic and granitic rocks collected from Carrock Fell, Cumbria. The results showed that the PXRF bias was approximately the same (0.82) as when measuring greenstone rock (0.88). In this case inductively coupled plasma – atomic emission spectrometry (ICP-AES) was used to obtain Ti concentrations for 8 rock samples which had also been analysed by the PXRF during Week 4 (Davis pers. com.). It is assumed that

the accuracy and precision of the Imperial College ICP-AES equipment used to analyse the samples is similar to that for the OU WDXRF and as reported in Ramsey et al. (1995). This data is displayed in Figure 57 and summarised in Appendix 23.

The conclusion drawn from these observations is that PXRF measurement of Ti is dependent on the form of the sample, whether pressed powder pellet or actual rock thus supporting the observations by Williams-Thorpe et al. (1999a). It appears that PXRF measurements on pelletised samples are overestimated, whilst measurements on rock are underestimated. Thus, the application of Bias (I) Ti regression coefficients as correction factors to rock samples may result in the Ti concentration being overstated by up to 40%. It is therefore decided that no adjustment to PXRF Ti measurements of rock (or axe) will be made and it will be noted that PXRF measurements may be 10 to 15% understated. For example, take a PXRF reported value for an exposure rock sample of 10,000ppm, then the value, for the rock sample, is calculated as 10,000/0.88 = 11,400ppm, where 0.88 is the PXRF bias for exposure samples (Bias (III)). This understatement, equivalent to 1,000 to 2,000ppm (0.1 to 0.3% oxide wt) must be borne in mind when using PXRF results.

Actual adjustments to PXRF data are covered in Section 6.17, at the end of this Chapter, after examining PXRF precision and the effect of non-ideal surfaces on PXRF measurements.

6.13 PXRF Proto Axe: Examining the effect of non-ideal surfaces on PXRF measurements

6.13.1 Introduction to the investigation

Unlike the exposure samples used in the Bias (III) investigations above, which all had flat and fresh surfaces, Neolithic axes possess surfaces that may be curved, polished, irregular or weathered (or any combination of these). It is therefore necessary to investigate how such variable surfaces affect PXRF measurements and to investigate if any restriction on the use of associated PXRF data is necessary. These investigations have been made possible through the manufacture of two 'proto-axes' from typical greenstone rocks: the 'proto-axes' and associated production waste (debitage) of the proto-axe providing various combinations of curved, polished, irregular and weathered surfaces for this investigation.

6.13.2 Source and description of proto-axes and associated samples

6.13.2.1 Proto-axe: MM3

Mr D Weddle discovered greenstone sample MM3 as a loose boulder at the site of a ditch (SW405321) being cut on the Land's End granite in the Penwith Peninsula. This large spheroidal boulder, greater than 30cm in diameter, was split (at the OU) to provide samples for petrological analysis and axe manufacture. Some pieces of MM3 were subsequently sawn to provide flat surfaces for PXRF measurement and the remaining pieces were given to Mr Weddle for the manufacture of a stone-axe. The shape and surface texture of the axe was to be loosely based on IPC Group I and ungrouped greenstones axes held at Truro Museum. As it turned out there was insufficient material to manufacture a whole axe from the pieces of MM3 provided, so the larger fragments were pecked, polished and ground to provide variable curved surfaces, typical to those found on axes.

In total five samples of MM3 were prepared:

1. A lapped flat piece with << 1 mm surface relief, of sufficient size for 4 non-overlapping PXRF measurements. (Referred to as 'Sawn & Polished')
2. A sawn flat piece with << 1mm surface relief, of sufficient size for 4 non-overlapping PXRF measurements. (Referred to as 'Sawn & Unpolished')
3. A piece with a fresh broken surface, away from weathered crust, leaving an irregular surface with estimated 1 to 3mm relief, sufficient for 4 non-overlapping PXRF measurements. (Referred to as 'Fresh, Flaked Blank')
4. A piece retaining its weathered surface. The weathered surface is lighter in colour than a fresh surface and is 'pock-marked' to 2mm depth. The 'crust' formed by

weathering had an overall penetration of approximately 3mm. This piece is slightly convex and of sufficient size for 4 non-overlapping PXRF measurements on the weathered surface. (Referred to as 'Weathered Surface')

5. A piece with a smooth curved surface similar to those surfaces found on polished greenstone axes which are approximately 10 cm long. The rock surface had been prepared by pecking with a hammerstone of similar material (greenstone) to obtain the desired shape and then polished and ground using coarse and fine quartz sand. The resultant surface is smooth to the feel and convex and large enough for 4 non-overlapping PXRF measurements. (Referred to as Pecked, Polished, Ground Curved')

6.13.2.2 Proto-axe: PTX002

PTX002 was collected from the foreshore on the western side of Mounts Bay, 50m south of Penlee Lifeboat station (SW475269). The brick-like cobble, measuring approximately 20cm x 10cm x 8cm was split and some pieces sawn and lapped flat (at the OU), whilst the remaining pieces were given to Mr Weddle for the manufacture of a stone axe. Subsequently PTX002 was found to contain many flaws, seen as light-coloured veins running through the fine-grained rock, making it difficult to craft a typical greenstone axe. Hence, the resultant PTX002 axe has a flatter, oval, cross section than most axes seen at Truro (and during this research). After polishing PTX002 the veining in the rock became clearer and the overall homogeneity of the rock was called into doubt. It was therefore decided to concentrate on measuring the more homogenous MM3. (However, measurements were made on PTX002 and are included in Appendix 18.2 for completeness.)

6.13.3 Methodology

All PXRF measurements on the various pieces of MM3 were taken on the same day, to minimise the potential for any time-related bias of the PXRF equipment. (Apart from two measurements (ref. OMM3#1V &2V in Appendix 18.1) which have not been used in the subsequent statistical analysis.) Four non-overlapping PXRF measurements were taken on each of the five pieces of MM3 in order to achieve a sample precision of better than 5% relative standard deviation of the mean as suggested by Potts et al. (1997a) for medium grained basaltic rocks.

6.13.4 Results

The resulting 20 PXRF measurements were statistically analysed to determine the nature of relationships between pieces of MM3 with flat surfaces and the three pieces with irregular, curved and weathered surfaces. The results of the measurements are contained in Appendix 18.1 and summarised in Table 38 below. Three statistical processes were used: Student's t-test (for comparing means), Mann-Whitney and two independent sample Kolmogorov-Smirnov. The null hypothesis in each case is that there was no difference between the means of each pair of measurements (e.g. flat – fresh, flaked; flat – weathered; flat – curved), with the alternative hypothesis was that there was a difference (using two tailed tests). A significance level of 5% was chosen for the tests. The results of the t-test and the Kolmogorov-Smirnov tests are summarised in Appendix 18.3, with the results from the t-test also included in Table 38. The Mann-Whitney tests gave similar results to the Kolmogorov-Smirnov tests are therefore not included in the tables or appendixes.

Table 38 below summarises the elemental averages for each set of measurements and report the associated sd, based on the number (n) of measurements. The value of significance is from Student's two-tailed t-test, assuming unequal variances. Values indicated in bold are greater than 0.050, indicating the null hypothesis: the means are equal using a 0.05 significance value, cannot be rejected.

MM3 t-test Result	Flat Surface (ppm ±1sd) (n=8)	Fresh, Flaked Blank (ppm ±1sd) (n=4) Between Flat & Fresh	Weathered Surface (ppm ±1sd) (n=4) Between Flat & Weathered	Pecked, Polished and Ground Curved (ppm ±1sd) (n=4) Between Flat and Pecked
K	8 384 ± 2 513	3 571 ± 1 190 0.001	10 575 ± 4 269 **0.396**	6 666 ± 1 737 **0.202**
Ca	76 315 ± 1 297	65 916 ± 13 410 **0.219**	43 981 ± 4 034 0.000	81 270 ± 4 215 **0.098**
Ti	13 689 ± 1 620	15 153 ± 6 581 **0.689**	12 157 ± 1 884 **0.220**	15 532 ± 2 655 **0.269**
Mn	1 514 ± 555	1 252 ± 347 **0.344**	1 368 ± 109 **0.493**	1 282 ± 238 **0.337**
Fe	85 367 ± 4 020	71 579 ± 18 420 **0.232**	87 094 ± 8 392 **0.718**	85 736 ± 2 225 **0.843**
Rb	86.0 ± 23.1	65.6 ± 14.0 **0.089**	29.9 ± 15.7 0.001	79.1 ± 23.2 **0.646**
Sr	713 ± 42.4	359 ± 74.7 0.001	283 ± 27.1 0.000	777 ± 51.8 **0.085**
Y	33.1 ± 4.3	27.1 ± 15.0 **0.490**	26.7 ± 6.2 **0.134**	37.8 ± 2.9 **0.052**
Zr	176 ± 15.6	128 ± 42.2 **0.107**	191 ± 11.8 **0.101**	176 ±20.0 **0.960**
Nb	4.9 ± 3.0	8.1 ± 5.1 **0.322**	7.5 ± 3.9 **0.304**	7.6 ± 6.3 **0.467**
Ba	144 ± 17.6	92.5 ± 10.6 0.000	104 ± 9.9 0.001	164 ± 33.7 **0.338**
Ce	-17.9 ± 6.5	-26.4 ± 15.5 **0.359**	-41.5 ± 3.9 0.000	-18.3 ± 7.5 **0.929**
Pb	-0.6 ± 15.0	3 ± 9.1 **0.621**	29.8 ± 12.4 0.007	19.3 ± 14.7 **0.070**

Table 38 Averages and associated sds of PXRF measurements made on pieces of greenstone MM3. Significance values are based on Student's two-tailed t-test, assuming unequal variances. Values indicated in bold are >0.05, thus indicating the null hypothesis: the means are equal using a 0.05 significance value, cannot be rejected

6.13.5 Discussion

6.13.5.1 Comparison between flat surfaces and fresh flaked blanks

Table 38 and Appendix 18.3 show that significance values for Ca, Mn, Ti, Fe, Rb, Y, Zr, Nb, Ce, Pb are all greater than 0.05, indicating that the null hypothesis cannot be rejected using a 0.05 significance value. Examination of the PXRF data shows that the third measurement taken on the fresh, flaked blank (Appendix 18.1: Reading RMM3#11) is noticeably different to the other three and has very low Fe backscatter (237 against 289 average), and was thought to be a contributory factor for rejection of the null hypothesis for K, Sr and Ba. However, repeated statistical calculations showed that if this measurement was ignored then K, Sr, and Ba levels of significance still remain below 0.05, thus supporting the rejection of the null hypothesis for these elements. The two-sample Kolmogorov-Smirnov tests confirm the t-test findings, however, in this case the anomalous reading, RMM3#11, calls into doubt the Fe comparison.

The mean measurement of K for the fresh flaked blank is significantly lower than for flat surfaces which is probably due to the absorption of the Mn Kα in the 1 to 3mm air gap between the sample and PXRF window. Similarly, the mean for Sr derived from measurements on fresh flaked blanks is significantly lower than the mean derived from flat surfaces, for possibly the same (air gap) reasons. Since the pieces measured were greater than 10 mm thick there should be no loss of response in fluorescent x-rays because of critical depth factors, thus the low Ba readings for fresh flaked blanks are probably not due to variable specimen thickness.

Average values of the PXRF measurements on the fresh, flaked blanks are often markedly lower than those obtained on the flat samples, apart from Ti, Nb & Pb. It can also be seen that the associated sd of measurements made on the 1 to 3mm irregular surface are often substantially greater than those from measurements on the flat surfaces (apart from K, Mn, Rb and Ba).

As the only physical difference between the three samples is the irregular 1 to 3mm surface it is concluded that a 1 to 3mm air gap generally reduces PXRF measurements and increases the associated sd, but that the reductions are only significant for K, Sr and Ba. This observation supports the findings reported by Potts et al (1997b) that air gaps effectively reduce the amount of x-rays reaching the detector, resulting in an underestimation of the concentration by the PXRF. The ability of the procedure proposed by Potts et al (1997b) to correct for reduction in PXRF measurements due to air gaps is examined later in this chapter (c.f. Section 6.14).

6.13.5.2 Comparison between flat surfaces and weathered surfaces

Table 38 shows that t-test significance values for Ca, Rb, Sr, Ba, Ce and Pb are all less than 0.05, hence allowing the rejection of the null hypothesis. Although inspection of Appendix 18.1 shows that measurement RMM3#14 has anomalous values and low Fe backscatter (246), it was calculated that the removal of this measurement does not significantly affect the statistical results. Kolmogorov-Smirnov supports the t-test results and further calls into doubt the similarity of Fe and Zr averages.

The significant difference revealed by the statistics for Ca, Rb, Sr, Ba and Ce probably reflects the combined effect of surface irregularity (pitting to <2mm deep randomly spaced over the surface of the sample) and, more importantly, element mobility in the rock surface

because of weathering. Pb and K have greater concentrations in the weathered surfaces than those found in the flat surfaces which is also probably related to weathering processes (or surface contamination, e.g. Pb from atmospheric pollution). The four high field strength (HFS) elements Ti, Y, Zr and Nb, have significance values greater than 0.05, indicating that the null hypothesis cannot be rejected (i.e. indicating there is no reason to doubt that the average PXRF measurements from weathered and flat surfaces for these elements are not the same).

It is concluded that PXRF measurements of Ca, Rb, Sr, Ba, Ce and Pb made on weathered surfaces must be treated with caution and that the more weathered the sample the less these element concentrations are likely to represent the whole rock values (which is not surprising). But for the level of weathering observed in the greenstone sample (pitting to 2mm and crustal thickness to 3 mm) PXRF measurements of Ti, Y, Zr and Nb, generally regarded as 'immobile elements', are statistically no different to those obtained on a fresh flat surface of the same rock.

6.13.5.3 Comparison between flat surfaces and pecked, polished and ground curved surfaces

Table 38 shows that t-tests significance values are all greater than 0.05 indicating that the null hypothesis is cannot be rejected: PXRF measurements on flat and curved surfaces (of the type encountered in the sample) are not statistically different. These results are supported by the Kolmogorov-Smirnov test, with the exception that Ca falls below the 0.05 significance level.

Means for Ca, Ti, Fe, Sr, Y, Zr, Nb, Ba and Pb for the curved polished surfaces are slightly higher than those reported from flat surfaces. This may be accounted for by the probe window to sample air gap being reduced by the convex nature of the curved surface sitting into the window, thus reducing the attenuation of x-rays through scatter/absorption in air and/or causing an increase in signal strength (i.e. reducing d, increases $1/d^2$). However the increase between the mean values is not large enough to drop the t-test value below 0.05 and indicate rejection of the null hypothesis.

It is concluded that curved and polished surfaces (as present on the sample) give statistically indistinguishable results to those that would be obtained from flat surfaces of the same sample. Although averages of K, Mn, Rb and Ce concentrations are lower for

curved surfaces than flat surfaces, the difference is small enough so that the null hypothesis cannot be rejected. For these 4 elements the difference between the two means is less than 1sd as calculated from the curved surface measurements and as such the minor differences in the results are probably due to the size of the sample precision.

6.13.6 Sample precision

Table 39 indicates the relative precision associated when measuring the various samples of MM3. Sample precision is calculated by dividing the sd by the average concentration shown in Table 38

MM3	concentrations based on flat surfaces	Flat Surface (n=8)	Fresh, Flaked Blank (n=4)	Weathered Surface (n=4)	Pecked, Polished and Ground Curved (n=4)
K	8 384	30.0%	33.3%	40.4%	26.1%
Ca	76 315	1.7%	20.3%	9.2%	5.2%
Ti	13 689	11.8%	43.4%	15.5%	17.1%
Mn	1 514	36.7%	27.7%	8.0%	18.6%
Fe	85 367	4.7%	25.7%	9.6%	2.6%
Rb	86.0	26.9%	21.3%	52.5%	29.3%
Sr	713	5.9%	20.8%	9.6%	6.7%
Y	33.1	13.0%	55.4%	23.2%	7.7%
Zr	176	8.9%	33.0%	6.2%	11.4%
Nb	4.9	61.2%	63.0%	52.0%	82.9%
Ba	144	12.2%	11.5%	9.5%	20.5%
Ce	-17.9	36.3%	58.7%	9.4%	41.0%
Pb	-0.6	2500%	303%	41.6%	76.2%

Table 39 Sample precision based on replicate measurements of MM3 samples. Sample precision is expressed as a percentage and is calculated by dividing the sd by the associated average.

The values clearly show that sample precision is poorest for measurements made on the fresh, flaked blanks with irregular surfaces and is probably related to the differences caused by the variable 1 to 3mm air gap between the sample and the PXRF window. Table 39 shows that sample precision obtained for flat surfaces and pecked, polished ground and curved surfaces are similar, noting the difference in the number of replicate measurements (8 and 4 respectively). Sample precision obtained on weathered surfaces is also similar to that achieved for flat surfaces, although the overall elemental concentrations differ, so they cannot be directly compared with the other sample precisions in Table 39.

In Section 6.4.4.3 it was stated that greenstones have a similar grain size to that of the Whin Sill sample used by Potts et al. (1997a: table 3) and that 2 PXRF measurements of greenstones should be sufficient to achieve a sample precision of better than 5% standard deviation of the mean for most elements whose concentration is greater than 10 times the PXRF SD. Table 40 below reports similar statistics to those used by Potts et al. to

determine the actual number of measurements to achieve 5% standard deviation of the mean (R) for greenstones calculated from the 8 PXRF measurements made on the two flat surfaced samples of MM3.

	MM3 (100s ^{109}Cd, 50s ^{55}Fe, 40s ^{241}Am count times)					Whin Sill (100s ^{109}Cd, 50s ^{55}Fe, 20s ^{241}Am count times) (from Potts et al. (1997a): table 3)				
	Conc. (n=8) (ppm)	SDM (ppm) (% rel.)	N for R=0.05	R when n=2	R when n=4	Conc. (n=10) (ppm)	SDM (ppm) (% rel.)	n for R=0.05	R when n=2	R when n=4
K	***8 384***	888 10.7%	***36***	21.0%	15%	608.3	69.2 11.4%	51.8	25.4%	18.0%
Ca	**76 315**	459 0.8%	**0.11**	1.2%	<1%	**16 200**	145.1 0.9%	**0.3**	2.0%	1.4%
Ti	**13 869**	573 4.1%	**5.6**	8.4%	5.9%	2 805	75.8 2.7%	2.9	6.0%	4.3%
Mn	1 514	196 12.9%	57.3	25.9%	18.3%	622	61.9 9.9%	39.6	22.2%	15.7%
Fe	**85 367**	1 421 1.7%	**0.89**	3.3%	2.3%	**56 104**	394.9 0.7%	**0.2**	1.6%	1.1%
Rb	86.0	8.2 9.5%	28.9	19.0%	13.4%	-5.3	2.0 -37.6%	565	83.7%	59.4%
Sr	**713**	15.0 2.1%	**1.4**	4.2%	3.0%	**368.3**	4.3 1.2%	**0.5**	2.6%	1.8%
Y	33.1	1.5 4.5%	6.7	9.2%	6.5%	13.6	1.4 10.4%	43.4	23.4%	16.5%
Zr	**176**	5.5 3.1%	**3.1**	6.3%	4.4%	**75**	1.5 2.0%	**1.7**	4.5%	3.2%
Nb	4.9	1.1 22.5%	150	43.3%	30.6%	0.4	1.0 757%	>100	>100%	>100%
Ba	**144**	6.2 4.3%	**6.0**	8.6%	6.1%	**230**	6.4 2.8%	**3.1**	6.2%	4.4%
Ce	-17.9	2.3 -12.8%	52.7	25.7%	18.2%	1.4	4.2 972%	>100	>100%	>100%
Pb	-0.6	5.3 >880%	>100	>100%	>100%	11.8	5.2 43.9%	>100	97.6%	69.1%

Table 40 Results from calculations to show the number of PXRF measurements (n) to achieve a 0.05 standard deviation of the mean (R) and R achieved by 2 and 4 PXRF measurements (see text for discussion). Values indicated in bold are where the concentration (conc.) is greater than 10 times the associated PXRF SD. (SDM = standard deviation of the mean)

The calculations in Table 40 are based on the following:

$R = s/(\sqrt{n} \times x_{bar})$

where n is the number of measurements, s is the standard deviation associated with x_{bar}, the average concentration ('conc'. in Table 40).

Potts et al. calculated that a mean of 1.2 'determinations' (i.e. 2 PXRF measurements) were required to achieve a precision for R = 5% (1997a: table 8). Using the same logic (n calculated for elements whose concentration is >10x PXRF SD) the equivalent value for greenstone is 2.9 'determinations' (i.e. 3 PXRF measurements) to achieve R = 5%. Note that K has not been included in the greenstone calculation since 2 of the measurements (c.f. Appendix 18.1) are just above 5,000ppm, and as noted (Section 6.12) PXRF measurements

of K for these concentrations may be understated by up to 1,000ppm. Rearranging the given formula to calculate R based on a given number of PXRF measurements of greenstone shows that when n = 2, R = 5.3% (again, using only concentrations greater than 10 times the PXRF SD and ignoring K). This is equivalent to R = 3.4% for 2 PXRF measurements on the Whin Sill sample.

6.13.7 Concluding remarks

In general, uneven surfaces with peak to pit differences between 1 to 3mm result in the PXRF underestimating concentrations, but apart from K, Sr & Ba, the reduction is not statistically significant (at a 0.05 significance value). However, the precision obtained from 4 replicate measurements made on irregular surfaces is worst of all four surface types. Weathered surfaces, not surprisingly, return the greatest differences in element concentration when compared to fresh, flat surfaces. This is almost certainly due to migration (in and out) of elements, thus changing the rock geochemistry. Therefore PXRF measurements of highly weathered axe surfaces should be treated with caution. However, it is noted that measurements of the four HFS elements, Ti, Y, Zr & Nb, on weathered surfaces are statistically indistinguishable from measurements made on ideal surfaces of the same greenstone rock. Thus PXRF measurements of these elements from (rare) axes with a similar degree of weathering seen in the MM3 sample (pitted to 1mm, crust to 2mm thick) can be directly compared with polished & curved axes and exposure samples. Sample precision obtained from measurements of weathered surfaces is similar to that of fresh, flat surfaces and suggests regular, not patchy, migration of minerals through weathering.

The findings above indicate that PXRF measurements from curved, polished greenstone axes are statistically indistinguishable to (theoretical) PXRF measurements made on an ideal sample of the axes and that the sample precision obtained for each case is also similar. This means that PXRF measurement of axes and exposure samples can be directly compared.

Calculations show that 2 PXRF measurements of MM3 return a standard deviation of the mean of 5.3%, close to the 5% anticipated (c.f. Section 6.4.4.3). This is seen as supporting the decision to take 2 PXRF measurements of greenstone axes to ensure a reasonable level of sample precision. However, if the two measurements are markedly different, then a 3rd measurement is considered necessary.

6.14 PXRF Fe backscatter correction: potential to adjust measurements on non-ideal surfaces

6.14.1 Introduction to investigation

Potts et al. (1997b) noted that 'quantitative results (from the PXRF) cannot be obtained directly from rock samples in the field that have irregular shaped surfaces' (1997b: p769). This is because the PXRF is calibrated assuming the sample to be measured is both flat and positioned in the PXRF reference plane and the presence of any gaps between the PXRF and an uneven sample would increase the x-ray path length. This increase in path length reduces the number of x-rays received by the detector owing to the inverse square law and increased absorption/scattering in air, and results in the underestimation of concentrations. Potts et al (op. cit.) went on to propose a normalisation procedure to counteract surface irregularity effects, based on the ratio of PXRF Fe backscatter intensities measured on a non-ideal surface with that on an ideal surface (i.e. flat and on the measuring plane).

Since greenstone axes are rarely flat and therefore present non-ideal surfaces for PXRF measurement the effectiveness of the proposed normalisation procedure is examined for greenstone axes.

6.14.2 Methodology

MM3 PXRF data (Appendix 18.1) was adjusted using the normalisation procedure proposed by Potts et al. (1997b) (Fe backscatter measured on a flat surface divided by Fe backscatter measured on a non-flat measuring surface, for a similar rock matrix). Statistical data similar to that obtained for the proto-axe experiment was calculated and is summarised in Table 41 and Appendix 18.4. The expectation is that application of the Fe backscatter correction would bring the actual PXRF measurements made on irregular and curved (not weathered) surfaces closer to equivalent measurements (hypothetically) made on flat surfaces of the same sample. Hence, if the proposed procedure for normalisation is helpful then the following would be observed:

1. The average of corrected PXRF measurements made on irregular surfaces would be closer to the average measurement made on the flat surface than the uncorrected average (indicated in Bold in Table 42 and denoted by a **C** when the corrected value is closer or ***F*** for further away in Appendix 18.5)
2. A reduction in the sd of the corrected measurements compared with the uncorrected sd (indicated as a positive value in Appendix 18.5 sd column)

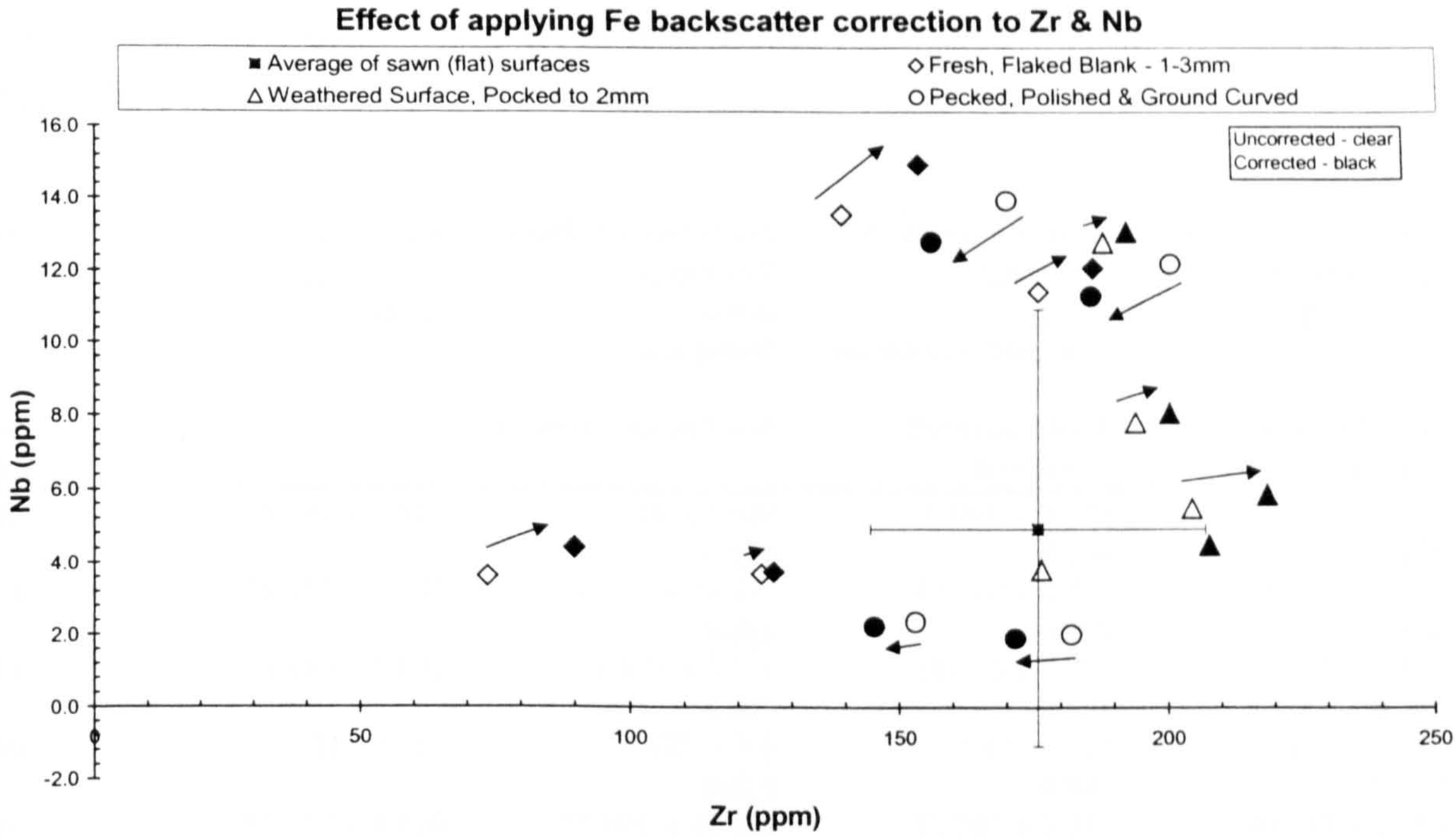

Figure 58 Chart illustrating the effect of applying the Fe backscatter normalisation procedure to PXRF made on non-ideal surfaces. (see text for discussion – note weathered surfaces are included for interest only)

3. A reduction in the standard error (se) of the corrected measurements compared with the uncorrected measurement (indicated as a positive value in Appendix 18.5 'se' column)
4. An improvement in the probability that the mean of the corrected measurements is the 'same' as for measurements on the flat surfaces (indicated in bold in Table 42 and shown as a negative value in the 'significance' column of Appendix 18.5)

6.14.3 Results

Bivariate charts provide a visual impression of the effect of applying the Fe backscatter correction. Figure 58 is extracted from Appendix 18.6 to illustrate the effect of applying the Fe backscatter correction to Zr & Nb measurements. The arrows in Figure 58 indicate the movement of data caused by applying the correction factor. The averages of PXRF measurements of Zr & Nb made on flat surfaces are shown along with error bars representing ±2sd of the average.

PXRF averages and associated sds after applying the Fe backscatter correction are reported in Table 41. In this table the average values for the non-flat samples have been normalised (corrected) using the Fe backscatter normalisation procedure described in Potts et al. (1997b). Significance values from comparing means of the flat and adjusted non-flat measurements are derived from Student's two-tailed t-test, assuming unequal variances. Values above 0.05 are indicated in bold in Table 41 and indicate that the null hypothesis:

that the means are equal, cannot be rejected. A full summary of the data is contained in Appendix 18.4.

MM3	Flat Surface (ppm ±1sd) (n=8)	Fresh, Flaked Blank (ppm ±1sd) (n=4) (corrected)	*Weathered Surface (ppm ±1sd) (n=4) (for information only)	Pecked, Polished and Ground Curved (ppm ±1sd) (n=4) (corrected)
t-test Result		Between Flat & Fresh	Between Flat & Weathered	Between Flat and Pecked
K	8 384 ± 2 513	3 998 ± 1 683	11 168 ± 4 078	6 222 ± 1 616
		0.006	**0.276**	**0.105**
Ca	76 315 ± 1 297	71 677 ± 10 472	47 210 ± 3 977	75 925 ± 3 940
		0.422	0.000	**0.858**
Ti	13 689 ± 1 620	16 427 ± 6 110	13 035 ± 1 781	14 505 ± 2 457
		0.467	**0.561**	**0.577**
Mn	1 514 ± 555	1 373 ± 368	1 471 ± 142	1 198 ± 214
		0.611	0.840	0.187
Fe	85 367 ± 4 020	77 603 ± 16 250	93 241 ± 3 515	80 110 ± 2 694
		0.412	0.010	0.026
Rb	86.0 ± 23.1	71.3 ± 10.9	31.8 ± 15.8	74.0 ± 21.9
		0.166	0.001	**0.411**
Sr	713 ± 42.4	391 ± 61.8	303 ± 15.5	726 ± 50.5
		0.000	0.000	**0.682**
Y	33.1 ± 4.3	28.9 ± 15.0	28.6 ± 5.6	35.3 ± 3.0
		0.620	**0.213**	**0.325**
Zr	176 ± 15.6	139 ± 40.7	205 ± 11.3	165 ± 17.7
		0.169	0.006	**0.333**
Nb	4.9 ± 3.0	8.8 ± 5.6	7.9 ± 3.8	7.0 ± 5.8
		0.265	**0.231**	**0.529**
Ba	144 ± 17.6	101.2 ± 7.8	111 ± 11.3	153 ± 32.0
		0.000	0.003	0.633
Ce	-17.9 ± 6.5	-28.6 ± 15.9	-44.6 ± 3.6	-17.2 ± 7.2
		0.276	0.000	**0.872**
Pb	-0.6 ± 15.0	3.4 ± 9.7	31.9 ± 12.8	18.1 ± 14.1
		0.596	0.006	**0.075**

*Table 41 Averages and sds of n PXRF measurements made on pieces of greenstone MM3, with the non-flat measurements adjusted using the Fe backscatter normalisation procedure (see text for discussion). V'alues reporting the significance are based on Student's two-tailed t-test, assuming unequal variances. V'alues indicated in bold are greater than 0.05 thus indicating the null hypothesis' that the means are equal at a 0.05 significance value' cannot be rejected. (*Note that the effect of adjusting measurements on weathered surfaces is presented for interest only as the difference in mineralogy precludes use of the correction procedure on weathered surfaces.)*

Table 42, extracted from Appendix 18.5, summarises the difference before and after using the Fe backscatter normalisation procedure. Values reported in bold in Table 42 indicate that the application of the procedure has improved the average value (brought it closer to that measured on flat surfaces) or has increased the significance value reported by Student's two-tailed t-test.

MM3 t-test Result	Flat Surface (ppm ±1sd) (n=8)	Fresh, Flaked Blank (ppm) (n=4) (corrected) Between Flat & Fresh	*Weathered Surface (ppm) (n=4) (for information only) Between Flat & Weathered	Pecked, Polished and Ground Curved (ppm) (n=4) (corrected) Between Flat and Pecked
K	8 384 ± 2 513	**427**	593	444
		0.005	0.120	0.097
Ca	76 315 ± 1 297	**5 761**	**3 229**	**5 345**
		0.223	0.000	**0.760**
Ti	13 689 ± 1 620	1 094	**878**	**1 027**
		0.222	**0.341**	**0.308**
Mn	1 514 ± 555	**121**	**103**	84
		0.267	**0.347**	0.150
Fe	85 367 ± 4 020	**6 024**	6 147	5 626
		0.180	0.708	0.817
Rb	86.0 ± 23.1	**5.7**	**1.9**	5.1
		0.077	0.000	0.235
Sr	713 ± 42.4	**31.6**	**20.1**	**51.0**
		0.001	0.000	**0.597**
Y	33.1 ± 4.3	**1.8**	**1.9**	**2.5**
		0.130	**0.079**	**0.273**
Zr	176 ± 15.6	**10.7**	14.1	11.7
		0.062	0.095	0.627
Nb	4.9 ± 3.0	0.7	0.4	**0.6**
		0.057	0.073	**0.062**
Ba	144 ± 17.6	**8.7**	**7.8**	**10.8**
		0.000	**0.002**	**0.295**
Ce	-17.9 ± 6.5	2.2	3.1	**1.1**
		0.083	0.000	**0.057**
Pb	-0.6 ± 15.0	0.4	2.1	**1.2**
		0.025	0.001	**0.005**

*Table 42 The moduli of the differences in PXRF measurements caused by applying the Fe backscatter normalisation process. Values in Bold indicate an improvement: average values are closer to the measured flat surface average by the amount shown and the significance value of the t-test is higher after applying the normalisation procedure by the amount shown. (*Note values for weathered surfaces are shown for interest only)*

6.14.4 Discussion and remarks

Table 41 and 42 (from Appendixes 18.4 & 18.5) show that the correction factor is not universally effective on irregular or polished and curved surfaces measured in this investigation: the application of the correction factor does not always bring the corrected results closer to those obtained on flat rock surfaces. The data in Table 42 show that the application of the Fe backscatter normalisation procedure to PXRF measurements obtained from irregular surfaces improves measurements for all elements, except Ti, Nb, (note Ce and Pb are only reported for interest). Similarly, application of the normalisation process improves measurements made on pecked, polished and ground surfaces for all elements except K, Mn, Fe and Zr.

It is noted that Potts et al. (1997) developed the Fe backscatter correction factor based upon effective air-gaps between PXRF probe window and the sample, and that the sample

surface was flat. In this experiment the measured surfaces were irregular and curved and it is not fully clear if the Fe backscatter correction proposed by Potts et al. should work in these situations. It can be seen, from the above observations, that the application of the Fe backscatter normalisation to non-flat irregular surfaces does not improve PXRF measurements for all elements. Therefore, it calls into doubt as to the universal usefulness of the Fe backscatter normalisation procedure when dealing with irregular or curved greenstone rock and axe surfaces.

Although it appears that the application of the procedure could be marginally advantageous at improving some measurements it is noted that Ti, Zr & Nb are amongst those elements where an improvement *was not observed*. As these HFS elements are important in geochemical analyses and are used extensively in characterisation of axes and subsequent geochemical provenancing (c.f. Chapters 7 & 8) it could therefore, be detrimental to this research to apply the Fe backscatter normalisation procedure.

A further difficulty with the Fe backscatter normalisation procedure is that the procedure is used to adjust measurements made on a similar rock matrix and requires an ideal sample of the rock to establish the reference Fe backscatter value. Assuming that MM3 is representative of a 'typical' greenstone then the 'ideal' Fe backscatter value is 289 ± 5 (Appendix 18.1) and ranges to 264 ± 20 for irregular and 310 ± 5 for polished & curved surfaces. However, field records note that Fe backscatter values for axes range from 260 to 350 for similar surfaces. This is interpreted as showing that it is probable that the MM3 Fe backscatter value may not be universally representative of the axe rock type. Additionally, inspection of Appendix 15.1 shows that Fe backscatter for the greenstone exposure samples ranges from 280 to 350, thus allowing the conclusion that use of a single Fe backscatter value to form the basis for adjusting axe measurements could lead to misleading results.

It appears that the use of an ideal normalising value may not be appropriate for all samples for which it would be thought to be acceptable. This, plus the observation that the Fe backscatter normalisation procedure does not universally improve measurements made on MM3 samples, indicates that there is no real benefit gained from using the Fe backscatter normalisation procedure in this work.

One observation about the Fe backscatter value that is worth reporting is that any Fe backscatter value which is significantly different (>10%) from others measured on the same sample indicates a possible problem with that set of data. For example RMM3#12 (Appendix 18.1) has Fe backscatter significantly lower than the other analyses on that surface. The reasons for this are not fully understood but are believed to indicate a significant difference in the composition of the sample or surface form beneath the PXRF probe window. This finding is supported by field tests: the Fe backscatter values changed markedly when the PXRF was used to measure over paper identification labels stuck to axes. Hence, any reading with markedly different Fe Backscatter to others from the same sample should be (and has been) eliminated.

6.15 PXRF SD: Examination of instrument precision and elemental detection limits.

6.15.1 Introduction to purpose of investigation

The PXRF supplies a value that represents the uncertainty associated with each measured element concentration. This value is referred to as the PXRF SD and is an estimate of instrument precision based largely on the statistics associated with the total number of x-ray counts that contribute to a measurement (Potts et al. 1997a: p39). The main factor determining the magnitude of the PXRF SD is the total count of x-rays arriving at the detector during the count time, which depends on the concentration of the element within the sample and the sensitivity of the instrument. Long count times should lead to reduced values of PXRF SD (according to the relationship PXRF SD $\propto \sqrt{n}$, where n = number of counts detected) as larger values of n will *proportionally* reduce the magnitude of the PXRF SD, hence improve instrument precision.

A second factor that affects PXRF results in the longer term is the reduction in primary x-ray intensity as the isotopic sources decay. A periodic PXRF 'energy calibration' process takes into account of the source age and decreasing x-ray intensity and recalibrates the PXRF by adjusting PXRF sensitivity (i.e. calibration) to counteract the reduction in counts. The reduction in instrument precision (as n decreases) witnessed by the increasing PXRF SD values can be partly counteracted by increasing the count time. The duration between the first and second fieldwork periods (Week1 and Week 2&3) is approximately one year (May 97 to May 98) and between the second and third fieldwork periods (Week 2&3 and Week 4) is approximately 8 months (May 98 to Jan 99). For the first fieldwork period and half of the second the PXRF count times were set at 100s (^{109}Cd), 50s (^{55}Fe) 40s (^{241}Am) and for the second half of Weeks 2&3 and Week 4 these times were increased to 110s, 60s, 50s respectively, to restore PXRF instrument precision. (Note: the same PXRF adjustment was used during all three fieldwork periods.)

The detection limit of the PXRF is believed to be related to the value of the PXRF SD at low concentrations. For example, assume the reported concentration (of an element) is 1ppm and the associated PXRF SD is reported at 10ppm. This is taken as indicating the true value is within 1 ± 10ppm for 67% of measurements (1sd, assuming normal distribution of data), 1 ± 20ppm for 95% of measurements (2sd) and 1 ± 30ppm for 99% (3sd) of measurements. Hence, 3 x PXRF SD is a value associated with the PXRF correctly detecting a low concentration in 99 out of 100 measurements and it is this value which is believed to represent, or be close to, the PXRF detection limit.

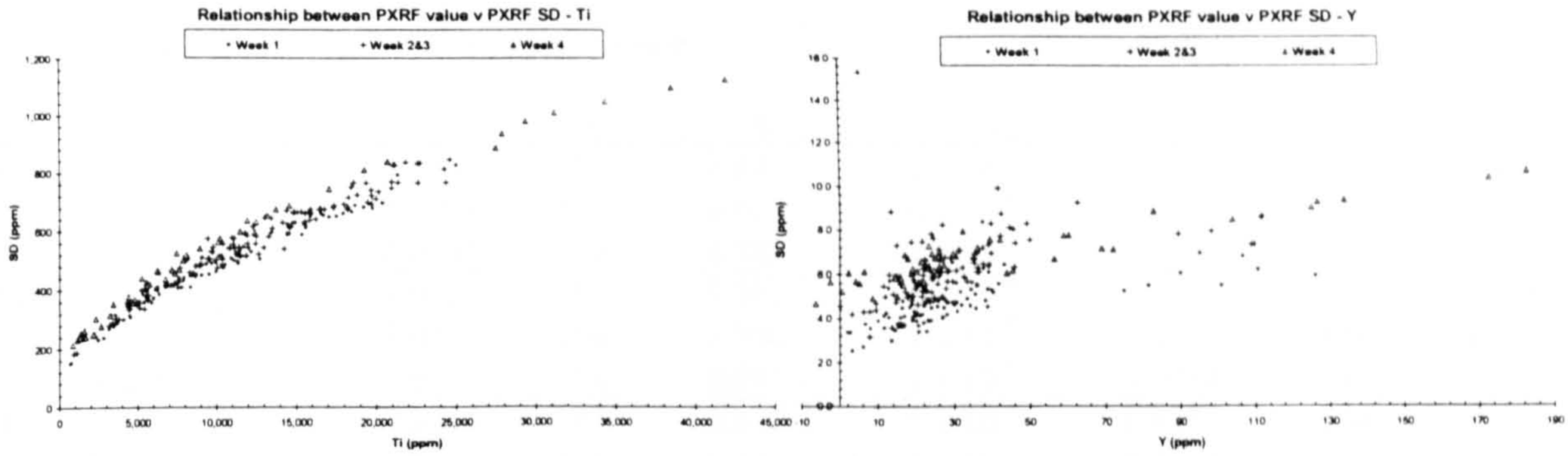

Figure 59 Illustration of charts with element concentrations plotted against PXRF SD values for the three fieldwork periods. Full-size charts are contained in Appendix 19.1

6.15.2 Results

PXRF data of 266 exposure samples and pellets measured during the three fieldwork periods is plotted for each element on the bivariate charts contained in Appendix 19.1, with data from each of the fieldwork period represented by a different symbol. Four of these charts, Ti, Y, Zr & Nb, are reproduced in Figure 59 for reference.

Linear and quadratic regression statistics are used to investigate the relationship of the data. The model for linear regression is $Y = b_1x + b_o$ and the quadratic model is $Y = b_2x^2 + b_1x + b_o$ The full set of results for each of the three analysis periods, for each element is contained in Table 43.

	Element & fieldwork period	Linear Regression			Quadratic Regression			
		b_1	b_0	R^2	b_2	b_1	b_0	R^2
K	Week 1	0.0085	225	0.801	-4×10^{-8}	0.0098	239	0.804
	Week 2&3	0.0101	255	0.807	-6×10^{-8}	0.0118	234	0.810
	Week 4	0.0064	422	0.888	3.2×10^{-8}	0.0053	327	0.890
Ca	Week 1	0.0046	159	0.967	-3×10^{-8}	0.0072	116	0.990
	Week 2&3	0.0051	166	0.936	-3×10^{-8}	0.0081	118	0.959
	Week 4	0.0057	154	0.981	-4×10^{-8}	0.0084	132	0.996
Ti	Week 1	0.0260	217	0.957	-5×10^{-7}	0.0380	164	0.972
	Week 2 & 3	0.0255	246	0.945	-5×10^{-7}	0.0394	172	0.961
	Week4	0.0238	274	0.952	-4×10^{-7}	0.0400	199	0.992
Mn	Week 1	0.0372	214	0.788	-5×10^{-6}	0.0673	182	0.849
	Week 2&3	0.0436	288	0.677	-4×10^{-6}	0.0793	242	0.777
	Week 4	0.0483	316	0.562	-1×10^{-5}	0.1347	228	0.726
Fe	Week 1	0.0078	361	0.934	-3×10^{-8}	0.0131	159	0.968
	Week 2&3	0.0094	487	0.943	-2×10^{-8}	0.0131	312	0.953
	Week 4	0.0144	408	0.986	-3×10^{-8}	0.0177	328	0.990
Rb	Week 1	0.0194	14.7	0.259	4.5×10^{-6}	0.0177	14.8	0.260
	Week 2&3	0.0269	19.6	0.405	1.3×10^{-5}	0.0151	20.2	0.426
	Week 4	0.0484	26.7	0.105	-3×10^{-5}	0.0425	26.5	0.105
Sr	Week 1	0.0158	7.6	0.919	-8×10^{-6}	0.0254	5.6	0.951
	Week 2&3	0.0221	9.7	0.827	-1×10^{-5}	0.0368	7.2	0.858
	Week 4	0.0366	8.2	0.810	-5×10^{-5}	0.0645	4.5	0.894
Y	Week 1	0.0270	3.9	0.388	-0.0005	0.0804	2.9	0.522
	Week 2&3	0.0338	5.2	0.204	-0.0004	0.0796	4.4	0.240
	Week 4	0.0282	5.7	0.837	-5×10^{-5}	0.0360	5.5	0.843
Zr	Week 1	0.0092	7.0	0.799	-4×10^{-6}	0.0143	6.3	0.835
	Week 2&3	0.0116	9.3	0.720	-1×10^{-5}	0.0282	6.8	0.826
	Week 4	0.0141	8.3	0.853	-1×10^{-5}	0.0189	8.1	0.858
Nb	Week 1	0.0290	2.6	0.826	-0.0002	0.0438	2.0	0.846
	Week 2&3	0.0400	3.4	0.709	-0.0006	0.0903	2.8	0.871
	Week 4	0.0389	3.6	0.598	-0.0005	0.0534	3.6	0.604
Ba	Week 1	0.0363	11.3	0.928	-3×10^{-5}	0.0525	10.3	0.953
	Week 2&3	0.0381	10.2	0.850	-4×10^{-5}	0.0591	9.1	0.893
	Week 4	0.0205	12.6	0.935	-1×10^{-5}	0.0318	11.2	0.950
Ce	Week 1	0.0340	10.7	0.835	2×10^{-5}	0.0325	10.7	0.836
	Week 2&3	0.0406	9.9	0.416	-0.0001	0.0482	10.1	0.428
	Week 4	0.0234	9.0	0.790	-4×10^{-5}	0.0256	9.1	0.796
Pb	Week 1	0.0468	14.1	0.403	3.0×10^{-5}	0.0435	23.6	0.404
	Week 2&3	0.0540	18.8	0.308	6.2^{-5}	0.0500	18.7	0.309
	Week 4	0.0318	20.5	0.057	0.0003	0.0193	20.5	0.062

Table 43 Linear and quadratic regression coefficients calculated from PXRF SDs obtained from 266 measurements

6.15.3 Discussion

6.15.3.1 Bivariate charts

Figure 59 and Appendix 19.1 Parts 1 to 13 clearly show that there are systematic differences in the values of PXRF SD for each fieldwork period. The main difference between the first fieldwork period and the first half of the second fieldwork period was the decay of the isotope sources (in 1 year) since the isotope count times were the same for both periods, hence the observed differences are probably related to a reduction in x-ray intensity. The main difference between the second half of Week 2&3 (from date letter V) and Week 4 and the other two analysis periods is both isotope decay (8 months) and an increase in the PXRF count times by 10 seconds per isotope. Figure 59 and Appendix 19.1

show that the effect of isotope age alone is to increase proportionally the PXRF SD (seen on the charts as a slight anticlockwise rotation of the data trend between the two periods, especially visible on the Fe Chart). A combined effect of source age and count time change (i.e. Week 4 data) reveals similar patterns to those seen for reduction in x-ray intensity (isotope decay only). However, in this case the observed slope of Week 4 data is distinctly different to the previous two periods for many elements (see Fe) and probably reflects the effect of increasing count times by 10s per isotope.

6.15.3.2 R^2 Coefficients of linear and quadratic regression

Observed evidence from the charts in Figure 59 and Appendix 19 clearly suggests that there is a non-linear relationship between the PXRF SD value and the associated concentration for each of the 13 elements measured. Regression analysis suggests this is so, as the majority of R^2 statistics in Table 43 are below 0.95, with Ca & Ti providing the exceptions. The quadratic R^2 statistic is generally larger than the equivalent linear R^2 statistic indicating that residual errors from a quadratic curve are lower than for a linear curve and thus quadratic regression better represents the relationship between the PXRF SD and associated concentration.

(Note that as the data contains zero and negative values so exponential and logarithmic regression could not be undertaken. The addition of constant to the PXRF SD data to eliminate the negative values was examined, but subsequent calculations indicated that this method to obtain curve-fit regression parameters was flawed and hence not used.)

Inspection of the bivariate charts indicates that the largest deviation from an approximately linear regression occurs at comparatively low concentrations, with a marked decrease in PXRF SDs recorded in this zone. Away from this zone the relationship between PXRF SD and concentration appear to be more linear.

6.15.3.3 b_0 coefficient of linear and quadratic regression

The b_0 coefficient (*y-axis* intercept) is representative of the PXRF SD given for zero elemental concentration. This, in turn, leads to an estimate of the PXRF detection limit as discussed above.

Comparing the calculated b_0 coefficients reported in Table 43 and the associated charts in Figure 59 and Appendix 19 indicates the value calculated from the quadratic regression

coefficient, b_0, is larger than the equivalent value deduced from the *y-axis* intercepts in the bivariate charts. For example the calculated b_0 for Ti for Week 1 is 164ppm and the best fit curve from Figure 59a (Appendix 19.1 Part 3/13) crosses the *y-axis* at approximately 120ppm. As mentioned above, this is due to the fact that the relationship between PXRF SD and associated concentration is only approximately quadratic. Therefore the calculated b_0 value is an overestimate of the PXRF SD at zero concentration. Thus 3 x b_0 (from the quadratic regression) gives an indication of the PXRF detection limit at *greater* than 99% probability. Table 44 below compares the PXRF detection limits based at 3 x b_0 and those published (c.f. Table 29)

	Week 1 (ppm)	Week 2&3 (ppm)	Week 4 (ppm)	*Thermo FI (ppm)	*Potts et al (1995) (ppm)
K	717	702	981	150	360
Ca	348	354	396	70	225
Ti	492	1182	597	55	120
Mn	546	726	684	200	354
Fe	477	936	984	110	424
Rb	44.4	60.6	79.5	5	13
Sr	16.8	21.6	13.5	4	14
Y	8.7	13.2	16.5	4	9
Zr	18.9	20.4	24.3	3	9
Nb	6.0	8.4	10.8	4	6
Ba	30.9	27.3	33.6	9	21
Ce	32.1	30.3	27.3	7	14
Pb	70.8	56.1	61.5	15	39

*Table 44 Comparison of PXRF detection limits. Values for Weeks 1, 2&3 and 4 are 3 times the b_0 value from quadratic regression analysis of PXRF measurements of mainly greenstone exposure and pellet samples using 100s (^{109}Cd), 50s (^{55}Fe) 40s (^{241}Am) (Week 1 and 2&3), and 110s (^{109}Cd), 60s (^{55}Fe) 50s (^{241}Am) (Week 4 only), count times. * indicates values from Table 29 based on 200s count times per isotope.*

Table 44 shows that the detection limits based on 3 times the PXRF SD at zero concentration are markedly larger than those published by Potts et al. (1995). Two reasons for this are: the smaller count times used in this examination and/or that 3 x PXRF SD at zero concentration is not related to PXRF detection limit. (Note that detection limits are normally specified as '3 standard deviations on the background signal' (Potts 1997: p 158)). Overall, and from working with the PXRF data, it is felt that the PXRF detection limit is probably closer to 1 to 2 times the PXRF SD at zero concentrations. Further work will be necessary to confirm this.

6.15.3.4 b_1 Coefficient of linear and quadratic regression

For linear regression the b_1 coefficient represents the relationship between the two sets of data being compared. As R^2 approaches one, b_1 approaches a value that represents a more accurate measure of the relationship between the two sets of data. As seen, R^2 values are

often <0.95, but >0.8, indicating that the b_1 coefficients can only be indicative of the relationship between PXRF SD and associated concentrations.

Inspection of Table 43 above shows that b_1 (linear regression) is less than 0.05 for all elements which is interpreted that PXRF instrument precision is generally better than 5% relative (1sd) over the range of concentrations measured. However, these results need to be tempered with the fact the relationship between the two data sets is not linear when the concentrations approach the PXRF detection limit (concentrations of approximately 5 to 10 times the PXRF SD) and therefore, should only be used as indicative for measurements away from the PXRF detection limit.

6.15.3.5 b_2 Coefficient

The quadratic regression b_2 coefficients are all smaller than 6×10^{-4} in Table 43 (above). When typical element concentrations are taken into account the magnitude of resulting term in the quadratic equation will be in the order of 10^{-1} to 10^{-3}. For example K concentrations for greenstones are around 3,000ppm and with the corresponding b_2 coefficient at 6×10^{-8}, which results in the x^2 term having a value of 18×10^{-2}. This, coupled with the generally higher R^2 values, suggests the quadratic curve (or regression) is both shallow and better approximates the relationship between the PXRF SD and the associated concentration.

6.15.3.6 Estimated PXRF instrument precision when measuring greenstones

Table 45 presents the instrument precision as a relative percentage, calculated from the linear and quadratic regression coefficients from the second fieldwork period and typical greenstone concentrations. For example, assuming a K concentration of 3,000ppm, and the associated linear regression coefficients from Table 43 we get (0.0101 x 3,000) + 255 = 285.3ppm, when divided by 3,000 gives 0.095, or 9.5%.

	Typical greenstone concentration (ppm)	Instrument precision (%) Linear regression Week 2&3	Instrument precision (%) Quadratic regression Week 2&3	Reported precision (Whin Sill dolerite using 100s (left) & 200s (right) count time)		
K	3 000	9.5%	9.0%	3.9%	1.6%	(8 302ppm)
Ca	60 000	0.8%	1.0%	1.1%	0.45%	(64 540ppm)
Ti	10 000	5%	5.6%	2.1%	1.8%	(14 560ppm)
Mn	1 500	23.5%	24.0%	24.5%	13.5%	(91 320ppm)
Fe	100 000	1.4%	1.6%	1.3%	1.5%	(93 380ppm)
Rb	50	42%	41.9%	21.4%	9.5%	(27ppm)
Sr	100	11.9%	10.9%	4.3%	2.2%	(442ppm)
Y	30	20.7%	14.6%	16.8%	14.0%	(34ppm)
Zr	200	5.8%	6.2%	3.4%	3.2%	(206ppm)
Nb	10	38.0%	37.0%	26.8%	29.4%	(18ppm)
Ba	250	7.9%	9.5%	7.2%	2.0%	(350ppm)
Ce	-30	36.9%	38.5%			
Pb	10	194%	193%			

Table 45 Estimated PXRF instrument precision based on linear and quadratic regression analysis of PXRF SD data for typical greenstone rock. (Reported precision from Potts et al. 1995).

Table 45 indicates that the PXRF instrument precision based on regression analysis of PXRF SD values for typical greenstone concentrations are generally larger than those previously reported, with Rb showing the largest difference. This increase is almost certainly due to the fact that the reported precisions are based on 100s and 200s count time per isotope Potts et al (1995), whereas count times of 100s (^{109}Cd), 50s (^{55}Fe) 40s (^{241}Am) and 110s (^{109}Cd), 60s (^{55}Fe) 50s (^{241}Am) were used in this work. Inspection of Table 43 indicates that the amount contributed to the overall precision value by the b_1 and b_2 coefficients is relatively small and that it is the offset (b_0) that contributes most to the calculated value for the typical concentrations measured.

6.15.4 Summary

This section has shown that the relationship between the PXRF SD and associated PXRF measured concentration can be best approximated by quadratic regression, although the relationship is roughly linear, for concentrations away from the detection limit. Detection limits, established from 3 x the b_0 coefficient, are higher than to those reported from other sources, possibly due to the lower count times used in this thesis and/or the possibility that there is no distinct relationship between PXRF SD and detection limits. Achieved instrument precision, based on PXRF SD measurements and after taking into account the shorter PXRF count times used in this work, are generally similar to those previously reported.

6.16 PXRF Repeatability: Assessment of long term accuracy and precision

6.16.1 Data

Two reference pellets, referred to as 'control pellets' were measured at least twice and often three times each day of the three analysis periods and on the same side. In total 80 PXRF measurements were made on both control pellets. The primary use of measuring the control pellets was to check that the operating performance of the instrument was within acceptable limits. The control pellets, ACE and WSE, were chosen because their range of concentrations bracketed the range of values expected from most silicate rocks. The resulting data are tabulated and plotted in full in Appendix 20 for ACE and Appendix 21 for WSE and are summarised below.

6.16.2 Results

Control pellet data is displayed graphically in Appendix 20.2 and 21.2, with examples Ti for both ACE & WSE shown in Figure 60. In these charts the value of each PXRF measurement is shown, with error bars equivalent to twice the average PXRF SD for the analysis period. The average value is shown for each fieldwork period as a horizontal line. Additionally, the conventional true value (published) value for the reference material is displayed as a dotted horizontal line.

Simple statistical parameters, namely average, sd, standard error (SE) and instrument/sample precisions are detailed in Appendix 20.3 for ACE and Appendix 20.3 for WSE, and are summarised in Tables 46, 47 & 48 below. SDs are calculated from the measurements made in each fieldwork period. SE is calculated by dividing the sd by $\sqrt{n}$, where n is the number of analyses in that period. Sample precision is calculated by dividing the sd by the average PXRF measured concentration, with the result expressed as a percentage. Instrument precision is presented as the average of the recorded PXRF SD values for measurements made in the period. The conventional true values are obtained from Potts et al. 1992 (ACE) and Govindaraju et al. 1994 (WSE).

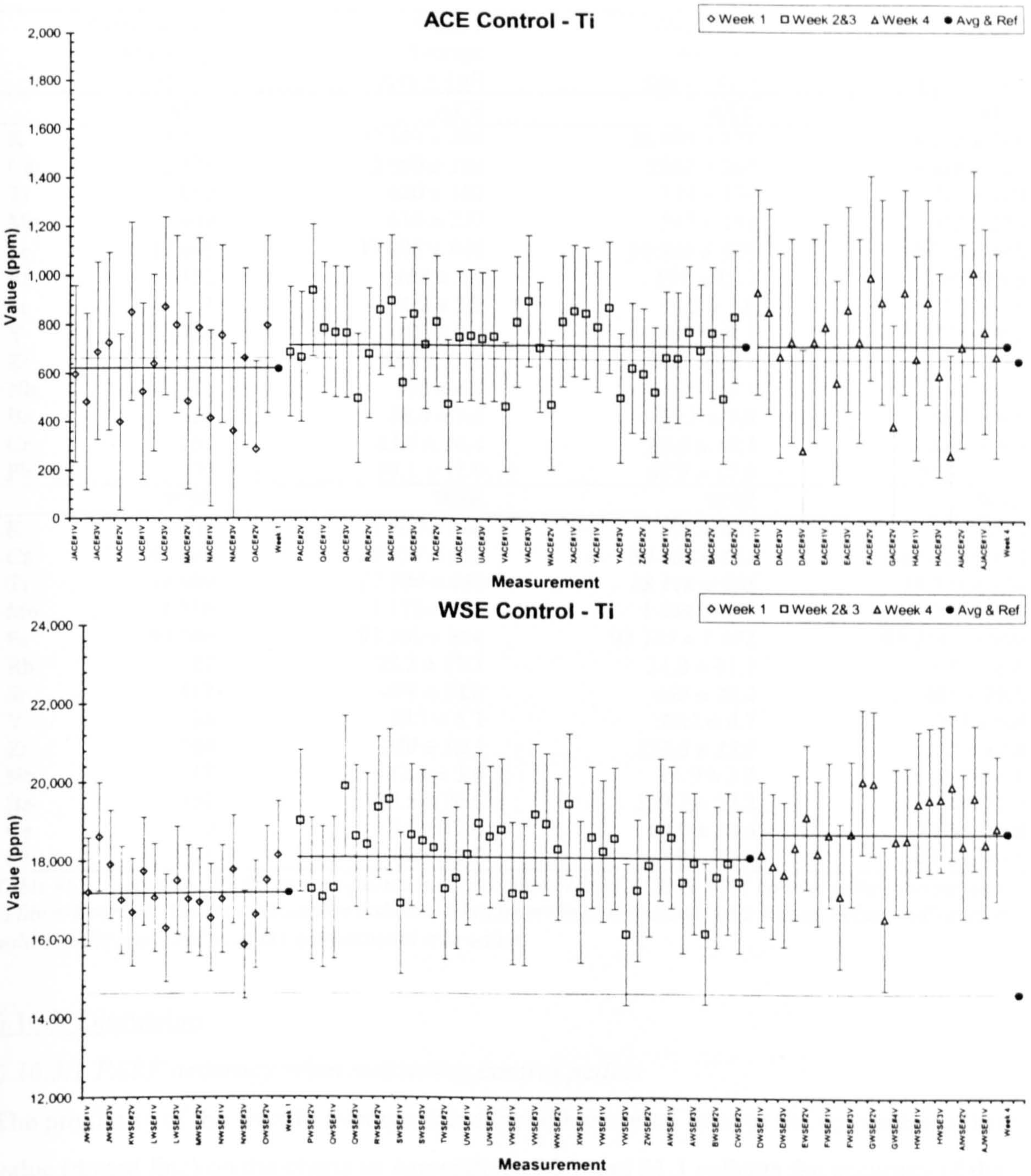

Figure 60 Example of ACE and WSE control pellet charts used to examine long term PXRF accuracy and precision. Conventional true value is shown as a dotted horizontal line, weekly average values are shown as horizontal black lines. Error bars represent ±2 average PXRF SD. Full-size charts and data are contained in Appendix 20 (ACE) & 21(WSE)

	Conventional true value (ppm)	Week 1 Average (ppm ± 1sd)	Week 2&3 Average (ppm ± 1sd)	Week4 Average (ppm ± 1sd)
	ACE	**ACE**	**ACE**	**ACE**
K	37 273	37 341 ± 504	36 999 ± 472	**38 282 ± 701**
Ca	2 429	**2 599 ± 154**	2552 ± 267	***3 480 ± 149***
Ti	659	620 ± 182	719 ± 134	722 ± 209
Mn	449	616 ± 237	545 ± 232	478 ± 276
Fe	17 696	17 298 ± 440	**16 816 ± 525**	**16 770 ± 448**
Rb	152	***188 ± 9.3***	159 ± 10.3	159 ± 16.6
Sr	3	4.2 ± 3.2	5.2 ± 4.0	5.2 ± 4.5
Y	184	180 ± 7.1	177 ± 9.2	178 ± 9.8
Zr	780	***887 ± 13.6***	***861 ± 19.1***	***852 ± 18.4***
Nb	110	**118 ± 4.9**	115 ± 7.1	116 ± 7.0
Ba	55	**38.4 ± 9.0**	**39.3 ± 7.8**	**38.6 ± 9.5**
Ce	154	***83.9 ± 10.4***	***87.5 ± 10.1***	***84.8 ± 9.6***
Pb	39	39.1 ± 11.9	45.9 ± 17.0	37.7 ± 18.7
	WSE	**WSE**	**WSE**	**WSE**
K	8 302	**7 860 ± 306**	**7 492 ± 411**	7 874 ± 473
Ca	64 608	***59 734 ± 392***	***59 569 ± 654***	***62 410 ± 612***
Ti	14 609	***17 194 ± 689***	***18 118 ± 905***	***18 724 ± 924***
Mn	1 316	1 175 ± 355	1 444 ± 439	1 350 ± 414
Fe	93 166	93 561 ± 854	92 745 ± 1 672	93 018 ± 1 800
Rb	27	25.2 ± 17.1	31.0 ± 31.1	23.4 ± 36.4
Sr	417	***479 ± 18.0***	***469 ± 20.2***	**461 ± 29.5**
Y	34	29.1 ± 5.1	**28.2 ± 4.7**	28.5 ± 6.8
Zr	204	***230 ± 10.3***	***223.6 ± 13.9***	***222 ± 12.8***
Nb	17	**12.1 ± 3.6**	14.9 ± 3.3	13.9 ± 6.4
Ba	354	330.5 ± 26.5	339.7 ± 27.2	340 ± 22.9
Ce	0	8.5 ± 12.4	**10.9 ± 10.6**	**12.3 ± 10.0**
Pb	11	-3.0 ± 18.7	-4.9 ± 19.0	-11.6 ± 19.8

Table 46 Average PXRF measurements and associated sds of ACE & WSE control pellets during each fieldwork period. Values indicated in bold are >1sd from the conventional true values, values indicated in bold + italic are >2sd from the conventional true value.

6.16.3 Discussion

6.16.3.1 PXRF accuracy when measuring control pellets

The proximity of the weekly average value (solid horizontal line) to the conventional true value (dotted line) on the charts in Appendixes 20.1 and 21.1 reflects the accuracy of the PXRF during that fieldwork period. Inspection of Table 46 above and Appendixes 20.3 & 21.3 show that the weekly averages are similar for each element, apart from ACE: K and WSE Ca, where the Week 4 average is markedly different. The consistency between measured averages and difference with the conventional true value indicates that there is probably a bias in the PXRF measurements (with respect to conventional true values). Table 47 compares the bias calculated from dividing the measured average control pellet value by the conventional true value and compares them with the bias obtained in Section 6.9, PXRF Bias (I) examination.

	ACE Week 1	Week2&3	Week 4	WSE Week 1	Week 2&3	Week 4	Bias (I) (min-max range)
K	1.002	0.993	1.027	**0.947**	**0.902**	**0.950**	0.983-1.055
Ca	**1.070**	**1.051**	**1.433**	0.925	0.922	0.966	0.909-0.988
Ti	**0.940**	**1.091**	**1.095**	1.177	1.240	**1.28**	1.170-1.312
Mn	1.372	1.213	1.064	**0.893**	1.097	**1.026**	1.005-1.381
Fe	0.978	**0.950**	**0.948**	1.004	0.995	0.998	0.977-1.029
Rb	1.106	1.047	1.049	**0.933**	1.146	0.865	0.991-1.147
Sr	**1.395**	1.138	**1.740**	1.150	1.126	1.107	1.075-1.167
Y	0.976	0.960	0.969	**0.858**	**0.831**	**0.842**	0.894-1.063
Zr	1.137	1.103	1.092	1.130	1.098	1.092	1.092-1.161
Nb	**1.070**	1.047	1.055	**0.698**	**0.862**	**0.806**	0.961-1.061
Ba	**0.698**	**0.714**	**0.702**	**0.934**	**0.960**	**0.959**	0.771-0.878
Ce	-						
Pb	-						

Table 47 PXRF bias based on the ACE & WSE control pellets. Bias values are derived by dividing the average fieldwork period measurement by the conventional true value. The min-max range of values obtained in the Bias (I) investigation is shown. Values indicated in bold are outside the Bias (I) range. Note Bias(I) values for linear regression through (0,0) have been used, hence values for Ce & Pb have not been reported.

Examination of Tables 46 and 47 show that ACE: Ca, Ti, Fe, Sr and Ba and WSE: K and Rb, have low concentrations compared to the range exhibited by the reference samples and the associated relative precision is low (see below), thus giving rise to slightly different bias values to those obtained in Bias (I). WSE: Y, Nb and Mn average values are associated with relatively large sds and this is probably the reason these values are slightly different to those obtained in Bias (I). ACE and WSE Ba bias values deviate the most, appearing to straddle the min-max range of Bias (I) values. Therefore, apart from Ba, the bias values obtained from replicate PXRF measurements of the control pellets are considered as being similar to those calculated using the reference sample (of which ACE & WSE were included).

Calculations show that using the Bias (I) values to adjust ACE and WSE average values results in improved accuracy (i.e. the adjusted value is closer to the conventional true value) in 42 of the possible 66 cases (11 elements x average value for each fieldwork periods x two pellets = 66 possible measurements). (Note Ce & Pb were ignored since linear regression cannot establish bias for these two elements.). In 21 of the remaining 24 cases no appreciable difference was observed, the corrected value was slightly further removed from the conventional true value by a few ppm or by a small relative value (e.g. 650ppm in 93 500ppm). In the last 3 cases application of Bias (I) moved WSE Ba values 25 to 50ppm further away from the conventional true value of 354ppm. Considering the PXRF SD at this concentration (approximately 25ppm) this movement is not considered significant, but is worth noting that for high Ba values Bias (I) correction factors do not appear to improve accuracy for ACE & WSE measurements.

6.16.3.2 Instrument precision

The repeatability of PXRF measurements (instrument precision) can be assessed through the size of the sd associated with calculating the fieldwork period averages. Table 48, below, reports the calculated sd associated with the average concentration for each fieldwork period and the average of the PXRF SD values for the same set of PXRF measurements (c.f. Appendix 20 & 21 for details).

	Conventional true value (ppm)	Fieldwork period Week 1		Fieldwork period Week 2&3		Fieldwork period Week 4		Average Sample precision	Average Instrument precision
		Av. sd	PXRF SD	Av. sd	PXRF SD	Av. sd	PXRF SD		
	ACE	ppm	ppm	ppm	ppm	ppm	Ppm		
K	37 273	504	508	472	549	701	572	1.5%	1.5%
Ca	2 429	154	148	267	159	149	176	7.8%	6.6%
Ti	659	182	160	134	174	209	178	26.6%	25.9%
Mn	449	237	191	232	238	276	266	55.3%	51.6%
Fe	17 696	440	412	525	516	448	588	2.7%	2.9%
Rb	152	9.2	10.1	10.3	12.6	16.6	14.4	7.9%	8.1%
Sr	3	3.6	3.2	4.0	4.1	4.5	4.8	134.4%	134.4%
Y	184	7.1	7.1	9.2	9.0	9.8	10.2	4.7%	4.8%
Zr	780	12.5	13.6	19.1	17.0	18.4	19.2	2.1%	2.1%
Nb	110	4.0	4.9	7.1	6.2	7.0	7.1	5.5%	5.5%
Ba	55	9.5	9.0	7.8	8.5	9.5	8.0	16.2%	15.5%
Ce	154	9.5	10.4	10.1	9.9	9.6	9.3	6.3%	6.4%
Pb	39	12.0	11.9	17.0	15.2	18.7	16.9	40.8%	37.6%
	WSE								
K	8 302	306	335	411	361	473	376	4.8%	4.3%
Ca	64 608	392	445	654	483	612	507	0.9%	0.7%
Ti	14 609	689	659	905	713	924	745	5.7%	4.8%
Mn	1 316	355	287	439	374	414	427	30.6%	27.6%
Fe	93 166	854	1 118	1 672	1 403	1 800	1 605	1.5%	1.5%
Rb	27	17.1	18.3	31.1	22.9	36.4	26.5	104.4%	83.6%
Sr	417	18.0	17.0	20.2	21.3	29.5	24.3	5.4%	5.0%
Y	34	5.1	4.8	4.7	6.1	6.8	7.0	16.3%%	17.5%
Zr	204	10.3	10.3	13.9	12.9	12.8	14.8	6.0%	6.2%
Nb	17	3.6	3.2	3.3	4.2	6.4	4.8	26.0%	23.9%
Ba	354	26.5	25.1	27.2	24.1	22.9	22.9	7.2%	6.8%
Ce	0	12.4	10.5	10.6	10.1	10.0	9.6	*	*
Pb	11	18.7	15.5	19.0	19.5	19.8	21.9	174.2%	172.4%

*Table 48 Comparison between calculated standard deviations, based on PXRF measurements of ACE & WSE control pellets during each fieldwork period and the average PXRF SD for the same period. Relative precision is obtained by dividing the average precision by the corresponding conventional true value. * indicates relative precisions cannot be calculated as the divisor is zero.*

It is clear from Table 48, above, that there is a close link between the PXRF SD and that calculated from replicate measurements of the same sample. In most cases the PXRF SD slightly is smaller than the associated calculated sd, suggesting that the PXRF SD may be an optimistic estimate of size of instrument precision (measuring pellets only). Equipment precision is better than 5% relative for elemental concentrations 10 times PXRF detection limits identified in Table 44 (Section 6.15.3.3) for K, Ca, Ti (5.2%), Fe, Sr, Y, Zr, Nb

(5.5%) and Ba (7.4%). Ce & Pb PXRF measurements are both relatively small and the PXRF measurements may be offset by some value and this probably accounts for the large relative precision calculated. The Mn calculated and PXRF SDs are large compared to the actual measurements and are possibly near the PXRF detection limits for the element. Rb concentration in WSE is small and the large sd results in the large relative precision. The relative precision improves to better than 8.1% for higher Rb concentrations in ACE. Likewise, Ba sds are comparatively large compared to the WSE measured concentration resulting in the approximate 7.2% value for equipment relative precision.

Figure 60 and Appendixes 20.2 and 21.2, show that precision and accuracy is maintained throughout the each of the three fieldwork periods. However, in the long term, equipment precision reduces. A simple average calculated from all 13 element's *average calculated sd* values for both ACE & WSE control samples increases from 165.1 to 227.9 to 240.2 for the three fieldwork periods Week 1, 2&3, and 4 respectively (c.f. Table 48). Similarly, the average of the *associated PXRF SD* values also increases, from 170.7 to 199.0 to 217.8 for the same sequence of fieldwork periods. This loss of precision is almost certainly due the decay of source isotopes and the associated reduction in primary x-ray intensity. It shows the extended count times used in the second half of Week 2&3 and Week 4 did not return precision to previously obtained levels.

6.17 Consolidation, interpretation and location of PXRF data for further work

The previous sections of this chapter have established the performance parameters of the PXRF when measuring greenstone rocks and axes. This section illustrates how this data is consolidated in preparation for use in Chapters 7 & 8. Table 49, below provides the key for Table 50 which uses PXRF measurements from 2 axes to illustrate the processing and interpretation of PXRF measurements.

Title	Content
Raw PXRF data (PXRF measurement reference)	PXRF reported concentrations and associated PXRF SD. These values originate from electronic file transfer from the PXRF to a portable computer on the day of measurement. The files are incorporated into a custom built relational database which allowed manipulation of the data, ultimately as formatted spreadsheet files. Hard copies of the formatted spreadsheet files are contained in the Appendices.
Average (Axe/sample name)	Simple average of the PXRF measurements. Note an average for the PXRF SD is not reported.
Bias	Bias (I) coefficient for appropriate week rounded are reported to three decimal places and then rounded to two decimal places prior to using them to adjust the PXRF measurements. Bias (I) coefficients are used throughout (Table 34, except Ti, Ce & Pb) as they are available for each fieldwork period and they represent the best estimate of PXRF accuracy. Ti, Ce and Pb averages measurements are not adjusted for bias: Ti due to the anomaly noted in measuring pellets and rock, Ce & Pb due to the fact that the PXRF does not appear to be linearly calibrated over the range of concentrations encountered..
Adjusted average	Achieved by dividing the Average by the appropriate PXRF Bias (I) value.
Conversion factors	Indication of the major oxide and the associated stoichiometric conversion factor used to convert ppm to wt% (Potts et al 1992: p xi). Major oxides are reported as %wt since concentrations of major elements are normally reported in this way. However, this work uses ppm measurements in all statistical calculations.
Reported data	This is the PXRF data reported as 'averaged and corrected for bias' in the various Appendixes and used in the statistical calculations in Chapters 7 & 8. Major elements reported to nearest 100ppm and 2 decimal places by weight oxide. Trace elements reported to nearest ppm for concentrations 100ppm and to 0.1ppm for concentrations <100ppm
Instrument precision	Calculated using the quadratic regression coefficients in Table 43 to show the instrument precision associated with the measurement. Value is reported as ppm and relative % based on the PXRF average (i.e. unadjusted) measurement.
Sample precision	From Table 40, using R achieved by 2 PXRF measurements. Reported value is % relative deviation of the mean (R). PPM values are calculated by multiplying R by the PXRF average.
Detection limit	This is the average detection limit calculated from Table 44 Week 1, 2&3, and 4.

Table 49 Key for Table 50, identifying and explaining how the values in Table 50 have been arrived at.

Example 1: Axe Co138/1527

	K			Ca			Ti			Mn			Fe			Rb		Sr		Y		Zr		Nb		Ba		Ce		Pb	
	wt%	ppm	SD	wt%	ppm	SD	wt%	ppm	SD	wt%	ppm	SD	wt%	ppm	SD	ppm	SD	ppm	SD	ppm	SD	ppm	SD	ppm	SD	ppm	SD	ppm	SD	ppm	SD
Raw PXRF data																															
NC318#1V		3 389 9	274 4		51 028 8	406 0		12,578 5	571 3		2,709 2	341 2		124,569 0	1,293 4	70 4	23 0	276 1	14 7	53 6	6 0	187 6	9 5	4 8	3 2	63 2	15 4	-40 9	10 3	80 5	19 9
NC318#2V		3,397 8	270 1		48 208 7	394 1		16,608 7	616 2		2,352 8	332 7		121,939 0	1,278 1	-3 9	21 9	240 0	14 3	40 6	5 7	223 3	10 2	2 0	3 0	42 9	14 4	-39 7	10 2	36 1	18 0
Average Co318/1527		3,393 9			49,618 8			14,593 6			2,531 0			123,254 0		33 3		258 1		47 1		205 5		3 4		53 1		-40 3		58 3	
Bias (I) Week 1		0 997			0 930			1			1 224			1 016		1 095		1 150		1 017		1 142		1 019		0 820		1		1	
Rounded 2dp		1 00			0 93			1			1 22			1 02		1 10		1 15		1 02		1 14		1 02		0 82		1		1	
Adjusted average		3,393 9			53,353 5			14,593 6			2,074 6			120,837 3		30 2		224 4		46 2		180 2		3 3		64 7		-40 3		58 3	
Conversion Factor	K_2O			CaO			TiO_2			MnO			FeO																		
Factor	1 2046			1 3992			1 6681			1 2912			1 2865																		
Reported data	**0.41**	**3,400**		**7.47**	**53,400**		**2.43**	**14,600**		**0.27**	**2,100**		**15.55**	**120,800**		**30.2**		**224**		**46.2**		**180**		**3.3**		**64.7**		**-40.3**		**58.3**	
Instrument precision			271 8			399 4			612 1			320 3			1317 9		15 4		11 6		5 6		9 1		2.1		13 0		9 4		26.2
			8 0%			0 8%			4 2%			12 7%			1 1%		46 3%		4 5%		11 8%		4 4%		63 1%		24 5%		-23 4%		45 0%
Sample precision			21 0%			1 2%			8 4%			25 9%			3 3%		19 0%		4 2%		9 2%		6 3%		43 3%		8 6%		25 7%		not
			712 7			595 4			1,225 9			655 5			4,067 4		6 3		0 0	10 8	4 3		12 9		1.5		4 6		-10 4		calc.
Average detection limit	0 10	800		0 05	366		0 13	757		0 08	652		0 10	799		61 5		17 3		12 8		21 2		8 4		30 6		29 9		62 8	

Example 2: Axe Wi74/291

	K			Ca			Ti			Mn			Fe			Rb		Sr		Y		Zr		Nb		Ba		Ce		Pb	
	wt%	ppm	SD	wt%	ppm	SD	wt%	ppm	SD	wt%	ppm	SD	wt%	ppm	SD	ppm	SD	ppm	SD	ppm	SD	ppm	SD	ppm	SD	ppm	SD	ppm	SD	ppm	SD
Raw PXRF data																															
MW74#1V		2,522 9	246 2		39,495 5	354 2		12,342 7	532 1		1,063 8	258 5		83,972 8	1,002 6	51 3	17 4	430 3	15 3	21 9	4 2	169 0	8 6	3 4	2 5	51 0	13 0	-38 2	8 6	52 2	16 1
MW74#2V		2,162 8	272 8		58,896 2	435 3		14,409 9	607 1		1,155 1	288 9		102,633 0	1,168 4	31 4	19 3	438 8	16.7	31 4	5 0	195 9	9 8	10.3	3 2	72 2	15 4	-12.2	11 3	42 5	17 4
MW74#3V		1,989 9	250 2		45,200 9	381 4		20,078 2	671 0		1,449 3	276 8		80,940 2	1,008 9	15 2	21 5	538.7	18 6	31.6	5.1	188 7	9 9	11.7	3 3	91 9	16 3	-41.0	9 5	63 5	18 4
Average Wi74/291		2,225 2			47,864 2			15,610 3			1,222 7			89,182 0		32 6		469 3		28 3		184 5		8 5		71 7		-30 5		52 7	
Bias (I) Week 1		0 997			0 930			1			1 224			1.016		1 095		1.150		1.017		1.142		1 019		0 820		1		1	
Rounded 2dp.		1 00			0 93			1			1 22			1 02		1.10		1.15		1 02		1.14		1 02		0.82		1		1	
Adjusted average		2,225 2			51,466 9			15,610 3			1,002 2			87,433.3		29 7		408 1		27.7		161.9		8.3		87 4		-30 5		52 7	
Conversion Factor	K_2O			CaO			TiO_2			MnO			FeO																		
Factor	1 2046			1 3992			1 6681			1 2912			1 2865																		
Reported data	**0.27**	**2,200**		**7.20**	**51,500**		**2.60**	**15,600**		**0.13**	**1,000**		**11.25**	**87,400**		**29.7**		**408**		**27.7**		**162**		**8.3**		**87.4**		**-30.5**		**52.7**	
Instrument precision			260 6			391 9			635 3			256 8			1088 7		15 4		15 8		4.8		8 8		2.4		13 9		9.7		26 0
			11 7%			0 8%			4 1%			21 0%			1 2%		47.1%		3.4%		16 9%		4 8%		27 8%		19 4%		-31 9%		49 3%
Sample precision			21 0%			1 2%			8 4%			25 9%			3 3%		19 0%		4 2%		9 2%		6.3%		43 3%		8 6%		25 7%		not
			467 3			574 4			1,311 3			316 7			2,943 0		6 2		0 0	19 7	2 6		11 6		3.7		6 2		-7 8		calc.
Average detection limit	0 10	800		0 05	366		0 13	757		0 08	652		0 10	799		61 5		17 3		12 8		21 2		8 4		30 6		29 9		62 8	

Table 50 Two examples illustrating how PXRF data is presented, processed and interpreted (see text for discussion, RAW PXRF data reported as presented by PXRF, c.f. Table 49)

Both axe examples in Table 50 were chosen at random and represent typical IPC Group I axe PXRF analyses. Example 1 illustrates the normal situation where two PXRF measurements were made; the second PXRF measurement being similar enough to the first not to warrant a third PXRF measurement. Example 2 illustrates the situation where the first two PXRF measurements are sufficiently different (Ca & Fe) to warrant a third being taken.

The consolidated PXRF axe measurements (in bold in Table 50) are used in Chapters 7 & 8, and reported in Appendix 23. Exposure measurements are similarly adjusted for bias and reported, however in this case every exposure PXRF measurement is used and not an average of readings, as for axes. Adjusted PXRF data for rock exposures are reported in Appendix 28. Unprocessed PXRF data is contained in Appendix 23 (axes) and 28 (exposures), and in these cases the whole of the PXRF output is shown, which include measurements for V, Cr, Ni, Cu, Zn, Ga and La. Information for these 7 elements is only included since it was readily available and may prove useful to future work: the measurements take no part in any discussion or analysis in this thesis.

7 Examination of British greenstone and Irish gabbro & dolerite axes using geochemical analyses supported by MS and petrographic data.

7.1 Introduction, axes examined and general aims

7.1.1 Introduction

Axe geochemistry has been used by several workers to aid provenancing studies of Neolithic axes through direct comparison of exposure and axe elemental concentrations (Williams-Thorpe et al. 1999a, Mandal 1996, Cooney & Mandal 1998, Meighan et al. 1993). The main reason that geochemical information has not, to date, been more widely used is that most current methods of obtaining geochemical analyses are partly destructive, which leads to a great reluctance by axe custodians to release their valuable implements for geochemical analysis.

Mandal (1996) obtained geochemical data using only 0.5g of axe material, which had been produced as a 'by product' of coring axes for the production of petrographic thin sections. The very small amount of axe material was subsequently mixed with 1g of cellulose to make pellets suitable for WDXRF analysis. Thus, in this case, the geochemical analysis was only possible since the axes were already being cored so that macroscopic examinations to identify axe rock type could be confirmed using petrographic thin sections. Subsequent examination of the WDXRF measurements obtained from the lightweight pressed powder pellets (normally 8g of material is used), found it was possible to assign a number of Irish porcellanite axes to one of two known porcellanite sources: Tievebulliagh and Rathlin Island, using Y and Sr ratios (Mandal 1996, p98). This allowed axe distribution patterns from each site to be discerned, hence quantifying the relative importance of the two exposures and illustrating the value of geochemical information in provenancing axes.

Similarly, but using non-destructive PXRF geochemical analyses, Williams-Thorpe et al. (1999a) supported the provenance of two IPC Group XIII axes to their hypothesised source at Preseli by identifying that the axe and outcrop shared similar elemental concentrations. Geochemical comparisons also showed that two other axes that had been assigned to IPC Group XIII on the basis of petrographic similarity were actually geochemically different to rock from the Preseli source, raising the distinct possibility that these two axes had been incorrectly assigned to IPC Group XII

In both examples above, the provenance of each axe group had previously been established, thus allowing a direct geochemical comparison between rocks from the source exposure and the axes. However, in the case of most Cornish IPC greenstone axe groups examined in this thesis it is not possible to obtain a direct geochemical comparison between axe group and source exposure for two main reasons. Firstly, the current provenance of IPC Group I, Ia, I/Ia, I(near) & IIIa axes contains many potential source exposures (c.f. Section 2.5 & Section 3.6.3). Secondly, as shown in Chapter 4, it is possible to recognise a number of petrographically distinct sub-groups within IPC Groups I, Ia, III & IIIa which lead to the suspicion that more than one greenstone exposure may have been used to provide axe material.

As part of the provenancing study, this chapter (7) uses geochemical data of axes, obtained by non-destructive PXRF analysis, in order to examine the geochemical relationships within and between IPC Groups I, Ia, I/Ia, I(near), III & IIIa, and to see if the petrographically determined sub-groups in Chapter 4 are also geochemically distinctive. The results from this part of the provenancing study will then be used in Chapter 8, where direct geochemical comparisons will be made between groups of axes (i.e. IPC axe groups, petrographic sub-groups, etc.) and greenstone exposures in order to determine the provenance of the axes.

7.1.2 Number of axes measured from each IPC group and axe sub-group

A primary objective of the fieldwork associated with this thesis was to undertake PXRF analysis of as many IPC Group I, Ia, I/Ia, I(near), III & IIIa axes as possible so that a meaningful sample size for subsequent statistical analysis could be attained (c.f. Section 2.8.3). In addition, every opportunity was taken to undertake PXRF analysis of other axes: IPC ungrouped greenstone, non-IPC (axes not yet examined by the IPC) and Irish gabbroic & doleritic axes. All this was successfully achieved as a total of 272 axes were measured at 14 field locations, during the three fieldwork periods. Table 51, below, summarises the number of axes measured from: each IPC group, each petrographically defined sub-group introduced Chapter 4 and from fieldwork carried out in Ireland. The total population of IPC groups is taken from Appendix 2. The population of Irish gabbroic and doleritic axes is taken from Mandal (1996). The number of thin sections examined is repeated from Chapter 4. The 'ungrouped' entry at the bottom of each IPC group section indicates the number of axes from that IPC group that were analysed by PXRF and for which no thin sections were available.

IPC or Irish group Sub-group	Total population	Thin sections examined	Analysed by PXRF	Proportion of population analysed by PXRF
IPC Group I	**369**	**119**	**149**	**40.4%**
GpI-1		59	29	49.1%
GpI-2		13	5	38.5%
GpI-3		6	2	33.3%
GpI-4		16	12	75.0%
GpI-5		2	None	-
GpI-6		13	6	46.2%
GpI-7		3	1	33.3%
GpI-8		2	2	100.0%
GpI-9		1	None	-
GpI-10		1	None	-
GpI-11		1	None	-
GpI-12		1	1	100.0%
GpI-13		1	1	100.0%
GpI-ungrouped		None	90	-
IPC Group Ia	**29**	**17**	**4**	**13.8%**
GpIa-1		5	2	40.0%
GpIa-2		4	None	-
GpIa-3		5	None	-
GpIa-4		1	None	-
GpIa-5		1	1	100.0%
GpIa-6		1	None	-
GpIa-ungrouped		None	1	-
IPC Group I/Ia	**8**	**None**	**6**	**75.0%**
IPC Group I(near)	**29**	**None**	**6**	**20.7%**
IPC Group III & IIIa	**22 + 7**	**11 + 3**	**11 + 1**	**41.4%**
GpIII-1		2	2	100.0%
GpIII-2		5	4	80.0%
GpIII-3		4	None	-
GpIII-4		1	None	-
GpIII-5		1	None	-
GpIII-ungrouped		None	6	-
IPC ungrouped greenstones	**426**	**None**	**55**	**12.9%**
Non-IPC greenstones	**17**	**None**	**17**	**100.0%**
Irish axes	**74**	**None**	**23**	**31.1%**
Gabbro I	14		5	35.7%
Gabbro II	19		5	26.3%
Ungrouped Gabbro	27		6	22.2%
Dolerite	13		6	46.1%
Miscellaneous	1		1	100.0%
Grand Totals	**981**	**149**	**272**	**27.7%**

Table 51 Number of axes analysed by PXRF and in thin section. Population data from Appendix 2 and Mandal (1996). Thin section data from Chapter 4. Note the 'ungrouped' line at the bottom of each IPC group (not in bold) indicates that the axes were analysed by PXRF for which no thin sections were available for examination. IPC Group III (22 axes) and IIIa (7 axes) are shown together since the two IPC Group IIIa thin sections examined are contained within GpIII-3 & 5, and 1 IPC Group IIIa axe is included in the 6 GpIII-ungrouped sub-group.

7.1.3 General aims

7.1.3.1.. Identification of groups of axes with similar geochemical characteristics

IPC Group I, Ia, I/Ia, I(near), III & IIIa axes have been found over a large part of England & South Wales and have been assigned to IPC groups on the basis of petrographical examination (c.f. Chapter 2). Further examination of axe thin sections, reported in Chapter 4, concluded that there are 24 petrographically recognisable sub-groups of axes within the

3 IPC groups examined: 13 in IPC Group I, 6 in IPC Group Ia and 5 in IPC Group III & IIIa (c.f. Table 51, no thin sections were available for IPC Groups I/Ia & I(near)). Thus, one aim of this chapter is to examine whether corrected PXRF measurements (c.f. Section 6.17), supported by MS measurements (where available), can be used to recognise the petrographically determined axe sub-groups and show if they are also geochemically distinct from each other.

Within each of the IPC Groups I, Ia, III & IIIa there are a number of axes that have only been analysed by the PXRF (c.f. Table 51). Thus, another aim will be to assess the potential of assigning these axes to the petrographically determined sub-groups using geochemical data alone. Similarly, as noted above, no thin sections from axes within IPC Groups I/Ia & I(near) have been examined. Hence, for these two groups, geochemical data will be used to examine the similarity of the axes within each group and with those sub-groups already established.

The 149 IPC Group I axes that have been geochemically analysed come from many parts of England and south Wales (c.f. Figure 3). Hence, a further aim of this chapter will be to examine the degree of similarity of geochemical data of axes from within and between their county of origin. This will lead to a discussion, for example, whether IPC Group I greenstone axes found in Yorkshire are geochemically the same as those found in Cornwall.

The final aim relating to the grouping of axes will be to assess the possibility of assigning individual IPC ungrouped axes (i.e. axes listed by the IPC, but not assigned to one of the IPC Groups) and non-IPC axes (i.e. not (yet) listed by the IPC) to IPC Group I or III using geochemical and MS information alone.

7.1.3.2 Comparison of Irish gabbroic & doleritic axes and British greenstone axes

Although the main aims of this work relate to British greenstone axes (of Cornish origin), advantage was taken of an opportunity to analyse a number of Irish gabbroic and doleritic axes. Consequently, this chapter includes a section that investigates the similarity of geochemical and magnetic data between these Irish gabbroic and doleritic axes and British greenstone axes. This complements work already carried out by Mandal (1996) who assigned 6 Irish gabbroic axes to IPC Group I through comparison of thin sections. If

geochemical and magnetic susceptibility matching were successful, then the hypothesis of Neolithic trade/migration between Ireland and Cornwall would be supported.

7.1.3.3 Determination of the tectonic setting for the source of axe material

Chapter 3 indicated that greenstone exposures in SW England originated from a range of tectonic settings, e.g. MORB, IAB, OIB etc (c.f. Appendix 30). It therefore follows that axes sharing similar rock characteristics to that found in SW England have potentially been derived from exposure(s) in SW England. Hence, using element discrimination diagrams it may be possible to identify the axe greenstone rock petrogenesis and thus relate it to a tectonic setting found in SW England. Consequently, the final aim of Chapter 7 is to identify the probable petrogenesis (specifically its tectonic origin) of axe material in preparation for Chapter 8.

7.1.4 Chapter 7 structure

Figure 61, overleaf, illustrates the structure and summarises the content of Chapter 7. The introduction to the chapter and its aims is followed by an overview of the activities within Sections 7.4 to 7.10. This is followed by a review of the two main statistical processes used in the Chapter: Simple Component Analysis (SCA) and Discriminant Analysis (DA). Sections 7.4, 5 & 6 examine the geochemical relationship of axes within IPC Groups I, IPC Groups Ia, I/Ia, I(near) and IPC Groups III & IIIa respectively. Section 7.7 examines the ability of DA to assign IPC grouped axes to one of the petrographically determined sub-groups, that were subsequently refined as apart of the exercises in Sections 7.4, 5, 6. The ability to allocate of IPC ungrouped and non-IPC listed axes to IPC groups using information produced in Sections 7.4 to 7.7 is assessed in Section 7.8. A small case study that examines the possible Cornish origin of Irish gabbroic and doleritic axes is contained in Section 7.9. Section 7.10 uses a selection of immobile and trace element discrimination diagrams to determine the most likely genesis that produced the greenstone axe material. The final section of the chapter summarises the major findings and conclusions.

Chapter 7
Examination of British greenstone and Irish gabbro & dolerite axes using geochemical analyses supported by MS and petrographic data

7.1 Introduction, axes examined and general aims

7.2 Rationale and methods underlying the examination of axe geochemistry

7.3 General description of SCA and DA statistical procedures and their interpretation

7.4 Examination of IPC Group I axe geochemistry

Examination of IPC Group I PXRF and MS data is used to identify any anomalous axes prior to determining the IPC Group I geochemical fingerprint. SCA, DA and comparative statistics are used to examine the reduced IPC Group I data set (i.e. after the removal of anomalous axes from the data set) to investigate the geochemical similarity of axes within and between petrographically determined axe sub-groups, and between counties where the axes were found

7.5 Examination of IPC Group Ia, I/Ia and I(near) geochemistry

PXRF and MS data is used to examine the relationship of axes within and between these three groups and IPC Group I. The geochemical make up for each group is established, as well as the identification of geochemically anomalous axes assigned to the groups.

7.6 Examination of IPC Group III and IIIa axe geochemistry

PXRF and MS data is used to examine the relationship of axes within IPC Group III and between IPC Group I The geochemical make up for IPC Group III is established, as well as the identification of geochemically anomalous axes assigned to the IPC Group III and IIIa.

7.7 Discriminant analysis of IPC grouped axes

Discriminate Analysis (DA) is used to examine the geochemical similarity between axes and axe sub-groups that have been established in Sections 7.4, 7.5 and 7.6

7.8 Allocation of IPC ungrouped and non-IPC greenstone axes to axe sub-groups using SCA and DA supported by MS measurements

This section examines the possibility of using non-destructive analyses to assign axes to IPC groups. The geochemical similarity of IPC ungrouped and non-IPC axes, supported by MS measurements, is used to determine whether any of these axes could be assigned to IPC Group I or IPC Group III.

7.9 Comparison between Irish gabbroic & doleritic axes and British greenstone axes using petrographic observations and PXRF & MS measurements

Previous petrographic analyses have suggested that a number of Irish gabbroic and doleritic axes are similar to ones in IPC Group I. PXRF and MS measurements of Irish gabbroic and doleritic axes are used to examine the reported petrographic similarities in order to further investigate the possibility of a Neolithic Cornish-Irish trade link.

7.10 Assessment of axe rock genesis using Immobile and trace element discrimination diagrams

This section establishes the petrogenesis of axe sub-groups using element discrimination diagrams, thus identifying the probable tectonic origin of axe greenstone.

7.11 Summary of chapter and main conclusions

Figure 61 Simplified structure of Chapter 7

7.2 Rationale and methods underlying the examination of axe geochemistry

7.2.1 Initial assumption and null hypothesis

The initial assumption is that IPC Groups I, Ia, I/Ia, I(near), III & IIIa are individually geochemically homogeneous: that axes within each of the IPC groups could have originated from a greenstone exposure unique to that group. It is acknowledged that examination of petrographic and MS data has already shown that this initial assumption is slightly flawed since Chapters 4 & 5 have shown that some IPC grouped axes have mineralogical, textural and magnetic characteristics that are notably different from others within the same IPC group. However, the initial assumption sets the criteria for the null hypothesis: that the axes and sub-groups of axes within an IPC group are petrographically, geochemically and magnetically the same.

7.2.2 Inspection of IPC Group I axe geochemistry

Initial inspection of the PXRF data for IPC Group I axes contained in Appendix 29.1 is carried out in order to identify axes which have elemental concentrations that are outside ±2sd of the average of the 149 IPC Group I axes analysed. The aim of this initial inspection is to discard 'anomalous' axes that have unusual elemental concentrations from the IPC Group I data set. Emphasis will be placed on the four immobile elements Ti, Zr, Y & Nb, with axes having one or more concentrations of these elements outside ±2sd likely to be discarded. Secondary importance is placed on mobile elements K, Ca, Fe, Rb, Sr, and Ba and axes with one or more of these elements outside ±2sd may be discarded after taking into account the immobile element concentrations. Axes with only Mn, Ce and Pb concentrations outside ±2sd are unlikely to be discarded. MS measurements will be used as an additional discriminant in determining whether to discard an axe from the IPC Group I data set. Axes with corrected maximum MS measurements below 0.23 x 10^{-3}SI (minimum IPC Group I average -2sd) I or above 1.89 x 10^{-3}SI (maximum IPC Group I average +2sd, from Table 23: range of IPC Group I MS values) will be considered as having unusual MS measurements and may be discarded after taking into account their elemental concentrations (Section 7.4.1).

7.2.3 Inspection of IPC Group Ia, I/Ia, I(near), III & IIIa axe geochemistry

A similar inspection of axe geochemical data to that undertaken for IPC Group I will be carried out for IPC Groups Ia, I/Ia, I(near), III & IIIa (data in Appendix 23.3 & 23.4). However, in these cases the relatively small number of PXRF analyses within each of these IPC groups means that the nominal criteria, that axes will be discarded if certain elemental

concentrations are outside ±2sd, used for IPC Group I, will not be used. Instead, a decision whether to discard an axe from a group will be made on the magnitude of its geochemical and MS difference from other members of the same group (Section 7.5.1 & 7.6.1).

7.2.4 Simple component analysis (SCA) of IPC Group I axe geochemistry

Simple component analysis (SCA) using IPC Group I geochemical data is carried out three times using different parts of the whole data set (SCA methodology is described in Section 7.3.1, below):

Firstly, SCA will be carried out on the immobile element (Ti, Y, Zr, Nb) PXRF measurements of the 59 axes that have been petrographically sub-grouped, with the results displayed as a scatter plot with the two main simple components (SC1 & SC2) forming the axes of the plot (c.f. Section 7.3.1.4). SC1 and SC2 components for the remaining 90 IPC Group I axes are calculated using the SCA statistics from the 59 axes above, and displayed on an additional scatter plot. These plots are used to illustrate and support the conclusions reached during the initial inspection the IPC Group I data by identifying those axes with anomalous immobile element geochemistry and so producing a reduced data set. (Section 7.4.1)

(Note that the data set after discarding anomalous axes is referred to as the 'reduced IPC Group I data set' or 'reduced IPC Group I'.)

Secondly, SCA is carried out using the immobile elements of those axes remaining within the IPC Group I data set after discarding the anomalous axes (i.e. the reduced IPC Group I data set). Results will be displayed as scatter plots illustrating the disposition of axes grouped by petrographic sub-groups and by county of origin. (Section 7.4.2)

Finally, SCA is carried out using mobile elements K, Ca, Fe, Rb, Sr and Ba from the reduced IPC Group I data set. As above, results are displayed as scatter plots illustrating the disposition of axes grouped by petrographic sub-groups and by county of origin. (Section 7.4.3)

7.2.5 SCA analysis of other IPC grouped, IPC ungrouped, non-IPC and Irish axe geochemistry

SCA is carried out using four immobile (Ti, Y, Zr & Nb) and five mobile (K, Ca, Fe, Sr & Ba) element concentrations from the:

1. 16 IPC Group Ia, I/Ia and I(near) axes (Section 7.5.2)
2. 11 IPC Group III axes (the 1 IPC Group IIIa axe is not included in this particular SCA calculation) (Section 7.6.2)

As for IPC Group I, the results are displayed as scatter plots using SC1 and SC2 as the chart axes.

In addition to the above, new SC1 and SC2 are calculated based on the results from SCA of the reduced IPC Group I data set and displayed as scatter plots for

1. IPC Group Ia, I/Ia and I(near) (Section 7.5.5)
2. IPC Group III (Section 7.6.3)
3. IPC ungrouped and non-IPC axes (Section 7.8.2)
4. Irish gabbroic and doleritic axes (Section 7.9.5)

The aim is to display all PXRF axe data using the same SCA so that direct observations can be made on the geochemical similarity between the groups listed above and IPC Group I.

7.2.6 Comparative statistics

ANOVA and MANOVA are used to test the null hypothesis between various groups of axes. A 0.05 significance value is chosen for the tests, hence probabilities greater than 0.05 indicate the null hypothesis: the values are the same, cannot be rejected. These tests are carried out after examination of the associated data using SCA.

7.2.7 Discriminant analysis (DA)

Two consequences of the initial inspection and SCA of axe geochemistry will be the refinement of the 13 (of 24) petrographically recognised axe sub-groups that are also geochemically represented, and the identification of new geochemically based sub-groups. Both the established petrographic axe sub-groups with geochemical data and the new geochemically defined axe sub-groups will, together, form the initial set of 'seed' groups used in DA of the 272 axes analysed by PXRF. (Section 7.7)

DA of the 272 axe PXRF measurements, based on the seed groups, is carried out three times: using immobile elements assuming equal prior probabilities, using mobile elements assuming equal prior probability and using immobile elements assuming unequal prior probability (c.f. Section 7.3.2 for a description of DA).

The results from DA are used in two ways. Firstly, to assess the geochemical similarity of axes within each of the IPC groups, and secondly, to examine the potential of assigning IPC ungrouped, non-IPC and Irish axes to one of the seed groups, hence ultimately to one of the IPC groups. In the latter case, MS data will also be used, where available, to assist in the assignment of axes. (Section 7.8 and 7.9)

7.2.8 Assessment of axe rock petrogenesis using element discrimination diagrams

Element discrimination diagrams are used extensively in geochemistry to assess the tectonic origins of rock samples (c.f. Appendix 30). Six such diagrams are used to display axe geochemistry in order to assess its tectonic origin and in prelude to provenancing studies in Chapter 8.

Two sets of the six geochemical discrimination diagrams are used: the first set of diagrams display geochemical data obtained from the existing petrographic and new geochemically defined axe sub-groups, and the second set displays data *derived* by DA based on these sub-groups. For example, in the first instance the average elemental concentration of GpI-1 axes, after eliminating any anomalous axes within the 29 examined, are used to draw the first set of discrimination diagrams. In the second instance, the average elemental concentrations from axes *assigned* to GpI-1 *by* DA is used (Section 7.10)

7.3 General description of SCA and DA statistical procedures and their interpretation

7.3.1 Simple component analysis (SCA)

7.3.1.1 Background and overview

Simple component analysis (SCA) (Vines 2000) is similar to principal component analysis (PCA). PCA is a statistical process that combines data sets such that Eigenvalues can be determined that relate to the maximum variance of the data sets being investigated. Hence, PCA has the ability to reduce the dimensionality of the data set making it simpler to analyse. Principal components are new variables, derived from the original data set, that express the variance of the data set in terms of the original variables. Although there are

the same number of principal components as there are variables, and providing the data is correlated and not spherically distributed, a small number of the principal components will account for the majority of the variance observed in the data sets. See Swan & Sandilands (1995) for further discussions on the use of multivariate analysis methods to investigate geological data.

Simple component analysis (SCA) is similar to PCA in that is reduces the dimensionality of a data set. The main difference from PCA is that SCA produces integer value *simple components* (SC) as opposed to decimal values produced by PCA. This makes it simpler to assess the contribution of each of the variables to the overall variance being examined and it also simplifies subsequent calculation of SC components used to draw scatter plots.

SCA is a new statistical procedure (Vines 2000) and it is believed this is the first time it has been used to examine geochemical data.

7.3.1.2 Presentation of SCA results and derivation of SC1 and SC2

Results from running SCA with SPSS V7.0 software are summarised and presented in tabulated form with a typical table shown below (which is a copy of Table 56).

Element	Average (ppm) (n = 59)	SD	Simple Components			
			1	2	3	4
Ti	14,408	4,209	1	0	2	-1
Y	33.2	9.3	1	-1	-1	-1
Zr	161	38.9	1	0	0	3
Nb	6.4	4.3	1	1	-1	-1
Standardised error			±1.62	±1.56		
Cumulative % of variance			57.4	80.1	92.8	100.0

Table 52 Illustration of how SCA statistics are presented (this table is a copy of Table 56). See text for discussion.

Data for each variable is displayed in a row and reports the average, associated sd and its associated simple component based on the number of measurements (n) indicated. SCs are thus arranged vertically with SC1 accounting for the maximum variance followed by SC2, 3 & 4. The cumulative amount of variance accounted for by the 4 SCs is shown at the bottom of each SC column. As an example to illustrate the derivation of SC1 & SC2: in Table 52 above, SC1 (plotted on the *x-axis* of the scatter plot) equals 'Ti + Y + Zr + Nb' and accounts for 57.4% of the variance seen in the data set. The second simple component, SC2 (plotted on the *y-axis* of the scatter plot) equals 'Nb - Y' and accounts for a further 22.7% of the variance seen in the data set. Hence, together SC1 and SC2 account

for 80.1% of the variance observed within the data set. The derivation of the actual value for Ti, Y, Zr and Nb and a description of how the 'standardised error' value is calculated are shown below.

7.3.1.3 'Standardisation' of variables

Each SC component value is generated by calculating the standardised variate, commonly known as the 'Z statistic' (Lucey 1979: p57) of the variable being considered, using the given data set results. The standardised variate (also called the 'Z statistic') is calculated from the equation "$(x-\mu)/\sigma$", where x is the axe variable value (e.g. an axe Nb concentration), μ is the data set average (e.g. average Nb calculated from n measurements) and σ is the standard deviation associated with the data set average. These 'standardised' variates are then used to calculate the SC value and plotted accordingly. Hence, in the example above the value for SC1 is obtained by adding the standardised variates of axe Ti, Y, Zr and Nb concentrations together (See Section 7.5.5 for a further example).

7.3.1.4 SC scatter plots

Scatter plots use SC1 as the *x-axis* component and SC2 as the *y-axis* component to display axe data. SC1 and SC2 are chosen since together they represent the maximum amount of variance that can be shown on a two-dimensional scatter plot.

The proximity of a data point (e.g. representing an axe) to the origin of the SC scatter plot (0,0) is believed to be *broadly* related to the degree of similarity between the axe values and the average values of the data set used for the SCA. For example, an axe with Ti, Y, Zr and Nb concentrations very close to the SCA averages would have small SC1 and 2 values (since $(x-\mu) \approx 0$, the associated standardised variate is small) and thus plot close to (0,0). This belief is only broadly true since the proximity of the data point to the origin of the scatter plot *x & y-axes* cannot always be taken as proof that axe and SCA average share similar values. This problem is illustrated by considering the SC component 'Ti + Zr': a **value of 0** can be achieved by **'0 + 0'** (i.e. the axe Ti and Zr values are the same as the SCA Ti and Zr average value) or by **'1 + (-1)'** (i.e. the axe value is +1sd above the SCA Ti average and -1sd below the SCA Zr average) (c.f. Table 69).

One aspect of SC scatter plots is that any data point that plots significantly (assessed as ±2 times the number of variables, e.g. SC2 above Nb - Y = ±4) away from the origin (0,0) is

expected to have at least one elemental concentration that is significantly different to the average from the SCA data set used as a basis for SC1 and SC2.

7.3.1.5 Calculation of error bars shown on simple component plots

Error bars are shown on all SC scatter plots in order to illustrate the relative precision of PXRF measurements. The size of each error bar is based upon: PXRF instrument precision (Section 6.15), the average composition of the reduced IPC Group I data set, and the associated SC.

The value for instrument precision is calculated using the average reduced IPC Group I value (see below) and the quadratic regression coefficients used to model instrument precision, reported in Section 6.15.2. The average reduced IPC Group I value is the average of all IPC Group I axe compositions, minus those axes that are deemed anomalous. The sd required to standardise values is the sd associated with same reduced IPC Group I average (c.f. Section 7.4.1).

The following example shows how the 'standardised error value' is calculated. The reduced IPC Group I average Zr concentration is 171 ± 29.2ppm (Table 53). Instrument precision associated with Zr concentrations of 171ppm is calculated as 11.6ppm (Chapter 6 Table 43: Zr quadratic regression Week 2 &3). The standardised value of 11.6ppm is (11.6/29.2) = 0.40. Hence the standardised error value for the 'reduced IPC Group I data set' Zr concentration is 0.39. Table 53 reports the standard error values for all elements used in SCA based upon the reduced IPC Group I elemental averages.

	Average (n=130) (reduced IPC Group I) (ppm)	Sd (reduced IPC Group I) (ppm)	Instrument precision (calculated) (ppm)	Standardised value of instrument precision
K	3 567	2 282	276	0.12
Ca	67 715	14 636	666	0.05
Ti	14 959	3 772	766	0.20
Fe	95 632	14 009	1 567	0.11
Rb	29.6	25.8	20.6	0.80
Sr	324	150	19.1	0.13
Y	35.7	6.8	7.0	1.03
Zr	171	29.2	11.6	0.40
Nb	6.7	2.9	3.4	1.17
Ba	104	64.3	15.3	0.24

Table 53 Standardised error values associated with average composition of the reduced IPC Group I data set (see text for discussion). Instrument precision is calculated from quadratic regression of PXRF SD values for Week 2 & 3 (c.f. Table 43)

The value of the error bars shown on the SC scatter plots is the square root of the sum of the squares of the standardised error values for each of the components in the SC. For example, using the information in Table 53 above, SC1 = Ti + Y + Zr + Nb, hence the associated value for the error bar is calculated as $\sqrt{(0.19^2 + 1.03^2 + 0.40^2 + 1.17^2)} = 1.62$. Similarly, SC2 = Y – Nb, so the associated value for the error bar is $\sqrt{(1.03^2 + 1.17^2)} = 1.56$. In order to reduce clutter on the SC scatter plots, the error bars are plotted away from the axe data and actually display ± the calculated standard error value.

Strictly speaking, the standard error values in Table 53 should be recalculated for every SCA as the reported averages and variance will be different for different data sets. However, the error bars are only meant to be *representative* of the achieved PXRF precision and further, it has been *assumed* that the individual standardised error values can be summed in quadrature, and that all data is normally distributed, so Table 53 values are used throughout.

7.3.2 Discriminant analysis (DA)

'Discriminant analysis (DA) is used to assign objects to one of two or more *groups* (through analysis of variances)' (Swan & Sandilands 1995: p352). In this work DA is carried out using SPSS v7.0 software and is based on data from the 272 axes analysed by PXRF. The initial (training) set of 'seed' groups consist of the 13 (of 24) petrographically recognised axe sub-groups that are also geochemically represented plus a further 3 sub-groups established during the examination of axe PXRF data. The names and members of each of the seed groups are reported, below, in Section 7.7.2, Table 76.

DA is carried out three times, once based on the immobile elements Ti, Y, Zr & Nb, once based on the mobile elements K, Ca, Fe, Rb, Sr & Ba. In both these cases the assumption is that the prior probability for objects to be assigned to each seed group is equal. The third DA is based on the immobile elements and this time assumes that the prior probability of assigning objects is related to the population of the seed groups. In all these cases the same set of seed groups is used.

Results from the three DA exercises are contained in Appendix 25 and summarised in the appropriate section. For each DA the first and second most probable assignments are listed along with P(G/D). P(D/G) is only identified if it is below 0.10 (see below).

P(G/D) is the probability that the axe is in the given seed group on the basis of the selected data used (e.g. the Ti, Y, Zr & Nb values). It is a measure of the confidence that can be given to the axe belonging to that seed group. Providing there is good discrimination between the seed groups (i.e. the axe sub-groups are geochemically distinct from each other) then P(G/D) will probably be high. However, if there is a considerable overlap of the range of geochemical data between the sub-groups then P(G/D) will probably be low.

The statistical process assumes that each axe in the data set has to belong to one of the seed groups identified, hence P(G/D) can approach 1 even if the axe is not similar to the other sub-group members: a high P(G/D) value means that the axe is unlikely to belong to any other of the seed groups.

P(D/G) is the probability for data arising for axes in a particular seed group. A low P(D/G) means that the axe does not really fit into the indicated seed group. Therefore, axes with $P(D/G) < 0.05$ (i.e. a significance value of 0.05) are indicated on the basis that they are unlikely to be similar to other axes within that particular seed group.

7.4 Examination of IPC Group I axe geochemistry

7.4.1 Initial examination of IPC Group I data to identify anomalous axes

7.4.1.1 Inspection of IPC Group I PXRF data

Table 54 reports the average, sd and ±2sd range of the 149 IPC group I axes analysed by the PXRF. The corrected PXRF axe data is reported in full in Appendix 23.1.

	IPC Group I average (n=149) (ppm)	IPC Group I sd (ppm)	Average -2sd (ppm)	Average +2sd (ppm)
K	3 811	2 898	-1 985	9 606
Ca	66 581	16 406	34 489	98 673
Ti	15 013	4 981	5 051	24 976
Mn	1 569	588	393	2 746
Fe	95 491	18 010	59 471	131 512
Rb	31.1	29.4	-27.8	89.9
Sr	318	163	-8.0	644
Y	35.9	9.0	17.8	53.9
Zr	170	39.3	91.8	249
Nb	6.9	3.9	-0.8	14.7
Ba	108	73.9	-39.9	256
Ce	-26.8	16.7	-60.0	6.5
Pb	365	1 593	-2 821	3 550

Table 54 Average geochemical composition of the 149 IPC Group I axes measured by PXRF.

Using the criteria set out in Section 7.2.2 each elemental concentration of the 149 axes was inspected and Table 55 lists those 48 axes that were found to have at least one elemental concentration outside ±2sd of the average of the 149 IPC Group I axes measured. In addition and where available, the associated axe MS measurement has been included in Table 55 (IPC Group I axe MS measurements are reported in Appendix 11.1).

Axe	Elements > ±2sd	MS range	Comment	Recommendation
Ca12	K	0.71-0.76	K exceeds ±2sd through first analysis, notes indicate measurement made near paper label	Retain
Cd13	Fe	0.79-1.05	2 of 3 Fe analyses very high (>170,000ppm), Low Sr & Rb. Field notes do not indicate anything else unusual	Retain Possibility of element migration
Co151/737	K, Mn	0.90-1.07	K & Mn just exceed >+2sd, Axe identified as a rough out – nothing else unusual	Retain
Co154/740	Y	Not measured	Y average just below –2sd, all other values acceptable. Partly weathered – nothing else unusual	Retain
Co166/761	Rb	0.70-0.92	Only one measurement taken, Rb >> group average. Weathered battle axe –nothing else is unusual	Retain Rb is mobile
Co180/783	Pb	0.96-1.14	Second measurement over lead based filler/paint	Retain Pb indicative only
Co358/1627	Ca, Y, Zr, Ba	0.65-0.69	Field notes state this axe is visually different to most examined. Y & Zr both below –2d limit	**Discard** **2 immobile >±2sd**
Co363/1632	Ba	0.52-0.68	Similar to Co358/1627. Field notes indicate axe is visually different to the majority examined. Zr is just on lower limit	**Discard** **Same as Co358/1627?**
Co398/1734	K, Rb, Ce	0.79-0.97	Axe has many veins suggesting high K, Rb and Ce values through enrichment	Retain Only mobile elements enriched
Co401/1737	Ti, Sr, Zr, Ce	0.53-0.61	Field notes indicate axe is visually different to majority examined. Sr is exceptionally high, Y is just within –2sd	**Discard** **2 immobile >±2sd**
Co92/659	Rb	0.88-0.94	Nothing unusual in Field notes. Rb exceeds limit on one measurement only	Retain Rb is mobile
CoGWA3	Ca, Ti, Y, Zr, Nb	**11.3-12.9**	All four immobile elements outside limits. MS outside expected range	**Discard** **All immobile >±2sd**
Do123/1648	Mn, Fe	Not measured	High Fe probably due to surface contamination (rust stain?).	Retain

			Mn high on one measurement only. Nothing unusual recorded in field notes	Fe high through surface contamination
Do127/660	Mn	Not measured	Weathered appearance – nothing else unusual	Retain
Do146/1762	Nb	Not measured	Axe fragment just covered PXRF window, only one analysis. K low, Zr high. Field note indicate alignment of minerals (sheared greenstone?)	**Discard Nb 5x group average**
Do62/656	Mn,	0.89-1.02	Pb high on one measurement, possibly through surface contamination. Field notes state overall pale brown/whitish colour to axe	Retain Surface contamination
DoT02	Ti	Not measured	Appearance recorded as similar to GpI	Retain
Es9	K, Fe, Ba	0.40-0.50	Field notes report overall orange colour, possibly through weathering. Ti, Mn & Y also towards lower sd limit	**Discard K value 4x average**
Gl44	Ba	Not measured	Both Ba values >+2sd. Nothing unusual reported in field notes	Retain Ba is mobile
Gm37	Ti	**3.51-7.02**	High MS value, possibly related to high Ti? Weathered surface distinctly brown. Borderline case	**Discard Ti & MS high**
Gm85	Ca, Ti, Fe, Y, Zr, Nb, Ce	**0.09-0.10**	Axe has schistose appearance and is not doleritic/greenstone	**Discard All immobile >±2sd**
Gm87	Ba, Ce	0.60-0.69	Ba just outside upper limit, Ce positive. Apart from overall black colour nothing unusual in field notes	Retain Ba is mobile Ce indicative only
Gm91	K, Ti, Fe, Rb, Zr	0.46-0.56	Axe covered in thin coat of protective wax, should not affect PXRF values to the extent indicated. Five elements exceed limits	**Discard 2 immobile >±2sd**
Ha10	Mn	Not measured	Mn exceeds average through one measurement. Apart from noting axe is finer grained than most nothing else is unusual	Retain Mn has large sd`
Ha23/330	Fe	**7.41-7.95**	High MS – related to high Fe? (possibly magnetite?) Borderline case	Retain
Li123	Ba	***1.71-1.97***	Ba slightly high. Nothing unusual in field notes	Retain
Li124	Ti, Fe	0.87-1.07	Has the highest Ti reading of all GP I axes analysed. Field note suggest that axe is less altered than most	**Discard Ti >2x average**
Li149	Ca, Sr, Nb	Not measured	Field notes state axe is visually different to majority of GpI	**Discard 1 immobile >±2sd**
Li2	Sr	1.10-1.36	Sr is high in both measurements. Nothing unusual reported in field notes	Retain Sr is mobile
Li357	K, Ti, Fe, Rb, Y, Zr,	0.32-0.39	Field notes indicate pale coloured axe, lighter than other Group I. All three measurements consistent	**Discard 3 immobile >±2sd**
Li4	Ca, Y, Pb	1.07-1.40	Pb high by measuring close to filler. Ca high on one of three readings, however Y >=2sd on two of three readings	**Discard 1 immobile>±2sd**
Li542	Y, Zr, Nb	Not measured	Filed notes state axe is visually different to majority of GpI	**Discard 3 immobile >±2sd**
Lo2(38)	Sr	1.13-1.30	Sr just >+2sd. Nothing unusual in field notes	Retain Sr is mobile
Lo21(69)	Ca	0.87-1.07	Ca exceeds limit through first measurement being high. Nothing else unusual reported in field notes	Retain
Mo3	Ti, Mn, Fe, Zr	0.79-0.92	High Fe possibly through surface contamination	**Discard 2 immobile >±2sd**
No46	Fe	0.57-0.66	Brown stains (rust?) noted, possible cause of high Fe. Nothing else unusual reported	Retain
Ox61	Sr	0.99-1.13	Sr just above upper limit. Field note suggests lighter than majority of GpI	Retain Sr is mobile
So21/232	Ti	Not measured	Ti just below lower limit. Small piece measured in same place, otherwise nothing else unusual noted	Retain Ti just outside limits
So60/1143	Mn, Y, Pb	0.80-0.85	High Mn, Y & Pb measurements on first of two analyses, possibly because of close proximity to writing on axe	**Discard 1 immobile>±2sd & 3rd reading not taken**
Wi209/937	Ca	1.11-1.36	One of two Ca measurements is high. Nothing else unusual noted	Retain
Yo116	Mn	0.69-0.90	Odd square-rectangular black grains – but generally like GpI	Retain
Yo118	Ba	0.73-0.90	Ba just above limit. Nothing else unusual reported	Retain
Yo352	Ti, Fe	**2.21-2.90**	High Fe may be due to surface contamination. Nothing else unusual recorded	**Discard 1 immobile >±2sd**
Yo454	Ba	Not measured	Ba just above limit. Ti on upper limit. Nothing unusual in field notes	Retain
Yo496	Zr, Nb	Not measured	Field notes suggest axe does not look like GpI	**Discard 2 immobile >±2sd**
Yo733	K	0.72-0.95	Nothing unusual in field notes	Retain
Yo800	Fe, Zr	**68.1-78.1**	Low Zr, Fe plus very high MS. Field note identifies axe as v fine grained, dissimilar to GpI	**Discard 1 immobile >±2sd**
Yo871	Ba	0.73-0.90	Ba just above upper limit. Nothing else usual reported	Retain

Table 55 List of axes that have one or more elemental concentrations outside ±2sd of the IPC Group I (n=149) average. Axes identified in bold are recommended to be discarded from the IPC Group I data during subsequent statistical analysis (see text for details).

The geographical distribution of axes that have one or more elemental concentrations outside ±2sd is revealing. Initial determination of IPC Group I was petrographically based on axes from Wiltshire (Keiller et al. 1941) and only Wi209/937 of the 18 Wiltshire axes measured by the PXRF has a concentration outside ±2sd (Ca). Of the 8 Welsh axes analysed, Gm37, Gm85, Gm87, Gm91, Mo3 have at least one elemental concentration outside ± 2sd and **Gm 37, Gm85, Gm91 & Mo3** are subsequently recommended for removal from further statistical analysis of IPC Group I (c.f. Section 7.4.1.3). Similarly, of 10 axes found in Lincolnshire, 7 (Li2, Li4, Li123, Li124, Li149, Li357, Li542) have at least one concentration outside prescribed limits with 5 of these **(Li4, Li124, Li149, Li357 & Li542)** being subsequently recommended for removal from further statistical analysis of IPC Group I. IPC serial numbers for the 6 Cornish, Dorset and Somerset axes **(Co358/1627, Co363/1632, Co401/1737, CoGWA3, Do146/1762, So60/1143)** that are recommended for removal are all greater than 1143 indicating that these axes have been recently allocated to IPC Group I, with 5/6 axes identified having IPC serial numbers greater than 1627 (note: CoGWA3 will have a serial number greater than 1627 once it is listed in the IPC database). The remaining 4 axes from the 19 indicated in bold in Table 55 are **Yo352, Yo496 and Yo800** from the 18 Yorkshire axes analysed and **Es9** from the 10 Essex axes analysed. Thus, the main observation resulting from the initial inspection of IPC Group I axe geochemistry is that axes from NE England and Wales, and those with a high IPC serial number appear to have an increased probability of being geochemically different to the majority of IPC Group I. The disposition of these anomalous axes is further examined using SCA below (Section 7.4.1.2).

It has been stated that MS could not be used to provenance axes on its own (Chapter 5). However, now that geochemical data is available, a comparison between axes with anomalous geochemical readings and their associated MS can be made. From Table 55 it can be seen that axes CoGWA3, Gm37, Gm85, Gm91, Li357, Yo352, & Yo800 have both geochemical and MS measurements that are outside ±2sd of the associated IPC Group I average. Only axes Ha23/330 and Li123 (just) have MS values outside ±2sd of the IPC Group I MS average and are not recommended for removal from the data set. (Recall the MS range for IPC Group I is defined as $1.09 + 0.80 \times 10^{-3}$ SI (maximum corrected average plus 2sd) to $0.95 - 0.72 \times 10^{-3}$SI (minimum corrected average minus 2sd): from Chapter 5, Table 23.)

7.4.1.2 SCA of IPC Group I PXRF data

SCA of the immobile element concentrations using the 59 (of the 149) axes that have been petrographically sub-grouped is summarised in Table 56 (c.f. Table 51 & 57, below, for details of the sub-group populations) with SC results displayed as scatter plots in Figure 62. Using SCA results from the 59 axes, SC1 and SC2 values for the remaining 90 IPC Group I axes that have not been petrographically examined as part of this work were calculated, with results being displayed in the SC scatter plot in Figure 63.

Element	Average (ppm) (n = 59)	SD	Simple Components 1	2	3	4
Ti	14,408	4,209	1	0	2	-1
Y	33.2	9.3	1	-1	-1	-1
Zr	161	38.9	1	0	0	3
Nb	6.4	4.3	1	1	-1	-1
Standardised error			±1.62	±1.56		
Cumulative % of variance			57.4	80.1	92.8	100.0

Table 56 Summary SCA calculations based upon immobile elements contained in the 59 axes that have both PXRF data and have been petrographically sub-grouped in Chapter 4 (see Table 51). Simple component 1 (SC1) = Ti + Zr + Y + Nb. Simple component 2 (SC2) = Nb - Y

Figure 62, below, clearly shows the 6 (of the 19) axes recommended for removal from further statistical analysis of IPC Group I and that have been petrographically examined plot away from the main cluster of the data and that the remaining 53 axes cluster within (±5, ±3) of the origin. A considerable overlap is also seen between the data cluster for GpI-1 (upper chart) and the associated data clusters for GpI-2, 3, 4, 6, and 7 (lower chart). So60/1143 and Co401/1737 plot away from their petrographic sub-groups (GpI-1 & GpI-2 respectively) supporting the recommendation to exclude them from further statistical analysis of IPC Group I by excluding them from their respective sub-groups. The lower chart in Figure 62 shows distinct separation of the GpI-8, GpI-12 & GpI-13 clusters from the remaining axes. It is noted that petrographic analysis of these 3 IPC Group I sub-groups indicated that they are also mineralogically and/or texturally different to the majority of the 119 IPC Group I axe thin sections examined (c.f. Chapter 5). GpI-2 appears on Figure 62 to be slightly different to GpI-3, 4, & 6 since the cluster of the 4 GpI-2 axes (excluding Co401/1737) does not overlap the clusters formed by GpI-3, 4 & 6 axes. This indicates that there is a possibility that GpI-2 is geochemically different to GpI-3, 4 & 6, but it cannot be conclusive evidence as the GPI-2 data set is small (n=4).

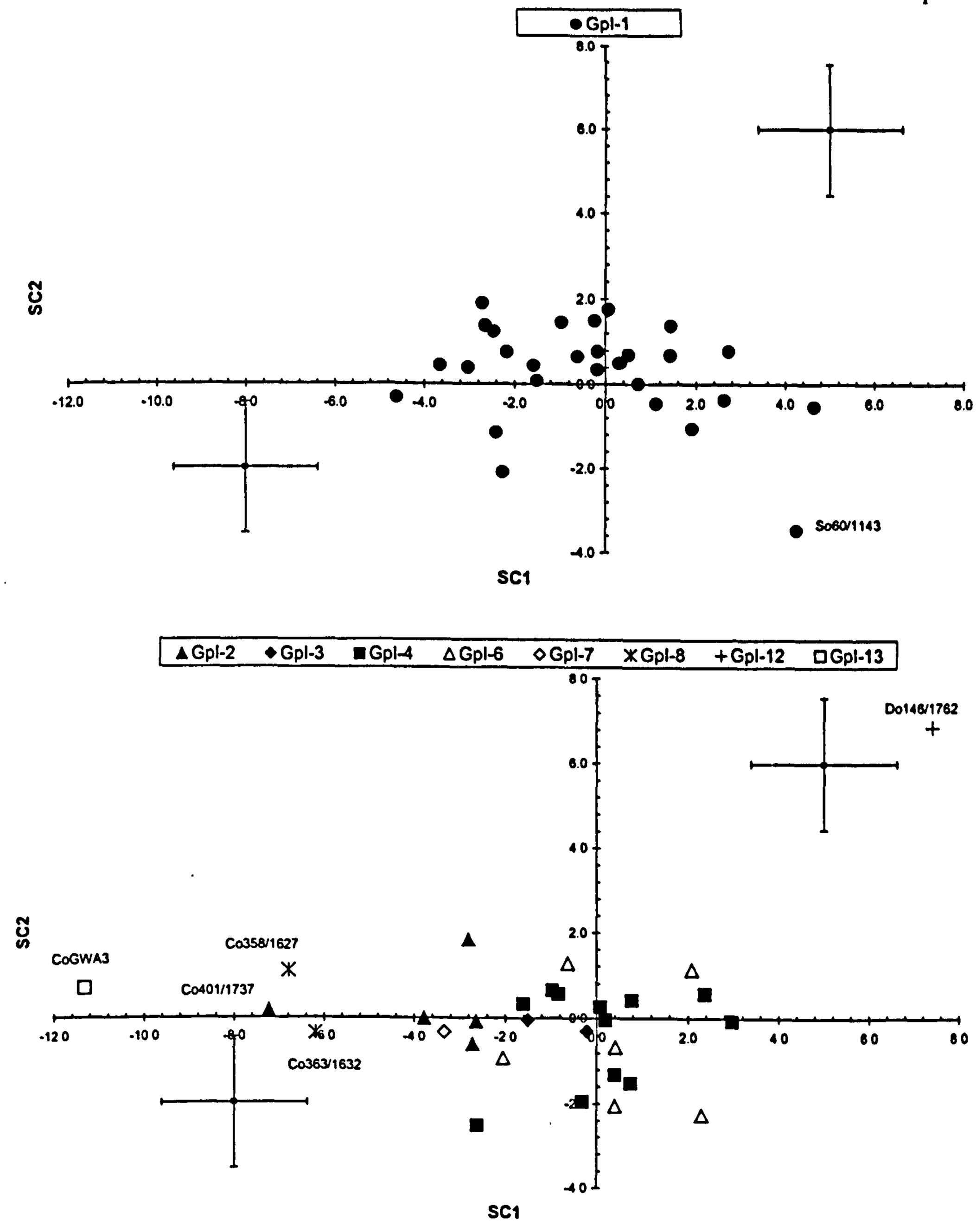

Figure 62 SC Scatter plots of SC1 against SC2 for IPC Group I sub-groups Gpl-1 (upper chart) and Gpl-2, 3, 4, 6, 7, 8, 12 & 13 (lower chart). SC1 (Ti+Y+Z+Nb) & SC2 (Nb-Y) account for 80.1% of the variance seen in the immobile element concentrations of the 59 axes included in the analysis. Axes that have been recommended for removal from further statistical analysis of IPC Group I are identified (c.f. Table 57). See text for discussion.

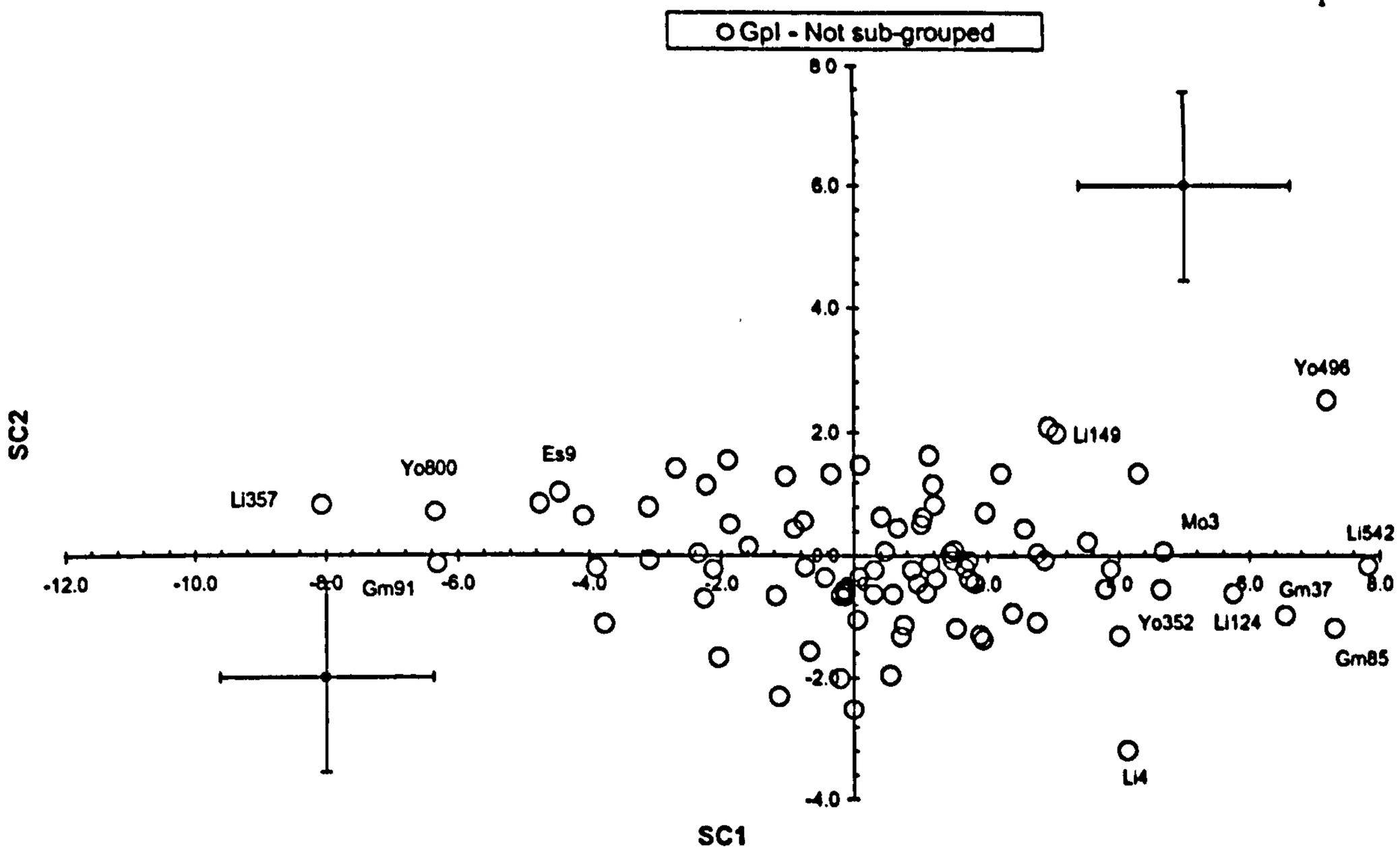

Figure 63 SC Scatter plots of SC1 against SC2 for the 90 IPC Group I axes that have not been petrographically examined as part of this thesis. Axe data has been standardised using SCA statistics detailed in Table 56 and plotted using the same simple components as in Figure 62: SC1 = Ti+Y+Zr+Nb; SC2 = Nb-Y. Axes identified in Table 55 as being recommended for removal from the statistical analysis of the IPC Group I data set are indicated

Geochemical data for the remaining 90 Group I axes that have not been petrographically examined (i.e. thin sections were not available) are displayed in Figure 63, above. The same SCA statistics calculated from the 59 IPC Group I sub-grouped axes are used to standardise the geochemical data for the remaining 90 IPC Group I axes analysed (Table 56). As discussed in Section 7.3.1.4, the proximity of the plotted point to the chart origin (0,0) probably indicates the geochemical similarity between the axe and the average of the 59 sub-grouped axes. Thus, examination of Figure 63 indicates that the distribution of the 90 axes generally falls within (±5, ±3) and is similar to the range observed for the 59 sub-grouped axes, therefore indicating that they are probably geochemically similar to the IPC Group I sub-grouped axes. The remaining 13 (of the 19) axes that are recommended for removal from the IPC Group I data set during further statistical analysis are identified in Figure 63, and are clearly seen to plot at, or near, the outer edges of the data cluster.

7.4.1.3 Anomalous axes within IPC Group I and implications for further geochemical analysis

Inspection of the geochemistry IPC Group I axes has shown that there are 48 of the 149 axes analysed that have one or more elemental concentrations outside ±2sd of the IPC Group I average (n=149), with 19 being recommended for removal from the data set. SCA, based on immobile element concentrations of the 59 IPC Group I axes that have been

both petrographically examined and analysed by PXRF, showed that these 19 axes plot at the outer edges of the associated data clusters, supporting the observations made during the examination of the axe geochemical data.

Table 57, below, summarises the IPC Group I sub-groups and identifies the 6 geochemically anomalous axes within the 59 axes contained in the sub-groups.

IPC Group I sub-group	Total in sub-group	Number analysed by PXRF	No with elements >±2sd	Number discarded	Comment on discarded axes
GpI-1	59	29	6	1	**So60/1143** discarded , Y twice average value
GpI-2	13	5	3	1	**Co401/1737** discarded through low Y & Ti
GpI-3	6	2	0	0	No geochemical anomalies
GpI-4	16	12	2	0	Co180/783 very high Pb due to surface contamination. Wi209/937 high Ca, above upper limit
GpI-5	2	None			Sub-group not analysed by PXRF
GpI-6	13	6	1	0	Gl103 has Ca slightly over +2sd limit
GpI-7	3	1	0	0	No geochemical anomalies
GpI-8	2	2	2	2	**Co358/1627 & Co363/1632** discarded, low Zr, Y and large negative Ba values
GpI-9	1	None			Subgroup not analysed by PXRF
GpI-10	1	None			Subgroup not analysed by PXRF
GpI-11	1	None			Subgroup not analysed by PXRF
GpI-12	1	1	1	1	**Do146/1762** discarded, Nb 4x average value
GpI-13	1	1	1	1	**CoGWA3 discarded**, very low Ti, Y, Zr & Nb values
Total	119	59	16	6	

Table 57 Summary of IPC Group I sub-groups axes with both thin section and PXRF data available, and identifying how many have elemental concentrations outside ±2sd of the IPC Group I (n=149) average, and those recommended for removal from the IPC Group I data set during subsequent statistical analysis.

Inspection of Table 57 and Figure 62 shows that three of the smaller IPC Group I sub-groups (GpI-8 (**Co358/1627 & Co363/1632**), GpI-12 (**Do146/1762**) and GpI-13 (**CoGWA3**) have both petrographic and geochemical anomalies that set them apart from the majority of IPC Group I. The remaining six IPC Group I sub-groups with geochemical data available, GpI-1, 2, 3, 4, 6, & 7, are noted in Chapter 4 as being petrographically 'similar' (although having at least one petrographic feature that is unique to the sub-group). This similarity is borne out by the fact that only one axe in GpI-1 (**So60/1143**) and one axe in GpI-2 (**Co401/1737**) are different to other members of the sub-group, and to IPC Group I in general.

A further thirteen IPC Group I axes, not petrographically examined, **Es9, Gm37, Gm85, Gm91, Li124, Li149, Li357, Li4, Li542, Mo3, Yo352, Yo496 and Yo800**, are also seen to be geochemically different to the majority of IPC Group I axes. These 13 and the 6

identified in the previous paragraph together constitute approximately 13% of the 149 IPC Group I axes geochemically examined. Since these 19 axes are believed to be sufficiently different to the other 130 IPC Group I axes examined, they will be removed from the IPC Group I data set used in subsequent statistical examinations of IPC Group I group geochemical data. Thus the *reduced IPC Group I data set* will comprise 130 axes, representing approximately 87% of IPC Group I axes measured by PXRF.

It is emphasised that the 19 'anomalous' axes identified above are still considered to be members of IPC Group I at this time. However, the petrographic, magnetic and geochemical evidence so far presented suggests that the IPC may wish to re-evaluate these axes with the possibility of formally removing them from IPC Group I.

7.4.2 SCA of the reduced IPC Group I data set using immobile elements

7.4.2.1 Reduced IPC Group I geochemical averages and immobile element SCA results

The aim of this part of the examination of IPC Group I axe geochemistry is to determine whether there is any identifiable geochemical variation between IPC Group I sub-groups and between counties of origin, using the reduced IPC Group I data set of 130 axes. Table 58, below, reports the average elemental, associated sd and the range of concentrations in the reduced IPC Group I data set

	Reduced IPC Group I average (n=130) (ppm)	Reduced IPC Group I sd (ppm)	Minimum value in data set (ppm)	Maximum value in data set (ppm)
K	3 567	2 282	100	12 500
Ca	67 715	14 636	39 700	102 600
Ti	14 959	3 772	4 700	26 300
Mn	1 532	521	800	3 800
Fe	95 632	14 009	67 900	155 300
Rb	29.6	25.8	-11.4	202
Sr	324	150	87.7	767
Y	35.7	6.8	17.6	48.9
Zr	171	29.2	96.2	245
Nb	6.7	2.9	-1.4	14.6
Ba	104	64.3	5.7	481
Ce	-27.1	11.4	-53.2	23.3
Pb	230	1013	-3.1	11 254

Table 58 Average and range of composition of the 130 axes in the reduced IPC Group I data set.

Table 59, below, reports the SCA statistics from calculations based on Ti, Y, Zr and Nb measurements of the 130 axes in the reduced IPC Group I data set.

Element	Average (ppm) (n = 130)	SD	Simple Components			
			1	2	3	4
Ti	14 959	3 772	1	0	2	1
Y	35.7	6.8	1	-1	-1	1
Zr	171	29.2	1	0	0	-3
Nb	6.7	2.9	1	1	-1	1
Standardised error			±1.62	±1.56		
Cumulative % of variance			47.0	70.5	88.8	100.0

Table 59 Summary of SCA calculations based upon immobile elements in the reduced data set of 130 IPC Group I axes. Simple component 1 (SC1) = Ti + Zr + Y + Nb. Simple component 2 (SC2) = Nb - Y

It is interesting to note that SC1, 2 & 3 for the reduced IPC Group I data set immobile elements are the same as for 59 sub-grouped axes detailed in Table 56, and that SC4 has the same values, but opposite signs. The other difference is that the average elemental values have changed slightly and that the associated sds for the reduced IPC Group I data set (n=130) are smaller than those for the IPC Group I sub-group data set (n=59). This latter observation, reduction in the sd values, is put down to the removal of the 19 anomalous axes from the IPC Group I data set (n=149), of which 6 (of 19) were originally included in the 59 that have been both petrographically and geochemically examined.

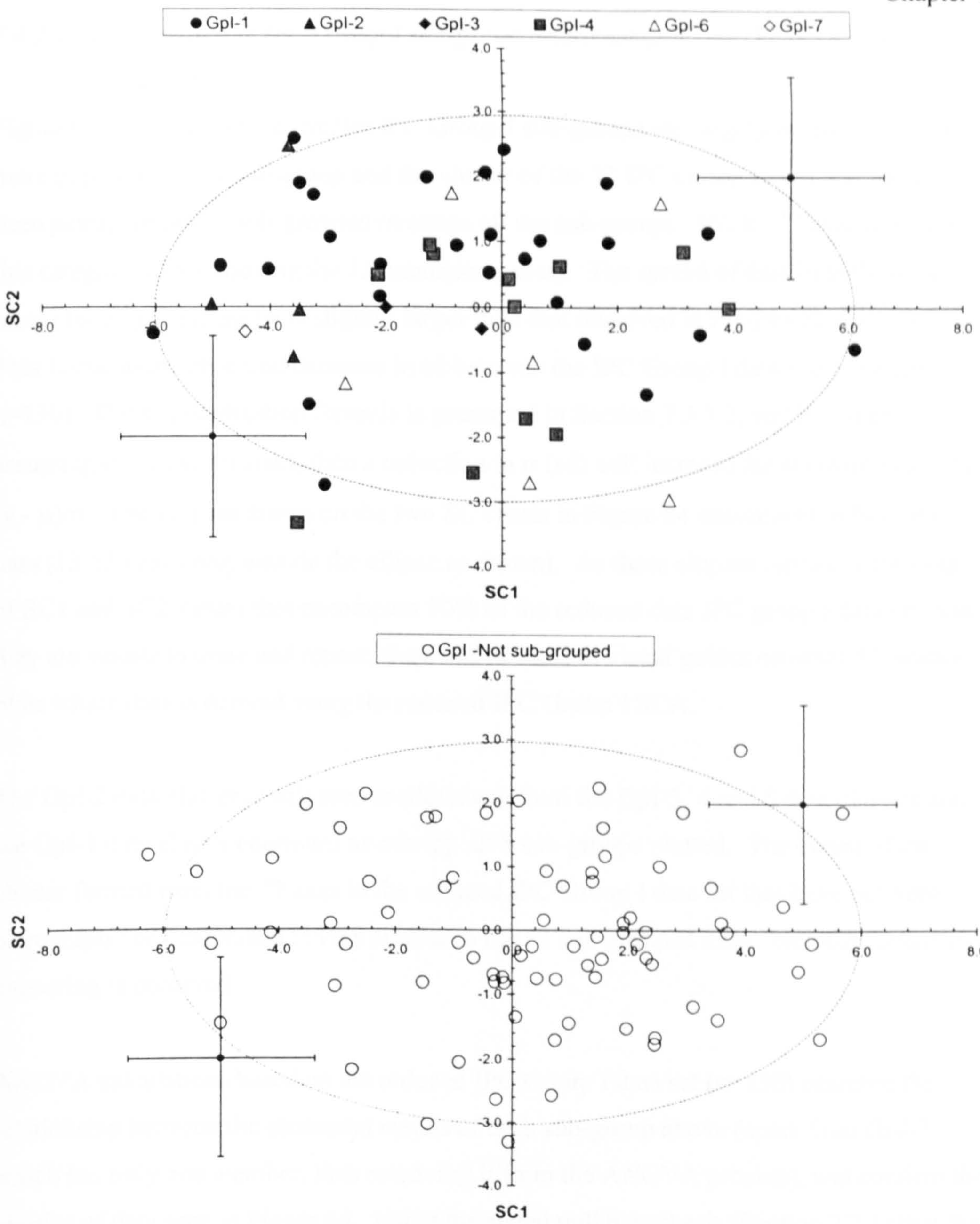

Figure 64 SC Scatter plots of SC1 against SC2 for the reduced IPC Group I data set of 130 axes based in immobile elements Ti, Y, Zr & Nb. Sub-groups Gpl-1, 2, 3, 4, 6, 7(upper chart) and IPC Group I – not sub-grouped (lower chart) are represented. SC1 (Ti+Zr+Y+Nb) & SC2 (Nb-Y) account for 70.5% of the variance seen in the immobile element concentrations of the 130 axes included in the analysis. There is considerable overlap between the sub and non-sub-grouped axes, although as seen in Figure 62 Gpl-2 is not overlapped by Gpl-3, 4 & 6. The ellipses encapsulate a total of 90% of the data points and are used as visual guides in other SC charts based on SC statistics calculated from Ti, Y, Zr, Nb concentrations in the reduced set of IPC Group I axes (see text for discussion)

7.4.2.2 Examination of IPC Group I sub-group relationships using the reduced IPC Group I data set

Figure 64 above shows the smaller IPC Group I sub-groups are largely overlapped by the more populous GpI-1 sub-group and the cluster of the 77 IPC Group I axes that have not been petrographically sub-grouped overlaps all the sub-groups. (Note: 77 axes remain in this category after removing the 13 anomalous axes). The spread of data in both SC scatter plots (±6, ±3) in Figure 64 is slightly larger than that observed in Figures 62 & 63 (±5, ±3). This is due to the observed decrease in sd between the IPC Group I data sets used (n=59, & n=130). The standardisation formula is presented in Section 7.3.1.3, and it is seen that, assuming $(x - \mu)$ is constant, then a reduction in σ (sd) will increase the standardised value $(x - \mu)/\sigma$. The ellipses drawn on the two SC charts in Figure 64 encompass 90% of the data (13/130 axes plot outside the ellipse as drawn). As these ellipses represent the range of SC1 and SC2 values that encompass 90% of the reduced data IPC group I data set, and they are simple to draw and repeat, they will be used as visual guides on other SC scatter plots where data is derived using the reduced IPC Group I SCA.

The GpI-2 data cluster is still seen to plot away from the GpI-3, 4 and 6 data clusters and the GpI-1 data cluster continues to overlap all 5 sub-groups plotted. The extent of the cluster formed from the 77 axes in the reduced IPC Group I data set that have not been petrographically examined is very similar to the 53 sub-grouped axes. No other distinctive clustering is observed.

ANOVA calculations based on the reduced IPC Group I data set (n=130) examine the relationship between the elemental means of each sub-group above (apart from GpI-7, which has only one member, thus removing it from the ANOVA process), and confirm the overlap of data seen in Figure 64. Using the stated null hypothesis (Section 7.2.1) that the means between each pair of sub-groups are equal; all of the significance values from ANOVA of Ti, Y, Zr & Nb between each pair of sub-groups is greater than 0.05, thus, not allowing the rejection of the null hypothesis at a 0.05 significance value. Therefore, ANOVA based on the reduced IPC Group I data set indicates that sub-groups GpI-1, GpI-2, GpI-3, GpI-4, GpI-6 and the ungrouped IPC Group I axes, cannot be statistically differentiated at a 0.05 significance value, using the immobile elements Ti, Y, Zr & Nb.

Results of MANOVA calculations based on the relationship of Ti, Y, Zr & Nb between each of the 9 IPC Group I sub-groups that are geochemically represented are contained in

Appendix 24 (note: the MANOVA data set comprises the reduced IPC Group I data set plus GpI-8, GpI-12 & GpI-13). Inspection of results indicates that the null hypothesis can only be rejected in one case: between GpI-2 & GpI-4 (GpI-8, 12 & 13 are discussed below). This complements the visual impression in Figures 62 & 64 that GpI-2 can be distinguished from GpI-3, 4, & 6. However it is noted that GpI-2 only contains 4 axes, therefore statistical results from this small data set need to be treated with caution.

MANOVA probabilities clearly show that the null hypothesis can be rejected between GpI-1, 2, & 4 and GpI-8, 12, & 13 at a 0.05 significance value (Appendix 24). This supports the observations made in Figure 62, that the axes within GpI-8 (Co358/1627, Co363/1632), GpI-12 ((Do146/1762) and GpI-13 (CoGWA3) are geochemically different to the majority of IPC Group I axes.

Hence, it is concluded that it is not possible to allocate IPC Group I ungrouped axes to Group I sub-groups GpI-2, 3, 4, 6, & 7 (recall, GpI-7 is not included in ANOVA) using SCA, ANOVA and MANOVA statistics with any confidence using immobile element geochemistry alone. The inability to reject the null hypothesis (apart from the cases cited) means that the sub-group populations may have originated from the same parent population.

7.4.2.3 Examination of the geochemical similarity of IPC Group I axes found in different counties

The geochemical relationship between IPC Group I axes found within various counties is investigated using SCA and MANOVA statistics. The SC scatter plots in Figures 65 & 66 have been generated from the same reduced IPC Group I data set (n=130) and SCA statistics used to generate the SC scatter plots in Figure 64.

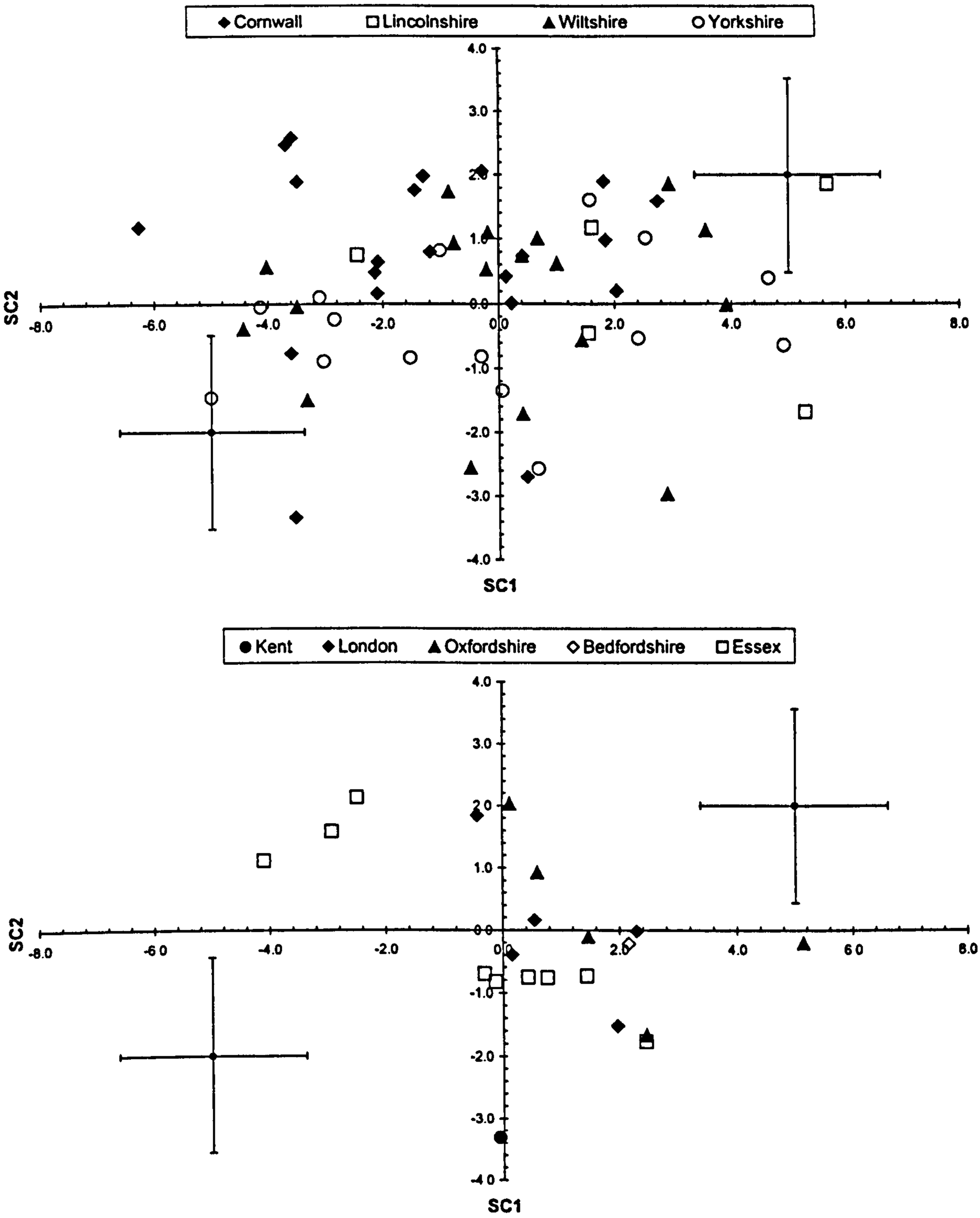

Figure 65 SC Scatter plots of SC1 against SC2 for the reduced IPC Group I data set of 130 axes subdivided into County (find location). SC1 (Ti+Y+Zr+Nb) & SC2 (Nb-Y) account for 70.5% of the variance seen in the immobile element concentrations of the 130 axes included in the analysis. The upper chart (Cornwall, Lincolnshire, Wiltshire & Yorkshire) shows considerable overlap of the data points and no readily apparent distribution patterns are seen. The lower chart (Kent, London, Oxfordshire, Bedfordshire & Essex) reveal that the axes found in Essex appear to form two sub-sets of data points. Axes from the remaining counties overlap to some degree, apart from the single representative from Kent (Ke56).

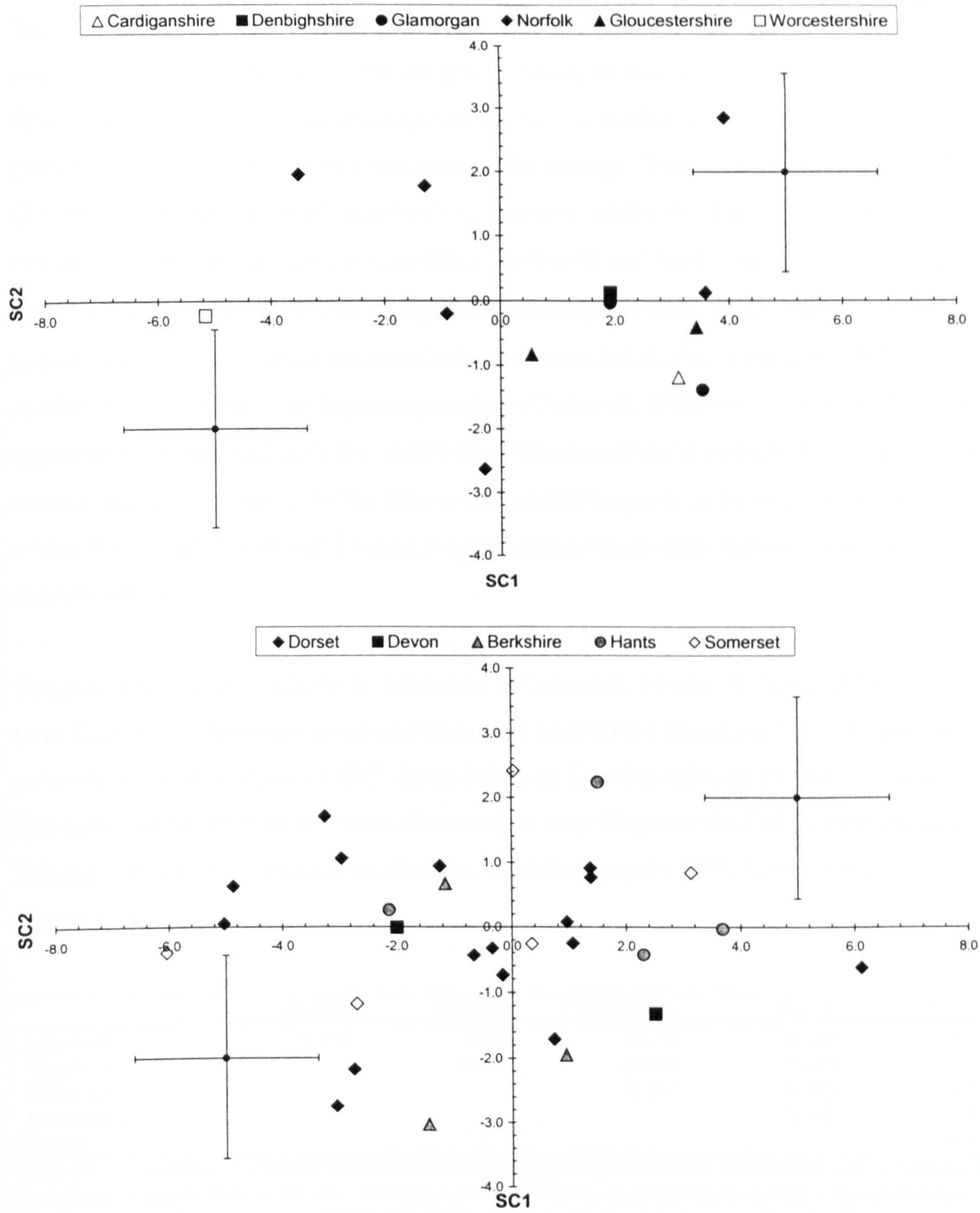

Figure 66 SC Scatter plots of SC1 against SC2 for the reduced IPC Group 1 data set of 130 axes subdivided into county (find location). SC1 (Ti+Y+Zr+Nb) & SC2 (Nb-Y) account for70.5% of the variance seen in the immobile element concentrations of the 130 axes included in the analysis. The upper chart (Cardiganshire, Denbighshire, Glamorgan, Norfolk, Gloucestershire and Worcestershire) shows possible cluster formed by axes from Wales. The lower chart (Dorset, Devon, Berkshire, Hants & Somerset) reveals no clustering of data points and too few axes to consider potential distribution of data points.

The four SC scatter plots contained in Figures 65 & 66 reveal that there is considerable overlap between the immobile element geochemistry of axes from 19 counties across Britain. In most counties, the axes appear to plot in a random pattern approximately centred on the origin; however some patterns do emerge. The Welsh axes (Cardiganshire, Glamorgan, Denbighshire) plot in the (+,-) quadrant, whilst the Essex axes appear to form two distinct sets, one group of 3 axes ((Es7, Es25/892, Es35) plotting in the (-,+) quadrant and all but one of the remaining axes plotting in the lower half of the chart. This could indicate a closer relationship between individual axes but further work is needed to confirm the similarity. The larger populations (Cornwall, Wiltshire, Yorkshire, Dorset) appear to be evenly and randomly distributed with a considerable mutual overlap. Some smaller data sets (London, Bedfordshire, Oxfordshire) appear to be restricted to regions within the overall IPC Group I range, suggesting that these axes may share similar characteristics.

The geochemical relationship of axes found in Cornwall, Dorset, Wiltshire, Norfolk, Lincolnshire and Yorkshire are examined using MANOVA based on Ti, Y, Zr and Nb concentrations of the reduced IPC Group I data set (n=130) with results detailed in Table 60 below. These six counties were chosen since they illustrate the SW (Cornwall, Dorset, Wiltshire) to NE (Yorkshire, Lincolnshire, Norfolk) spread of IPC Group I axe distribution.

	Yorkshire	Wiltshire	Lincolnshire	Dorset	Norfolk
Cornwall	0.196	0.056	0.176	0.160	0.256
Yorkshire		0.416	0.484	0.698	0.228
Wiltshire			0.474	0.763	0.386
Lincolnshire				0.300	0.845
Dorset					0.381

Table 60 Summary of MANOVA statistics investigating the geochemical relationships of axes found in six different counties around the UK. Thevalue quoted is the significance of the variance based on Pillais, Hostellings and Wilks tests using SPSS V7.0 Multivariate Analysis routine testing for significance between two sets of data (counties) based on Ti, Zr, Y, Nb. (All three tests gave the same significance value)

The null hypothesis for the MANOVA test is that there is no difference between the means of the groups. As all significance values in Table 60 are greater than 0.05, there is no reason to reject the null hypothesis and therefore there it is not possible to distinguish between axes found in these six counties using a 0.05 significance value (noting that Cornwall/Wiltshire value is only just >0.05 at 0.056). Hence, the statistics suggest that Group I axes found in Cornwall, Dorset, Wiltshire, Norfolk, Lincolnshire and Yorkshire may have all originated from the same parent population. However, it must be emphasised

that the data sets are small and thus the inability to reject the null hypothesis cannot be taken as *definite proof* that the axes come from a single parent population.

7.4.3 SCA of the reduced IPC Group I data set using mobile elements

In order to support the conclusions based on the four immobile elements, SCA analysis is carried out using K, Ca, Fe, Rb, Sr and Ba concentrations of the reduced IPC Group I axe data set with the results shown in Table 61 below and displayed in Figures 67, 68 and 69.

It is noted that the elements selected are 'mobile' within the metamorphic and weathering regimes encountered by Cornish greenstones and as such a greater variation in axe geochemistry can be expected (c.f. Chapter 6). In addition, the generally low K and Rb measurements mean that the PXRF is working close to its detection limits and spurious results may be included in the data set. However, it is still believed that examination of mobile element geochemistry is useful and has the potential to reveal useful information.

Element	Mean (ppm) (n=130)	SD	Simple Component 1	2	3	4	5	6
K	3 567	2,282	-1	1	-1	-1	1	1
Ca	67 715	14 636	1	1	0	-1	-1	2
Fe	95 632	14 009	0	-1	-1	-2	-1	-1
Rb	29.6	25.8	-1	1	1	-1	-1	-1
Sr	324	150	1	1	0	-1	1	-2
Ba	104	64.3	0	1	-1	2	-1	-1
Standardised error			±0.82	±0.86				
Cumulative % of variance			30.5	51.1	67.5	82.6	93.6	100.0

Table 61 Summary of SCA calculations based upon selected mobile elements contained in the reduced data set of 130 IPC Group I axes. Simple component 1 (SC1) = Ca + Sr - K - Rb. Simple component 2 (SC2) = K + Ca – Fe +Rb + Sr + Ba.

Figure 67 shows that the IPC Group I sub-groups continue to overlap with no obvious distribution patterns emerging. Co398/1734 plots well off the chart due to its comparably large K & Rb. GpI-2 appears to form an elongate cluster, above and to the left of the main concentration of data points and does not overlap the cluster formed by the 6 GpI-6 data points and is only partly overlapped by the 12 GpI-4 data points. IPC Group I axes not sub-grouped appear randomly distributed and appear to be more evenly spread within the ellipse than do the sub-grouped axes. The ellipses encapsulate 90% of the data points, that generally fall within (±6, ±5). As before the ellipse will be used to illustrate the range of reduced IPC Group I SC1 & SC2 values when the associated SCA (Table 61) is used to generate the scatter plot.

Figure 68 and 69 based on SCA using K, Ca, Fe, Rb, Sr & Ba, suggest some delineation of axes by county. The majority of Cornish axes plot to the left of the *y-axis*, whilst the majority of Wiltshire axes plot to the right of the *y-axis*, this is not seen for immobile elements in Figure 65. Inspection of the Appendix 23.1 shows that Cornish axes appear to have slightly less Ca and more Sr than Wiltshire axes. As seen in Figure 68 (lower), the positioning of Oxfordshire, London, Kent and Bedfordshire axes in the (+,+) quadrant suggest that the concentrations of the 6 mobile elements in these axes are probably similar. The 9 Essex axes (Figure 68 lower) do not form into two distinct clusters as in Figure 65 and the Welsh axes appear more randomly distributed in Figure 69 (upper) than in Figure 66 (upper).

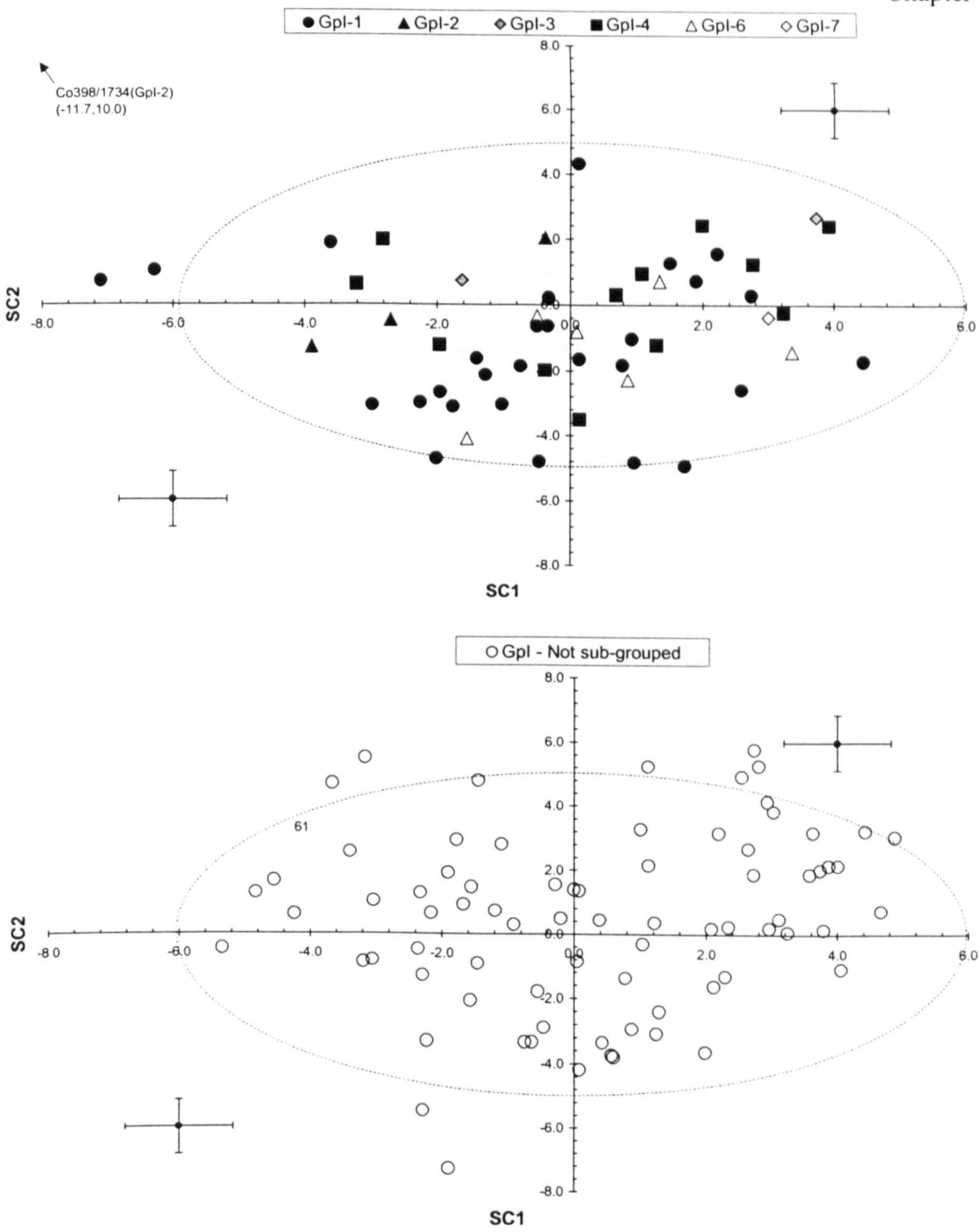

Figure 67 SC scatter plots of SC1 against SC2 for the reduced IPC Group I data set of 130 axes based on mobile elements K, Ca, Fe, Rb, Ba & Sr. GpI-1, 2, 3, 4, 6, 7(upper chart) and IPC Group I – not sub-grouped (lower chart) are represented. SC1 (Ca+Sr-K-Rb) & SC2 (K+Ca-Fe+Rb+Sr+Ba) account for 51.1% of the variance seen in the mobile element concentrations of the 130 axes included in the analysis. There is considerable overlap between the sub and non-sub-grouped axes. Unlike Figure 64, GpI-2 is only overlapped by GpI-6 and part of GpI-4. The ellipses encapsulate a total of 90% of the data points and will be used as visual guides in other SC charts based on SC statistics calculated from mobile element concentrations in the reduced set of IPC Group I axes.

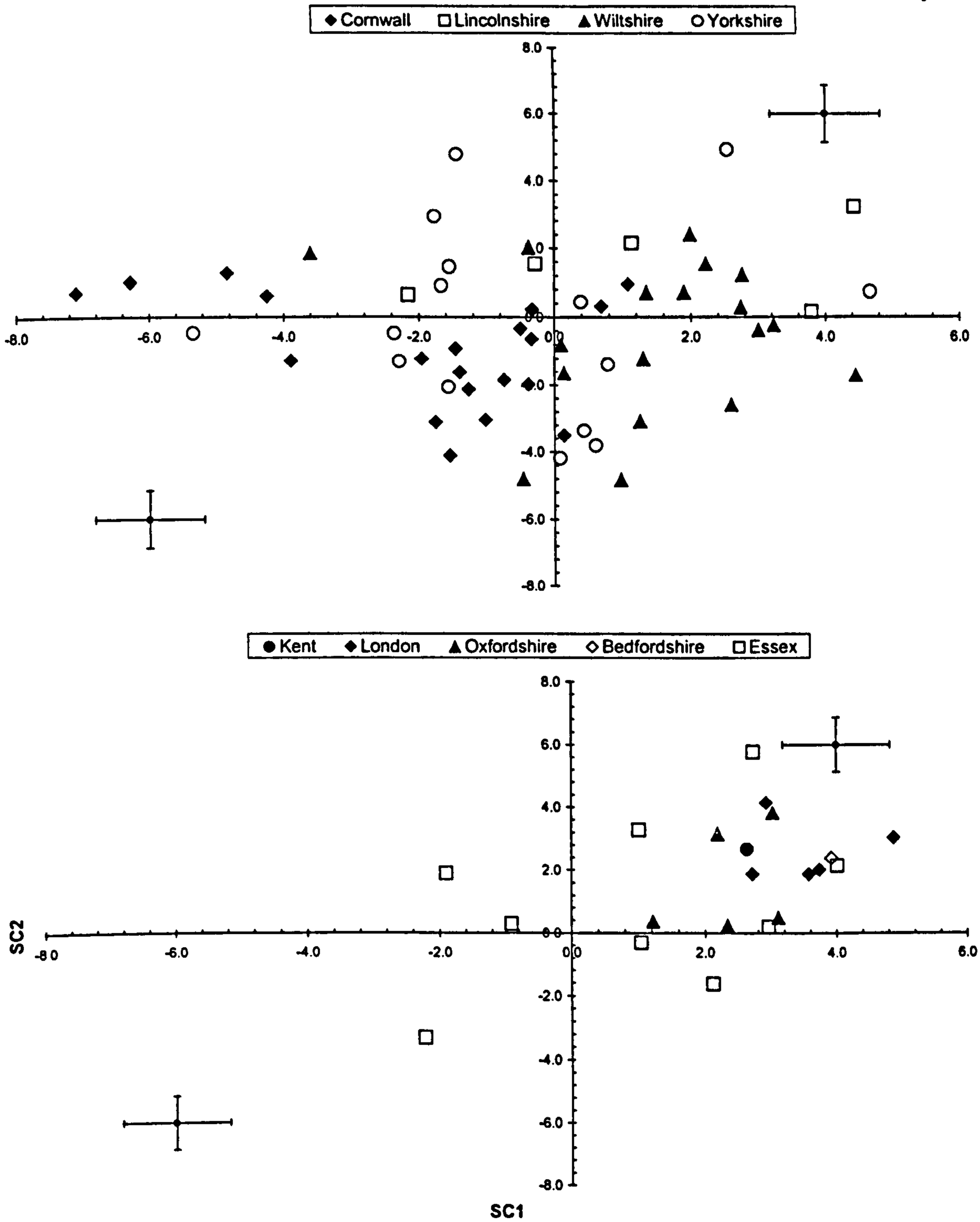

Figure 68 SC Scatter plots of SC1 against SC2 for the reduced IPC Group I data set of 130 axes based on mobile element concentrations subdivided into county (find location). SC1 (Ca+Sr-K-Rb) & SC2 (K+Ca-Fe+Rb+Sr+Ba) account for 51.1% of the variance seen in the mobile element concentrations of the 130 axes included in the analysis. The upper chart (Cornwall, Lincolnshire, Wiltshire & Yorkshire) shows considerable overlap of the data points although Cornwall and Wiltshire axes appear to form two distinct and only partly overlapping clusters. The lower chart (Kent, London, Oxfordshire, Bedfordshire & Essex) reveals that the axes found in Essex do not form the two clusters seen in the immobile element SC scatter plot (Figure 65). Axes from London, Oxfordshire, Bedfordshire and Kent form a relatively small, but overlapping cluster in the (+,+) quadrant.

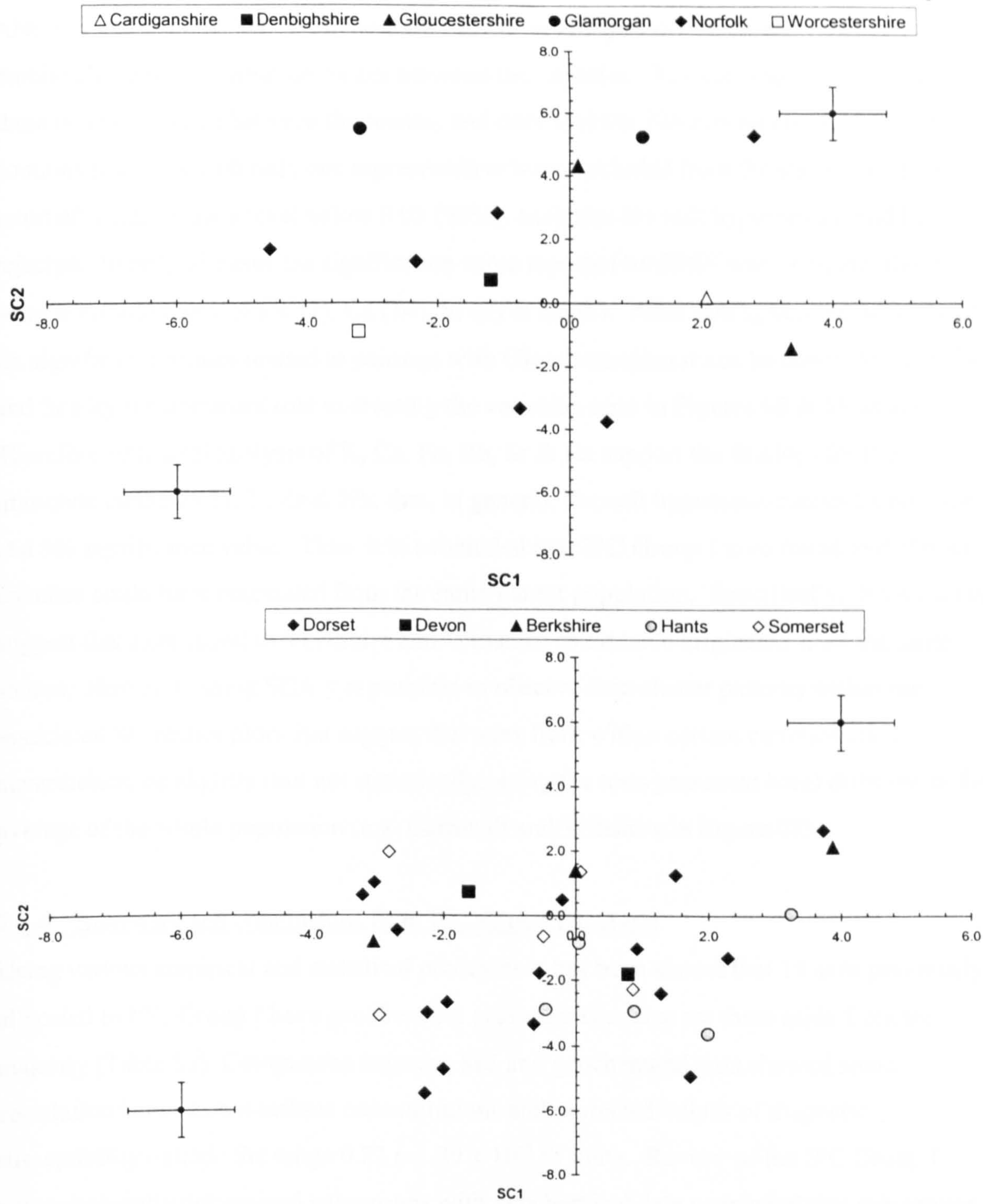

Figure 69 SC Scatter plots of SC1 against SC2 for the reduced IPC Group I data set of 130 axes based on mobile element concentrations subdivided into county (find location). SC1 (Ca+Sr-K-Rb) & SC2 (K+Ca-Fe+Rb+Sr+Ba) account for 51.1% of the variance seen in the mobile element concentrations of the 130 axes included in the analysis. The upper chart (Cardiganshire, Denbighshire, Glamorgan, Norfolk, Gloucestershire and Worcestershire) shows no clear distribution patterns, unlike those seen in Figure 66. The lower chart (Dorset, Devon, Berkshire, Hants & Somerset) reveals a relatively even distribution of data points and too few axes to consider potential clustering of data.

ANOVA and the post hoc Sheffe test are used to investigate the relationship between the mobile element concentration means between the counties. The null hypothesis is that there is no difference between the means, and only 1 of the 720 combinations ($^{16}C_2$ x 16 counties (counties with only one representative were excluded from the statistical process) returned a significance level below 0.05 (95%), such that the null hypothesis could be rejected. In only 35 cases the significance value reported by SPSS was <0.9, and these were distributed between K (3), Ca (14), Sr (9) & Ba (9). After noting that the majority of Ba significance values related to pairings with Gloucestershire it can be concluded that Ca and Sr play the dominant role in creating the variation seen in Figures 68 & 69 above. Therefore statistical analysis of K, Ca, Fe, Rb, Sr & Ba support the findings for the immobile elements Ti, Y, Zr & Nb: that, in general, the null hypothesis cannot be rejected at a 5% significance value. Thus, it is concluded that IPC Group I axes found in different counties could have originated from the same parent population. Specifically, these results suggest that axes found in Yorkshire and Wiltshire could have originated from the same source. However, using SCA it is possible to observe data cluster patterns within the associated SC scatter plots that suggest that axes from within certain counties may, nevertheless, be slightly (but not statistically, using the tests presented here) different to the average of the whole population (e.g. Cornwall and Wiltshire in Figure 68).

7.4.4 Summary and conclusions from IPC Group I analysis

Using various empirical and statistical processes it has been shown that 19 axes previously allocated to IPC Group I have geochemical characteristics that set them aside from the majority (Table 55). Comparison between MS and geochemical data showed some correlation between anomalous concentrations and corrected values of magnetic susceptibility outside the range 0.23 to1.89 x 10^{-3} SI units. Review of the IPC Group I petrographically determined sub-groups with geochemical data concluded that sub-groups GpI-8, GpI-12 & GpI-13 with mineralogical and/or textural differences also have geochemical differences that set them apart from the majority of IPC Group I axes examined. The remaining 6 sub-groups could not be distinguished using ANOVA statistics based on geochemical data although MANOVA statistics based on immobile elements suggested GpI-2 was statistically different from GpI-4 and that GpI-8, 12, & 13 are statistically different to GpI-1, 2, 4 & 6 at a 5% significance value.

SCA, MANOVA and ANOVA processes showed that axes from different counties share similar geochemistry as the null hypothesis could not be rejected at the 0.05 significance

level. Hence, statistically, axes from the 19 counties represented could have originated from the same parent population. This, in part, confirms the observation that the majority of IPC group I axes share petrological similarities and goes some way to suggesting axes may have been dispersed by along trade/migration routes to the counties in which they were found.

A geochemical 'fingerprint' for IPC Group I is derived from the reduced data set of 130 IPC Group I axes and detailed in Table 62, below. Whilst there remain some axes within this data set (e.g. Ha23/330) that are 'borderline' using the rejection criteria set out above, it is concluded that the elemental averages and associated sds calculated from the reduced IPC Group I data set of 130 axes are representative of the greenstone used to manufacture the axes. The relatively even spread of the geochemical data in the associated SC charts strongly suggests a single parent population, although there is visual evidence of clustering within the sub-group and county SC scatter plots that may indicate deliberate selection of material from a single greenstone exposure, or several exposures that are geographically close.

A summary of all the averages & sds for the various data sets referred to in this section (7.4) is contained in Appendix 23.9 with key ones reported in Table 62, below.

	IPC Group I (ppm ± 1sd) (n=130)	GpI-1 (ppm) (n=28)	GpI-2 (ppm) (n=4)	GpI-3 (ppm) (n=2)	GpI-4 (ppm) (n=12)	GpI-6 (ppm) (n=6)	GpI-7 (ppm) (n=1)	IPC Group I (n=149)
K	**3 567 ± 2 282**	3 025	6 100	4 200	3 533	3 217	1 700	3 811
Ca	**67 715 ± 14 636**	62 454	53 625	75 700	72 417	71 850	80 500	66 581
Ti	**14 959 ± 3 772**	15 343	10 875	14 550	15 325	15 517	10 400	15 013
Mn	**1 532 ± 521**	1 668	1 100	1 500	1 483	1 700	1 300	1 569
Fe	**95 632 ± 14 009**	97 600	77 375	91 050	95 533	103 083	89 400	95 491
Rb	**29.6 ± 25.8**	27.3	77.9	24.4	28.1	22.2	-3.7	31.1
Sr	**324 ± 150**	247	211	405	342	299	317	318
Y	**35.7 ± 6.8**	32.1	28.9	33.9	36.8	40.1	30.7	35.9
Zr	**171 ± 29.2**	165	135	164	178	169	133	170
Nb	**6.7 ± 2.9**	6.9	5.0	5.4	5.8	6.4	3.4	6.9
Ba	**104 ± 64.3**	103	102	117	88.1	70.4	134	108
Ce	**-27.1 ± 11.4**	-32.0	-14.0	-22.0	-27.4	-29.5	-30.6	-26.8
Pb	**230 ± 1013**	107	79.1	51.3	1052	160	109.3	365

Table 62 Reduced IPC Group I data set elemental averages which are considered to constitute the 'geochemical fingerprint' for IPC Group I (in bold). Also shown are IPC Group I sub-group average concentrations (after anomalous axes have been removed) and the average elemental concentrations of all 149 axes measured by PXRF (c.f. Table 51, Table 57, Appendix 23.9 for further information)

7.5 Examination of IPC Group Ia, I/Ia and I(near) axe geochemistry

The IPC recognises three categories of axes as being petrographically similar to IPC Group I, but with sufficient difference to be designated separately (c.f. Chapter 1 & 2). This section investigates these three IPC designations: IPC Group Ia, I/Ia and I(near).

7.5.1 Inspection of IPC Group Ia, I/Ia and I(near) data

The low numbers of axes (4, 6, & 6 respectively) precludes the initial investigation of elemental concentrations outside ±2sd (c.f. Section 7.2.3). Hence, SCA is used to visualise the intra and inter geochemical relationship of these three IPC axe groups after the data set of 16 axes is first examined for anomalous measurements. The average elemental concentration of the 16 axes in the data set is reported in Table 63 below, along with the averages for each of the three IPC groups. Appendix 23.3 contains the corrected and summarised PXRF data for each of the 16 axes.

	Combined IPC Group Ia, I/Ia & I(near) (n=16) (ppm ± 1sd))	IPC Group Ia (n=4) (ppm ± 1sd)	IPC Group I/Ia (n=6) (ppm ± 1sd)	IPC Group I(near) (n=6) (ppm ± 1sd)
K	7 044 ± 6 002	8 950 ± 3 861	7 000 ± 8 960	5 817 ± 3 756
Ca	70 106 ± 18 350	66 950 ± 18 228	73 500 ± 19 290	68 817 ± 20 369
Ti	14 944 ± 5 424	15 825 ± 3 738	15 137 ± 4 956	13 983 ± 7 308
Mn	1 556 ± 528	1 750 ± 1 002	1 533 ± 273	1 450 ± 339
Fe	94 363 ± 23 176	109 450 ± 30 635	81 500 ± 21 256	97 167 ± 14 705
Rb	49.9 ± 42.6	75.2 ± 51.6	36.3 ± 41.8	46.7 ± 36.7
Sr	281 ± 176	201 ± 88.9	404 ± 230	212 ± 80.4
Y	36.8 ± 10.7	33.8 ± 8.0	44.9 ± 5.4	30.6 ± 12.0
Zr	159 ± 50.2	170 ± 40.0	187 ± 27.3	124 ± 58.2
Nb	6.4 ± 4.2	7.1 ± 2.5	9.7 ± 3.3	2.6 ± 2.9
Ba	163 ± 153	204 ± 214	148 ± 190	151 ± 72.6
Ce	-24.0 ± 15.1	-24.7 ± 19.0	-18.3 ± 14.4	-29.2 ± 13.8
Pb	224 ± 317	152 ± 129	364 ± 486	133 ± 133

Table 63 Average composition of the 16 IPC Group Ia, I/Ia & I(near) axes measured by PXRF and the associated IPC group averages.

In IPC Group Ia, axe Co152/738 has similar immobile elements concentrations to the others in the group, apart from Y which is slightly lower, but has significantly different K, Fe, Rb, Ce concentrations. Field notes indicate that there is nothing visually unusual about this axe and that it is visually similar to the IPC Group I axe Co151/737. The axe thin section was placed in GpIa-1 and is therefore petrographically similar to GpI-1 (Chapter 4). IPC Group Ia axe So50/939 has higher Ti, Mn, Fe and Ba than other group members although the axe appears to be macroscopically comparable to the majority of greenstone axes examined. However, this axe is the sole representative of the petrographic sub-group GpIa-5, which has been assessed as being mineralogically different to the other IPC Group Ia axe thin sections examined.

Axe Lo114 is geochemically different to the others measured in IPC Group I/Ia by having very high K, Rb, Ba, relatively high Ce and very low Ca, Ti, Fe. Field notes support the geochemical analysis by noting that the axe is macroscopically different to the majority of greenstone examined. Also Lo114 MS is (uncorrected) 0.17 x 10^{-3} SI, it is therefore possible that Lo114 has been mis-categorised as IPC Group I/Ia.

Examination of immobile element concentrations in the 6 axes measured from IPC Group I(near) suggests Yo99 & Li94 are different to the other 4 axes, having lower Ti, Y, Zr concentrations than the other 4 axes in the group. Field notes report that these two axes have pitted/eroded surfaces and relatively low (corrected) MS of between 0.49 and 0.66 x 10^{-3} SI. It is concluded that these two axes are atypical of IPC Group I(near) and are probably not related to IPC Group I either.

Initial examination and recommendations regarding the 16 IPC Group Ia, I/Ia & I(near) axes is summarised in Table 64, below.

Short Name	Anomalous Elements	Magnetic Susceptibility	Comment	Recommendation
Group Ia				
Es10	None	0.90-0.96	Nothing unusual reported in field notes	Thin section not examined: do not allocate to Gpla sub-groups
Co145/731	None	0.77-1.02	Nothing unusual reported in field notes	Retain in Gpla
Co152/738	K, Fe, Rb, Ce	Not measured	Nothing unusual reported in field notes	Retain in Gpla at this time (possibly anomalous?)
So50/939	Fe, Ba	1.39-1.70	Macroscopically typical greenstone, microscopically unique.	Retain in Gpla-5 (sole member)
Group I/Ia				
Lo113	None	0.66-0.76	Nothing unusual reported in field notes	Retain in GpI/Ia
Lo114	K, Ca, Ti, Fe, Y, Ba, Ce	0.34-0.41	Conchoidal impact marks noted, field notes suggest not typical greenstone	**Discard Anomalous elements, relatively low MS & unusual macroscopic features**
Lo115	None	0.65-0.80	Nothing unusual reported in field notes	Retain in GpI/Ia
Lo116	None	1.59-1.95	Nothing unusual reported in field notes	Retain in GpI/Ia
Lo16(63)	None	0.89-1.17	Macroscopically not similar to GpI, overall darker colour, with indistinct grains. Surface finish may mask macroscopic features	Retain in GpI/Ia
Lo52(263)	None	0.97-1.12	Macroscopically not similar to GpI, overall darker colour, with indistinct grains. Surface finish may mask macroscopic features	Retain in GpI/Ia
Group I(near)				
Yo99	K, Ti, Y, Zr, Nb	0.49-0.60	Nothing unusual reported in field notes. Geochemically similar to Li94	**Sub-group with Li94 GpI(near)1**
Li94	Ca, Ti, Y, Zr, Nb	0.53-0.66	Heavily eroded, but similar to majority of greenstone axes viewed. Geochemically similar to Yo99	**Sub-group with Yo99 GpI(near)1**
Yo102	None	0.75-0.98	Nothing unusual reported in field notes	GpI(near)2
Yo123	None	1.18-1.45	Nothing unusual reported in field notes	GpI(near)2
Es18	None	0.85-0.91	Nothing unusual reported in field notes	GpI(near)2
Es25	None	1.17-1.33	Nothing unusual reported in field notes	GpI(near)2

Table 64 Summary of review of IPC Group Ia, I-Ia & I(near) axes and identification of the axe sub-groups used to investigate inter sub-group relationships and in discrimination calculations. Note the indicated 'anomalous elements' are not necessarily outside ± 2d of the mean of all 16 axes, just that they appear different to other members within their IPC Group.

7.5.2 SCA of IPC Group Ia, I/Ia and I(near) data

SCA statistics were calculated using both immobile and mobile elements in order to investigate the inter and intra geochemical relationship of the three groups. The SCA statistics in Tables 65 and 66 are derived from using all 16 axes in the three groups. Standardised errors are calculated as described in Section 7.3.1.5. Rb has been omitted due to its large variation across the three groups.

Element	Average (ppm) (n = 16)	SD	Simple Components 1	2	3	4
Ti	14,944	5,424	1	-2	1	0
Y	36.8	10.7	1	0	-3	0
Zr	159	50.2	1	1	1	-1
Nb	6.4	4.2	1	1	1	1
Standardised error			±1.62	±1.27		
Cumulative % of variance			67.0	88.0	96.8	100.0

Table 65 Summary of SCA calculations based upon Ti, Y, Zr & Nb elements concentrations in IPC Group Ia, I/Ia and I(near). Simple component 1 (SC1)= Ti + Y +Zr + Nb. Simple component 2 (SC2) = Zr + Nb - 2Ti.

Element	Average (ppm) (n=16)	SD	Simple Component 1	2	3	4	5
K	7,044	6,002	1	2	-4	-31	-938
Ca	70,106	18,350	-1	0	-14	187	-154
Fe	94,363	23,176	0	-3	-2	-336	-618
Sr	281	176	-1	2	1	-473	11
Ba	163	153	1	0	-9	-225	795
Standardised error			±0.30	±0.32			
Cumulative % of variance		46.5	72.1	88.4	98.3	100.0	

Table 66 Summary of SCA calculations based on selected mobile element concentrations in IPC Group Ia, I/Ia, I(near) axes. Simple component 1 (SC1) = K + Ba - Ca - Sr. Simple component 2 (SC2) = 2K + 2Sr - 3 Fe

7.5.2.1 Group Ia

All four members of IPC Group Ia appear evenly, but widely, distributed on both SC scatter plots in Figure 70. In Chapter 4, axe So52/939 is noted as being microscopically distinct and thus forms GpIa-5. Co145/731 & Co152/738 are members of GpIa-1, and are therefore petrographically similar to sub-group GpI-1. (See Table 51 for summary of IPC Group Ia sub-groups represented.) Thin section for axe Es10 was not available. The range of corrected MS for So50/939 is 1.39 to1.70 x10^{-3} SI, with the other two axes measured in the group ranging from 0.77 to 1.02 x 10^{-3} SI. Field notes reports note no macroscopic anomalies with any IPC Group Ia axe examined. Based on the inspection of geochemical data and supported by MS values it appears that So50/939 is petrographically, magnetically and geochemically different to the remainder of the group. Since there are only two representatives from GpIa-1 it cannot be known which one is typical of the sub-group. However, using the observed petrographical similarities between GpIa-1 and GpI-1 it can be reasonably assumed that the geochemical measurements of Co145/731 represents

the GpIa-1 on the basis of it having similar geochemical values to the IPC Group I average (n-130). But, the immobile element concentrations of Co152/738 are also within ±2sd of the IPC Group I geochemical average (just). As such, both GpIa-1 axes will be assumed to represent (possibly end member of) the GpIa-1 sub-group, at this time.

7.5.2.2 Group I/Ia

SC based on Ti, Y, Zr & Nb appears to divide IPC Group I/Ia into three clusters in Figure 70 (upper chart): Lo114; Lo115 & Lo52(263) and Lo113, Lo116 & Lo16(63). In part, this is borne out by Figure 70 (lower chart), based upon SC derived from K, Ca, Fe, Sr & Ba, with Lo114 an outlier in both cases. Coupled with a low corrected MS measurement of approximately 0.4 $x10^{-3}$SI, makes Lo114 dissimilar to other IPC Group I/Ia axes. Field notes record that Lo114 is macroscopically different to other axes in that it has conchoidal fracture patterns, not seen on any other greenstone axe.

The second IPC Group I/Ia cluster in Figure 70 (upper chart) is Lo52(263) & Lo115, which is not repeated in the mobile element (lower) SC scatter plot. After inspecting MS measurements it is concluded that these two axes are similar to the remaining three, Lo113, Lo16(62) & Lo116 in IPC Group I/Ia. Field notes indicate Lo16(62) & Lo52(268) are macroscopically different to the majority of IPC Group I & I/Ia axes with both having polished dark surfaces. However the polished surfaces may have obscured the mineralogy and hence it is not macroscopically conclusive that these axes are petrologically different to other GpI-Ia axes.

Therefore only axe Lo114 is anomalous and unlike any other Group I/Ia (or Group Ia or I(near) axe) and it is removed from further statistical evaluation of IPC Group I/Ia.

7.5.2.3 Group I(near)

Li94 and Yo99 plot away from the main IPC Group I(near) cluster in Figure 70 (upper) as a result of their comparatively low Ti, Zr, Y & Nb concentrations. These two axes also have the lowest MS readings of all 6 IPC Group I(near) axes measured (<0.66 x 10^{-3} SI). The 4 remaining IPC Group I(near) axes have no reported anomalous macroscopic, geochemical or magnetic anomalies. The geochemical similarity between Li94 & Yo99 suggest that IPC Group I(near) is divided into two sub-groups: Li94 & Yo99, and Yo102, Yo123, Es18 & Es25. Hence in further statistical analyses 'GpI(near)1' consists of Li94 & Yo99 and 'GpI(near)2' consists of Es18, Es25, Yo102 & Yo123

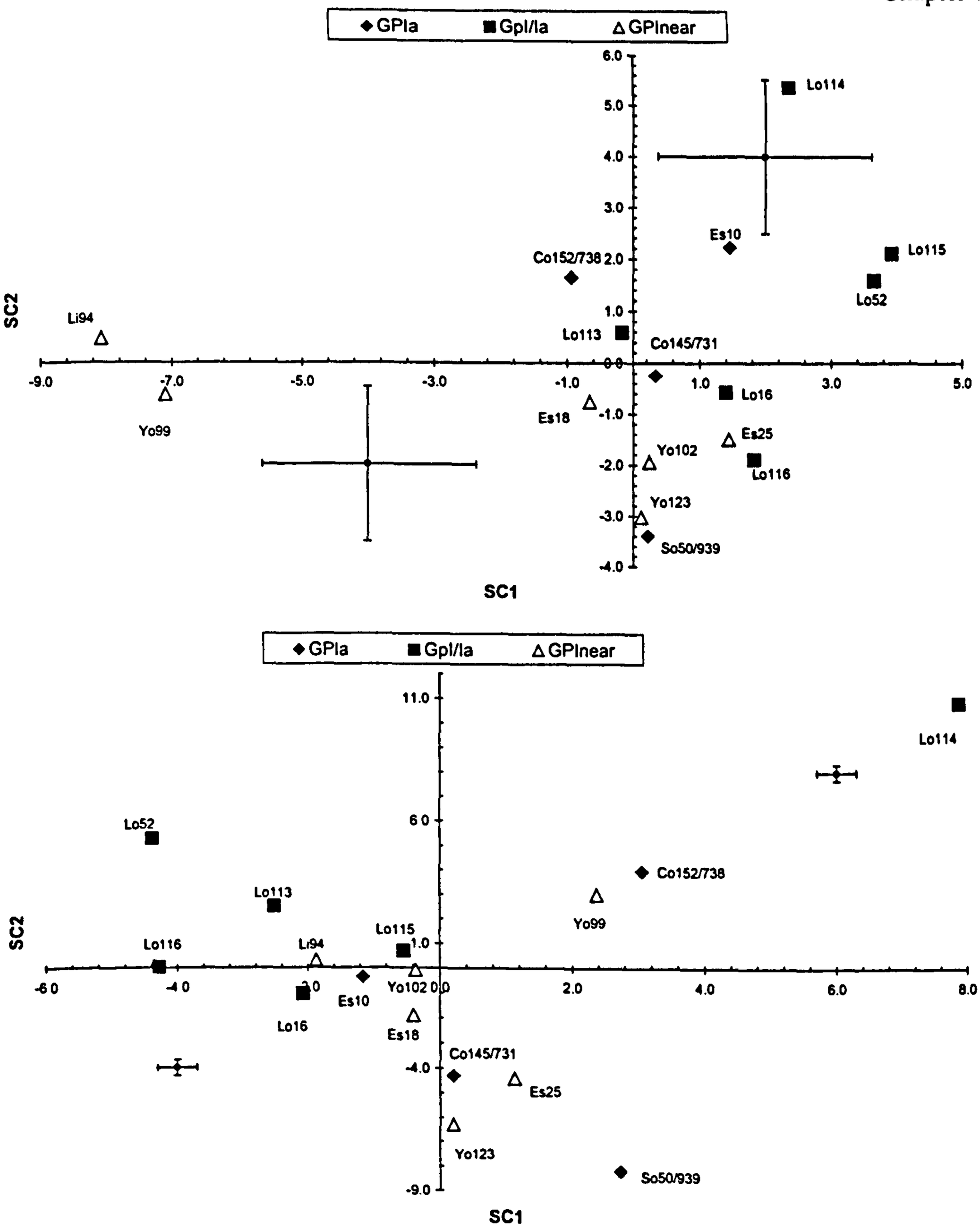

Figure 70 SC Scatter plots of SC1 against SC2 for IPC Groups Ia, I/Ia and I(near) based on Ti, Y, Zr & Nb (immobile) elements (upper chart) and K, Ca, Fe , Sr & Ba (mobile) elements (lower) chart. SC1 (Ti+Y+Zr+Nb) & SC2(Zr+Nb-2Ti) (upper) account for 88.0% of the variance seen in the immobile element data and SC1 (K-Ca-Sr+Ba) and SC2 (2K-3Fe+2Sr) account for 72.1% of the variance seen in mobile element data of the three IPC groups. IPC Group Ia axes are widely distributed with So50/939 standing apart from the other members in both charts. IPC Group I/Ia appears to divide into three clusters in the immobile element chart (upper) with Lo114 easily identified as an outlier. IPC Group I(near) divides into two clusters on the immobile element char: Li94 & Yo99 separate from Es18, Es 25, Yo102 & Yo123, although this division is not clear in the mobile element chart

7.5.3 Re-definition of IPC Group Ia, I/Ia and I(near) sub-groups.

The above examination of geochemical and MS data has resulted in identifying a further 3 axe sub-groups: GpI/Ia, GpI(near)1, and GpI(near)2. These, along with the existing axe sub-groups, are reported in Table 67 below and will be included in the set of seed groups used in DA.

Sub-group name	Members
GpIa-1	Co145/731, (Co152/738 - but see comment in Section 7.5.5)
GpIa-5	So50/939
GpI/Ia	Lo113, Lo115, Lo116, Lo16(63), Lo52(263)
GpI(near)1	Li94, Yo99
GpI(near)2	Yo102, Yo123, Es18, Es25

Table 67 Summary of IPC Group Ia, I/Ia, I(near) sub-groups and their members. Note GpIa-2, 3, 4 & 6 petrographic sub-groups are not geochemically represented.

7.5.4 Statistical investigation of the relationship between IPC Groups Ia, I/Ia and I(near) sub-groups and GpI-1

Taken as a whole, and ignoring the 3 anomalous axes identified above (Lo114, Yo99, Li94), the range of geochemical concentrations for each IPC group overlap to some extent. However, when inspected at sub-group level using SC scatter plots there appears to be the potential to recognise distinct clusters. These two observation are partly borne out through MANOVA. MANOVA results are detailed in Table 68, below. In three cases, (GpI/Ia & GpI(near)2, GpI/Ia & GpI-1 and GpI(near)1 & GpI-1: indicated in bold in Table 68), a significance value less than 0.05 is returned, indicating that there is sufficient evidence to reject the null hypothesis (null hypothesis is that there is no difference between the means).

	Gp1a-5	GpI/Ia	GpI(near)1	GpI(near)2	GpI-1
Gpla-1	*	0.325	*	0.433	0.972
Gpla-5		0.288	*	*	0.110
GpI/Ia			0.058	**0.022**	**0.017**
GpI(near)1				0.123	**0.001**
GpI(near2					0.092

Table 68 Summary of MANOVA statistics investigating the geochemical relationships of IPC Group Ia, I/Ia & I(near)sub-groups and IPC Group I sub-group GpI-1. The value quoted is the significance of the variance based on Pillais, Hostellings and Wilks tests using SPSS V7.o Multivariate Analysis routine testing for significance between two sets of data (groups) and with four variables (Ti, Zr, Y, Nb) (All three tests gave the same significance value). '' indicate that there were insufficient cases to calculate the MANOVA statistics.*

There are only enough axe measurements to investigate the relationship in 11 of the possible 15 pairing between the six sub-groups: GpIa-1, GpIa-2, GpI/Ia, GpI(near)1, GpI(near)2 and GpI-1. In 8 pairings the calculated MANOVA probability is greater than 0.05, indicating that the null hypothesis cannot be rejected. As before, it is emphasised

that the small numbers axes in each MANOVA calculation means that the results need to be treated with caution.

7.5.5 Comparison between IPC Groups Ia, I/Ia, I(near) and IPC Group I sub-groups

Petrographic, MS and geochemical properties of a number of Group Ia, I/Ia and I(near) axes appear similar to those encountered in IPC Group I axes. Geochemical similarities are examined further by standardising the geochemical values in IPC Group Ia, I/Ia and I(near) subgroups, based on SCA statistics from the reduced IPC Group I data set (c.f. Tables 59 & 61) and using the process described in Section 7.3.1.3. SCs are then calculated from these standardised variates using SC1 and 2 in Tables 59 & 61. It is therefore expected that IPC Group Ia, I/Ia, I(near) axes with similar elemental concentrations to IPC Group I axes will plot close to the origin of the associated SC chart and within the ranges (illustrated as ellipses) seen for IPC Group I axes. The distribution of the standardised data is displayed as SC scatter plots in Figure 71.

Figure 71 (upper) clearly shows the majority of axes plotting inside the reduced IPC Group I ellipse, suggesting similarity to IPC Group I. GpI(near)1 plot reasonably close together, but outside the ellipses supporting the decision to generate a new sub-group from these axes, and that they are different to the majority of IPC Group I axes. Lo114 does not plot outside the upper chart ellipse as might have been expected since it has been excluded from the GpI/Ia sub-group. This highlights the problem of using this method alone to indicate axe relationships (c.f. Section 7.3.1.4) and can be illustrated by comparing elemental concentrations and associated standardised variates between axes Lo114 and Lo115 (the latter selected as a representative member of IPC Group I/Ia). Table 69 shows that it is the negative standardised variate for Ti that reduces SC1 (SC1= Ti + Y + Zr + Nb) to 3.52, thus countering the effect of Y and Nb variates.

	Ti	Y	Zr	Nb	SC1 = Ti + Y + Zr + Nb	SC2 = Nb - Y
Lo114 (ppm)	6,500	54.6	200	12.4		
Standardised variate	-2.19	2.77	0.95	1.99	3.52	-0.79
Lo115 (ppm)	17,300	42.2	224	13.5		
Standardised variate	0.54	0.94	1.77	2.36	5.62	1.42

Table 69 Comparison of immobile elemental concentrations and associated standardised values (based on IPC Group I reduced data set) to show how two different sets of concentrations can return similar SC values.

The decision to exclude Lo114 from GpI/Ia is supported in the lower chart in Figure 71 where the axe is seen to plot well outside the ellipse and away from other IPC group I/Ia

members. Figure 71 (upper) shows that Co152/738 is geochemically different to IPC Group I and the other IPC Group Ia axes that are represented. This observation is used to decide that Co152/738 is to be removed from GpIa-1 and therefore, its geochemical data will not be used in DA calculations.

Comparison between Figures 65, 66 and 71 shows that axes from Essex (Es10, Es25) and London (Lo113, Lo115, Lo116, Lo16(63) Lo52(263)) share geochemical similarities with some IPC Group I axes from Essex, London, Oxfordshire, Gloucestershire and Wales. This is not as clearly seen between mobile element Figures 68, 69 and 71 (lower chart), but there is some visual evidence to support a similar, county related, distribution pattern. Again, attention is drawn to the limited data set used in the analysis which allows no definite conclusions may be made.

7.5.6 Summary and conclusion from IPC Group Ia, I/Ia & I(near) examination

It has been shown that within each of IPC Group Ia, I/Ia and I(near) there is at least one anomalous member, suggesting it has been incorrectly assigned. Inspection of the geochemical data, supported by MS and petrographic examination (where available) resulted in the formation of 5 sub-groups: GpIa-1, GpIa-5, GpI/Ia, GpI(near)1 and GpI(near)2 (Table 67 and Table 70 below) MANOVA statistics between the IPC Groups as a whole suggest the some of the groups may be statistically different at a 5% level of confidence, but there are too few cases in each sub-group to allow any definite conclusions to be drawn. MANOVA analysis did indicate similarity between GpIa-1, Ia-5, I(near)2 and IPC Group I. This was borne out in SCA, where clusters for these 3 sub-groups fall within the IPC Group I ellipses indicating potential geochemical similarity.

	GpIa-1 (n=1) (ppm)	GpIa-5 (n=1) (ppm)	GpI/Ia (n=5) (ppm)	GpI(near)1 (n=2) (ppm)	GpI(near)2 (n=4) (ppm)
K	4 700	9 200	3 360	9 850	3 800
Ca	57 600	85 100	80 100	85 500	60 475
Ti	15 800	21 100	17 080	4 900	18 525
Mn	1 500	3 200	1 600	1 450	1 450
Fe	110 400	149 000	88 880	81 650	104 925
Rb	18.9	60.5	21.6	90.9	24.5
Sr	155	117	458	201	218
Y	37.9	38.9	42.9	16.0	37.9
Zr	175	123	184	52.2	160
Nb	5.4	4.6	9.1	-0.7	4.2
Ba	40.3	510	71.0	188	132
Ce	-31.8	-21.6	-23.4	-42.3	-23.2
Pb	34.6	267	429	37.0	180

Table 70 Average elemental composition of the 5 IPC Group Ia, I/Ia & I(near) sub-groups. (Note axe Co152/738 is removed from Gpla-1 as identified in Table 67)

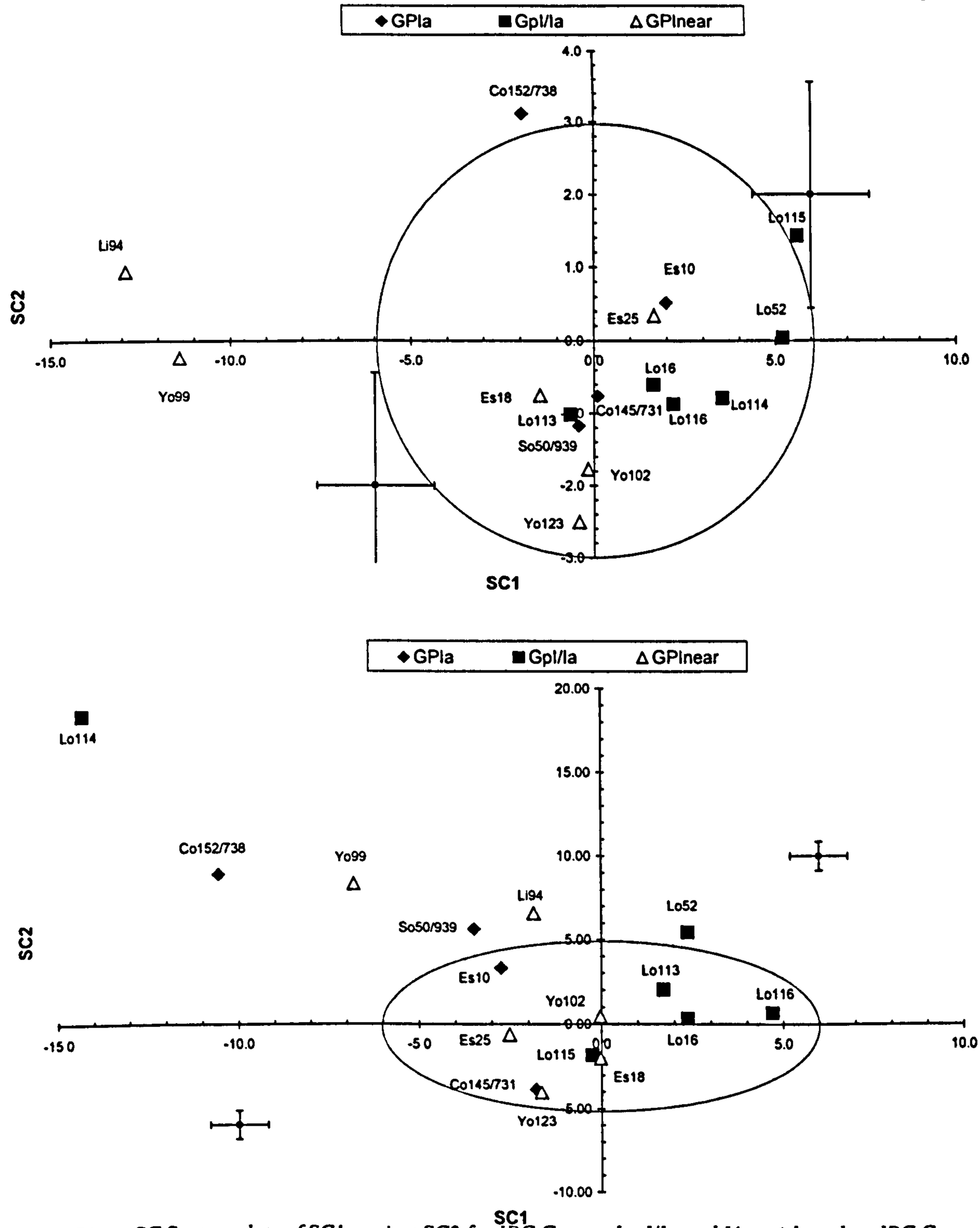

Figure 71 SC Scatter plots of SC1 against SC2 for IPC Groups Ia, I/Ia and I(near) based on IPC Group I SCA analysis of Ti, Y, Zr & Nb (immobile) elements (upper chart) and K, Ca, Fe , Rb , Sr & Ba (mobile) elements (lower) chart. The position of Co152/738 is used to decide that it is atypical of Gpla-1 and will be removed from the discriminant analysis exercise. Li94 & Yo99 (GpI(near)1) are seen to plot well away from other IPC Group I(near) axes confirming that they are significantly different to IPC Group I and other IPC Group I/Ia members. It is already decided to eliminate Lo114 plots from GpI/Ia, however it plots inside the upper ellipse suggesting it has similar immobile element geochemistry to its IPC Group I/Ia members. This situation illustrates the difficulty of using SCA alone to assess similarity between axes (see text for further discussion).

7.6 Examination of IPC Group III and IIIa axe geochemistry

7.6.1 Inspection of IPC Group III and IIIa axe data

Table 71, below, reports the average elemental concentration and associated sd of the 11 IPC Group III axes measured by PXRF and reports the corrected PXRF measurement of the single IPC Group IIIa axe (Wi119/402) measured.

	IPC Group III (n=11) (ppm ±1sd)	IPC Group IIIa (Wi119/402) (ppm)
K	5 773 ± 4 697	4 500
Ca	89 055 ± 14 922	86 900
Ti	16 527 ± 6 704	17 300
Mn	2 000 ± 548	1 600
Fe	102 391 ± 13 211	94 500
Rb	61.5 ± 47.7	75.5
Sr	413 ± 110	497
Y	35.1 ± 13.5	50.2
Zr	177 ± 57.0	181
Nb	9.9 ± 5.7	10.2
Ba	105 ± 115	168
Ce	-24.1 ± 18.5	-13.3
Pb	76.7 ± 56.2	283

Table 71 Average composition of the 11 IPC Group III and one IIIa axes measured by PXRF

Inspection of corrected PXRF measured elemental concentrations of IPC Group III reported in Appendix 23.4 reveals that many axes have at least one unusual elemental concentration compared to the others in the group. This, coupled with the range of corrected MS values for 7 of the 11 IPC Group III axes (0.52 to 1.72 x 10^{-3} SI) means that it is difficult to see if there are any anomalous IPC Group III axes by inspection of data alone.

Five petrographic sub-groups were identified during the examination of IPC Group III thin sections (Chapter 4) and members of two of these sub-groups have been analysed by PXRF (c.f. Table 51). GpIII-1 (Wi4/4 & Wi110/393) appear to have different elemental concentrations to GpIII-2 (Do156/1784, So22/267, Wi199/648, Wi205/687), especially Ti, Rb, Zr and in a few axes Ca, which support the observations that the two sub-groups are different. No members of the other 3 sub-groups (GpIII-3 to 5) were geochemically analysed. Table 72, below, summarises the results from inspecting IPC Group III and IIIa data.

Short Name	Anomalous Element	Magnetic Susceptibility	Comment	Recommendation
Do156/1784	Ca	Not measured	Nothing unusual in field notes. Very high Ca on both measurements taken for axe.	Retain in GpIII-2
Ha107	Ca,	0.91-1.05	Nothing unusual in field notes. Appears similar to GpIII-1	Thin section not examined: do not allocate to sub-group:
Ha8/69	Ti, Fe	Not measured	Nothing unusual in field notes. High Ti & Zr not seen in any other GpIII axe	Thin section not examined: do not allocate to sub-group:
Lo18(65)	Zr, Nb, Ba	0.82-0.94	Alignment of grains seen. High Zr & -ve Ba not seen in any other GpIII axe.	Thin section not examined: do not allocate to sub-group:
So22/267		0.81	Distinctive lath-like feldspars noticed in field observation	Retain in GpIII-2
Wi107/390	Nb, Ce	Not measured	Nothing unusual in field notes. Geochemically similar to Wi376/1453	Thin section not examined: do not allocate to sub-group:
Wi1110/393	Ti, Zr	0.70	Nothing unusual in field notes	Retain in GpIII-1
Wi199/648	K, Y, Ce	0.52	Nothing unusual in field notes. High Y & +ve Ce not seen in any other GpIII axe	Discard from GpIII-2
Wi205/687		1.05-1.12	Nothing unusual in field notes	Retain in GpIII-2
Wi376/1453	Nb, Ce	1.41-1.72	Nothing unusual in field notes. Geochemically similar to Wi107/390	Thin section not examined: do not allocate to sub-group:
Wi4/4	K, Ti, Zr	Not measured	Small fragment, paler in colour than most greenstones. Founder of IPC Group III	Retain in GpIII-1

Table 72 Summary of the inspection of geochemical and MS values seen in IPC Group III axes (see text for discussion and details of the sub-groups)

7.6.2 SCA of IPC Group III PXRF data

SCA analysis of the 11 IPC Group III axes was carried out in two stages, using Ti, Y, Zr & Nb and then K, Ca, Fe, Sr, Ba. Results are contained in Tables 73 & 74 and displayed in Figure 72 below. Standardised errors are calculated as described in Section 7.3.1.5. Rb has been omitted due to its large variation across the group. (Note IPC Group IIIa axe Wi119/402 was not included in the data used for SCA.)

Element	Average (ppm) (n = 11)	SD	Simple Components			
			1	2	3	4
Ti	16,527	6,704	1	0	2	1
Y	35.1	13.5	1	-1	-1	1
Zr	177	57.0	1	0	0	-3
Nb	9.9	5.7	1	1	-1	1
Standardised error			±1.62	±1.56		
Cumulative % of variance			60.5	86.2	95.2	100.0

Table 73 Summary of SCA calculations based upon immobile element concentrations contained in the 11 IPC Group III axes measured by PXRF. Simple component 1 (SC1) = Ti + Y + Zr + Nb. Simple component 2 (SC2) = Nb - Y.

Element	Average (ppm) (n=11)	SD	Simple Component				
			1	2	3	4	5
K	5,773	4,697	1	-1	10	59	-299
Ca	89,055	14,922	-1	4	10	106	-10
Fe	102,391	13,211	-1	-4	-3	141	3
Sr	413	110	1	2	-15	129	15
Ba	105	115	1	-1	12	59	277
Standardised error			±0.32	±0.40			
Cumulative % of variance			44.6	71.1	85.8	97.1	100.0

Table 74 Summary of SCA calculations based upon selected mobile element concentrations contained in the 11 IPC Group III axes measured by PXRF. Simple component 1 (SC1) = K + Sr + Ba - Ca - Fe. Simple component 2 (SC2) = 4Ca + 2Sr - K - 4Fe – Ba

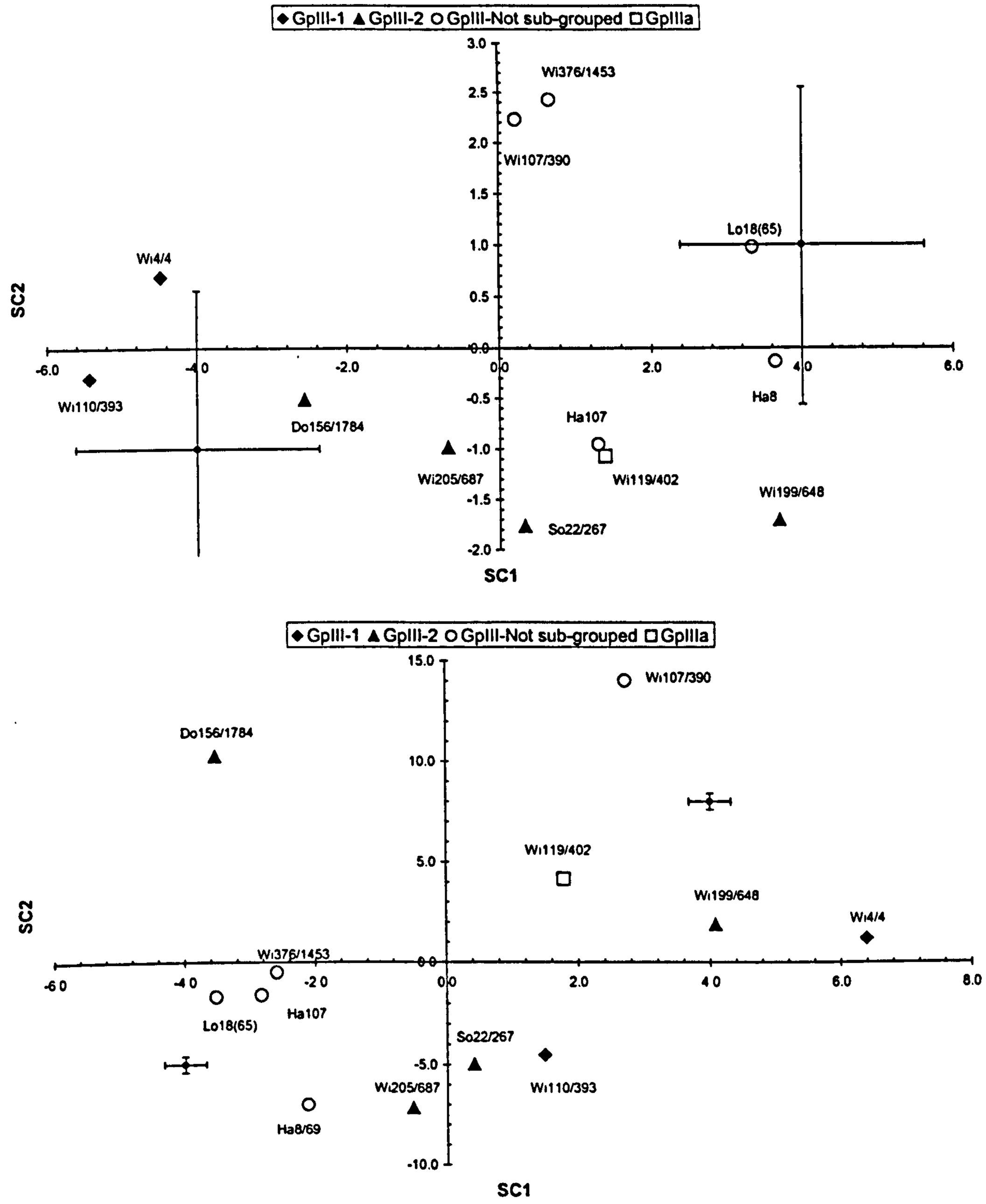

Figure 72 SC Scatter plots of SC1 against SC2 for IPC Groups III & IIIa based on Ti, Y, Zr & Nb (immobile) elements (upper chart) and K, Ca, Fe, Sr & Ba (mobile) elements (lower) chart. SC1 (Ti+Y+Zr+Nb) & SC2 (Nb-Y) (upper) account for 86.2% of the variance seen in the immobile element data, and SC1 K-Ca-Fe+Sr+Ba) and SC2 (4Ca-K-4Fe+2Sr-Ba) (lower chart) account for 71.1% of the variance seen in the selected mobile element data. Low number of data points makes it difficult to see clusters, however, GpIII-1 (Wi4/4 & Wi110) and GpIII-2 (Do156/1784, So22/267, Wi199/648 & Wi205/687) do appear in similar areas of the upper (immobile element) chart. This chart also suggests Wi376/1453 & Wi107/390 share similar immobile element geochemistry. These 'clusters' are not seen in the mobile element (lower) chart.

The immobile element SC scatter plot (Figure 72: upper chart) shows a distribution pattern covering (±6, ±2.5) and the mobile element SC scatter plot shows a distribution covering (±7, ±15) (Figure 72: lower chart). Inspection of the immobile element SC scatter chart shows that GpIII-1 forms a cluster that is separated from GpIII-2 and the other IPC Group III and IIIa axes measured. This is seen as supporting the petrographic observation that GpIII-1 and GpIII-2 are mineralogically different (Section 4.5). Do156/1784, Wi205/687, So22/267, Wi199/648 (sub-group GpIII-2) cluster together in the lower half of the immobile element SC scatter plot, again seen as supporting the petrographic observations of GpIII-2 (Section 4.5).

Inspection of elemental concentrations of the non-sub-grouped IPC Group III axes Wi376/1453 and Wi107/390 that plot in the (+,+) quadrant reveals that these two axes share similar Ti, Y and Nb values. Wi376/1453 has the highest magnetic susceptibility of all Group III axes measured. Do146/1784 plots away from the other IPC Group III axes in the mobile element SC scatter plot due to a very high Ca value, as does Wi107/390 through relatively low Fe and high Ba. However, noting the heavily altered state of Group III thin sections, the large range and variability of mobile element concentrations observed in Appendix 23.4 and illustrated in Figure 72 (lower) is not surprising. The IPC Group III non-sub-grouped axes will not be assigned to any sub-groups at this stage of the examination due to the inconclusive clustering of SC data points.

7.6.3 Comparison between IPC Group III, IIIa and IPC Group I

Figure 73 plots SC1 and SC2 for the IPC Group III and IIIa geochemical data after it has been standardised using the reduced IPC Group I SCA details (Table 59 and 61, c.f. Section 7.5.5, 1st paragraph)

Only four IPC Group III axes fall within both IPC Group I ellipses for both immobile and mobile element plots. Of these, Do156/1784, Wi205/687 & So22/267 are members of GpIII-2. The remaining axe, Ha107, has not been petrographically examined. Wi4/4 is believed to be the founding member of IPC Group III (c.f. Chapter 1 & 4) and, along with Wi110/393, plots well outside the immobile element ellipse indicating a statistical difference with IPC Group I geochemistry (i.e. comparably lower Ti, Y & Zr). Wi107/390 & Wi376/1453 have higher Nb than the reduced IPC Group I accounting for their vertical separation with the immobile element ellipse (recall SC2 = Nb - Y). The only member of

IPC Group IIIa analysed, Wi119/402, shows similarities with both GpIII-2 and IPC Group I and not GpIII-1.

Thus, it appears that GpIII-2 is geochemically similar to IPC Group I and that GpIII-1 is not geochemically similar to IPC Group I. The other IPC Group III axes measured by PXRF, Wi199/648, Wi376/1453, Wi107/390, Lo18(65) and Ha8 also appear to be geochemically different to IPC Group I. Finally, the single IPC Group IIIa axes measured by PXRF, Wi119/402, does appear to be geochemically similar to IPC Group I.

7.6.4 Summary and conclusions from IPC Group III analysis

The 11 IPC Group III and 1 IPC Group IIIa axes can be divided into at least three distinct sub-groups using geochemical and MS measurements, hence questioning the homogeneity of the group. It can be concluded that IPC Group III axes that have been petrographically and geochemically analysed consist of two sub-groups: GpIII-1 and GpIII-2, with the possibility of a 3rd sub-group made up from axes Wi107/390 & Wi376/1453. As GpIII-1 contains Wi4/4 (believed to be the founding member of IPC Group III) it is concluded that the IPC Group III geochemical fingerprint is obtained from the average of Wi4/4 and Wi110/393 PXRF data. The geochemical similarity between GpIII-2 (except Wi199/648) and IPC Group I suggests that these three axes may have previously been incorrectly categorised as IPC Group III. Similarly, the remaining five axes examined (Wi107/390, Wi376/1453, Lo18(65), Ha8, Wi199/648) are sufficiently geochemically different to both IPC Group III and the reduced IPC Group I geochemical averages to suggest they have also previously been incorrectly assigned to IPC Group III, and also that they are not geochemically similar to the reduced IPC Group I set of axes. Table 75 summarises the geochemical composition of the IPC Group III sub-groups used in DA.

	GpIII-1 (Wi4/4 & Wi110/393) (ppm ±1sd)	GpIII-2 (Do156/1784, So22/267, Wi205/687) (ppm ± 1sd)
K	10 400 ± 5 657	4 100 ± 2 800
Ca	73 800 ± 6 223	91 933 ± 25 736
Ti	5 800 ± 3 253	16 633 ± 5 382
Mn	2 200 ± 1 273	1 600 ± 300
Fe	96 550 ± 636	105 867 ± 8 871
Rb	107 ± 9.6	39.7 ± 8.3
Sr	430 ± 82.6	381 ± 33.9
Y	21.0 ± 3.4	37.0 ± 7.4
Zr	93.4 ± 0.1	165 ± 15.5
Nb	5.0 ± 2.6	4.5 ± 0.5
Ba	259 ± 216	93.3 ± 33.3
Ce	-43.4 ± 12.7	-35.9 ± 9.3
Pb	66.1 ± 0.6	98.8 ± 90.4

Table 75 Average geochemical composition of GpIII-1 and GpIII-2.

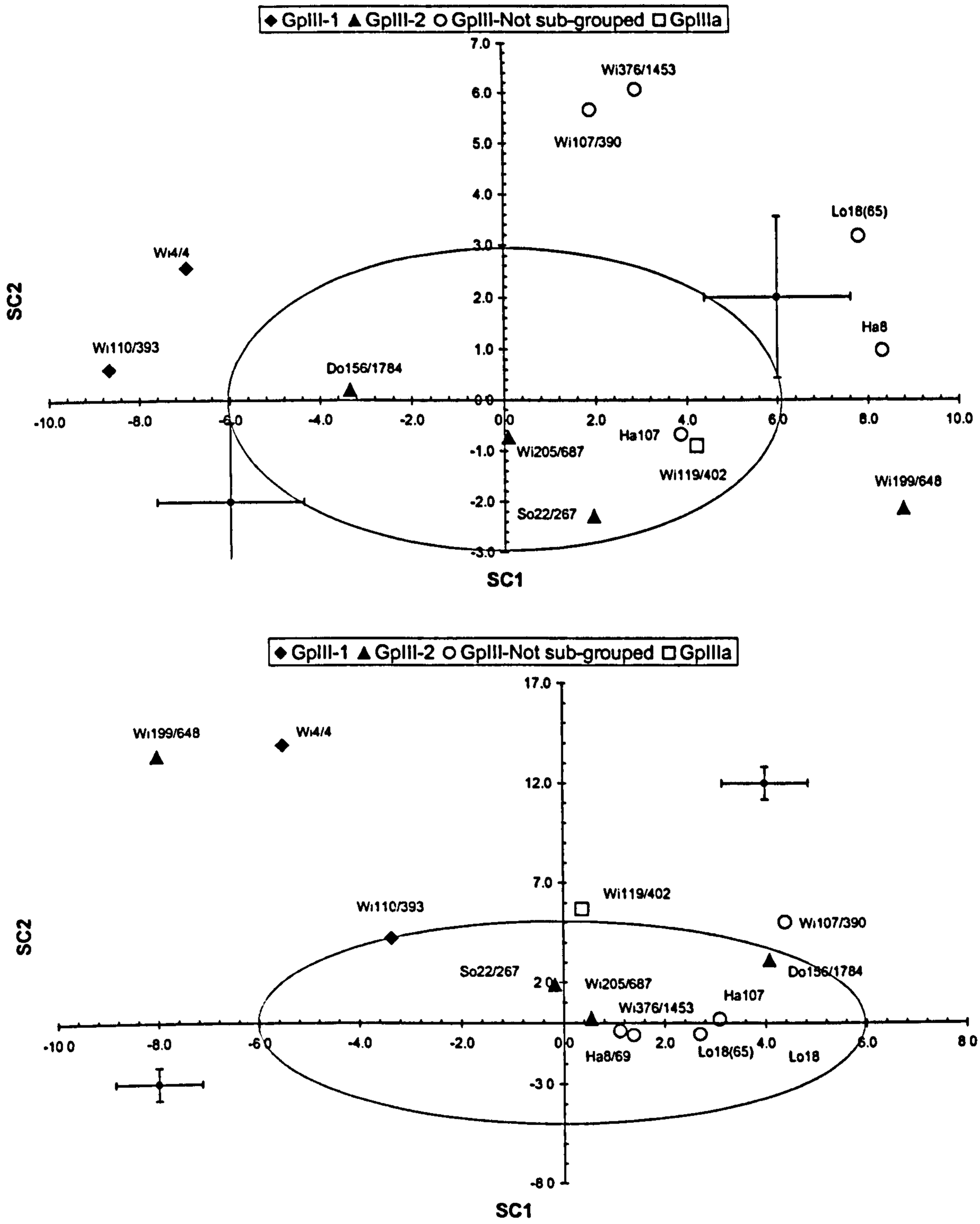

Figure 73 SC scatter plots of SC1 against SC2 for IPC Groups III & IIIa based on IPC Group I SCA analysis of Ti, Y, Zr & Nb (immobile) elements (upper chart) and K, Ca, Fe , Sr & Ba (mobile) elements (lower) chart. GpIII-1 (representative of IPC Group III) appears to be different to IPC Group I as would be expected given that they form different IPC Groups. However, GPIII-2, except Wi199/648, appears to share geochemical similarities with IPC Group I, along with Ha107 & Wi119/402 (IPC Group IIIa). On the basis of SC evidence Wi199/648 is different to other GpIII-2 axes and is therefore excluded from further statistical analyses.

7.7 Discriminant analysis of IPC grouped axes using PXRF data

7.7.1 Overview of discriminant analysis (DA) exercise

Discriminant analysis (DA) is used to assign each of the 272 grouped and ungrouped axes analysed by PXRF to one of the 16 seed groups identified in Sections 7.4, 5 & 6 and listed in Table 76 below. DA is carried out three times:

1. Based on elements Ti, Y, Zr, Nb and assuming prior probability of allocation to seed groups is equal
2. Based on elements K, Ca, Fe, Rb, Sr, Ba and assuming prior probability of allocation to seed groups is equal
3. Based on elements Ti, Y, Zr, Nb and assuming prior probability relates to seed group population.

As discussed in Section 7.3.2, the last of the three analyses is not used in further examination of data and is provided for information only.

Results from all three analyses are detailed in Appendix 25.1, with the two DA assuming equal prior probability reviewed in this section. These results have been further condensed, sorted into IPC grouped, ungrouped and Irish axes and have had associated MS values reported to form Appendixes 25.2 to 6. Within these Appendices, seed group and P(G/D) data highlighted in **bold** text indicates that P(D/G) is less than 0.05. The same data in ***bold*** and ***italic*** text indicates that P(D/G) is less than 0.10. Axe MS range outside the 0.23 to 1.89 x 10^{-3} SI is also highlighted in bold text (c.f. Section 7.2.2)

This section covers DA of IPC Groups I, Ia, I/Ia, I(near), III and IIIa. DA for IPC ungrouped and non-IPC axes is covered in the next section (7.8) and DA of the Irish doleritic and gabbroic axes is covered in Section 7.9. The same seed groups and assessment criteria detailed below is used in all three sections.

7.7.2 Identification of seed groups and DA assessment criteria

The seed groups used in DA are those petrographic sub-groups and new geochemically determined sub-groups that have been (re-)defined in Sections 7.4, 5 & 6. Table 76 summarises these seed groups and provides details on the membership of each group.

Seed group	Members	Notes
GpI-1	28	Axes listed in Appendix 25.1. (c.f. Section 7.4.4 & Table 62)
GpI-2	4	Co154/740, Co398/1734, Do2/50, Wi101/384 (c.f. Table 62)
GpI-3	2	De49/820, Do15/94 (c.f. Table 62)
GpI-4	12	Axes listed in Appendix 25.1 (c.f. Table 62)
GpI-6	6	Axes listed in Appendix 25.1 (c.f. Table 62)
GpI-7	1	Wi244/966 (c.f. Table 62)
GpI-8	2	Co358/1627, Co363/1632 (c.f. Section 7.4.1, Table 51)
GpI-12	1	Do146/1762 (c.f. Section 7.4.1, Table 51)
GpI-13	1	CoGWA3 (c.f. Section 7.4.1, Table 51)
GpIa-1	1	Co145/731 (c.f. Section 7.5.6 Table 70)
GpIa-5	1	So50/939 (c.f. Section 7.5.6, Table 70)
GpI/Ia	5	Lo113, Lo115, Lo116, Lo16(63) Lo52(263) (c.f. Section 7.5.6, Table 70)
GpI(near)1	2	Yo99, Li94 (c.f. Section 7.5.6, Table 70)
GpI(near)2	4	Yo102, Yo123, Es18, Es25 (c.f. Section 7.5.6, Table 70)
GpIII-1	2	Wi4/4, Wi110/393 (c.f. Section 7.6.4, Table 75)
GpIII-2	3	Do156/1784, So22/267, Wi205/687 (c.f. Section 7.6.4, Table 75)

Table 76 List and size of the 16 seed groups used to form the basis (i.e. training se)t for DA

Taking previous petrographical, geochemical and MS data into account, it is felt that there are insufficient numbers of axes within all seed groups, except GpI-1, GpI-4 and possibly GpI-6, such that assignment of an axe by DA to a seed group cannot be taken as definite proof that the axe is geochemically the same as others in that seed group. However, it is felt that there is sufficient data to confidently state whether axes are geochemically similar to the reduced IPC Group I sub-groups (defined below). Hence, the following criteria is used to assess geochemicai similarity using DA:

1. IPC Group I is deemed to comprises seed groups GpI-1, GpI-2, GpI-3, GpI-4, GpI-6, GpI-7 (Section 7.4). Axes with both first and second highest allocations to any of these seed groups using DA of the immobile and mobile elements are considered to be geochemically similar to the reduced IPC Group I set of axes (n=130).
2. Sub-groups GpIa-1, GpIa-5, GpI/Ia, GpI(near)2 and GpIII-2 have been identified as being petrologically and/or geochemically similar to the reduced IPC Group I set of axes. Hence axes with both first and second highest allocations to any of these seed groups (or the 6 IPC Group I sub-groups) using DA of the immobile and mobile elements are considered to be geochemically similar to IPC Group I.
3. IPC Group III is represented by GpIII-1 only. Axes need to be assigned to this seed group by both immobile and mobile element DA in order for it to be considered to be geochemically similar to IPC Group III.
4. Sub-groups GpI-8, GpI-12, GpI-13, and GpI(near)1 are petrographically and geochemically different to the reduced IPC Group I and IPC Group III (as represented by GpIII-1). Therefore, axes assigned to any of these 4 seed groups using immobile element DA are considered to be geochemically different to IPC Group I or III.

The criteria above are also subject to the following two observations:

1. Axes with P(D/G) less than 0.05 are almost certainly unlike other members of the assigned seed group (c.f. Section 7.3.2). This means that these axes may not be assigned on the basis of DA results, as they are sufficiently geochemically different to other members of that seed group.
2. Ungrouped axes with MS values outside the IPC Group I corrected minimum to maximum MS range (0.23 to 1.89 x 10^{-3} SI) (c.f. Section 7.2.2) are unlikely to be recommended for placement in IPC Group I, even if DA indicates that they are geochemically similar to the reduced IPC Group I data set.

Finally, immobile element DA results are given the most weighting for those cases where one or more of the 4 assignments (1st & 2nd highest probability for immobile & mobile element DA) is not to a reduced IPC Group I or the GpIII-1 seed group.

7.7.3 DA of IPC Group I PXRF data

Appendix 25.2 summarises the results of DA of the 149 IPC Group I axes analysed by PXRF using the 16 seed groups identified (data from Appendix 25.1).

Inspection of Appendix 25.2 shows that all 19 axes identified for exclusion during the initial inspection of geochemical data have anomalous DA results (as would be expected since the inspection procedure and discriminant analysis share similar processes). In addition to these 19 axes (detailed in Table 55), axe Co398/1734 is recommended for exclusion from the reduced IPC Group I and axes Ca15 and Ha23/330 are considered as borderline cases. In these three cases the IPC may want to re-examine the classification of these axes.

In summary, 20 of the 149 IPC Group I axes analysed by PXRF have been identified as having some elemental, and/or MS, values noticeably different to the majority of IPC Group I axes examined to question their continued inclusion in IPC Group I. Two further axes are borderline cases and a second examination is really necessary before assignation can be concluded either way. Of the axes examined it appears that approximately 13 to 15% may have been mis-categorised as IPC Group I. If it is assumed that the 149 axes examined are representative of the whole IPC Group I, then it is therefore possible that 13 to 15% of IPC Group I (52 axes) may have been incorrectly assigned.

7.7.4 DA of IPC Groups Ia, I/Ia & I(near) PXRF Data

It is already apparent through inspection of geochemical data and SCA statistics that some axes within these three IPC groups share similarities with axes within IPC Group I (c.f. Section 7.5). Reviewing the results in Appendix 25.3 and using the criteria set out above, it is judged that axes Es10, Co145/731 (IPC Group Ia), Lo113, Lo115, Lo16(63), Lo52(263) (IPC Group I/Ia) and Es18, Es25, Yo102, Yo123 (IPC Group I(near)) have sufficiently similar geochemical and MS characteristics with IPC Group I to indicate that they are probably closely related to IPC Group I. Two other axes, So50/939 and Lo116 are only possibly related to IPC Group I, whereas IPC Group I(near) axes Li94 & Yo99 share some geochemical similarities with GpIII-1 (i.e. IPC Group III). IPC Group Ia axes Co152/738 and IPC Group I/Ia axe Lo114 are geochemically different to conclude that they are probably not related to IPC Groups I or III.

It is therefore concluded that the IPC may wish to re-examine the classification of all 16 axes assigned to IPC Groups Ia, I/Ia and I(near) as 10 are geochemically (and have MS) similar to IPC Group 1, 2 are probably related to IPC Group 1, 2 share geochemical similarities with IPC Group III (GpIII-1) and 2 may have been incorrectly assigned. If it is assumed that the number of axes examined for each of the three IPC groups is representative of the whole group then it follows that there is an approximately 62.5 to 75% chance that axes within IPC Groups Ia, I/Ia and I(near) are geochemically and magnetically similar to IPC Group I. Conversely, there is an approximate 12.5% (2/16) chance that an axe within these IPC groups has been mis-categorised as they are geochemically (and/or magnetically) unlike the majority of other IPC Group Ia, I/Ia and I(near) axes.

7.7.5 DA of IPC Group III PXRF data

Inspection and SCA of geochemical data has shown that IPC Group III is heterogeneous (c.f. Section 7.6). This is borne out by the IPC Group III DA results in Appendix 25.4. Wi4/4 and Wi110/393 are the only IPC Group III axes (as expected since they form GpIII-1 the archetypal IPC Group III). Sub-group GpIII-2 (Do156/1784, So22/267, Wi205/687) is seen to share geochemical similarities with IPC Group I, except Wi199/648 which is unlike IPC Group I or III seed groups. Ha107 and possibly Lo18(65) from those IPC Group III axes not sub-grouped (i.e. not petrographically examined as part of this work) are similar to IPC Group I. The remaining three IPC Group III axes examined, Ha8/69,

Wi107/390, W376/1453, cannot be assigned to either IPC Group I or III on the basis of their geochemical make up.

Wi119/402, the only representative of IPC Group IIIa analysed, has geochemical characteristics that indicates it is probably related to IPC Group I than IPC Group III (Appendix 25.4).

With 11 of the 20 axes assigned to this Group by the IPC having been measured by the PXRF, DA results indicate that IPC Group III axes stand a better chance of being similar to IPC Group I than IPC Group III. Of the axes examined, which represent over 50% of axes currently catalogued as IPC Group III, there is only an approximately 18% chance that an IPC Group III axe is similar to Wi4/4 and Wi110/393 (GpIII-1).

7.7.6 Review of DA on established IPC Groups

DA has shown that many IPC grouped axes have sufficiently anomalous geochemical concentrations to exclude them from the reduced IPC Group I or IPC Group III. In part, the discrimination exercise is a similar process to inspecting and analysing the data by SCA, ANOVA and MANOVA, hence similar results were expected and have been observed. This means that it is eminently feasible to develop a system whereby an axe could be statistically categorised using geochemical and magnetic data that has been obtained without harming the axe. This process of DA being used to assess the geochemical similarity of axes is developed further in the next section where IPC ungrouped and non-IPC axes are considered.

The 16 axe seed groups originated as petrographically or geochemically distinct sub-sets of their original IPC groups and, in total, the seed groups account for 75 of the 272 axes measured by PXRF. DA has statistically assigned all 272 axes to these 16 seed groups and as such the population of a seed group after DA is likely to be different, as previously ungrouped axes are now assigned and original members excluded. This is illustrated in Table 77, below, where the geochemical composition for the original seed groups GpI-1, GpI/Ia and GpIII-1 are shown alongside the geochemical composition of the seed group after DA, hence including new members (and possibly excluding original members). The details for the seed groups after DA are taken from the immobile element DA, and exclude any axes assigned to the seed groups with P(D/G) less than 0.05.

	GpI-1 before DA (n=28) (ppm±1sd)	GpI-1 after DA (n=23) (ppm ±1sd)	GpI/Ia before DA (n=5) (ppm ± 1sd)	GpI/Ia after DA (n=37) (ppm ± 1sd)	GpIII-1 before DA (n=2) (ppm ±1sd)	GpIII-1 after DA (n=12) (ppm ± 1sd)
K	3 025 ± 2 183	4 152 ± 3 850	3 360 ± 994	4 365 ± 2 917	10 400 ± 5 657	8 225 ± 5 962
Ca	62 454 ± 11 622	60 943 ± 13 747	80 100 ± 11 765	72 975 ± 11 183	73 800 ± 6 223	64 008 ± 24 215
Ti	15 343 ± 3 872	15 957 ± 2 685	17 080 ± 2 718	16 989 ± 2 602	5 800 ± 3 253	6 091 ± 2 638
Mn	1 668 ± 584	1 470 ± 407	1 600 ± 245	1 746 ± 542	2 200 ± 1 273	1 383 ± 622
Fe	97 600 ± 13 521	95 517 ± 10 753	88 880 ± 12 502	98 924 ± 13 084	96 550 ± 636	79 975 ± 22 658
Rb	27.3 ± 27.3	34.2 ± 39.9	21.6 ± 24.0	30.9 ± 31.2	107 ± 9.6	58.5 ± 60.3
Sr	247 ± 104	284 ± 152	458 ± 210	351 ± 160	430 ± 82.6	319 ± 182
Y	32.1 ± 6.7	29.5 ± 4.2	42.9 ± 2.9	43.7 ± 5.3	21.0 ± 3.4	23.4 ± 3.7
Zr	165 ± 31.0	172 ± 18.7	184.2 ± 29.7	198 ± 23.4	93.4 ± 0.10	83.6 ± 23.9
Nb	6.9 ± 2.7	8.5 ± 1.7	9.1 ± 3.4	10.9 ± 1.8	5.0 ± 2.6	4.8 ± 2.5
Ba	103 ± 82.1	89.2 ± 43.5	71.0 ± 30.5	120 ± 118	259 ± 216	154 ± 154
Ce	-32.0 ± 9.4	-25.4 ± 9.6	-23.4 ± 8.4	-26.1 ± 12.6	-43.4 ± 12.7	-36.3 ± 22.6
Pb	107 ± 98.6	122 ± 106	429 ± 513	136 ± 203	66.1 ± 0.6	116 ± 213

Table 77 Table illustrating the difference in seed group membership and geochemical composition before and after DA

In general, it can be seen in Table 77 above and in Appendix 23.9 that the sd associated with Ti, Y, Zr and Nb seed group averages are mainly smaller after DA using these elements and subsequently removing axes with P(D/G) less than 0.05. This reduction in sd has increased the statistical separation between seed groups for the 4 elements and this useful increase in *discrimination* between groups is utilised in Section 7.10 where Ti, Y, Zr and Nb are used in geochemical element discrimination diagrams.

7.8 Allocation of IPC ungrouped and non-IPC greenstone axes to axe sub-groups using SCA and DA supported by MS measurements

7.8.1 IPC ungrouped and non-IPC axes

IPC ungrouped axes (identified in Table 51 and listed in Appendix 23.5) are those 55 greenstone axes measured by PXRF that have not been assigned by IPC workers to one of the IPC greenstone groups. Clough & Cummins (1988) list these axes as 'greenstone' and it is not known if thin sections are available for these axes, or that examination of thin sections has proved inconclusive. This means that it cannot be assumed that these axes will have similar geochemical characteristics to any IPC group, or even with any other ungrouped greenstone axe. Non-IPC axes includes 8 that have been made recently as part of ongoing experiments by Mr D Weddle into axe manufacturing processes and are included here since the material used was collected from local Cornish sources. In addition, 9 'non-IPC' greenstone axes that have yet to be listed by the IPC have been analysed by PXRF and are included in this examination (details in Appendix 2.7 and 2.8)

Examination of the geochemistry of the 72 IPC ungrouped and non-IPC axes is carried out by standardising the axe data using the SCA results from the reduced IPC Group I data set (Tables 59 & 61)). The results are plotted on 4 SC scatter plots by county of origin; two using immobile element concentrations (Figure 74) and two using mobile element concentrations (Figure 75). As discussed (Section 7.3.1.4) the proximity of the axe data to the origin (0,0) of the SC scatter plot axes is potentially indicative of the similarity of the axe to the reduced IPC Group I average.

DA, using the 16 seed groups detailed in Table 76 is carried out to complement to observations made using the SC scatter plots. DA results are detailed in Appendix 25.1, summarised in Appendix 25.5, with relevant results reported in Table 78.

7.8.2 Examination of IPC ungrouped and non-IPC axe geochemistry using established SCA statistics

Figures 74 and 75 contain the SC scatter plots based on the standardisation of IPC ungrouped and non-IPC axes.

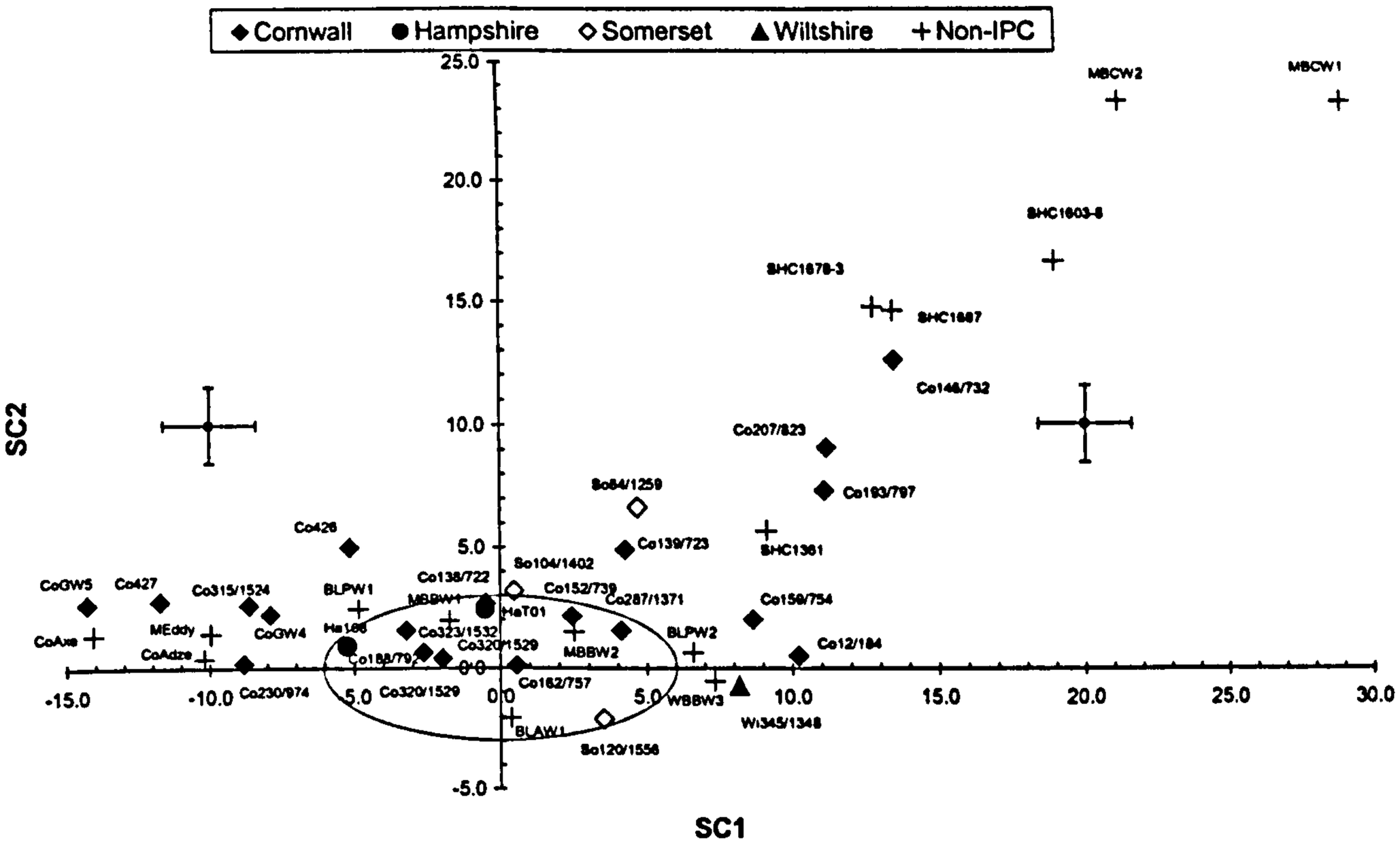

Figure 74 SC scatter plots of SC1 against SC2 for IPC ungrouped and non-IPC axes based on IPC Group I SCA analysis of Ti. Y. Zr & Nb (immobile) elements. No clear patterns emerge from the two charts except an increasing trend to higher values is observed the (+,+) quadrant, reflecting overall increased immobile element concentrations, with increase in Nb>> increase in Y for axes plotting in this area. (SC2 = Nb - Y). In total 30 axes plot inside or close to the ellipse.

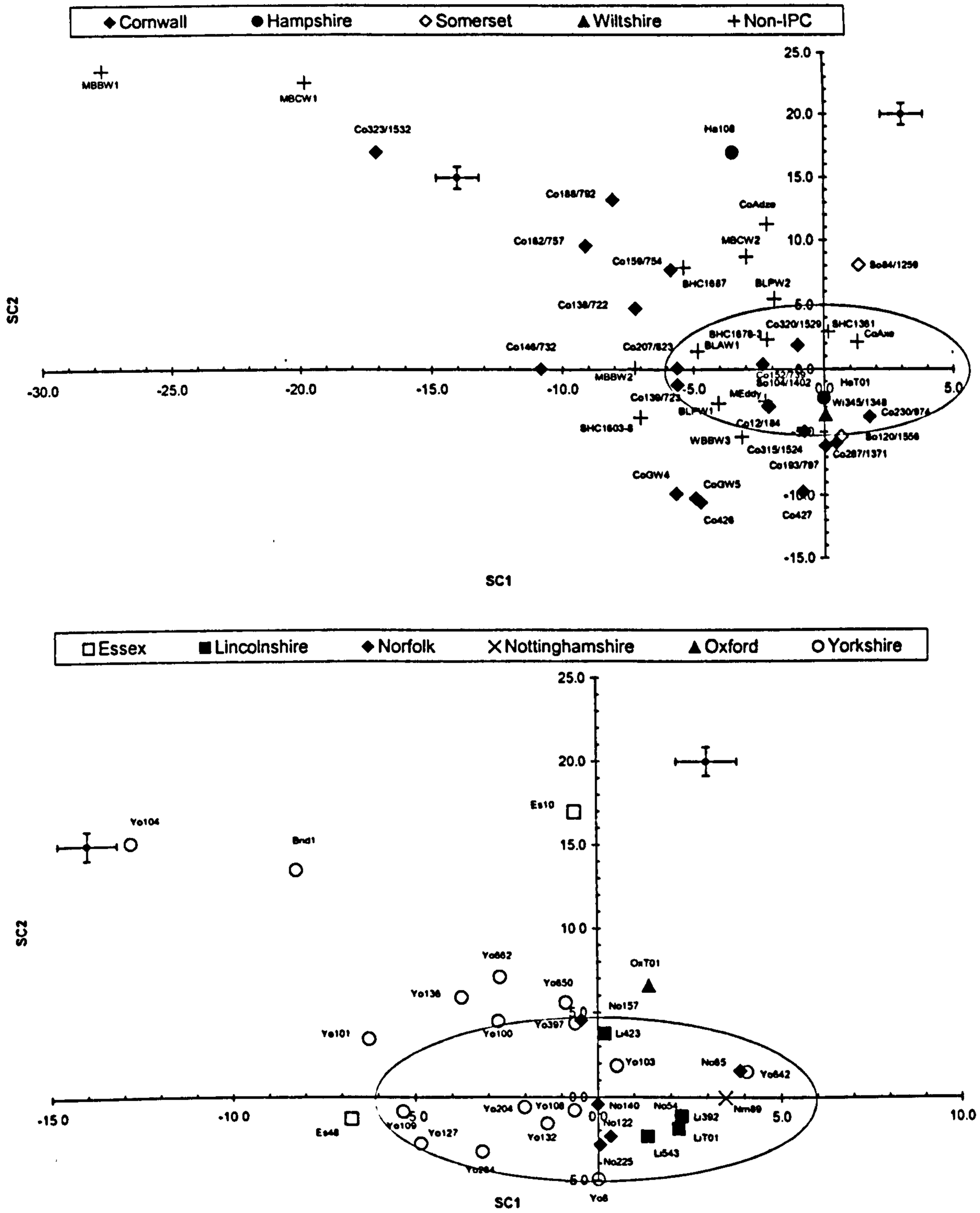

Figure 75 SC scatter plots of SC1 against SC2 for IPC ungrouped and non-IPC axes based on IPC Group I SCA analysis of K, Ca, Fe, Rb, Sr & Ba (mobile) elements. All axes from Norfolk and Lincolnshire as well as the majority from Yorkshire fall within the ellipse suggesting a regional similarity with IPC Group I. Axes in the (-,+) quadrant show a trend of increasingly negative SC1 and positive SC2, thus having comparably higher K and Ba than axes in the other three quadrants.

As indicated in Section 7.3.1.4, axes that plot within or close to the ellipses, indicating the 90% range that the reduced IPC Group I data falls within, potentially have elemental compositions similar to the reduced IPC Group I average. This potential is further examined using DA (Section 7.8.3 below))

Examinations of Figures 74 & 75 show that there are 30 axes that appear to be geochemically similar to the average reduced IPC Group I geochemistry. All 5 ungrouped Norfolk (**No122, No140, No157, No225, No54 and No65**) and 4 Lincolnshire (**Li392, Li423, Li543, LiT01**) axes fall within, or very close to the ellipses in Figures 74 and 75 indicating a potential geochemical similarity with the average reduced IPC Group I geochemical composition. Likewise **Yo100, Yo103, Yo132, Yo204, Yo284** and possibly **Yo108, Yo642 and Yo397** appear to have similar geochemistry to that of IPC group I. **Co320/1529, Co153/739 and Co287/1371** are the only 3 of the 18 Cornish axes examined in this section that fall in or are close to mobile and immobile element ellipses. The small number of representatives from Nottinghamshire (**Nm89**), Oxfordshire (**OxT01**), Hampshire (**HaT01** only), Wiltshire (**So120/556, Wi345/1348** only) also appear to have similar elemental concentrations to IPC Group I. Finally, **BLAW1 and BLPW1** from the non-IPC collection fall within both ellipses with **BLPW2 and WBBW3** plotting just outside both ellipses.

7.8.3 DA of IPC ungrouped and non-IPC greenstone axes

Following on from Section 7.7, each of the axes within the two ungrouped categories are assigned to one of the 16 seed groups using DA. The results of the analysis are contained in Appendix 25.1 and summarised in Appendix 25.5, which includes MS values where available. Table 78, below identifies those IPC ungrouped and non-IPC groups meeting or coming close to meeting the criteria set out in Section 7.7.2.

	Immobile 1st	2nd	Mobile 1St	2nd	MS	Indication
Co153/739	*GpI-4*	GpI-1	GpI-1	GpI(near)2	0.87 – 1.06	? IPC Group I
Co287/1371	GpI/Ia	GpI-6	GpIa-1	GpI-6	1.06 - 130	? IPC Group I
Co320/1529	**GpIa-5**	GpI(near)2	GpI-12	GpI-7	2.90 – 3.30	Not IPC Group I
HaT01	GpI-1	GpI-3	GpI-1	GpI(near)2	**3.92 – 4.49**	?IPC Group I
Li392	GpI-2	GpIII-1	GpI/Ia	GpI-6	0.77 – 0.83	**IPC Group I**
Li423	*GpI/Ia*	GpIa-5	GpIII-2	GpI-6	0.69 – 0.79	? IPC Group I
Li543	GpI/Ia	GpI-6	GpI-6	GpI-4	0.75 – 0.91	**IPC Group I**
LiT01	GpIa-1	GpIII-2	GpI/Ia	GpI-4	1.32 – 1.61	**IPC Group I**
Nm89	GpI-2	GpIII-1	GpI/Ia	GpI-3	0.70 – 0.80	? IPC Group I
No122	GpI/Ia	GpI-6	GpI(near)2	GpI-1	0.66 – 0.87	**IPC Group I**
No140	GpI-4	GpIa-1	GpI-4	GpI-1	-	**IPC Group I**
No157	GpI-4	GpI-1	GpIII-2	GpI-3	0.55 – 0.68	**IPC Group I**
No225	GpI-1	GpI-3	GpI-6	GpI-1	0.73 – 0.84	**IPC Group I**
No54	**GpIII-1**	GpI-2	GpI-6	GpI-2	-	Not IPC Group I or III
No65	GpIII-1	GpI-2	GpI/Ia	GpI-3	-	? IPC Group III
OxT01	GpI-2	GpI-1	GpI-3	GpI-7	-	**IPC Group I**
So120/1556	GpI/Ia	GpI-6	GpIa-1	GpI-6	-	**IPC Group I**
Wi345/1348	GpI/Ia	GpI-6	GpIa-1	GpI-6	**87.3 – 93.4**	Not IPC Group I
Yo100	GpI/Ia	GpI-6	GpIII-1	GpI(near)2	0.95 – 1.16	**IPC Group I**
Yo103	GpI-7	GpI-2	GpI-7	GpI-1	-	**IPC Group I**
Yo108	GpI/Ia	GpI-6	GpI-6	GpI-4	0.63 – 0.83	**IPC Group I**
Yo132	GpI-6	GpI/Ia	GpI-1	GpI(near)2	0.57 – 0.66	**IPC Group I**
Yo204	GpI-4	GpIa-1	GpI-1	GpI(near)2	0.67 – 0.77	**IPC Group I**
Yo284	GpIa-5	GpI(near)2	*GpIa-1*	GpI(near)2	1.60 – 1.84	? IPC Group I
Yo397	GpIa-5	GpI-7	GpIII-2	GpI(near)1	0.91 – 1.05	Not IPC Group I
Yo642	GpI-4	GpI/Ia	GpI-7	GpI-3	0.56 – 0.65	**IPC Group I**
BLAW1	GpIa-1	GpIII-2	GpI-2	GpI-1	0.87 – 0.99	**IPC Group I**
BLPW1	GpI-2	GpI-8	GpI-2	GpI-1	1.51 – 1.72	? IPC Group I
BLPW2	GpI/Ia	GpI-6	GpI-2	GpI-3	1.51 – 1.72	**IPC Group I**
WBBW3	GpI/Ia	GpI-4	GpIa-1	GpI(near)2	1.50 – 1.61	**IPC Group I**

Table 78 Summary of DA results for the 30 IPC ungrouped and non-IPC axes identified in Section 7.8.3. Axes that are geochemically similar to the reduced IPC Group I data set are indicated in bold. DA assignments indicated in bold have associated P(D/G) less than 0.05. MS indicated in bold is outside the range determined for IPC Group I.

Inspection of Table 78 shows that there are 18 axes that meet the criteria for assignment to IPC Group I set out in Section 7.7.2 and can therefore be declared as being geochemically (and magnetically) similar to the reduced IPC Group I elemental composition. In addition there are 8 'borderline cases that may be IPC Group I and one axe (No65) that is borderline for IPC Group III. Inspection of Appendix 25.1 and 25.5 further reveals that there are several axes that share similarities with the non-IPC Group I sub-groups: GpI-8, GpI-12, GpI-13 & GpI(near)1 indicating the possibility that these axes may form discrete sub-sets of greenstone axes not yet recognised. The assignment of 3 non-IPC axes BLAW1, BLPW1 and WBBW3 to IPC Group I provides some clues as to the origin of the IPC Group since these axes were collected as loose cobbles from beaches on the northern coast of Penwith Peninsula.

7.8.4 Comments on the assignment of IPC ungrouped and non-IPC axes

The process followed in this section uses data that has been obtained using non-destructive PXRF and MS methods. But, the basis for selecting the seed groups used for DA is partially through petrographic examination of thin sections, a partly destructive process. So it cannot be stated that the assignment of axes to petrological groups using this method is *totally* non-destructive. Further, as this is the first time the two non-destructive processes have been used to indicate the similarity of axes to existing petrological groups, further checks relating to the accuracy of the process in correctly assigning axes may be required before it is adopted. This could be achieved by petrographically examining the 18 axes identified in Table 78 as being geochemically similar to IPC Group I to see if they are also mineralogically and texturally similar to IPC Group I axes.

7.9 Comparison between Irish gabbroic & doleritic axes and British greenstone axes using PXRF & MS measurements and petrographic observations

7.9.1 Introduction

Mandal (1996) reports a similarity between 6 thin sections of Irish dolerite and gabbro axes and IPC Group I axes, reaching the conclusion that some Irish axes could have been sourced from Cornish exposures (Mandal op. cit.: table 6.4 and p 154). This section complements Mandal's work using PXRF and MS measurements of 22 Irish doleritic and gabbroic axes and compares them with PXRF and MS measurements made on IPC grouped axes. (Note that all but 2 Irish axes also have WDXRF analyses using the method described in Section 7.1.1. However, Mandal's WDXRF data is not used as the relationship between PXRF and WDXRF measurements using the 'thin' pellets has yet to be established.)

Although axe NMI 1908-3 is included in Appendix 27 (and Appendix 23.7: PXRF data) it has not been thin sectioned and has therefore not been allocated to any of the Irish groups discussed below.

Names and short petrographic descriptions of the Irish dolerite and gabbro axes that have been examined as part of this work is followed by a short discussion on the possibility of Irish axes being related to IPC Group I & III. A comparison between Irish and Group I geochemistry is carried out by standardising Irish axe PXRF elemental values using SCA values established for the reduced IPC Group I data set (n=130). Finally discriminant analysis is used to ascertain the best matches between Irish axes and the 16 axe seed groups identified in Table 76.

7.9.2 Irish dolerite axes: Overview (after Mandal 1996: section 6.3)

Mandal (1996: table 6.5) identified 27 doleritic axes using petrographic thin sections. Generally, Mandal states Irish dolerite axes to be medium grained, ophitic to sub-ophitic *olivine* dolerites that have a large range of textures from fresh to amphibolised. Primary axe mineralogy consists of plagioclase, pyroxene, *minor* olivine with secondary amphibole, epidote and chlorite. The most common oxide present is ilmenite, commonly altered to sphene. Mandal sub-divided these 27 doleritic axes into 2 main sub-groups: 9 Dolerite I and 18 Ungrouped dolerite (which are further sub-divided into 5 sub-sub-groups) on the basis of petrographic similarity. Six of the 27 Irish doleritic axes listed by Mandal were made available at the National Museum of Ireland for PXRF and MS analysis (see

Appendix 27.1 for a list of Irish gabbroic and doleritic axes and Mandal's (1996) sub-groups).

NMI E610:441 is the sole representative of a small sub-group within the Ungrouped dolerites (Ungrouped dolerite 1) that is recognised by a sub-ophitic texture with intergranular olivine and isolated growths of blue & brown amphibole in addition to the primary mineralogy described above. **NMI R1926** represents a small sub-group of the Ungrouped dolerites (Ungrouped dolerite 3) where partly amphibolised, sub-ophitic pyroxenes are present. **NMI 1958:95, NMI 1958:2, NMI 1958:1 and NMI R2574** form a sub-group of the Ungrouped dolerite axes (Ungrouped dolerite 4) where plagioclase and/or pyroxene is considerably altered (data from Mandal 1996: section 6.3c).

Mandal (op. cit.: p154) indicated that geochemical evidence suggested that the dolerites originated from an evolved MORB source. Mandal ruled out the Upper Palaeozoic dolerites in Ireland as the potential source region since the axes contained both ortho- and clinopyroxene. Two axes (NMI1958:1 and NMI 1958:82 (latter not analysed by PXRF)) showed similarities with thin sections from "ungrouped British altered dolerite axes of presumed Cornish origin" (= greenstone?), resulting in the possibility that the source of the some of the Irish dolerite axes could be Cornwall.

7.9.3 Irish gabbro axes: Overview (after Mandal 1996 section 6.2)

Mandal found a wide range of textures in the 46 gabbroic axes identified through examination of axe thin sections (Mandal op. cit.: table 6.3). Generally, all Irish gabbroic axes contained plagioclase feldspar, often altered to epidote and chlorite, ortho and clinopyroxene with rare ophitic texture and often totally altered to amphibole. Primary hornblende and secondary tremolite amphibole is common. Granophyric texture is found in 21 of the 46 axes. Ilmenite is the most common oxide, with magnetite seen in 8 of the 47 axes. Both ilmenite and magnetite are often altered to sphene (Mandal 1966: section 6.2).

On the basis of mineralogy, Mandal divided the 46 gabbro axes three sub-groups: Gabbro I (14), Gabbro II (19) and Ungrouped gabbro (13). **Sixteen** axes, representing all three gabbroic sub-groups, were made available at the National Museum of Ireland for PXRF and MS analysis. Appendix 27.1 lists all 46 gabbroic axes by sub-group.

NMI 1898:23, NMI 1931:164, NMI 1960:506, NMI 1962:240 and NMI W299 were selected, on the basis of availability, from **Gabbro I.** This sub-group is characterised by fresh pyroxene and fibrous uralite radiating from the coarse opaque assemblages. Most plagioclase is altered to epidote/chlorite and accessory quartz is present in all 14 members of the sub-group. Graphic quartz is seen in 8 axes and magnetite is present in most of the sub-group.

NMI 1897:313, NMI 1916:67, NMI 1916:69, NMI 1929:1694 and NMI 1931:143 are from **Gabbro II**, differentiated from other gabbros by the presence of primary amphibole in addition to the general gabbroic mineralogy of plagioclase, altered pyroxene and amphibole. In Gabbro II the main oxide is ilmenite and not magnetite as seen in Gabbro I. Graphic intergrowths of quartz and alkali feldspar are present in 11 of the 19 axes assigned to this sub-group.

The remaining 13 gabbroic axes, **Ungrouped gabbro**, were left ungrouped as they did not share any granophyric texture or secondary amphibole as seen in Gabbro I or II axes, and were sufficiently mineralogically diverse to preclude formation of another gabbroic sub-group. **NMI 1915:25, NMI 1897:311, NMI 1929:1127, NMI 1956:5, NMI 1957:164 and NMI P1954:14** were measured as part of this work.

Geochemically the Irish gabbros are tholeiitic with evolved MORB to within plate basalt affinities. Their level of alteration and mineralogy suggested a non-Irish origin and 17 Irish gabbroic axe thin sections were compared with IPC Group I and IPC ungrouped greenstone axes from Cornish origins. Petrographical comparisons revealed that 5 Gabbro II and 1 Gabbro I axe were similar to IPC Group I and Mandal concluded that these axes **(NMI 1897:313, NMI 1916:67, NMI 1916:69, NMI 1929:1694, NMI 1931:43 and NMI 1931:164)** could be classified as IPC Group I. The remaining 11 Irish gabbroic axes have petrographic similarities to ungrouped Cornish axes, but could not be assigned to an IPC group using petrographic comparisons. On the basis of these results Mandal concluded that there is a distinct possibility that some of the Irish Gabbro axes came from Cornwall, supporting Irish-Cornish trade concepts.

7.9.4 Preliminary discussion of petrographic similarity between Irish dolerite & gabbro axes and IPC Groups I & III

Olivine has not been identified in any IPC Group I and III axe thus the fresher Irish dolerites (Dolerite I, Ungrouped dolerite 1, 2) with accessory olivine are probably not related to IPC Group I & III. Mandal does not make it clear whether olivine is present in the more altered dolerites (Ungrouped dolerite 3, 4 & 5), so assuming that there is no olivine then the remaining mineralogy and texture appears to be petrographically similar IPC Group I & III, thus indicating potentially similar sources.

Magnetite is very rare in IPC Group I or III (Chapter 4 & 5) and primary amphibole has only been found in one thin section examined as part of this work: from Cudden Point (CUD003). In addition, graphic intergrowths of quartz and alkali feldspar have not been noted in IPC Group I or III thin sections. Hence the mineralogy of the Irish Gabbro I and II appears to be dissimilar to IPC Group I and III, the two Cornish groups being considered. However, primary amphibole is found from some exposures on the north coast of Cornwall (Floyd pers. com.) and high MS readings for some axes suggest magnetite is present in a few cases. Hence, Irish gabbroic axes appear to be mineralogically different to IPC Group I or III, but Mandal determined that six of the Irish Gabbro I & II axes share mineralogical similarities with IPC Group I thin sections sufficiently to conclude that they may be IPC Group I. This mineralogical contradiction will need to be examined further and forms a future research topic.

All IPC Group I and III thin sections contain altered pyroxene hence it is not expected that any Irish Ungrouped gabbro axe is similar to axes from these two Cornish groups.

7.9.5 Examination of Irish axe geochemical data using SCA values established for IPC Group I

Irish axe PXRF data (Appendix 23.7) is standardised using average and standard deviations calculated from elemental concentrations of the reduced IPC Group I axe data sets and plotted using simple components (defined in Tables 59 & 61). The ellipses plotted on both charts represent the range of standardised values for IPC Group I axes within which 90% of the 130 IPC Group I axes plotted. As discussed (Section 7.3.1.3), it is assumed that axes that Irish axes that plot within the ellipses probably have similar geochemical concentrations to the average composition of the reduced IPC Group I axes.

Table 79 below reports the average composition of each of the 4 Irish axe groups examined in this work.

	Gabbro I (n=5) (ppm ± 1sd)	Gabbro II (n=5) (ppm ± 1sd)	Ungrouped Gabbro (n=6) (ppm ± 1sd)	Dolerite (n=6) (ppm ± 1sd)
K	7 020 ± 1 840	3 780 ± 1 840	6 200 ± 2 687	2 733 ± 1 912
Ca	82 600 ± 34 185	80 800 ± 5 037	73 100 ± 13 400	76 617 ± 6 368
Ti	15 400 ± 3 269	12 000 ± 4 282	11 417 ± 4 317	13 717 ± 3 519
Mn	1 420 ± 370	1 540 ± 207	1 383 ± 248	1 533 ± 493
Fe	89 280 ± 14 947	96 560 ± 9 827	95 467 ± 9 895	87 133 ± 4 259
Rb	35.1 ± 15.3	13.8 ± 19.5	24.6 ± 42.1	15.0 ± 21.9
Sr	300 ± 76.0	227 ± 21.4	237 ± 66.6	274 ± 85.3
Y	37.8 ± 11.2	34.9 ± 7.1	34.4 ± 16.9	41.9 ± 6.6
Zr	193 ± 75.1	116 ± 39.9	93.3 ± 56.3	146 ± 28.5
Nb	5.2 ± 5.0	2.2 ± 4.1	1.7 ± 2.5	5.7 ± 5.4
Ba	336 ± 164	166 ± 54.3	120 ± 58.9	155 ± 171
Ce	-29.2 ± 15.1	-47.5 ± 6.3	-52.9 ± 13.1	-45.7 ± 5.9
Pb	510 ± 662	120 ± 91.2	196 ± 354	148 ± 167

Table 79 Average geochemical composition of Irish gabbroic and doleritic axes measured by PXRF

Inspection of Figure 76, below, shows the data clusters for the three gabbroic sub-groups and ungrouped dolerite axes overlap to some extent and it is probable that the groups cannot be differentiated by statistical means (hence MANOVA analysis was not carried out).

The four heavily altered Irish dolerite (Ungrouped dolerite 4) axes NMI 1958:1, NMI R2574, NMI 1958:95 & NMI1958:2 plot apart from axes representing the other two dolerite sub-groups on the mobile element SC chart (Figure 76: upper), but close to or within both immobile and mobile element ellipses (apart from NMI 1558:2, which is outside the mobile element ellipse) indicating geochemical similarity with IPC Group I. The fourth heavily altered doleritic axe, NMI 1958:2 stands apart from its co-members as it has Ba concentration twice that of the other doleritic axes (435ppm). The remaining two axes NMI E610:441 & NMI R1926, from separate Irish dolerite sub-groups (Ungrouped dolerite 1 and 3 respectively) appear geochemically similar to each other and have slightly high Y and Nb compared to the other dolerite axes measured. On the basis of SCA, by plotting inside both immobile and mobile element ellipses, axes NMI E610:441, NMI R2574 and NMI 1958.1 appear to be geochemically similar to the reduced IPC Group I average.

Gabbro I axes NMI W299, NMI 1898:23 and NMI 1962:240 plot outside one of the two ellipses, because of high Y, high K & Ba and high Ca & Ba respectively. It is therefore concluded that these axes are not geochemically similar to IPC Group I. Both NMI

1960:506 and NMI 1931:164 plot within both ellipses indicating they are potentially geochemically similar to IPC Group I, although it is noted NMI 1960:506 has high Zr, outside 2sd of reduced IPC Group I average.

Three of the five Irish Gabbro II axes analysed plot outside the immobile element ellipse (Figure 76, upper). NMI 1916:69 & NMI 1916:67 have low Zr and negative Nb, whilst NMI 1931:143 has slightly high Y compared with IPC Group I. On balance the first two axes are unlike IPC Group I, whilst NMI 1931:143 is close to IPC Group I averages with Y being just within 2 sds of the reduced IPC Group I (n=130) average. The two remaining axes, NMI 1929:1694 & NMI 1897:313, plot inside both ellipses indicating potential geochemical similarity with IPC Group I.

All Irish ungrouped gabbros plot outside the immobile element chart ellipse (Figure 76: upper) indicating that these axes are geochemically unlike IPC Group I. Inspection of the PXRF data (Appendix 23.7) confirms this, with three ungrouped gabbros having very low Zr, two with high Y and one with negative Nb. In addition the Zr/Y ratios for Irish ungrouped gabbros is less than 3.2, lower than IPC Group I, which are usually greater than 4. On the basis of this evidence none of the Irish Ungrouped gabbros appear geochemically similar to IPC Group I or III.

In conclusion, inspection of geochemical data using SCA is not conclusive, however it appears that 4 Ungrouped dolerite axes, 2 Gabbro I and 3 Gabbro II axes share similar geochemical compositions with the reduced IPC Group I axes. The possibility of geochemical similarity is examined further using DA supported by MS measurements in the next section.

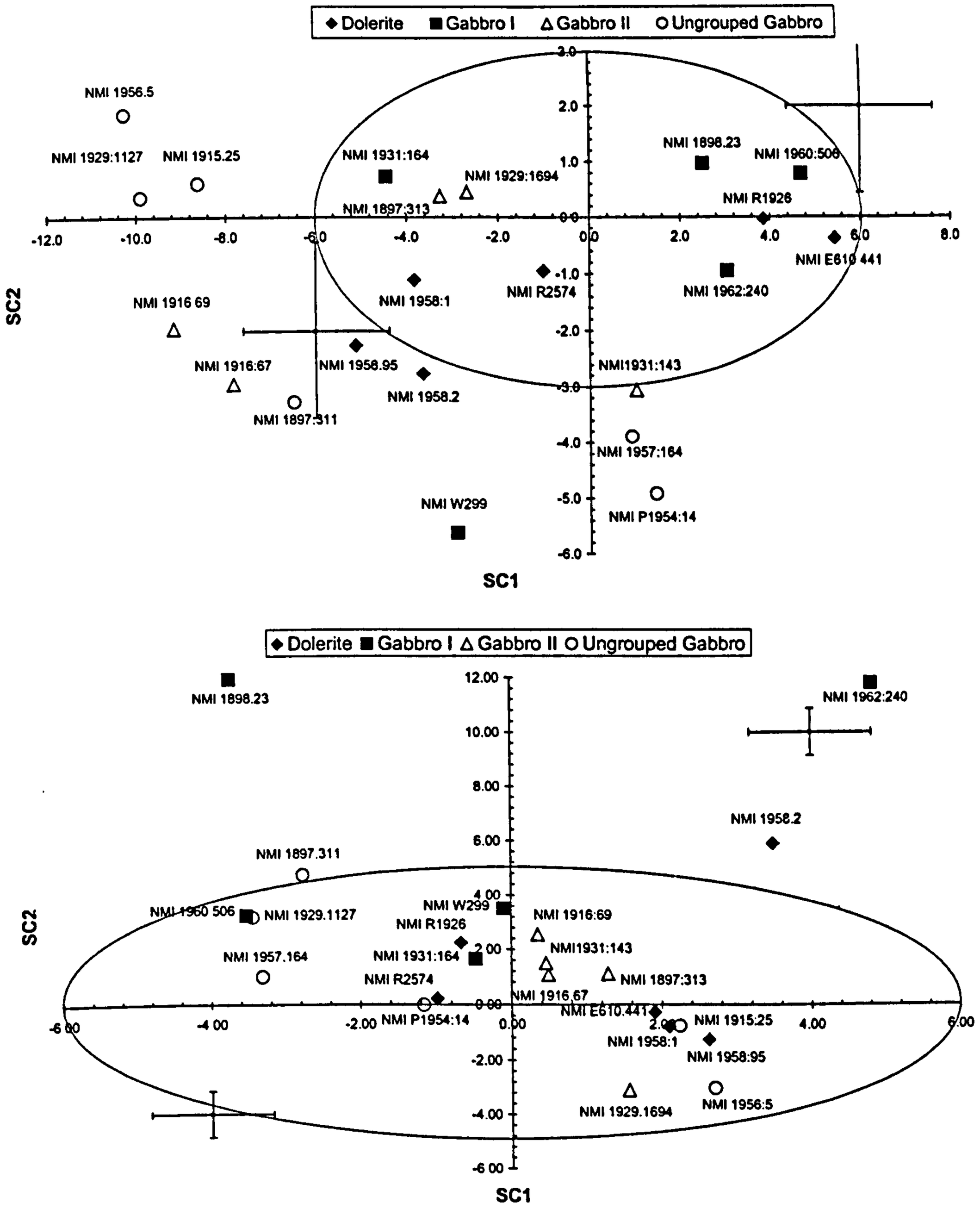

Figure 76 SC scatter plots of SC1 against SC2 for Irish gabbro and dolerite axes based on IPC Group I SCA analysis of Ti, Y, Zr & Nb (immobile) elements (upper chart) and K, Ca, Fe, Sr & Ba (mobile) elements (lower) chart. Although sub-grouped by Mandal, the four axe groups do not appear to form discrete clusters, although smaller pairings between axes within groups is seen (e.g. Gabbro II axes NMI 1916:69 & NMI 1916:67). Whilst not totally conclusive several Irish axes appear within both ellipses and therefore have apparently similar element concentrations to those found in IPC Group I axes, sufficient to indicate these axes may actually be IPC Group I.

7.9.6 DA of Irish axe PXRF data

DA of the 23 Irish axes is carried out using the 16 seed groups introduced in Section 7.7.2. Results from DA are detailed in Appendix 25.1, summarised in Appendix 25.6 and in Table 80 below. Magnetic susceptibility results for the Irish axes are contained in Appendix 27.2)

	Immobile		Mobile		MS	Indication
	1st	2nd	1st	2nd		
Irish Dolerite						
NMI 1958:1	GpI-7	GpI-2	GpI-7	GpI-4	0.70 – 0.75	**IPC Group I**
NMI 1958:2	GpI-7	GpI-6	GpI-12	GpI-7	0.65 – 0.80	? IPC Group I
NMI 1958:95	GpI-7	GpIII-2	GpI-7	GpI-4	0.98 – 1.20	**IPC Group I**
NMI E610:441	GpI/Ia	GpI-6	GpI-7	GpI(near)2	1.77 – 2.34	? IPC Group I
NMI R1926	GpI/Ia	GpI-6	GpI-4	GpIII-2	0.76 – 1.14	**IPC Group I**
NMI R2574	GpI-6	GpI/Ia	GpI-4	GpI-1	0.63 – 0.83	**IPC Group I**
Irish Gabbro I						
NMI 1898:23	GpI/Ia	GpI-6	**GpIII-1**	GpI(near)1	**28.8 – 35.3**	Not IPC Group I
NMI 1931:164	GpI-2	GpI-8	GpI(near)2	GpI-7	**4.78 – 6.30**	? IPC Group I
NMI 1960:506	**GpI-4**	GpIa-1	GpI-2	GpI-3	**14.0 – 18.4**	Not IPC Group I
NMI 1962:240	GpI-4	GpIa-1	**GpIa-5**	GpI(near)1	**21.1 – 29.8**	Not IPC Group I
NMI W299	**GpI(near)2**	GpIII-2	GpI-7	GpI(near)2	**17.4 – 21.4**	Not IPC Group I
Irish Gabbro II						
NMI 1897-313	GpI-2	GpI-7	GpI-7	GpI(near)2	0.50 – 0.66	**IPC Group I**
NMI 1916:67	GpI-7	GpI-8	GpI-7	GpI-4	0.93 – 1.07	? IPC Group I
NMI 1916:69	GpI(near)1	GpI-7	GpI-7	GpI-4	0.65 – 0.80	Not IPC Group I
NMI 1929:1694	GpI-2	GpI-1	GpI(near)2	GpI-6	0.77 – 0.88	**IPC Group I**
NMI 1931:143	GpIa-1	GpIII-2	GpI-7	GpI(near)2	0.48 – 0.58	**IPC Group I**
Irish Ungrouped Gabbro						
NMI 1897:311	GpI-7	GpI-8	GpI(near)1	GpIII-2	0.62 – 0.76	Not IPC Group I
NMI 1915:25	GpIII-1	GpI(near)1	GpI-7	GpI-4	0.65 – 0.98	Not IPC Group I
NMI 1929:1127	GpI(near)1	GpI-8	GpI-2	GpI-1	0.57 – 0.75	Not IPC Group I
NMI 1956:5	GpIII-1	GpI(near)1	GpI-6	GpI-4	0.60 – 0.69	Not IPC Group I
NMI 1957:164	GpI-6	GpI/Ia	GpIa-1	GpIII-2	**19.4 – 22.1**	Not IPC Group I
NMI P1954:14	**GpI-6**	GpIa-1	GpIa-1	GpI-6	1.05 – 1.37	? IPC Group I
Irish Unknown						
NMI 1908:3	**GpI-1**	GpI/Ia	GpIII-1	GpI(near)1	3.09 – 4.05	Not IPC Group I

Table 80 DA results for Irish gabbroic and doleritic axes. Axes indicated in bold appear to share similar geochemical and MS characteristics with the reduced IPC Group I. Sub-group and MS values in bold and/or in boxes indicate P(D/G) is <0.05, that the sub-group is not a recognised IPC Group I sub-group or that the MS values are outside the IPC Group I average range 0.23 to 1.89 x10^{-3} SI..

Four of the six Irish dolerite axes analysed are geochemically and magnetically similar to IPC Group I, and in particular, that they may be related to GpI-7. NMI 1958:2 has mobile element concentrations that assign it to GpI-12, which is not an IPC Group I sub-group (c.f. Section 7.7.2). Magnetically, NMI E610:441, is on the edge of the upper limit the prescribed MS range for IPC Group I.

It is therefore concluded that Irish dolerite axes **NMI 1958:1, NMI 1958:95, NMI R1926 and NMI R2574 are geochemically and magnetically similar to IPC Group I.** Axe NMI E610:441 is geochemically similar to IPC Group I, but has high MS, thus this axe is possibly related to IPC Group I. Finally, NMI 1958:2 has immobile element concentrations similar to IPC Group I, but has Ba concentration of 435ppm, almost 4 times the IPC Group I average of 104 ± 64ppm. Hence this axe may nevertheless be related to IPC Group I, if it is assumed that the high Ba concentration is due to localised enrichment of the source exposure.

Mandal only compared NMI 1958-1 & NMI 1958-2 (of the axes examined here) with IPC thin sections and concluded that they have petrographical similarities with 'ungrouped British dolerite axes of presumed Cornish origin' (Mandal 1996: p 155), although not stating which IPC ungrouped axes.

Mandal (1996) reports that Irish Gabbro I axes contain magnetite and this is supported by the MS measurements (Appendix 27.2 & 27.3) where these axes have distinctly higher MS than all but 3 of the other Irish axes examined. In addition DA results indicate that all Gabbro I axes, apart from NMI 1931:164 appear geochemically different to the average composition of the reduced IPC Group I data set (n=130). These findings complement those given by Mandal (1996: table 6.6, p142) where axe NMI 1931:164 is described as being petrographically similar to (undefined) IPC Group I axes (but it is known the same IPC Group I thin sections examined by Mandal have also been examined in this work). **Hence NMI 1931:164 is possibly related to IPC Group I** and appears to be geochemically and magnetically different to other members of Gabbro I examined here.

DA of Irish Gabbro II axes identified **NMI 1897:313, NMI 1929:1694 and NMI 1931:143 as being geochemically similar to the reduced IPC Group I** (and possibly GpI-7?). These three axes also have MS within the 0.23 to 1.89 $x10^{-3}$ SI range established for membership of IPC Group I. NMI 1916:69 and NMI 1916:67, both have negative PXRF measured Nb and comparatively low Zr, Ti and Y concentrations compared to the reduced IPC Group I averages and are thus NMI 1916:67 is only possibly related to IPC Group I, whilst it is unlikely that NMI1916:69 is related to IPC Group I.

Mandal (1996: table 6.4) indicates that all 5 Irish Gabbro II axes share petrographical similarities with IPC Group I and this observation is geochemically supported for 3 axes and possibly supported in the other two.

DA of the 6 Ungrouped Gabbro supported by MS indicates only NMI P1954:14 appears to be possibly similar to the reduced IPC Group I although this axe has higher Y concentrations than most IPC Group I axes and has P(D/G) <0.05 based on the immobile element DA. Mandal did not find any direct similarities with Ungrouped Gabbro and IPC Group I, other than to suggest that four (NMI 1915:25, NMI 1897:311, NMI 1929:1128, NMI 1956:5) were 'Cornish' in origin and thus related to the ungrouped greenstone axes listed.

7.9.7 Remarks on the comparison between Irish and British axes

SCA and discriminant analysis of the 23 Irish doleritic and gabbroic axes analysed as part of this work shows that 7 of them are geochemically and magnetically similar to the reduced IPC Group I. From the results above, there is very good correlation between conclusions drawn by Mandal (op. cit.) and those arrived out through statistical analysis of the geochemistry of the axes supported by MS.

Table 81 summarises the geochemical and MS supported conclusions reached in this section with those put forward by Mandal. There are 14 cases where axes have been examined by both Mandal and in this work. In six cases, full agreements is reached and seven cases, provisional agreement is reached. There is only one case, axe NMI1916:69, where there is disagreement: petrographically the axe appears similar to IPC Group I, whereas geochemically it is different to the reduced IPC Group I data set.

The discussion above reveals that there is petrographical, geochemical and magnetic evidence that 7 of the Irish doleritic and gabbroic axes examined above are similar enough to IPC Group I greenstone axes to strongly suggest they were sourced from the similar greenstone rock outcrop(s). SCA and DA results compare favourably with those previously obtained through petrographic analysis, with full or provisional agreement reached in 13 out of the 14 cases examined in this work and by Mandal. DA results indicate a strong resemblance between GpI-7 and the Irish axes that are geochemically similar to IPC Group I and this suggests that a closer inspection between Co64/588, Wi244/966 & Wi49/172A (GpI-7) and the Irish '*IPC Group I*' designates is carried out.

Although the results above are encouraging, and show the potential of using totally non-destructive techniques to assign axes to IPC groups, a few questions remain. These relate to the slight differences in observed mineralogy between IPC Group I axes and the geochemically similar Irish gabbroic and doleritic axes. The reported presence of olivine in Irish dolerites, and graphic quartz-alkali feldspar intergrowths in gabbroic axes, is not seen in IPC Group I thin sections.

As a final remark, a number of Irish axes were geochemically analysed using WDXRF and it will be interesting to note how the PXRF and the WDXRF analyses made by Mandal (1996) compare.

Irish axe	Mandal (1996)	This work	Agreement ?
Irish dolerite			
NMI 1958:82	Cornish	Not examined	n/a
NMI 1958:1	Cornish	**IPC Group I**	Provisional
NMI 1958:2	Not examined	Possibly IPC Group I	n/a
NMI 1958:95	Not examined	**IPC Group I**	n/a
NMI E610:441	Not examined	Possibly IPC Group I	n/a
NMI R1926	Not examined	**IPC Group I**	n/a
NMI R2574	Not examined	**IPC Group I**	n/a
Irish Gabbro I			
NMI 1898:23	Ungrouped	Not IPC Group I	**Yes**
NMI 1931:164	**IPC Group I**	Possibly IPC Group I	Provisional
NMI 1960:506	Ungrouped	Not IPC Group I	**Yes**
NMI 1962:240	Ungrouped	Not IPC Group I	**Yes**
NMI W299	Not examined	Not IPC Group I	n/a
Irish Gabbro II			
NMI 1897:313	**IPC Group I**	**IPC Group I**	**Yes**
NMI 1916:67	**IPC Group I**	Possibly IPC Group I	Provisional
NMI 1916:69	**IPC Group I**	Not IPC Group I	No
NMI 1929:1533	Ungrouped	Not examined	n/a
NMI 1929:1694	**IPC Group I**	**IPC Group I**	**Yes**
NMI 1931:143	**IPC Group I**	**IPC Group I**	**Yes**
Irish Ungrouped Gabbro			
NMI 1897:311	Cornish	Not IPC Group I	Provisional
NMI 1915:25	Cornish	Not IPC Group I	Provisional
NMI 1929:1127	Not examined	Not IPC Group I	n/a
NMI 1929:1128	Cornish	Not examined	n/a
NMI 1956:5	Cornish	Not IPC Group I	Provisional
NMI 1957:164	Ungrouped	Not IPC Group I	Provisional
NMI P1954:14	Ungrouped	Possibly IPC Group I	n/a

Table 81 Comparison between assignation of axes by Mandal and as part of this work. It is seen that there is agreement that 3 of the 6 axes identified as IPC Group I by Mandal (indicated in bold) are also geochemically and magnetically similar to the reduced IPC Group I derived in this work. ('Ungrouped' indicates similarity between Irish axes and ungrouped greenstone axes in the IPC collection (Mandal 1996: table 6.4), suggesting a Cornish origin only.)

7.10 Assessment of axe rock petrogenesis using immobile and trace element discrimination diagrams

7.10.1 Initial considerations when using element discrimination diagrams

This section uses six established immobile and trace element discrimination diagrams (collectively referred to as 'element discrimination diagrams') (after Rollinson 1993) in order to examine the potential petrogenesis of the greenstone rock used to make axes. As noted in Chapter 2, element discrimination diagrams are to be used with care as it is not always known whether the criteria for using the discrimination diagram have been met. Specifically:

1. Samples should be from fresh, unaltered exposures of basalt
2. Ti-Y, Ti-Y-Zr and Ti-Y-Sr element discrimination diagrams apply to tholeiitic basalts with the compositional range 20%> CaO + MgO >12% by weight (Rollinson 1993: p 174)
3. Basaltic rocks with cumulate phases may give erroneous classification
4. Recalculating to 100% for plotting on ternary element discrimination diagrams may cause samples to be grouped when no real relationship exists (Butler & Woronov 1986)

It is known that greenstones are altered basalts and dolerites, but that the level of alteration is unlikely to have mobilised the four immobile elements Ti, Y, Zr and Nb (Chapter 4). Thus, although criterion 1 above is not met, it is not thought to pose major problems in relation to conclusions drawn from the examination of greenstone geochemistry. However, Sr is deemed as being relatively mobile (Rollinson 1993; p 120) as it belongs to the LFS (low field strength) group of elements. Therefore the Ti–Y–Sr element discrimination diagram will not be used to determine the genesis of greenstones.

MgO concentrations have not been determine by the PXRF, hence it is not known if criterion 2 above has been met. However, evidence from previous analyses of Cornish greenstones does show that all altered tholeiitic basalts and dolerites from Cornwall do meet the criteria 20% > CaO + MgO >12% (Floyd pers. com.). So it is assumed that criterion 2 above has been met for IPC Group I and III axes, since they have already been assessed as being tholeiitic (Section 4.6.2).

No evidence of cumulate phases has been seen within macroscopic and microscopic examination of IPC grouped axes. Thus it is assumed criteria 3 is not relevant to this work.

Criterion 4 above, that clusters on ternary diagrams may be seen where there are none, can only be noted at this stage.

Finally, it was reported in Chapter 6 (Section 6.12.4) that there may be some anomaly in PXRF measurements of Ti concentrations. Up to now, this has not been a problem since only PXRF Ti measurements have been used, and as such the relative differences between Ti measurements only has been examined. In using element discrimination diagrams to identify the petrogenesis of a particular rock, the absolute value of Ti is required. As noted in Section 6.12.4 PXRF Ti measurements of rock samples may be 10 to 15% understated, representing approximately 1,000 to 3,000ppm when considering the average Ti concentrations reported by the PXRF for axes (10,000 to 20,000ppm). Thus, conclusions drawn from examination of element discrimination diagrams that use Ti will take note of the potential understatement of Ti.

This section provides the link to Chapter 8 where axe and exposure geochemistry is compared using six immobile element discrimination diagrams (c.f. Appendix 30). Figures 77 to 80 are included in this chapter as they continue to illustrate the geochemical relationships between axe sub-groups. Using 3 binary and 3 ternary element discrimination diagrams described below, the likely petrogenesis for each axe sub-group will be assessed. This will allow the geographical location of potential exposures to be restricted to those exposures that produce rocks from similar tectonic settings (thus narrowing the provenancing search parameters). It will also display elemental ratios (e.g. Nb:Zr) which are not seen through SCA and DA statistical methods above, but commonly used to distinguish igneous rock types.

7.10.2 Element discrimination diagrams

Figures 77 to 80 contain the 6 immobile element discrimination diagrams: three binary: **Zr v Ti, Zr v Nb and Zr v Zr/Y** and three ternary: **Zr-Ti-Y, Zr-Nb-Y and Zr-Ti-Sr** (note Zr-Ti-Sr is included as 2 of the 3 elements are immobile, but see comment above). IPC group sub-group averages (i.e. seed groups) are plotted in Figures 77 and 78, whereas IPC group sub-groups determined after DA (i.e. seed groups with new membership after DA) are shown in Figures 79 and 80 (see Section 7.7.6, Table 77). As shown in Section 7.7.6 the sub-group immobile element sds are generally smaller after DA, and thus the sub-groups are more statistically distinct from each other. Sub-group averages prior to DA are

reported in Tables 62, 70 and 75 and summarised, along with averages after DA, in Appendix 23.9. **All element discrimination diagrams in Figures 77 to 80 are produced full size in Appendix 26.3.**

The error bars plotted on Ti–Zr and Nb–Zr element discrimination diagrams represent ±2sd of the associated sub-group average or ±2 PXRF SD where there is only one measurement. Error bars are not included in the Zr/Y v Zr binary plot and the three ternary plots since elemental *ratios* are plotted and not absolute values.

Inspection of Figures 77 to 80 show:

1. IPC Group I sub-groups GpI-1, 3, 4 & 6 form a cluster on Zr–Ti and Zr-Nb charts by virtue of similar Zr, Ti, & Nb values.
2. IPC Group I sub-groups GpI-2 & 7 form a small cluster on Zr –Ti and Zr-Nb charts, separated from other IPC Group I sub-groups by differing Zr & Ti.
3. IPC Group I (minus GpI-8, 12, 13) generally falls into the 'within plate tholeiite' and MORB fields of the three ternary diagrams.
4. GpI-13 (CoGWA3) plots well away from the other sub-groups, its position suggesting it is tholeiitic and originated within an oceanic arc
5. GpI-8 plots away from IPC Group I sub-groups (as expected) and within the MORB/within plate fields on Zr–Ti & Zr–Zr/Y charts.
6. GpI-12 (Do146/1762) has high Zr, Ti & Nb accounting for its position, which suggests alkali affinities (Zr-Nb-Y diagram)
7. GpIa-1, GpIa-5, GpI(near)2, GpI/Ia and GpIII-2 form a loose cluster on all binary charts and in a similar position to IPC Group I sub-groups.
8. GpI(near)1 appears to have Island Arc affinities, possibly volcanic arc type tholeiite.
9. GpIII-1 has low immobile elements and is probably a primitive tholeiite with MORB-type affinities.
10. An increase in separation of the data clusters is seen on charts plotting sub-group averages after DA (discrimination). (Note GpI-12 & 13 have moved the most since they now contain a comparatively large number of axes).
11. Low Nb averages indicate that all sub-groups (apart from GpI-12 (high Nb), GpI-13 (very low Nb) probably source from the South Cornish melange (Roseland Breccia formation) or possibly from within the Mylor Slate Formation (after Floyd 1993).

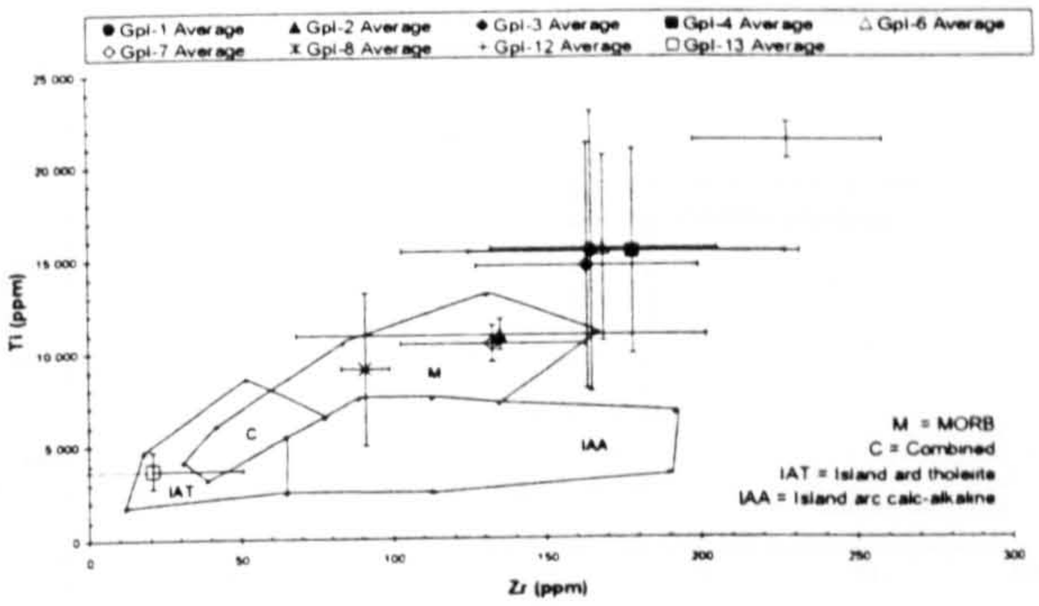

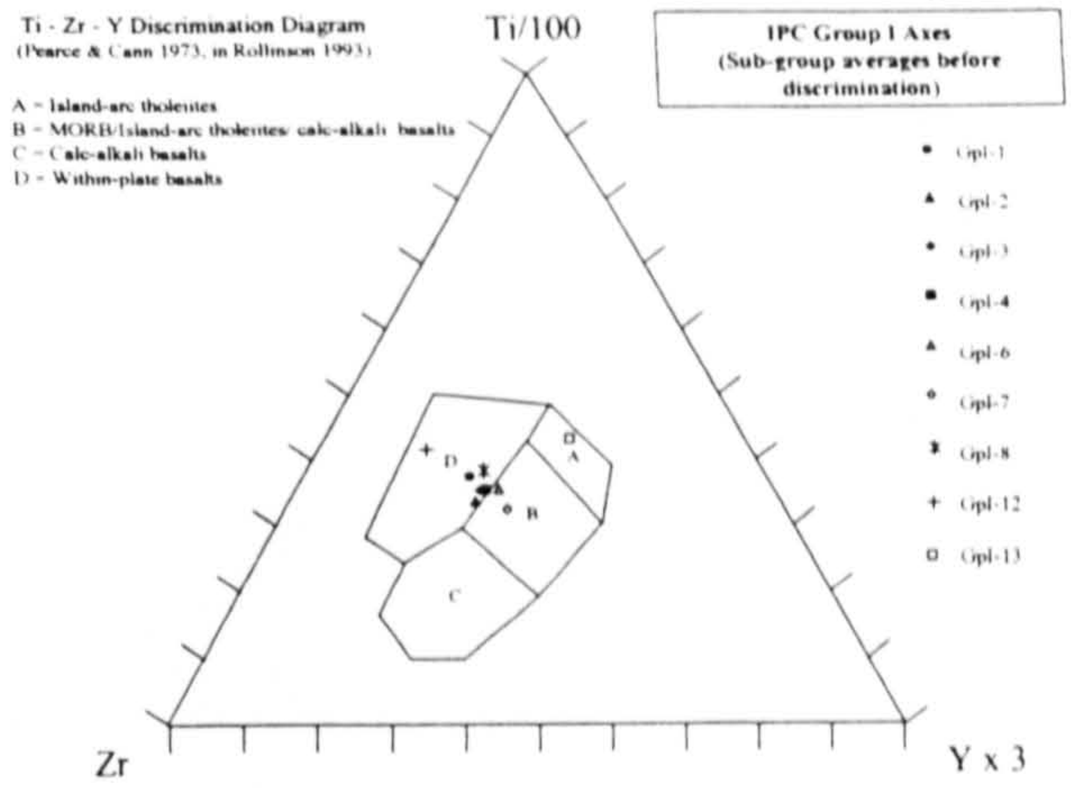

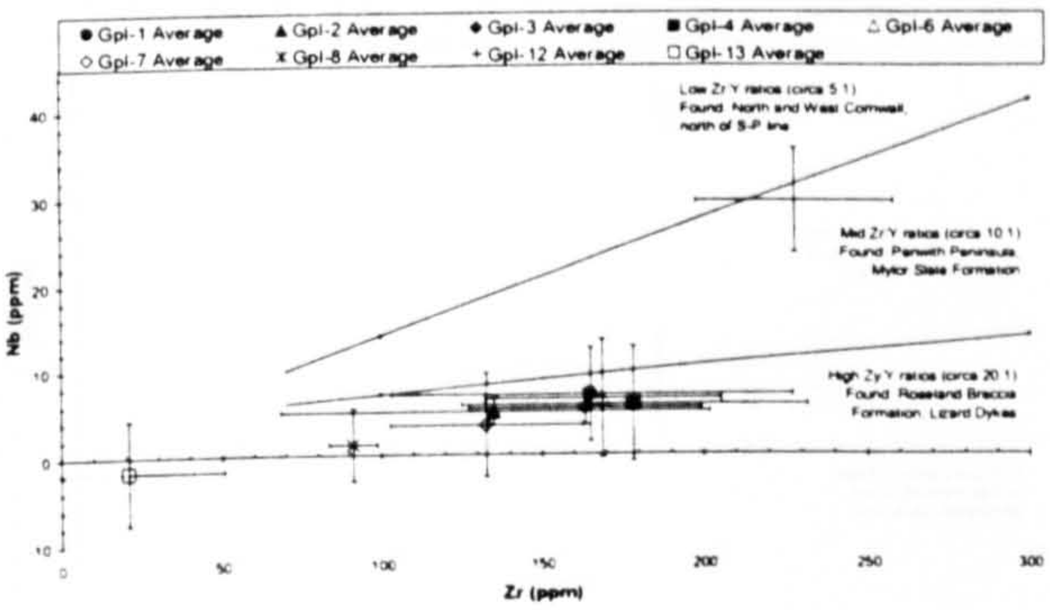

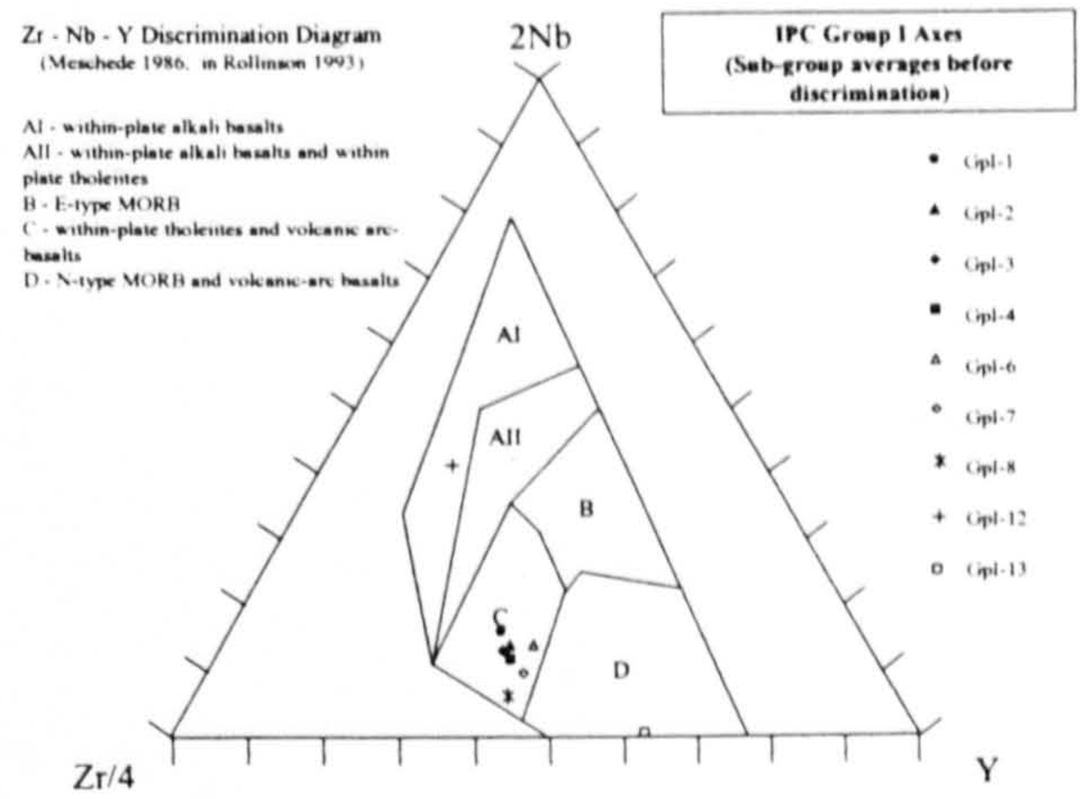

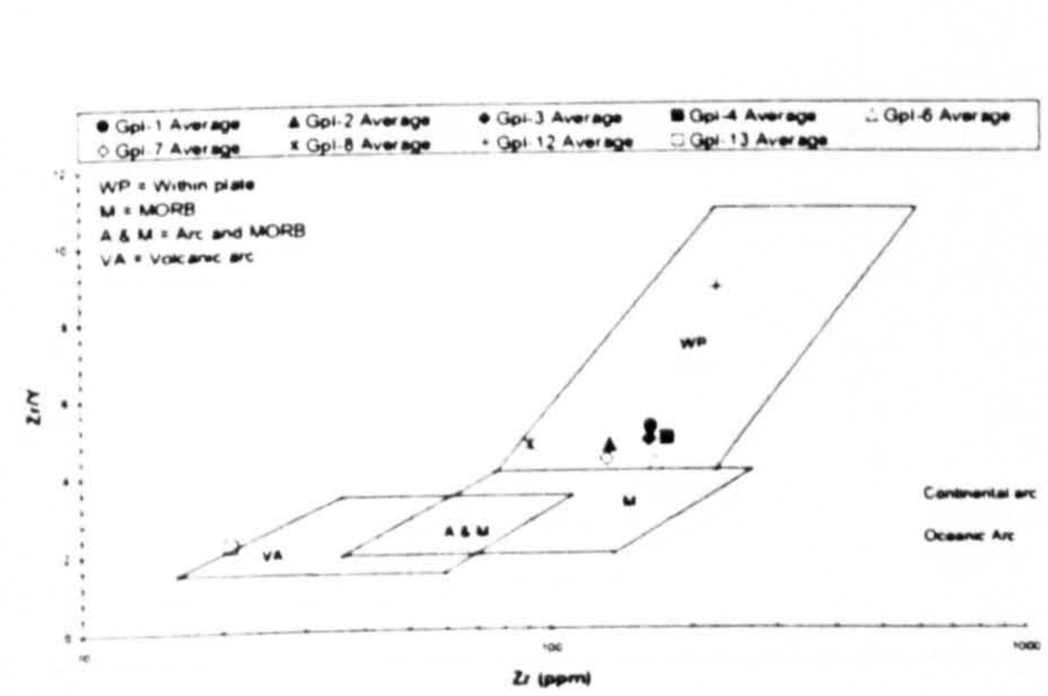

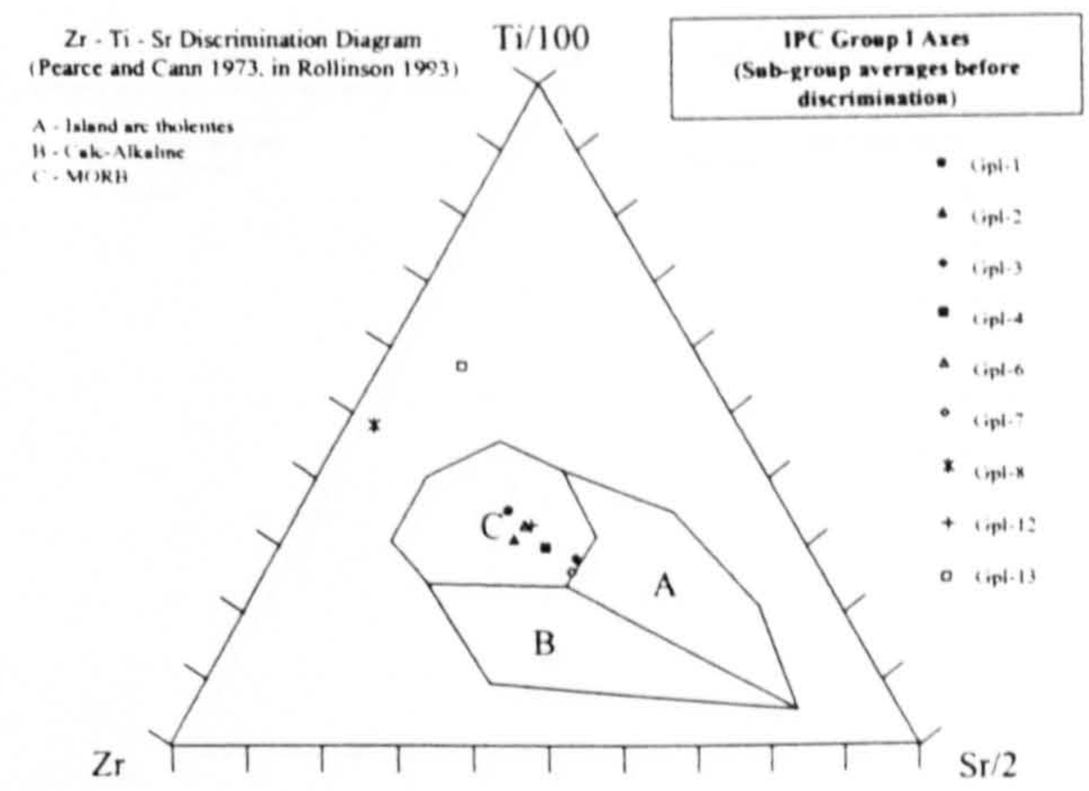

*Figure 77 Six binary and ternary element discrimination diagrams(after Rollinson 1993 & Floyd 1996) showing the position of **IPC Group I sub-group** immobile element averages and associated ±2sd error bars (c.f. Appendix 23.9, 26.1 & Appendix 30 for details). See text for discussion. Note that these diagrams are intended to discriminate between fresh and unaltered basalts meeting certain criteria so due consideration is necessary when using these charts to determine the genesis of greenstones (c.f. Section 7.10.1)*

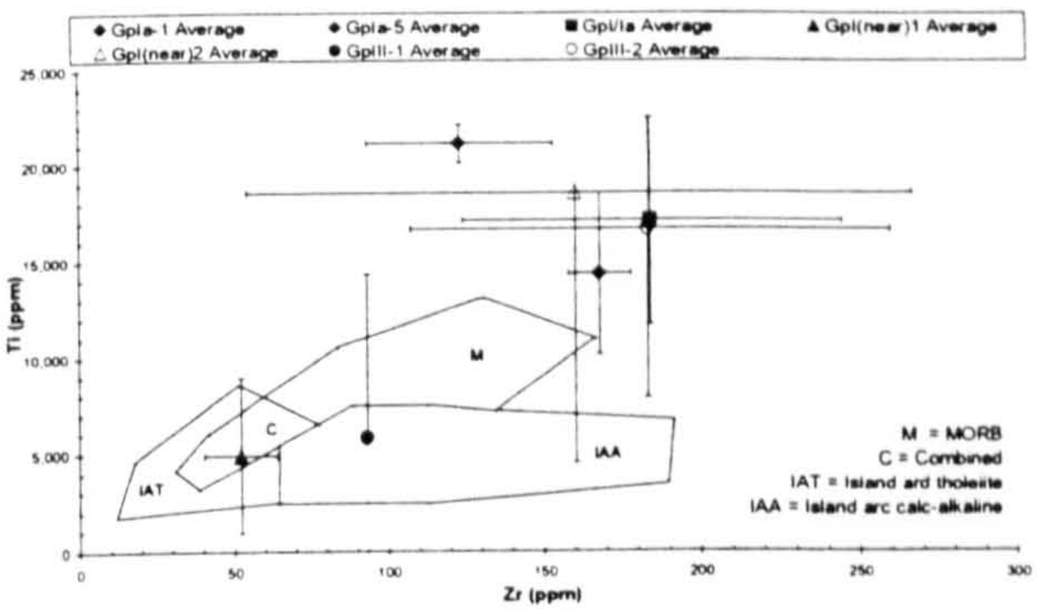

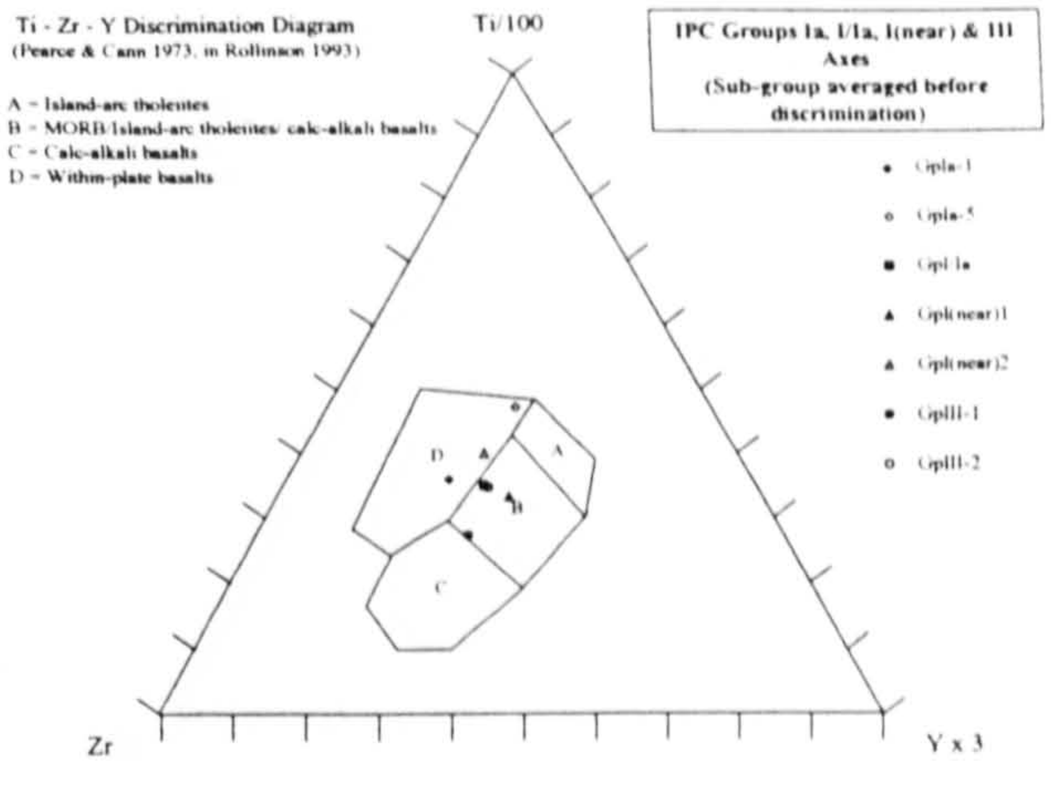

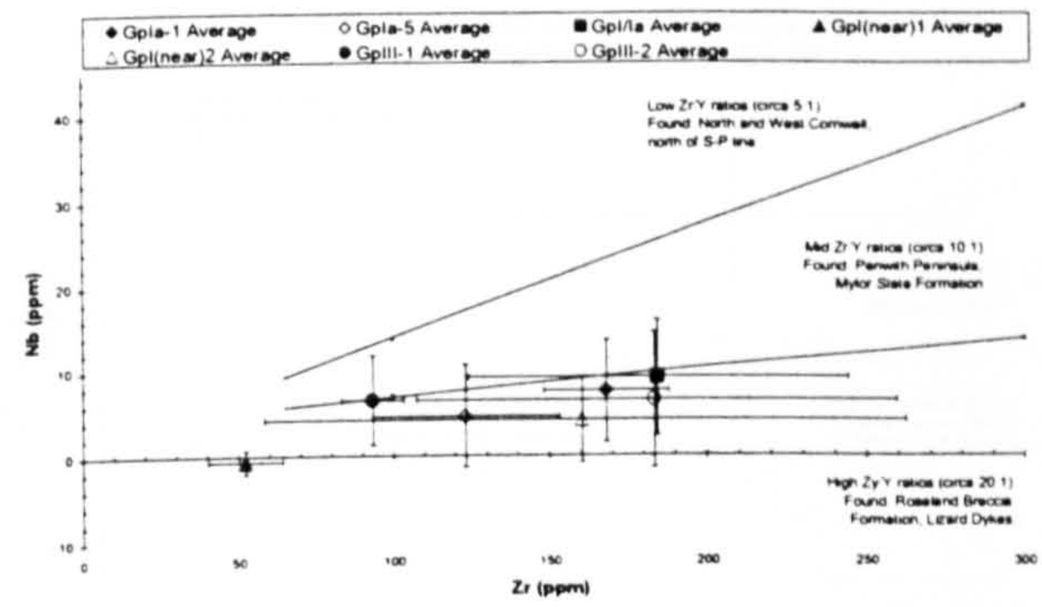

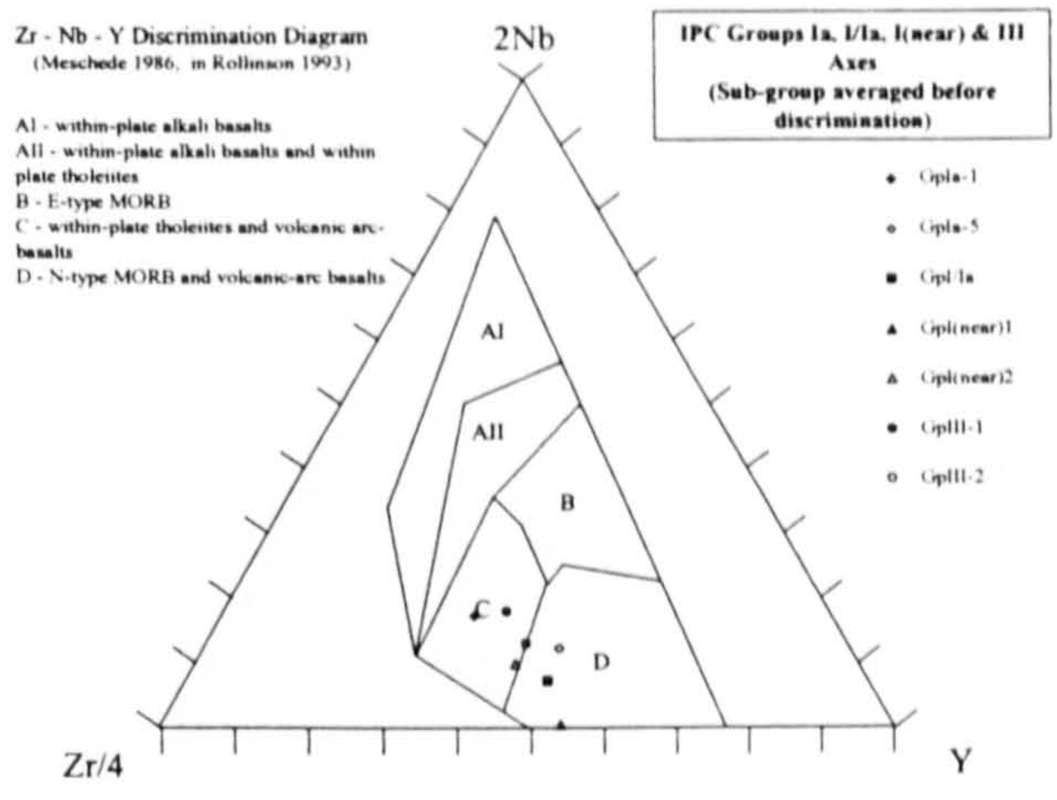

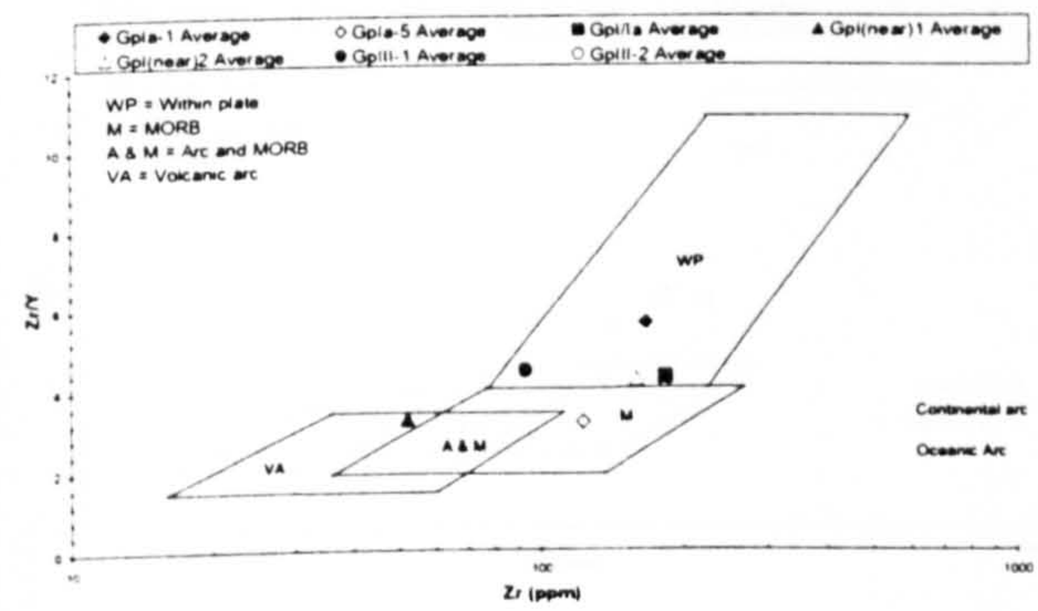

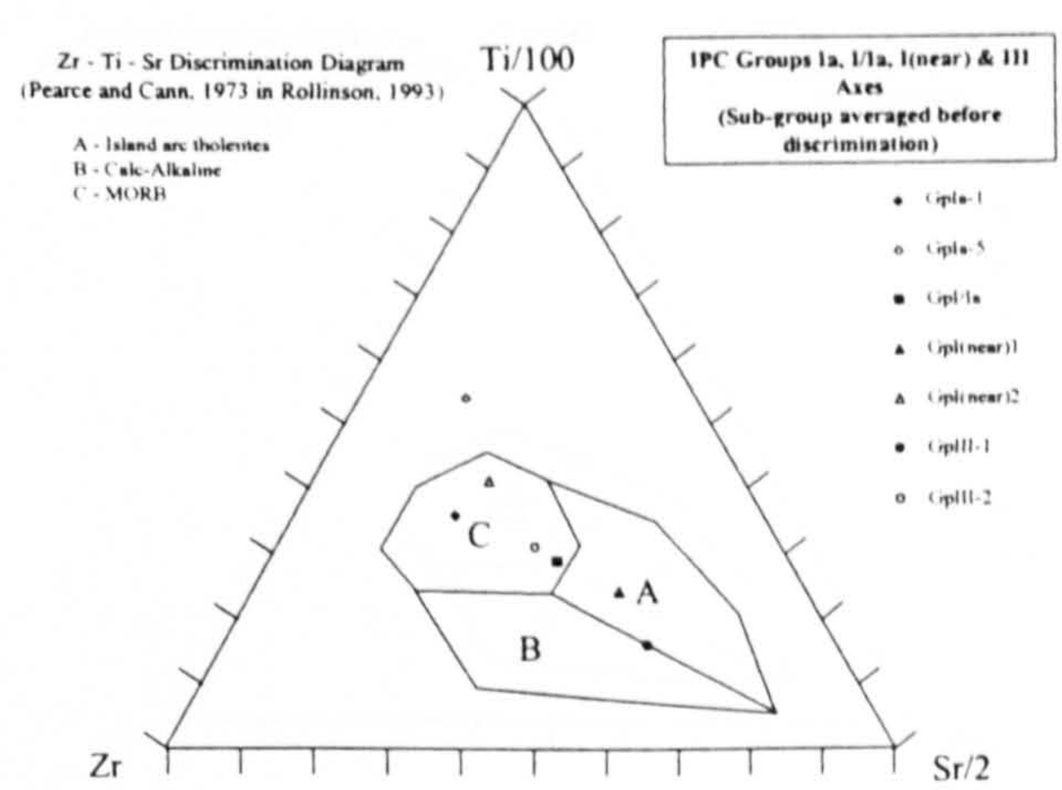

*Figure 78 Six binary and ternary element discrimination diagrams(after Rollinson 1993 & Floyd 1996) showing the position of **IPC Group Ia, I/Ia & I(near) and III sub-group** immobile element averages and associated ±2sd error bars (c.f. Appendix 23.9, 26.2 & Appendix 30 for details). See text for discussion. Note that these diagrams are intended to discriminate between fresh and unaltered basalts meeting certain criteria so due consideration is necessary when using these charts to determine the origin of greenstones (c.f. Section 7.10.1)*

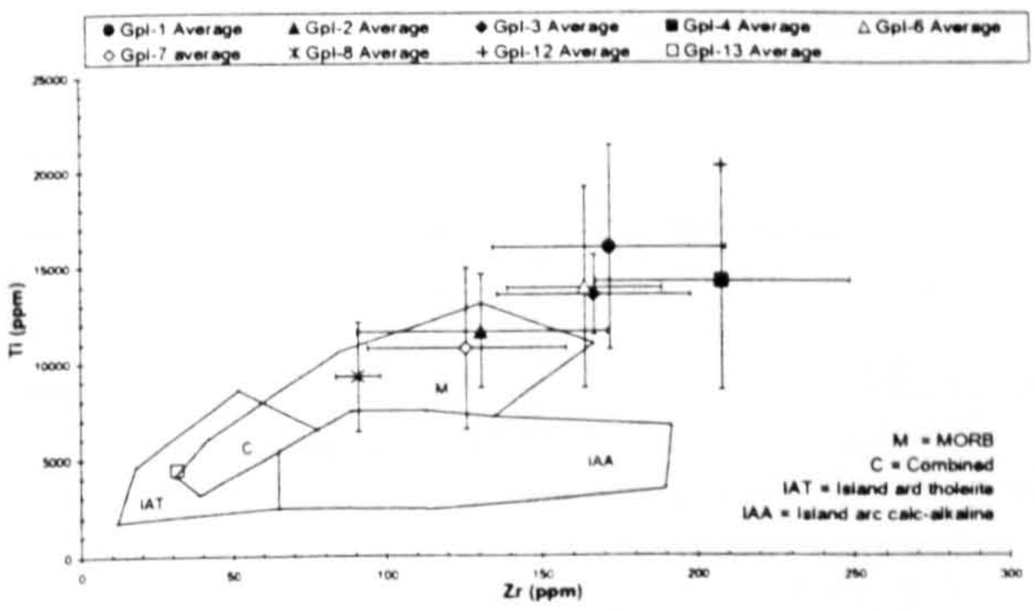

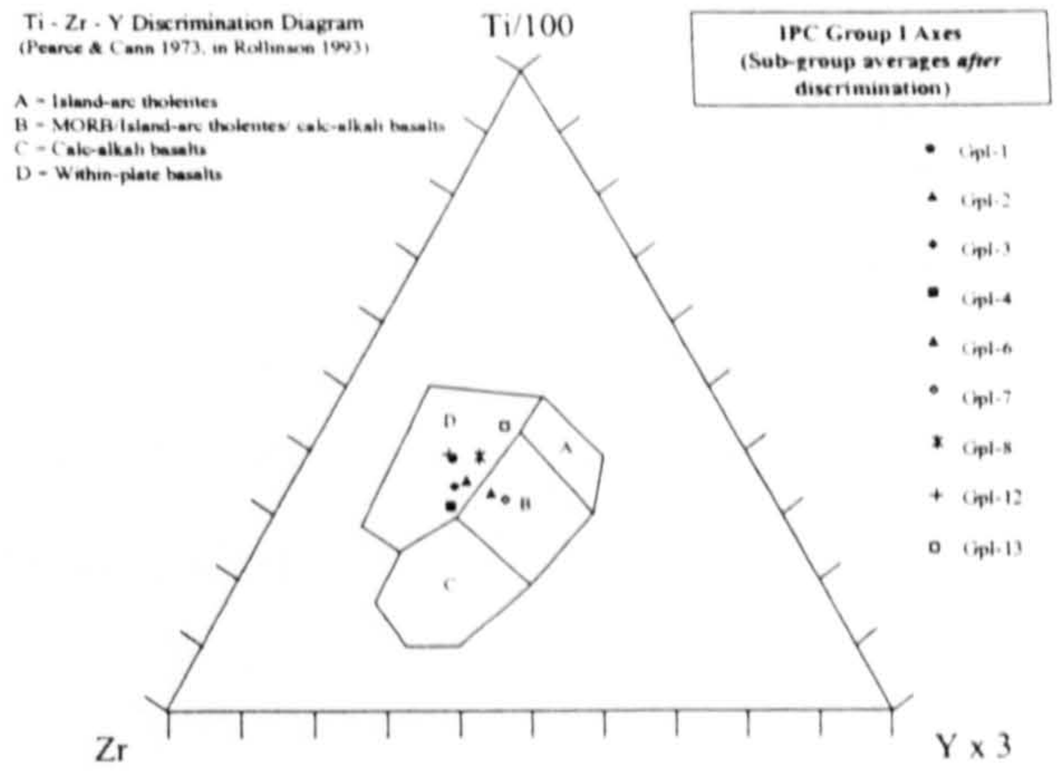

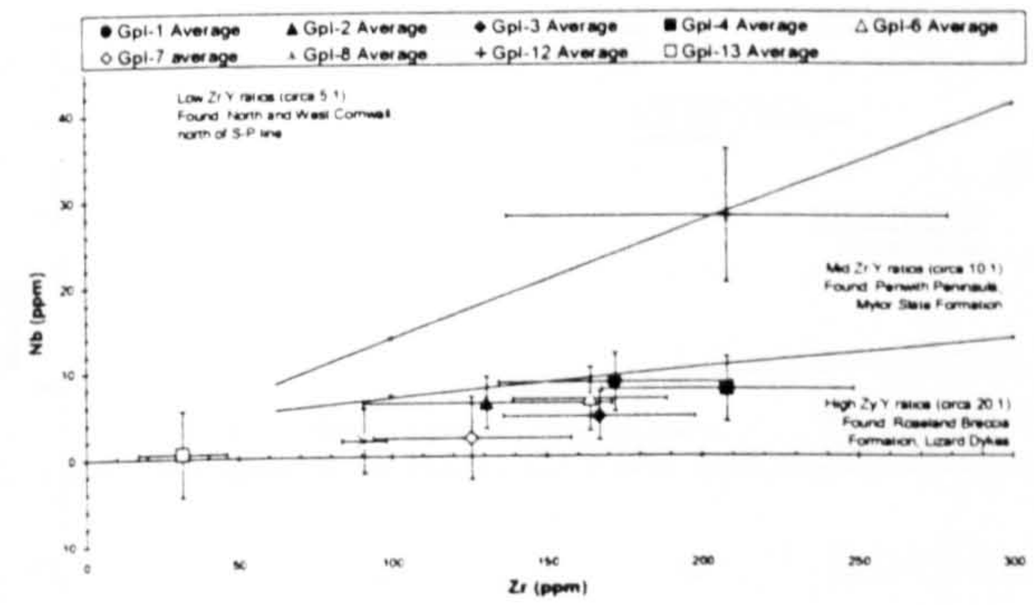

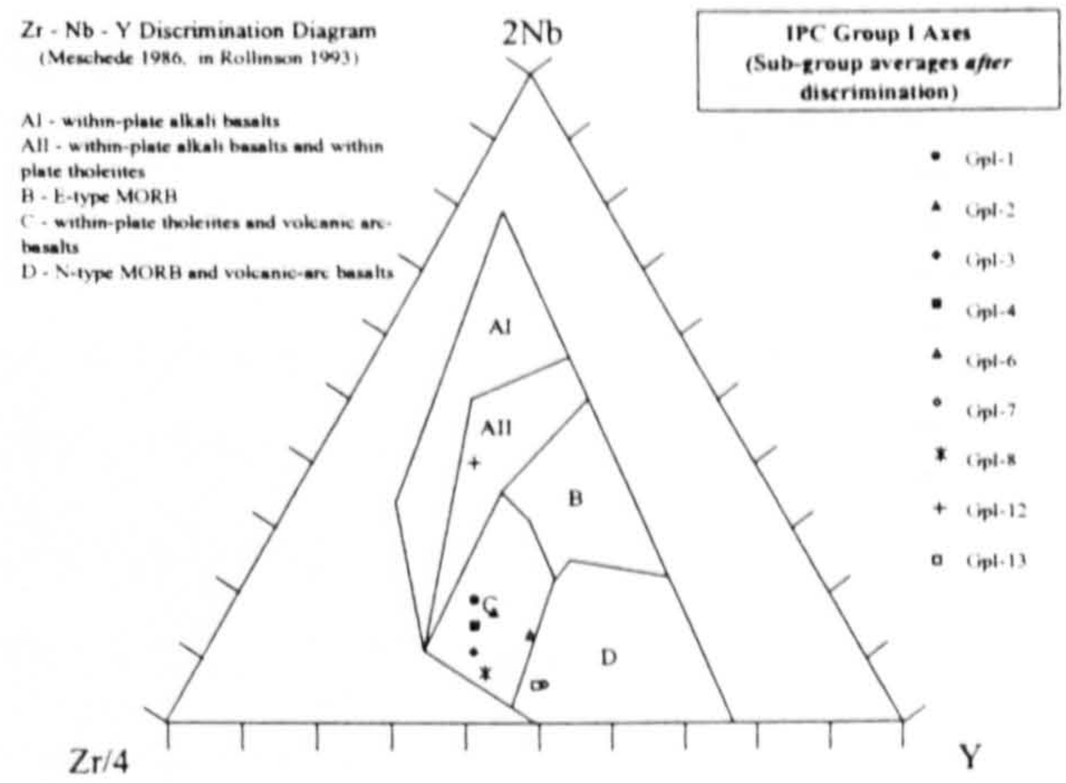

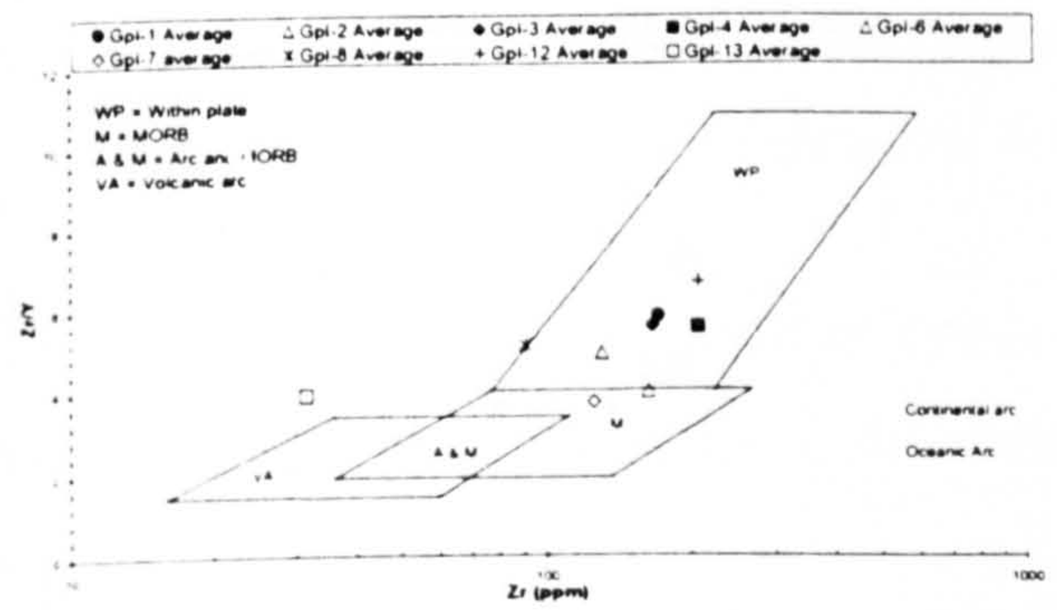

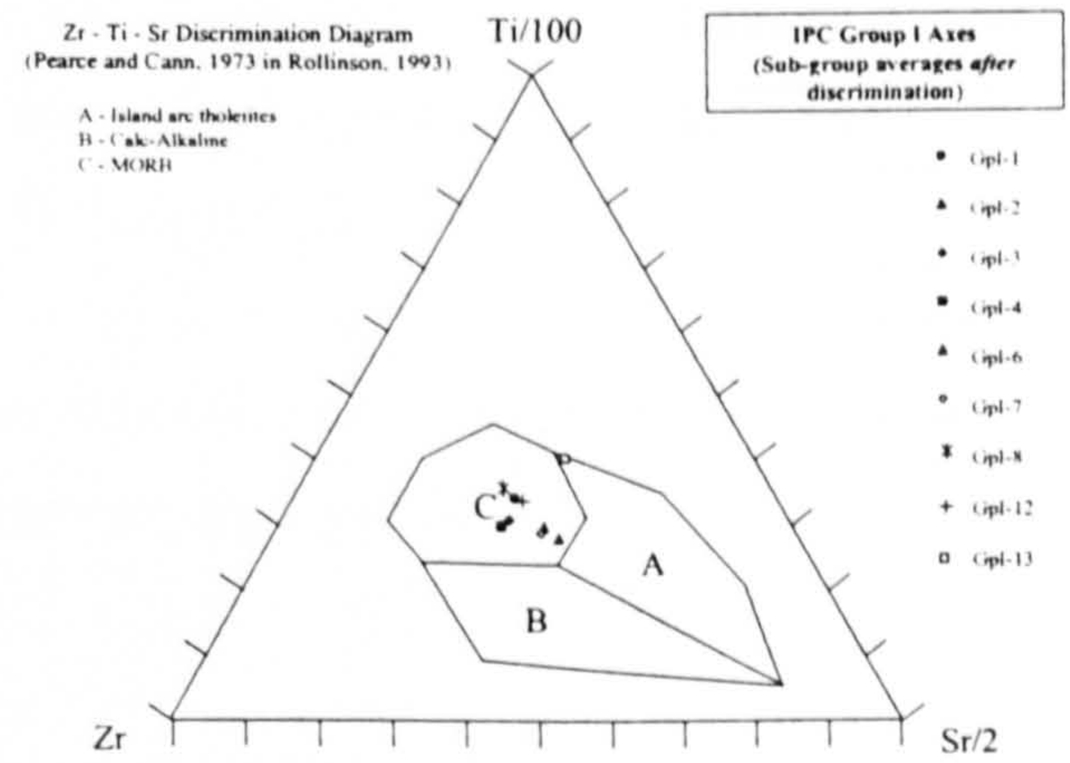

Figure 79 Six binary and ternary element discrimination diagrams(after Rollinson 1993 & Floyd 1996) showing the position of ***IPC Group I sub-group*** *immobile element* ***averages after discrimination*** *and associated ±2sd error bars (c.f. Appendix 23.9, 26.3 & Appendix 30 for details). See text for discussion. Note that these diagrams are intended to discriminate between fresh and unaltered basalts meeting certain criteria so due consideration is necessary when using these charts to determine the origin of greenstones (c.f. Section 7.10.1)*

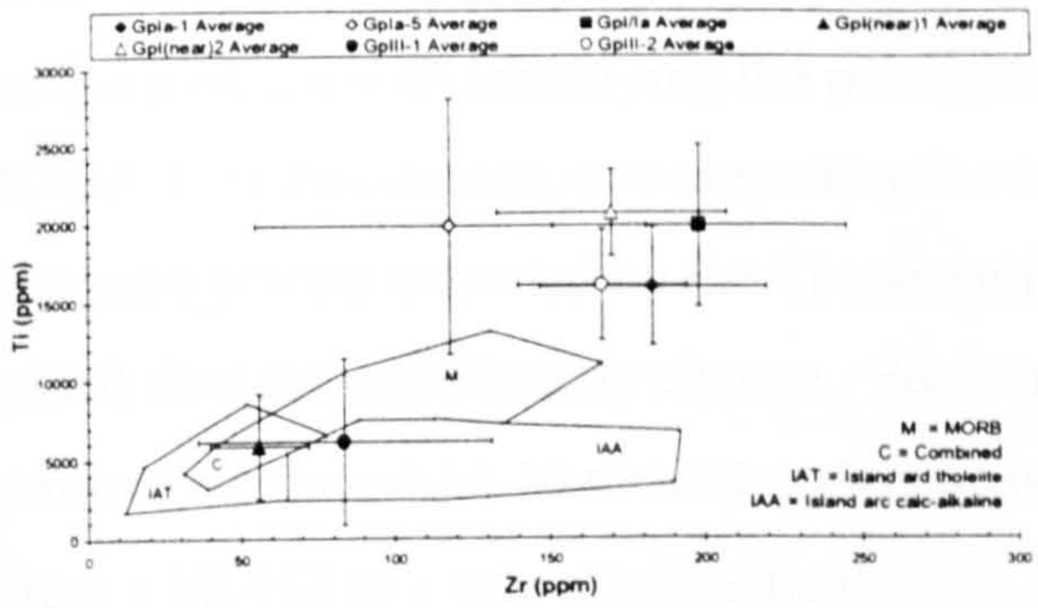

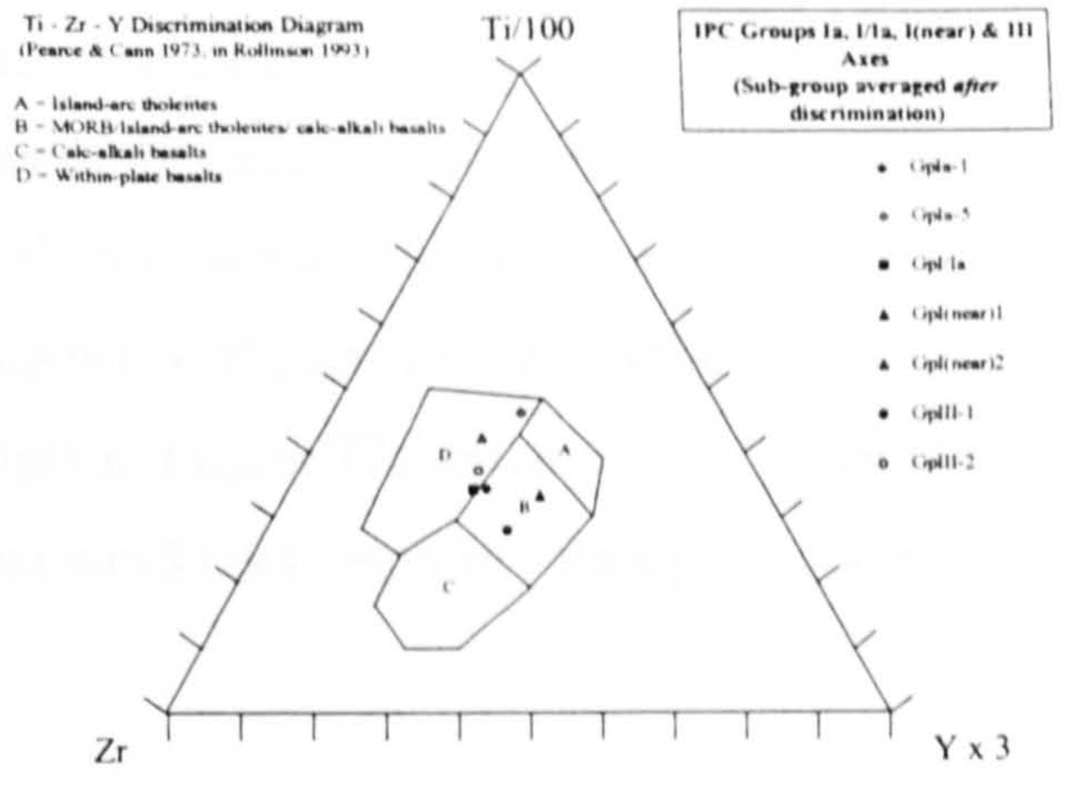

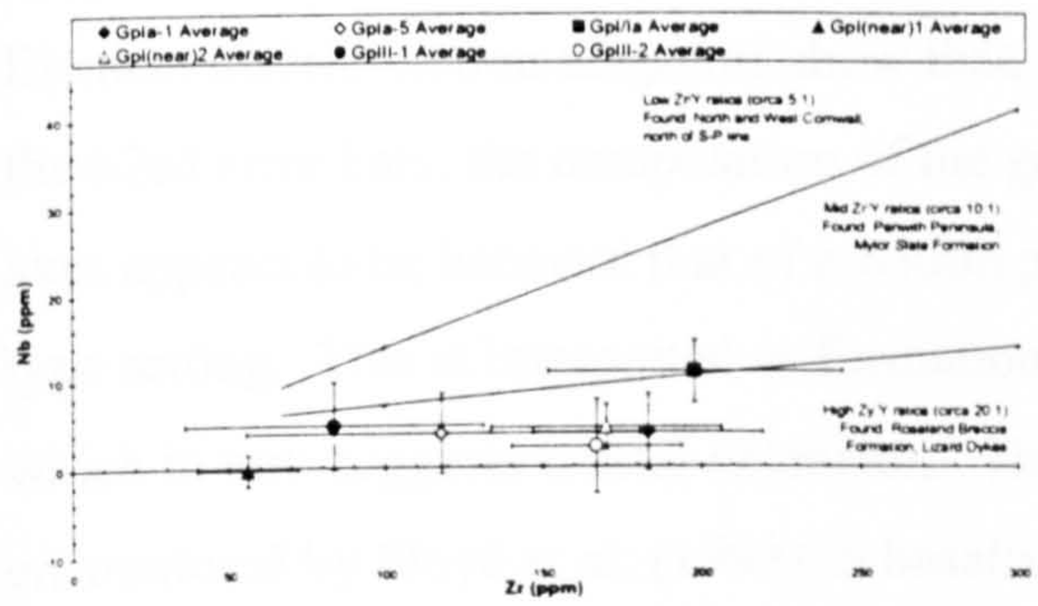

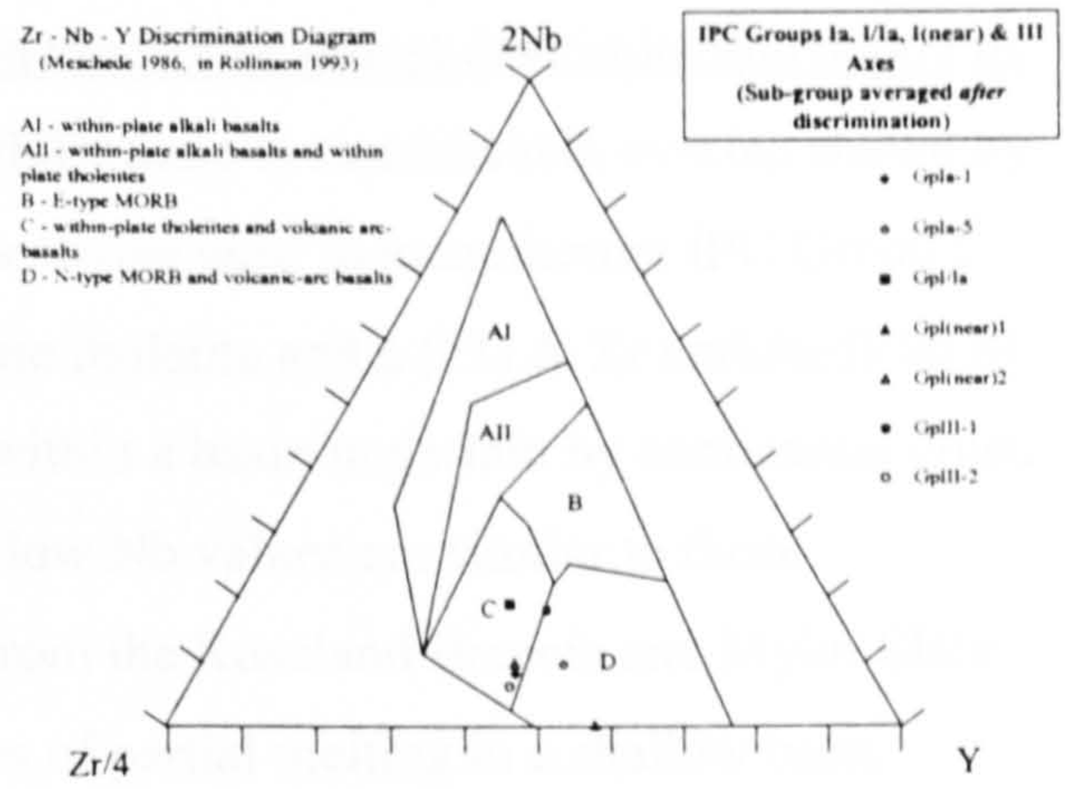

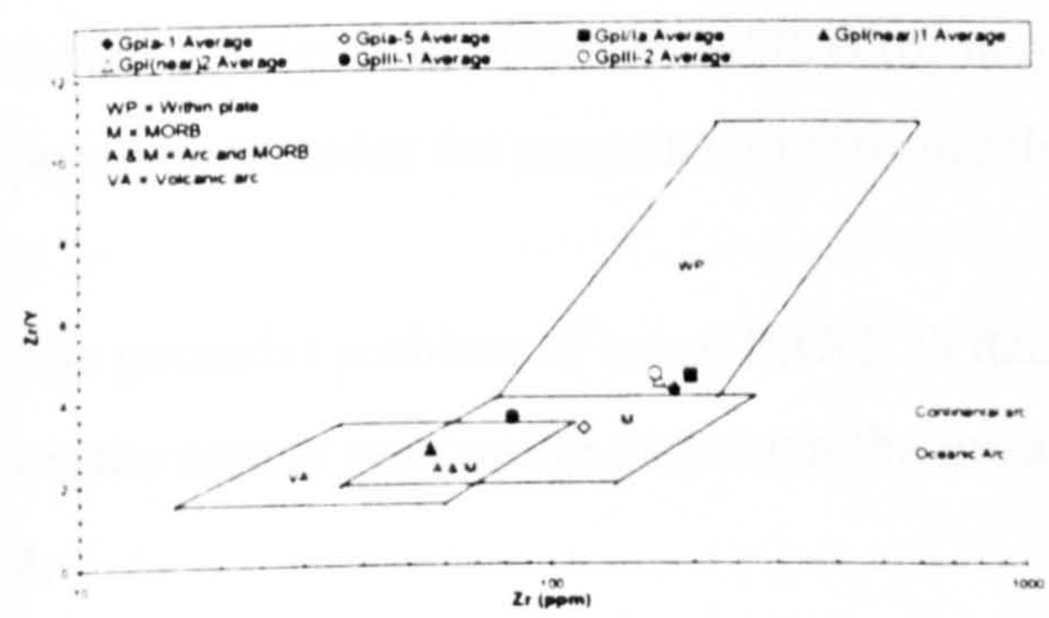

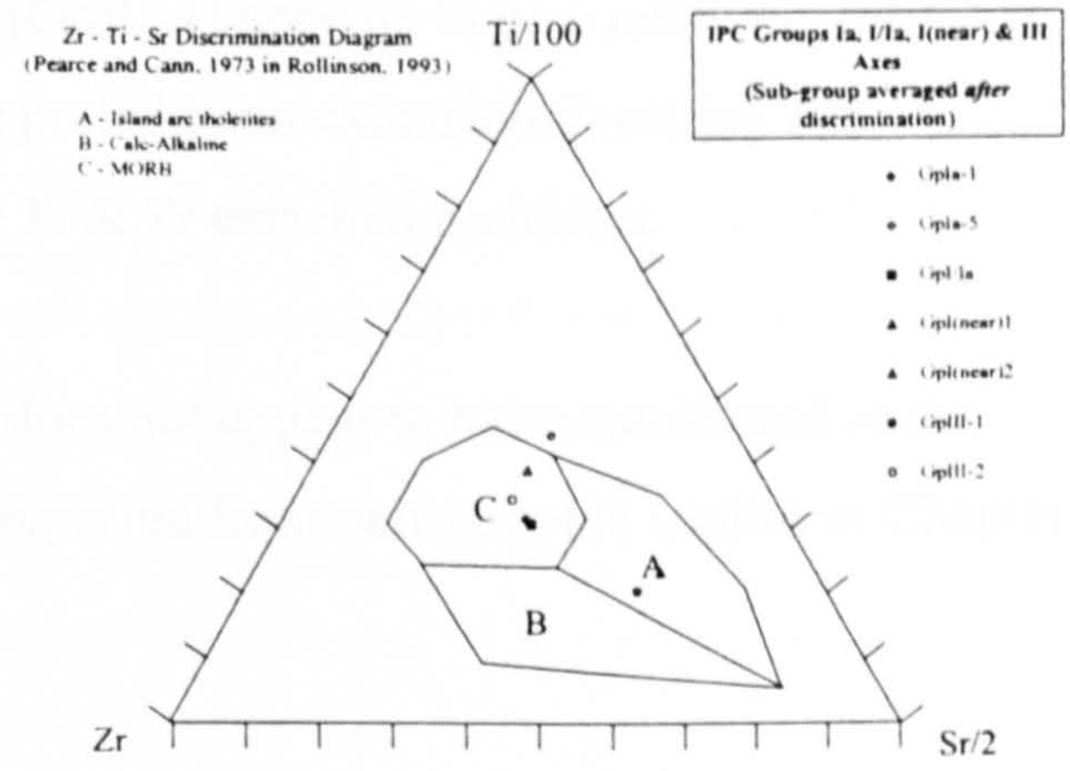

Figure 80 *Six binary and ternary element discrimination diagrams(after Rollinson 1993 & Floyd 1996) showing the position of* ***IPC Group Ia, I/Ia & I(near) and III sub-group*** *immobile element* ***averages after discrimination*** *and associated ±2sd error bars (c.f. Appendix 23.9, 26.4 & Appendix 30 for details). See text for discussion. Note that these diagrams are intended to discriminate between fresh and unaltered basalts meeting certain criteria so due consideration is necessary when using these charts to determine the origin of greenstones (c.f. section 7.10.1)*

It is noted the potential understatement of Ti measurements does not appear to cause a major problem with identifying the petrogenesis of the greenstone. Firstly, the possible PXRF Ti underestimate is swamped by the ±2sd error bars and secondly, if Ti is adjusted, the petrogenesis indicated by the Ti concentrations (i.e. the zone in which the data point plots) does not significantly change. For example in Figure 77, increasing the Ti data to remove the (possible) 10 to 15% understatement would not result in a data point moving from a MORB to a calc-alkaline field.

7.10.3 Summary of petrogenesis of axe greenstone from element discrimination diagrams

Element discrimination diagrams show that, whilst there is considerable overlap shown by the ±2sd error bars, the composition of the greenstone used to manufacture IPC Group I axes appears to be between that of a within plate tholeiite and a (?Ti & Zr enriched) MOR type setting. This is interpreted as formation within a basin underlain by continental crust, which in turn suggests crustal extension. The low Nb values are similar to those encountered by Floyd et al. (1993) in basalts from the Roseland Breccia and Mylor Slate Formations that were attributed to high degrees of partial melting in a shallow basin underlain by continental crust. IPC Group III (GpIII-1) appears to be a relatively primitive tholeiite, originating from an MORB (or more probably an extensional) setting and possibly precedes the magmatism forming the Ti & Zr enriched tholeiites.

The potential problem of using PXRF Ti data does not appear to have manifested as the results appear reasonable and along the lines expected from petrographic studies in Chapter 4.

7.11 Summary of chapter findings and main conclusions

Two hundred and seventy two axes representing approximately 29 % of the target population have been measured by PXRF during the three fieldwork periods. IPC Group I provided 149 of these axes, representing 40% of the current population of 369 IPC Group I axes. IPC Groups Ia, I/Ia, I(near), III, IIIa, IPC ungrouped, non-IPC and Irish gabbro & dolerite axes made up the other 123 axes.

Four statistical processes, ANOVA, MANOVA, SCA and DA analysis were used to examine the inter and intra group relationships. Initial grouping of the axes was based on the petrographically determined sub-groups defined after examination of existing thin sections in Chapter 4.

Initial inspection of IPC Group I axe PXRF analyses, supported by MS data, revealed 19 axes within the 149 that had elemental concentrations outside ±2sd to suggesting that they were not IPC Group I. Four of these axes formed GpI-8, GpI-12 & GpI-13 sub-groups that had already been determined as petrographically different to the majority of IPC Group I. A further two axes belonged to petrographic sub-groups (GpI-1 & GpI-2) and the remaining 13 had not been petrographically examined. Perusal of the 19 axes indicated that they predominantly originated from NE England (Lincolnshire & Yorkshire) and Wales, or that they had high (>1143) IPC serial numbers. This indicates a potential geographical and temporal variation in accurately assigning axes.

The 19 anomalous axes were removed from the IPC Group I data set and the Group average re-calculated and SCA statistics generated. The reduced IPC Group I data set (n=130) was subsequently used in the remainder of the Chapter as the benchmark with which to compare other axes.

SCA statistics showed considerable overlap between the 6 IPC Group I sub-groups remaining after anomalous axes had been discarded from the data set (GpI-1, 2, 3, 4, 6, & 7) and MANOVA statistics were used to show that the null hypothesis could not be rejected: that the geochemical means between sub-groups were not shown to be different (apart from between GpI-2 and GpI-4). Although not conclusive, because of small axe numbers, the results indicate the geochemical similarity of the reduced IPC Group I (n=130) sub-groups.

SCA and MANOVA were used to examine the relationship between axes found in different counties. Again the MANOVA statistics were inconclusive, suggesting little, if no difference between county populations. However, SC scatter plots did reveal the possibility of geographically based clusters of axes, indicating that they possibly shared similar geochemistry. This possibility will need to be investigated in depth, with access to petrographic thin sections required in order to confirm the observed relationships (which are most visible in the mobile element SC scatter plots). But, at this time, it appears that axes from Yorkshire and Cornwall (the two most geographically separated counties providing axes) share similar immobile and mobile element concentrations and the same range of MS measurements indicating probable origin from a single greenstone outcrop.

The relatively concentrated distribution of axe data points around the origin (0,0), seen in the IPC Group I (n=130) SC scatter plots, suggests the probability of a single greenstone source outcrop since there is only a single discernible cluster of data.

The same statistical processes used to examine IPC Group I were used to investigate IPC Groups Ia, I/Ia, I(near), III and IIIa. Inspection of the data, SCA analysis supported by MS and MANOVA statistics resulted in the division of these three IPC groups into 7 sub-groups: GpIa-1, GpIa-5, GpI/Ia (all GpI/Ia analysed except Lo114), GpI(near)I, GpI(near)2, GpIII-1, and GpIII-2. GpIa, GpIa-5, GpIII-1 & GpIII-2 were based, initially, on petrographic sub-groups determined in Chapter 4 and subsequently re-defined using geochemical characteristics. GpI/Ia, GpI(near)1 & GpI(near)2 were derived from examination of geochemical data alone as no thin sections were available. It was found that GpIa-1, GpIa-5, GpI(near)2 and GpIII-2 shared similar geochemical and MS values with IPC group I (n=130). GpI/Ia was found to be close to IPC Group I and GpI(near)1 & III-1 were statistically different to IPC Group I.

The conclusion of the investigation within and between IPC Grouped axes indicated that :

1. GpI-1, GpI-2, GpI-3, GpI-4, GpI-6, GpI-7, GpIa-1, GpIa-5, GpI(near)2 & GpIII-2 were considered to form IPC Group I
2. GpI/Ia is close to IPC Group I and is possibly related.
3. GpI-8, GpI-12, GpI-13, GpI(near)1 are not related to IPC Group I or III
4. GpIII-1 represents IPC Group III
5. There is a 13 to 15% chance that an IPC Group I axe has been previously incorrectly assigned to the group
6. There a 25% chance axes have been previously incorrectly assigned to IPC Group Ia, I/Ia and I(near)
7. There is an 80% chance that IPC Group III axes are dissimilar to Wi4/4, the founding member of the Group.

The 16 (of 24) axe sub-groups introduced in Chapter 4 which have been geochemically refined in Sections 7.4, 5 & 6 were used as the 'seed' groups in DA. The results of this statistical process, assigning axes to the seed groups based on the similarity of immobile and mobile elements indicated that Co398/1734 had sufficient geochemical anomaly to warrant its exclusion from IPC Group I and that Ca15, and Ha23/330 were 'borderline cases' for exclusion.

SCA and discriminant analysis of 72 axes from IPC ungrouped (55) and non-IPC axes (17) showed that 18 shared sufficient geochemical and magnetic similarity to warrant their inclusion to IPC Group I and 1, borderline, for inclusion to IPC Group III. Assuming the IPC ungrouped axes were selected at random, this indicates that approximately 27% (15/55 (note 3 axes assigned to IPC Group I are non-IPC axes (c.f. Table 78)) of IPC ungrouped greenstones could belong to IPG Group I. The allocation of three non-IPC axes, BLAW1, BLPW1 and WBBW3 (manufactured recently from beach pebbles collected from Mount's Bay and North Penwith) to IPC Group I is the first modern evidence that IPC Group I originated from rock found within Cornwall.

Sixteen Irish gabbro (5 Gabbro I, 5 Gabbro II, 6 Ungrouped Gabbro) and 6 Irish Ungrouped dolerite axes were analysed (sub-groups as per Mandal 1996). Results from SCA and discriminant analysis of the Irish PXRF and MS data coincided with those proposed by Mandal (1996). Specifically:

1. Irish Gabbro I axes have high MS coinciding with magnetite found in their mineralogy.
2. 4/5 Gabbro I axes are geochemically and magnetically different to IPC Group I
3. 1/5 Gabbro I axes (NMI 1931:164) has high MS but is possibly geochemically related to IPC Group I
4. 3/5 Gabbro II axes share similar geochemical and magnetic values to those of IPC Group I, sufficient to recommend their inclusion to the IPC Group.
5. All Ungrouped gabbro axes do not share similarities with IPC Group I or III, except possibly NMI P1954:14
6. All Ungrouped Dolerite axes (6) are probably or possibly related to IPC Group I

The agreement between Mandal (1996) and this work, reached using two independent processes, one partially destructive using petrographical thin sections and the other using non-destructive techniques, supports the possibility of assigning axes on the basis on non-destructive analysis. Additionally, the findings in Section 7.10 supports the hypothesised Cornish origin of certain Irish doleritic and gabbroic axes.

Element discrimination diagrams were used to display the averages of the 16 axe sub-groups as defined before and after DA. Acknowledging the restrictions placed on using the element discrimination diagram to interpret altered, mafic rocks, the diagrams show

IPC Group I greenstone falls between that of MORB and a within plate tholeiite, thus probably originating from an extensional type environment. The Zr-Nb discrimination chart suggests a Cornish melange (= Roseland Breccia Formation) or possibly Mylor Slate Formation source (based on Floyd et al. 1993). These charts and Chapter 7 findings provide the link to Chapter 8, where the provenancing of the axe sub-groups using geochemical, magnetic and petrographic data is carried out.

8 Provenancing of greenstone axes to source outcrops using geochemical analyses supported by MS and petrographic data

8.1 Introduction

8.1.1 Overview

This chapter examines the provenance of IPC Cornish greenstones axes to source exposures using geochemical data that, for axes, has been obtained using totally non-destructive methods. Chapter 7 examined the geochemical relationship of greenstone axes and identified a total of 16 geochemically defined axe sub-groups (also referred to as 'DA seed groups' or 'seed groups') within the 6 Cornish IPC Groups reviewed (IPC Groups I, Ia, I/Ia, I(near), III and IIIa) (c.f. Section 7.7.1, Table 76). In this chapter, these 16 axe sub-groups are compared to each of the ten geographical collections of greenstone exposures introduced in Chapter 3 (and identified in Table 85 below) in turn, in order to examine the degree of geochemical similarity between axe sub-group and greenstone exposure. Where available, measurements of MS (Chapter 5) and petrographic observations (Chapter 4) are used to supplement the geochemical comparisons.

This chapter is divided into two main parts. Firstly, a review of the provenancing methodology used and its associated limitation/restrictions is followed by a resume of the petrography, MS and rock petrogenesis of IPC Group I, the location of the greenstone exposures and the source and adjustment of geochemical data used in this chapter. The second part of this chapter uses the described methodology to systematically compare axe sub-group geochemistry to greenstone exposure geochemistry for each of the ten geographical collections of greenstone exposures for which geochemical data is available.

Provenancing is primarily aimed at identifying the source exposure for IPC Group I axes. Secondary aims include identifying the source exposure for the other IPC Groups considered in this thesis (IPC Groups Ia, I/Ia, I/(near), III and IIIa), provenancing IPC ungrouped axes and provenancing Irish doleritic and gabbroic axes.

8.2 Provenancing methodology and associated limitations/restrictions

8.2.1 Introduction to provenancing methodology

Provenancing of greenstone axes to greenstone exposures is carried out by comparing geochemical data obtained from axes and exposures using 5 separate methods: inspection, element discrimination diagrams, SCA, DA and comparative statistics (MANOVA and/or

Student's t-test). These individual methods are described below, along with any associated limitations or restrictions particular to the process.

As this work is predominantly geochemically orientated, emphasis is placed on the matching of geochemical data between axe and exposure in order to establish provenance. Hence, all of the individual methods used employ geochemical data. However, MS and petrographic information is used to supplement the geochemical data where it is available.

Each of the 10 chapter sections, 8.4 and 8.6 to 8.14, examining the provenance of axes uses the same sequence of examination methods as followed in Sections 8.2.2 to 8.2.6 below.

8.2.2 Inspection of geochemical, petrographic and magnetic data

8.2.2.1 Inspection of exposure and axe geochemical data

Geochemical measurements of greenstone exposure samples are compared with the reduced IPC Group I elemental averages (Table 58) and to each of the 16 axe sub-group elemental averages (Tables 62, 70, 75 and Appendix 23.9) by inspection. The inspection is aimed at identifying the degree of similarity between the elemental concentrations observed in the exposure and the elemental averages of the axe groups. These observations will then 'set the scene' for subsequent examination of the data using SCA and DA analysis. As discussed in Section 7.2.2, most emphasis will be placed on comparing immobile element (Ti, Y, Zr, Nb) measurements, as axe and exposure concentrations for these four elements will need to be similar before the exposure can seriously be considered as a potential source of axe material.

8.2.2.2 Inspection of exposure and axe petrography

Comparison between IPC Group I, Ia and III axe thin sections and greenstone exposures has already been undertaken in Chapter 4 (Section 4.7). The conclusions from these comparisons will be briefly restated in the appropriate sections. Published and unpublished petrographic information from Cornish greenstone samples will also be used to supplement the petrographic comparison of axe and exposure petrography. Details of all petrographic information used in this chapter are contained in Appendixes 4 and 5. It is noted that petrographic information is not available for every greenstone exposure/sample used in this work.

As with the analysis of geochemical data above, similarity of mineralogical and textural features between axe and exposure are required before the exposure can be considered to be a potential source of axe material.

8.2.2.3 Inspection of exposure and axe magnetic susceptibility values

MS measurements taken at the Cudden Point, Trenow Cove, Penzance, Gurnard's Head and Zennor Point greenstone exposures have already been compared to axe MS measurements in Chapter 5. Conclusions from these comparisons are used as supplementary evidence in the provenancing process.

8.2.3 Element discrimination diagrams

Greenstone exposure geochemical data is displayed using six elemental discrimination diagrams based on elements Ti, Y, Zr, Nb and Sr (c.f. Section 7.10 and Chapter 30). As identified in Section 7.10, these bivariate and ternary element discrimination diagrams distinguish basalts from differing tectonic-magmatic settings (Rollinson 1993) and are therefore potentially useful in matching the IPC Group I axe rock type (tholeiitic, with MOR and within-plate characteristics, Section 7.12.3) with exposures that have a similar tectonic setting.

In order to use the discriminant plots to identify the genesis of a basalt a number of pre-conditions need to be met, hence conclusions drawn from any geochemical data not meeting these pre-conditions must be treated with caution. Specifically (and as already stated in Section 7.10.1):

1. Samples should be from fresh, unaltered exposures of basalt
2. Ti-Y, Ti-Y-Zr & Ti-Y-Sr discrimination diagrams apply to *tholeiitic basalts* in the range 20% > CaO + MgO > 12% (Rollinson 1993)
3. Rocks containing cumulate phases give erroneous classification
4. Recalculating to 100% for plotting on ternary discrimination diagrams may cause samples to be grouped when no real relationship exists (Butler & Woronov 1986)

As discussed in Chapter 3, the majority of greenstone exposures in SW England have been altered to some degree: by varying grades of contact metamorphism and metasomatism through proximity to the local Cornubian granite batholith, low-grade regional metamorphism caused by the Variscan orogeny, and possibly by hydrothermal alteration through contact with sea water during the emplacement/eruption of the magma.

Section 7.10.1 points out that criteria 1, 2 and 3 above are not problematic for axe measurements of Ti, Y, Zr and Nb, since the degree of alteration of the axe greenstone is not thought to have mobilised these elements. However, the same cannot be said for all exposure samples since these include non-tholeiitic and intermediate rocks, and possibly cumulates. Hence, care will be taken in reaching conclusions regarding the petrogenesis of greenstone exposures. But, as the main aim is to compare axe and exposure geochemistry, spatial (i.e. cluster) comparison between data plotted on axe and exposure element discriminant diagrams can be used to assist the provenancing exercise by recognising data cluster overlaps.

The 6 geochemical discrimination diagrams (Zr–Ti, Zr–Nb, Zr–Zr/Y, Zr–Ti–Y, Zr–Nb–Y, Zr–Ti–Sr) are reproduced together in a single collage in the appropriate section **and in full size in Appendix 29.1 to 29.9**. Appendix 30 contains descriptions of all 6 element discrimination diagrams identifying what each of the delineated fields represents. In addition, Appendix 30 reproduces information identifying the relative mobility of elements and typical concentrations of MORB, OIB and crustal rocks (from Rollinson 1993).

8.2.4 SCA

Geochemical data from each greenstone exposure is plotted on SC scatter plots that are based on the simple components and associated averages & sds generated from the reduced IPC Group I (n=130) data set (see Tables 82 and 83). As before (Section 7.3.1.4) the assumption is that exposure samples that plot close to the origin of the SC scatter plots probably have similar elemental concentrations to the reduced IPC Group I average. Ellipses representing the area enclosing 90% of all IPC Group I axes (excluding anomalous axes, c.f. Section 7.4.2.2 and 7.4.3) are drawn on each SCA chart as a visual guide to the geochemical similarity between exposure and IPC Group I geochemistry. These charts also allow direct comparison between geochemistry of exposure and IPC Group Ia, I/Ia, I(near) (Section 7.5.5, Figure 71), IPC Group III & IIIa (Section 7.6.3, Figure 73), IPC and non-IPC ungrouped axes (Section 7.8.2, Figures 74, 75) and Irish axes (Section 7.9.5, Figure 76) since all these charts are drawn using the same SCA statistics and SC components (reproduced below in Tables 82 and 83).

(The SCA method is described in Section 7.3.1)

Element	Average (ppm) (n=130)	SD (ppm)	SC1	SC2	Ellipse range
Ti	14 959	3 772	SC1= Ti + Y + Zr + Nb	SC2= Nb – Y	x-axis = ±6
Y	35.7	6.8			y-axis = ±3
Zr	171	29.2	SC1 error bars = ±1.62	SC2 error bars = ±1.56	
Nb	6.7	2.9			

Table 82 Summary of SCA statistics based on IPC Group I axe Ti, Y, Zr & Nb immobile element concentrations used in the calculations generating SC1 & SC2 for exposures (from Section 7.4.2.1, Table 59)

Element	Average (ppm) (n=130)	SD (ppm)	SC1	SC2	Ellipse range
K	3 567	2 282	SC1= Ca + Sr – K – Rb	SC2= K + Ca –Fe +Rb	x-axis = ±6
Ca	67 715	14 636		+ Sr + Ba	y-axis = ±5
Fe	95 632	14 009			
Rb	29.6	25.8	SC1 error bars = ±0.82	SC2 error bars = ±0.86	
Sr	324	150			
Ba	104	64.3			

Table 83 Summary of SCA statistics based on IPC Group I axe mobile elements K, Ca, Fe, Rb, Sr & Ba concentrations used in the calculations generating SC1 & SC2 for exposures (from Section 7.4.3, Table 61)

SC scatter plots displaying the averages of the 16 axe sub-groups after (axe) DA, based on IPC Group I (n=130) SCA parameters are shown in Figure 81 after Section 8.2.5 (from sub-group average concentrations contained in last section of Appendix 23.9).

8.2.5 DA

DA is used to assign exposure samples to one of 16 DA seed groups. Unlike in Section 7.7.2, the 16 seed groups used in this DA are those obtained after immobile element DA of the 272 greenstone axes carried out in Section 7.7 (results in Appendix 25) and illustrated in Section 7.7.6, Table 77 and Figure 81. This approach has been taken so that the increased statistical discrimination of axe sub-groups achieved by DA of the axes (in section 7.7) is fully utilised when assigning exposure samples. Table 84, below identifies the DA seed groups used in this chapter.

Averages and associated sds for the 'seed' groups used in this Chapter are contained in Appendix 23.9 and displayed, using the reduced IPC Group I SCA statistics (n=130) in Figure 81 below. Results from DA of exposure samples are detailed in Appendix 31 and summarised, where appropriate in this chapter.

As discussed in Section 7.7.1 exposure samples will need to be matched to recognised IPC Group I sub-groups for both mobile and immobile elements, and have P(G/D)>>0.05, in order for the exposure to be considered as being geochemically similar to IPC Group I.

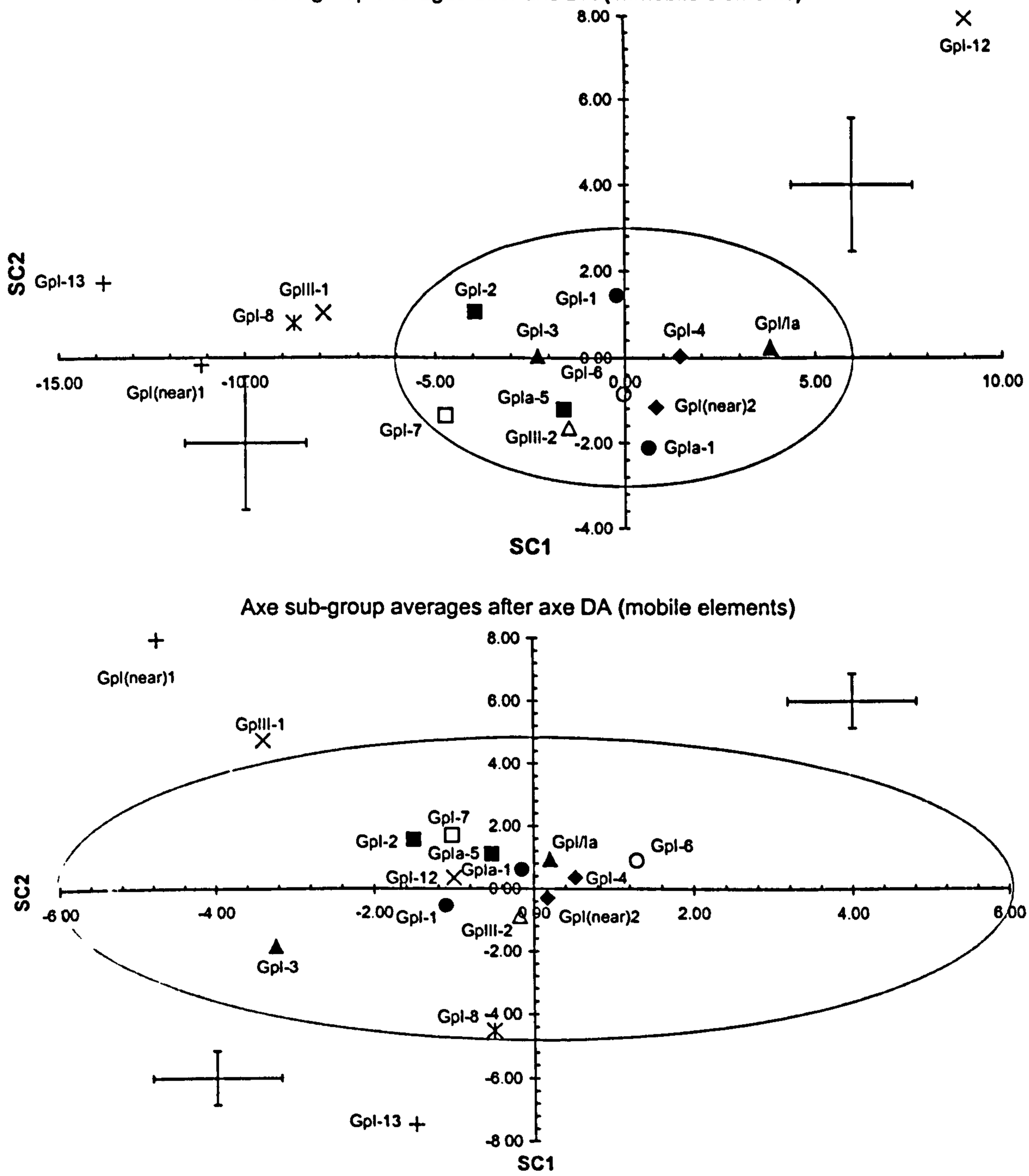

*Figure 81 Scatter plot of SC1 against SC2 for the 16 axe sub-group elemental averages based on IPC Group 1 (n=130) analysis of Ti, Y, Zr & Nb (immobile) elements (upper chart) and K, Ca, Fe, Rb, Ba, & Sr (mobile) elements (lower chart). The ellipses represent the region that 90% of IPC Group 1 axes fall within and are the same on all IPC Group 1 SC based scatter plots to provide a common frame of reference. The plotted points represent **averages** of axe sub-groups **after axe DA**. Error bars illustrate the estimated PXRF precision based on the reduced IPC Group 1 average elemental compositions. See text for discussion.*

Sub-group (seed group)	n before axe DA	n after axe DA	Average element composition ± 1sd after DA (ppm)			
			Ti	Y	Zr	Nb
GpI-1	28	23	15 956 ± 2 685	29.5 ± 4.2	172 ± 18.7	8.5 ± 1.7
GpI-2	4	24	11 570 ± 1 499	26.6 ± 4.1	131 ± 20.1	6.2 ± 1.5
GpI-3	2	6	13 483 ± 1 038	29.9 ± 1.6	167 ± 15.4	4.6 ± 1.4
GpI-4	12	25	14 192 ± 2 869	37.4 ± 4.1	208 ± 20.3	7.7 ± 1.9
GpI-6	6	20	13 835 ± 2 648	41.0 ± 4.7	164 ± 12.4	6.6 ± 1.7
GpI-7	1	16	10 681 ± 2 110	33.7 ± 4.1	126 ± 16.0	2.1 ± 2.5
GpI-8	2	5	9 220 ± 1 436	17.8 ± 4.1	90.7± 3.7	1.9 ± 1.9
GpI-12	1	4	20 225 ± 1 931	31.1 ± 5.3	208 ± 35.4	28.0 ± 3.9
GpI-13	1	4	4 425 ± 939	8.1 ± 2.8	31.5 ± 7.3	0.5 ± 2.5
GpIa-1	1	14	15 929 ± 1 906	43.5 ± 3.2	183 ± 18.1	4.0 ± 2.2
GpIa-5	1	6	19 800 ± 4 179	37.0 ± 3.9	118 ± 31.6	3.9 ± 2.3
GpI/Ia	5	37	16 989 ± 2 602	43.7 ± 5.3	198 ± 23.4	10.9 ± 1.8
GpI(near)1	2	7	5 800 ± 1 675	19.5 ± 5.5	56.0 ± 8.1	-0.2 ± 0.9
GpI(near)2	4	14	20 607 ± 1 388	38.3 ± 6.0	170 ± 18.4	4.6 ± 1.3
GpIII-1	2	12	6 092 ± 2 638	23.4 ± 3.7	83.6 ± 23.9	4.8 ± 2.5
GpIII-2	4	7	16 000 ± 1 787	36.4 ± 2.8	167 ± 13.5	2.4 ± 2.7

Table 84 List of seed groups used in DA of exposure samples. Seed group composition after axe DA are used in Chapter 8. Immobile element averages for seed groups after axe DA are repeated from Appendix 23.9

8.2.6 MANOVA and Student's t-test

MANOVA and Student's t-test are used to further test the geochemical relationship between exposure and axe sub-groups observed through inspection, SCA and DA examination. Considering the potential for 1280 MANOVA analyses (16 axe sub-groups x 40 (+ depending on geographical resolution) exposures x immobile & mobile element elements = 1280), MANOVA will only be used where previous methods have indicated similarity between axe sub-group and exposure. Specifically, MANOVA is used to establish the degree of statistical similarity between the two groups of geochemical data being considered. Student's t-test is used to compare means of the two groups concerned, element by element. In both cases the null hypothesis is that the elemental means of the data sets being examined are equal, and since a 0.05 value for confidence has been chosen, the null hypothesis can be rejected for significance values below 0.05.

8.3 Brief resume of IPC Group I petrographic, magnetic and geochemical properties, location of greenstone exposures and associated geochemical data

8.3.1 IPC Group I

This section is included to provide a simple overview of IPC Group I petrography, MS and axe rock petrogenesis that has already been established elsewhere in this thesis, in preparation for the provenancing activities undertaken in Sections 8.4 to 8.14.

8.3.1.1 IPC Group I petrography

IPC Group I axes generally consist of ophitic and non-ophitic clinopyroxene (& rare orthopyroxene) showing alteration to fibrous amphibole and sometimes chlorite. Plagioclase feldspar is almost totally altered to mica/clay (sericite, chlorite), epidote (usually granular, rarely discrete grains) and/or amphibole (actinolite) with ilmenite as the most common oxide present. Secondary alteration products include minor biotite. No olivine and only small amounts of very fine apatite are seen (Section 4.4.3.1). The mineralogy is consistent with an evolved tholeiite and lack of evidence of volcanic glass coupled with a (primary) medium grain size indicates shallow, not extrusive, emplacement (Section 4.6.2).

8.3.1.2 IPC Group I MS

IPC Group I axes have an average uncorrected MS of $0.65 \pm 0.50 \times 10^{-3}$ SI (Section 5.9.3.1, Table 23). This rises to a lower estimate of $0.95 \pm 0.72 \times 10^{-3}$ SI and upper estimate of $1.09 \pm 0.80 \times 10^{-3}$ SI when corrected (Section 5.9.3.1, Table 23). These values are encompassed by the 0.23 to 1.89×10^{-3} SI *range* of MS values used to recognise potential IPC Group I axes (Section 7.2.2).

8.3.1.3 IPC Group I greenstone petrogenesis

Element discrimination diagrams for all axe sub-groups are produced in Figures 77 to 80 (Chapter 7) and in full size in Appendix 26.3. Noting the limitations for interpreting these diagrams (Sections 7.10.1 and 8.2.3), IPC Group I sub-groups appear to be tholeiites originating from a MOR type tectonic setting but also having within-plate characteristics. IPC Group I has generally high Zr/Nb ratios (20:1) suggesting a south Cornish melange origin (Floyd et al. 1993) and Zr/Y ratios greater than 3 indicating continental influence on the petrogenesis of the original magma (Rollinson 1993; figure 5.5).

8.3.2 Location of greenstone exposures and associated data

Using the hypothesised provenance regarding the probable location of the source of IPC Group I axes (Chapter 2) over 15 greenstone exposures surrounding Mount's Bay and along the North Penwith coast have been sampled and petrographically (Chapter 4), magnetically (Chapter 5) and geochemically examined (this chapter) as part of this work. Additional petrographical and geochemical data from some of these exposures and a further 14 Cornish greenstone exposures, totalling over 100 previously published and unpublished geochemical WDXRF analyses, are available thanks to Dr. P. A. Floyd of

Keele University. All greenstone samples are geologically and geographically located in Chapter 3, detailed in Appendixes 3 & 4, with geographical locations summarised in Table 85 below.

Geological Unit (Chapter 3)	Collective location name used in this Chapter	Greenstone exposures sampled within geological unit	Section
Normannia Basement	*No samples taken*	*N/A*	
Lizard Ophiolite	**Lizard Dykes**	Porthoustock	**8.4**
Portscatho Formation	*No greenstones in unit*	*N/A*	
Pendower Formation	**Tubbs Mill Unit**	Tubbs Mill	**8.6**
Carne Formation	**Carne Formation**	Cury	**8.7**
Roseland Breccia Formation	**Roseland Breccia Formation**	Mullion Island, Nelly's Cove, Belossack, Tredawargh, Tregadjack Tregidden, Nare Head	**8.8**
Dodman Formation	*No greenstones in unit*	*N/A*	
Porthtowen Formation	*No greenstones in unit*	*N/A*	
Mylor Slate Formation	**Camborne Group**	Camborne	**8.9**
Mylor Slate Formation	**Cudden Point Group**	Cudden Point	**8.10**
Mylor Slate Formation	**Perranuthnoe Group**	Trenow Cove, Perran Sands, Perranuthnoe, Great Hogus, Marazion	**8.11**
Mylor Slate Formation	**Penzance Group**	Carn Gwavas, Gulval, Penlee, Penzance, Mousehole, Long Rock, Polkinhorne, Tredavoe	**8.12**
Mylor Slate Formation	**North Penwith Group**	Kenidjack, Zennor Point, Gurnards Head, St Ives, Clodgy Point, Carrick Dhu, Trowan	**8.13**
Dartmouth Group	*No samples taken*		
Meadfoot Group	*No samples taken*		
Middle-Upper Devonian	**South Hams Group**	Ansty Cove (Torquay), Pople's Bridge, Bow Bridge, Dorsley Barton, Luscombe Cross	**8.14**
Lower Carboniferous	**South Hams Group**	Ivybridge	**8.14**

Table 85 List of greenstone exposures referred to in this Chapter, their associated geological unit and location name (c.f. Chapter 3 for geological discussion and identification of samples)

8.3.3 Exposure geochemical data

Geochemical data for all greenstone exposure samples is summarised in Appendix 28.1. Appendix 28.2 is a sub-set of Appendix 28.1, listing the previously published or unpublished geochemical analyses from greenstone samples collected and measured by other workers.

In all PXRF measurements reported in Appendix 28.1 (and, where repeated, in this chapter) the corrected average values calculated from the individual measurements of the sample are shown. Each average elemental concentration has been adjusted using the Bias (I) coefficients reported in Chapter 6 apart from Ti, Ce and Pb. In the case of Ti, only PXRF measurements of pressed powder pellets have been adjusted using Bias I coefficients; all Ti measurements of actual rock samples have not been adjusted.

Similarly, no adjustments have been made to PXRF measurements of Ce and Pb (c.f. Section 6.17).

Geochemical analyses obtained using the OU WDXRF are reported as averages of the measured values; no adjustment to the data is made.

Previously published or unpublished geochemical analyses (from other workers) were obtained using WDXRF equipment located at Keele University. It has been assumed that this equipment has been calibrated to a similar accuracy and precision to that of the OU WDXRF, hence no adjustment to the data values has been made. This assumption is supported by work published by Markham & Floyd (1998) which indicates a significant overlap between PXRF and Keele WDXRF measurements of samples from the same exposure (Markham & Floyd op. cit.: figure 2). This assumption is further supported as there is considerable evidence of similarity between the Keele data and PXRF data seen in the element discrimination diagrams within this chapter.

Major element concentrations are reported in the relevant appendixes as both ppm and %wt of the major oxide. Conversion between the two is achieved using stoichiometric conversion factors (Potts et al. 1992)

8.4 Lizard Dykes (Porthoustock)

8.4.1 Overview of samples and localities

Two samples (MM1 & MM2) of the slightly altered plagioclase-phyric dolerite dykes found at Manacles Point, Porthoustock are used to represent the Lizard ophiolite dyke swarm. The dykes are MORB related tholeiites and are *geochemically different* to the pillow lavas found at Mullion Island and Nare Head, once thought to represent the (now missing) pillow lava carapace (Section 3.6.2.2.2 and Floyd et al. 1993). The dykes are well exposed along the west-side of the Lizard Peninsula (Chapter 3 Figure 17) and have been extensively quarried to provide roadstone (e.g. large roadstone quarry at Porthoustock was re-opened in 1998). Carn Brea, an important Neolithic habitation site is 20km north of Porthoustock, across the Helford River.

8.4.2 Inspection of petrographic, magnetic and geochemical data

Thin sections from MM1 & MM2 have *some* petrographic similarities with GpI-11 and GpIII-5 (both sub-groups have not been geochemically analysed), although the plagioclase

dominant mineralogy observed in MM1 and MM2 is different to all IPC Group I, Ia and III thin sections examined (Section 4.7.2).

MS data is not available.

	Reduced IPC Group I (n=130) (ppm ± 1sd)	Lizard sample MM1 (n=4) (ppm ± 1sd)	Lizard sample MM2 (n=4) (ppm ± 1sd)
K	3 567 ± 2 282	599 ± 802	35 ± 978
Ca	67 715 ± 14 636	67 698 ± 8 486	76 357 ± 1 502
Ti	14 959± 3 772	6 703 ± 1 008	7627 ± 449
Mn	1 532 ± 521	1031 ± 211	969 ± 226
Fe	95 632 ± 14 009	57 762 ± 5 598	61 741 ± 1 468
Rb	29.6 ± 25.8	2.2 ± 3.5	-0.5 ± 4.5
Sr	324 ± 150	268 ± 16.2	176 ± 4.3
Y	35.7 ± 6.8	23.4 ± 4.4	26.8 ± 2.7
Zr	171 ± 29.2	109 ± 4.6	101 ± 4.1
Nb	6.7 ± 2.9	0.1 ± 2.3	-0.1 ± 2.6
Ba	104 ± 64.3	9.1 ± 15.3	12.4 ± 18.6
Ce	-27.1 ± 11.4	-30.2 ± 2.4	-42.5 ± 20.1
Pb	230 ± 1013	-6.3 ± 12.7	-3.2 ± 10.7

Table 86 Average elemental composition of Lizard dyke (Porthoustock) samples and reduced IPC Group I average elemental composition. Lizard dyke data is from Appendix 28.1. Reduced IPC group I data is from Table 58.

Table 86 shows that both Porthoustock samples appear geochemically dissimilar to the reduced IPC Group I composition by having low concentrations of immobile (especially Ti, Zr and Nb) and mobile (especially K, Fe, Ba) elements. The slight differences between individual WDXRF and PXRF measurements of the same sample, reported in Appendix 28.1, are probably due to the precision of the PXRF. These differences give rise to the clusters in Figure 82 and 83 and illustrate the potential variation in measurements is reflected in the size of the error bars (which represent instrument precision, c.f. Section 7.3.1.5 (SCA charts only)). Appendix 15.2 (OU WDXRF results) reports SiO_2 levels for MM1 and MM2 are approximately 50% by wt and combined MgO + CaO at approximately 19% by wt indicating the interpretation of the element discrimination diagrams is valid for this tholeiitic rock.

8.4.3 Element discrimination diagrams

MM1 & MM2 Zr-Ti values support the accepted classification for the Lizard dykes as tholeiitic with slightly evolved N-MORB characteristics. The Zr/Y ratio is greater than 3 which suggests a 'within plate' setting for the original igneous activity. K (<0.2%) and Rb (<6ppm) concentrations are similar to those expected for MORB-type rocks (Rollinson 1993: table 4.8, repeated in Appendix 30.1) and suggest that these elements have not been mobilised during post-emplacement events (e.g. regional & contact metamorphism (or

marine weathering)). The bivariate and ternary element discrimination diagrams in Figure 82, below, (reproduced in full size in Appendix 29.1) show a reasonably tight cluster of the analyses apart from the Ti-Zr-Sr ternary diagram. In this case the effect of difference between MM1 and MM2 Sr concentrations (≈270ppm to ≈175ppm respectively) is clearly seen.

Comparison of Figure 82 with Figures 77 to 80 (Chapter 7, illustrating axe sub-group geochemistry) shows that there is some similarity in plotted position between GpI-8 and MM1 & 2, although the Lizard dykes contain significantly more Sr (>176ppm) than Co358/1627 & Co363/1632 (petrographic GpI-8: 13.0 ± 5.9ppm Sr). Examination of GpI-8 petrography (Section 4.5.3.8) indicates that this axe sub-group is petrographically different to the two Lizard Dyke samples, in that there is no visible feldspar in GpI-8.

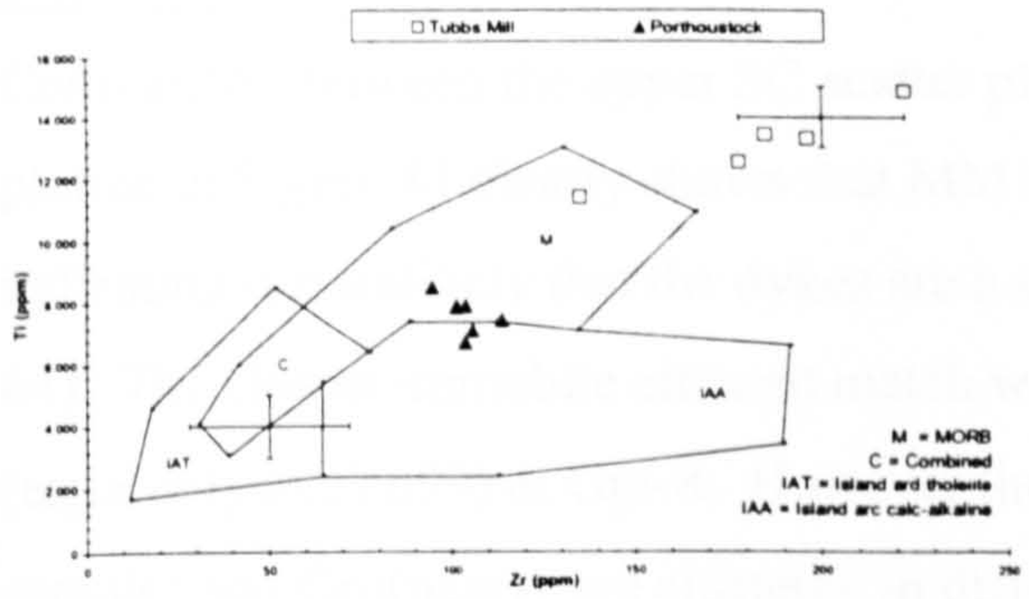

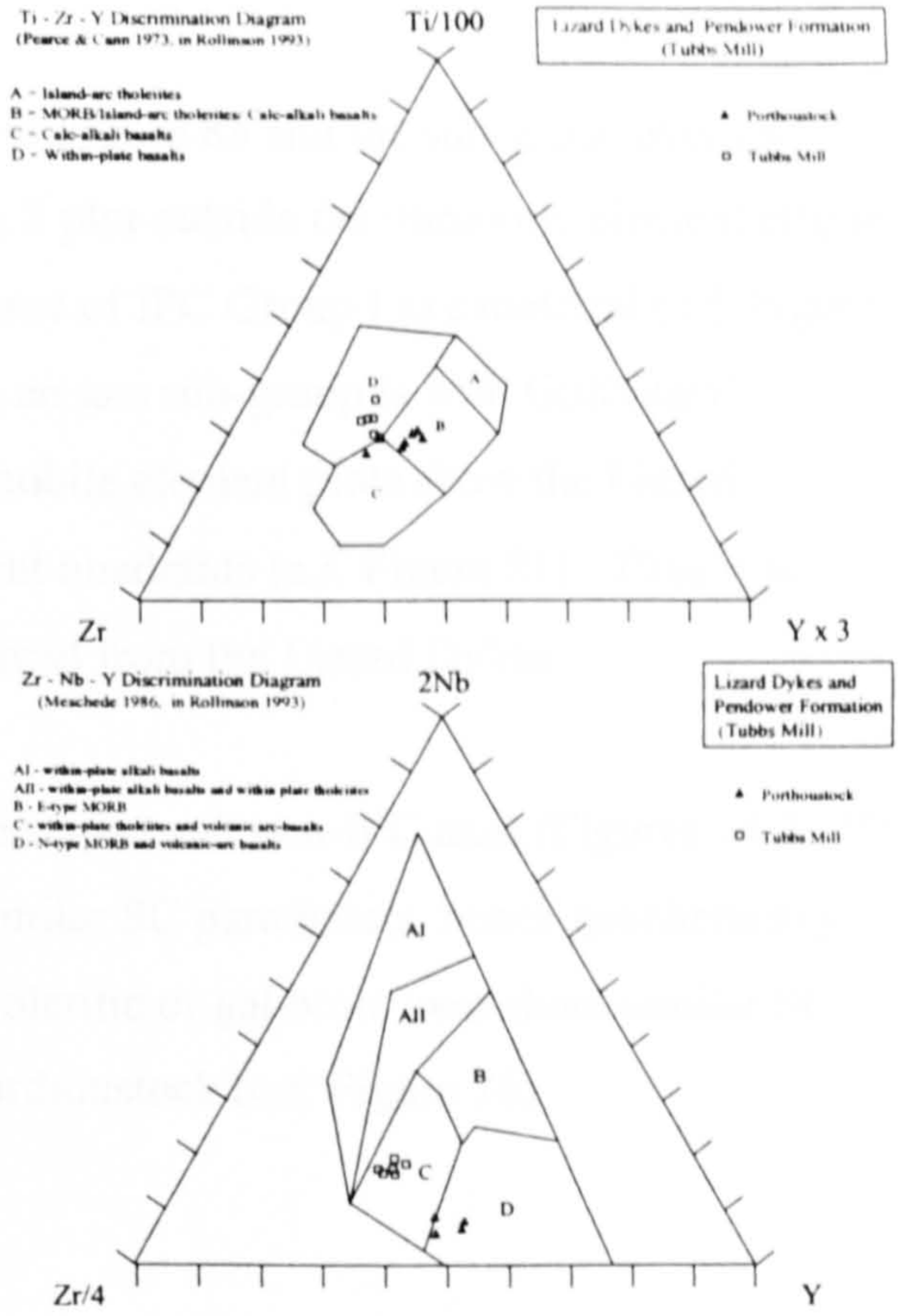

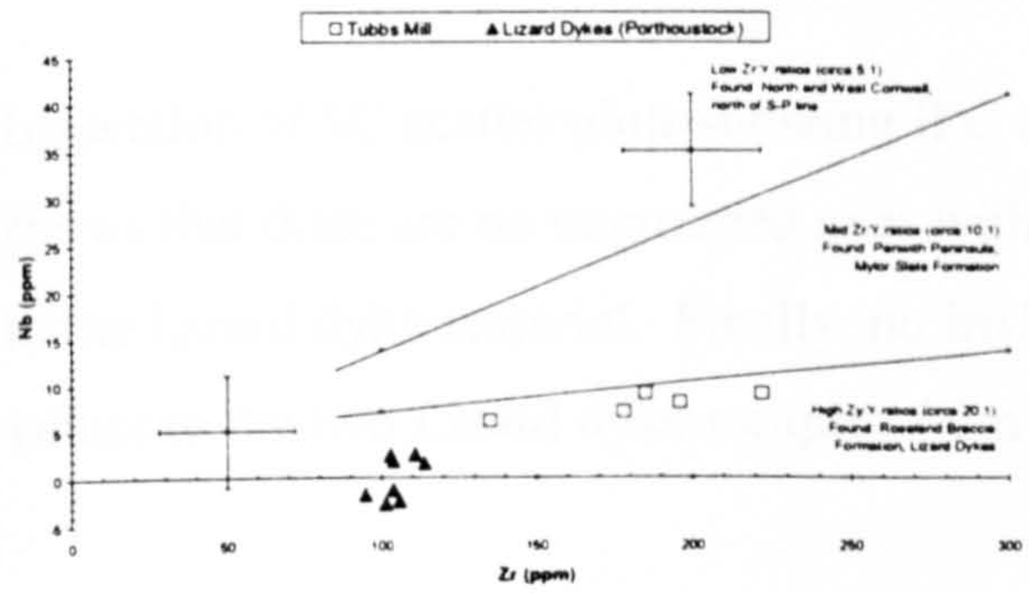

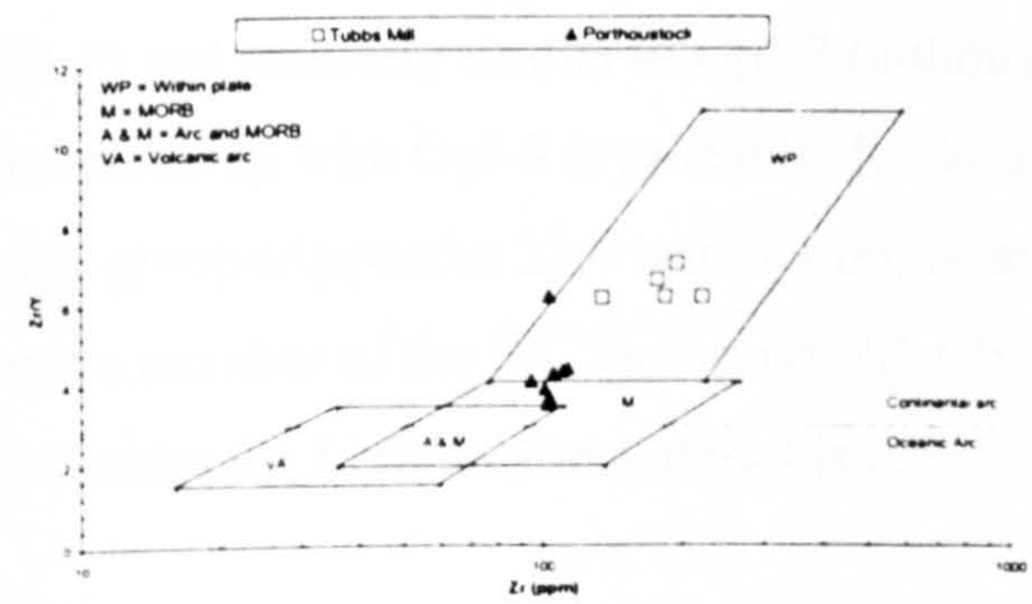

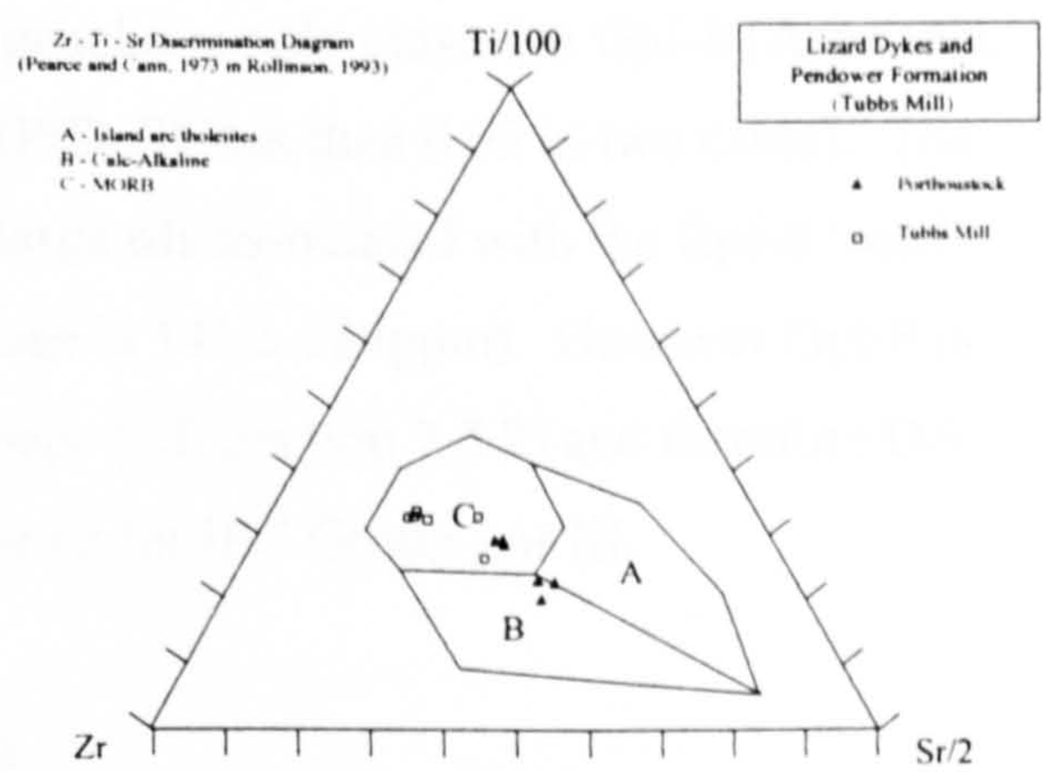

Figure 82 Immobile element discrimination diagrams for the Lizard Dykes (Porthoustock) and Pendower Formation (Tubbs Mill) greenstone samples. Lizard Dyke samples are clearly tholeiitic and N-MORB related whereas the Tubbs Mill are more evolved within plate tholeiites, geochemically different to the Lizard dyke samples

8.4.4 SCA

Comparison between the upper SC scatter plot in Figure 83 and the sub-group averages plotted in Figure 81 clearly shows that MM1 & 2 plot outside the immobile element ellipse indicating it is unlikely that the dykes are a source of IPC Group I axe material (c.f. Figure 64). The closest immobile element match with an axe sub-group is with GpI(near)1 (especially axeYo99) & GpI-8. However the mobile element plots show the Lizard samples and GpI(near)1 are clustered in different quadrants (c.f. Figure 81). Thus it is unlikely any IPC Group I axe sub-group is sourced from the Lizard Dykes.

Inspection of SC scatter plots showing IPC ungrouped and non-IPC axes (Figures 74 & 75) shows that there are no ungrouped axes with similar SC parameters, hence geochemistry, to the Lizard dyke material. Finally, no Irish doleritic or gabbroic axes share similar SC values to the two Lizard dyke samples from Porthoustock (c.f. Figure 76)

8.4.5 DA

DA indicates that the Lizard dyke samples are geochemically closest to GpI-8 (Appendix 31.1) and remotely similar to GpI-7 (although (P(D/G) less than 0.05 in two cases). The relationship with GpI-8 is probably due to the large sds associated with the GpI-8 'seed' sub-group (Appendix 23.9 last section, Sr average is 141 ± 184ppm). However GpI-8 is not a member of the IPC Group I or III sub-groups (c.f. Section 7.7.2) and therefore DA indicates the Lizard dyke material is not the source for IPC Group I or III.

8.4.6 MANOVA and Student's t-test analysis

MANOVA is not carried out since all evidence points to no match between axe and exposure.

8.4.7 Discussion

Assuming the two Lizard Dykes samples are representative of the outcrop, then the evidence above clearly shows that IPC Groups I, Ia, I/Ia, I(near), III or IIIa cannot be geochemically provenanced to the greenstone outcrop at Manacle Point, Porthoustock on the east side of the Lizard Peninsula.

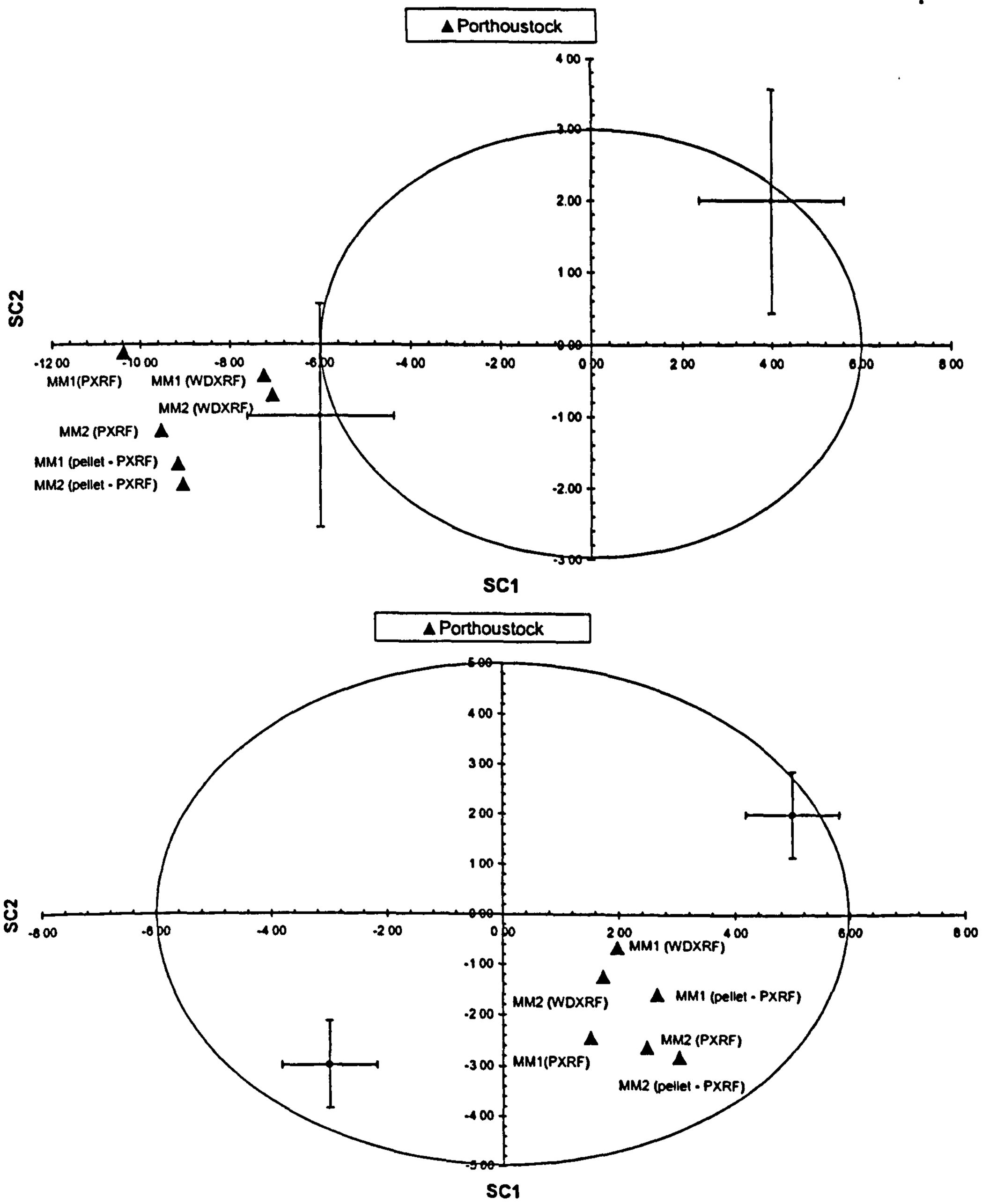

Figure 83 SC scatter plots of SC1 against SC2 for Lizard Dyke (Porthoustock) greenstone exposure based on IPC Group I SCA analysis of Ti, Y, Zr, & Nb (immobile) elements (upper chart) and K, Ca, Fe, Rb, Sr, Ba (mobile) elements (lower chart). The position occupied by the samples is outside the immobile element ellipse indicating the samples are not related to IPC Group I. Additionally, the combination of positions occupied by the greenstone within immobile and mobile element scatter plots is unique and not matched by any axe allowing the conclusion that the Lizard dyke exposure at Porthoustock is not the source of any axes examined in this work.

8.5 Gramscatho Group - overview

The allochthonous sediments of the Pendower, Carne, Roseland Breccia and Dodman Formations were deposited into the Gramscatho Basin during Mid-Late Devonian – Early Carboniferous (Selwood et al. 1998, Section 3.6.2.3). Interbedded with these sediments are shallow level and extrusive N- to T-MORB tholeiitic basalts thought to originate in a back arc or extensional environment that have been subsequently altered to greenstone (Barnes & Andrews 1986, Floyd et al. 1993, Section 3.6.2.3). Southward dipping thrust faults separate the Gramscatho Group into five Formations: Portscatho (Carrick Thrust), Pendower Formation, Carne Formation and Roseland Breccia Formation (Veryan Thrust) and the Dodman Formation bounded below by the Dodman Thrust and above by the Lizard Basal Thrust (Evens 1990, Selwood et al. 1998, Figure 16). The Portscatho and Dodman Formations do not contain any greenstone bodies, the remaining three formations are dealt with in Section 8.6 to 8.8 below.

8.6 Pendower Formation -Tubbs Mill Unit

8.6.1 Overview of samples and localities

WDXRF analyses from five samples of the T-MORB related extrusive Tubbs Mill pillow lava that outcrops on the west-side of the steep-sided valley leading up from Porthluny Cove have been provided (Floyd et al. 1993, Floyd pers. com. and Section 3.6.2.5). This exposure at the base of the Pendower Formation (c.f. Figure 15 & 16) is believed to represent the earliest phase of volcanics in the Gramscatho Basin. Geographically, the exposure is approximately 5km from prehistoric (unidentified) tumulus sites found near Veryan (north of Nare Head) (Appendix 3 & OS 1:50 000 Map 204). Tubbs Mill is less than 10km from the hypothesised origin of IPC Group XVII at Terras Mill (Section 2.5.12).

8.6.2 Inspection of petrographic, magnetic and geochemical data

Although no thin sections have been examined it is presumed that the rocks at Tubbs Mill were once fine grained and probably contained volcanic glass since they are recognised as being pillow lavas. However, since their emplacement in the Eifelian (Figure 15) any volcanic glass has almost certainly devitrified and the original mineralogy and texture has probably been altered to some degree.

No MS measurements are available for this exposure.

	Reduced IPC Group I (n=130) (ppm ± 1sd)	Tubbs Mill (n=5) (ppm ± 1sd)	Sample RV27 (ppm)	Sample RV28 (ppm)	Sample RV29 (ppm)	Sample RV30 (ppm)	Sample RV31 (ppm)
K	3 567 ± 2 282	7 703 ± 5 841	13 780	5 064	4 981	830	13 863
Ca	67 715 ± 14 636	56 871 ± 8 996	53 840	63 206	58 630	65 709	42 972
Ti	14 959± 3 772	13 116 ± 1 278	14 880	13 320	12 540	13 440	11 400
Mn	1 532 ± 521	1 194 ± 354	1 163	1 550	1 550	930	775
Fe	95 632 ± 14 009	78 442 ± 7 309	70 770	82 460	80 570	87 360	71 050
Rb	29.6 ± 25.8	12.8 ± 9.0	25	12	9	1	17
Sr	324 ± 150	178 ± 15.2	180	168	179	161	201
Y	35.7 ± 6.8	28.6 ± 5.1	36	28	27	30	22
Zr	171 ± 29.2	183 ± 31.7	222	196	178	185	135
Nb	6.7 ± 2.9	7.8 ± 1.3	9	8	7	9	6
Ba	104 ± 64.3	104 ± 66.8	207	115	75	25	97
Ce	-27.1 ± 11.4	Not recorded	-	-	-	-	-
Pb	230 ± 1013	Not recorded	-	-	-	-	-

Table 87 Average and individual elemental compositions of samples collected from the Tubbs Mill Unit and the reduced IPC Group I average composition. Tubbs Mill data is in Appendix 28.1 & 28.2 (reported here to nearest ppm) ,reduced IPC Group I data from Table 58.

The five (Keele) WDXRF analyses (Floyd pers. com. and summarised in Table 87) have immobile element concentrations similar to the reduced IPC Group I (n=130) average. Ti (11,400 to 14,880ppm) and Nb (6-9ppm) are within 1sd and, Y (22-36pm) and Zr (135-222ppm) are within 2sd of the reduced IPC Group I average (Table 58). Two samples (RV27 & RV31) have higher K concentrations (~13,750ppm), nearly 3 times that of the other samples, suggesting that some alteration through submarine weathering or contact metamorphism may have occurred (Rollinson 1993; table 3.4). Tubbs Mill Fe is greater than 1sd below the IPC Group I average, all other mobile elements are within 1sd of the reduced IPC Group I average. SiO_2 ranges between 49-51.3% (basalt) by weight and MgO + CaO is between 15 and 18% by weight (Floyd pers. com.). $Na_2O + K_2O$ is approximately 4 to 5% by wt, placing the rock on the boundary between tholeiitic and alkaline (MacDonald & Katsura 1964).

8.6.3 Element discrimination diagrams

Element geochemical discrimination diagrams, Figure 82 above (and Appendix 29.1) indicate the Tubbs Mill samples are Ti and Zr enriched within plate tholeiites. High Zr/Nb ratios (>20:1, Zr-Nb chart Figure 82) suggests that the rock belongs to the South Cornish Melange suite as identified by Floyd et al. (1993 & Appendix 30.2 part 2/6)). Ternary discrimination charts indicate the Tubbs Mill pillow lavas have slightly evolved MORB affinities, with Ti concentrations (13,116 ± 1,278) above the N-MORB norm of 8,400ppm (Saunders & Tussey 1984, Appendix 30.1). The Zr/Y ratio (>5) indicates formation in a 'within plate' setting.

Comparison between Figure 82 and Figures 77 to 80 (Chapter 7) shows the Tubbs Mill cluster occupies the same position as GpI-1, 3, 4 & 6, GpIa-1,GpI/Ia, GpI(Near)2 & GpIII-2 on the Zr-Ti & Zr-Nb discrimination diagrams (after taking into account the error bars of the latter). Tubbs Mill Zr/Y ratios are between 6-8, higher than all axe sub-groups except GpIa-1 (Zr/Y = 6) and GpI-12 (Zr/Y = 9). Although the Tubbs Mill cluster is close to the sub-groups on the three ternary diagrams the cluster does not clearly or consistently overlap any one sub-group. These observations indicate, that whilst there is a geochemical similarity between the Tubbs Mill and IPC Group I elemental concentrations (especially Zr, Ti, Nb), the ratios of these elements are slightly different.

8.6.4 SCA analysis

Figure 84, below, shows the Tubbs Mill samples all plot within the immobile element ellipse (upper chart) and comparison with Figure 81 shows the Tubbs Mill data cluster overlaps with GpI-1, 2, & 4 axe sub-group clusters. The overlap with GpI-1 is repeated within the mobile element (lower) chart (RV28 & 29 and Figure 81 lower), although the two high K samples (RV27 & 31) plot well away from the sub-group cluster. This suggests a potentially close geochemical match between Tubbs Mill and IPC Group I, and a possible relationship with GpI-1, 2 & 4.

Comparison between SC scatter plots in Figure 84 and county based SC scatter plots in Figures 65, 66, 68 and 69 (Chapter 7) shows that axes from Cornwall, Yorkshire and Essex (in part) cluster in comparable positions on the immobile and mobile element SC scatter plots. The low number of axes preclude the certainty that other counties may overlap Tubbs Mill, however it is clear that axes from Wiltshire, and the Thames Valley (Oxford, Kent, London, Bedford & Essex) do not share similar mobile element concentrations to those found at Tubbs Mill (Figure 84 lower).

After taking into consideration the calculated error bars it is found that only three IPC ungrouped axes (Co138/722, Co152/739 & HaT01 (Figure 74, & 75) and that no Irish axes (Figure 76) share similar positions to Tubbs Mill on both immobile and mobile SC scatter plots.

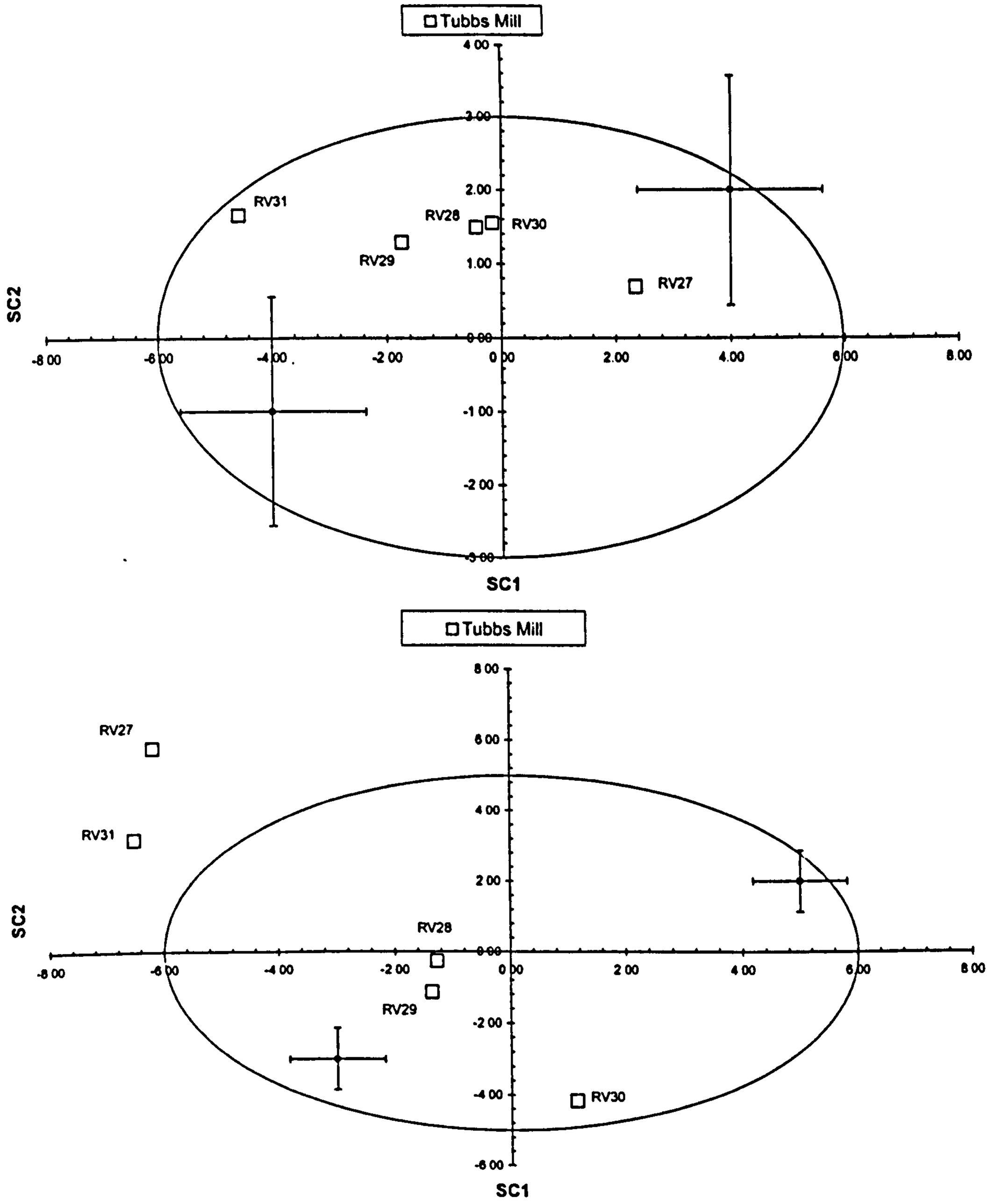

Figure 84 Graphs of SC1 against SC2 for Pendower Formation (Tubbs Mill) greenstone exposure based on IPC Group I SCA analysis of Ti, Y, Zr, & Nb (immobile) elements (upper chart) and K, Ca, Fe, Rb, Sr, Ba (mobile) elements (lower chart). Apart from RV27 & RV31 the points plot inside the two ellipses indicating a potential geochemical similarity with IPC Group I, and especially GpI-1.

8.6.5 DA

DA matches the Tubbs Mill samples to axe sub-groups GpI-1, 2, 3 & 4 based on similarity of immobile element concentrations (Table 88), which is as expected from the data inspection and SCA results described above. RV27 & 31 are assigned to non IPC Groups I sub-groups (GpIII-1 & GpI(near)1) on the basis of their high K, low Fe and Sr values compared to those observed in the IPC Group I sub-groups. Similarly, the three remaining Tubbs Mill samples are statistically closer to GpI-8 (not a IPC Group I sub-group), but have low P(G/D) values indicating they share similarities with at least one other sub-group, with GpI-2 & 7 cited as the second highest probabilities (both IPC Group I sub-groups) (Appendix 31.1).

Sample	Immobile DA 1st	2nd	Mobile DA 1st	2nd	Indication
RV27	GpI-4	GpI-3	GpI(near)1	GpIII-1	Not IPC Group I
RV28	GpI-3	GpI-4	GpI-8	GpI-2	? IPC Group I
RV29	GpI-3	GpI-1	GpI-8	GpI-2	? IPC Group I
RV30	GpI-1	GpI-4	GpI-8	GpI-7	? IPC Group I
RV31	GpI-2	GpI-3	**GpIII-1**	GpI(near)1	Not IPC Group I

*Table 88 Summary of DA of Tubbs Mill samples against 16 axe sub-groups (sub-groups **after** axe DA). DA indicates the Tubbs Mill immobile element concentrations are similar to IPC Group I, but that mobile element concentrations are unlike IPC Group I. Matches in bold indicate P(D/G) is less than 0.05. Non-IPC Group I sub-groups are indicated in boxes.*

Using the criteria set out in Section 7.7.2, DA results suggest that Tubbs Mill is possibly a candidate for the source of IPC Group I axe material, but immobile element concentrations and ratios are sufficiently different to the reduced IPC Group I to conclude it is only a remote possibility.

8.6.6 MANOVA and Student's t-test analysis

MANOVA calculations between the Tubbs Mill samples and the *petrographic sub-groups* using immobile elements Ti, Y, Zr & Nb were undertaken to further examine the relationship between petrographic axe sub-groups and Tubbs Mill samples. MANOVA results support the DA results by indicating that the average immobile element concentrations from Tubbs Mill and GpI-2 (0.197), GpI-7 (0.182) and GpIa-1 (0.175) could have been derived from the same data set. The significance values (reported in brackets in the previous sentence) for these three sub-groups are greater than 0.05 indicating that the null hypothesis cannot be rejected. Significance values, calculated from the same MANOVA test, were less than 0.05 for comparisons between Tubbs Mill and GpI-6, GpIa-2, GpI/Ia, GpI(near)1, GpI(near)2 and GpIII-2 indicating that the null

hypothesis can be rejected in these cases : the elemental concentrations in these axe sub-groups probably do not originate from Tubbs Mill.

Student's 't-test' was used to compare means between Tubbs Mill and GpI-2, GpIa-1 and GpI-7. This time the *discriminant-derived sub-groups* were used to further examine the degree of similarity indicated by DA results and the above MANOVA. The results are summarised in Table 89 below.

	K	Ca	Ti	Fe	Rb	Sr	Y	Zr	Nb	Ba
GpI-2	0.311	0.315	**0.042**	0.052	0.241	0.231	0.343	**0.000**	**0.034**	0.603
GpI-7	0.184	0.113	**0.026**	0.110	0.262	**0.026**	**0.032**	**0.000**	**0.000**	0.533
GpIa-1	**0.042**	**0.004**	**0.002**	**0.002**	0.208	**0.022**	**0.000**	0.205	**0.001**	0.762

Table 89 Summary of Student's t-test between Tubbs Mill and GpI-2, GpI-7 and GpIa-1 for immobile and mobile elements (sub-groups after discrimination). Values in bold indicate the null hypothesis: that the means are equal, can be rejected using a 0.05 value for significance

The above tests indicate that the null hypothesis: that the means of the two data sets are equal, cannot be rejected in 15 of the 30 cases. In these 15 cases only 2 relate to comparisons between immobile element concentrations thus giving rise to question the degree of similarity indicated by DA and MANOVA. Comparing elemental averages (Table 87 and Appendix 23.9) shows that Tubbs Mill and GpI-2 Ti values are 13,116 ±1,278ppm and 11,571 ±1,499ppm respectively and that the Tubbs Mill *Zr* average (183 ± 31.7ppm) is higher than GpI-2 (131 ± 20.1ppm) by 52ppm. This comparison illustrates that one reason for the low t-test significance value is the relatively small size of the sd associated with the average values.

The MANOVA and t-test calculations do go some way to showing that there is a similarity between the elemental composition or rocks from Tubbs Mill and IPC Group I (recall that GpI-2, GpI-7 and GpIa-1 are all considered representative of IPC Group I), but that a specific relationship with a single axe sub-group is not found.

8.6.7 Discussion

The Tubbs Mill greenstone exposure is a mildly enriched tholeiitic pillow lava, which means it should have originally been a fine grained rock, with interstitial volcanic glass. It has been assumed that the primary mineralogy and texture has not been completely replaced since the rocks have only been subjected to pumpellyite to low amphibolite levels of metamorphism (Floyd 1984, Floyd et al. 1993). Fine-grained textures have not been observed in the vast majority of IPC Group I, Ia or III thin sections examined. Thus the

petrographic evidence suggest the extrusive igneous rocks found at Tubbs Mill are unlikely to be the source of IPC Group I.

Geochemically, inspection, SCA and DA have shown that element concentrations found in the Tubbs Mill samples are similar to the average reduced IPC Group I values, although no specific match with an axe sub-group could be established. Although sharing similar levels of immobile elements, Tubbs Mill contains less Fe, Sr and more K compared to the average reduced IPC Group I value (Table 87).

Thus petrographically, the greenstone at Tubbs Mill is believed to be different to IPC Group I, yet geochemically the greenstone at Tubbs Mill has similar element concentrations to IPC Group I, especially immobile elements. Further inspection of the immobile element concentrations and associated ratios show that Tubbs Mill has, on average slightly less Ti and Y than the reduced IPC Group I suggesting that the pillow lavas at Tubbs Mill are probably less evolved than the average axe material. The difference in mobile element concentrations could be due to submarine weathering (increasing K) or/and low grade metamorphism (K, Fe and Sr are mobile at low grades of metamorphism). This dichotomy leads to the proposition that **Tubbs Mill is probably not the source of IPC Group I axes**, but that it is probably geochemically related to the actual source.

8.7 Carne Formation – Cury

8.7.1 Overview of samples and localities

Two samples, CUR001 & 002 were collected as loose material from within the Cury greenstone outcrop as indicated on the Lizard geological map (BGS Sheet 349). Flett (1946) indicated that the outcrop is 'ill exposed' and made of intrusive ophitic dolerite (Section 3.6.2.6). The fact that no exposure was found supports the first of Flett's observations, and the mineralogy described by Flett is not seen in the CUR001 and CUR002 thin sections (see below), indicating that the two samples did not come from the exposure. However, even thought the samples are not representative of the Cury greenstone body examination of the samples is presented here to provide a complete record of samples taken.

8.7.2 Inspection of petrographic, magnetic and geochemical data

CUR001 contains abundant clinozoisite and epidote set in a heavily altered chloritic matrix and CUR002 is a very fine-grained mineralogically immature sandstone (and thus not considered further, other than to report the observations made). Hence both rocks appear to be petrographically unlike any IPC Group I, Ia or III axe thin section examined (Section 4.8.3).

No MS measurements are available.

	Reduced IPC Group I (n=130) (ppm ± 1sd)	CUR001 (ppm)	CUR002 (ppm)
K	3 567 ± 2 282	-32	12 871
Ca	67 715 ± 14 636	13 390	1 589
Ti	14 959± 3 772	744	3 570
Mn	1 532 ± 521	1 057	383
Fe	95 632 ± 14 009	64 581	31 084
Rb	29.6 ± 25.8	-7	54
Sr	324 ± 150	8	74
Y	35.7 ± 6.8	5	23
Zr	171 ± 29.2	4	249
Nb	6.7 ± 2.9	-3	13
Ba	104 ± 64.3	-30	316
Ce	-27.1 ± 11.4	-47	25
Pb	230 ± 1013	-18	15

Table 90 Elemental compositions of samplesCUR001 & CUR002 and the reduced IPC Group I average composition. CUR001 & CUR 002l data is in Appendix 28.1 & 28.2 (reported here to nearest ppm) ,reduced IPC Group I data from Table 58.

Geochemically, CUR001 has small concentrations of immobile elements and CUR002 has very low concentrations of Ti and very low Fe (3,570 & 31,084ppm respectively) compared to the reduced IPC Group I values. Thus, on balance, both samples are distinctly geochemically different to IPC Group I. (Note: the geochemistry of CUR001 is similar to that expected from sandstone, e.g. CUR002. A trace to the original data records showed no crossover in the results so it is assumed the analyses correctly represent the two samples.)

8.7.3 Element discrimination diagrams

Cury samples are included in the Carne and Roseland Breccia Formation geochemical discrimination diagrams in the next section (Figure 85). The samples plot well away from any axe sub-group, confirming their different geochemistry. The discrimination plots cannot be used to identify rock petrogenesis, because they do not meet the qualifying criteria for interpretation of the element discrimination diagrams used (c.f. Section 8.2.3).

8.7.4 SCA

CUR001 & CUR002 are plotted with the Roseland Breccia Formation SC scatter plots, Figure 86 (in Section 8.8.4 below). The two samples plot well away from any axe sub-group, IPC ungrouped or Irish axe analysed as part of this work.

8.7.5 DA

DA clearly indicates the two Carne Formation samples are not IPC Group I. CUR001 is matched with GpI-13 (for immobile and mobile element DA) and CUR002 has P(D/G) less than 0.05 for both mobile and immobile DA. This suggests CUR001 is geochemically most similar to GpI-13 (which is not a recognised IPC Group I sub-group).

8.7.6 MANOVA and Student's t-test analysis

Not carried out.

8.7.7 Discussion

CUR001 is probably not representative of the Carne Formation greenstone body **at Cury and is petrographically different to the axes examined within this work.** DA indicates that CUR001 shares similar geochemistry to GpI-13, but inspection of geochemical data (Table 90) clearly shows CUR001 is distinctly different to GpI-13 (Appendix 23.9) which is due to the fact that DA always assigns to a group, even if it is a very poor match. Therefore, whilst it is possible to state that CUR001 is non representative of IPC Group I greenstone, it is not possible to eliminate the Cury greenstone body from the search for the source of IPC Group I.

8.8 Roseland Breccia Formation

8.8.1 Overview of samples and localities

Seven locations; Mullion Island, Belossack, Tregadjack, Tredawargh, Tregidden, Nelly's Cove and Nare Head, within the Roseland Breccia Formation have been previously sampled, providing a total of 30 individual (Keele) WDXRF geochemical analyses (Floyd 1984, pers. com, details in Section 3.3.7.2, Figure 17 and Appendix 4). Considerable contemporaneous tholeiitic, broadly N-MORB, extrusive and shallow level intrusives are found in the Roseland Breccia Formations (Holder & Leveridge 1986) and these seven locations represent exposures across the formation outcrop (Section 3.6.2.7 & Figure 17). Mullion Island, on the east side of Mount's Bay, consists of hyaloclastite and mildly aphyric tholeiitic vesicular pillow lavas. Belossack, Tregadjack, Tredawargh, and

Tregidden are all south of the Helford River and consist of often brecciated, vesicular pillow lavas/extrusive basalts. Nelly's Cove pillow lavas are MORB related and found exposed on the west-side of the Lizard Peninsula. The Nare Head greenstone body juts out into Gerrans Bay and is topped with pillow lavas of similar mineralogy and texture to those found at Mullion Island. (Details above summarised from Floyd 1984, et al. 1993, Flett 1946 and Appendix 4.) Nare Head is probably a major olistholith (large km sized block of igneous rock that has slid down the front of the northward prograding allochthonous block) within the Roseland Breccia Formation and contains pillow lavas, sheeted dolerites and gabbro (Holder and Leveridge 1986). Floyd (1984) indicates the Nare Head greenstone is tholeiitic with MORB affinities and suggests that Nare Head represents the most primitive igneous rock found in the Roseland Breccia Formation. Note that only the pillow lavas within these exposures have been sampled.

The coastal exposures at Mullion Island, Nare Head and Nelly's Cove are easily reached by boat. The inland exposures at Belossack, Tregadjack, Tredawargh, and Tregidden are all relatively well exposed along the northern Lizard Boundary thrust fault scarp. The Carne Brea Neolithic site is less than 20 km due north of these exposures.

8.8.2 Inspection of petrographic, magnetic and geochemical data

The author has examined no thin sections from any of the seven exposures so the discussion here uses existing published petrographic descriptions (Floyd et al. 1993, Flett 1946).

Mullion Island pillow lavas contain varying amounts of vesicles and have a primary mineralogy of plagioclase, clinopyroxene and ilmenite which has been altered by pumpellyite facies metamorphism to include chlorite, pumpellyite, and amphibole (Floyd et al. 1993). This mineralogy is generally similar to IPC Group I, although the pillow lavas appear to be finer grained and with vesicles, the latter not being observed in any of the axe thin sections examined. Belossack, Tregadjack, Tredawargh, Tregidden and Nelly's Cove pillow lavas are petrographically similar to those found at Mullion Island with plagioclase, pyroxene (augite) and iron oxide as the primary mineralogy (no olivine) and varying amounts of vesicles, apparently more pronounced to the west (Belossack) reducing eastwards to Nelly's Cove (Flett 1946). Again, this mineralogy is similar to IPC Group I. Nare Head is petrographically similar to Mullion Island, and consists of a fine grained

texture with primary plagioclase, clinopyroxene and ilmenite altered by pumpellyite facies metamorphism to amphibole, chlorite and pumpellyite.

No MS measurements are available.

Table 91 summarises the geochemical data for the Roseland Breccia samples and IPC Group I (n=130). Sample MZ03 from Belossack is atypical and appears to be a cumulate as it contains 35% MgO by weight and 2,450ppm Cr & 2,200ppm Ni (Floyd pers com.) and has been omitted from Table 91. Apart from this sample, immobile elemental concentrations from all seven exposures are generally within ±2sd of the reduced IPC Group I (n=130) average. Average Nb concentrations for each of the 7 exposures (Table 91 below) are within 1sd of the reduced IPC Group I average (6.7 ± 2.9ppm). Similarly, all exposure Ti and Y averages are within 1sd of the IPC Group I average (14,959 ± 3,772ppm and 35.7 ± 6.8ppm respectively) apart from Nelly's Cove and Nare Head where Ti is within ±2sd, Nelly's Cove where Y is within ± 2sd and Belossack where the reported Y concentration is 52ppm, greater than +2sd of the IPC Group I average (Table 91). Average exposure Zr concentrations are all within ±2sd of the reduced IPC Group I average (171 ± 29.2ppm) except for Belossack and Tregadjack.

Exposure mobile element concentrations are more variable between exposures, but are similar to the reduced IPC Group I (n=130). Exposure sample K & Ca concentrations range from approximately 1,000 to 15,000ppm and 25,00 to 157,000ppm respectively, probably due to varying degrees of metasomatism from the nearby Carnmenellis and Godolphin granites. Exposure Fe concentrations are generally lower than the reduced IPC Group I average (95,632 ± 14,009ppm) at between 60,000 –90,000ppm. Rb, Sr and Ba concentrations are likewise lower, but generally within 2sds of the reduced IPC Group I average.

Major element concentrations of the Roseland Breccia exposure samples range between 48 to 52% wt SiO_2, 4 to 5% wt $Na_2O + K_2O$ and 16 to 18% wt MgO + CaO (Floyd pers. com.) confirming the evolved tholeiitic, calc-alkaline nature of the exposures and indicating that the rocks meet the criteria for use of the element discrimination diagrams.

	Reduced IPC Group I (n=130) (ppm ± 1sd)	Mullion Island (n=5) (ppm ± 1sd)	Belossack (n=1) (ppm)	Tregadjack (n=3) (ppm ± 1sd)	Tredawargh (n=2) (ppm ± 1sd)
K	3 567 ± 2 282	7 936 ± 4 353	11 455	12 313 ± 1 750	3 652 ± 0.0
Ca	67 715 ± 14 636	78 907 ± 18 644	52 695	64 064 ± 18 222	55 949 ± 7 330
Ti	14 959± 3 772	11 616 ± 911	15 300	13 400 ± 2 042	13 710 ± 297
Mn	1 532 ± 521	1 147 ± 149	1 085	1240 ± 134	1 201 ± 164
Fe	95 632 ± 14 009	82 880 ± 7 561	81 340	74 690 ± 6 986	81 235 ± 1 633
Rb	29.6 ± 25.8	18.2 ± 10.6	38	20.0 ± 7.0	6.5 ± 0.7
Sr	324 ± 150	277 ± 45.6	50	65.7 ± 15.9	104 ± 5.7
Y	35.7 ± 6.8	29.8 ± 2.2	52	38.7 ± 2.1	38.0 ± 4.2
Zr	171 ± 29.2	152 ± 16.3	268	249 ± 17.7	206 ± 19.1
Nb	6.7 ± 2.9	6.2 ± 0.4	8	8.3 ± 1.2	7.0 ± 1.4
Ba	104 ± 64.3	48.6 35.1	72	45.3 ± 8.3	55.5 ± 10.6
Ce	-27.1 ± 11.4	Not measured	Not measured	Not measured	Not measured
Pb	230 ± 1013	Not measured	Not measured	Not measured	Not measured

	Reduced IPC Group I (n=130) (ppm ± 1sd)	Tregidden (n=2) (ppm ± 1sd)	Nelly's Cove (n=3) (ppm ± 1sd)	Nare Head (n=12) (ppm ± 1sd)
K	3 567 ± 2 282	2 878 ± 1 155	2 767 ± 1 790	5 368 ± 3 300
Ca	67 715 ± 14 636	63 182 ± 2 713	44 711 ± 4 252	69 784 ± 29 667
Ti	14 959± 3 772	13 020 ± 722	8 240 ± 386	10 730 ± 2 076
Mn	1 532 ± 521	1 163 ± 63.3	1 317 ± 77.5	917 ± 303
Fe	95 632 ± 14 009	78 726 ± 3 960	82 273 ± 1 680	72 969 ± 11 488
Rb	29.6 ± 25.8	6.0 ± 2.9	3.3 ± 4.0	10.5 ± 5.6
Sr	324 ± 150	77.7 ± 2.6	152 ± 5.5	173.5 ± 90.4
Y	35.7 ± 6.8	37.0 ± 2.9	27.3 ± 0.6	30.2 ± 4.5
Zr	171 ± 29.2	205 ± 8.3	132.3 ± 3.5	119.8 ± 24.2
Nb	6.7 ± 2.9	6.7 ± 0.5	4.7 ± 0.6	6.5 ± 1.3
Ba	104 ± 64.3	28.3 ± 17.9	219 ± 94.0	32.8 ± 15.8
Ce	-27.1 ± 11.4	Not measured	Not measured	Not measured
Pb	230 ± 1013	Not measured	Not measured	Not measured

Table 91 Average elemental compositions of the seven Roseland Breccia greenstone exposures and the reduced IPC Group I average composition. Roseland Breccia Formation data is in Appendix 28.1 & 28.2, reduced IPC Group I data from Table 58.

8.8.3 Element discrimination diagrams

Element discrimination diagrams are reproduced in Figure 85, below and in full size in Appendix 29.2. Immediately obvious on the binary discrimination diagrams is that the exposures appear to form an evolving trend Nare Head – Mullion Island – Tredawargh/Tregidden – Tregadjack/Belossack, with Nelly's Cove off the trend on account of lower Ti (see Zr – Ti chart top-left in Figure 85). Inspection of each exposure cluster also suggests an evolving trend within the exposure, although there are insufficient samples to confirm this observation. The element discrimination charts, therefore, support the published findings that the Roseland Breccia greenstones are tholeiites with an evolved (or evolving?) MORB affinity. The Floyd et al. (1993) Zr-Nb diagram was developed using this data, with the high Zr/Nb ratios used to distinguish the Roseland Breccia volcanics from the more evolved Mylor Slate and mid-Upper Devonian alkali basalts (Floyd pers. com.).

Comparing Figure 85 with Figure 77 to 80 reveals a considerable overlap between IPC Group I sub-groups and the exposures. Specifically GpI-1, 3, 4 & 6 overlap Mullion Island, Tredawargh, Tregidden and the upper part of the Nare Head data cluster. The most consistent overlap is between Mullion Island and IPC Group I sub-groups GpI-1, 3, 4 & 6. GpIa-1, GpI/Ia and GpIII-2 also overlap the position of the Mullion Island cluster.

Conversely, there appears to be no overlaps between the Roseland Breccia Formation greenstones and GpI-12, 13, GpI(near)1 and GpIII-1 indicating that these axe sub-groups do not originate from within the Roseland Breccia Formation.

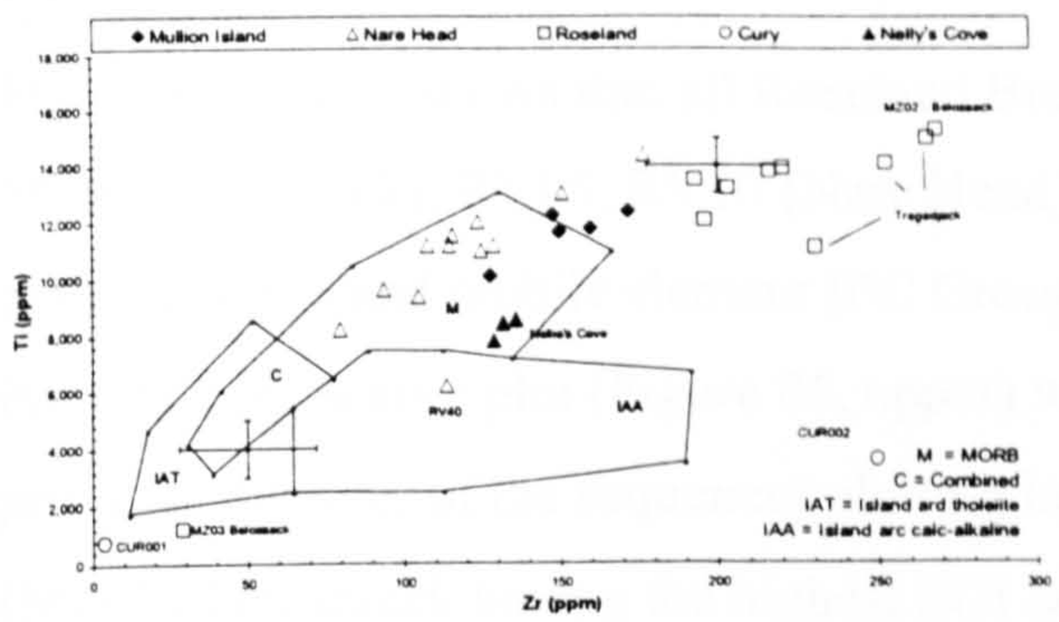

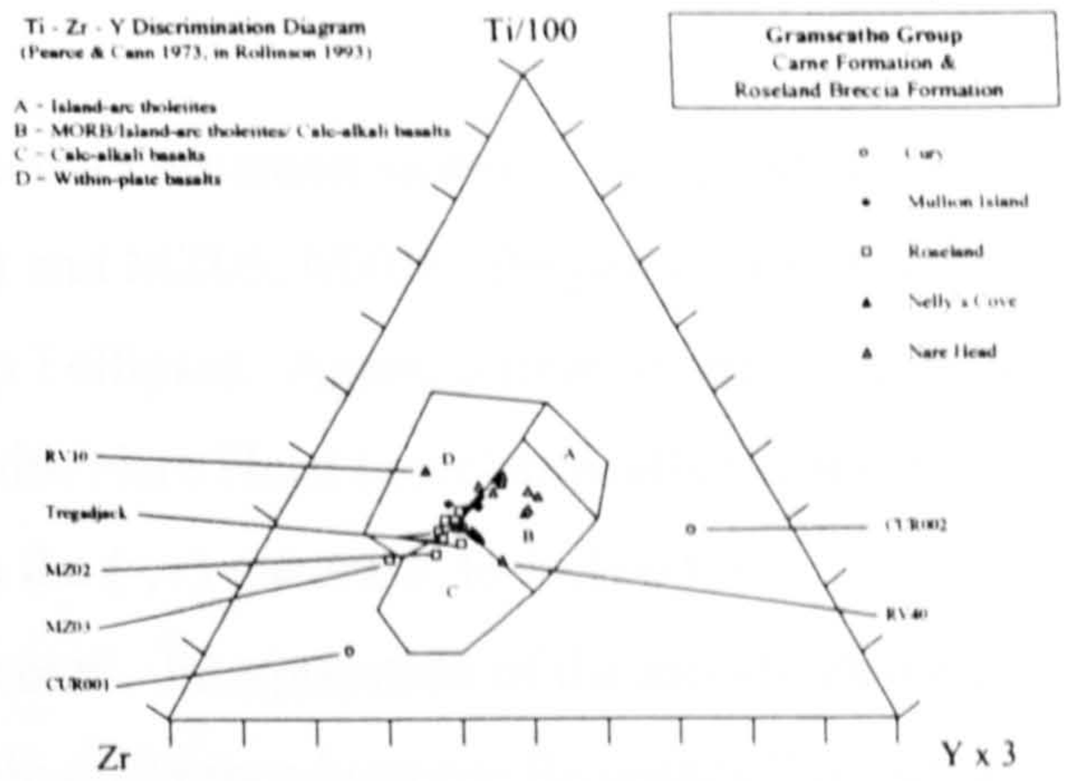

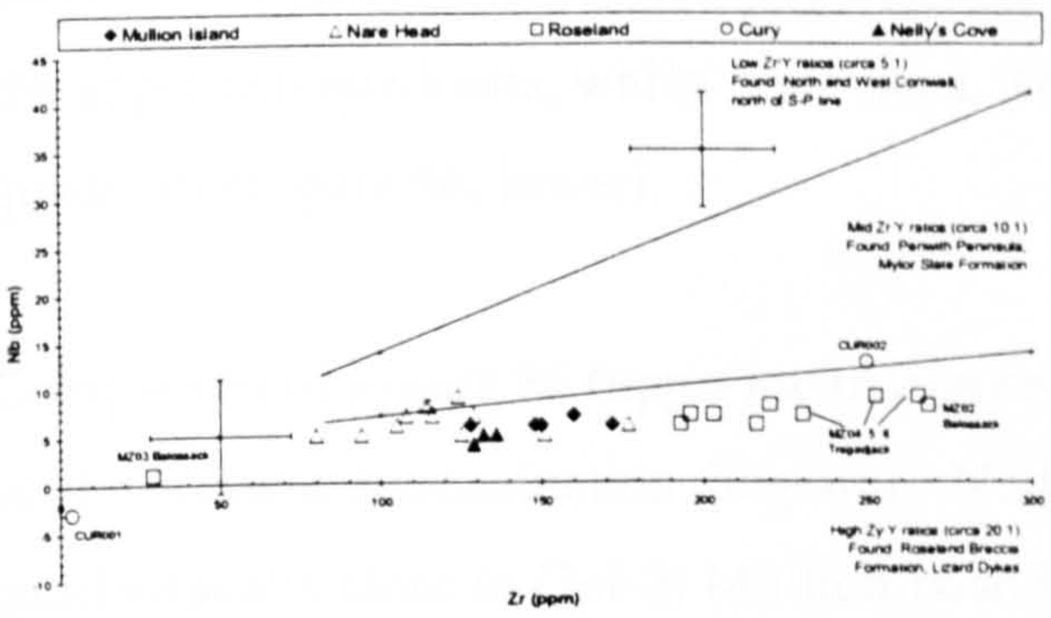

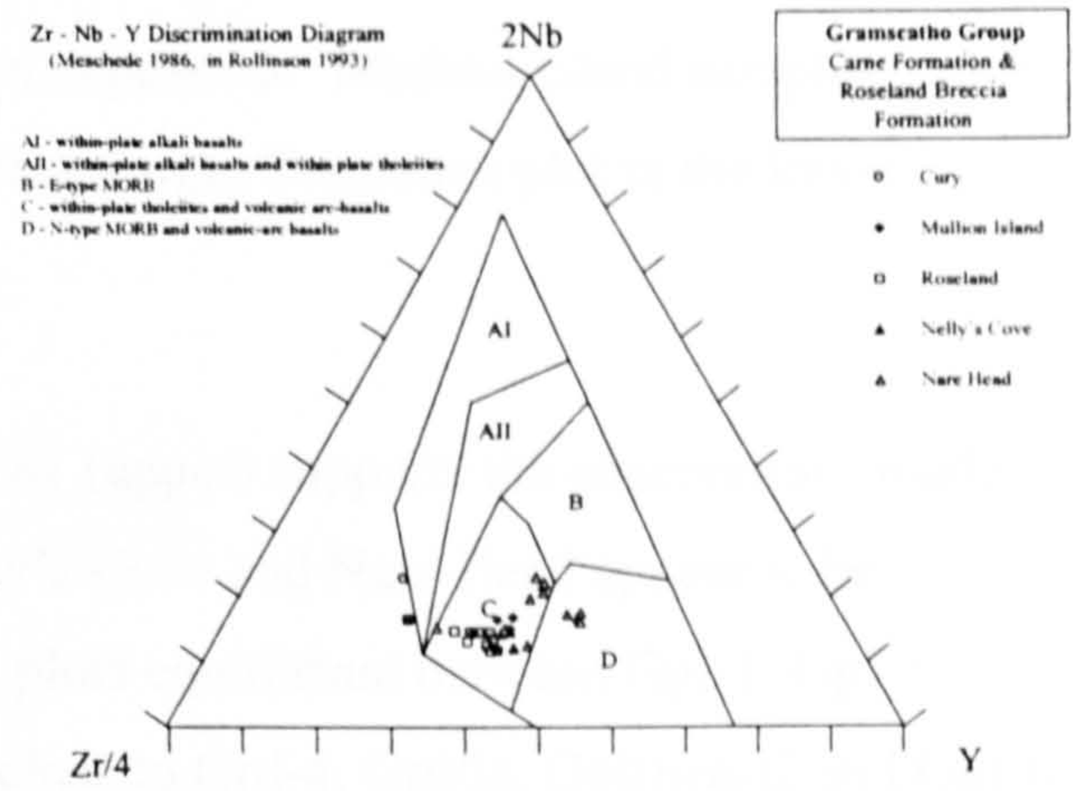

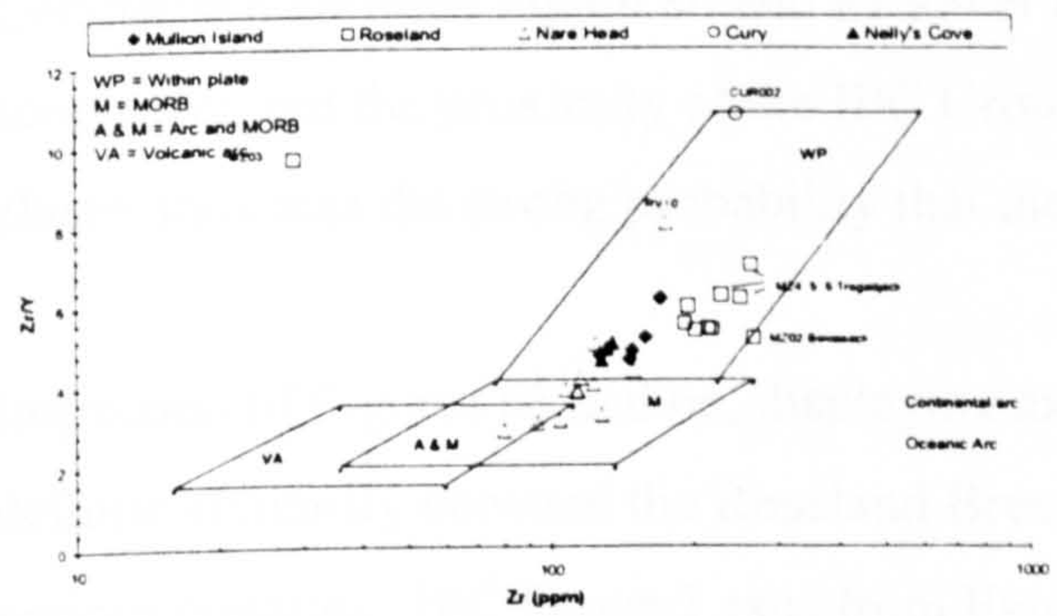

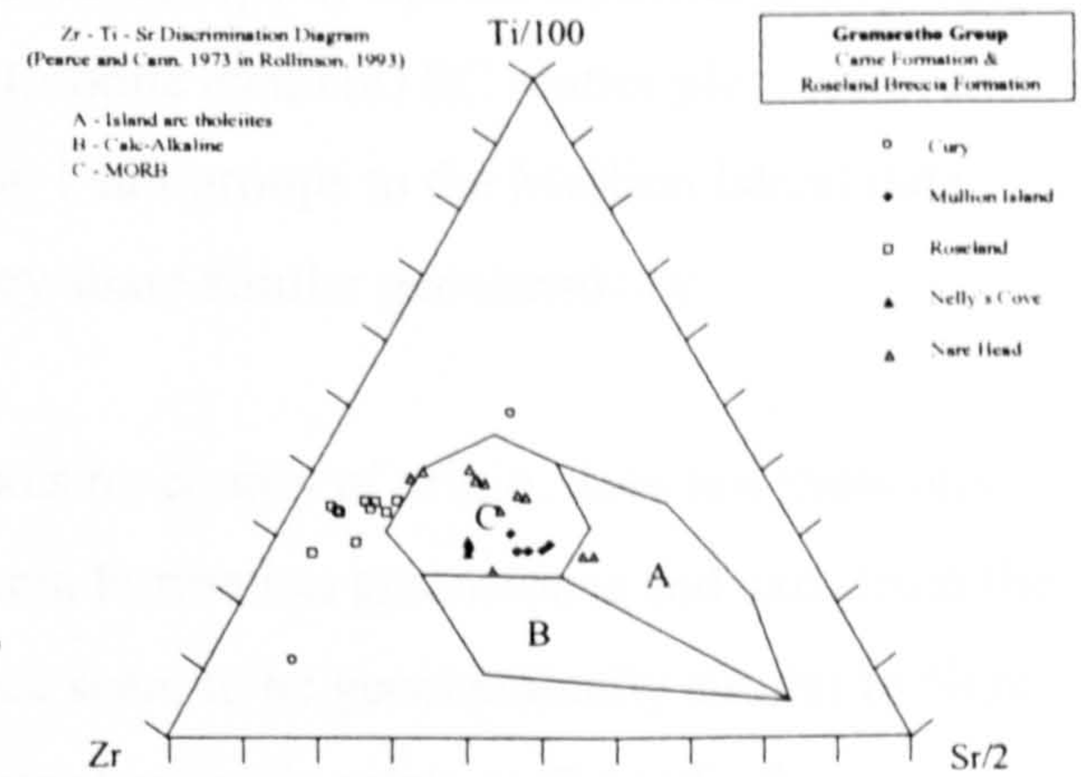

Figure 85 Element discrimination diagrams for Carne Formation (Cury) and Roseland Breccia Formation. Two Carne Formation samples are clearly not basaltic and are not similar to any axe sub-group. Roseland Formation exposures form elemental trends and therefore appear to be related, with Nare Head the most primitive and Tregadjack the most evolved. There is considerable overlap between the Roseland Breccia greenstone exposures and axe sub-groups (see text for discussion). Data from previous published and unpublished WDXRF analyses.

8.8.4 SCA

Figure 86, below, shows that all Roseland Breccia Formation samples, except MZO2, MZ03 (Belossack), RV05, RV10 (Nare Head) and MZ05, MZ06 (Tregadjack) plot within both immobile and mobile element IPC Group I ellipses. Again, a trend is seen within the immobile SC scatter plot (Figure 86, upper) with Nare Head (geochemically the most primitive member of the sequence) plotting in the (-,+) quadrant, to Belossack (MZ03)/Tregadjack having the highest SC1 scores. Interpretation of the mobile element SC scatter plot is not clear, but there is a visible difference between Belossack/Tregadjack and the remaining Roseland Breccia Formation exposures. Mullion Island samples plot in the upper two quadrants, whilst Nare head, Tredawargh, Tregidden plot in the lower two quadrants (Figure 86, lower).

Comparison of Figure 86 (upper) with Figure 81 (upper) supports the observations made on the element discrimination diagrams. Nelly's Cove and Nare Head appear to be geochemically close to GpI-2; Mullion Island plots equidistant between GpI-1, GpI-3; Tredawargh , Tregidden and Tregadjack plot close to GpI-4, GpI/Ia, GpI(near)2 and GpI-6. Comparison between Figure 86 and 81 lower (mobile element) SC scatter plots is not as conclusive, but the proximity of the IPC Group I sub-groups to the Mullion Island data cluster indicates the strong probability that they share similar geochemistry.

Inspection of Figures 65 and 66, displaying axes by county of origin, does not show any definite similarity between the Roseland Breccia Formation greenstones and axes from the various counties. IPC Group I axes from Essex seem to be geochemically similar to Nare Head and other Thames valley axes seem to geochemically relate to Tregadjack, Tregidden, Tredawargh. However, these patterns are not repeated in Figures 68 & 69 (mobile elements) where the Thames Valley and most of the Essex axes seem to concentrate in the (+,+) quadrant, whilst the exposure mobile elements congregate in the (-,+) and (-,-) quadrants. IPC Group I axes found in Cornwall, Dorset and Somerset appear to have the closest geochemical relationship with to Tregadjack, Tregidden, Tredawargh.

Ungrouped axes from Hampshire, Norfolk, Lincolnshire and Yorkshire share potentially similar mobile and immobile element concentrations with Tregadjack, Tregidden and Tredawargh (Figure 74, 75). No Irish axes plot in the same positions on both immobile and mobile SC scatter plots (Figure 76).

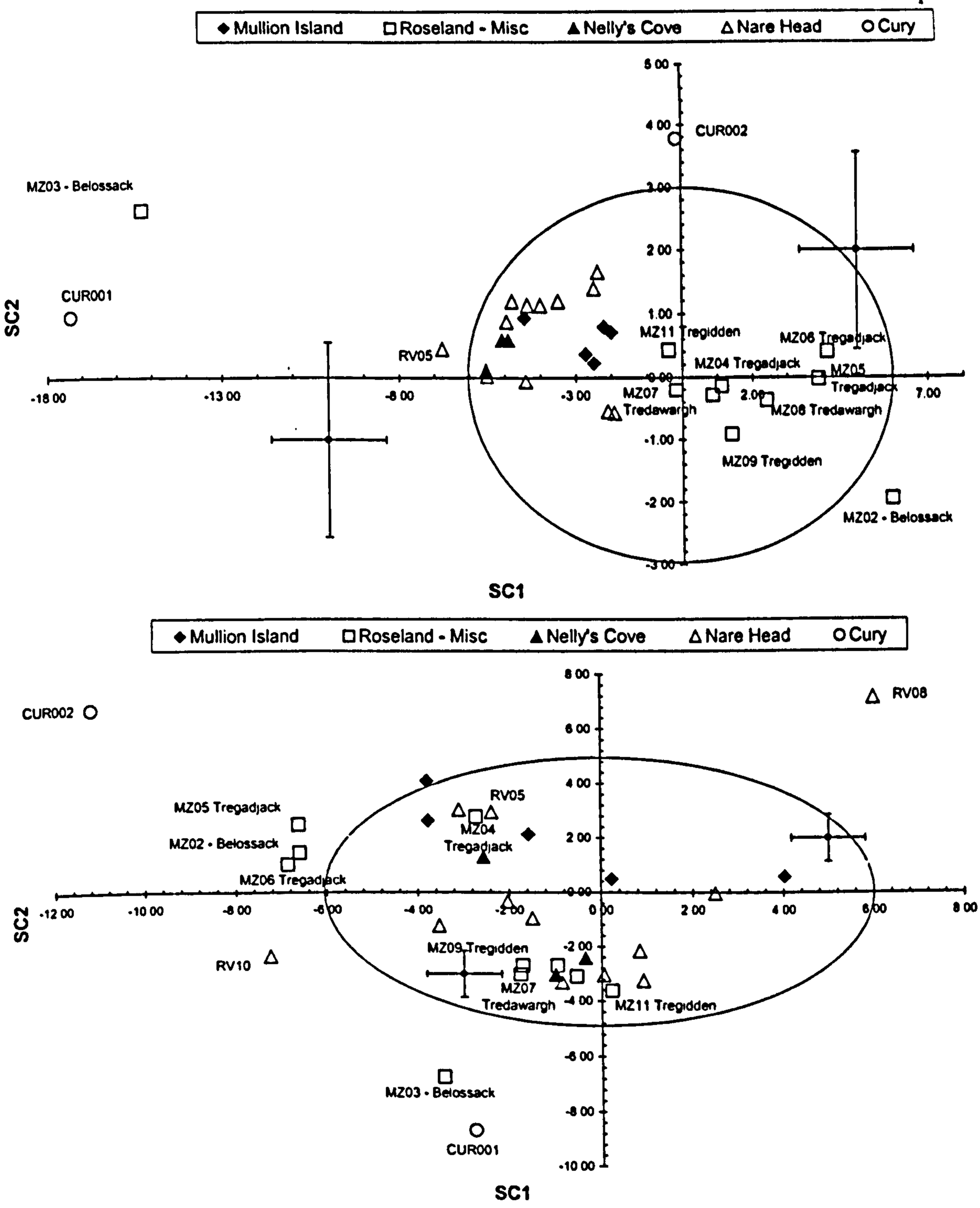

Figure 86 SC scatter plots of SC1 against SC2 for Roseland Breccia Formation greenstone exposures based on IPC Group I SCA analysis of Ti, Y, Zr, & Nb (immobile) elements (upper chart) and K, Ca, Fe, Rb, Sr, Ba (mobile) elements (lower chart). The majority of analyses plot within both ellipses indicating a potentially strong geochemical similarity with IPC Group I.

8.8.5 DA

Inspection of Table 92 and Appendix 31.1 shows that all but six samples from exposures within the Roseland Breccia Formations appear geochemically similar to IPC Group I sub-groups, and GpI-2, 3, & 4 in particular, on the basis of sharing similar immobile element concentrations (immobile elements, best (1st) match). There is some partitioning within the immobile element matches with Mullion Island, Nare Head and Nelly's Cove being matched mainly with GpI-2, Belossack (not MZ03), Tregadjack, Tregidden & Tredawargh matched with to GpI-4. This partitioning supports the visual clustering seen in the SC scatter plots (Figure 86) and the immobile element discrimination charts (Figure 85).

Sample location and number	Immobile DA 1st	2nd	Mobile DA 1st	2nd	Indication
Mullion Island					
MI01	GpI-2	GpI-3	GpIII-1	GpI-6	? IPC Group I
MI02	GpI-2	GpI-3	GpIII-1	GpI(near)1	Not IPC Group I
MI03	GpI-2	GpI-7	**GpI-6**	GpI-7	? IPC Group I
MI04	GpI-2	GpI-3	GpIII-1	GpI(near)1	Not IPC Group I
MI05	GpI-3	GpI-1	GpIII-1	GpI(near)1	Not IPC Group I
Belossack					
MZ02	**GpI-4**	GpIa-1	GpI(near)1	GpIII-1	Not IPC Group I
MZ03	GpI-13	GpI(near)1	GpI-8	GpI-13	Not IPC Group I
Tregadjack					
MZ04	GpI-4	GpIa-1	GpI(near)1	GpIII-1	Not IPC Group I
MZ05	GpI-4	GpIa-1	GpI(near)1	GpIII-1	Not IPC Group I
MZ06	**GpI-4**	GpIa-1	GpIII-1	GpI(near)1	Not IPC Group I
Tredawargh					
MZ07	GpI-4	GpIa-1	GpI-8	GpI-2	? IPC Group I
MZ08	GpI-4	GpIa-1	GpI-8	GpI-2	? IPC Group I
Tregidden					
MZ09	GpI-4	GpIa-1	GpI-8	GpI-2	? IPC Group I
MZ10	GpI-4	GpIa-1	GpI-8	GpI-2	? IPC Group I
MZ11	GpI-4	GpI-3	GpI-8	GpI-7	? IPC Group I
Nelly's Cove					
MZ13	GpI-2	GpI-7	GpI-7	GpI-3	**IPC Group I**
MZ14	GpI-2	GpI-7	GpI-13	GpI-8	Not IPC Group I
MZ15	GpI-7	GpI-2	GpI-8	GpI-7	? IPC Group I
Nare Head					
RV05	GpIII-1	GpI-2	**GpI(near)1**	GpIII-1	Not IPC Group I
RV06	GpI-6	GpI-2	GpI-8	GpIII-1	Not IPC Group I
RV07	GpIII-1	GpI-2	GpI-8	GpIII-1	Not IPC Group I
RV08	GpI-2	GpIII-1	**GpI(near1**	GpI-6	Not IPC Group I
RV09	GpI-2	GpI-7	GpI(near)1	GpIII-1	Not IPC Group I
RV10	GpI-3	GpI-1	GpI-8	GpIII-1	Not IPC Group I
RV11	GpI-6	GpI-7	GpI-6	GpI/Ia	**IPC Group I**
RV36	GpI-2	GpIII-1	GpI-8	GpI-2	Not IPC Group I
RV37	GpI-2	GpIII-1	GpI-8	GpIII-1	Not IPC Group I
RV38	GpI-2	GpI-1	GpI-8	GpI-7	? IPC Group I
RV39	GpI-2	GpIII-1	GpI-8	GpI-7	Not IPC Group I
RV40	GpIII-1	GpI-2	GpI-8	GpI-2	Not IPC Group I

Table 92 Summary of DA based on immobile and mobile elements using axe seed groups after axe DA. Matches in bold indicate P(D/G) is less than 0.05. Non IPC Group I sub-groups are indicated in boxes. Following the criteria set out in Section 7.7.2, a good geochemical match to IPC Group I is achieved when all individual matches are to a recognised IPC Group I sub-group.

Matching on the basis of mobile element discrimination using the axe sub-groups after axe DA is not as clear, with half the samples assigned to GpI-8 (15/30) and only MI03 and MZ13 matched with recognised IPC Group I sub-groups, GpI-6 & GpI-7 respectively. However, review of Figure 81 (lower) shows that IPC Group I averages form a relatively small cluster and that the assignments have been made to sub-groups on the extremities of this cluster: GpIII-1, GpI-8, GpI-6 and GpI-7. It should also be noted that the SC scatter plots only shows 2 of the 4 *simple components*, whilst the discrimination process uses all 4 *principal components* in matching exposure samples to seed groups and this may account for the match with sub-groups that plot on the extremities of the SC scatter plot (Figure 81, lower).

Samples MZ13 (Nelly's Cove) and RV11 (Nare Head) are geochemically the closest to IPC Group I as they meet the criteria set out in Section 7.7.2. As they are among samples from the same exposure that are deemed not to be IPC Group I (c.f. Table 92), this illustrates that a small variation in elemental composition can significantly alter the DA match (e.g. compare RV11 with other samples from Nare Head detailed Appendix 28.1).

8.8.6 MANOVA and Student's t-test analysis

Selected multivariate MANOVA tests were carried out between Mullion Island, Tredawargh & Tregidden, Nelly's Cove and Nare Head, and *petrographically determined* sub-groups in order to further examine the geochemical relationship between exposure and IPC Group I sub-groups observed above. Table 93 below summarises the findings of the MANOVA results by indicating the highest three significance values reported, hence indicating the best match, found for each of the exposures based on immobile elements.

	1st (significance)	2nd (significance)	3rd (significance)
Mullion Island	GpI-1 (0.415)	GpIa-1 (0.421)	GpI-3 (0.320)
Tredawargh & Tregidden	GpIa-1 (0.391)	GpIa-3 (0.284)	GpI-4 (0.156)
Nelly's Cove*	GpI-6 (0.142)	GpI-1 (0.080)	No 3rd value
Nare Head	GpI-7 (0.409)	GpI-4 (0.308)	GpI-3 (0.187)

Table 93 Summary of selected multivariate MANOVA calculations between Roseland Breccia Formation greenstone outcrops and petrographically determined sub-groups, based on Ti, Y, Zr & Nb concentrations (Nelly's Cove analysis was restricted due to the small number of cases). The value in brackets is the value of significance reported by the MANOVA calculation.*

Table 93 indicates that the null hypothesis: that the concentrations of Ti, Y, Zr and Nb found in the exposure samples and those found in the axe sub-groups are potentially from the same population, cannot be rejected at a 0.05 significance value. Thus MANOVA broadly supports findings detailed in Table 92, and the interpretations of the SC scatter

plots (Figure 86) and DA results: that the null hypothesis (immobile element averages found in the Roseland Breccia Formation greenstone exposures are the same as those found in IPC Group I sub-groups) cannot be rejected.

Student's t test for comparing means was used as a final investigation into the relationship between elemental concentrations found in axe sub-groups and Roseland Breccia Formation greenstones. Table 94 summarises the results of the t-test examination, which was based on the axe sub-groups as *determined after DA* (in order to maximise statistical resolution of the sub-groups) and quotes the 2-tailed significance level assuming equal variance of test groups.

	K	Ca	Ti	Fe	Rb	Sr	Y	Zr	Nb	Ba
Mullion Island										
GpI-1	0.062	**0.019**	**0.002**	**0.020**	0.389	0.924	0.286	**0.033**	**0.008**	0.063
GpI-2	0.249	0.185	0.949	0.256	0.347	0.904	0.101	**0.040**	0.977	0.163
GpI-7	0.127	0.199	0.354	0.401	0.374	0.638	0.056	**0.006**	**0.002**	0.206
Tredawargh & Tregidden										
GpI-2	0.391	0.523	**0.020**	0.079	0.146	**0.022**	**0.000**	**0.000**	0.382	0.123
GpI-3	0.229	0.695	0.744	**0.003**	**0.000**	**0.003**	**0.001**	**0.001**	**0.011**	0.057
GpI-4	0.762	0.199	0.499	**0.035**	**0.021**	**0.001**	0.982	0.823	0.308	0.079
Nelly's Cove										
GpI-2	0.421	0.073	**0.001**	0.314	0.220	0.236	0.760	0.902	0.100	0.316
GpI-3	0.249	**0.001**	**0.000**	**0.032**	**0.002**	0.085	**0.031**	**0.007**	0.916	0.233
Nare Head										
GpI-2	0.885	0.658	0.182	**0.000**	0.050	0.071	**0.024**	0.164	0.540	**0.012**
GpI-3	0.548	0.534	**0.010**	**0.001**	**0.000**	0.058	0.900	**0.001**	**0.013**	**0.002**
GpI-7	0.529	0.874	0.953	**0.003**	0.059	**0.011**	**0.042**	0.433	**0.000**	**0.026**

Table 94 Summary of Student's t test for comparing means between Roseland Breccia greenstone exposures and selected axe sub-groups (after DA). Null hypothesis is that the means are equal. Values indicated in bold are where the null hypothesis may be rejected at a 0.05significance value. The results show that the best geochemical match between a Roseland Breccia Formation greenstone exposure and IPC Group I sub-group is between Mullion Island and GpI-2.

Inspection of Table 94 reveals a large number of comparisons where the null hypothesis cannot be rejected: that elemental means for each case originate from the same parent population. The best geochemical match is between samples collected from the Mullion Island pillow lavas and GpI-2, although the significance values are still rather low.

However, the results in Table 94 need to be taken in context of the elemental concentration (value) and the relatively small number of samples for this type of statistical comparison. For example Student's t-test reports a significance of 0.008 for Nb concentrations between GpI-1 and Mullion Island. Actual measured values are 8.5 ± 1.7ppm for GpI-1 and 6.2 ± 0.4ppm for the 5 Mullion Island samples. This is a difference of 2.3ppm which is considered to be small for this particular element considering the data is from different

sources and the PXRF precision for Nb is approximately ±3ppm at these concentrations (Table 48). The small number of exposure samples (generally <30 is considered statistically small (Lucey 1996)) means that it is not known if the samples are normally distributed – a prerequisite for this type of statistical analysis. Noting these limitations of the t-test, the results still support the observations made using SCA and DA.

GpI-2 and Mullion Island elemental concentrations are within 1sd (based on GpI-1) of each other for all 10 elements considered (recall t-test uses standard error, not standard deviation). GpI-4 and Tredawargh & Tregidden (apart from Sr < ± 2sd), GpI-2 and Nare Head (apart from Fe < ± 2sd) elemental concentrations are also within 1sd. (Appendix 23.9 last section shows average elemental concentrations for sub-groups as determined by discriminant analysis).

8.8.7 Discussion

Petrographically , the reported fine grained vesicular texture of the samples collected from within the Roseland Breccia Formation means that it is unlikely any of these provided the material for the manufacture of IPC Cornish axes considered in this thesis as these textures are not found in IPC Group I, Ia or III axe thin sections. However, the reported mineralogy of amphibolised pyroxene, altered plagioclase feldspar and accessory ilmenite is similar to that observed in IPC Group I axe thin sections.

Geochemically, immobile element concentrations found in Roseland Breccia Formation greenstones are very similar to IPC Group I and to sub-groups GpI-2, 3, 4 & 7 especially. This suggests that it is probable that the source of IPC Group I axes is closely related to the Roseland Breccia Formation pillow lavas. Specifically, **Mullion Island provides the closest geochemical match with IPC Group I axes** and the zone beneath the pillow lavas (assuming the exposure is similar to Nare Head, with pillows overlaying coarser shallow level intrusives) is well worth investigating further as a source for IPC Group I–type greenstone. (Coarser grained greenstones thought to be beneath the Mullion Island pillow lavas have not been examined for three reasons: they are underwater; it is not known if they are exposed; and it is assumed the shallow intrusive dykes/sills are still in place beneath the pillow lavas noting that it is not known if Mullion Island is an olisthostrome like Nare Head.)

8.9 Mylor Slate Formation: Camborne Group

8.9.1 Overview of samples and localities

The Mylor Slate Formation contains numerous shallow level and extrusive tholeiitic greenstone bodies related to extensional tectonics during the development of the Gramscatho Basin during the Devonian. The Camborne Group is a co-magmatic series of shallow level intrusives outcropping near Camborne, Cornwall that show MOR to intraplate affinities that are *different* to those seen within the Roseland Breccia Formation (Floyd & Al Samman 1980, Section 3.6.3.2). The fourteen geochemical analyses used in this section are taken from Al Samman (1980) and are sub-divided into fine grained extrusive basalts found close to the Camborne Railway Station (NG2, 5, 6 & 9), coarser intrusive dolerites found at an exposure near the Camborne Railway viaduct (NG13, NG22, NG 24, NG26, NG29 & NG32) and a miscellaneous group consisting of NG39 (pillow lava), NG43 (loose boulder), NG50 (vesicular & foliated pillow lava) and NG65 (intrusive) (Appendix 4). These samples are from the closest greenstone exposures to the important Neolithic (and later) occupation site at Carn Brea, which is less than 2km from the exposures.

8.9.2 Inspection of petrographic, magnetic and geochemical data

Petrographic descriptions for the Camborne Group reported below are summarised from Al Samman (1980) and listed in Appendix 4.

NG2, 5, 6 & 9 (Camborne Station) are finely foliated and banded lavas, possibly sub-aerial, containing plagioclase, hornblende and sphene with secondary chlorite and epidote.

NG13, 22, 24, 26, 29 & 32 (Camborne Viaduct) and are from a 'massive intrusive basalt-dolerite' that has been altered by contact metamorphism to a low-grade hornfels containing altered plagioclase, fibrous amphibole, sphene and secondary epidote.

NG39, 50, 43 & 65 (Camborne others (or miscellaneous)) are from *other* greenstone exposures in the Camborne area. NG39 & 50 were originally pillow lavas, now altered to low-grade hornfels. NG43 & 65 are both intrusive rocks, the former now described as a low-grade hornfels and the latter as 'greenstone'.

Hence, mineralogically and texturally the Camborne Group differ from GpI-1 in that they are reported to be predominantly hornfelsic and appear to contain no remnant clinopyroxene or ilmenite commonly seen in IPC Group I, Ia or III thin sections.

No MS measurements are available.

	Reduced IPC Group I (n=130) (ppm ± 1sd)	Camborne Station (n=4) (ppm ± 1sd)	Camborne Viaduct (n=6) (ppm ± 1sd)	Sample NG39 (ppm)	Sample NG43 (ppm)	Sample NG50 (ppm)	Sample NG65 (ppm)
K	3 567 ± 2 282	8 695 ± 1 792	15 426 ± 5 975	17 847	6 392	1 743	913
Ca	67 715 ± 14 636	108 340 ± 19 846	72 203 ± 10 739	52 982	67 782	64 708	54 269
Ti	14 959± 3 772	18 690 ± 1 002	9 350 ± 1 457	12 180	11 880	13 200	13 440
Mn	1 532 ± 521	1 589 ± 313	2 235 ± 256	1 938	2 093	1 318	1 473
Fe	95 632 ± 14 009	89 860 ± 16 634	72 814 ± 10 302	69 923	82 261	76 121	83 029
Rb	29.6 ± 25.8	53.5 ± 12.6	90.0 ± 60.4	87	33	11	3
Sr	324 ± 150	496 ± 82.1	390 ± 72.0	583	395	237	587
Y	35.7 ± 6.8	40.8 ± 2.8	32.5 ± 4.8	38	31	33	36
Zr	171 ± 29.2	195 ± 24.4	65.2 ± 30.5	74	76	86	75
Nb	6.7 ± 2.9	17.3 ± 3.5	4.2 ± 2.9	4	4	5	3
Ba	104 ± 64.3	104 ± 84.4	117 ± 61.9	181	25	0	11
Ce	-27.1 ± 11.4	Not measured	Not measured	-	-	-	-
Pb	230 ± 1013	Not measured	Not measured	-	-	-	-

Table 95 Average and individual elemental compositions of samples collected from exposures in and around Camborne and the reduced IPC Group I average composition. Camborne data is in Appendix 28.1 & 28.2 and reduced IPC Group I data from Table 58.

Table 95 indicates that the three Camborne sub-groups: Station, Viaduct & miscellaneous, appear to be geochemically different to the reduced IPC Group I average. Zr concentrations in samples collected from the Viaduct are all less than 60ppm (apart from NG24), hence considerably lower than IPC Group I average of 171 ± 29.2ppm, giving Zr/Y rations of approximately 1 to 2, less than the 4 to 6 expected for IPC Group I. NG24 has 2 to 3 times Zr & Nb than its co-group members, giving a Zr/Nb ratio of approximately 13, less than the 18+ ratio seen for IPC Group I axes. Immobile element concentrations in samples from the extrusive basalts found at Camborne Station are higher than the reduced IPC Group I average, but only by 1 to 2sd, apart from Nb (greater than 3sd). The remaining four samples have immobile element concentrations slightly higher than the coarse, hornfelsic samples from the Camborne Viaduct exposure. Mobile element concentrations in the Camborne Group samples are more variable, probably reflecting varying amounts of alteration through contact metamorphism from the nearby Carnmenellis Granite. In comparison with reduced IPC Group I averages, Camborne samples generally have higher K, Rb, Sr and Mn.

Samples from the Camborne Station exposure have 43 to 45% wt SiO_2, 2 to 4% Na_2O + K_2O and 17 to 21% wt MgO + CaO which classifies them as ultra basic (Le Maitre et al. 1989) and tholeiitic. The 6 samples from the Viaduct exposure have 45 to 50% SiO_2, 3 to 4% wt Na_2O + K_2O and 15 to 18% wt MgO + CaO, hence are basaltic/gabbroic (depending on grain size) and tholeiitic. The remaining 4 samples have similar major element concentrations to the Viaduct group. (Data from Al Samman 1980.)

8.9.3 Element discrimination diagrams

The six element discrimination diagrams in Figure 87 clearly show that the four Camborne Station samples form a cluster away from the other samples showing that they are comparatively more evolved (higher Ti, and Zr) than the four miscellaneous samples and the Viaduct greenstone exposure. The ternary diagrams indicate that the intrusive Viaduct greenstone exposure is a Ti enriched island arc related tholeiite, with Zr/Y ratios less than 3 indicating an oceanic arc origin. The extrusive igneous exposure at Camborne station appears to be a within plate basalt with N to T-MORB affinities. This suggests two different tectonic settings as arc basalts are generally subduction related, whilst MOR type basalts are generally formed in extensional regimes. Their geographical proximity illustrates the difficulty in understanding the geological evolution of the region and the need to date the emplacement/eruption of the exposures.

The six samples from Camborne Viaduct and four from other Camborne locations (apart from NG24) do not consistently share geochemical similarities with any axe sub-group based on the position of the data clusters (Figures 77 to 80) indicating that it is very unlikely these samples originate from the IPC Group I source. NG24 plots away from any single axe sub-group. The four samples from Camborne Station appear closest to GpI/Ia and GpI-4, although the exposure samples contain relatively more Nb, Zr & Ti. These four samples are certainly not related to GpI-2, 7, 8, 12, 13, GpIa-5, GpI(near)1, GpIII-1.

8.9.4 SCA

Inspection of Figure 88, below, shows only 3 Camborne Group samples only just plot within both SC scatter plot ellipses: NG5, NG43 and NG65 (NG50 has no recorded Ba value so its position within the mobile element ellipse is questionable.)

A comparison between Figures 81 and 88 shows the Camborne Station cluster is closest to GpI/Ia and that the Viaduct cluster is closest to GpI(near)1 and possibly GpI-7.

Comparison between Chapter 7 Figure 74 and 75 and Figure 88 fails to find any IPC ungrouped or non-IPC axe that shares similar positions to the Camborne groups.

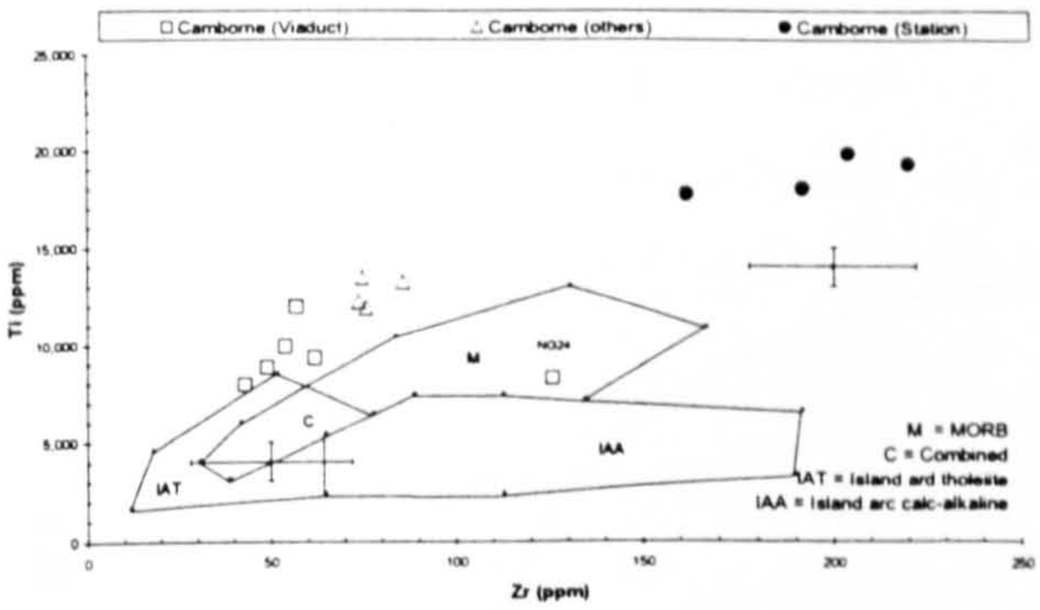

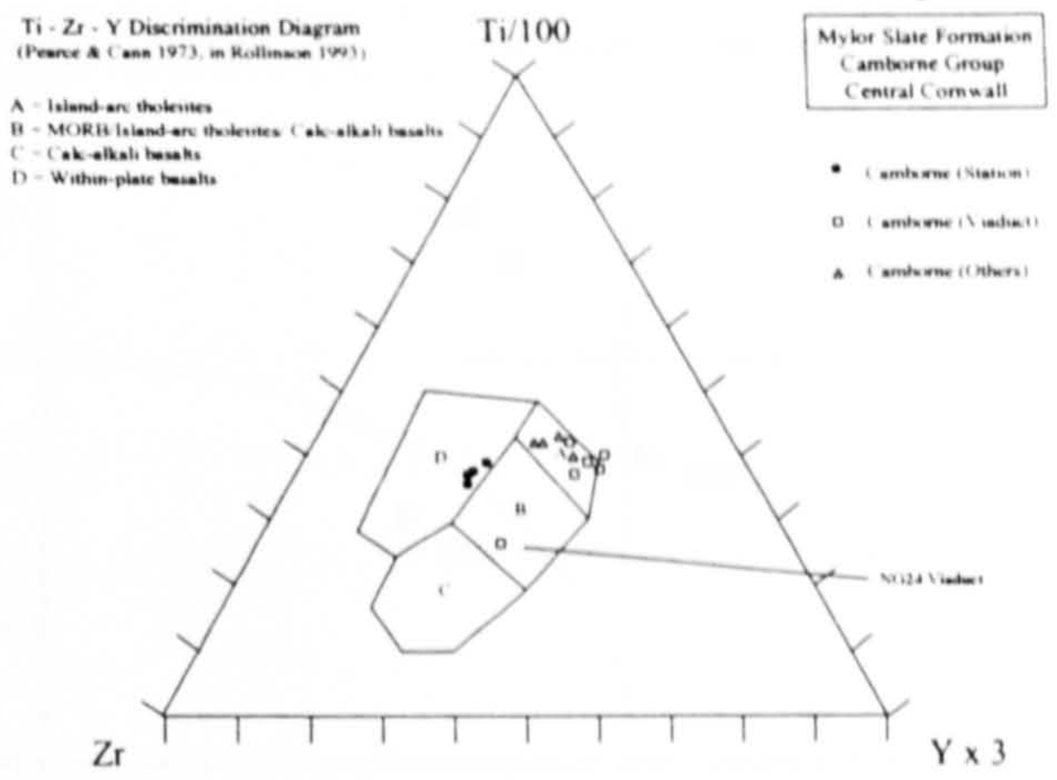

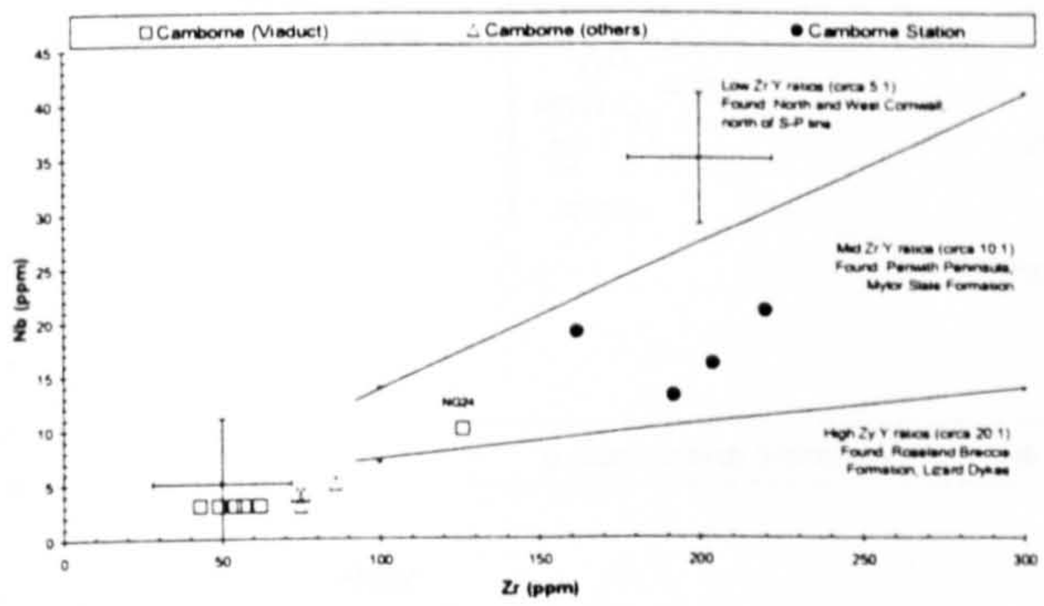

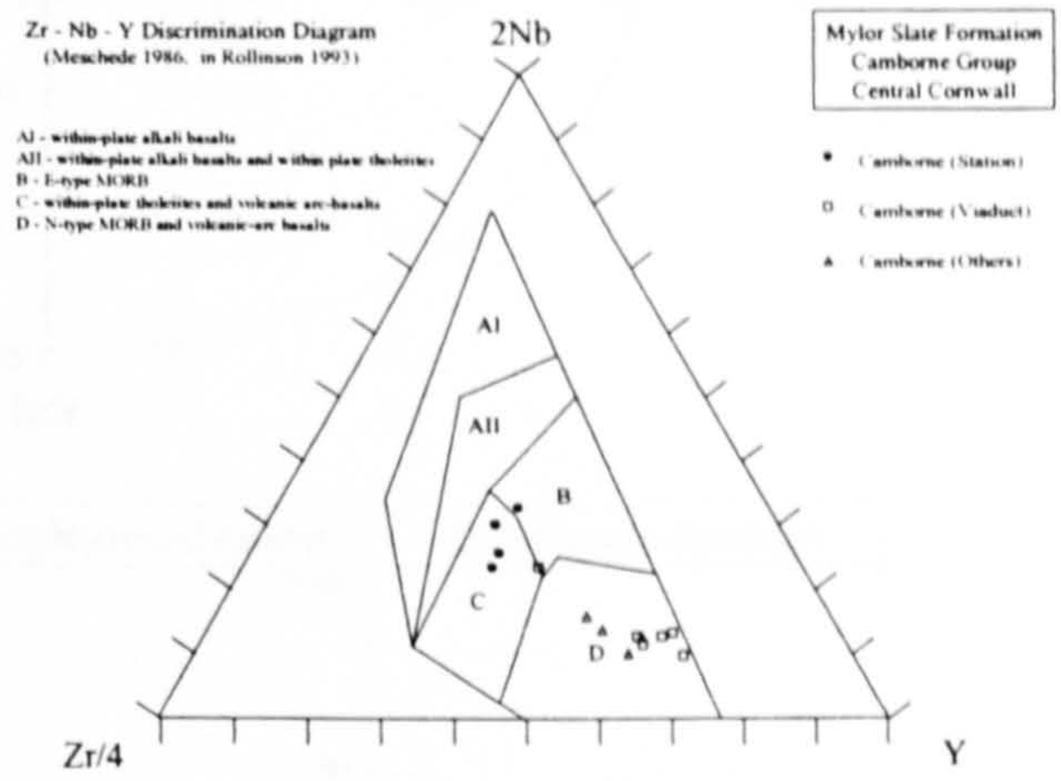

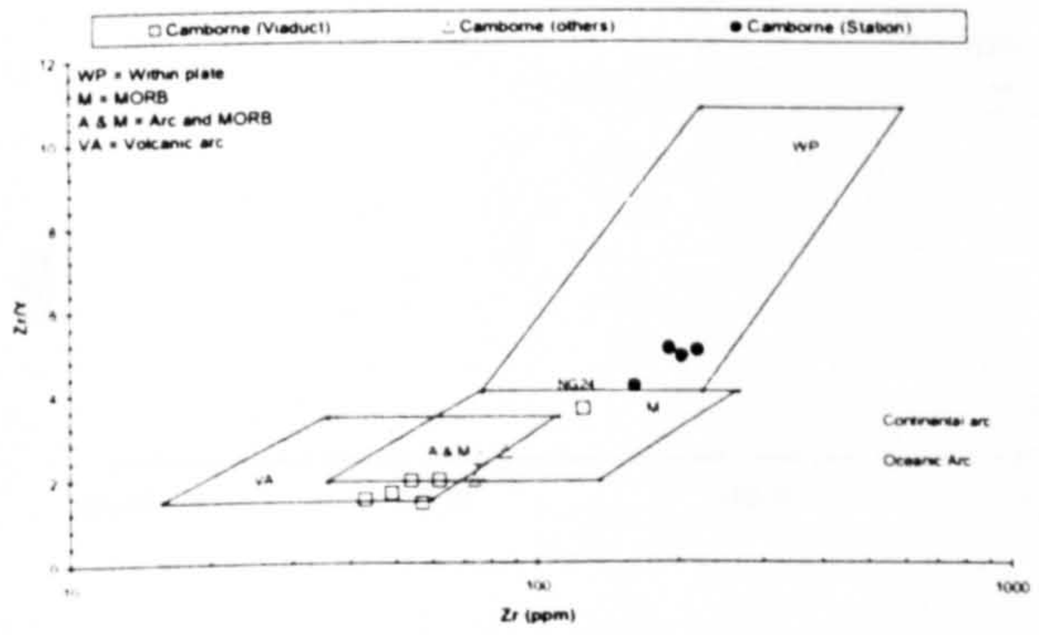

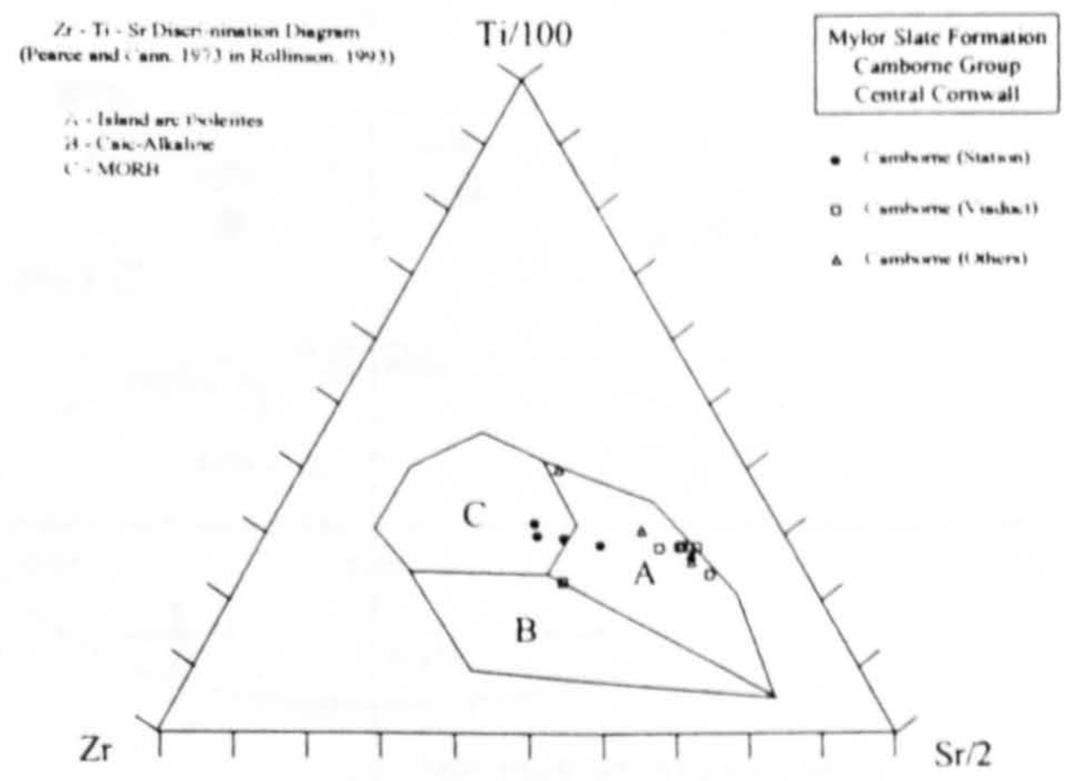

Figure 87 Element discrimination diagrams for the Camborne Group, within the Mylor Slate Formation. The divisions between the extrusive fine grained and foliated samples from Camborne station are clearly separate to the coarser grained hornfels from the Camborne railway viaduct. There is some overlap between Camborne station and IPC Group I, but the former has far higher Nb concentrations

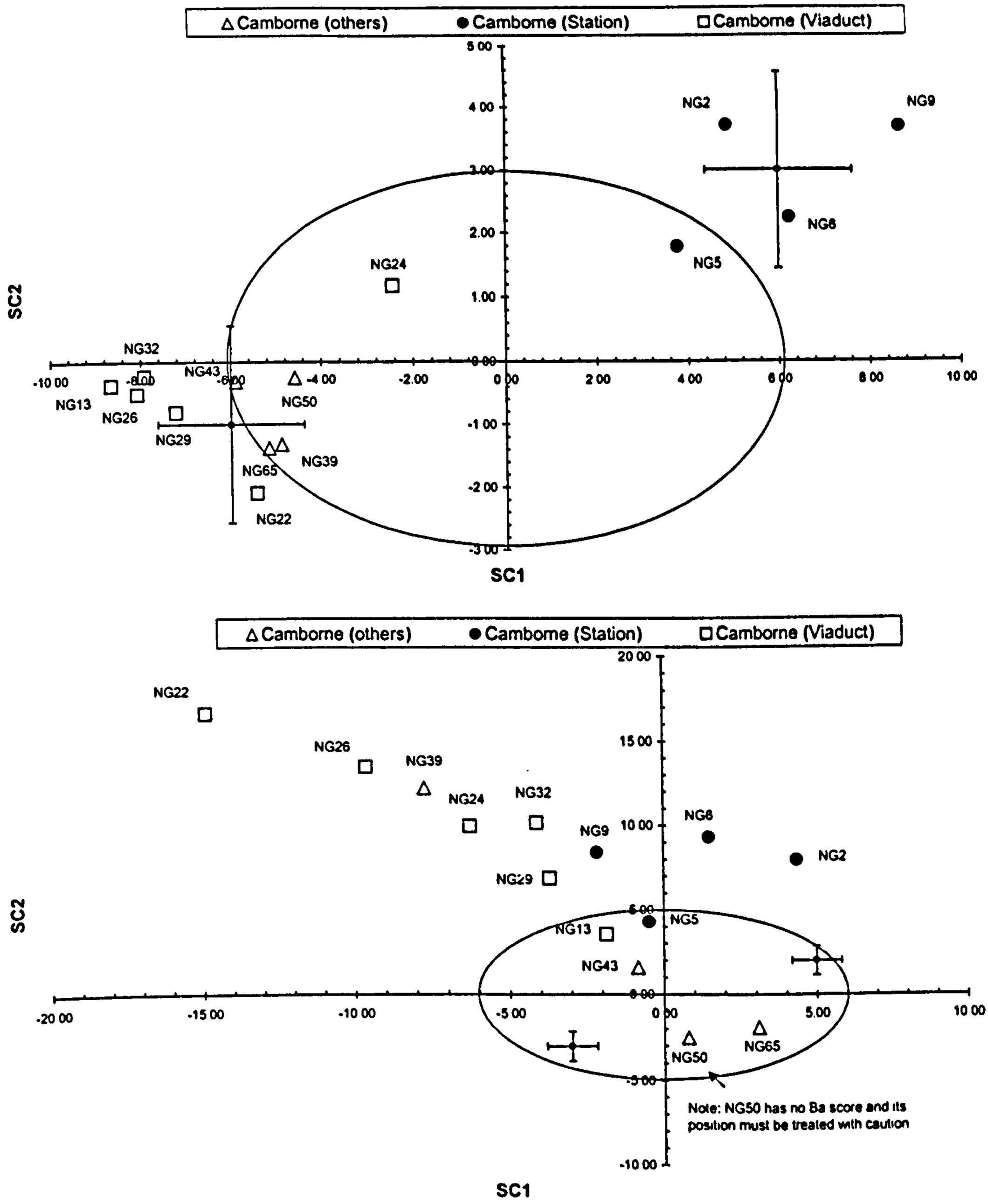

Figure 88 SC scatter plots of SC1 against SC2 for Mylor Slate Formation – Camborne Group greenstone exposures based on IPC Group I SCA analysis of Ti, Y, Zr & Nb (immobile) elements (upper chart) and K, Ca, Fe, Rb, Sr, Ba (mobile) elements (lower chart). Most samples plot outside ellipses indicating small probability of being geochemically related to IPC Group I. Extrusive samples from Camborne Station and intrusive samples from Camborne railway Viaduct (and others) form two distinct clusters indicating there is a marked geochemical difference between them.

8.9.5 DA

Appendix 31.1 (summarised in Table 96) shows that only NG5 has P(D/G) greater than 0.10 for both immobile and mobile element DA and is best matched with GpI/Ia by both immobile and mobile element discrimination. NG5 was collected from the same exposure as NG2, 6, & 9 which all return P(D/G) less than 0.05, but similarly match GpI/Ia. Hence it is a remote possibility that GpI/Ia could have originated from Camborne, although the evidence is very weak.

Sample location and number	Immobile DA 1st	2nd	Mobile DA 1st	2nd	Indication
Camborne Station					
NG2	**GpI-12**	GpI/Ia	GpI(near)1	GpI-6	Not IPC Group I
NG5	GpI/Ia	GpI-1	GpI/Ia	GpI(near)2	**IPC Group I**
NG6	**GpI/Ia**	GpI-1	GpI(near)1	GpI-6	Not IPC Group I
NG9	GpI-12	GpI/Ia	GpI/Ia	GpI(near)1	Not IPC Group I
Camborne Viaduct					
NG13	GpIII-1	GpI(near)1	GpIII-1	GpI(near)1	? IPC Group III
NG22	**GpIa-5**	GpIa-7	**GpI(near)1**	GPIII-1	Not IPC Group I
NG24	**GpI-2**	GpI-6	**GpI(near)1**	GpIII-1	Not IPC Group I
NG26	GpIII-1	GpI(near)1	GpI(near)1	GpIII-1	? IPC Group III
NG29	GpIII-1	GpI(near)1	GpI(near)1	GpIII-1	? IPC Group III
NG32	GpIII-1	GpI(near)1	GpI(near)1	GpIII-1	? IPC Group III
Camborne – misc.					
NG39	**GpIa-5**	GpIII-1	**GpIII-1**	GpI(near)1	Not IPC Group I
NG43	**GpIII-1**	GpI-2	GpIII-1	GpI-6	? IPC Group III
NG50	**GpIa-5**	GpI-2	GpI-8	GpI-2	Not IPC Group I
NG65	**GpIa-5**	GpI-7	GpI-12	GpI-1	Not IPC Group I

Table 96 Summary of DA based on immobile and mobile elements of Camborne Group samples using axe seed groups after axe DA. Matches in bold indicate P(D/G) is less than 0.05. Non IPC Group I sub-groups are indicated in boxes. Following the criteria set out in Section 7.7.2, a good geochemical match to IPC Group I is achieved when all individual matches are to a recognised IPC Group I sub-group.

Inspection of Table 96 suggests that the samples from the Camborne Viaduct exposure are geochemically similar to those of IPC Group III, although this is not obvious from the collage of element discrimination diagrams in Figure 87 and Figure 77 to 80. This is explained by examining Table 97 below, which compares GpIII-1 compositional averages, before and after axe DA, with Camborne samples. It is clear that the mobile element DA matches are in part due to the large sds associated with GpIII-1 values after axe DA. The reason that the element discrimination diagrams did not indicate any similarity between samples from the viaduct exposure at Camborne and GpIII-1 is that the immobile element ratios in particular are significantly different. For example, the Zr/Y ratio for GpIII-1 is approximately 4.3 (n=2) and 3.6 (n=12) compared with 2.0 calculated from the average of the five Camborne Viaduct samples.

	GpIII-1 (before DA) (n=2) (ppm ± 1sd)	GpIII-1 (after DA) (n=12) (ppm ± 1sd)	Camborne Station (n=4) (ppm ± 1sd)	Camborne Viaduct (n=5) (ppm ± 1sd)	Sample NG43 (ppm)
K	10 400 ± 5 657	8 255 ± 5 962	8 695 ± 1 792	15 426 ± 5 975	6 392
Ca	73 800 ± 6 223	64 008 ± 24 215	108 340 ± 19 846	72 203 ± 10 739	67 782
Ti	5 800 ± 3 253	6 091 ± 2 638	18 690 ± 1 002	9 350 ± 1 457	11 880
Mn	2 200 ± 1 273	1 383 ± 622	1 589 ± 313	2 235 ± 256	2 093
Fe	96 550 ± 636	79 975 ± 22 658	89 860 ± 16 634	72 814 ± 10 302	82 261
Rb	107 ± 9.6	58.3 ± 60.3	53.5 ± 12.6	90.0 ± 60.4	33
Sr	430 ± 82.6	319 ± 182	496 ± 82.1	390 ± 72.0	395
Y	21.0 ± 3.4	23.4 ± 3.7	40.8 ± 2.8	32.5 ± 4.8	31
Zr	93.4 ± 0.1	83.6 ± 23.9	195 ± 24.4	65.2 ± 30.5	76
Nb	5.0 ± 2.6	4.8 ± 2.5	17.3 ± 3.5	4.2 ± 2.9	4
Ba	259 ± 216	154 ± 154	104 ± 84.4	117 ± 61.9	25
Ce	-43.4 ± 12.7	-36.3 ± 22.6	Not measured	Not measured	-
Pb	66.1 ± 0.6	116 ± 213	Not measured	Not measured	-

Table 97 Average and individual elemental compositions of samples collected from exposures in and around Camborne and GpIII-1 compositions before and after axe DA. Camborne data is in Appendix 28.1 & 28.2, GpIII-1 data from Table 75 and Appendix 23.9.

8.9.6 MANOVA and Student's t-test analysis

MANOVA is not carried out as the only likely geochemical match is between one sample from the Camborne station exposure and GpI/Ia. The results from comparing elemental averages between these two groups using Student's t-test are given in Table 98 below.

	K	Ca	Ti	Fe	Rb	Sr	Y	Zr	Nb	Ba
GpI/Ia	**0.001**	**0.032**	0.303	0.922	**0.049**	0.745	0.291	0.597	**0.010**	0.441

Table 98 Summary of Student's t test for comparing means between Mylor Slate Formation – Camborne (Station) and GpI/Ia (after axe DA). Null hypothesis is that the means are equal. Values indicated in bold are where the null hypothesis may be rejected at a 0.05 significance value.

Camborne Station samples have an average Nb of 17.3 ± 3.5ppm and GpI/Ia axes have a Nb average of 9.2 ± 3.4ppm. This is the only one of the four immobile elements to be different by greater than 1sd (based on GpI/Ia average, n=5). There is a large difference between respective K (3,360 to 8,695ppm) and Ca (80,100 to 108,340ppm), but the remaining mobile element pairs are different by less than 1sd.

8.9.7 Discussion

The hornfels texture seen in Camborne Viaduct and others has not been seen in any axe thin section examined and the petrographic differences are such that it is highly improbable that IPC Group I or III axes originate from these Camborne greenstone exposure.

There is a limited possibility of geochemical similarity between the fine grained, foliated, lavas from the greenstone exposure near the Camborne railway station and IPC Group I/Ia. However, the large difference between Nb, K and Ca concentrations mean that this exposure is unlikely to have provided the material for the IPC Group I axes. Elevated K

could be explained by enrichment though contact metasomatism. However, Ca can be depleted by metasomatism (Rollinson 1993: table 3.4) and as the exposure samples contain considerably more K & Ca than GpI/Ia it is improbable GpI/Ia is a less affected part of the Camborne Station greenstone exposure. Nb is immobile in the regimes discussed above, and its elevated level in the exposure indicates the two rocks (Camborne Station and GpI/Ia) originated from different tectonic regimes.

Therefore, on balance of geochemical evidence and also on the supposition that petrologists assigning axes to GpI/Ia would recognise and report a hornfelsic texture **it is improbable that any IPC Group I, Ia, I/Ia, I(near) or III axes originated from the exposures sampled within the Mylor Slate Formation at Camborne.** An examination of GpI/Ia thin sections would be of great help in testing this hypothesis, although field notes taken when measuring the axes indicate that GpI/Ia axes were medium grained and macroscopically similar to other IPC Group I axes examined.

8.10 Mylor Slate Formation: Cudden Point Group

8.10.1 Overview of samples and localities

A total of thirty-six geochemical analyses have been obtained from the chemically primitive olivine bearing tholeiitic intrusive greenstone body jutting out into the east side of Mount's Bay at Cudden Point (Floyd et al. 1993). This exposure of massive intrusive greenstone within the Mylor Slate Formation probably originated from high degrees of partial melting (Floyd et al. 1993). Incompatible element ratios can be matched with the extrusive rocks found in South Cornwall (Floyd 1984). Contact metasomatism has taken place on the outer edge of the Cudden greenstone body where high levels of K, Rb are found (Floyd & Lees 1972). The exposure has mineral grain sizes ranging from medium at the periphery to coarse grained at the centre and has been slightly altered by low-grade (prehnite-pumpellyite facies) regional metamorphism (Floyd et al. 1993, Section 3.6.3.2). The geochemical analyses come from three different sources: Floyd (pers. com.), Al Samman (1980) and the author, and represent all areas of the exposure (c.f. Figure 19 Chapter 3). New thin sections were made from the three samples collected by the author. Additional petrographical data has been gathered from published sources (Floyd et al. 1993, Floyd & Al Samman 1980, Al Samman 1980).

Geographically, the Carn Brea Neolithic occupation site is approximately 20km north-east of Cudden Point and the extensive series of Neolithic tombs on the Penwith Peninsula are

20km to the north-west. The Cudden Point greenstone exposure is on the Cornish Coastal Path and easily accessible by foot or boat.

8.10.2 Inspection of petrographic, magnetic and geochemical data

Clinozoisite and epidote are plentiful within the Cudden Point greenstone, along with ophitic and occasional euhedral clinopyroxene and plagioclase feldspar. Secondary amphibole and chlorite complete the main mineralogy observed (Appendix 4, Section 4.8.4). Cudden Point is the only tholeiitic exposure in Cornwall to contain primary brown amphibole indicating the magma became (or was) hydrated during cooling (Floyd et al. 1993) and brown amphibole was found in thin section CUD003. Floyd et al. (Op. Cit.) reports olivine as being found in Cudden Point rocks although none has been seen in thin sections examined from this work. The overall texture and mineralogy is dissimilar to any seen during the examination of IPC Group I, Ia and III thin sections (Chapter 4).

Cudden Point MS was measured at 5 locations and from one sample (Appendix 9.3) and produced corrected values ranging between 0.33 to 0.57 x 10^{-3} SI (Section 5.8.3, Table 22). This is at the lower end of that expected for IPC Group I axes (0.23 to 1.89 x 10^{-3} SI).

Apart from samples CG13 and SG57, all Cudden Point immobile element concentrations are low (<10ppm Nb, < 70ppm Zr, < 20ppm Y and < 9,000ppm Ti (apart from CG14, SG48, CG13)) supporting the observation that the exposure is geochemically primitive (has relatively low immobile element concentrations). Mobile element concentrations are variable, having a wide range of values (e.g. K 600 to 12,500ppm, Fe 53,000 to 147,000ppm). Inspection of the geochemical data in Table 99, Appendix 28.1 and geographical locations in Figure 19 reveals no clear geographically centred clusters within the Cudden Point greenstone and also shows that the corrected PXRF values are similar to those obtained from Keele University, supporting the assumption that the Keele data is of similar precision and accuracy to the OU WDXRF and corrected PXRF data (c.f. Markham & Floyd 1998). Sample SG57 was collected from close to the boundary between the greenstone body and the country rock and is almost certainly a greenschist (Floyd pers. com.). Rocks within this zone are probably contaminated by metosomatic fluids from the nearby Godolphin Granite. CG13 was collected from the end of the Cudden Point promontory where a raft of baked shales is present, possibly part of the relict roof of the sill, and therefore may have been contaminated in a similar manner as SG57. The increased average value of Fe measured within the author's sample as compared to the

other analyses is due to the exceptionally high Fe recorded for sample CUD003. There is no obvious reason for this and it is probably due to a higher than average presence of ilmenite.

OU and Keele WDXRF analyses show that Cudden Point greenstones contain between 44 to 50% wt SiO_2, 18 to 22% wt MgO + CaO and 2 to 4% K_2O + Na_2O, with generally less than 0.5% wt K_2O (Appendix 15.2, Al Samman 1980, Floyd pers. com.). This confirms their gabbroic and tholeiitic nature. This also indicates that metasomatic alteration does not appear to have affected the rock at the localities where the majority of samples were collected (c.f. Figure 19).

	Reduced IPC Group I (n=130) (ppm ± 1sd)	Cudden Point (author, n=12) (ppm ± 1sd)	Cudden Point (Arch Zawn, n=6) (ppm ± 1sd)	Cudden Point (Zawn Susan n=8) (ppm ± 1sd)	Cudden Point (Zawn Harry n=2) (ppm ± 1sd)
K	3 567 ± 2 282	1 935 ± 1 945	2 560 ± 876	4 160 ± 4 570	5 479 ± 5 283
Ca	67 715 ± 14 636	64 710 ± 18 338	80 831 ± 12 215	78 301 ± 21 623	49 335 ± 25 077
Ti	14 959± 3 772	5 822 ± 1 968	4 710 ± 1 292	5 077 ± 915	5 760 ± 1 782
Mn	1 532 ± 521	1 475 ± 429	1 382 ± 173	1 269 ± 290	969 ± 54.8
Fe	95 632 ± 14 009	84 690 ± 25 816	69 578 ± 7 336	67 230 ± 16 446	61 702 ± 9 920
Rb	29.6 ± 25.8	21.7 ± 19.1	18.3 ± 12.4	26.1 ± 25.4	30.5 ± 31.8
Sr	324 ± 150	609 ± 321	478 ± 321	464 ± 370	419 ± 250
Y	35.7 ± 6.8	12.1 ± 5.7	8.5 ± 2.3	10.5 ± 5.0	17.0 ± 1.0
Zr	171 ± 29.2	52.9 ± 11.4	41.5 ± 8.9	45.8 ± 9.9	53.0 ± 0.0
Nb	6.7 ± 2.9	5.0 ± 3.0	5.0 ± 0.6	3.3 ± 0.5	4.0 ± 1.4
Ba	104 ± 64.3	95.3 ± 66.6	112 ± 18.4	139 ± 87.8	213 ± 287
Ce	-27.1 ± 11.4	-39.7 ± 11.9	-	-	-
Pb	230 ± 1013	6.2 ± 19.6	35.8 ± 19.6	36.9 ± 37.9	-

Table 99 Average elemental composition of samples collected from the Cudden Point Greenstone and the reduced IPC Group I average composition. Cudden Point data is in Appendix 28.1 & 28.2, reduced IPC Group I data from Table 58. Note Cudden Point analyses for Arch Zawn, Zawn Susan and Zawn Harry are from Floyd (pers. com. measured using Keele U. WDXRF). Cudden Point analyses by author are from PXRF and OU WDXRF. The increased average Fe in the author's Cudden Point analysis is due to the exceptionally high Fe concentrations measured in sample CUD003.

The inspection of mineralogical, magnetic and geochemical data strongly indicates that that the exposure greenstone is different to IPC Group I greenstone and therefore unlikely to be a source for the axes.

8.10.3 Element discrimination diagrams

The low immobile element concentrations within the Cudden Point greenstone samples means that the spread seen in ratio based immobile element discrimination plots (e.g. ternary diagrams and Zr/Y) may be relatively large, hence interpretations from these charts should be treated with caution. The six immobile element discrimination diagrams in Figure 89 indicate the Cudden Point greenstone is tholeiitic with Zr/Y ratios greater than 3

suggesting a continental plate-volcanic arc basalt setting, hence possibly representing early stages of subduction related, or more likely, early stages of extensional tectonics.

The Cudden Point data cluster in Figure 89 does not overlap the plotted positions occupied by IPC Group I sub-groups (Figures 77 to 80), but does partly overlap the GpI(near)1 cluster on the element discrimination diagrams. CG13 and SG57 do not consistently overlap any sub-group positions indicated in Figures 77 to 80 supporting the observations that these two samples are probably not greenstone from the Cudden Point exposure.

The lack of similarity in plots of Cudden Point and axe sub-group data supports the results from the inspection of data (above) that the Cudden Point greenstone is probably not the source of material for IPC Group I, Ia, I/Ia or III axes. However, there appears to be some similarity between the Cudden Point geochemistry and axes GpI(near)1 (axes Yo99 & Li94).

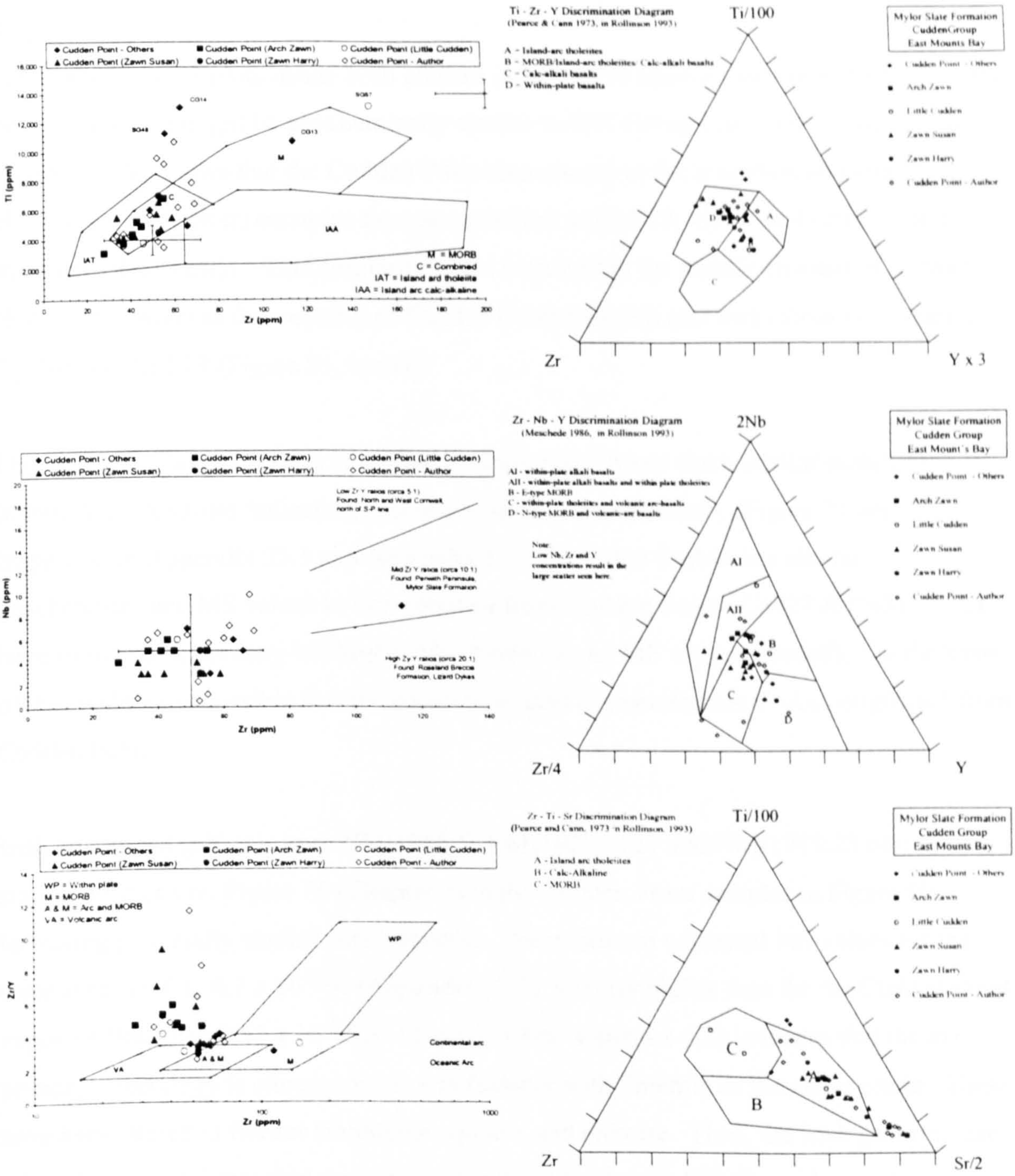

Figure 89 Element geochemical discrimination diagrams for Mylor Slate Formation – Cudden Point Group. The low concentrations of immobile elements result in the wide spread of data in the ratio ternary and Zr – Zr/Y charts. Charts show Cudden Point to be generally homogeneous and related to continental volcanic arc origins. The Cudden Point cluster of points does not overlap any IPC Group I or III axe sub-groups, but does share a similar position to GpI(near)I (already eliminated from the IPC Groups). The overlap in data from PXRF, OU WDXRF and Keele WDXRF supports the assumption that the accuracy of the Keele data is comparable with that established for the PXRF and OU WDXRF.

8.10.4 SCA

Only sample CG13 plots inside both ellipses in Figure 90 (below) indicating that this is the only sample that might be geochemically similar to IPC Group I (n=130). Comparison with Figure 81 shows that the Cudden Point data cluster in the immobile element SCA chart (Figure 90 upper) occupies the same position as GpI-13, GpI-8 and GpIII-1, and marginally GpI(near)1. This similarity is not seen within the mobile element SCA chart (Figure 90, lower) as the majority of Cudden Point Samples plot away from GpI(near)1, GpIII-1 and GpI-13 (Figure 81, lower).

Ungrouped IPC axes Co315/1524, Co427, No65 and CoAxe share similar mobile and immobile SCA values indicating potentially similar geochemistry (Figure 74 and 75). Inspection of Appendix 23.5 and Appendix 11.3 show that CoAxe has similar geochemistry and MS values to that obtained from Cudden Point. Co427 & Co315/1524 have similar geochemistry but higher MS (No65 has no MS value recorded). On the basis of this evidence is possible that the greenstone used to manufacture CoAxe originated from Cudden Point.

Irish ungrouped gabbroic axes NMI1956:5, NMI1929:1127 and NMI1915:25 plot in similar positions on Figure 76 (Chapter 7) to the Cudden Point samples in Figure 90 indicating potentially similar geochemistry. The minimum corrected MS values for the three axes is 0.6 to 0.7 x 10^{-3} SI (Appendix 27.2), slightly higher than for the Cudden Point exposure (less than 0.57 x 10^{-3} SI). Mandal (1996: appendix 6.2) indicates that the axe primary mineralogy is clinopyroxene and feldspar with ilmenite as the major oxide. These have been altered to fibrous amphibole, epidote and chlorite. Thus, the Irish gabbroic axe mineralogy is similar to that seen at Cudden Point (and most IPC Group I axes) however, Mandal makes no mention that euhedral clinozoisite or primary amphibole is present in the axes as it is within the Cudden Point greenstone thin sections. Thus it is plausible that the gabbro used to manufacture these three axes originated from Cudden Point, but a re-examination of thin sections would be needed to evaluate the provenance.

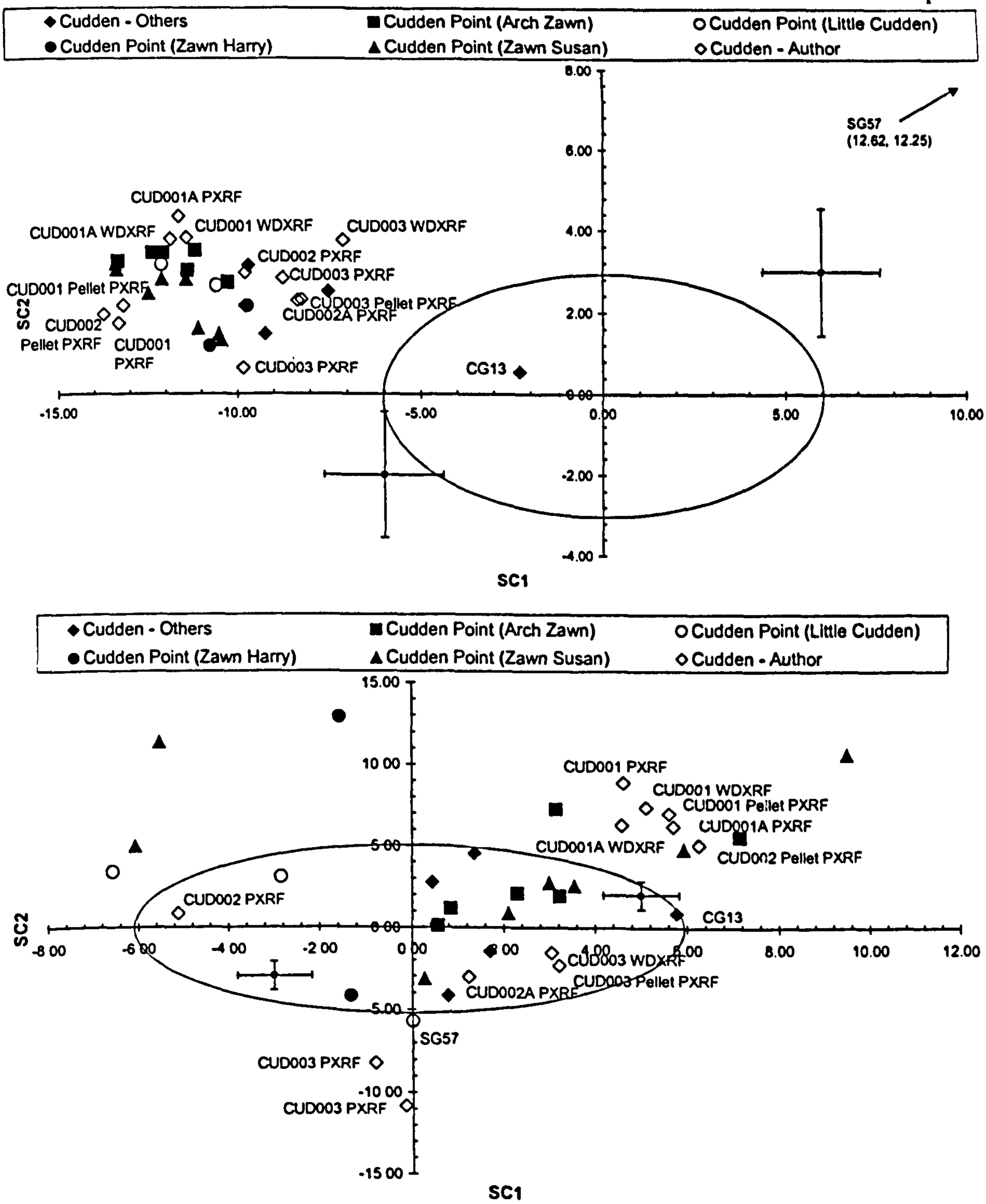

Figure 90 SC scatter plots of SC1 against SC2 for Mylor Slate Formation – Cudden Point greenstone exposures based on IPC Group I SCA analysis of Ti, Y, Zr & Nb (immobile) elements (upper chart) and K, Ca, Fe, Rb, Sr, Ba (mobile) elements (lower chart). Most samples plot outside ellipses indicating small probability of being geochemically related to IPC Group I. There is some similarity in plotted positions between some ungrouped IPC and ungrouped Irish gabbroic axes (see text for discussion).

8.10.5 DA

DA indicates that the Cudden Point samples are geochemically best matched with non-IPC Group I sub-groups (Table 100). The relatively high immobile element P(G/D) probabilities (often >0.9) indicate a strong match with the given sub-group. Mobile element discrimination give smaller significance values, but matches are still generally to non-IPC Group I sub-groups. Only one sample (SG52) is assigned to the same sub-group (GpIII-1) by both immobile and mobile element discrimination.

Sample reference (Appendix 28.1)	Immobile DA 1st	P(G/D)	Mobile DA 1st	P(G/D	Indication
CG1	GpI-13	0.99	GpI-6	0.33	Not IPC Group I
CG10	GpI-13	0.67	GpI-6	0.21	Not IPC Group I
CG11	GpI-13	0.97	**GpI-12**	0.37	Not IPC Group I
CG12	GpI-13	0.94	GpIII-2	0.12	Not IPC Group I
CG13	**GpI-2**	0.44	GpI-6	0.20	Not IPC Group I
CG14	**GpI-8**	0.59	GpI-7	0.13	Not IPC Group I
CG15	GpI-13	0.97	GpIII-1	0.21	Not IPC Group I
CG16	GpIII-1	0.88	GpI-(near)1	0.32	Not IPC Group I
CG2	GpI-13	0.95	GpI-7	0.19	Not IPC Group I
CG3	GpI-13	0.93	GpI-7	0.22	Not IPC Group I
CG4	GpI-13	0.99	GpI-8	0.20	Not IPC Group I
CG5	GpI-13	0.99	GpI-7	0.26	Not IPC Group I
CG6	GpI-13	1.00	GpIII-1	0.59	Not IPC Group I
CG7	GpI-13	1.00	GpI-(near)1	0.68	Not IPC Group I
CG8	**GpIII-1**	0.86	GpI-7	0.17	Not IPC Group I
CG9	GpI-13	1.00	**GpI-12**	0.47	Not IPC Group I
SG43	GpI(near)1	0.42	GpI-8	0.28	Not IPC Group I
SG44	GpI(near)1	0.37	GpI-7	0.25	Not IPC Group I
SG47	GpI(near)1	0.39	GpI-6	0.45	Not IPC Group I
SG48	GpI-8	0.66	GpI-7	0.33	Not IPC Group I
SG51	GpIII-1	0.86	GpI-8	0.30	Not IPC Group I
SG52	GpIII-1	0.50	GpIII-1	0.37	**? IPC Group III**
SG54	GpIII-1	0.71	GpI-8	0.44	Not IPC Group I
SG57	**GpI-12**	1.00	GpI-8	0.14	Not IPC Group I
CUD001	**GpI-13**	0.95	**GpI-6**	0.37	Not IPC Group I
CUD001A	**GpI-13**	0.99	GpI-6	0.38	Not IPC Group I
CUD003	**GpIII-1**	0.99	GpI-12	0.41	Not IPC Group I
CUD003	GpIII-1	0.99	GpI-13	0.26	Not IPC Group I
CUD001	GpI-13	0.91	**GpI-12**	0.59	Not IPC Group I
CUD002	**GpI-13**	0.61	GpI-2	0.15	Not IPC Group I
CUD001(A)	**GpI-13**	1.00	**GpI-12**	0.34	Not IPC Group I
CUD002A	**GpIII-1**	0.81	GpI-8	0.20	Not IPC Group I
CUD003	GpI(near)1	0.51	**GpI(near)2**	0.20	Not IPC Group I
PEL CUD001	GpI-13	0.96	**GpI-12**	0.39	Not IPC Group I
PEL CUD002	GpI-13	0.99	**GpI-6**	0.34	Not IPC Group I
PEL CUD003	GpIII-1	0.99	GpI-12	0.61	Not IPC Group I

Table 100 DA results for Cudden Point (data from Appendix 31.1). (see text for discussion.)

DA supports the findings that Cudden Point greenstone is geochemically different to IPC Group I axe sub-groups, but appears geochemically (but inconsistently) similar to GpI-8, GpI-13, GpIII-1 and GpI(near)1.

8.10.6 MANOVA and Student's t-test analysis

Not carried out.

8.10.7 Discussion

It is clear from the petrographic and geochemical observations above that **the Cudden Point greenstone is not the source for IPC Group I, Ia, I/Ia or I(near) axes.** Although DA indicates that there are geochemical similarities between Cudden Point and sub-groups GpI(near)1 (Yo99, Li94) and GpIII-1 (Wi4/4 & Wi110/393), it is thought unlikely that axes from these two sub-groups originate from this exposure since their petrographic texture is probably completely different to the samples from Cudden Point (c.f. Section 4.7.4 and 4.5.2). As stated, DA and SCA evidence suggests that GpIII-1 and GpI(near)1 are both similar to Cudden Point samples and this, in turn, suggests that GpIII-1 and GpI(near)1 are also geochemically similar, all three groups having low concentrations of immobile elements (c.f. Sections 7.4 and 7.5). But, as no IPC Group I(near) axe thin sections have been examined and only 4 axes have been geochemically analysed (2 axes for each GpIII-1 and GpI(near) 1) further work is required to establish the degree of similarity between these two axe sub-groups. However it appears plausible that the Cudden Point greenstone is geochemically related to the source of IPC Group III (as defined by GpIII-1).

The geochemistry of sample CG13 is markedly different to other samples collected from Cudden Point and it is strongly suspected that this sample is not representative of Cudden Point and may have been collected from loose material along the shorefront (note: this sample was not collected by the author.)

There is sufficient geochemical and magnetic similarity to indicate that IPC ungrouped axe 'CoAxe' and Irish ungrouped gabbro axes NMI1956:5, NMI1929:1127 and NMI1915:25 are possibly provenanced to the Cudden Point greenstone. A re-examination of the Irish axe thin sections and examination of CoAxe (it has not been sectioned) would confirm this observation.

8.11 Mylor Slate Formation: Perranuthnoe Group

8.11.1 Overview of samples and localities

The Perranuthnoe Group is represented by thirty-two analyses of twenty-four samples of greenstone from five possibly separate greenstone outcrops along the east side of Mount's

Bay near Perranuthnoe village. The greenstone exposures emerge from a thick, to 5m, glacial 'head' (a drift deposit) so it is not known whether the exposures form one large sill-like body or several smaller sills (Figure 20, Chapter 3). The largest mapped outcrop is south-west of Perranuthnoe village, and it includes 'The Greeb' (a headland jutting out into Mount's Bay), the northern edge of Perran Bay, and the southern edge of Trenow Cove (collectively called *Perranuthnoe*). This tholeiitic intrusive greenstone is geochemically more evolved than the primitive tholeiite found at Cudden Point approximately 1km to the south-east, and contains the exposure believed to have provided the material for IPC Group III axes (Keiller et al. 1941; Chapter 2) (located by a 'star' on Figure 20, Chapter 3). Four samples (TRE001, 010, 011 and 012) were collected from this exposure and are collectively referred to as *Perranuthnoe (Quarry)* and are considered as part of the Perranuthnoe collection. Geochemical data for a further eight samples (SG6, 9, 10, 13, 16, 22, 25 and 29) from the Perranuthnoe exposure have been obtained from Al Samman (1980). A headland 0.5km north-west of Perranuthnoe, 25m above sea level, contains an exposure of a greenstone outcrop and yielded six samples (called *Trenow Cove*) (TRE002, 003, 005, 006, 007 and SG35). Another outcrop (called *South Perran Sands)*, exposed at beach level and in 5m high cliffs at the southern edge of Perran Sands provided a further 2 samples (TRE013 and SG39). Two samples from Great Hogus (SG40 & 42), west of Marazion, are described as hornfels, originally pillow lavas (Al Samman 1980) and are the only extrusive rocks encountered in this area (Section 3.6.3.2). The fifth, and geographically the smallest exposure sampled (SG32) is on the coast south of Marazion. (c.f. Figure 20 for geographical orientation.)

The greenstone exposures in the Perranuthnoe area are easily accessible by land or sea and are closer to the Neolithic habitation sites of Penwith than to those of Camborne (Figure 2 Chapter 2).

8.11.2 Inspection of petrographic, magnetic and geochemical data

Thin sections from Perranuthnoe (Quarry) (TRE001, 010, 011, 012) have variable texture and mineralogy, with primary mineralogy of ophitic clinopyroxene and plagioclase feldspar altered, totally in some cases, to chlorite, amphibole (fibrous tremolite-actinolite and euhedral actinolite) and epidote. Samples collected by Al Samman (1980) to the south of the exposure (Perranuthnoe (near Perran Sands)) are similar but with the additional presence of abundant apatite. Thin sections from the Trenow Cove outcrop directly north-west of Perranuthnoe (TRE002, 003, 006 & 007) have coarse tabular plagioclase and

abundant apatite. Consequently, the amount of feldspar suggests that this exposure is more intermediate than basic. The two samples from Great Hogus are vesicular pillow lavas with abundant amphibole, epidote and iron ore (Al Samman 1980). The abundance of apatite and the overall texture of samples from the greenstone exposures has not been seen in any axe thin section examined, although the primary pyroxene - plagioclase mineralogy is similar (Section 4.7.5).

Corrected maximum MS measurements from the Trenow Cove exposure range between 0.44 to 0.75 x 10^{-3} SI, covering the lower part of the range expected for IPC Group I axes (0.23-1.89 x 10^{-3} SI). The only GpIII-1 axe measured for MS is Wi110/393, returning a corrected MS value of 0.70 x 10^{-3} SI, but this axe is thought to come from the Perranuthnoe (Quarry) exposure (see below), which has not been measured for its MS.

	Reduced IPC Group I (n=130) (ppm ± 1sd)	Perranuthnoe (Quarry) n=6 ppm ± 1sd	Perranuthnoe (others) n=9 ppm ± 1sd	Trenow Cove (n=10) (ppm ± 1sd)	South Perran Sands (n=2) (ppm ± 1sd)
K	3 567 ± 2 282	13 913 ± 11 056	4 773 ± 2 182	7 334 ± 2 323	17 696 ± 1 782
Ca	67 715 ± 14 636	47 030 ± 17 914	54 975 ± 8 149	26 963 ± 14 303	53 361 ± 24 197
Ti	14 959± 3 772	9 092 ± 2 273	14 625 ± 3 941	9 448 ± 1 684	16 533 ± 3 516
Mn	1 532 ± 521	3 589 ± 858	1 830 ± 323	1 900 ± 414	1 940 ± 333
Fe	95 632 ± 14 009	92 014 ± 19 358	88 936 ± 9 070	74 263 ± 11 172	68 625 ± 15 957
Rb	29.6 ± 25.8	101 ± 80.7	50.4 ± 46.6	46.2 ± 20.4	95.2 ± 21.5
Sr	324 ± 150	522 ± 183	477 ± 204	441 ± 90.6	647 ± 467
Y	35.7 ± 6.8	18.9 ± 3.9	29.9 ± 7.1	31.6 ± 4.0	45.5 ± 12.1
Zr	171 ± 29.2	95.5 ± 9.9	93.4 ± 50.4	376 ± 137	218 ± 85.0
Nb	6.7 ± 2.9	13.0 ± 6.3	20.5 ± 7.5	52.9 ± 18.6	51.6 ± 26.0
Ba	104 ± 64.3	224 ± 208	100 ± 61.8	202 ± 72.9	327 ± 63.1
Ce	-27.1 ± 11.4	-32.3 ± 10.1	-	50.4 ± 25.8	-5.6 ± 0.0
Pb	230 ± 1013	49.6 ± 29.3	-	26.0 ± 15.6	34.4 ± 48.7

Table 101 Average elemental compositions of samples collected from exposures in and around Perranuthnoe and reduced IPC Group I (n=130). Perranuthnoe data is summarised from that in Appendix 28.1 & 28.2, reduced IPC Group I is from Table 58.

Table 101 and inspection of Appendix 28.1 shows that immobile element concentrations are different between the Perranuthnoe and Trenow Cove exposures. Trenow Cove samples have 3 to 4 times the Zr concentrations present in most Perranuthnoe and Perran Sands samples (approximately 400ppm v 100ppm), but less Ti, circa 9,500ppm in Trenow Cove to mainly 11,000+ ppm in Perranuthnoe, although there is some overlap in the range of Ti values. Nb levels are relatively high in all exposure samples (mostly >12ppm) compared with the IPC Group I average (6.7 ± 2.9ppm). Mobile element concentrations are widely variable, especially K (ranging from 2,000 to 33,000ppm) and Ca (ranging from 17,000 to 127,000ppm), showing that there has been variable alteration, probably due to metasomatic fluids from the Godolphin granite as well as low-level prehnite-pumpellyite phase regional metamorphism. Major oxides generally range between 48 to 51% wt for

SiO_2, 12 to 16% wt MgO + CaO and 4 to 8% wt $Na_2O + K_2O$ (Al Samman 1980, Appendix 15.2) indicating a basic-intermediate tholeiite to sub-alkali rock type. However, Trenow Cove samples have MgO + CaO of between 7 to 9% wt indicating that the Ti, Y based element discrimination diagrams chosen should not be used to assess the petrogenesis of this rock.

When compared to IPC Group I (n=130), the rocks from the Perranuthnoe Group have generally higher Nb and different Zr/Ti and Zr/Y ratios indicating that they are geochemically dissimilar. However, immobile element concentrations from GpIII-1 (Appendix 23.9 and Table 103 in Section 8.11.5, below) are similar to those from Perranuthnoe, although the rock samples contain more Nb than the axes (GpIII-1: 5.0 ± 2.6ppm, Perranuthnoe Quarry samples range from 6 to 23ppm Nb) and this is discussed further below.

8.11.3 Element discrimination diagrams

Inspection of Figure 91, below, clearly suggests that the Trenow Cove and Perranuthnoe samples represent different tectonic settings. Noting the restriction on interpretation, Trenow Cove samples indicate that the exposure is a within-plate alkali rock and is therefore different to the tholeiitic nature of the IPC Group I and III axes. The Perranuthnoe outcrop appears to be an evolved, E-MORB tholeiitic rock (both oceanic & continental arc are suggested by the discrimination diagrams?). South Perran Sands has some similarities with Perranuthnoe, although this is not certain, with only two samples analysed. Similarly, the two samples from Great Hogus appear to be different from each other, their positions within the element discrimination diagrams supporting this by showing that the two Great Hogus samples are from different tectonic settings. These observations support the findings reported by Al Samman that Great Hogus is a volcanic agglomerate (Al Samman 1980) and represents an olisthostrome, with different volcanic rocks deposited after sliding down a basinal slope from two different sources/magmatic events (Floyd pers. com.).

Comparison between Figure 91 and Figures 77 to 80 (Chapter 7) shows the closest sub-groups to the Perranuthnoe Group are GpI-8 and GpIII-1. On closer inspection GpI-8 has markedly different Zr-Ti-Sr and Zr-Nb-Y values from the Perranuthnoe exposure and so is only remotely similar (c.f. Appendix 15 and 23). The main difference between GpIII-1

and Perranuthnoe is the comparatively high Nb in the rock compared to the axes causing a mismatch in plotted positions on the Zr-Nb-Y ternary diagram.

There are no consistent overlaps between analyses from the Perranuthnoe Group and any IPC Group I axe sub-group, supporting the observations above that these exposures did not provide the material for IPC Group I axes.

8.11.4 SCA

Figure 92, below, clearly shows that no sample from the Perranuthnoe Group falls within both ellipses and that the immobile element geochemistry of the Perranuthnoe Group is different to all of the identified IPC Group I axe sub-groups. This supports the findings above, that it is very unlikely that the greenstone exposures around Perranuthnoe provided the material for IPC Group I axes.

The closest match in plotted positions on the immobile element SCA chart is between GpIII-1 & GpI-8 and samples from Perranuthnoe outcrop. This is restricted to similarity between GpIII-1 and Perranuthnoe (Quarry) when both the immobile and mobile element charts are viewed (Figure 81 & 92 lower). It should be noted that only sample TRE001 was actually extracted from the quarry (marked on Figure 92), TRE010, 011, 012 were collected as loose boulders from very close to the quarry.

There is some similarity between the plotted positions of IPC ungrouped axe Co207/823 and the 4 SHC (non-IPC) axes (c.f. Appendix 23; SHC = axes from the Saltash Heritage Centre) and samples from Trenow Cove. However, on closer inspection these axes do not have the high (>300ppm) Zr concentrations possessed by the Trenow Cove samples (Figure 74 & 75, Chapter 7). There are no definite overlaps between any Perranuthnoe Group sample and any of the Irish doleritic or gabbroic axes.

Overall, SCA charts indicate that the samples from Perranuthnoe Quarry share geochemical similarities with GpIII-1, this being the closest match between samples from the Perranuthnoe Group and axe sub-groups.

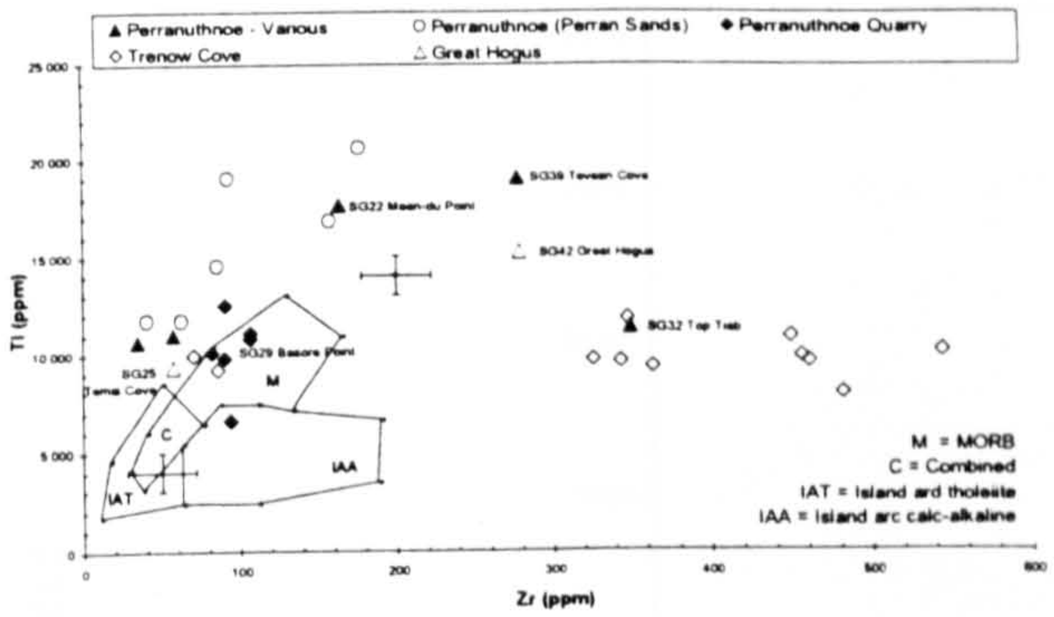

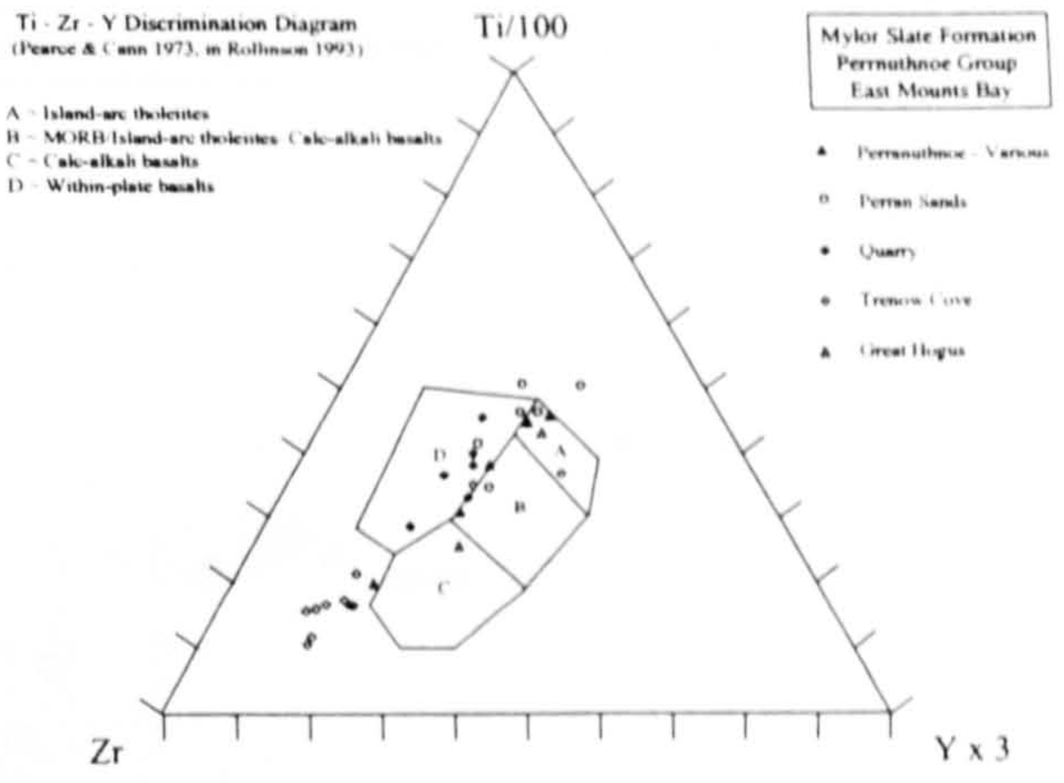

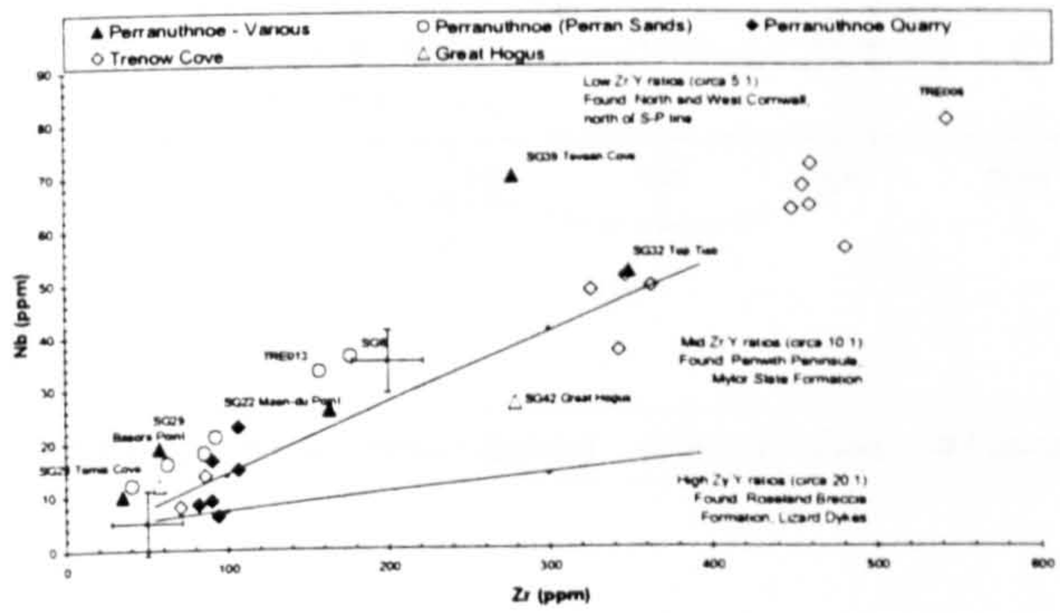

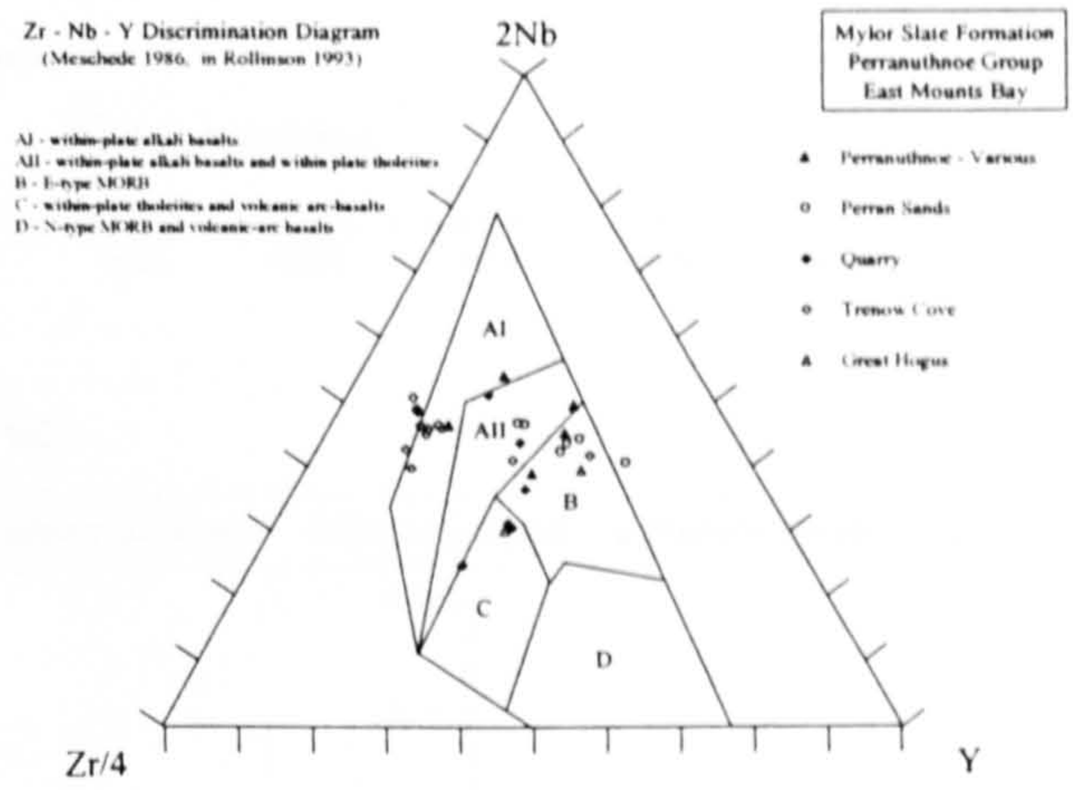

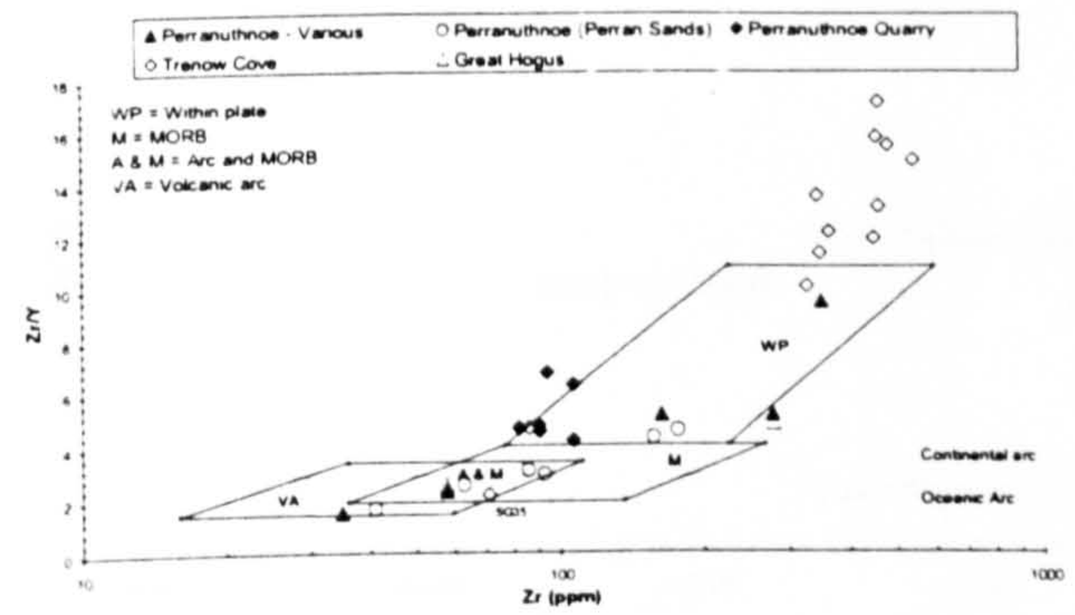

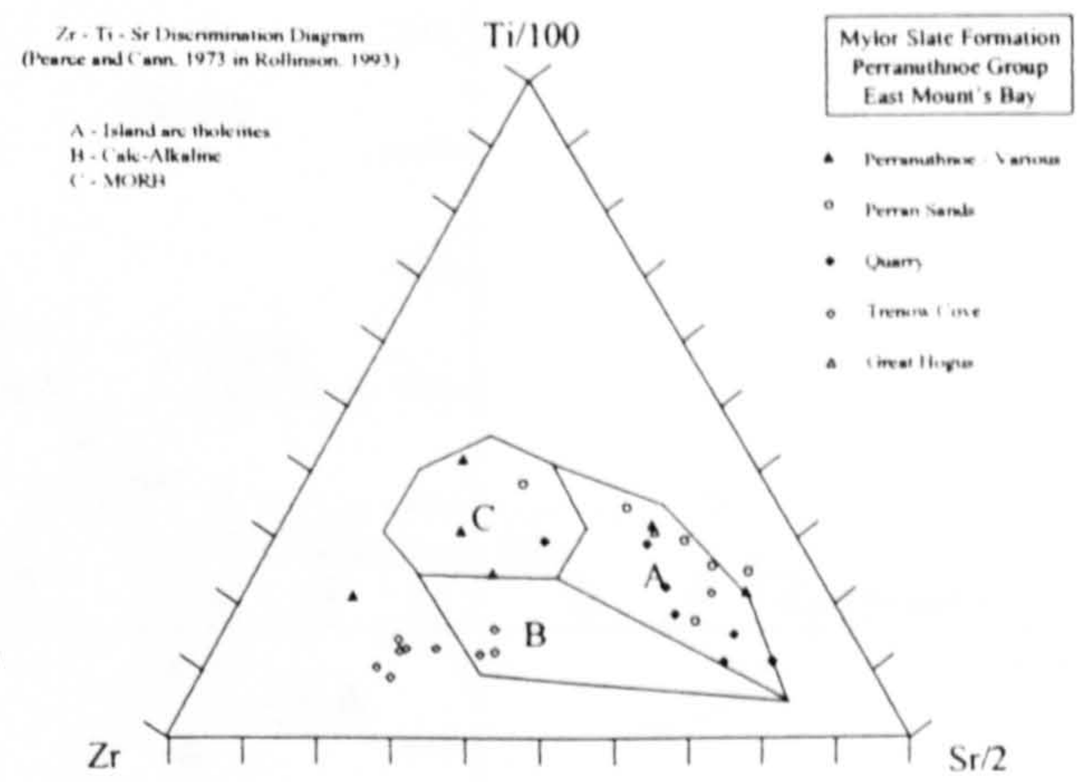

Figure 91 Element geochemical discrimination diagrams for Mylor Slate Formation – Perranuthnoe Group. The relatively low Ti & Zr concentrations coupled with comparatively high Nb results in a generally wide spread of data points, away from positions occupied by IPC Group 1 sub-groups. The Trenow Cove exposure is alkaline in nature, opposed to the predominantly E-MORB characteristics possessed by the Perranuthnoe and Perran Sands exposures.

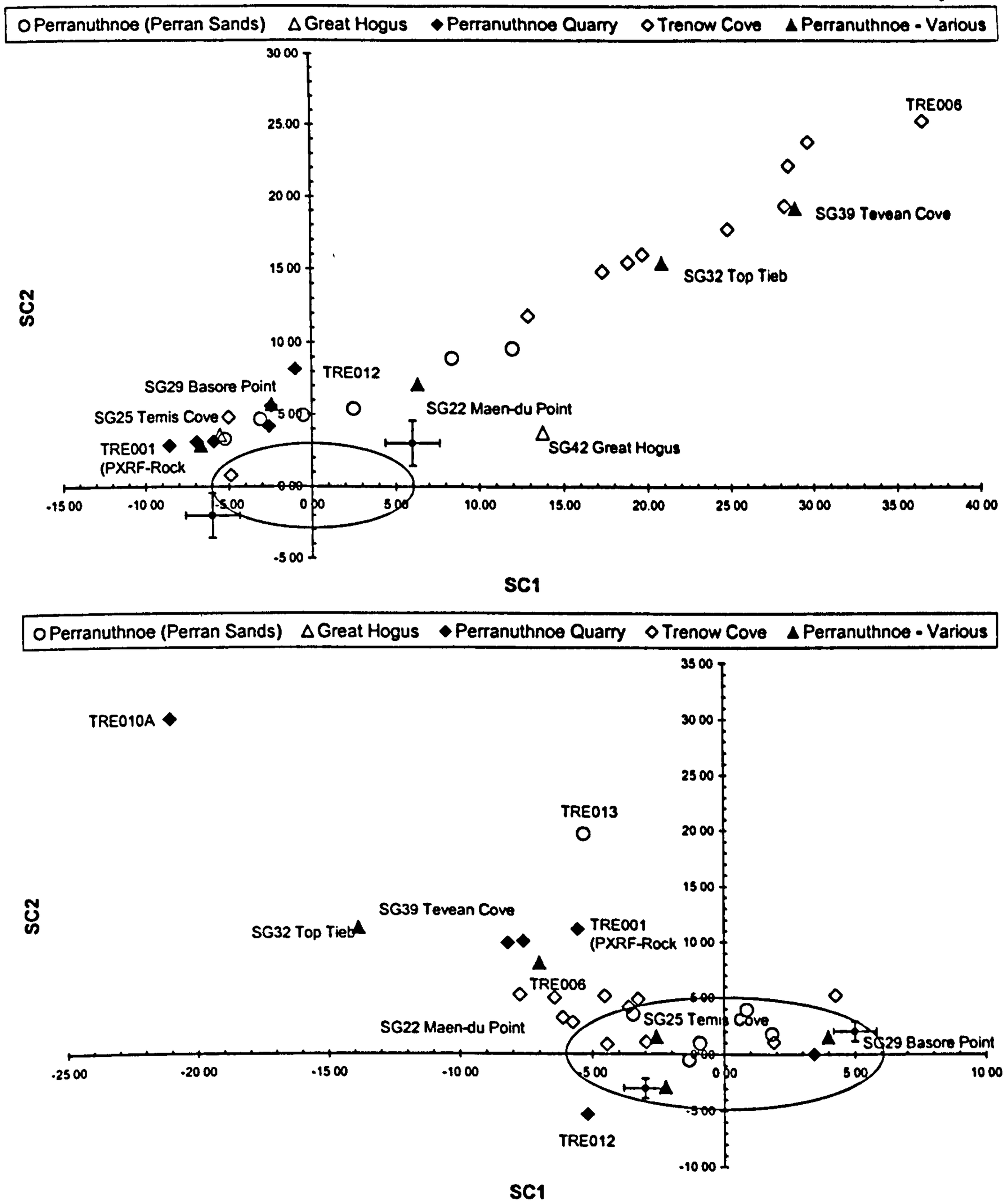

Figure 92 SC scatter plots of SC1 against SC2 for the Mylor Slate Formation – Perranuthnoe Group greenstone exposures based on IPC Group I SCA analysis of Ti, Y, Zr & Nb (immobile) elements (upper chart) and K, Ca, Fe, Rb, Sr & Ba (mobile) elements (lower chart). All but one samples plot outside the immobile element ellipse (upper chart) indicating a small probability of being geochemically related to IPC Group I. There is some similarity in plotted positions between GpIII-1 and Perranuthnoe (Quarry) (see text for discussion). Note that 'Perranuthnoe (Various)' refers to samples collected from the Perranuthnoe exposure by other workers.

8.11.5 DA

Table 102, below, summarises DA results for the samples collected from the five greenstone exposures near Perranuthnoe (compare with Table 101, indicating average elemental compositions).

Sample number and location	Immobile DA 1st	2nd	Mobile DA 1st	2nd	Indication
Perranuthnoe Quarry					
TRE001 (WDXRF)	**GpIII-1**	GpI-12	GpIII-1	GpI(near)1	Not IPC Group I
TRE001 (PXRF)	GpIII-1	GpI-8	GpIII-1	GpI-12	? IPC Group III
PEL TRE001	GpIII-1	GpI-2	GpIII-1	GpI(near)1	**IPC Group III**
TRE010(A)	**GpIII-1**	GpI-2	**GpI-(near)1**	GpIII-1	Not IPC Group I
TRE011(B)	**GpIII-1**	GpI-2	GpI-6	GpI-4	Not IPC Group I
TRE012	**GpI-12**	GpIII-1	GpI-12	GpI-13	Not IPC Group I
Perranuthnoe (others)					
SG6	**GpI-12**	GpI-12	GpI-1	GpI-3	Not IPC Group I
SG9	**GpI-12**	GpI-12	GpI-12	GpI/Ia	Not IPC Group I
SG10	**GpIII-1**	GpI-12	GpI-12	GpI-1	Not IPC Group I
SG13	**GpI-12**	GpI-13	GpI-12	GpI-1	Not IPC Group I
SG16	**GpIII-1**	GpI-2	GpI-12	GpI-6	Not IPC Group I
SG22	GpI-12	GpI-12	GpI-13	GpI-12	Not IPC Group I
SG25	**GpIII-1**	GpI-2	GpIII-1	GpI-1	Not IPC Group I
SG29	**GpI-12**	GpIII-1	GpI-12	GpI-6	Not IPC Group I
Trenow Cove					
TRE002	**GpI-12**	GpI-12	GpI-12	GpIII-1	Not IPC Group I
TRE003	**GpI-12**	GpI-12	GpI-12	GpIII-1	Not IPC Group I
TRE003A	No DA				Insufficient data
TRE004	No DA				Insufficient data
TRE002	**GpI-12**	GpI-12	GpI-12	GpI-13	Not IPC Group I
TRE003	**GpI-12**	GpI-12	GpI-12	GpIII-1	Not IPC Group I
TRE005	**GpIII-1**	GpI-2	**GpI-12**	GpI-6	Not IPC Group I
TRE006	**GpI-12**	GpI-12	**GpIII-1**	GpI-12	Not IPC Group I
TRE007	**GpI-12**	GpI-12	GpI-12	GpIII-1	Not IPC Group I
PEL TRE002	**GpI-12**	GpI-12	GpI-12	GpIII-2	Not IPC Group I
PEL TRE003	**GpI-12**	GpI-12	GpI-12	GpIII-2	Not IPC Group I
PEL TRE004	**GpI-12**	GpI-12	GpI-12	GpI-13	Not IPC Group I
SG35	**GpIII-1**	GpI-2	GpI-6	GpI-12	Not IPC Group I
South Perran Sands					
SG39	**GpI-12**	GpI-12	GpIII-1	GpI(near)1	Not IPC Group I
TRE013	**GpI-12**	GpI-12	**GpIII-1**	GpI(near)1	Not IPC Group I
Great Hogus					
SG40	**GpIII-1**	GpI-2	**GpI-5**	GpI(near)2	Not IPC Group I
SG42	**GpI-12**	GpI/Ia	GpI/Ia	GpI-6	Not IPC Group I
Marazion					
SG32	**GpI-12**	GpI-12	GpI-(near)1	GpIII-1	Not IPC Group I

Table 102 Summary of DA of Perranuthnoe Group showing that the best geochemical matches are with GpIII-1 and GpI-12.

Immobile element DA reveals that only SG22 & TRE001 (PXRF & Pellet) have P(D/G) greater than 0.05 indicating the majority are matched with GpIII-1 and GpI-12 with very low probability of actually being related to GpIII-1 or GpI-12, but with almost certain probability these exposure samples are not related to any other sub-group. This point is re-enforced by noting that the first and second best matches for many samples are both GpI-12, suggesting that GpI-12 this is the only possible statistical match. SG22 is matched

with GpI-12 (immobile) and GpI-13 (mobile) and therefore not geochemically similar to either axe sub-group since they are separated by a considerable margin (compare Figure 81). TRE001 (PXRF and Pellet) is matched with GpIII-1 using both immobile and mobile elements, with one immobile element match P(D/G) less than 0.05 and one less than 0.10. Mobile element matches for TRE001 have P(D/G) < 0.10 for one of the two comparisons. Inspection of TRE001 (other analyses) and TRE010(A), TRE011(B) shows sub-group GpIII-1 is the best match, however, in these cases immobile element DA has P(D/G)<0.05. Overall, the matches found by immobile and mobile element DA indicate that there is a potential geochemical match between rocks from Perranuthnoe (Quarry) and GpIII-1.

	GpIII-1 (before DA) (n=2) (ppm ± 1sd)	GpIII-1 (after DA) (n=12) (ppm ± 1sd)	Perranuthnoe (Quarry) n=6 (ppm ± 1sd)	Sample TRE001 (PXRF) (ppm)	Sample TRE001 (PXRF pellet) (ppm)
K	10 400 ± 5 657	8 255 ± 5 962	13 913 ± 11 056	13 012	14 006
Ca	73 800 ± 6 223	64 008 ± 24 215	47 030 ± 17 914	51 724	52 378
Ti	5 800 ± 3 253	6 091 ± 2 638	9 092 ± 2 273	5 475	9 797
Mn	2 200 ± 1 273	1 383 ± 622	3 589 ± 858	2 959	3 655
Fe	96 550 ± 636	79 975 ± 22 658	92 014 ± 19 358	74 477	83 901
Rb	107 ± 9.6	58.3 ± 60.3	101 ± 80.7	100	110
Sr	430 ± 82.6	319 ± 182	522 ± 183	678	488
Y	21.0 ± 3.4	23.4 ± 3.7	18.9 ± 3.9	14	19
Zr	93.4 ± 0.1	83.6 ± 23.9	95.5 ± 9.9	95	91
Nb	5.0 ± 2.6	4.8 ± 2.5	13.0 ± 6.3	6	9
Ba	259 ± 216	154 ± 154	224 ± 208	202	200
Ce	-43.4 ± 12.7	-36.3 ± 22.6	-32.3 ± 10.1	-29	-20
Pb	66.1 ± 0.6	116 ± 213	49.6 ± 29.3	50	36

Table 103 Average and individual elemental compositions of samples collected from Perranuthnoe (Quarry) and GpIII-1 compositions before and after axe DA. Perranuthnoe data is in Appendix 28.1 & 28.2, GpIII-1 data from Table 75 and Appendix 23.9

Table 103, above, illustrates the similarity of elemental concentrations between IPC Group III (as indicated by GpIII-1) and samples from the Perranuthnoe (Quarry). Taking note of the PXRF precision (Section 6.15) the immobile element concentrations recorded for TRE001 are very close to the average of the 2 axes making up GpIII-1.

8.11.6 MANOVA and Student's t-test analysis

MANOVA is not carried out as there is insufficient data to produce statistically meaningful MANOVA analyses.

	K	Ca	Ti	Fe	Rb	Sr	Y	Zr	Nb	Ba
GpIII-1	0.595	0.084	0.095	0.159	0.912	0.180	0.637	0.973	0.146	0.963

Table 104 Results of carrying out Student's t-test for equality of means between GpIII-1 (Wi4/4 & Wi110/393) and Perranuthnoe Quarry samples TRE001, 010, 012. Value reported is the 2-tailed significance value assuming equal variance. With this number of samples it is not possible to reject the null hypotheses at a 0.05 significance value: that the means of the two groups being examined are equal.

Student's t-test is carried out between GpIII-1 and Perranuthnoe (Quarry), with results reported in Table 104, above. The results show that the null hypothesis, that the means of both groups are equal, cannot be rejected at a 0.05 significance value.

8.11.7 Discussion

Geochemically, it is clear that the **Mylor Slate Formation – Perranuthnoe Group greenstone outcrops did not provide the raw material for IPC Group I axes.**

Although no exact petrographical matches are recorded, inspection of geochemical data reveals that the Perranuthnoe (Quarry) sample TRE001 is similar to the two IPC Group III (GpIII-1, Wi4/4 & Wi110/393) axes analysed. This seems to supports the hypothesis that IPC Group III is provenanced to this area, a hypothesis based on the match of axe thin section Wi4/4 with one from a greenstone exposure near Perranuthnoe (Keiller et al. 1941). The failure to repeat the petrographic match is put down to the varied level of alteration encountered in the greenstone exposures and the small number of in situ samples (1) from the actual quarry. SCA, DA and t-tests supports the suggestions of geochemical similarity between GpIII-1 (representing IPC Group III) and samples collected from the Perranuthnoe (Quarry), although the matches are not definitive. **Noting Keiller et al.'s hypothesis, that IPC Group III originated from Perranuthnoe, the petrographic and geochemical evidence presented in this thesis cannot disprove that IPC Group III is provenanced to Perranuthnoe Quarry, but does go some way to supporting the published provenance of the group.**

Immobile and mobile element geochemistry of the Trenow Cove greenstone appears to be similar to that of GpI-12 (Do146/1762). However, immobile DA matches GpI-12 with the exposure samples giving P(D/G) less than 0.05, hence indicating that GpI-12 is a very poor match. Petrographical observations reveal Do146/1762 has no primary feldspar remaining, whilst feldspar dominates the Trenow Cove rock samples. With no additional evidence (unlike above) it is therefore probable that GpI-12 is unlikely to have originated from the Trenow Cove greenstone body. Further, the lack of another consistent immobile element DA match indicates that the **Trenow Cove greenstone body did not provide material for any other axe sub-group examined in this work.**

Finally, there is **no geochemical evidence to support that greenstone exposures at Great Hogus, South Perran Sands and Marazion provided material for IPC Group I axes.**

8.12 Mylor Slate Formation: Penzance Group

8.12.1 Overview of samples and localities

In order to test the hypothesis that IPC Group I axes originate from the 'Penzance area' (Keiller et al. 1941) over sixty geochemical analyses from forty-seven samples originating from ten locations around Penzance have been obtained (c.f. Figures 21 & 22, Section 3.6.3.2.3). These locations include readily accessible and well exposed greenstones at Long Rock (low tide only), Penzance (near the open air swimming pool), Carn Gwavas (including the large roadstone quarry), Penlee (including the two small disused quarries at Penolva less than 100m north-west of Penlee Point) and at Mousehole. These locations consist of shallow and deep level intrusive, evolved tholeiitic, rocks with intraplate-MORB affinities, apart from the Carn Gwavas exposure which is a diorite (Al Samman 1980, Floyd et al. 1993). The Carn Gwavas diorite exposure has been included in the data set to further show similarity between published WDXRF and new PXRF geochemical analyses over a different range of elemental concentrations to that encountered with greenstones. Inland sites include the alkali pillow lavas at Gulval and the fine grained vesicular, tholeiitic lavas at a small quarry (near Bennet's Coal Yard) within Penzance and from two poorly exposed intrusive outcrops at Tredavoe and Polkinhorne (Section 3.6.3.2 and Figures 21 and 22). (Note: samples are identified in Appendix 4, with geochemical analyses in Appendix 15)

Note that the only sample measured from a greenstone outcrop near Porthleven (PLN001) is included in charts within this section.

8.12.2 Inspection of petrographic, magnetic and geochemical data

Long Rock appears to consist of two petrographically different exposures, one with almost fresh, coarse ophitic, clinopyroxene (LNR001b & LNR004) and one very fine grained with no readily visible primary mineralogy (LNR002 & LNR003). The style of alteration, rather than the primary mineralogy, seen in LNR001b & LNR004, is reminiscent of GpI-5 & GpI-11. Penlee samples PEN003 and PEN004 are petrographically similar to GpI-6, sharing heavily altered clinopyroxenes, altered feldspars, ilmenite, accessory apatite and plentiful secondary fibrous and euhedral amphibole (Section 4.8.6). Published

petrographic observations for samples WG2 &WG4 (Gulval), WG11, WG12, WG13 WG16 and WG18 (Penzance (Bennet coal yard)) report a plagioclase-amphibole rich vesicular lava, hence dissimilar to IPC Group I which is not found to contain vesicles. WG20, WG22, WG23 and WG 24 (Penzance swimming pool) are reported as coarse grained with tabular plagioclase, prismatic actinolite and *abundant apatite*, hence also dissimilar to IPC Group I as the dominant plagioclase and abundant apatite are not found in axe thin sections examined as part of this work (Al Samman 1980, Figure 21, Appendix 4). Polkinhorne and Tredavoe thin sections either contain free quartz (Polkinhorne) or are hornfelsed (Tredavoe), thus are unlike any axe thin sections examined (Section 4.7.6)

MS measurements are available from the shore at Carn Gwavas, Penlee Point and Mousehole (Appendix 9.5 & Table 7 Chapter 5). The corrected range lies between 0.60-0.78 x 10^{-3} SI, towards the lower end of the IPC Group I axe range of 0.23 to 1.89 x 10^{-3} SI.

Immobile element concentrations summarised in Table 105 below and detailed in Appendix 28.1 clearly show a division between the dioritic Carn Gwavas and the doleritic rocks at Long Rock, Penzance, Penlee and Mousehole. Carn Gwavas Zr (circa 1,000ppm), Y (generally >100ppm), Nb (>75ppm) and Ti (<5,000ppm) are all significantly different to greenstone. SiO_2 ranges between 60 to 65% wt for Carn Gwavas samples, with total alkalis ($Na_2O + K_2O$) between 7 to 9%wt clearly placing this rock into the syeno-diorite field of the TAS diagram (Cox et al. 1979).

The petrographic division of Long Rock is also seen within immobile element concentrations with LNR001 & LNR004 having less Ti, Y, Zr & Nb than LNR002 & LNR003. The greenstone exposure at Penzance swimming pool is enriched in Ti, Y, Zr and Nb compared to greenstone exposures further south along the coast at Penlee and Mousehole. Samples collected at Polkinhorne and Tredavoe are geochemically different within and between the two locations, indicating these samples may not be indicative of the greenstone outcrops at these locations indicated on the geological map.

When compared to the reduced IPC Group I (n=130) average all Penzance Group greenstone samples appear to possess more Nb (generally >20ppm) than IPC Group I (n=130) (6.7 ± 2.9ppm). Ti, Y & Zr concentrations at Mousehole and Penlee Point are similar to the reduced IPC Group I (n=130). All mobile element concentrations vary

widely between and within greenstone exposures as could be expected with the proximity to the Lands End granite. Greenstones in the Penzance area contain 45 to 52%wt SiO_2 and 4 to 5% wt $Na_2O + K_2O$, hence are basic, and tholeiitic to mildly alkaline.

	Reduced IPC Group I (n=130) (ppm ± 1sd)	Penlee Point (n=8) (ppm ± 1sd)	Mousehole (n=6) (ppm ± 1sd)	Long Rock (A) (n=3) (ppm ± 1sd)	Long Rock (B) (n=3) (ppm ± 1sd)
K	3 567 ± 2 282	13 880 ± 6 365	15 077 ± 2 675	7 079 ± 8096	7 522 ± 3 920
Ca	67 715 ± 14 636	51 394 ± 6 615	65 971 ± 13 110	64 100 ± 30 922	50 157 ± 6 998
Ti	14 959± 3 772	16 779 ± 5 150	12 461 ± 1 172	20 070 2 609	11 187 ± 1 616
Mn	1 532 ± 521	1 549 ± 603	1 591 ± 413	3 236 ± 669	1 988 ± 1 059
Fe	95 632 ± 14 009	89 013 ± 11 358	84 244 ± 7 878	158 036 ± 50 153	86 444 ± 16 001
Rb	29.6 ± 25.8	174 ± 123	165 ± 39.9	416 ± 477	107 ± 29.9
Sr	324 ± 150	262 ± 82.6	308 ± 47.3	576 ± 373	459 ± 72.7
Y	35.7 ± 6.8	34.4 ± 11.1	24.4 ± 2.9	24.5 ± 1.4	19.2 ± 10.0
Zr	171 ± 29.2	186 ± 62.3	140 ± 22.9	226 ± 22.9	117.3 ± 25.9
Nb	6.7 ± 2.9	46.8 ± 7.8	29.1 ± 5.5	57.2 ± 3.7	16.2 ± 5.5
Ba	104 ± 64.3	131 ± 46.5	170 ± 47.7	1.0 ± 21.4	187 ± 156
Ce	-27.1 ± 11.4	18.0 ± 9.8	2.6 ± 3.7	62.1 ± 52.9	-13.9 ± 15.8
Pb	230 ± 1013	6.4 ± 4.4	1.4 ± 18.8	53.1 ± 23.8	17.2 ± 5.9

	Reduced IPC Group I (n=130) (ppm ± 1sd)	Penzance (swimming pool) (n=4) (ppm ± 1sd)	Penzance (Gulval) (n=2) (ppm ± 1sd)	Penzance (Bennet coal yard) (n=5) (ppm ± 1sd)	Carn Gwavas (Floyd pers.com.) (n=9) (ppm ± 1sd)
K	3 567 ± 2 282	11 310 ± 4 419	11 995 ± 10 859	27 261 ± 18 501	19 461 ± 13 473
Ca	67 715 ± 14 636	47 941 ± 4 711	90 626 ± 29 374	72 487 ± 17 989	16 072 ± 5 958
Ti	14 959± 3 772	21 630 ± 1 663	21 810 ± 1 315	15 756 ± 2 385	3 973 ± 470
Mn	1 532 ± 521	1801 ± 337	1 628 ± 329	2 185 ± 726	1 137 ± 384
Fe	95 632 ± 14 009	99 899 ± 11 890	65 088 ± 4 044	141 005 ± 32 182	59 935 ± 14 112
Rb	29.6 ± 25.8	207 ± 81.4	121 ± 102	511 ± 497	109.4 ± 148
Sr	324 ± 150	300 ± 81.2	425 ± 21.2	180 ± 147	122 ± 35.4
Y	35.7 ± 6.8	63.3 ± 7.6	34.5 ± 0.7	34.4 ± 9.8	134 ± 25.5
Zr	171 ± 29.2	312 ± 45.5	269 ± 23.3	192 ± 49.7	995 ± 276
Nb	6.7 ± 2.9	37.5 ± 8.6	69.5 ± 7.8	31.8 ± 10.4	*90.7 ± 6.5
Ba	104 ± 64.3	82.5 ± 50.1	Not measured	Not measured	387 ± 471
Ce	-27.1 ± 11.4	Not measured	Not measured	Not measured	Not measured
Pb	230 ± 1013	Not measured	Not measured	Not measured	Not measured

*Table 105 Summary of average compositions of samples collected from greenstone exposures near Penzance and the reduced IPC Group I(n=130). Data in table is summarised from data in Appendix 28.1 and 28.2 and Table 58. Penlee, Mousehole are averages from combined data from author and Floyd (pers. com.). Long Rock (A) consists of samples LNR001 & 004, Long Rock (B) consists of samples LNR002 & 003). Polkinhorne and Tredavoe are not reported above since they appear to be petrographically different to IPC Group I and also, were not collected from in-situ exposure material. * indicates the author's Nb average Carn Gwavas concentration (n=10 analyses) as none were available from Floyd (pers. com.). Also note n=number of analyses made and not the number of samples.*

Inspection shows that, whilst there is some petrographic similarity between IPC Group I and greenstone samples from the Penzance Group, they appear to be geochemically different, especially noting the high Nb values possessed by the Penzance greenstones.

8.12.3 Element discrimination diagrams

Figures 93 & 94 contain the immobile element discrimination diagrams for the Penzance Group greenstone exposures and the Carn Gwavas diorite exposure. Nb values for Floyd's

Carn Gwavas samples are not recorded, hence not displayed on the associated discrimination chart. Where available, geochemical data for the Carn Gwavas samples measured by the author (samples PEN001 and PEN002) and by Floyd is seen to overlap on the element discrimination diagrams, hence supporting the accuracy of the Bias (I) correction factors and the compatibility of data from different sources. The greenstone exposures plot (e.g. Penlee, Mousehole, Penzance) as Ti, Zr, Nb enriched within plate basalts, with the Nb values indicating that both evolved tholeiitic (Penzance swimming pool, Penlee Point and Mousehole) and alkali (Gulval, Long Rock) rock types are present.

Comparing Figures 93 & 94 with Figures 77 to 80 (Chapter 7) reveals no consistent overlap in plotted position between any axe sub-group and Penzance Group exposure. This includes all IPC Group I sub-groups, suggesting that IPC Group I sub-groups are geochemically dissimilar to rocks from the Penzance area. GpI-12 (not an IPC Group I sub-group) has the closest similarity with Penlee Point and Long Rock, having comparable Ti, Zr, Nb values, but with a Zr/Y ratio of 9 compared to less than 8 for Penlee, and Nb of 30ppm compared to Long Rock (LNR002 & LNR003) with more than 50ppm. (IPC Group I axe Zr/Y ratio is approximately 5 and associated Nb average is 6.7 ± 2.9.) Hence it is observed that all Penzance Group exposures have sufficiently different immobile element geochemistry to axe sub-groups to preclude any of the Penzance Group exposures being the source of IPC Group I axe material.

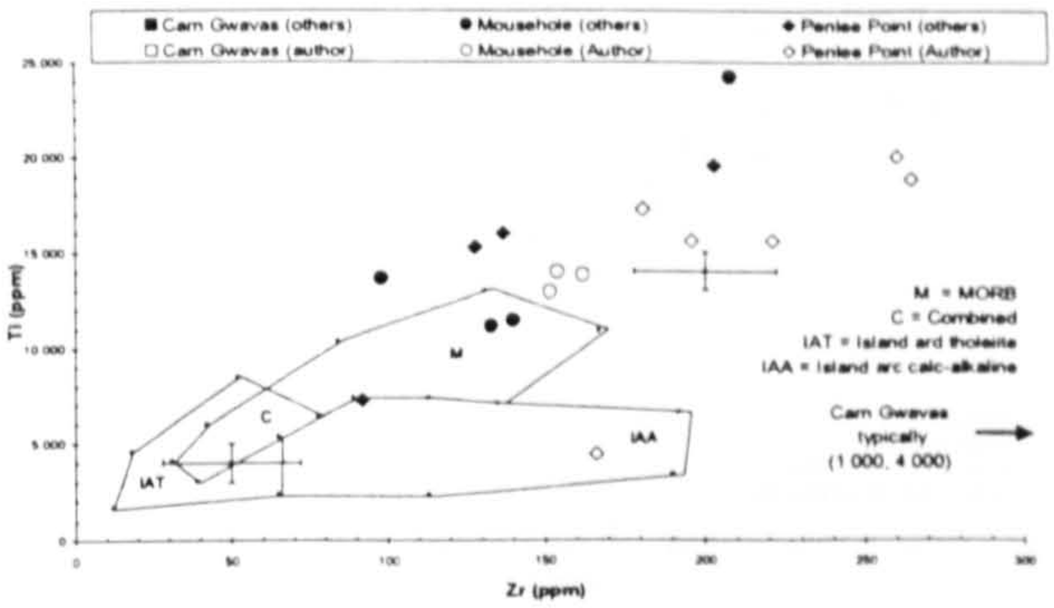

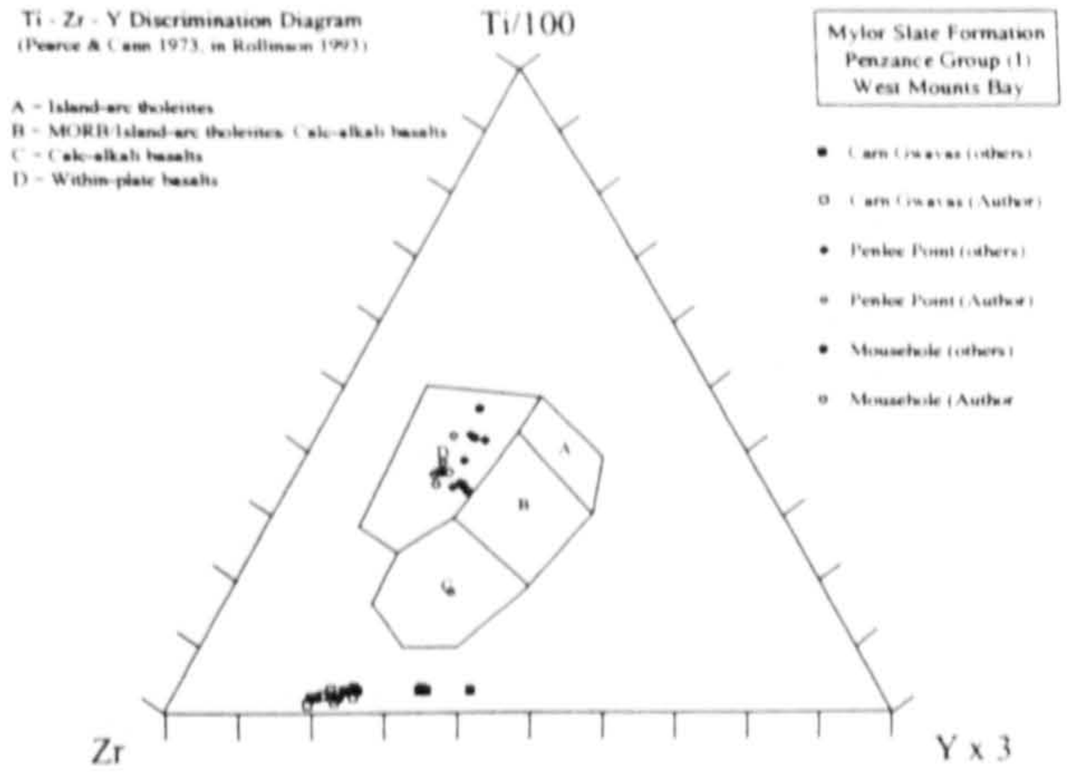

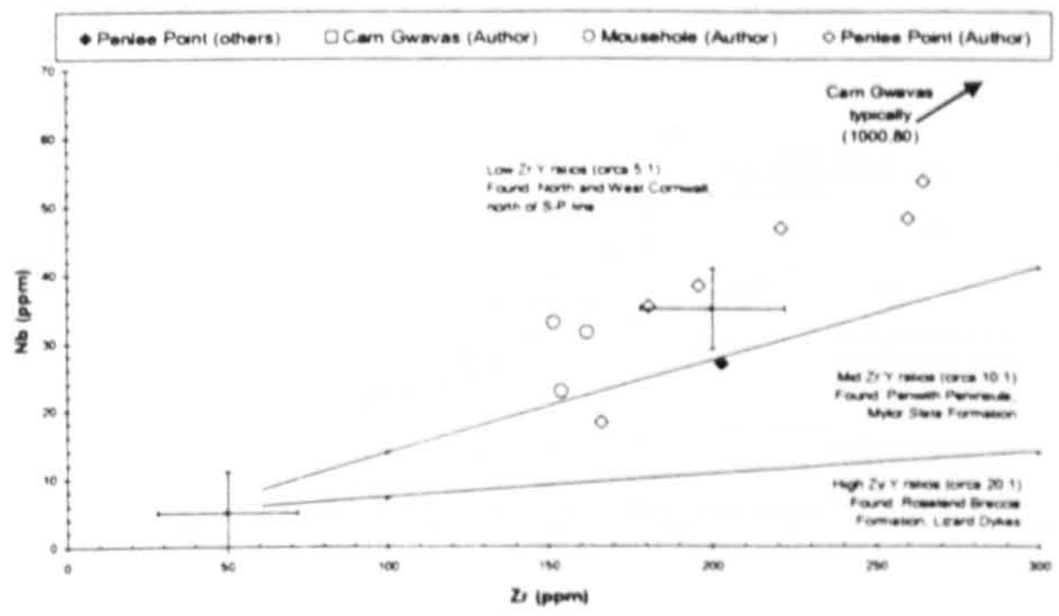

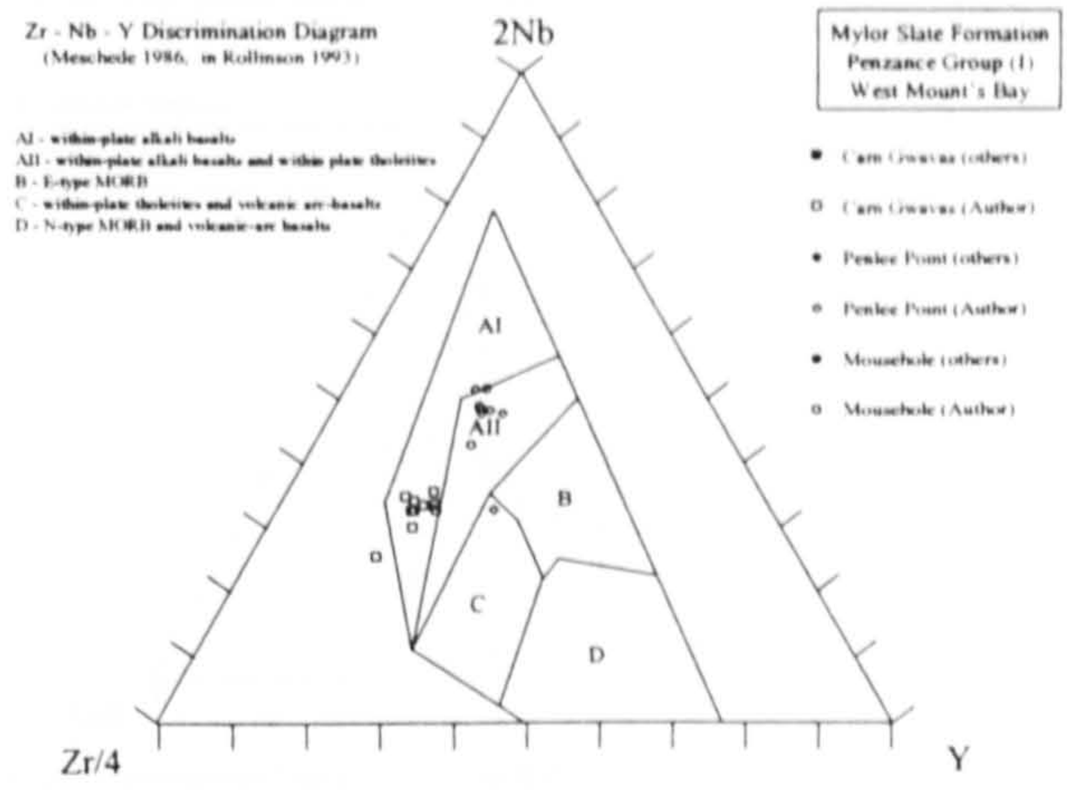

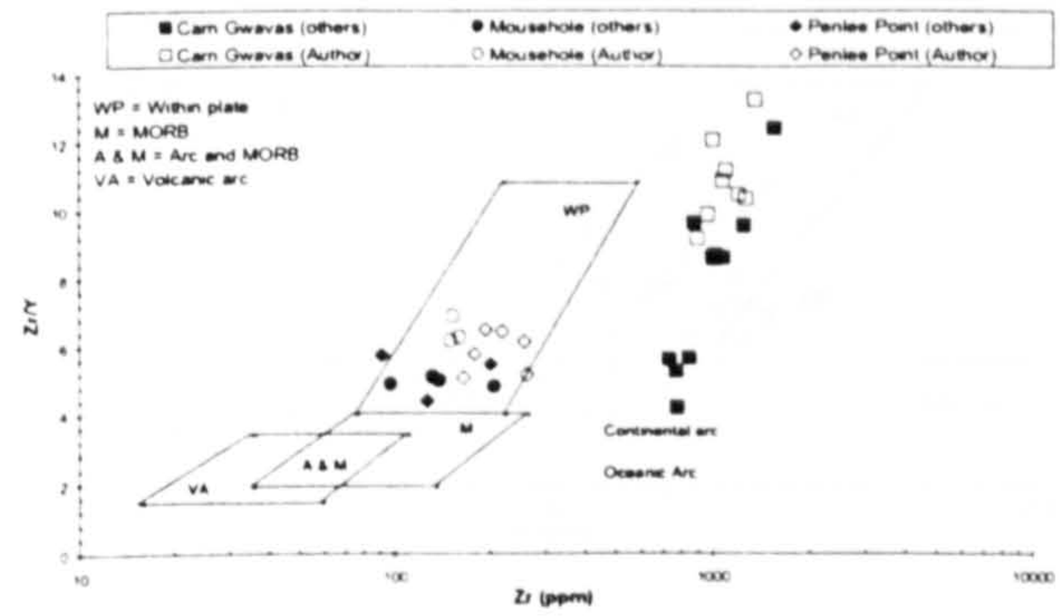

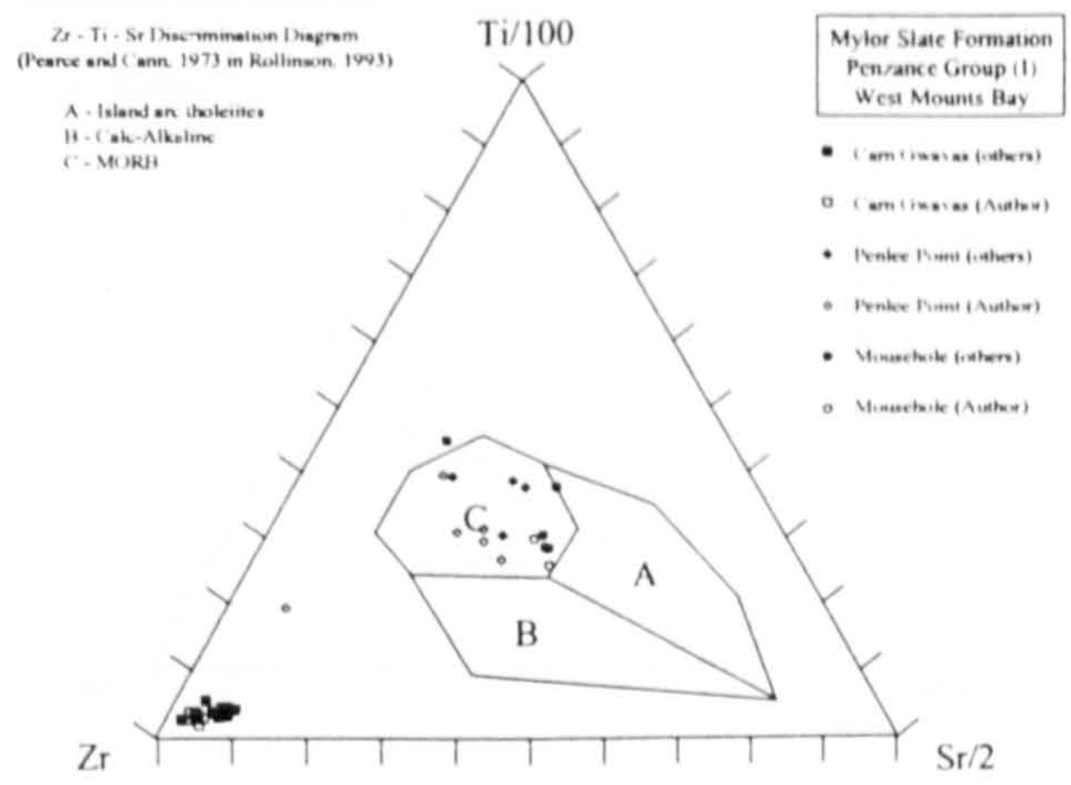

Figure 93 Element geochemical discrimination diagrams for Mylor Slate Formation Penzance Group (Carn Gwavas, Penlee & Mousehole). The dioritic Carn Gwavas exposure is clearly geochemically different to all greenstone exposures. Penlee and Mousehole greenstone exposures are evolved and Ti, Y, Nb enriched within plate tholeiites and are geochemically different to all axe sub-groups.

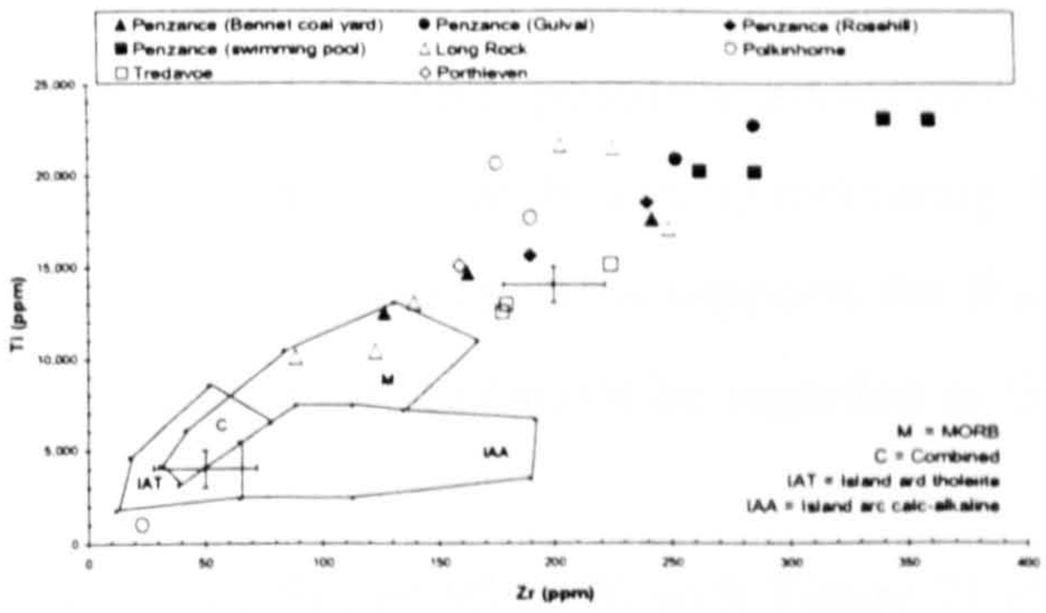

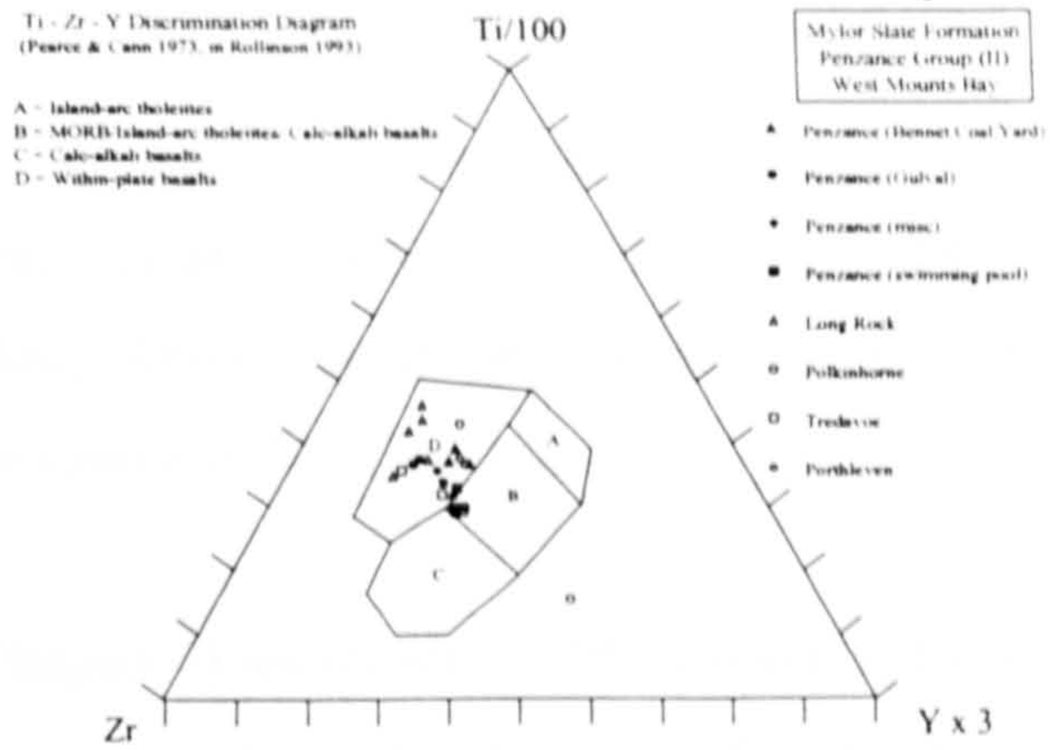

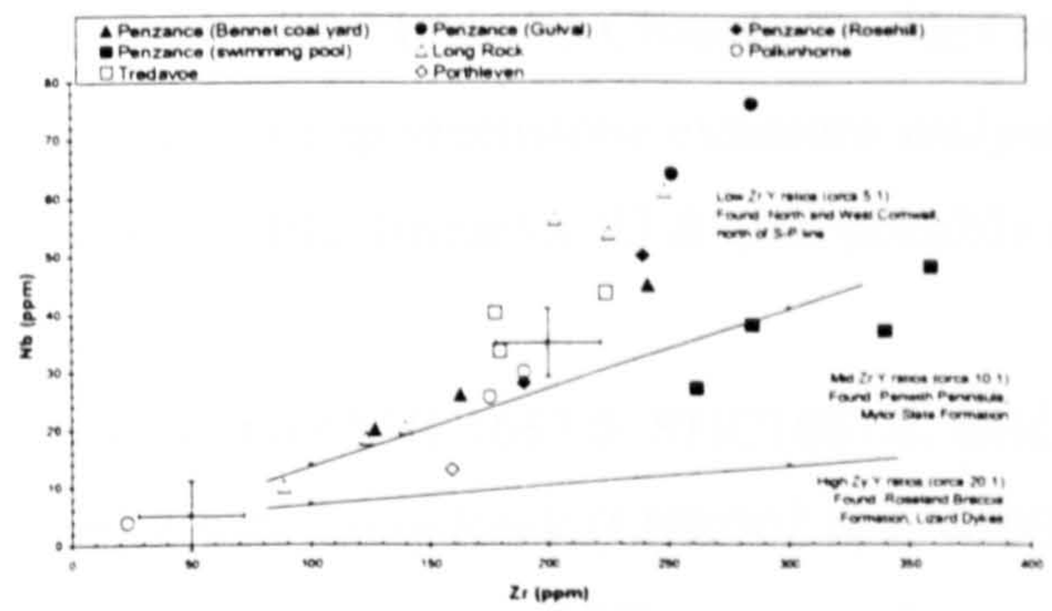

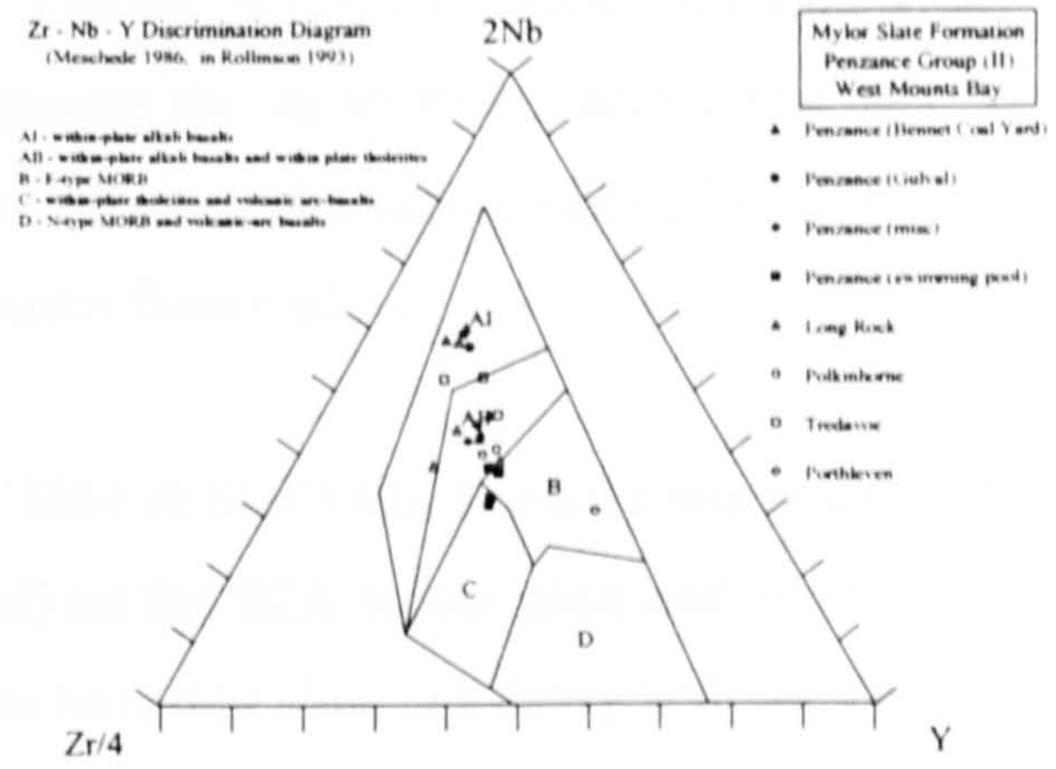

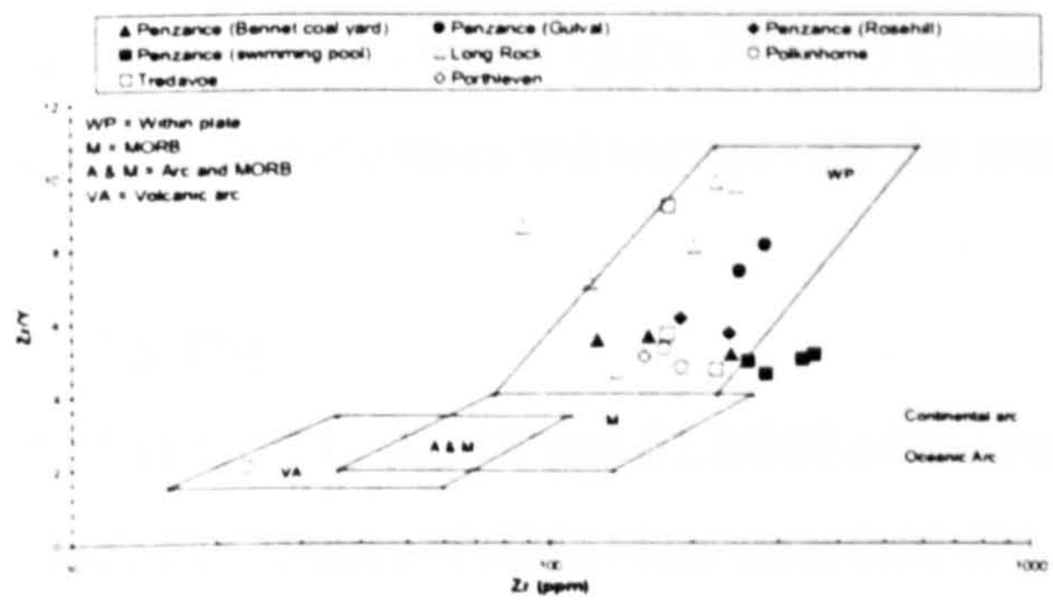

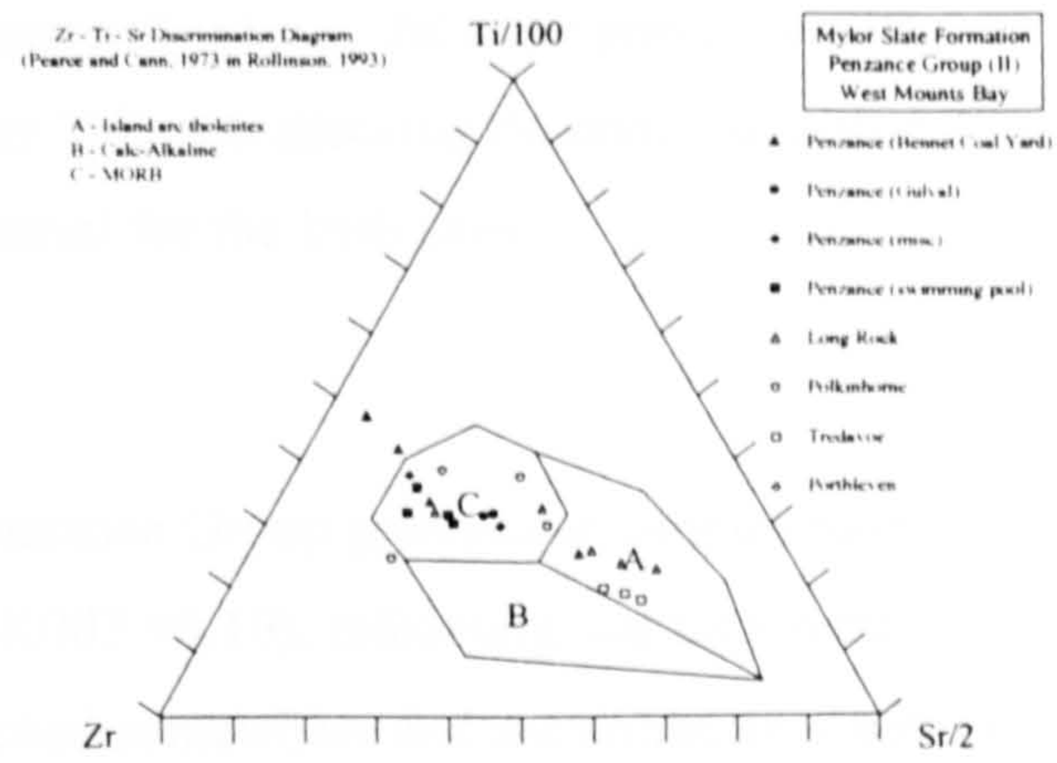

Figure 94 Element geochemical discrimination diagrams for Mylor Slate Formation - Penzance Group (Penzance, Long Rock, Tredavoe & Polkinhorne). All greenstones are Ti, Y, Nb enriched tholeiites or alkali basalts and appear unrelated to each other. All exposures are geochemically different to all axe sub-groups, especially IPC Group I axe sub-groups, indicating that it is very unlikely any exposure provided the source material for IPC Group I axes.

8.12.4 SCA

No Penzance Group exposure analyses plot within the immobile element SC scatter plot ellipses (Figures 95 & 96 upper) indicating that they are geochemically different to IPC Group I (n=130) axes. This supports the findings above: that the greenstone exposures in the Penzance Group cannot be regarded as the source of IPC Group I.

Comparing Figure 95 & 96 with Figure 71 (Chapter 7) shows that no IPC Group Ia, I/Ia or I(near) consistently plots within any exposure cluster. A similar situation is found with IPC Group III (Figure 73 Chapter 7). This supports the observations, above, that no Penzance Group greenstone exposure analysed provided the source material for IPC Groups Ia, I/Ia, I(near)or III & IIIa, possibly apart from GpI-12.

Non-IPC axes SHC1687.6, SHC1687.8, SHC1361 & SHC1603-8 share some positional overlap with Long Rock (LNR002 & LNR003) on the SCA scatter plots and are the only non-catalogued axes or IPC ungrouped axes to have any clear similarity with the Penzance Group. No Irish gabbro or doleritic axes consistently plot in the same positions on the associated SCA chart (Figure 74 & 75 Chapter 7) hence allowing the conclusion that these greenstone exposures did not provide the material for the Irish axes.

8.12.5 DA

All but WG11, WG18 and PLK002 of the Penzance Group greenstone samples have immobile element P(D/G) less than 0.05 (PLK003 <0.10), indicating that they were matched on the basis that they had to be matched somewhere and are unlike axes within the indicated 'best match' sub-group (Appendix 31.1). Mobile element discrimination produces similar, low probability assignments, for the majority of samples. Inspection of Appendix 31.1 reveals no consistency in assignment of exposure samples to axe sub-groups.

Therefore, discriminant analysis supports the findings in the above sections: that no Penzance Group exposure sample is statistically similar to any axe sub-group. (Note that there is insufficient geochemical data from some of Floyd's analyses to carry out DA (c.f. Appendix 31 and Appendix 15 for details.)

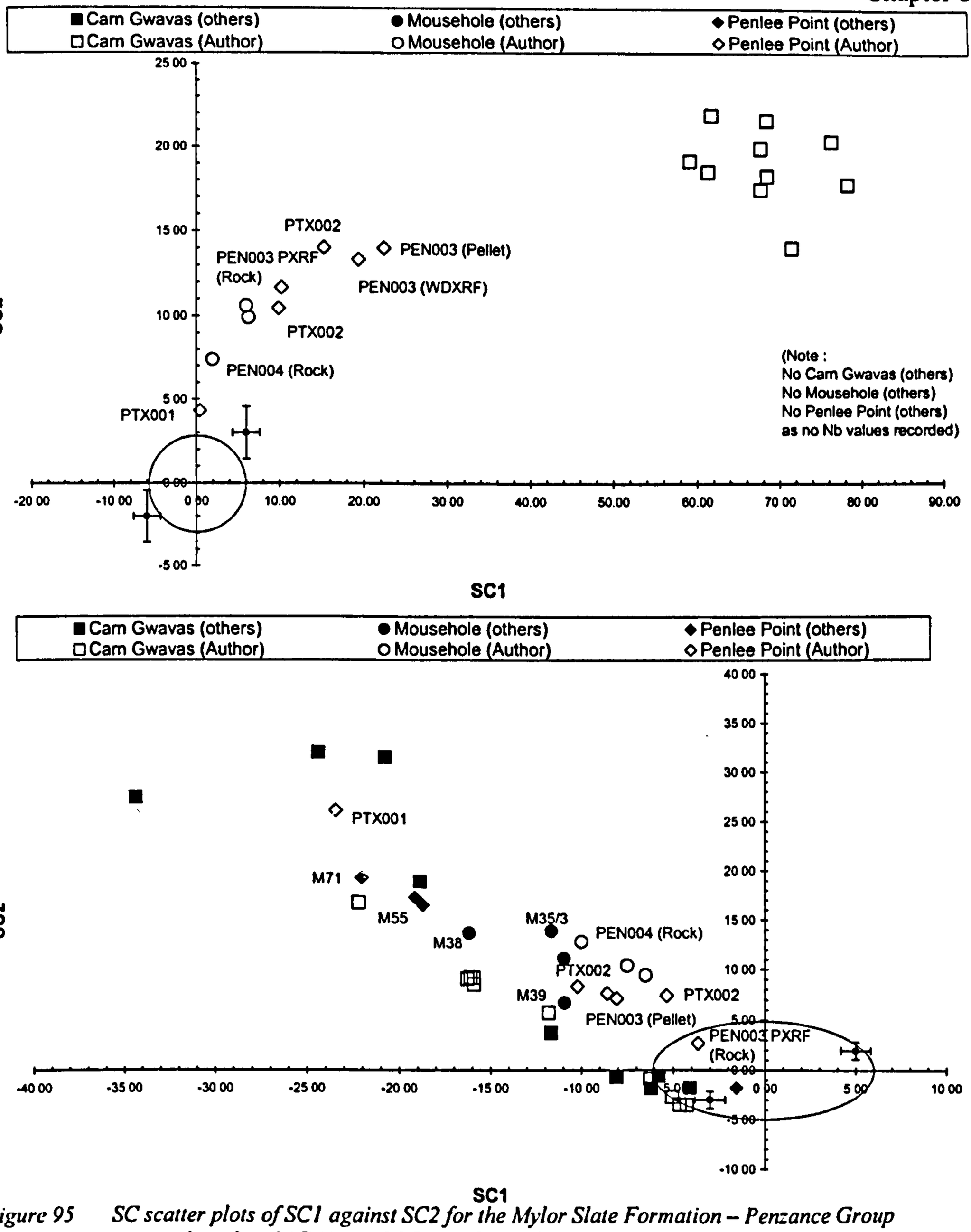

Figure 95 SC scatter plots of SC1 against SC2 for the Mylor Slate Formation – Penzance Group greenstone exposures based on IPC Group I SCA analysis of Ti, Y, Zr & Nb (immobile) elements (upper chart) and K, Ca, Fe, Rb, Sr & Ba (mobile) elements (lower chart). No exposure sample plots within the immobile SCA ellipse indicating immobile element geochemistry is different to IPC Group I.

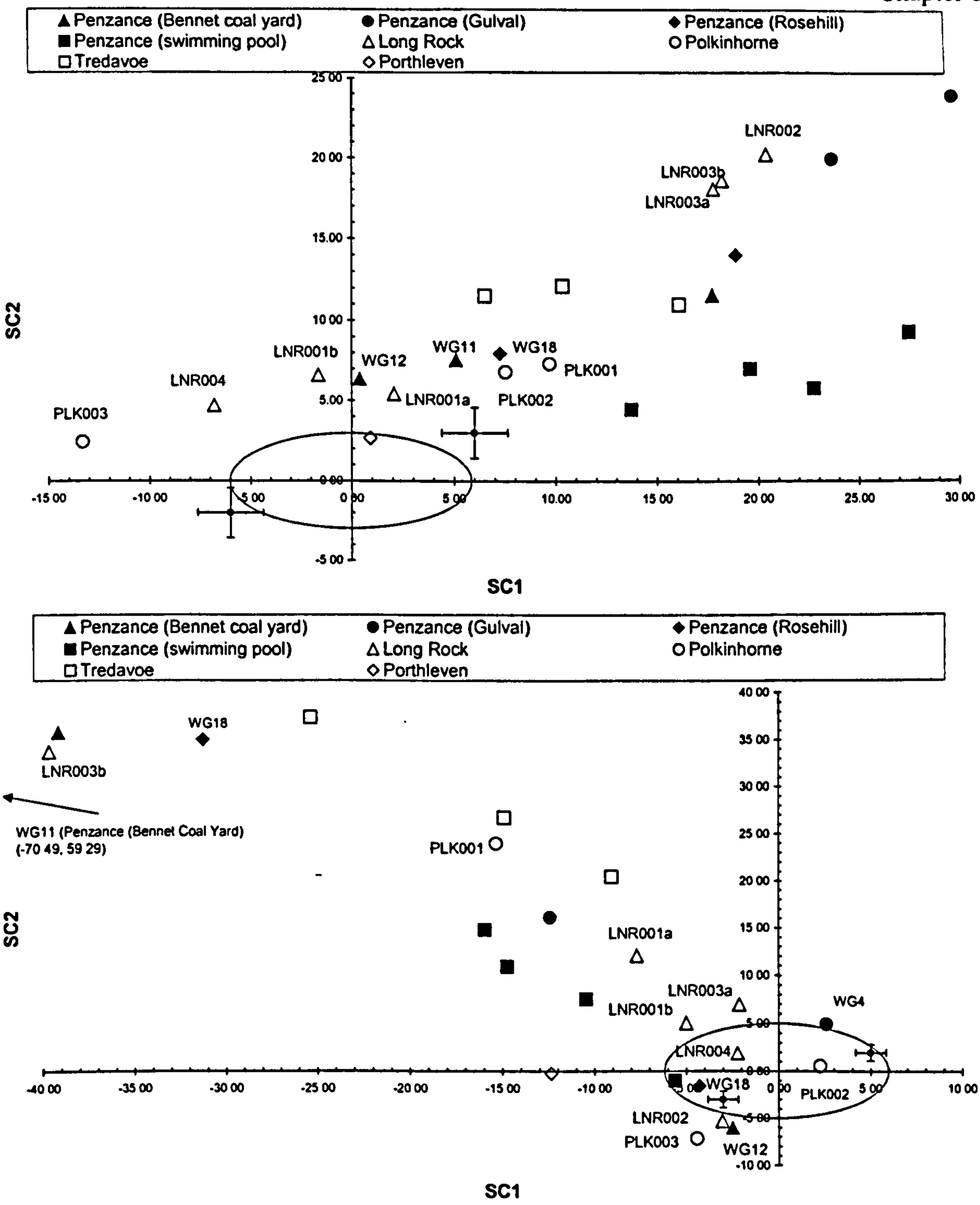

Figure 96 SC Scatter plots of SC1 against SC2 for the Mylor Slate Formation – Penzance Group greenstone exposures based on IPC Group I SCA analysis of Ti, Y, Zr & Nb (immobile) elements (upper chart) and K, Ca, Fe, Rb, Sr & Ba (mobile) elements (lower chart). No exposure sample plots within the immobile SCA ellipse indicating immobile element geochemistry is different to IPC Group I. (Note the sample to plot in the immobile ellipse is from Porthleven, and is included in this chart for reference only as it does not clearly fit in with any other section of this chapter.)

8.12.6 MANOVA and Student's t-test analysis

No MANOVA or statistical comparison on geochemical data is carried out as the findings in the above three sections are that there is no match between axe sub-groups and Penzance Group exposures.

8.12.7 Discussion

There are some marginal petrographic and magnetic similarities between axe sub-groups and greenstone exposures found in and around Penzance noted but there are clearly no associated geochemical similarities. The most significant difference between Penzance Group exposures and the IPC Groups examined is the evolved tholeiitic to alkali nature of the exposures, indicated by the relatively high Nb values. Mobile element concentrations are variable, not only between, but within greenstone exposures strongly suggesting variable alteration, probably associated with intrusion of the Land's End granite.

It is therefore concluded on the basis of geochemical differences that the greenstone exposures sampled in the Penzance area are unlikely to have provided the material for the manufacture of IPC Group I, Ia, I/Ia, I(near) or III & IIIa axes, most of the IPC and non-IPC axes and none of the Irish dolerite or gabbro axes.

8.13 Mylor Slate Formation: North Penwith Group

8.13.1 Overview of samples and localities

The north coast of the Land's End peninsula between St Ives in the east, to Kenidjack in the west, has numerous resistant headlands of shallow intrusive and submarine extrusive tholeiitic to intermediate within plate basalts/dolerites that have been altered through regional and contact metamorphism to greenstone (Floyd et al. 1993). Twenty greenstone samples yielding thirty-two geochemical analyses have been obtained from headlands at St Ives, Clodgy Point, Trowan, Carrick Dhu, Zennor Point, Gurnard's Head and Kenidjack. Invariably these headlands consist of shallow level sill-like bodies, often associated with pillow lavas and are not comagmatic, representing separate volcanic centres (Floyd pers. com.). The grade of contact metamorphism increases westwards towards Kenidjack and Botallack where Mg (cordierite) and Ca (garnet) rich hornfels are found (Floyd et al. 1993, Section 3.6.3.2).

The headlands are all easily accessible by foot or boat and are relatively close to a number of Neolithic tombs along the northern edge of the Land's End granite (Figure 2 Chapter 2).

8.13.2 Inspection of petrographic, magnetic and geochemical data

Pillow lavas exposed at Clodgy Point and Carrick Dhu (LE86, LE87, LE90 & LE 89) contain a low-level hornfelsed assemblage of albite-epidote (Floyd et al. 1993), dissimilar to GpI-1, which has relict pyroxene and is not hornfelsed. ZEN001 was found to be a laminated fine grained rock, possibly sedimentary, unlike any axe thin section examined. The medium grained intrusive greenstone at Zennor Head (ZEN002) contains secondary biotite in a heavily altered epidote-amphibole-plagioclase groundmass, again unlike any axe thin section examined. Pyroxenes replaced by secondary tremolite-actinolite, with altered acicular plagioclase feldspar and secondary biotite found at Gurnard's Head are similar, but not the same, as GpI-7 and GpIa-3 thin sections and is the only North Penwith greenstone exposure to share any similarities with axe thin sections (Section 4.7.7). Andalusite and staurolite present in the KEN001, KEN002 & KEN003 reflect the increased grade of contact metamorphism westwards towards Land's End. Published petrographic descriptions for intrusive greenstones near St Ives have not been found, but it is assumed that they are potentially medium grained.

Corrected MS values from Zennor Point range between 0.50 to 0.72 x 10^{-3} SI and from Gurnard's Head between 0.60 to 0.78 x 10^{-3} SI. As for all other greenstone exposures measured (Penlee, Trenow Cove and Cudden Point) these values are at the lower end of the IPC Group I axe range (0.23 to 1.89 x 10^{-3} SI) and are therefore compatible but inconclusive.

	Reduced IPC Group I (n=130) (ppm ± 1sd)	Gurnard's Head (n=8) (ppm ± 1sd)	Zennor Point (n=7) (ppm ± 1sd)	St Ives (n=3) (ppm ± 1sd)	Carrick Dhu (n=2) (ppm ± 1sd)
K	3 567 ± 2 282	11 242 ± 3 207	721 ± 1 041	5 036 ± 1 490	5 064 ± 1 526
Ca	67 715 ± 14 636	79 676 ± 8 747	95 109 ± 3 243	76 887 ± 18 031	93 772 ± 2 882
Ti	14 959± 3 772	13 270 ± 871	8 376 ± 614	9 660 ± 1 157	13 410 ± 1 315
Mn	1 532 ± 521	2 534 ± 411	1 161 ± 153	2092 ± 676	2 015 ± 767
Fe	95 632 ± 14 009	86 813 ± 3 219	72 273 ± 6 369	88 439 ± 14 209	96 200 ± 21 420
Rb	29.6 ± 25.8	88.2 ± 16.9	10.7 ± 8.0	27.7 ± 6.7	22.5 ± 16.3
Sr	324 ± 150	250 ± 64.0	201 ± 28.4	278 ± 138	316 ± 106
Y	35.7 ± 6.8	36.3 ± 3.7	20.7 ± 3.4	29.3 ± 2.1	35.0 ± 0.0
Zr	171 ± 29.2	142 ± 12.8	104 ± 6.7	103 ± 26.6	200 ± 20.5
Nb	6.7 ± 2.9	9.8 ± 2.2	7.2 ± 2.4	7.0 ± 2.6	13.0 ± 1.4
Ba	104 ± 64.3	130 ± 30.1	6.5 ± 16.6	80.0 ± 29.5	75.0 ± 9.9
Ce	-27.1 ± 11.4	-28.3 ± 8.9	-39.1 ± 6.9	Not measured	Not measured
Pb	230 ± 1013	4.2 ± 8.4	0.5 ± 10.2	Not measured	Not measured

Table 106 Average elemental compositions of selected samples collected from exposures along the North Penwith Peninsula and reduced IPC Group I (n=130). North Penwith data is summarised from that in Appendix 28.1 & 28.2. reduced IPC Group I is from Table 58. The three St Ives measurements reported here are from samples LE 92, LE125 and LE152.

Table 106 and Appendix 28.1 show that immobile element concentrations from the samples collected in the St Ives area (LE81 Trowan Cliff; LE86 & LE87 Clodgy Point; LE89 & LE90 Carrick Dhu; LE92 St Ives; LE125 Carbis Bay (St Ives) and LE152 St Ives Head) and Gurnard's Head (GUR001 & GUR002) are generally within 2sd of the IPC Group I average (Appendix 23.9). However, in both cases Ti is consistently less and Nb slightly higher in the exposure samples compared with the axe Group average. Nb concentrations at Zennor Point are within 1sd of the IPC Group I average (6.7 ± 2.9ppm) but the Zr, Y and Ti concentrations are all greater than 1sd lower than IPC Group I averages. The hornfels at Kenidjack has comparatively high Nb (>17ppm) and slightly high Ti (>16,100ppm) compared to the reduced IPC Group I (n=130) averages. Mobile element concentrations, especially K and Ca are variable indicating the probable effect of metasomatism. Interestingly, Mn concentrations at St Ives and Gurnard's Head are also generally higher than the reduced IPC Group I (n=130) average of 1,532 ± 521ppm. Major element oxides for all samples range between 44 to 48% wt SiO_2, 1.5 to 3.5% wt total alkali ($Na_2O + K_2O$) and 9 to18% wt MgO + CaO. This places the rocks as marginal tholeiitic/alkaline on the TAS (total alkalis v silica) discrimination diagram (Le Maitre et al. 1989; in Rollinson 1993), hence similar to other greenstones within the Mylor Slate Formation (Appendix 15.2 and Floyd pers. com.).

Thus it appears that there are some petrographic, magnetic and geochemical similarities between IPC Group I and greenstones from the North Penwith coast, especially with exposures around St Ives and Gurnard's Head.

8.13.3 Element discrimination diagrams

The six immobile element geochemical discrimination diagrams in Figure 97, below, show that the exposures around St Ives and at Gurnard's Head and Zennor Point plot as within plate tholeiites. Zr–Nb ratios clearly fall in Floyd's 'South and West Cornwall' Group (Floyd et al. 1993, Appendix 30) as would be expected since some of the data reported here was used to generate figure 4.2 in Floyd et al. (op. cit.).

Comparing Figure 97 with Figures 77 to 80 reveals some, but not consistent, overlap between axe sub-groups and samples from North Penwith. GpI-2 & GpI-7 plot in similar positions to two St Ives greenstone samples (LE81, LE125) and Gurnard's Head samples (GUR001, 002), whilst GpI-8 and GpIII-1 plot close to St Ives samples (LE92, LE87, LE152 and LE86) and Zennor Head (ZEN002). However, in the first case Gurnard's Head

and LE81 & LE125 have different Zr-Ti ratios than GpI-2 &GpI-7 and in the second case GpI-8 and GpIII-1 differ from Zennor Point and LE92, LE87, LE152 and LE86 by having lower Nb and generally higher Sr. Hence, on balance, whilst there is some geochemical similarity between North Penwith and IPC Group I (n=130), the samples from North Penwith greenstones cannot be clearly related to any one sub-group.

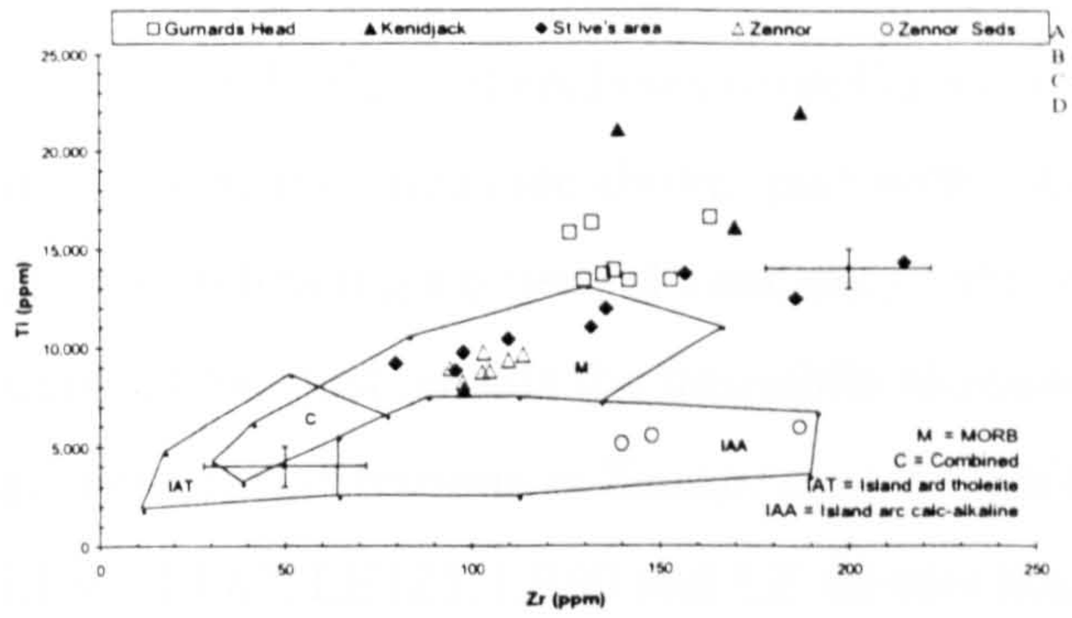

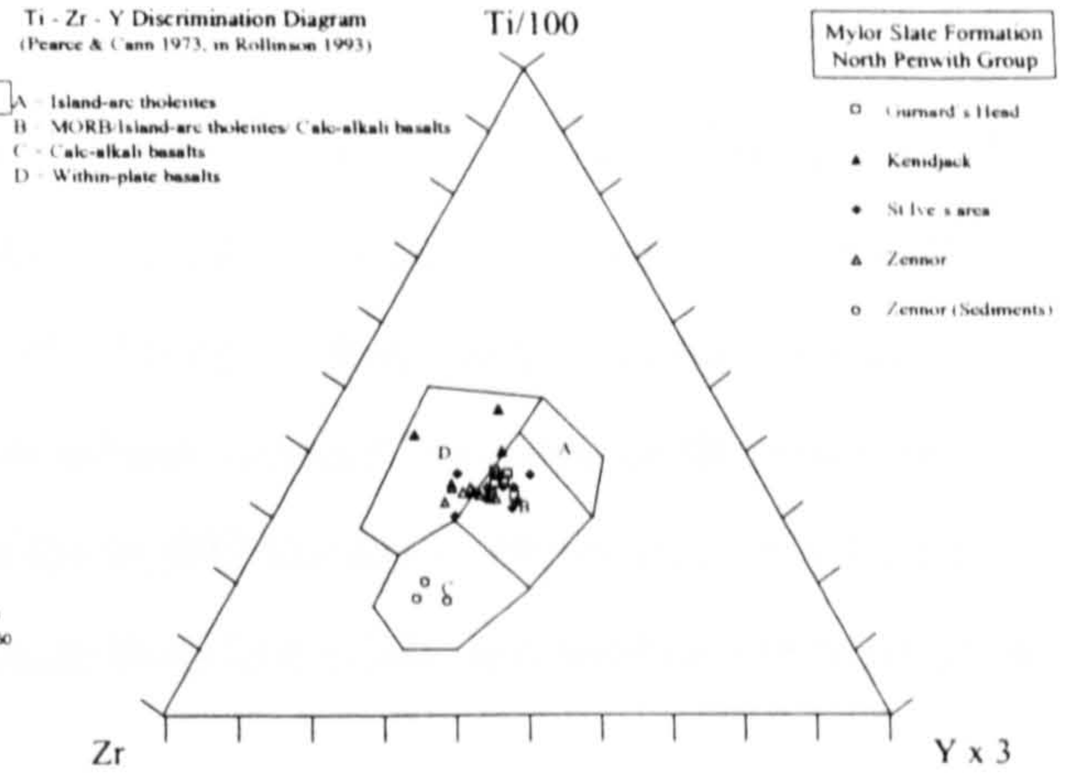

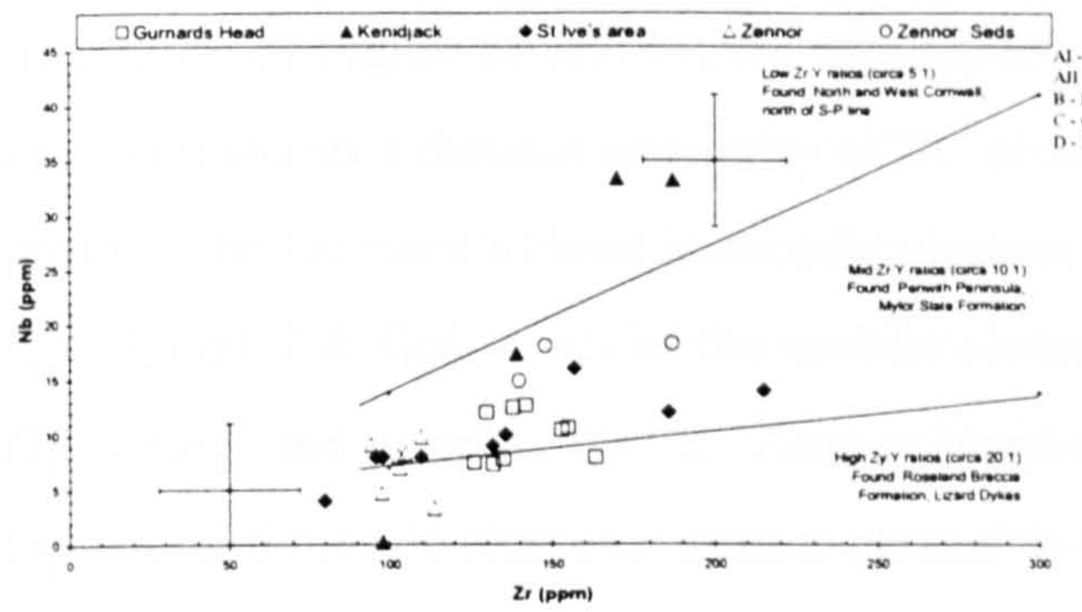

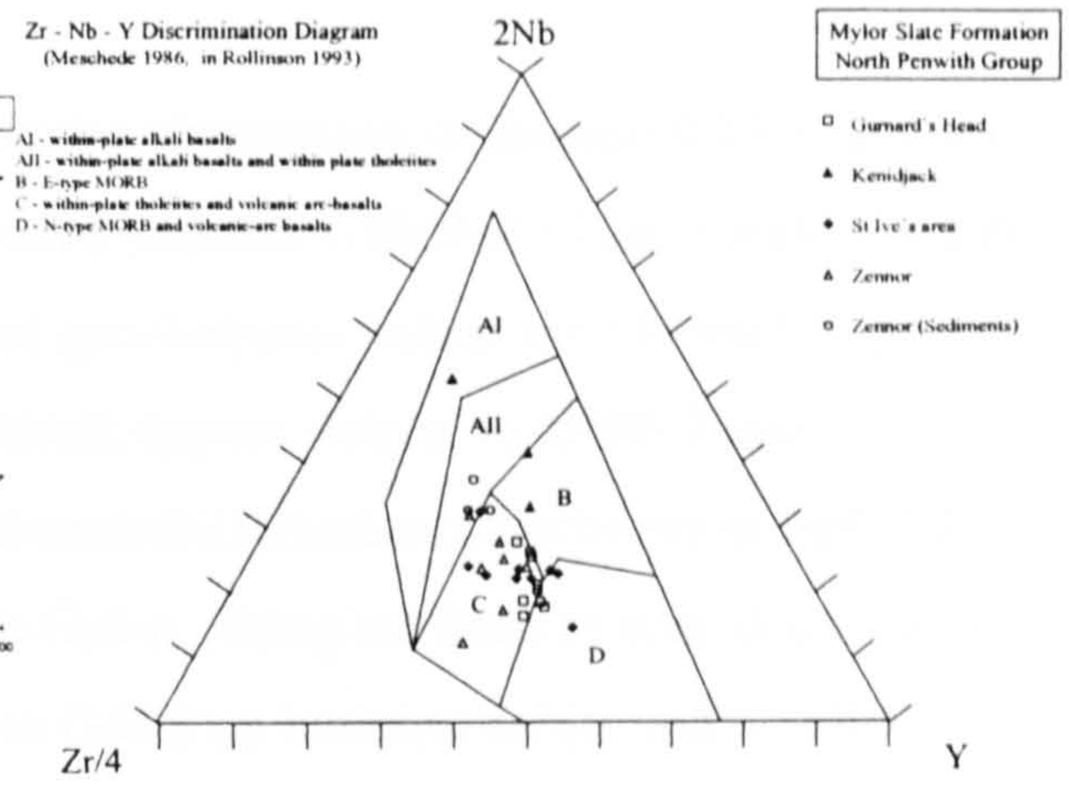

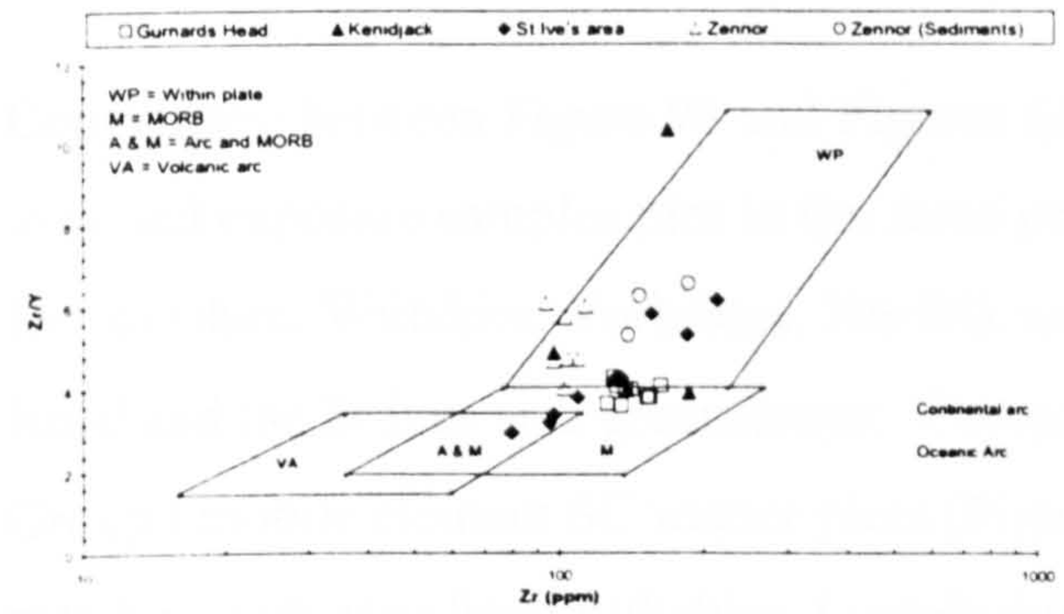

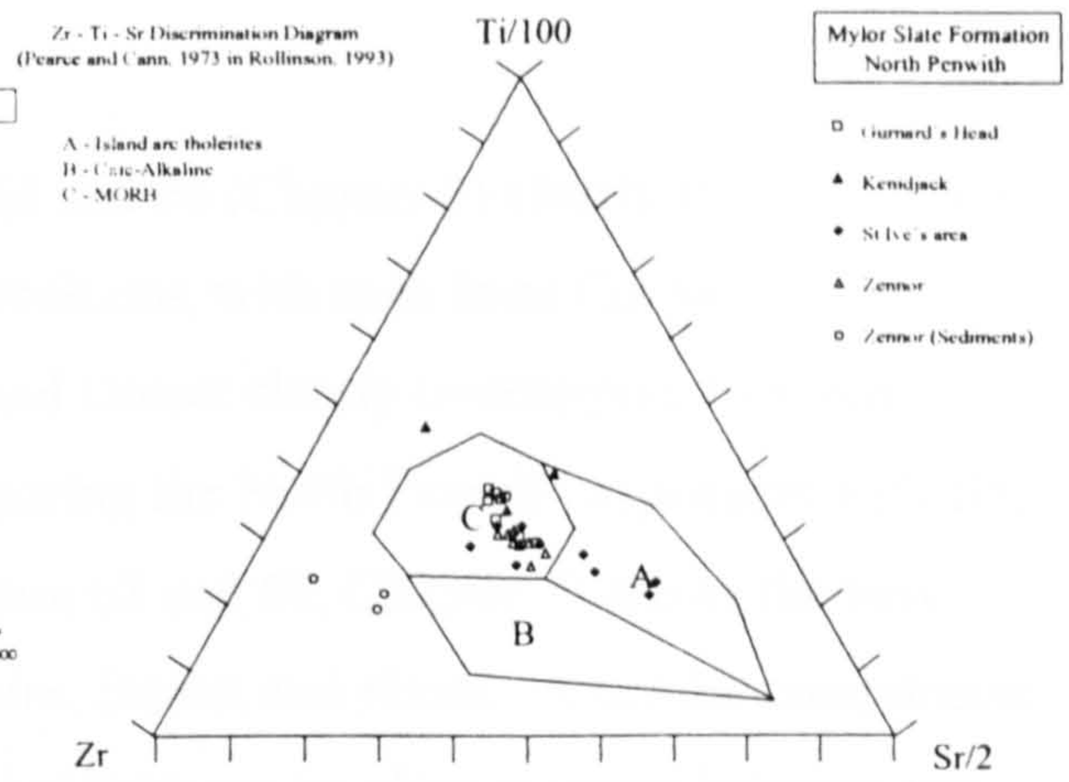

Figure 97 Element geochemical discrimination diagrams for Mylor Slate Formation North Penwith Group. There is some similarity with IPC Group 1 sub-groups, but the exposure appears enriched in Nb compared to the axe sub-groups.

8.13.4 SCA

All immobile element analyses from Gurnard's Head samples and all but LE86 & LE152 from the St Ives area (see above) plot within the immobile element ellipse on Figure 98 (upper) indicating a potential similarity with IPC Group I. Analyses of Zennor Head samples plot just outside the immobile element ellipse suggesting some of the immobile element concentrations in Zennor may be similar to IPC Group I. However, only LE110, LE92, LE87, LE125, LE90 and LE 89 plot inside both immobile and mobile element SCA ellipse (Figure 98, upper & lower).

Inspection of Figure 81 and Figure 98 supports the observation in Section 8.13.3, that no exposure shares a distinct similarity of SC plotted position with that of any single axe sub-group. The Gurnard's Head immobile element geochemical values are closest to GpI-1, GpI-3, GpI-2 & GpI-4, whilst the mobile elements appear similar to GpIII-1 and GpI(near)1 and possibly GpI-2. Zennor Head immobile elements fall between GpI-2 & GpIII-1 and mobile elements cluster closest to GpI-6. Samples from St Ives share a similar dichotomy, except LE125, which plots close to GpI-2 on both immobile and mobile element SC scatter plots.

Comparison between Figure 98 and Figures 65 and 66 (Chapter 7) clearly shows that some axes and exposure samples plot in the same positions, with axes from Cornwall, Lincolnshire, Wiltshire, Yorkshire, Norfolk and Dorset clearly overlapping Gurnard's Head and the St Ives area greenstones. Comparing the North Penwith exposures with IPC Group I mobile element SC scatter plots (Figure 68 and 69, Chapter 7) shows the best match is with axes from Wiltshire, Lincolnshire, Dorset and Hants. A similar comparison with IPC Groups Ia, I/Ia and I(near) reveals that there are no clear matches between axe and exposure, especially noting the almost empty (-,+) quadrant in Figure 71 (Chapter 7) and comparing it with the same, highly populated quadrant in Figure 98 (upper). Figure 73 (Chapter 7) also shows that there is no obvious relationship in plotted positions between IPC Group III and North Penwith greenstones.

Based on similarity of plotted position on SC scatter plots (Figure 98 and Figures 74 & 75 Chapter 7) IPC ungrouped axes Co188/792, Co323/1532 and Co162/757 appear to have potentially similar immobile and mobile element geochemistry to that found at Gurnard's Head. Likewise, IPC Ungrouped axes Co320/1529, HaT01, Li392, No28, No65, No225,

No157 and Nm89 appear to share potential similar geochemistry to greenstones found near St Ives.

Four Irish axes, NMI1929:1694, NMI1897:313, NMI1951:164 and NMI1915:25, share similar positions on SC scatter plots indicating potential geochemical similarity with samples from greenstone exposures near St Ives (c.f. Figure 76 and 98).

Comparison of North Penwith SCA values based on IPC Group I (n=130) using graphical methods has shown that greenstones from near St Ives and from Gurnard's Head are potentially geochemically similar to IPC Group I, although not to a specific IPC Group I related sub-group. However, comparison between axe and exposure SC scatter plots confirms some similarity in plotted positions, and reveals a potential geographical link between exposures near St Ives and Gurnard's Head, and axes found in Wiltshire, Lincolnshire and Yorkshire. No obvious relationship is established between the exposures and any non-IPC Group I sub-group. Eleven IPC ungrouped and four Irish axes can be seen to have potentially similar geochemical concentrations with greenstones from the St Ives area and Gurnard's Head.

8.13.5 DA

Immobile and mobile element discriminant analysis based on discriminated axe sub-groups often matches LE125 (Carbis Bay, near St Ives), LE87 (Clodgy Point), LE89 & LE90 (Carrick Dhu) with IPC Group I sub-groups (Table 107 and Appendix 31.1).

This observation supports the findings in the previous two sections, that these exposures are geochemically similar to IPC Group I axes. However, the lack of consistency between immobile and mobile element matches indicates that the exposure samples cannot be related to any one axe sub-group, again, confirming the findings in Sections 8.13.3 & 4.

It is, therefore, statistically possible that greenstone material from Clodgy Point, Carrick Dhu, and Carbis Bay is geochemically similar with that found within IPC Group I axes.

DA fails to consistently match any other exposure sample, including Gurnard's Head, to IPC Group I, Ia, I/Ia, I(near) or III.

Sample name and location	Immobile DA 1st	2nd	Mobile DA 1st	2nd	Indication
Trowan Cliff					
LE81	GpI-2	GpI-1	GpIII-1	GpI(near)1	Not IPC Group I
Carrick Dhu					
LE89	GpI/Ia	GpI-4	GpI-6	GpIII-1	? IPC Group I
LE90	GpI/Ia	GpI-1	GpI-5	GpI(near)2	**IPC Group I**
Clodgy Point					
LE86	**GpI-1**	GpI-2	GpI-6	GpI-4	? IPC Group I
LE87	GpI-2	GpIII-1	GpI-6	GpI-2	? IPC Group I
St Ives					
LE125	GpI-2	GpI-1	GpI/Ia	GpI(near)2	**IPC Group I**
LE152	GpIII-1	GpI-2	GpI-6	GpI-2	? IPC Group I
LE92	GpIII-1	GpI-2	GpI-8	GpI-2	Not IPC Group I
Gurnard's Head					
GUR001(i)	**GpI/Ia**	GpI-1	GpI-(near)1	GpIII-1	Not IPC Group I
GUR001(ii)	**GpI/Ia**	GpI-1	GpI-(near)1	GpIII-1	Not IPC Group I
GUR002(i)	GpI-6	GpI/Ia	GpIII-1	GpI(near)1	Not IPC Group I
GUR002(ii)					
GUR001	GpIa-5	GpI-2	GpI-(near)1	GpIII-1	Not IPC Group I
GUR001(1)	**GpI-2**	GpI-1	GpI-(near)1	GpIII-1	Not IPC Group I
GUR001(11)	GpI-1	GpI-2	GpI-(near)1	GpI-7	? IPC Group I
GUR002	GpI-6	GpI/Ia	GpIII-1	GpI(near)1	Not IPC Group I
PEL GUR001	GpI-6	GpI-2	GpI-(near)1	GpIII-1	Not IPC Group I
Zennor Point					
ZEN001	**GpI/Ia**	GpI-1	**GpI-(near)1**	GpIII-1	Not IPC Group I
ZEN001A	**GpIII-1**	GpI-2	**GpI-(near)1**	GpIII-1	Not IPC Group I
ZEN001B	GpIII-1	GpI-2	**GpI-(near)1**	GpIII-1	Not IPC Group I
ZEN002	GpIII-1	GpI-2	GpI-6	GpI-7	Not IPC Group I
ZEN002A	GpIII-1	GpI-2	GpI-7	GpI-8	Not IPC Group I
ZEN002B	GpIII-1	GpI-2	GpI-7	GpI-8	Not IPC Group I
ZEN002	GpI-8	GpI-2	GpI-8	GpI-6	Not IPC Group I
ZEN002A	GpIII-1	GpI-2	GpI-7	GpI-8	Not IPC Group I
ZEN002B	**GpIII-1**	GpI-2	GpI-8	GpI-7	Not IPC Group I
PEL ZEN002	GpIII-1	GpI-8	GpI-6	GpI-7	Not IPC Group I
Kenidjack					
KEN001	**GpI-12**	GpI/Ia	GpI-6	GpI-4	Not IPC Group I
KEN002	**GpI-12**	GpI-12	**GpI-(near)1**	GpIII-1	Not IPC Group I
KEN003	**GpI-12**	GpI-12	GpI-12	GpI-1	Not IPC Group I
GEEV1	GpI-8	GpIII-1	GpI-8	GpI-7	Not IPC Group I
Botallack					
LE110	GpIII-1	GpI-2	GpI-6	GpI-4	? IPC Group I

Table 107 Summary of immobile and mobile element DA using axe sub-groups (after axe DA) as seed groups. See text for discussion. Note samples from Trowan Cliff, Carrick Dhu, Clodgy Point and St Ives are collectively referred to as being near St Ives. Values in bold indicate the P(D/G) < 0.05.

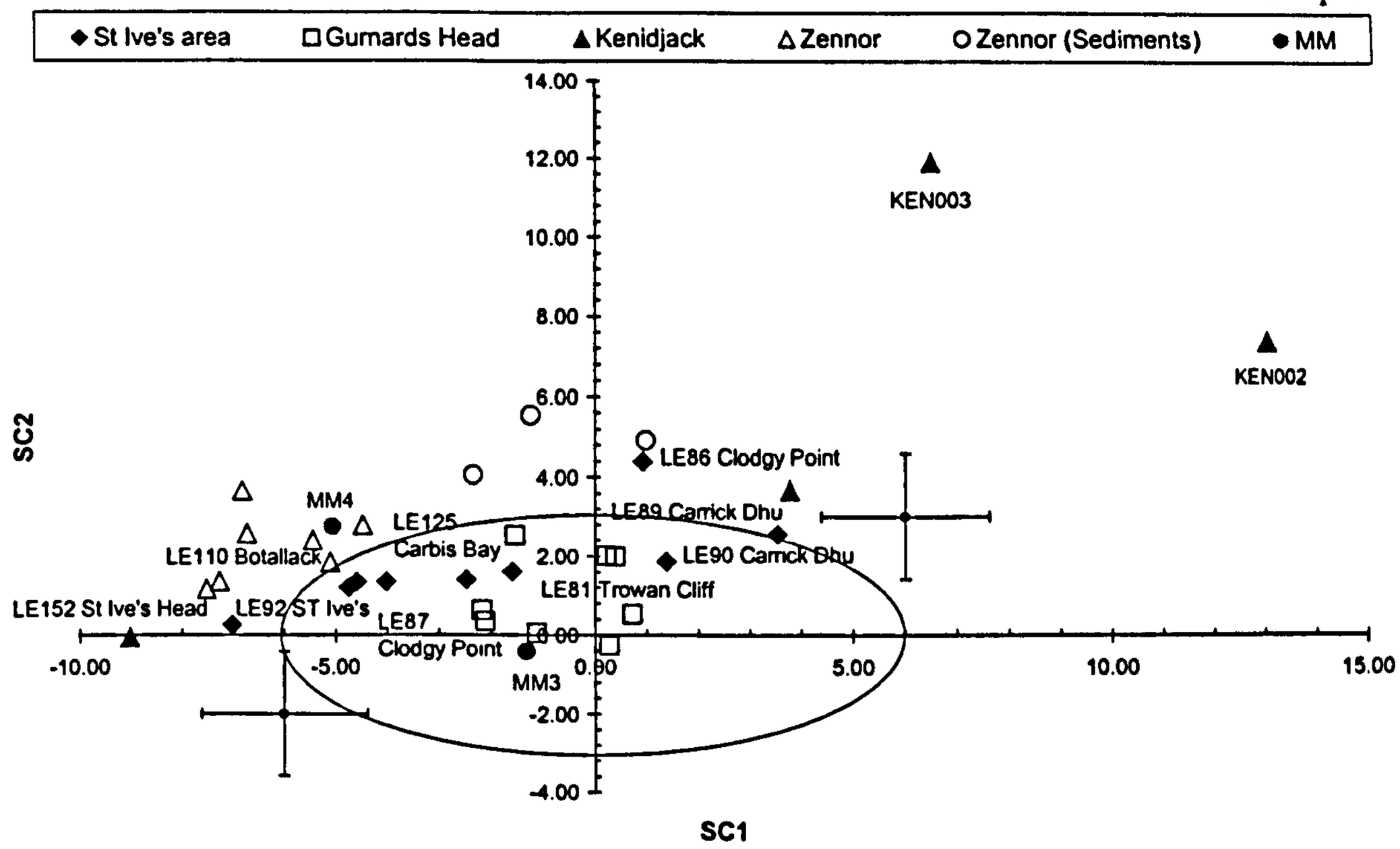

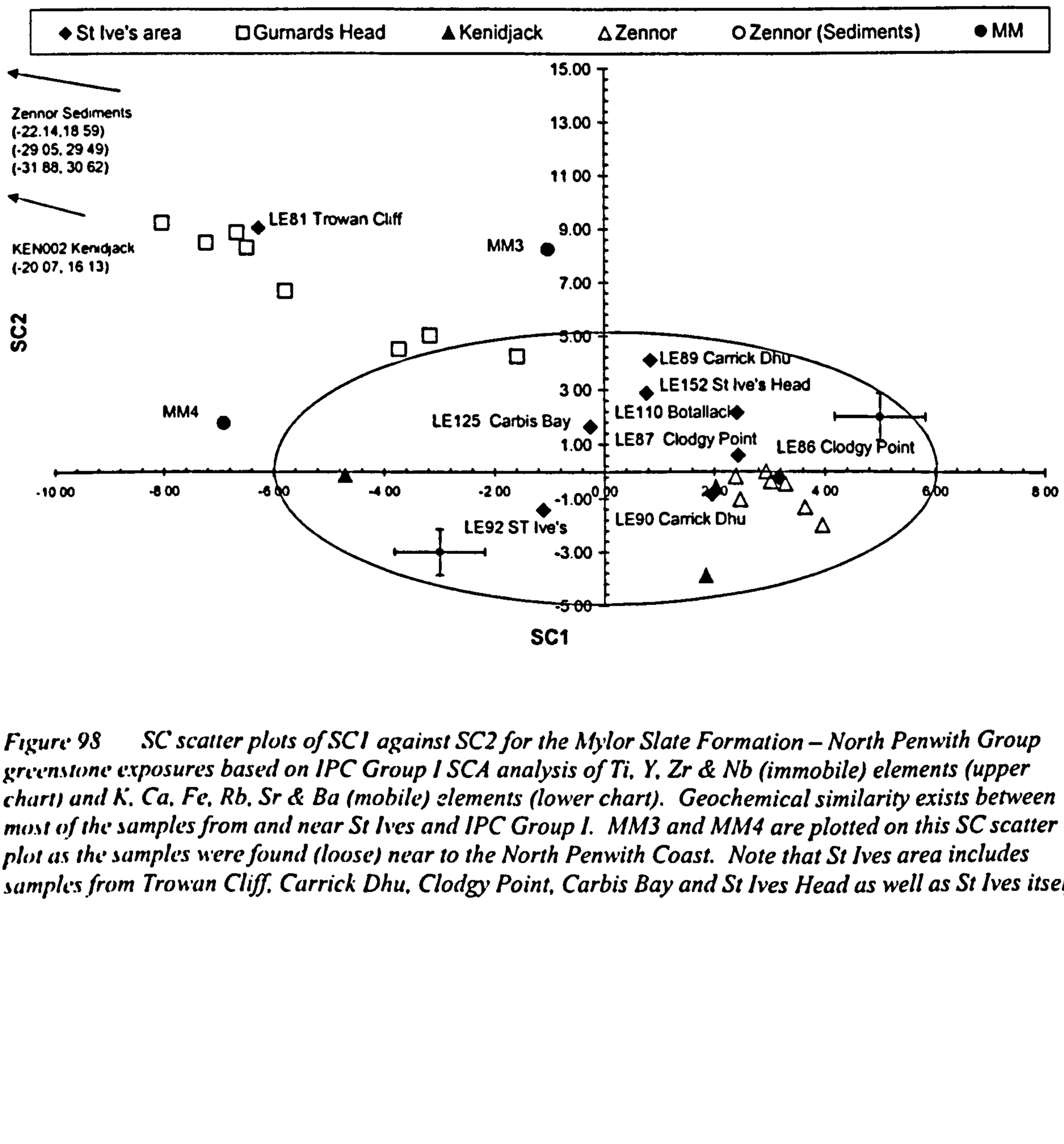

Figure 98 SC scatter plots of SC1 against SC2 for the Mylor Slate Formation – North Penwith Group greenstone exposures based on IPC Group I SCA analysis of Ti, Y, Zr & Nb (immobile) elements (upper chart) and K, Ca, Fe, Rb, Sr & Ba (mobile) elements (lower chart). Geochemical similarity exists between most of the samples from and near St Ives and IPC Group I. MM3 and MM4 are plotted on this SC scatter plot as the samples were found (loose) near to the North Penwith Coast. Note that St Ives area includes samples from Trowan Cliff, Carrick Dhu, Clodgy Point, Carbis Bay and St Ives Head as well as St Ives itself.

8.13.6 MANOVA and Student's t-test analysis

MANOVA based on Ti, Y, Zr and Nb concentrations is carried out to determine the statistical similarity between Clodgy Point, Carrick Dhu and Gurnard's Head greenstone samples and all sixteen petrographically determined axe sub-groups after DA. Results indicate the highest significance value is found between Gurnard's Head and GpI-3 (0.281); Clodgy Point and GpI-6 (0.308): Carrick Dhu and GpI-6 (0.392). Thus the null hypothesis cannot be rejected at a 0.05 significance value, hence the chosen exposure average geochemistry and average axe group geochemistry could have originated from the same parent population. However, these results are based on small numbers of samples and therefore cannot be deemed conclusive.

The relationships found using the MANOVA investigation are investigated further using Student's t-test for comparing means.

	K	Ca	Ti	Fe	Rb	Sr	Y	Zr	Nb	Ba
Clodgy Point (n=2)										
GpI-2	0.504	0.112	0.671	0.648	0.403	0.517	0.637	0.864	**0.000**	0.319
GpI-6	0.734	0.196	0.375	0.602	0.171	0.800	**0.001**	**0.009**	**0.002**	**0.047**
Carrick Dhu (n=2)										
GpI-2	0.984	0.058	0.107	0.394	0.634	0.691	**0.008**	**0.000**	**0.000**	0.531
GpI-6	0.235	0.086	0.828	0.444	0.861	0.618	0.092	**0.001**	**0.000**	0.410
Trowan Cliff (n=1)										
GpI-2	0.118	0.990	0.811	0.345	0.233	0.296	.205	0.804	**0.020**	0.837
St Ives Head (n=1)										
GpI-2	0.897	0.696	0.132	0.397	0.865	0.321	0.923	**0.021**	0.168	0.842
Carbis Bay (n=1)										
GpI-2	0.754	0.140	0.703	0.164	0.861	0.715	0.299	0.956	0.078	0.689
St Ives (n=1)										
GpI-2	0.807	0.785	0.085	0.502	0.699	0.637	0.420	0.102	0.246	0.534
Gurnard's Head (n=8)										
GpI-2	**0.007**	0.087	**0.000**	0.558	0.017	0.821	**0.000**	0.141	**0.000**	0.869
GpI-3	**0.001**	**0.001**	0.121	**0.024**	**0.000**	0.707	**0.003**	**0.007**	**0.000**	0.902
Zennor Point (n=6)										
GpI-2	**0.044**	**0.001**	**0.001**	**0.000**	0.191	0.297	**0.003**	**0.005**	0.073	**0.028**

Table 108 Summary of Student's t test for comparing means between selected North Penwith greenstone exposures and selected axe sub-groups (determined by DA). Null hypothesis is that the means are equal. Values indicated in bold are where the null hypothesis may be rejected at a 0.05 significance value. The results indicate that it is not possible to reject the null hypothesis for greenstone samples from Carbis Bay and St Ives, and GpI-2

Inspection of Table 108 reveals that the null hypothesis cannot be rejected between sub-group GpI-2 and sample LE125 (Carbis Bay). Zr significance for similarity of St Ives Head (LE 152) GpI-2 is 0.021 reflecting the difference in Zr concentrations (80ppm and 131 ± 20.1ppm respectively). Nb is the only element to fall below 0.05 significance value for Clodgy Point samples (LE86 & LE87) and Trowan Cliff (LE81). In these two cases the difference between the two corresponding Nb values is 6ppm (GpI-2 (6.2 ± 1.5) and

Clodgy Point (12.0 ±5.7ppm)) and 4ppm (GpI-2 and Trowan Cliff (10ppm)) respectively. Gurnard's Head and Zennor are statistically different to GpI-2, and from GpI-3 (Gurnard's Head only) at a 0.05 significance value for at least 4 elements, 2 of which are immobile.

It is emphasised that these statistical comparisons are based on small sample sizes and cannot be deemed conclusive for a match between the greenstone exposure and the axe sub-group, but the indications are that exposures near to St Ives in North Penwith share similar geochemical values to one of the main IPC Group I sub-groups: GpI-2.

8.13.7 Discussion

Greenstones in North Penwith show an increased metamorphic grade westwards from St Ives, evidenced by the increasing presence of hornfels texture and associated contact metamorphic minerals (e.g. cordierite) towards Lands End. Thin sections from Gurnard's Head have some petrographic similarities with GpI-7 and GpIa-3. No thin sections were available from the pillow lavas sampled near St Ives, but published petrographic descriptions indicate that the rocks lack pyroxene, and contain altered plagioclase feldspars and secondary amphibole & epidote. Hence the extrusive greenstones near to St Ives appear to be petrographically different to GpI-1, which is observed to contain relict pyroxenes and is also medium grained. However, it is possible that all the pyroxene in the St Ives greenstone has been completely altered to secondary chlorite and/or amphibole.

Element discrimination and SC scatter plots indicate that there is some geochemical similarity between North Penwith exposures and axe sub-groups. But, immobile element ratios from North Penwith greenstones appear different to IPC Group I axe sub-groups, as seen in the Zr-Nb chart and Zr-Nb-Y ternary diagram since the exposures appear to contain proportionally more Nb than IPC Group I axes.

MANOVA and Student's t test calculations indicate that a sample from the Carbis Bay greenstone exposure (LE125) near St Ives cannot be statistically separated from GpI-2 at a 0.05 significance value. Associated t-test results also indicate the possibilities of matches between GpI-2 and samples from Clodgy Point, St Ives Head and Trowan Cliff, all within a few kilometres of St Ives town and thus close to the numerous Neolithic sites along the north Penwith coast.

On balance, geochemical evidence suggests that it is highly probable that some, especially GpI-2, of the IPC Group I axe population originates from coarser grained greenstone rocks near St Ives. Additional greenstone thin sections and samples from the coarser grained greenstone bodies would be needed in order to confirm this.

8.14 Mid-Upper Devonian & Lower Carboniferous: South Hams Group

8.14.1 Overview of samples and localities

The reason for collecting greenstone samples from the South Hams area of South Devon was to provide a 'contrast' with those collected from a relatively small area of Cornwall. Little published work has been found regarding the South Hams locations sampled in this thesis. Work carried out on the thick sequence of pillow lavas at Chipley Quarry, north of the sample area, but within the same geological setting, determined that the lavas are alkaline and have intraplate characteristics (Floyd et al. 1993). Ten samples were obtained from five exposures of intrusive medium-coarse grained greenstone (Pople's Bridge, Ansty Cove, Ivybridge, Luscombe Cross & Bow Bridge) and one vesicular extrusive sub-aerial lava in the mid-upper Devonian slates (Dorsley Barton) within the South Hams region of South Devon (Section 3.7.3).

There are no IPC axe Groups associated with the South Hams and few Neolithic sites, the closest being on Dartmoor (Figure 2, Chapter 2).

8.14.2 Inspection of petrographic, magnetic and geochemical data

Examination of thin sections from the South Hams exposures revealed no petrographic similarity with any axe thin section examined (Section 4.8.7).

No MS measurements of greenstone within South Hams have been made.

Table 109 indicates that immobile element concentrations for (randomly) selected South Hams samples are generally different to IPC Group I (n=130) with difference in the Nb concentrations being most noticeable (Table 109 and Appendix 28.1). Apart from Pople's Bridge (IVY001 & IVY002), South Hams samples have greater than 22ppm Nb, compared to the reduced IPC Group I average of 6.7 ± 2.9ppm. Ivybridge samples IVY003 & IVY004 have Zr concentrations greater than 357ppm and Nb concentrations greater than 71ppm indicating it is possibly intermediate in nature (note: no SiO_2 oxide %wt

measurements have been made). Pople's Bridge appears to be the most primitive and tholeiitic with comparatively low immobile element concentrations.

	Reduced IPC Group I (n=130) (ppm ± 1sd)	Ansty Cove (n=2) (ppm ± 1sd)	Pople's Bridge (n-2) (ppm ± 1sd)	Ivybridge (n=2) (ppm ± 1sd)	Dorsley Barton (n=1) (ppm)
K	3 567 ± 2 282	7 528 ± 1 283	473 ± 2 002	20 454 ± 2 413	1 906
Ca	67 715 ± 14 636	43 243 ± 10 265	46 800 ± 11 740	59 982 ± 9 669	15 023
Ti	14 959± 3 772	839 ± 1 884	5 974 ± 1 555	16 215 ± 1 412	15 472
Mn	1 532 ± 521	1 106 ± 214	696 ± 180	1 376 ± 291	1 409
Fe	95 632 ± 14 009	88 971 ± 5 003	72 873 ± 995	94 787 ± 13 035	94 560
Rb	29.6 ± 25.8	39.8 ± 33.3	7.9 ± 10.2	225 ± 111	-5.6
Sr	324 ± 150	296 ± 64.0	520 ± 36.1	839 ± 221	459
Y	35.7 ± 6.8	20.3 ± 1.4	21.2 ± 0.5	37.2 ± 3.6	24.1
Zr	171 ± 29.2	121 ± 19.5	89.2 ± 0.1	371 ± 20.1	176.4
Nb	6.7 ± 2.9	23.5 ± 2.1	1.9 ± 0.2	91.0 ± 13.6	26.1
Ba	104 ± 64.3	367 ± 155	57.8 ± 45.9	598 ± 378	137.4
Ce	-27.1 ± 11.4	-14.9 ± 3.1	-35.3 ± 6.9	161 ± 55.1	-9.9
Pb	230 ± 1013	10.7 ± 8.2	-5.2 ± 8.8	0.1 ± 1.9	13.6

Table 109 Average elemental compositions of selected samples collected from exposures within South Hams and reduced IPC Group I (n=130). South Hams data is summarised from that in Appendix 28.1 & 28.2, reduced IPC Group I is from Table 58.

It is concluded that there is no petrographic or geochemical similarity between any South Hams greenstone and IPC Group I.

8.14.3 Element discrimination diagrams

The element discrimination diagram Y/Nb v Ti (Floyd & Winchester 1974) in Figure 99 (lower left hand side) indicate all the samples collected are alkaline with the exception of the two collected from the very large greenstone quarry at Pople's Bridge, south of Ivybridge (IVY001, IVY002). This fact precludes use of Zr–Y–Ti discrimination diagram to tectonically define the rock as this diagram is for tholeiitic rocks only (Rollinson 1993). The alkali rocks plot in the North Cornwall and Devon sector of the Zr–Nb discriminant diagram as anticipated (Floyd et al. 1993).

Pople's Bridge samples (IVY001, IVY002) plot as tholeiitic, with low incompatible elements suggestive of N-MORB, but with unusually high Sr. The source of the Sr could be original as the low levels of K & Rb suggest little if any hydrothermal alteration caused by the nearby Dartmoor granite (Rollinson 1993; table 3.4).

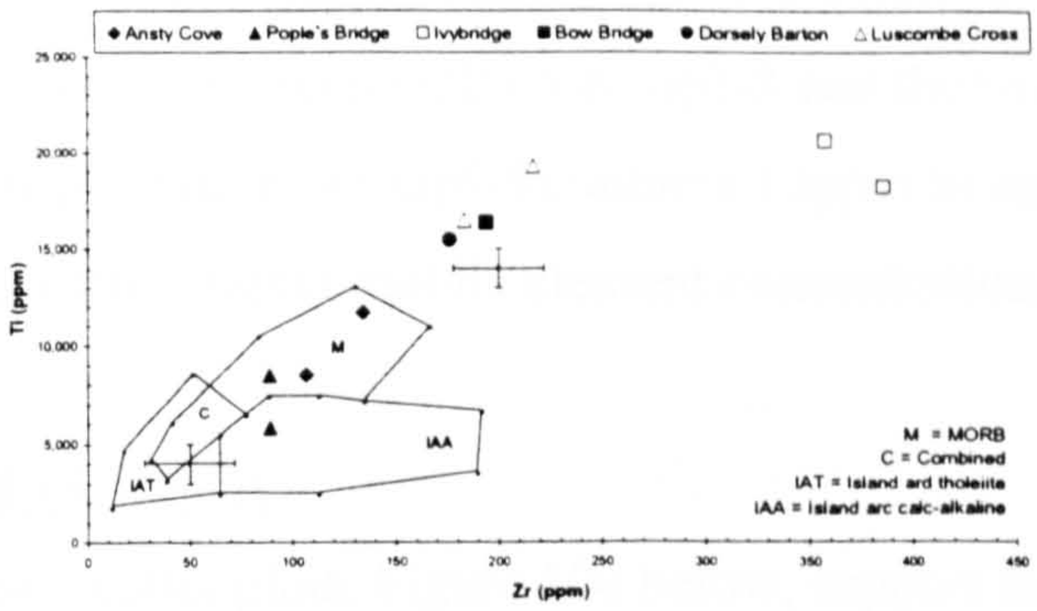

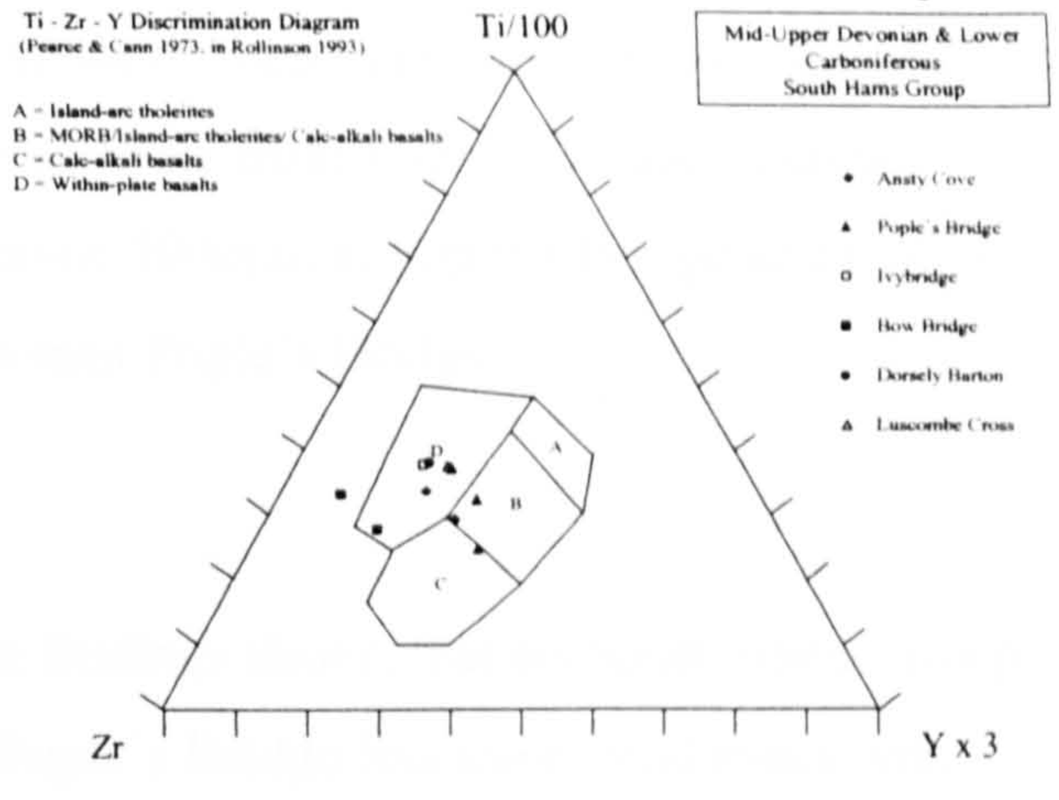

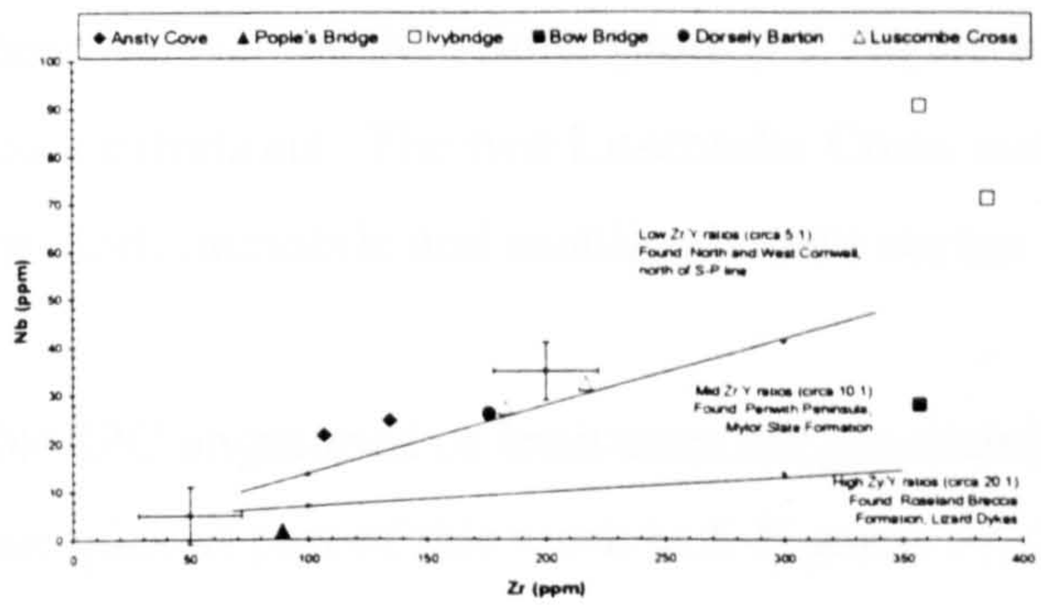

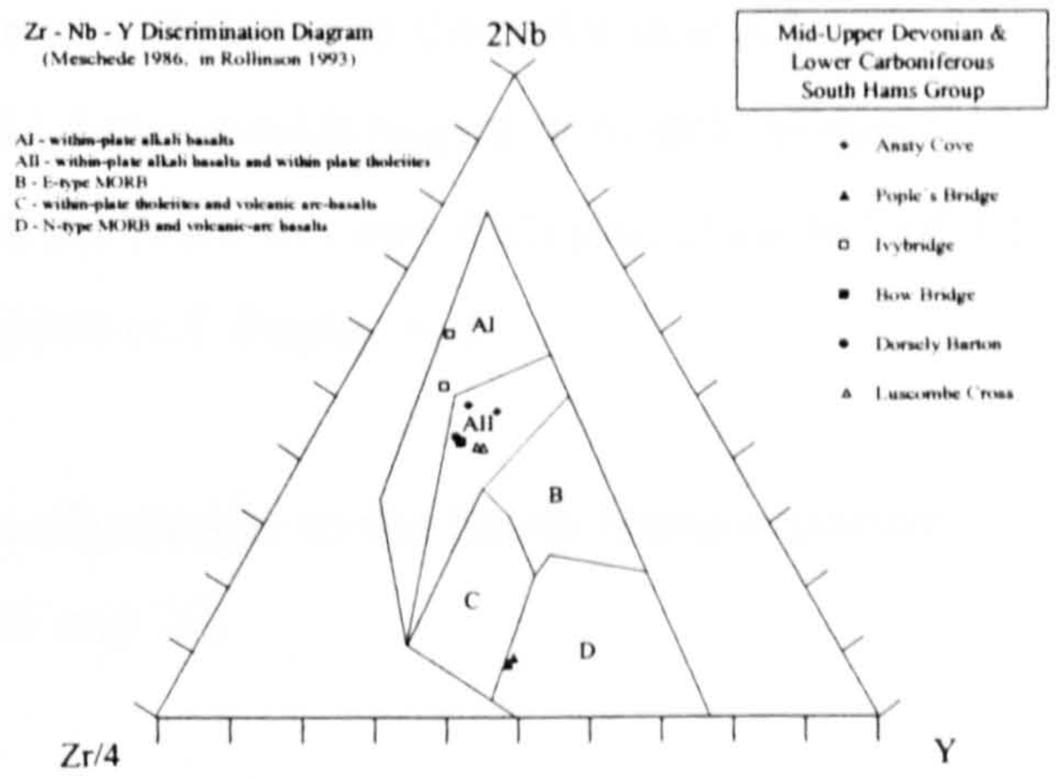

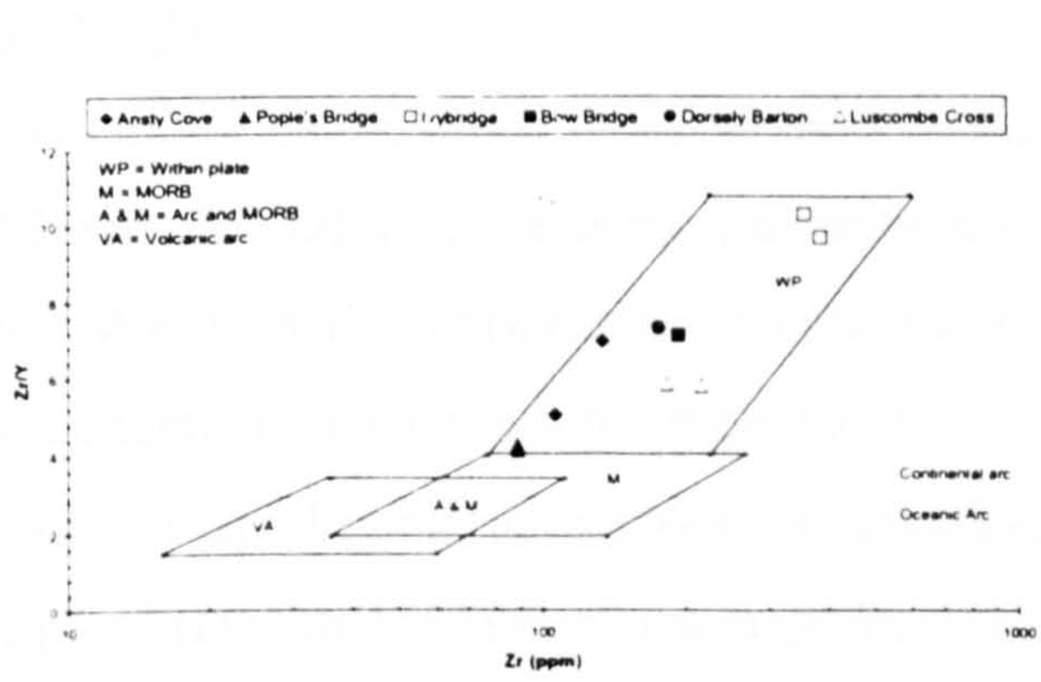

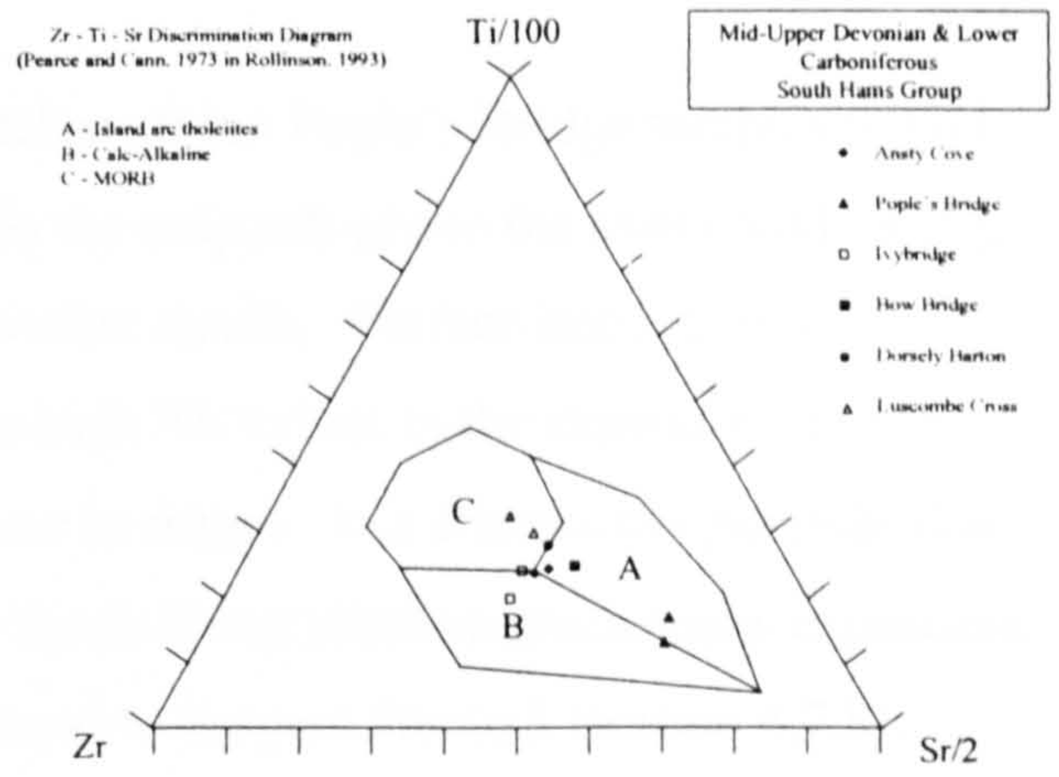

Figure 99 Element geochemical discrimination diagrams for South Hams Group. All exposures apart from Pople's Bridge plot as alkali. Pople's Bridge is tholeiitic and appears to have MORB affinities.

The only similarity between plotted positions of South Hams samples and axe sub-groups is found between GpIII-1 & GpI-8 and the two samples from Pople's Bridge. Further inspection shows GpI-8 contains 13ppm Sr against 500ppm at Pople's Bridge and GpIII-1 contains higher mobile element concentrations than Pople's Bridge.

8.14.4 SCA

SC scatter plots, Figure 100 below, support the findings above, that no South Hams Group greenstone sample is similar to IPC Group I. Pople's Bridge has some similarities with GpI(near)1 with regards to immobile element concentrations at they plot in similar positions on the SC scatter plots (c.f. Figure 81), but not with regard to mobile element concentrations. The two Luscombe Cross samples (LSC001 and 002) plot close to GpI-12 on both immobile and mobile element scatter plots (c.f. Figure 81).

No IPC ungrouped or Irish axes are geochemically similar to the South Hams exposures samples as part of this work (c.f. Figures 74, 75 and 76)

8.14.5 DA

Immobile element discrimination analysis matches all but Pople's Bridge samples to GpI-12 with P(G/D) in all cases =1 indicating this is the only sub-group the axes could belong to. Mobile element discrimination produces similar results. Further inspection of the geochemical data reveals the main factor is the high Nb values in the exposures, and the fact that GpI-12 and these exposures are alkaline in nature. It is statistically possible that GpI-12 (Do146/1762) may originate from the South Hams alkaline greenstones exposures, although no petrographic evidence has been found to support this (c.f. Section 4.7.8).

Immobile element discrimination analysis matches the Pople's Bridge tholeiite to GpI(near)1 and GpI-8, both not recognised as IPC Group I sub-groups (c.f. Section 7.7.2), hence it is not the source for IPC Group I. It is further unlikely that Pople's Bridge is the source of GpI(near)1 or GpI-8 as the mobile element DA matches the two exposure samples with GpI-12, which has a distinctly different mobile element geochemistry to both GpI(near)1 and GpI-8 (c.f. Figure 81).

8.14.6 MANOVA and Student's t-test analysis

Not carried out.

8.14.7 Discussion

No South Hams Group exposure is petrographically or geochemically similar to IPC Group I. The statistical relationship between GpI-12 and the exposures (excluding Pople's Bridge) does indicate potential similarity, but there are no petrographical similarities noted. On closer inspection, GpI-12 is found to contain significantly less K and relatively more Ti & Zr than the South Hams alkali rocks. Hence it is unlikely that GpI-12 originated from the exposures sampled.

The Pople's Bridge exposure is geochemically unlike GpI(near)1 or GpI-8 as it does not share similar mobile and immobile element concentrations with the two axe sub-groups.

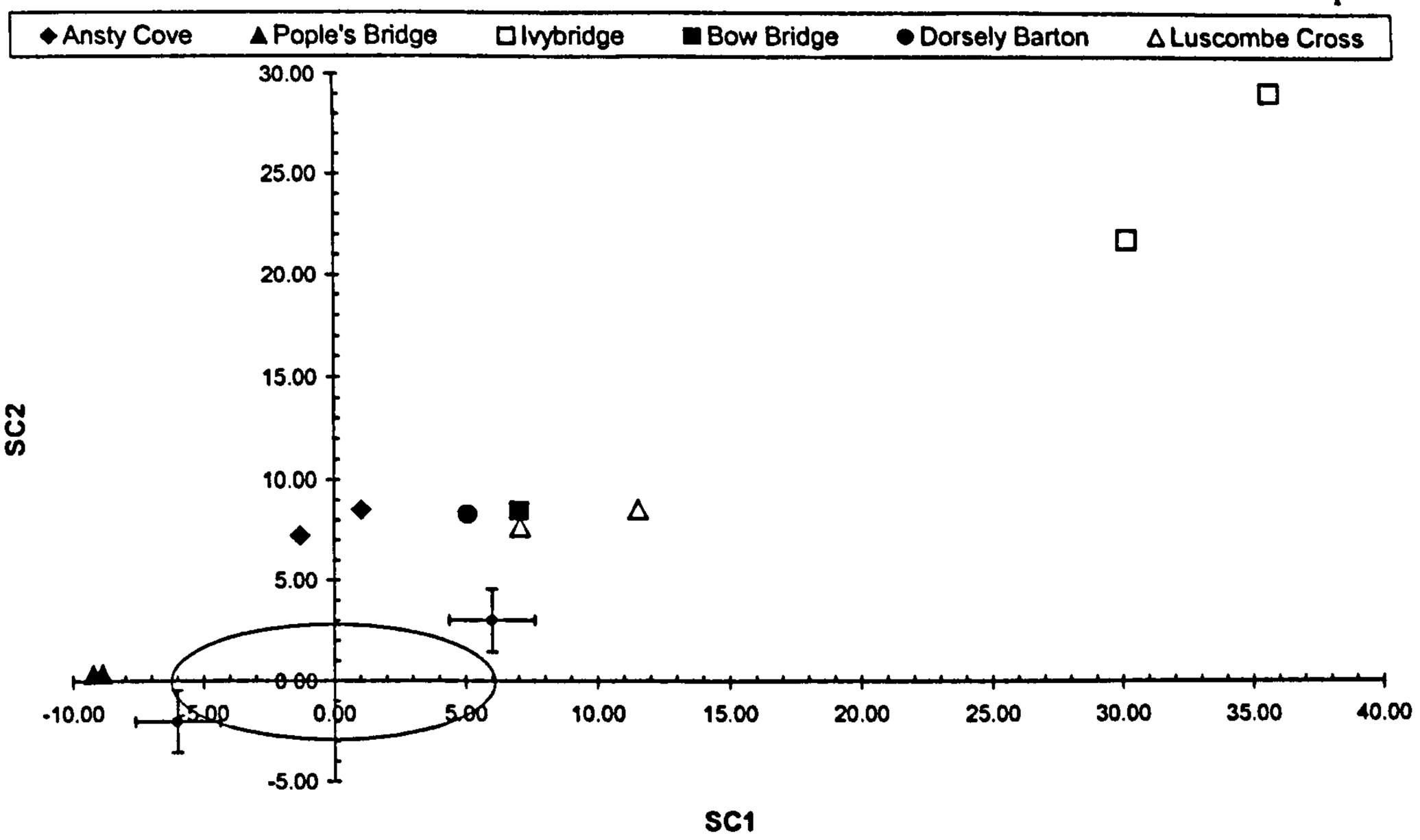

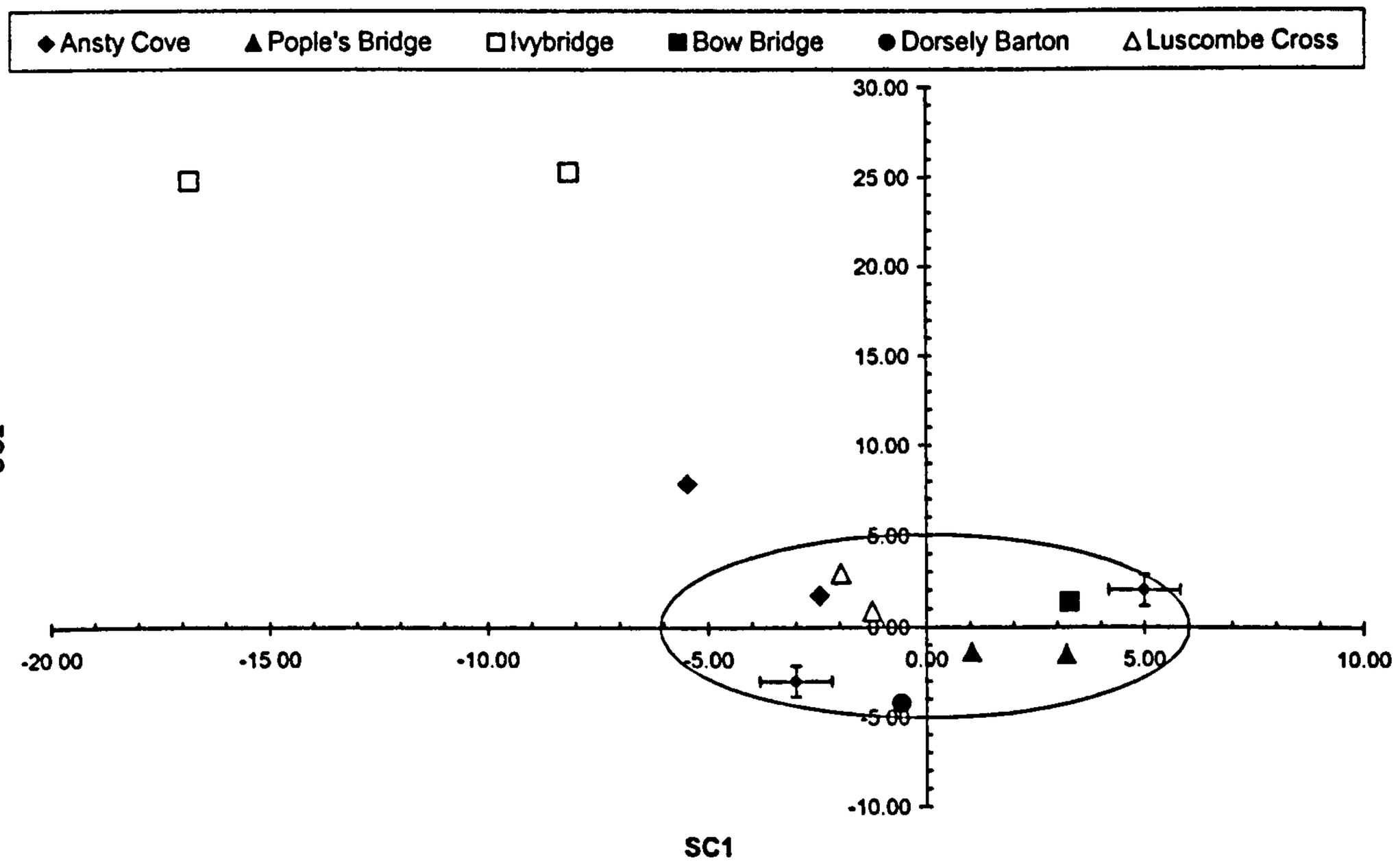

Figure 100 SC scatter plots of SC1 against SC2 for the South Hams Group greenstone exposures based on IPC Group I SCA analysis of Ti, Y, Zr & Nb (immobile) elements (upper chart) and K, Ca, Fe, Rb, Sr & Ba (mobile) elements (lower chart). As expected none of these exposures is geochemically similar to IPC Group I.

8.15 Summary and conclusions

This Chapter brought together the petrographical, magnetic and geochemical information and analytical data for greenstone axes and exposures presented in Chapters 3, 4, 5, & 7 and, with new, published and unpublished greenstone exposure geochemical data, examined the provenance of IPC Group I, Ia, I/Ia, I(near), III & IIIa axes. A series of five procedures has been used to investigate the geochemical relationship between the axe sub-groups recognised and defined in Chapter 7 and greenstone exposures from ten geographical areas within SW England.

As expected, the **Lizard Dyke** greenstone was found to be MORB related. The two samples were found to be petrographically and geochemically different to all IPC groups examined: IPC Group I, Ia, I/Ia, I(near), III & IIIa.

The pillow lavas at **Tubbs Mill**, within the Gramscatho Basin - Pendower Formation, are geochemically similar to IPC Group I, but are less enriched in Ti and Zr than IPC Group I. However, petrographically, the Tubbs Mill greenstone is thought to be finer grained than most IPC Group I axes and it is therefore unlikely that any IPC group axes originated from the Tubbs Mill exposure. But, it is possible that the Tubbs Mill pillow lava is related to the actual source of greenstone used to manufacture IPC Group I axes.

The two samples collected from the **Cury** greenstone outcrop are almost certainly not from the Cury greenstone body, hence this outcrop cannot be eliminated as a potential source of IPC Group I.

Samples from greenstones within the **Roseland Breccia Formation** are geochemically very similar to IPC Group I, with the pillow lava at Mullion Island providing the closest geochemical match. There are geochemical similarities between Roseland Breccia Formation exposures at Tregadjack, Tredawargh and Tregidden and axes found in Cornwall, Dorset and Somerset. Similarly, there is a geochemical similarity between the Nare Head greenstone body and some of the IPC Group I axes found in Essex. The main problem with provenancing IPC Group I to the Roseland Breccia Formation and Mullion Island in particular is the fact that the majority of exposures are fine grained pillow lavas. A coarse grained dolerite associated with (beneath?) Mullion Island that may have been exposed during marine regressions would be a likely candidate for the source of IPC Group I axes.

The co-magmatic **Camborne** greenstones within the Mylor Slate Formation are the closest greenstone exposures to the important Neolithic settlement at Carn Brea, but are petrographically and geochemically dissimilar to any axe sub-group examined.

The primitive tholeiite at **Cudden Point** has some geochemical similarity with IPC Group III, non-IPC axe 'CoAxe' and three Irish gabbroic axes (NMI1956:65, NMI1929:1127 and NMI1915:25), but not with IPC Group I, Ia, I/Ia or I(near).

Two types of greenstones are found near **Perranuthnoe.** The Perranuthnoe greenstone outcrop includes the quarry that provided the thin section used to provenance IPC Group III to the exposure. Statistical analysis of this exposure (the Quarry at GR SW534297) generally concluded that the null hypothesis: that the means are equal between the exposure and GpIII-1 (i.e. IPC Group III) could not be rejected using a 0.05 significance value; although samples from the two groups were observed to be petrographically different. The outcrop at Trenow Cove is geochemically distinct and different to all axe sub-groups except GpI-12 (Do146/1762).

The area around **Penzance** is the hypothesised source of IPC Group I (Keiller et al. 1941; Chapter 2). But this work has failed to find an exact petrographical match between exposures in the area and IPC Group I axes, although some similarities were observed. The geochemical evidence supports the petrographic evidence: that the greenstone exposures sampled near Penzance appear to be geochemically different to the reduced IPC Group I. Assuming the sampled exposures are typical of greenstones in the area then it is probable that the Penzance area does not contain the source greenstone exposure for IPC Group I. Similarly, no positive petrographic or geochemical match was found between greenstones near Penzance and IPC Groups Ia, I/Ia, I(near), III or IIIa.

Greenstone exposures along the **North Penwith** coast are close to numerous Neolithic burial sites, and exposures around St Ives appear to be geochemically similar to GpI-2. However, the samples with the best geochemical match are reported to be predominantly fine-grained pillow lavas, different to the doleritic axe greenstone. As the pillow lava exposures are often associated with shallow level intrusive rocks, it is possible that a greenstone outcrop near St Ives provided the raw material for the manufacture of some IPC Group I axes (especially GpI-2).

Greenstones within the **South Hams** area were chosen as their geographical distance from Cornwall and the Gramscatho Basin meant they were expected to have a different tectonic origin to the greenstones in west Cornwall. As anticipated, no South Hams exposure was found to be geochemically (possibly apart from GpI-12) or petrographically similar to any axe sub-group. However, finding the primitive MORB related tholeiite at Poples Bridge, outside the Gramscatho Basin and away from the Lizard Ophiolite, was a surprise.

Examination of axe and greenstone petrography and geochemistry therefore concludes

1. The most likely provenance for the majority of IPC Group I is to an exposure within the Roseland Breccia Formation, possibly local to Mullion Island.
2. Some IPC Group I axes are geochemically very similar to greenstones found near St Ives suggesting that this may be the provenance for some IPC Group I axes.
3. Greenstones within the Penzance area are unlikely to be the source of IPC Group I material.
4. IPC Group III is geochemically similar to greenstone rock from the small disused quarry approximately 1km south-west from Perranuthnoe Village (GR SW534297) which is believed to be the provenance of IPC Group III:
5. Inconclusive evidence suggests that some Irish axes may originate from the Cudden Point greenstone.

9 Discussion

9.1 Introduction

The non-destructive nature of the techniques used in this research made it possible to undertake the largest study of the geochemistry and magnetic susceptibility of British Prehistoric greenstone implements so far carried out in Britain. This discussion reviews the practicalities and potential of the analytical methods, before considering the archaeological implications of this research.

Implement petrology (IP) in Britain is largely based on examination of petrographic thin sections, a methodology established in the first half of the 20th Century and used by the Implement Petrology Committee (IPC) to recognise 39 petrological axe groups (e.g. Warren 1919, Keiller et al. 1941, North 1942, Grimes 1979, Davis 1997). One of the main aims of the IPC is to provide a provenance for British stone axes (Keiller et al. op. cit.), and new analytical techniques, such as laser microprobe, XRF and magnetic susceptibility, have been proposed to advance the aims of the IPC as well as providing a clearer understanding of axe petrology (Davis 1985, 1997). The potential of two of the proposed techniques, reflected light microscopy and XRF analysis, has been clearly demonstrated by the Irish Stone Axe Project (Mandal 1996). But, both reflected light microscopy and XRF analysis (as carried out by Mandal (op. cit.)) and most of the other techniques proposed by Davis (1997) are partially destructive in nature. This disadvantage can be overcome by using new non-destructive XRF and MS techniques as shown by Williams-Thorpe et al. (1999a) and Williams-Thorpe & Thorpe (1993). This thesis expands on the methodology proposed by Williams-Thorpe et al. (op. cit.) and Williams-Thorpe & Thorpe (op. cit.) to show that non-destructive analytical techniques can be used to advance the aims of the IPC.

The non-destructive and portable nature of the PXRF and MS equipment is fundamental to the successful characterisation of the large number of axes measured in this work. Axe custodians actively assisted this project by making axes and facilities available, once they were certain that the axe was not damaged during analysis. This is opposed to the reluctance shown by custodians in sending valuable axes away for thin section analysis (author's observation) as their axes often returned with a visible scar where the section was extracted. As the approximately eight thousand British stone axes registered by the IPC (Clough & Cummins 1988) are held at a large number of locations in Britain (c.f.

Appendix 2), the portability of the PXRF and MS equipment was (and is) a distinct advantage. It was logistically simpler to take the equipment to a regional centre, as opposed to arranging for the axes to be loaned to the OU for analysis.

The main disadvantage encountered in this work was the relatively high cost of hiring the PXRF. The cost (£1,000 per week) effectively restricted the number of museum visits and thus limited the number of axes examined. However, in terms of cost per analysis, it is estimated that the average PXRF analysis of an axe cost £10 and took approximately ten minutes. This compares favourably with the cost for production of thin sections (approximately £7) and WDXRF analysis (approximately £20 per analysis), although these two procedures may take days, even weeks, to produce data.

9.2 Discussion on specific aspects of the chosen methodology

The chosen methodology is based upon linking the petrographic work already carried out by the IPC to the results of the two non-destructive techniques, PXRF and MS, using various forms of statistical analysis in order to investigate continuity between the established and new methodologies. The four main techniques of the chosen methodology: petrography, magnetic susceptibility, portable x-ray fluorescence analysis and statistical analysis, are discussed below.

9.2.1 Petrography

Examination of one hundred and forty-nine IPC Group I, Ia, III and IIIa axe thin sections took place over a period of two years and resulted in the recognition of a total of twenty-four petrographically recognisable sub-groups within the four IPC groups examined. This is compared to the examination of over eight thousand axes by the IPC over the past sixty years, resulting in the recognition of thirty-nine petrographically distinguishable axe groups (Clough & Cummins 1988). This implies that a re-examination of other, established, IPC axe groups may result in the recognition of additional petrographic sub-groups and thus, raises two important questions. Firstly, if it is possible to recognise sub-groups then should the main IPC group be reclassified, and secondly, have the petrographic criteria for allocating axes to IPC groups altered, or 'drifted' during the past sixty years? These questions are dealt with in turn, below.

The recognition of distinct petrographic sub-groups within the four IPC groups examined suggests that primary petrographic descriptions are rather imprecise and do not allow the

recognition of subtle variations of thin section petrography. This is not to say that the early pioneers assessing axe petrology, for example Doctor Wallace, Alexander Keiller, Sir Kingsley Dunham, were incapable of recognising subtle petrographic differences, but that their individual type specimens and understandings probably differed slightly. These slight differences are probably the major contribution to the mineralogical and textural variation observed in the one hundred and forty-nine thin sections examined. A re-classification, or more precisely, a re-definition, of the range of mineralogy and texture which defines an IPC axe group should be considered, along with the establishment of type specimens and provision of reference samples to all IP assessors and researchers.

There is evidence that the criteria for allocating axes to IPC Group I have drifted over the sixty years since the group petrography was defined in the first IPC report (Keiller et al. 1941). It is seen in Chapter 4 that there are more anomalous axes (i.e. axes that are petrographically different to the majority) with IPC serial numbers greater than 1,000, indicating that the criteria used to allocate these axes may be different from those previously used. (Note; less than 2,000 axes have been given IPC serial numbers, most are recognised by their county number.) Geochemical analysis (c.f. Chapter 7) also suggests that there are relatively more anomalous IPC Group I axes from Wales and northeast England (no thin sections having been examined from these locations). In total, approximately 10% of IPC Group I axes examined in this thesis were found to be petrographically and/or geochemically different to the majority of IPC Group I axes examined. Hence, not only does it appear that there is variability in assigning axes over time, but there also appears to be a regional bias. Noting the limited published petrographic descriptions in the six reports of the IPC and the observed petrographic variability of axes from IPC Group I, Ia, III, & IIIa it is quite possible that distinct mineralogical and textural variability will be observed in other IPC axe groups. To improve the accuracy of assigning axes to groups it appears necessary that the criteria for allocation are both clarified and more effectively disseminated.

One reason behind the apparent temporal and regional discrepancies of assigning axes is the current wide-ranged distribution of axe thin sections. This has made it difficult for past, and will make it difficult for future IP researchers to compare directly, for example, Welsh, Yorkshire and Cornish IPC Group I axes. It is believed that the widely distributed nature of axe thin sections has inadvertently increased the possibility of incorrect identification through local researchers using local, non-representative, collections, as the

basis for assignment. It is acknowledged that a centralised collection of all axe thin sections is logistically and politically very difficult to achieve, but it is recommended that all greenstone axe thin sections are collected together and re-examined. This activity would reveal the extent of variance in allocation to the Cornish IPC groups examined and could be used to examine the provenance of the greenstone groups not examined here (IPC Groups II, IV, XVI and XVII).

Provenancing stone artefacts through petrographic analysis of axe and exposure thin sections is likely to remain the most accurate way to provenance axes for the foreseeable future. However, the advent of non-destructive provenancing methods means that the partially destructive practice of coring axes will probably become a last resort in the provenancing process and will probably not be necessary in the majority of cases, providing a large enough geochemical and MS axe and exposure database can be established. As the database grows in size and coverage it is anticipated that the need for axe thin sections will proportionally reduce. Ultimately it may be possible to provenance all stone implements using non-destructive methods.

Whilst the required database mentioned above is being generated, if it is necessary to obtain a thin section then it should be noted that additional and valuable petrographic information can be obtained through reflected light microscopy and microprobe analysis. It is therefore highly recommended that any new axe (or exposure) thin sections produced are prepared as polished thin sections as required for these two processes. The additional cost involved in producing polished thin sections would be outweighed by the extra petrographic information gained.

The new quantitative petrographic analysis system developed in Chapter 4 has considerable potential to IP since it is quick and easy to undertake. The system was developed to enhance and standardise the petrographic descriptions of greenstone axes and exposures so that they could be graphically and statistically compared, but without the need for a full modal analysis of the thin section, which would take approximately ten times longer to do. (Timing based on 45 minutes per modal analysis (Mandal pers. com.) and approximately 5 minutes to record the scores needed for the analysis system.) The visual representation of the data using bivariate and profile plots proved very useful in assessing the differences between greenstone sub-groups. The main disadvantage of the system is that, although quantitative, it is still subjective and largely dependent on the

observer's skills and interpretation of the criteria. The inclusion of photomicrographs in this thesis (as CD-ROMs) along with assigned scores (in Appendix 5) is aimed at overcoming these shortcomings by providing relatively simple access to reference material. It is thought that the present system could easily be improved by recording additional criteria, such as simple modal analysis (i.e. estimating the relative proportions of each of the main minerals) and by identifying the opaque minerals. Additionally, the scope of the system could be widened to include non-greenstone axe groups through the recognition of minerals common to other axe groups, such as quartz, olivine, orthoclase and feldspar.

9.2.2 Magnetic Susceptibility

This work constitutes the largest study of stone axe magnetic susceptibility (MS) so far carried out, measuring a total of 252 axes, and has shown that MS is a very useful technique for provenancing studies. Previous archaeological work utilising MS has shown that it is possible to characterise and provenance Roman granite columns (Williams-Thorpe and Thorpe 1993, Williams-Thorpe et al. 1996), and that the same potential existed for axes (Markham 1997). Similar to the work of Williams-Thorpe & Thorpe, a correction procedure needed to be developed in order to adjust the MS measurements made on artefacts.

The new method used to generate correction factors for MS measurements of stone axes is based on data contained in the MS instrument handbook (Exploranium 1990), as expanded by Williams-Thorpe & Thorpe (1993) and by Williams-Thorpe et al. (2000). It is seen that the method generally proved to be effective in adjusting the measured axe MS to bring it closer to the true value, but that the maximum correction factor produced MS values closest to the true rock value, and was not achieved using a factor mid-way between the maximum and minimum correction factors, as anticipated. The model could be improved by making a more accurate estimate of surface relief, although this, as noted by Williams-Thorpe et al. (2000), is difficult practically to achieve. Similarly, better estimations of axe curvature would also improve the model as the effect of the 'missing' material between the KT5 sensor head and the curved surface of the axe could be better determined. A simple improvement to the overall accuracy of the technique would be to measure dimensions to the nearest mm instead of 5mm, and use interpolated correction factors from the correction factor charts in Appendix 7. But, improving the accuracy of dimensional measurement

would increase the time taken to measure axe MS, and a study of the benefits gained in the accuracy of corrected MS values against the increased time taken is needed.

Overall, it is not possible to provenance greenstone axes using MS alone. The main reason why is not because of the precision of the KT5 MS meter, but that the overlap of the range of MS exhibited by the axes and the five greenstone exposures sampled proved to be too great to allow axes to be provenanced to a single outcrop with any statistical certainty. However, it is clear that MS can be used to assist with stone axe provenancing studies. There is a clear correlation between anomalous IPC Group I axes and MS values outside the group average, and that Irish Gabbro I axes have markedly higher MS than Gabbro II axes, reflecting the presence of magnetite in Gabbro I axes.

To assess the full potential in being able to provenance axes using this quick and simple analytical method it is necessary to increase the database of axe MS measurements and to include IPC axe groups that have yet to be extensively measured (i.e. IPC Group VI).

9.2.3 Portable x-ray fluorescent spectrometry

Production of geochemical data using the Spectrace TN9000 PXRF has proved to be relatively quick and cost effective when compared against other common, partially destructive, analytical techniques. The potential to use PXRF as an aid to provenancing studies was first presented by William-Thorpe et al. (1999a), after conducting various experiments examining the performance of the PXRF (Potts et al 1995, 1997a, 1997b). The work in this thesis clearly demonstrates the usefulness of PXRF in provenancing studies associated with Cornish greenstone axes and has advanced the use of the PXRF for archaeological work well beyond that previously carried out.

Overall, the bias in PXRF accuracy when measuring K, Ca, Fe, Rb, Sr, Y, Zr, Nb & Ba on a series of reference materials (c.f. Bias (I), Chapter 6) is of a similar magnitude to that published by Potts et al. (1995) and summarised in Williams-Thorpe et al. (1999a). But, it is noted that the accuracy of the PXRF, based on results from the Bias (I) examination, varied slightly between each of the three fieldwork periods, something that had not been noted before. This variation in accuracy appears to be random (e.g. examine Table 34) and therefore unpredictable, and indicates the need to check the calibration of the PXRF at the beginning of measurement activity and at regular periods thereafter. The reason behind the variation in accuracy may be related to the x-ray counting statistical uncertainty in a

similar manner to that for PXRF precision suggested by Williams-Thorpe et al. (1999a: p233). But, it is believed that the reduction in activity due to the age of the isotopic sources and associated, automatic, compensation carried out by the PXRF may be also be a contributory factor to the overall variation in accuracy.

PXRF Bias (III) results show a distinct PXRF Ti bias when measuring rock samples and the degree of bias was confirmed using ICP-AES data. This is similar to the effect reported by Williams-Thorpe (1999a), and probably for the same reasons: "preferential absorption of Ti Kα x-rays within the Fe-Ti oxides, which have a relatively high density compared with the silicate rock matrix" (Williams-Thorpe op. cit.: p224). However, what is not noted by Williams-Thorpe (op. cit.) or by previous workers (Potts et al. 1995, 1997a, 1997b), but which is clearly evident in the results for Bias (I) is that there is a large bias (overestimates of between 19 to 28%) in PXRF measurements of Ti within powdered samples (i.e. pressed powder pellets used for WDXRF analysis). It is unlikely that the magnitude of the observed PXRF Ti bias is due to random fluctuations within the PXRF equipment or process. This suggests a different bias mechanism is affecting PXRF Ti measurements and, as such, will need further examination to determine what it is. However, the bias observed in PXRF Ti measurements does not appear to have caused any problems with interpretation of Ti data in Chapters 7 and 8. After correcting PXRF Ti measurements of powdered samples using the results of Bias (I), and not correcting PXRF Ti measurements of rock samples, it is clearly seen in the various element discrimination diagrams and SC scatter plots in Chapter 8 that there is considerable overlap in (corrected) PXRF Ti data with WDXRF Ti data from Floyd and Al Samman, from the same greenstone exposure. This supports the observations made by Markham & Floyd (1997) on the similarity of PXRF and WDXRF data and thus allowed the simultaneous examination of PXRF and WDXRF Ti data.

PXRF instrument precision, based on K, Ca, Ti, Mn, Fe, Rb, Sr, Y, Zr, Nb & Ba measurements of greenstone is found to be similar to the instrument reported PXRF SD, and approximately one order of magnitude larger than the precision achieved by WDXRF equipment (Potts et al. 1995, c.f. Table 45). Similarly, instrument precision calculated from PXRF measurements of ACE and WSE reference samples is similar (K, Fe, Rb, Y, Nb) or larger (Ca, Ti, Mn, Sr, Zr, Ba) than reported by Potts et al (1995), based upon element concentrations greater than three times the PXRF detection limit (c.f. Table 48). The reason for the difference between Potts et al (op. cit.) and that reported in Table 48 is

almost certainly due to the longer count times used by Potts et al (200s against 110s used in this research), with a further contributory factor being the decrease in activity of the radioactive sources. Thus, PXRF instrument precision could be improved simply by extending the count times and/or ensuring that new radioactive sources are fitted. There is a balance to be maintained between increasing the count time, increasing the PXRF maintenance cost and the improvement in precision. The Spectrace TN9000 PXRF lacks the same precision as laboratory based XRF equipment, but it is believed that the non-destructive nature and portability of the PXRF far outweighs the reduction in precision compared with laboratory based XRF equipment.

Two PXRF measurements of a typical fine to medium grained greenstone rock achieved a sample precision of 5.3% relative standard deviation of the mean (calculated as the average of the relative standard deviations of the mean for those elements whose concentrations were ten times the PXRF detection limit, c.f. Table 40). This is comparable to the 5% relative standard deviation of the mean calculated by Potts et al from 1.2 (i.e. 2) measurements of Whin Sill dolerite using the same criteria (Potts et al. 1997a; p39, table 8). Sample precision can be improved by increasing the number of measurements taken, but this would result in reducing the number of samples measured in a given period of time. The main reason for not increasing the number of measurements taken per sample (i.e. axe) in this research was that the PXRF was only available for a limited time and it was decided to concentrate on maximising throughput using count times suggested by the thesis supervisors, at the cost of achieving optimum sample precision. For future work on greenstone axes it is recommended that three to four measurements be taken to improve sample precision, and consequently improve geochemical discrimination between axes.

PXRF detection limits reported in Chapter 6 are approximately two to four times those obtained by Potts et al (1995) and up to eight times those published by the PXRF manufacturer. Although the methodology used to calculate PXRF detection limits by Potts et al. (detection limit = 3 x fitting error) and in this work (detection limit = 3 x PXRF SD) are different, it is probable that the majority of the observed difference between Potts et al. (op. cit.) and this work is due to the shorter count times used here and most likely, the reduced intensity of excitation due to the age of the PXRF isotopes. However, based upon examination of PXRF measurements of Nb, which are often reported by the PXRF lower than the detection limit of 9ppm, it is probable that the detection limits ascertained by using three times PXRF SD are still higher than those published by Potts et al. (op. cit.),

even after taking count time and radioactive source age into account. Further work is required to explain this anomaly and requires a full understanding of how the PXRF actually generates the PXRF SD value.

The investigation of the effect of non-flat, axe-like, surfaces on PXRF measurements had not been done before and it was necessary to understand any limitations/corrections that might be necessary when measuring greenstone axes. As it turned out, it was not possible to distinguish statistically between PXRF measurements made on flat surfaces and polished axe-like surfaces made from the same greenstone. This means that PXRF measurements of polished greenstone axes can be readily compared with each other and measurements made on ideal samples (after adjusting for instrument bias). It is believed that this finding can be extended to PXRF measurements of any fine to medium grained igneous, basic to intermediate rock type, providing the sample's surface morphology is similar to those of sample MM3 examined in Chapter 6.

It was also found that PXRF measurements of immobile element Ti, Y, Zr and Nb concentrations made on weathered greenstone rocks are similar to those made on fresh, flat samples. This is slightly different to weathered surface effects on PXRF measurements reported by Williams-Thorpe et al (1999a), who indicate that PXRF measurements of lighter elements in weathered rhyolites, such as K, Ca, Ti and Fe, are generally lower than expected and that measurements of heavier elements Rb, Sr, Zr and Ba are mainly similar to those anticipated. The difference in response between the two sets of elements was, in part, put down to the greater critical penetration depths of the heavier elements (exceeding the weathered layer), although it was noted that Y measurements were lower than expected, even after considering critical penetrations depths. It is clear that weathered surfaces of both rhyolite and greenstone can result in anomalous PXRF measurements, depending on the element considered, and that the differences reported above are probably due to response of the different mineralogy of the two rock types to weathering. Whatever the situation, the effect of weathering must be considered on each rock type examined if it is likely that weathered samples will be encountered.

Overall, the non-destructive nature and portability of the PXRF equipment outweighs the reduction in precision and detection limits, compared with laboratory based XRF equipment, when the rapid and non-destructive geochemical analysis of axes is required. The range of variations of greenstone exposures and the reduced IPC Group I set of axes

meant that it was not possible to provenance the group to a single exposure, with the majority of the observed geochemical variability almost certainly caused by the natural mineralogical variability in greenstone rock coupled with the relatively small number of geochemical analyses made at each exposure, and not due to the precision of the PXRF. Hence, the limiting factor in using the PXRF to provenance axes is the variability of the rock being examined, since it is relatively simple to increase the number of exposure and axe measurements made.

9.2.4 Statistical methodology

The sequence of analytical and statistical methods used in this thesis was designed to compare the geochemical data of axes and exposures in a number of ways: to present the data in a geochemically recognisable format (element discrimination diagrams), to observe graphically the relationship of data (SC scatter plots), and to measure statistically the similarity of data (discriminant analysis (DA) & comparative statistics (e.g. Students t-test)). Individually, each methodology has its own advantages, but viewed collectively they provide a comprehensive attempt at geochemical matching leading to provenancing.

The use of element discrimination diagrams for assessing affinities to tectonic settings is well established and documented (c.f. Rollinson 1993). The diagrams chosen for this work use the four immobile elements Ti, Y, Zr and Nb, plus the mobile element Sr, because they minimised the potential difficulties with mobile elements (caused by weathering and mobility under metamorphic or hydrothermal conditions). There are three reasons for using element discrimination diagrams. Firstly, they give an indication of the tectonic setting of formation and this can quickly narrow down the search for prospective provenance locations (given the availability of adequate background knowledge). Secondly, they are useful in presenting data in a visual manner, thus allowing the direct comparison of data on separate diagrams by examining data cluster size and position (i.e. they show axes with the same geochemical parameters). Finally, element discrimination diagrams are widely used and recognised by other workers, so provide a common frame of reference for future investigations. The main drawback with using element discrimination diagrams based on PXRF data is that it is not always certain whether essential discrimination criteria have been met as the PXRF does not measure, for example, Si, Mg, Al, for which certain criteria (e.g. 20%> CaO + MgO >12% for tholeiitic rocks) must be satisfied in order for the diagram to be usefully interpreted.

SCA is based on the widely known PCA (e.g. Swan & Sandilands 1995) and its use here to examine geochemical data is its first application since the methodology was published (Vines 2000, Vines pers. com.). SCA and associated SC scatter plots provide a useful graphical representation of the data, based on the combined variance of the elements being considered and is therefore a valuable tool in revealing data clusters (hence data sub-groups). It is believed that using the same SCA statistics to plot different (non-associated) data may be controversial, but this has been done before with PCA (e.g. Rollinson 1993; p194, figures 5.19a & b). The ability to compare data to a common frame of reference (in this case the reduced IPC Group I SCA) was found to be invaluable. The main restriction in interpreting SC scatter plots, as produced in this work, is that any overlapping data clusters, or data points, do not necessarily share the same geochemistry (for the reasons stated in Section 7.3). This means that it is not possible to use SCA (or even PCA) alone to provenance axes, but that SCA does provide an excellent visual indicator of geochemical similarity.

DA cannot be used to generate primary groupings of data, which means the data must already have been examined and initial seed groups (i.e. axe sub-groups) determined prior to DA. Once seed groups are defined, in this work the petrographically determined axe sub-groups, then DA can be employed to statistically match individual axes to axe seed groups. The quality of the match is dependent on two things: the degree of variance within and between the seed groups, and the number of individuals in the seed group. In this work, there is little variance between many of the seed groups (i.e. the seed groups have similar geochemistry) and this made it difficult to assign axes to seed groups and seed groups to exposures with any certainty. Similarly, there are generally less than 10 members in most seed groups and this means that the seed group variance is relatively large, which again makes it difficult to definitively assign axes to seed groups. Both of these shortcomings will be overcome as the number of axes geochemically analysed increases, hence it is believed that there is great potential in using DA to provenance axes. It is noted that DA produced comparable results to those from SCA, especially relating to the anomalous axes in IPC Group I, and this is taken as supporting the use of the new SCA methodology.

Previous workers used bivariate element discrimination diagrams as an aid to provenancing studies. For example, Williams-Thorpe et al. (1999a) used Sr v Zr and Y v Zr bivariate plots to illustrate the origins of a total of seven Neolithic Welsh axes (4 IPC

Group XIII, 2 IPC Group VIII and one ungrouped axe), and Mandal used Sr v Y bivariate plots to determine the origins of twenty-three porcellanite axes (Mandal 1996). It was decided not to rely on bivariate diagrams in this thesis for two main reasons. Firstly, there are eleven elements which were found to be useful (K, Ca, Ti, Mn, Fe, Rb, Sr, Y, Zr, Nb and Ba) and this would have required a large number of bivariate plots in order to fully examine the geochemical relationships between axes and then between axes and exposure. As such, there was insufficient scope in this thesis to include all the potential bivariate plots alongside the element discrimination diagrams and the SC scatter plots. Secondly, in order to examine the potential of geochemical provenancing it was necessary to examine the match all of eleven elements between axe and exposure and the element discrimination diagrams and the SC scatter plots were required to achieve this. Bivariate diagrams will continue to feature in papers where there are restrictions on length, however, the use of SC scatter diagrams is encouraged as these can be used statistically to compare several elements on one graph, thus increasing the amount of information available to the reader.

9.3 Archaeological Implications

This thesis has examined ways in which the study of implement petrology (IP), and provenancing in particular, could take advantage of new, non-destructive, analytical techniques. It has only superficially considered axe distribution, morphology, usage and exchange in order to provide a background to the research. This part of the discussion covers the archaeological implications of the research findings and how the techniques developed here may be used in future work.

Archaeological research into Neolithic stone implements and subsequent interpretation of the results has undergone a considerable change in the past twenty years, as shown by the works of Clough & Cummins (1979 & 1988), Bradley (1984) and Cooney & Mandal (1998). As the database of axe information and provenance grew, researchers began to interpret the data in several ways: to infer on trade and distribution (e.g. Bradley & Edmonds 1993, Bradley 1984); to infer on social behaviour and usage of the environment (e.g. Tilley 1994); and to infer on the religious beliefs of Neolithic communities (e.g. Bewley 1994, Gron et al. 1991). The large amount of information on British Neolithic implements has come about through persuing the prime aims of the IPC: to catalogue and provenance axes (Keiller et al. 1941). Many works have been based on, or have extensively used, the output of the IPC (e.g. Hodder & Lane 1982, Cummins 1980) and give the impression that archaeological researchers are apparently satisfied with the

information available, that its sufficiency allows for the deduction of various aspects of Neolithic societies and groups. The question thus arises as to whether the IPC should continue to catalogue and provenance Neolithic stone axes, or especially, to periodically review its data. Bradley & Edmonds illustrate this question by homology with Italo Calvino's version of 'The Count of Monte Cristo'. The two prisoners wish to escape Chateau d'If, Abbe Faria unsuccessfully tries to dig his way out, whilst Edmonde Dantes adopts an intellectual approach using logic, and the information provided through Faria's diggings (Calvino 1969, Bradley & Edmonds1993). The inference by Bradley & Edmonds is that it is more important to use the data than gather it, illustrating their point with the statement '... tunnelling energetically and getting nowhere.' (Bradley & Edmonds, op. cit.: p4). To be fair to Bradley & Edmonds, they do not decry the collection of data, just the lack of interpretation. The author supports a view, that whatever hypotheses are constructed, to last, they must be on firm foundations. Therefore, the IPC must continue to examine new artefacts and re-evaluate old information with new methods (see below). Faria and Dante can only escape by combining their approaches.

The IPC and others have established provenances for all major axe groups, with eight groups provenanced to axe factories (c.f. Table 1, Chapter 2) and the remaining groups assigned to geographical locales (Clough & Cummins 1988). An ancillary aim of the IPC at its outset was to use the provenance of axes to determine Neolithic trade routes in Britain, and between Britain, Ireland and the near continent (e.g. Brittany) (Keiller et al. 1941; p50) and such work has been undertaken (e.g. Bradley & Edmonds 1993, Hodder & lane 1982, Cummins 1980). The implications of the findings presented in this thesis regarding the distribution of greenstone axes are considered on a large scale (10km), and a small scale (0.1km).

IPC Group I is geochemically best matched with two geographically separate locales: St Ives and Mullion Island. This, geochemically inferred, provenance does not support that published by Stone & Wallis (1951). On a large scale, the lack of agreements has minimal impact on published work regarding axe distribution and trade, as St Ives and Mullion Island are less than 20km away from the petrographically determined Penzance to Mousehole provenance. More so, the conclusions of published works considering the exportation of greenstone axes from Cornwall are strengthened, as there is now geochemical evidence to support the petrographic evidence: that a large number of greenstone axes found in Britain originated from Cornwall.

The distribution of IPC Group I axes was briefly considered in Chapter 2, where it was concluded that the distribution pattern was not random. Neither is the distribution of IPC Group I seen to follow the Law of Monotonic Decrement (Renfrew 1977), as there is not a steady decline in the number of axes found proportional to the distance from their origin. The use of the random walks to model axe distribution (Elliott et al. 1978) is believed to be flawed, simply because actual physical distribution of axes cannot be random: distribution is restricted by geology and available 'energy'. Geology is seen to affect the choice of transport routes in many ways: high dry chalk downs are preferred over marshy bog-laden ground (e.g. North 1938). Similarly, the use of navigable rivers (e.g. Rivers Severn, Thames, Trent, Ouse, Humber) to transport goods would require less 'energy' than walking. Hodder & Lane (1982) and Chappell (1986) can be interpreted as inferring that the distance travelled related to value: the higher the perceived value of the axe the greater the distance it would be carried. Hodder & Lane suggested a relationship between distance carried and implicit value of the axe (i.e. place value, a standard economic descriptive used today) (Hodder & Lane op.cit.). Whilst Chappell noted greenstone axes further from Cornwall were likely to be smaller than those found in Cornwall, suggesting that either the axes had been frequently reworked or that they started out small. So, in both cases, the distance travelled relates directly to the investment in energy to carry the axes. This latter, morphological, phenomena is noted in this research, as IPC Group I axes examined in Yorkshire were found to be generally smaller and a different shape to those found in Cornwall (c.f. Section 2.9.2 & 2.7). SC scatter plots do hint at the possibility that axes found in certain parts of Britain may be geochemically recognisable (within the overall IPC Group I geochemical range), however, further work is required to examine this potential, which could lead to the recognition of individual trade routes. A further examination between geochemistry and morphology may provide additional insight into the possibility of an age-related distribution and would also support Cummins' (1980) observations on the spatial distribution of Neolithic axes being used to delineate Neolithic boundaries in England.

On a smaller scale, the search for an IPC Group I axe factory should be redirected from the west side of Mount's Bay to St Ives and Mullion Island. It is the author's opinion that the best way to start the evaluation should begin with an analysis of exposures near St Ives. This opinion is based upon two main reasons: IPC Group II has already been provenanced to near St Ives (Keiller et al. 1941) and examination of IPC Group II axe thin sections

would quickly establish similarity with any of the recognised petrographic sub-groups identified in this work. Secondly, there appears to be more evidence of Prehistoric, mainly Neolithic, habitation near St Ives than Mullion Island (c.f. Figure 2, Chapter 2 and Pearce 1981).

As mentioned in Section 2.6.2, it is unlikely that the site of a greenstone axe factory would be found, even if there were one (c.f. Berridge 1993). The likely remains of such a factory would only be evident through the remains of quarrying activities as the debitage, largely dust, would be readily eroded from a factory site. The relatively narrow geochemical range of the reduced IPC Group I axes (consisting of approximately 90% of IPC Group I axes examined) suggest a single greenstone exposure produced the material for a large number of IPC Group I (and probably IPC Group Ia, I/Ia, I(near) & III) axes. It could be concluded that this supports the likelihood that the greenstone was quarried. However, along the Cornish coast, and especially near St Ives, there are a number of small-secluded coves filled with potential axe blanks (D. Weddle pers. com. and author's observations). The indented nature of some of these coves means that the beach material within the cove probably only originated from exposures surrounding the cove. Hence, it is plausible that a significant proportion of greenstone used to manufacture axes may have been taken from a small cove. This could help to explain the relatively large range of greenstone axe morphologies observed, which may have been determined by the range of beach material available. Further, it is speculated that Neolithic artisans would not undertake the risks associated with quarrying when the raw material already existed in a useable form.

The ability to petrographically and geochemically recognise axe sub-groups within a single IPC petrographic axe group, plus the indication that approximately 10% of IPC Group I axes examined are anomalous (which in turn suggests that 10% of the whole group may be incorrectly classified) indicates that it may be time for the IPC to re-examine its petrological groupings. Pitts (1996) argues that Neolithic axes can be divided into six 'rock classes' based on rock composition and working properties and that this 'framework' would reduce the emphasis placed on petrographic examination of axes in favour of 'organisation and technology of manufacture, style or value, an how such things changed over time." (Pitts op. cit.: p311). Taking these two points together, a re-examination of IPC axe groupings is probably needed, but that the criteria and objectives for allocation to each axe group needs to be clearly established before the exercise is conducted. The advent of non-destructive analytical methods gives an extra dimension to the fundamental

petrographic determination of group membership and the use of geochemical fingerprints and MS is likely to improve the precision in assigning axes to groups, as well as probably increasing the number of axe groups. Whilst morphology is a valuable indicator as to the technology and use of axes, Pitts proposed framework, based on morphology and simplifying the petrographical grouping, misses the fundamental need to provenance axes to a source. Without a known source any discussion regarding the origin and evolution of axe morphology, use and technology is weakened, as there is no firm basis for inference. The value of the current petrographic grouping, and the potential added precision through using extra geochemical and MS criteria, is that the basis for examining technology, style and value is strengthened. The IPC should consider establishing new criteria alongside the existing petrographic criteria for use when assigning axes to IPC groups and it should consider re-evaluating existing petrological groups to examine petrographic, geochemical and MS homogeneity of axe groups. The anticipated improved provenance could then be used as a firm basis to further the investigation of axe morphology in relation to origin and evolution of prehistoric axes.

The appropriateness of the techniques and methodology developed in this thesis to archaeology is considered using three examples: greenstone axes, IPC Group VI, and Irish porcellanite axes.

This work uses several methods to determine the provenance of IPC Group I and III axes (c.f. Chapter 7 & 8). Now that a more extensive greenstone database is available, it is not thought necessary to use every technique developed in this thesis for further work examining greenstone axes. Although it remains necessary to gather more geochemical data from greenstone exposures in Cornwall, to increase the number of exposure geochemical fingerprints available, this can be achieved using normal WDXRF analyses or using PXRF, depending on which is easiest and available. PXRF and MS data from other greenstone axes, both grouped and ungrouped can be compared with the existing database (i.e. this work) in order to establish provenance, with detailed work using all the techniques covered here required only if the new data is significantly different to that in the database.

It has been speculated that the exposure of volcanic tuff in the Great Langdale and Scafell Pike areas is not the source of all IPC Group VI axes (Davis pers. com.). PXRF derived geochemical data of IPC Group VI axes could be readily compared using SCA to identify the geochemical range exhibited by IPC Group VI axes, and thus to explore the potential

for matching exposures to material found at the many axe working sites as well as examining the geochemical homogeneity of the IPC group. This concept stands for all axe groups with known axe factories: the full range of techniques developed here is not needed to explore the provenance of the group, but SCA based on PXRF data would allow the heterogeneity of the axes to be determined.

Irish porcellanite axes are known to originate from two porcellanite exposures: Tievebulliagh and Rathlin Island, and it has been shown that axes can be provenanced to one or other of these sources using Sr & Y concentrations (Mandal 1996). Thus, PXRF measurements of porcellanite axes could be used to determine a secure provenance. As it is already known that Sr & Y are the key elements it is not necessary to use the SCA or DA techniques developed here; simple bivariate diagrams, supported by comparative statistics (e.g. Student's t-test) is enough to determine provenance. The non-destructive nature of PXRF, coupled with the availability of existing data, produces the exciting possibility of provenancing the important Malone Hoard of porcellanite axes to Tievebulliagh or Rathlin Island, without the need to deface the axes.

The three examples above illustrate that not all the techniques developed in this work are necessary when investigating the provenance of stone axes. The main considerations are: the amount of existing geochemical data; the current provenance of the axes being examined; and the actual question being ansewed (e.g are these axes geochemically the same, or what is the exact provenance for the axe group?). Whatever the questions, the non-destructive nature of the PXRF and MS techniques furnishes answers without damage to the unique implements.

10 Thesis findings and conclusions

10.1 Geology & Petrography

Petrographic and geochemical data for over 40 greenstone exposures within Cornwall and Devon has been used in this thesis. Seventy-three new samples from 21 exposures at a total of 6 outcrops: Cudden Point, Perranuthnoe (including Trenow Cove), Penzance, Gurnards Head, Zennor Point and South Hams. Further petrographical and geochemical information has been provided by Dr P. A. Floyd of Keele University for a further 23 greenstone exposures at Camborne, St Ives and within the Roseland area of Cornwall, as well as for 5 outcrops visited as part of this research.

Greenstone exposures in West Cornwall are mineralogically similar to each other (altered clinopyroxene, altered plagioclase feldspar and ilmenite), but their variability in degrees of alteration, plus the presence of secondary minerals (e.g. amphibole, apatite, biotite), makes it possible to distinguish between all 6 greenstone outcrops sampled.

Mineralogical and textural difference within the total of 149 IPC Group I (119), Ia (17), III (11) and IIIa (2) thin sections examined enabled the recognition of 24 sub-groups (IPC Group I: 13, IPC Group Ia: 6, IPC Group III & IIIa: 5).

The great majority of IPC Group Ia axe thin sections (15/17) are petrographically similar to many of those in IPC Group I. Six IPC Group III thin sections are also similar to many of those in IPC Group I. Seven of the 149 axe thin sections are individually unique and unlike any other axe thin section examined.

The primary mineralogy and texture of the vast majority of IPC Group I axe thin sections comprises medium-grained Ca poor clinopyroxene (occasionally ophitic), plagioclase feldspar and titano-ferrous opaques, rare apatite and rare orthopyroxene. This mineralogy and the lack of olivine & orthoclase feldspar indicate tholeiitic chemistry. Alteration of the primary mineralogy: pyroxene to fibrous amphibole, plagioclase to sericite and actinolite and the growth of secondary chlorite and sphene, corresponds to low-grade regional pumpellyite-prehnite facies metamorphism. The presence of secondary biotite suggests influence of contact metamorphism. Both of these metamorphic regimes are recognised in the igneous rocks found in Cornwall and strengthen the likelihood that the axe material originated from Cornish greenstone exposures.

No definite petrographic matches are found between greenstone material examined and axe thin sections. However, petrographic similarities between IPC Group I axe thin sections and rocks from Penlee, Mousehole and Gurnards Head are noted. The closest petrographic match is between greenstone found out of context (sample MM3), but near to the North Penwith coastline.

Results of a new quantitative petrographic analysis procedure developed for greenstone rocks supported the qualitative petrographic observations and showed that there is a potential to use it in assigning and provenancing greenstone axes and eventually other IPC axe groups.

10.2 Magnetic Susceptibility

A relative precision of 1.5% is established when using the Exploranium KT5 magnetic susceptibility meter to measure typical a greenstone rock (having a value 0.61 x 10^{-3} SI) and compares favourably with the published relative precision of 5% and 0.2% for MS values of 0.2 x 10^{-3} SI and 7 x 10^{-3} SI respectively.

A correction procedure taking account of sample surface relief, curvature and overall dimension (length, width, thickness), using published correction factors, results in a minimum-maximum range of MS which generally contains the true sample value. Empirical evidence suggests that the true value is probably closer to the maximum corrected value than the minimum corrected value. Duplicate MS and dimensional measurements of 21 axes indicated that the correction procedure is robust, with differences in corrected replicate MS values being generally less than 0.1 x 10^{-3} SI.

A total of 252 axes have been measured for MS (IPC Group I: 127, IPC Group Ia: 5, IPC Group I/Ia: 6, IPC Group I(near): 7, IPC Group III: 7, IPC Group IIIa: 1, IPC ungrouped & non-IPC: 76 and Irish doleritic & gabbroic axes: 23). After removing MS measurements for 8 axes with anomalous MS, but including duplicate measurements, a corrected minimum to maximum range of 0.95 ± 0.36 to 1.09 ± 0.40 x 10^{-3} SI (1sd) was established from a total of 131 measurements of IPC Group I axes. The IPC Group I range of corrected MS measurements is similar to IPC Group Ia (0.97 ± 0.31 to 1.10 ± 0.40 x 10^{-3} SI, n=7), IPC Group I/Ia (0.95 ± 0.38 to 1.16 ± 0.48 x 10^{-3} SI, n=5 (axe Lo114 omitted)), IPC Group I(near) (0.83 ± 0.27 to 0.99 ± 0.31 x 10^{-3} SI, n=7), IPC Group III (0.89 ± 0.28

to 0.98 ± 0.39 x 10^{-3} SI, n=7) and IPC Group IIIa (1.08 to 1.16 x 10^{-3} SI, n=1) (note n = the number of MS measurements). The range of corrected MS values for axe sub-groups and axes grouped by county of origin overlap to such an extent that it is not possible to statistically recognise individual sub-groups or counties of origin.

Thirteen IPC ungrouped and non-IPC axes (17%) recorded MS values outside the average IPC Group I minimum to maximum range ±2sd (0.23 to 1.89 x 10^{-3} SI) and 36 axes (47%) recorded MS values outside the average IPC Group I minimum to maximum range ± 1sd (0.69 to 1.49 x 10^{-3} SI). It is not possible to assign axes to IPC groups with any statistical certainty, but 83% of IPC ungrouped and non-IPC axes measured have MS values within ±2sd of the average IPC Group I minimum to maximum range indicating that it is possible that up to 83% of ungrouped greenstone axes are related IPC Group I, using a 0.05 value for significance.

MS measurements at five locations: Cudden Point, Trenow Cove (near Perranuthnoe), Penlee (near Penzance), Gurnards Head and Zennor Point produced a minimum to maximum range of corrected MS values from 0.44 to 0.78 x 10^{-3} SI.

Overall MS can aid provenancing but, as yet, cannot be used alone to provenance greenstone axes to exposures because of the significant overlap in ranges of MS values. Similarly, greenstone axes cannot be assigned to greenstone IPC axe groups using MS data alone with any degree of certainty.

10.3 Portable Fluorescence X-Ray Spectroscopy

The PXRF equipment generally takes less than one hour to set up, calibrate and to set count times, and approximately 5 minutes for each measurement. A total of over 1,300 PXRF measurements were made during the 28 days the PXRF equipment was available.

The PXRF is linearly calibrated, with zero offset for elements K (>10,000ppm), Ca, Ti, Fe, Rb, Sr, Y, Zr, Nb and Ba. K is linearly calibrated, but at measured concentrations of less than 10.000ppm a static offset of up to –1,300ppm is observed. Linearity could not be established for Ce and Pb over the range of concentrations encountered (generally less than 60ppm). However, results indicate a potential –40ppm offset for both Ce and Pb.

A systematic bias in PXRF measurements is found for each fieldwork period for elements K, Ca, Ti, Fe, Rb, Sr, Y, Zr, Nb and Ba. The range of values of this bias when measuring international reference samples is, in relative terms, K: 0 to 4%; Ca: -2 to -7%; Ti: 20 to 28%; Mn:9 to 22%; Fe: 0 to 2%; Rb: 3 to 10%; Sr: 10 to 15%; Y: -6 to 2%; Zr: 12 to 14%; Nb: 0 to 2%; Ba: -17 to -19% (negative values representing that the PXRF underestimates the true concentration). Values for bias identified when measuring greenstone samples are generally close to or within the range of bias established using the international reference samples, apart from Ti. Measurement of bias using uncrushed rock samples was masked by the variable mineralogy within the excited volume.

PXRF overestimates Ti concentrations by 20 to 28% relative when measuring pressed powder pellets and underestimates Ti concentrations by 12% when measuring uncrushed rock samples. ICP-AES analyses were used to confirm that the PXRF underestimated Ti in uncrushed rock

Typical uncrushed greenstone rock composition is measured to a sample precision of 5.3% relative standard deviation of the mean based on 2 PXRF measurements, using the same basis as Potts et al. (1997a). PXRF measured concentrations made on polished and curved surfaces (similar to the surfaces encountered on greenstone axes) cannot be statistically separated from those measured on an equivalent flat surface (using a 0.05 value for significance) of the same composition. PXRF measured concentrations of irregular surfaces with 1 to 3mm peak to pit differences are generally lower than concentrations measured on an equivalent flat sample of the same composition, with K, Sr and Nb concentrations found to be significantly different (using a 0.05 value for significance). Immobile element (Ti, Y, Zr and Nb) concentrations measured on weathered greenstones (pitting to 2mm and weathered crust to 3mm thick) cannot be statistically separated from those measured on an equivalent flat surface (using a 0.05 level of significance) of the same composition.

The Potts et al. (1977b) proposed Fe backscatter normalisation procedure is not regarded universally effective for irregular and curved surfaces and is not used to adjust PXRF measurements of rock and axes in this work.

PXRF precision achieved on replicate measurements of pelletised samples is slightly greater than the automatically reported PXRF SD value (a value indicating the uncertainty

associated with the measured element concentration). Instrument relative precision based on typical greenstone elemental concentrations are: K: 9.0% (3,000ppm); Ca: 1.0% (60,000ppm); Ti: 5.6% (10,000ppm); Mn: 24.0% (1,500ppm); Fe: 1.6% (100,000ppm); Rb: 41.9% (50ppm); Sr: 10.9% (50ppm); Y: 14.6% (30ppm), Zr: 6.2% (200ppm); Nb: 37.0% (10ppm); Ba: 9.5% (250ppm), Ce: 38.5% (-30ppm); Pb: 193% (10ppm). Ageing of the PXRF isotopes resulted in an observable worsening of instrument precision (the same PXRF equipment is used throughout this research).

PXRF detection limits calculated as 3 times the PXRF SD at 0ppm concentration are approximately K: 900ppm, Ca: 375ppm, Ti: 700ppm, Mn: 700ppm, Fe: 900ppm, Rb: 70ppm, Sr: 20ppm, Y: 15ppm, Zr: 22ppm, Nb: 9ppm, Ba: 30ppm, Ce: 30ppm, Pb: 60ppm. These limits are more than 3 times those indicated by the PXRF manufacturer and approximately twice those published (Potts et al. 1995). The larger detection limits obtained in this work are attributed to the reduced count time and greater age of the radioactive isotope source.

PXRF data is directly comparable with WDXRF data, providing the PXRF data has been corrected for bias, with the exception of Ti. However, adjusted PXRF measurements of Ti were not seen to cause noticeable problems during analysis of the geochemical data.

PXRF measurements of 272 axes have been made (149 IPC Group I; 4 IPC Group Ia; 6 IPC Group I/Ia; 6 IPC Group I(near); 11 IPC Group III; 1 IPC Group IIIa; 55 IPC ungrouped; 17 non-IPC and 23 Irish axes).

The geochemical fingerprint for IPC Group I, based on 130 axes is: K: 3,567 ± 2,282ppm; Ca: 67,715 ± 14,636ppm; Ti: 14,959 ± 3,772ppm; Mn: 1,532 ± 521ppm; Fe: 95,632 ± 14,009ppm; Rb: 29.6 ± 25.8ppm; Sr: 324 ± 150ppm; Y: 35.7 ± 6.8ppm; Zr: 171 ± 29.2ppm; Nb: 6.7 ± 2.9ppm; Ba: 104 ± 64.3ppm.

Nineteen IPC Group I axes have anomalous elemental concentrations, strongly suggesting that they may have been mis-categorised as IPC Group I. The origin and date of IPC examination of these axes indicates regional and temporal bias in petrographically assigning axes to IPC Group I, with 12 (of 19) anomalous axes originating from Wales (4), Lincolnshire (5) and Yorkshire (3), and 6 with IPC serial numbers greater than 1000.

IPC Group I petrographically determined sub-groups GpI-8, GpI-12 and GpI-13 contained anomalous axes and are therefore considered not to be IPC Group I. Geochemically, IPC Group I consists of sub-groups GpI-1, GpI-2, GpI-3, GpI-4, GpI-6 and GpI-7. SCA and DA of the geochemical data indicates that the IPC Group I sub-groups are not individually distinct from each other (using a 0.05 value for significance). Similarly, statistical analysis cannot, in general, distinguish axes by county of origin. However, SC scatter plots indicate a potential for geographical separation of axe geochemistry.

Petrographic axe sub-groups GpIa-1, GpIa-5 are geochemically similar to IPC Group I, indicating that some of IPC Group Ia axes are geochemically similar to IPC Group I. Axe sub-groups GpI/Ia, GpI(near)1 and GpI(near)2 were geochemically determined only, since thin sections were not available. GpI/Ia and GpI(near)2 appear geochemically similar to IPC Group I. Sub-group GpI(near)1 is geochemically unique.

Petrographic axe sub-group GpIII-1 is geochemically different to other IPC Group III axes, but contains the founding member of IPC Group III (Wi4/4) and is therefore deemed to be geochemically representative of IPC Group III. Sub-group GpIII-2 is geochemically similar to IPC Group I. The only GpIIIa axe examined (Wi119/402) is geochemically similar to IPC Group I. The remaining five IPC Group III axes are geochemically different to GpIII-1 and GpIII-2, and therefore probably different to IPC Group I or III.

SCA based on the reduced IPC Group I population (n=130) and DA based on the 16 geochemically recognised axe sub-groups (called seed groups) suggested that 15 IPC ungrouped axes are geochemically similar to IPC Group I and one axe is geochemically similar to IPC Group III (as defined by GpIII-1).

SCA and DA matches three non-IPC axes with IPC Group I. These axes were made recently, as part of an ongoing study into axe manufacture, from rocks collected along the North Penwith coast and from within Mount's Bay.

Seven Irish axes (4 Ungrouped dolerite and 3 Gabbro II) are geochemically similar to IPC Group I, supporting the hypothesis that these axes found in Ireland originated in Cornwall.

In total, 14 Irish axes have been both petrographically (Mandal 1996) and geochemically examined (this work) and compared to Cornish greenstone groups. Full agreement

between both methods on the match between Irish and Cornish axes is reached in 6 cases, partial agreement in 7 cases and disagreement in only 1 of the 14 cases examined. Irish Gabbro I axes are magnetically distinct from other Irish gabbros, having high MS (generally greater than 10 x 10^{-3} SI units).

Element discrimination diagrams show that IPC Group I sub-groups plot in the within-plate tholeiite and MORB sectors of the diagrams. Hence, the tectonic setting of IPC Group I greenstone is probably related to an area of crustal extension, with high degrees of partial melting beneath a thinned crust erupted/emplaced into a shallow water filled basin. IPC Group III (GpIII-1) appears to be a primitive tholeiite, possibly related to the earliest stages of crustal extension and associated partial melting.

10.4 Provenancing results

The number of IPC Group I axes examined is representative of the whole range of regional distribution apart from The English Midlands (e.g. Derbyshire, Nottinghamshire) Axes from the whole geographical distribution of IPC Group III have been examined. IPC ungrouped axes examined are largely from Cornwall and Yorkshire.

The predominantly MORB-related tholeiitic greenstone exposures in Cornwall and south Devon examined as part of this thesis can be individually distinguished using WDXRF and PXRF geochemical data.

Greenstone from the Lizard ophiolite dyke swarm at Porthoustock is geochemically different to IPC Groups I, Ia, I/Ia, I(near), III and IIIa indicating that this greenstone exposure did not provide the material for the axes.

Pillow lavas exposed at Tubbs Mill (within the Pendower Formation of the Gramscatho Group) have immobile and mobile element concentrations similar to the reduced IPC Group I average, but are unlikely to be petrographically similar as the axe material is doleritic not basaltic. However, it is possible that the pillow lavas are geochemically related to the actual source of axe greenstone.

Pillow lavas from Mullion Island (within the Roseland Breccia Formation of the Gramscatho Group) provide the closest geochemical match with the reduced IPC Group I set of axes. However, the fine-grained greenstone from Mullion Island is unlikely to be

texturally similar to the coarser grained axes. It is plausible that shallow intrusive igneous bodies (feeder dykes?) associated with the Mullion Island Pillow lavas would be geochemically and petrographically similar to IPC Group I axe greenstone. Other pillow lavas within the Roseland Breccia Formation also share geochemical similarities with the reduced IPC Group I.

Extrusive and intrusive Mylor Slate Formation greenstones sampled in the Camborne area are petrographically and geochemically different to IPC Groups I, Ia, I/Ia, I(near), III and IIIa, indicating that these exposures are highly unlikely to have provided material for axes within these six IPC groups.

The large intrusive Cudden Point greenstone within the Mylor Slate Formation is petrographically and geochemically different to IPC Groups I, Ia, I/Ia, I(near). There is some geochemical evidence, which indicates that the Cudden Point greenstone may be geochemically related to the source of IPC Group III.

Material from the greenstone quarry at GR SW534297 near Perranuthnoe, on the eastern side of Mount's Bay, which is believed to have provided the petrographic evidence to allow the provenance of IPC Group III is geochemically similar to IPC Group III axes. Whilst not a definitive match, the geochemical data supports the previously hypothesised provenance.

It is unlikely that the Mylor Slate Formation greenstone exposures sampled within and near to Penzance and Mousehole on the west side of Mount's Bay provided the material for IPC Group I, Ia, I/Ia, I(near), III and IIIa axes.

Greenstone exposures within the Mylor Slate Formation near to St Ives, on the North Penwith coastline are geochemically similar to the reduced IPC Group I average geochemistry. Petrographically, the greenstones sampled near St Ives are all fine grained and these exposures are unlikely to be the provenance of IPC Groups I, Ia, I/Ia, I(near), III and IIIa. However, known coarser grained igneous bodies associated with the pillow lavas may have provided material for some IPC Group I axes.

The late Devonian to early Carboniferous greenstone exposures sampled within the South Hams area of Devon are petrographically and geochemically different to IPC Groups I, Ia, I/Ia, I(near), III and IIIa, as expected.

10.5 Archaeological observations and implications

Simplified cumulative frequency-distance charts for IPC Group I axes, based loosely on those presented by Cummins (1979), indicate a non-random dispersal of IPC Group I axes, but do not show the two-stage distribution pattern suggested by Cummins (1979).

IPC Group I axes found in Yorkshire are generally smaller than those found in Cornwall and a different shape (adze-like). SC scatter plot suggest that there may be a regional bias in IPC Group I axe geochemistry.

On a 10km geographic scale, the provenance of IPC Group I based on PXRF and MS support the published work: that IPC Group I is very likely to have originated from West Cornwall. On a smaller, 0.1km, scale it is concluded that the most probable provenance for IPC Group I is to either St Ives, or Mullion Island. St Ives is considered as being the most likely provenance.

It is a recommendation that all greenstone axe thin sections are collected together and re-examined to reveal the extent of inaccuracy in allocation to Cornish IPC groups. There is an observed regional and temporal variability in accurately assigning axes to IPC Group I, with approximately 10% of IPC Group I probably incorrectly assigned. Serious consideration should be given to the provision of type specimens and reference samples to all IP assessors and researchers, as well as improving and expanding the criteria for allocating an axe to a particular petrographic group.

There is considerable potential to use non-destructive PXRF and MS data to provenance implements, with the accuracy of provenancing increasing in line with the database of PXRF and MS data. The methodologies developed in this work may be used selectively in provenancing studies, depending on the amount and type of petrographic, magnetic and geochemical data that is available. However until a comprehensive geochemical and MS database is available, assignment of implements to IPC petrographic groups by thin section analysis is likely to remain the most accurate way to provenance axes for the foreseeable future.

Bibliography

Al Samman. 1980. Petrology and geochemistry of some volcanic rocks from S Cornwall. Unpublished MSc Thesis – University of Keele

Balfour, M. 1992. Megalithic Mysteries. Parkgate Books (ISBN 1-85585-355-8)

Barnatt, J. 1982. Prehistoric Cornwall. Turnstone Press Ltd.

Barnes, R.P. 1984. Possible Lizard-derived material in the underlying Meneage Formation. Journal of the Geological Society **141**, 71-79

Barnes, R.P., Andrews, J.R. 1986. Upper Palaeozoic ophiolite generation and obduction in South Cornwall. Journal of the Geological Society **143**, 117-124

Berridge, P. 1993. Cornish Axe Factories; fact or fiction? In Stories in Stone 45-56.Lithic Studies Society Occasional Paper 4

Bewley, R. 1994. Prehistoric Settlements. Batsford/English Heritage (ISBN 0-7134-6853-X)

Bradley, R. 1978. The prehistoric settlement of Britain. Routledge & Keegan Paul (ISBN 0-7100-8993-7)

Bradley, R, 1984. The social foundations of prehistoric Britain. Longman (ISBN 0-582-49163-0

Bradley, R., Edmonds, M. 1993. Interpreting the axe trade: Production and exchange in Neolithic Britain. Cambridge University Press (ISBN 0-521-43446-7)

Briggs, C.S. 1976. Notes on the distribution of some raw materials in later prehistoric Britain. In Burgess, C., Miket, R. (eds) Settlement and economy in the third and second millennia B.C. British Archaeological Reports 33.

Bristow, C.M. 1996. Cornwall's geology and scenery: An introduction. Cornish Hillside Publications (ISBN 1-900147-00-9)

British Geological Survey. 1994b. Trevose Head and Camelford. England and Wales Sheet 335 & 336, Solid and drift geology. 1:50 000. BGS, Keyworth, Nottingham.

British Geological Survey. 1994a. Tavistock. England and Wales Sheet 337, Solid and drift geology. 1:50 000. BGS, Keyworth, Nottingham.

British Geological Survey. 1976. Newton Abbot. England and Wales Sheet 339, Solid and drift geology. 1:50 000. BGS, Keyworth, Nottingham.

British Geological Survey. 1974. Ivybridge. England and Wales Sheet 349, Solid and drift geology. 1:50 000. BGS, Keyworth, Nottingham.

British Geological Survey. 1976. Torquay. England and Wales Sheet 350, Solid and drift geology. 1:50 000. BGS, Keyworth, Nottingham.

British Geological Survey. 1984. Penzance. England and Wales Sheet 351 & 358, Solid and drift geology. 1:50 000. BGS, Keyworth, Nottingham.

British Geological Survey. 1975. Lizard, England and Wales Sheet 359, Solid and drift geology. 1:50 000. BGS, Keyworth, Nottingham.

Bunch, B., Fell, C. 1949. A stone axe factory at Pike of Stickle, Great Langdale, Westmorland. Proceedings of the Prehistoric Society **15**, 1-20

Butler, J.C., Woronov, A. 1986. Discrimination among tectonic settings using trace element abundances of basalts. Journal of Geophysical Resources **91**, B10289-B10300

Chappell, S. J. 1987. Stone axe morphology and distribution in Neolithic Britain. B.A.R., Oxford. (ISBN 0 86054 489 3)

Chen, Y., Clarke, A.H., Farrar, E., Wasteneys, H.A.H.P., Hodgeson, M.J., Bromley, A.H. 1993. Diachronous and independent histories of plutonism and mineralisation in the Cornubian Batholith, southwest England. Journal of the Geological Society **150**, 1183-1191.

Chesley, J.T., Halliday, A.N., Snee, L.W., Mezger, K., Shepherd, T.J., Scrivener, R.C. 1993. Thermochronolgy of the Cornubian batholith in southwest England: Implications for pluton emplacement and protracted hydrothermal mineralisation. Geochemica et Cosmochimica Acta **57**, 1817-1835

Clough, T.H.McK., Cummins, W.A. (eds.). 1979. Stone Axe Studies Vol. 1 (CBA Research Report No 23). Henry Ling Ltd, Dorchester (ISBN 0-900312-63-7)

Clough, T.H.McK., Cummins, W.A. (eds.). 1988. Stone Axe Studies Vol. II (CBA Research Report No 67)

Cooney, G., Mandal, S. 1995. Getting to the core of the problem: Petrological results from the Irish Stone Axe Project. Antiquity **69**, 969-980

Cooney, G., Mandal, S. 1998. The Irish stone axe project – Monograph 1. Wordwell Ltd, Bray, Co. Wicklow, Eire (ISBN 1 869857 23 2)

Coope, G.R. 1979. The influence of geology on the manufacture of Neolithic and Bronze Age stone implements in the British Isles. In Clough, T.H.McK., Cummings, W.A. (eds.). 1979. Stone Axe Studies Vol. 1 (CBA Research Report No 23). Henry Ling Ltd, Dorchester (ISBN 0-900312-63-7)

Cummins, W.A. 1979. Neolithic stone axes: distribution and trade in England and Wales. In Stone Axe Studies (CBA Research Report 23) (ed Clough T H & Cummins W A). Henry Ling Ltd, Dorchester (ISBN 0-900312-63-7)

Cummins, W.A. 1980. Stone Axes as a guide to Neolithic Communications and Boundaries in England and Wales. Proceedings of the Prehistoric Society, **46**, 45-60

Darbyshire, D.P.F., Shepherd, T.J. 1987. Chronology of magmatism in southwest England: the minor intrusions. Proceedings of the Ussher Soc. **64**, 431-438

David, A., Williams, G. 1995. Stone axe-head manufacture: new evidence from the Preseli Hills, West Wales. Proceedings of the Prehistoric Soc. **61**, 433-460

Davis, R.V. 1985, Implement petrology: the state of the art. In CBA Research Report 58: The archaeologist and the laboratory. Unwin Brothers Ltd. (ISBN 0 906780 45 4)

Davis, R.V. 1997. Implement Petrology: 60 Years of Service to the Archaeological Science. In Proceedings of a conference on the application of scientific techniques to the study of archaeology. Archaeological Sciences 1995 (eds Sinclair A, Slater R, Gowlett J). Oxbow Books (ISBN 1-900188-04-X)

Davis, R.V., Howard, H., Smith, I.F. 1988. The petrological identification of stone implements from southwest England. 6th Report of the Sub-Committee of the South-Western Federation of Museums and Art Galleries. In Stone Axe Studies Vol. II (CBA Research Report No 67) Clough & Cummings (eds)

Davies. G. 1984. Isotopic evolution of the Lizard Complex. Journal of the Geological Society **141**, 3-14

Deer, W.A., Howie, R.A., Zussman, J. 1992. The rock forming minerals. Longman (ISBN 0-582-30094-0)

Edmonds, E.A., McKeown, M.C., Williams, M. 1975. British regional geology: South-West England (4th Edition). HMSO (ISBN 00-11-880713-7)

Edmonds, M. 1995. Stone tools and society. Batsford (ISBN 0-7134-7141-7)

Edmonds, M., Sheridan, A. 1993. Survey and excavation at Creag na Caillich, Perthshire. Proceedings of the Society of Antiquaries of Scotland **121**

Elliott, K., Ellman, D., Hodder I. 1978. The simulation of Neolithic axe dispersal in Britain. In Hodder, I. Simulation studies in Archaeology, University Press, Cambridge, 79-87. (ISBN 0 521 22025 4)

Evans, J. 1872. The ancient stone implements, weapons and ornaments of Great Britain. Longmans, Green, Reader and Dyer: London

Evans, C.D.R. 1990. The geology of the western English Channel and its western approaches. HMSO (ISBN 0-11-884475-X)

Evans, E.D., Grinsell, L.V., Piggott, S., Wallis, F.S. 1962. Fourth report of the sub-committee of the South Western Group of Museums and Art Galleries on the Petrological Identification of Stone Axes. The Prehistoric Society **XXVIII**, 209-266

Evans, E.D., Smith, I.F., Wallis, F.S. 1972. Fifth report of the sub-committee of the South Western Group of Museums and Art Galleries on the Petrological Identification of Stone Axes. The Prehistoric Society **XXXVIII**, 235-275

Fenton, M.B. 1984. The nature of the source and the manufacture of Scottish battle-axes and axe-hammers. Proceedings of the Prehistoric Society **50**, 217-243

Fenton, M.B., Travis, R.J.A. 1988. A method for taking petrological samples from stone implements. In Clough & Cummings (eds), CBA Research Report 67: Stone Axe Studies II

Fitton, G. 1997. X-ray fluorescence spectrometry. In Gill, R. (ed) Modern Analytical Geochemistry. Longman Scientific (ISBN 0 582 099447)

Fleming, A. 1988. The Dartmoor reaves: Investigating prehistoric land divisions. Batsford (ISBN 0-7134-5665-5)

Flett, J.S. 1946. Geology of the Lizard and Meneage. HMSO (ISBN 0-11-880618-1) (Second edition)

Floyd, P.A. 1976. Review of geochemical data on rocks from the Lizard Complex, Cornwall. Proceedings of the Ussher Soc. **3.3**, 402-413

Floyd, P.A. 1982. The Hercynian Trough: Devonian and Carboniferous volcanism in SW England. In Sutherland, D.S. (ed), Igneous Rocks of the British Isles, 217-225. Wiley, Chichester

Floyd, P.A. 1984. Geochemical characteristics and comparison of the basic rocks of the Lizard Complex and the basaltic lavas within the Hercynian troughs of SW England. Journal of the Geological Society **141** 53-61

Floyd, P.A. 1995. Igneous activity : Basaltic volcanism in the Rhenohercynian Zone N. Europe. In Dallmeyer, R.D., Franke, W., & Weber, K. (eds.), Pre Permian geology of central and eastern Europe. SpringerVerlag, Berlin, 59-81

Floyd, P.A., Al-Samman, M. 1980. Primary and secondary chemical variation exhibited by some west Cornish volcanic rocks. Proceedings of the Ussher Soc. **5.1**, 68-75

Floyd, P.A., Lees, G.J., Parker, A. 1976. A preliminary geochemical twist to the Lizard's new tale. Proceedings of the Ussher Soc. **3.3**, 414-425

Floyd, P.A., Fuge, R. 1973. Distribution of F and Cl in some contact and regionally metamorphosed Cornish greenstones. Proceedings of the Ussher Society **2 6**, 483-488

Floyd, P.A., Exeley, C.S., Styles, M.T. 1993. Igneous rocks of south west England. Chapman and Hall (ISBN 0-412-48850-7)

Floyd, P.A., Lees, G.J. 1972. Preliminary petrological data on the Cudden Point greenstone. Proceedings of the Ussher Soc.

Gill, R. (ed). 1997. Modern analytical geochemistry: An introduction to quantitative chemical analysis. Longman (ISBN 0-582-09944-7)
Goode, A.J.J., Taylor, R.T. 1988. Geology of the country around Penzance. HMSO (ISBN 0-11-884388-5)
Govindaraju, K., Potts, P.J., Webb, P.C., Watson, J.S. 1994. Report on Whin Sill Dolerite WS-E from England and Pitscurrie Microgabbro from Scotland: Assessment by one hundred and four International Laboratories. Geostandards Newsletters **18** (2), 211-300
Grimes, W. F. 1979. The history of implement petrology in Britain. In Clough, T.H., Cummins, W. A. (eds) Stone Axe Studies I. CBA Research Report 23. Henry Ling Ltd, Dorchester (ISBN 0-900312-63-7)
Gron, O. 1991. A method for reconstruction of social organisation in prehistoric societies and examples of practical application. In Gron, O., Engelstad, E., Lindblom, I. (eds). Social Space. Odense University Press (ISBN 87 7492 842 2)
Hancock, P.L. (ed.). 1983. The Variscan fold belt in the British Isles. Adam Hilger (ISBN 0-85274-383-1)
Harland. 1984. A geological timescale. Cambridge University Press (ISBN 0 521 247284)
Harmer, F.W. 1928. The distribution of erratics and drift. Proceedings of the Yorkshire Geological Society **21**, 83-150
Hawkes, C.F.C. 1954. Archaeological theory and method: some suggestions from the old world. American Anthropology **56**, 155-68
Hodder, I., Lane, P. 1982. A contextual examination of Neolithic axe distribution in Britain. In Ericson, J.E., Earle, T.K (eds) Contexts for prehistoric exchange. Academic Press Inc., London & New York (ISBN 0 12 241580 9)
Holder, M.T., Leveridge, B.E., 1986. A model for the tectonic evolution of South Cornwall. Journal of the Geological Society **143**, 125-134
Holdsworth , R.E. 1989. The Start-Perranporth Line: a Devonian terrane boundary in the Variscan orogen of SW England. Journal of the Geological Society **146**, 419-421
Hope, -Sanderson, M.A. 1971. Bulletin of the Geological Survey of Great Britain. Science and Archaeology **8**
Houlder, C.H. 1961. The excavation of a Neolithic stone implement factory on Mynytt Rhiw in Caernarvonshire. Proceedings of the Prehistoric Society **XXVII**, 108-43
Hutton, D.H.W., Sanderson, D.J. (eds). 1984. Variscan Tectonics of the north Atlantic region. Geological Society Special publication No 14, Blackwell (ISBN 0-632-01203-X)
Jope, E.M. 1952. Porcellanite axes from factories in north-east Ireland: Tievebulliagh and Rathlin. Part 1. Archaeological survey. Ulster Journal of Archaeology **15**, 31-35
Keiller, A. 1937a. Petrological analysis. An appeal on behalf of the sub-committee of the south-western group of museums and art galleries. Antiquity **XI**, 484-485
Keiller, A. 1937b. The petrology of the stone implements. Scheme for the examination of stone implements. Museums Journal **37**, 295-296
Keiller, A., Piggott, S., Wallis, F.S. 1941. First Report of the sub-committee of the South Western Group of Museums and Art Galleries on the Petrological Identification of Stone Axes. The Prehistoric Society
Keen, L., Radley, J. 19??. Report on the petrological identification of stone axes from Yorkshire. The Prehistoric Society
Kerr, P.F. 1942. Optical Mineralogy. McGraw-Hill, Inc (ISBN 0-07-034218-0) (1977 re-print)
Kinnes, I. 1988. The cattleship potemkin: reflections on the first Neolithic in Britain. In Barret, J., Kinnes I. (eds) The Archaeology of Context. University of Sheffield
Kirby, G.A. 1979. The Lizard Complex as an ophiolite. Nature, London **282**, 58-61
Knowles, W.J. 1906. Stone axe factories near Cushendall. Journal of the Royal Society of Antiquaries or Ireland **36**, 383-94
Le Gaul, B., Le Herrisse, A., Deunff, J. 1985. New palynological data from the Gramscatho Group at the Lizard front (Cornwall): paleaogeographical and geodynamical implications. Proceedings of Geologist's Association **96**, 237-253
Le Maitre, R.W., Bateman. P., Dudec. A., Keller, J., Lameyre Le bas, M.J., Sabine, P.A., Schmid, R., Sorenson, H., Streckeisen, A., Wooley, A.R., Zanettin, B. 1989. A classification of igneous rocks and glossary of terms. Blackwell, Oxford.
Le Roux, C.T. 1971. A stone axe factory in Brittany. Antiquity **45**, 283-288
MacDonald, G.A., Katsura, T. 1964. Chemical composition of Hawaiian Lavas. Journal of Petrology **5**, 83-133
MacKenzie, W.S., Donalson, C.H., Guilford, C. 1982. Atlas of igneous rocks and their textures. Longman (ISBN 0-582-30082-7)
van Marcke-deLummen, G. 1985. Mineralogy and geochemistry of scarn deposits in the Land's End aureole. Proceedings of the Usher Society **6** (2), 211-217
Mandal, S. 1996. The petrology of the Irish stone axe. (Unpublished) PhD Thesis – University of Dublin
Mandal, S. 1997. Striking the balance: The roles of petrography and geochemistry in stone axe studies in Ireland. Archaeometry **39**, 289-308

Mandal, S., Cooney, G., Meighan, I.G., Jamison, D.D. 1997. Using geochemistry to interpret porcellanite stone axe production in Ireland. Journal of Archaeological Science **24**, 757-763
Manley, J. 1989. Atlas of prehistoric Britain. Phaidon Press (ISBN 0-7148-2569 7)
Markham, M.C. 1997. Geology and Archaeology: a search for the source rock used by British Neolithic Axe makers. Journal of the Open University Geological Society, 25 Anniversary Edition, 48-57. (ISSN 0143-9472)
Markham, M.C., Floyd, P.A. 1998. Geochemical fingerprinting of west Cornish greenstone as an aid to provenancing Neolithic axes. Proceedings of the Ussher Society **9**.
Meighan, I.G., et al. 1993. Trace element and isotopic provenancing of north Antrim porcellanites: Portrush-Tievebulliagh-Brockley (Rathlin Island). Ulster Journal of Archaeology **56**
North, F.J. 1938. Geology for the archaeologist. Archaeological Journal **XCIV**
North, F.J. 1942. Unpublished letter to the Museums Journal. IPC Archives
Ordnance Survey. 1998. The elipsoid and the transverse mercator projection. Geodetic information paper No 1. Ordnance Survey, Southampton
Pearce, S.M. 1981. The archaeology of south west Britain. Collins (ISBN 0-00-216219-9)
Pearson, M.P. 1993. Bronze Age Britain. Batsford (ISBN 0-7134-6856-4)
Pitts, M. 1996. The stone axe in Neolithic Britain. Proceedings of the Prehistoric Society, **61**, 311-371
Potts, P.J. 1997. A glossary of terms and definitions used in analytical chemistry. Geostandards Newsletters **21-1**, 157-161
Potts, P.J., Tindle, A.G., Webb, P.C. 1992. Geochemical Reference Materials. Whittles Publishing (ISBN 1-870325-40-0)
Potts, P.J., Webb, P.C. 1992. X-ray fluorescence spectrometry. Journal of Geochemical Exploration **44**, 251-296
Potts, P.J., Webb, P.C., Williams-Thorpe, O. 1995. Analysis of silicate rocks using field-portable X-Ray Fluorescence Instrumentation incorporating a Mercury (II) Iodide Detector: A preliminary assessment of analytical performance. Analyst **120**, 1273-1277
Potts P.J., Williams-Thorpe, O., Webb, P.C. 1997a. The bulk analysis of silicate rocks by portable X-ray fluorescence: effect of sample mineralogy in relation to the size of the excited volume. Geostandards Newsletter **21-1**, 29-41
Potts, P.J., Webb, P.C., Williams-Thorpe, O. 1997b. Investigation of a correction procedure for surface irregularity effects based on scatter peak intensities in the field analysis of geological and archaeological rock samples by portable x-ray fluorescence spectrometry. Journal of Analytical Atomic Spectrometry **12**, 769-776
Ramsey, M.H., Potts, P.J., Webb, P.C., Watkins, P., Watson, J.S., Coles, B.J. 1995. An objective assessment of analytical method precision: comparison of ICP-AES and XRF for the analysis of silicate rocks. Chemical Geology **124**, 1-19
Renfrew, C. 1977. Alternative models for exchange and spatial distribution. In Earle, T. K., Eriscson, J.E. (eds) Exchange Systems in Prehistory, New York. p71-79.
Renfrew, C. (ed). 1973. The explanation of culture change: models in prehistory. Gerald Duckworth & Co (ISBN 0 7156 1141 0)
Ritchie, P.R. 1968. The stone implement trade in 3rd Millennium Scotland. In Coles, J.M., Simpson, D.D.A. Studies in Ancient Europe: essays presented to Stuart Piggott, 117-36
Ritchie, P.R., Scott, J.G. 1988. The petrological identification of stone axes from Scotland In Clough & Cummins (eds) Stone Axe Studies Vol. II
Robinson, D., Sexton, D. 1987. Geochemistry of the Tintagel volcanic formation. Proceedings of Ussher Soc. 6 4, 523-528
Robson, J. 1957. The Cornish Greenstones. Transactions of The Royal Geological Society, Cornwall
Roe, F.E.S. 1966. The battle-axe series in Britain. Proceedings of the Prehistoric Society **32**, 199-245
Roe, F.E.S. 1988. Typology of stone implements with shaftholes. (In Cough & Cummings (eds) Stone Axe Studies Vol. II)
Rollinson, H. 1993. Using Geochemical Data; evaluation, presentation, interpretation. Longman Scientific (ISBN 0 582 06701 4)
Sadler, P.M. 1974. An appraisal of the 'Lizard-Dodman-Start thrust' concept. Proceedings of the Ussher Society **3**, 71-81
Sandeman, H.A., Clarke, A.H., Styles, M.T., Scott, D.J., Malpas, J.G., Farrar, E. 1997. Geochemistry and U-Pb and ^{40}Ar-^{39}Ar geochronology of the Man of War gneiss, Lizard Complex, SW England: pre-Hercynian arc-type crust with a Sudentan-Iberian connection. Journal of the Geological Society **154**, 403-411.
Saunders, A.D., Tarney, J. 1984. Geochemical characteristics of basaltic volcanism within back-arc basins. In Kokelaar, B.P, Howells, M.F. (eds) Marginal basin geology. Special publication of the Geological Society, **16**, 59-76
Schick, K.D., Toth, N. 1993. Making silent stones speak. Wiedenfield & Nicolson, (ISBN 0-297-81452-4)
Selwood, E.B., Durrance, E.M., Bristow, C.M. 1998. The Geology of Cornwall. University of Exeter Press (ISBN 0 85989 432 0)

Sharma, P.V. 1976. Geophysical methods in geology. Elsevier Scientific Publishing Company
Sheridan, J.A. 1986. Porcellanite artefacts: a new survey. Ulster Journal of Archaeology 49, 19-32
Simmons, I., Tooley, M. 1981. The environment in British prehistory. Gerald Duckworth (ISBN 0-7156-1362-6)
Smith, I.F. 1979. The chronology of British stone implements. In Clough, T. H. & Cummins, W. A. (eds) Stone Axe Studies (CBA Research Report 23). Henry Ling Ltd, Dorchester (ISBN 0-900312-63-7)
Spectrace. 1994 TN9000 Operators Manual
Stone, J.F.S., Wallis, F.S. 1947. Second report of the sub-committee of the South Western Group of Museums and Art Galleries on the Petrological Identification of Stone Axes. The Prehistoric Society
Stone, J.F.S., Wallis, F.S. 1951. Third report of the sub-committee of the South Western Group of Museums and Art Galleries on the Petrological Identification of Stone Axes. The Prehistoric Society
Styles, M.T., Kirby, G.A. 1980. New investigations of the Lizard Complex, Cornwall, England and a discussion of an ophiolite model. Proceedings of the International Ophiolite Symposium, Cyprus 1979. Geological Survey Dept. Nicosia, 517-526
Styles, M.T., Rundle, C.C. 1984. The Rb-Sr isochron age of the Kennack Gneiss and its bearing on the age of the Lizard Complex, Cornwall. Journal of the Geological Society **141**, 15-19.
Swan, A.R.H., Sandilands, M. 1995. Introduction to geological data analysis. Blackwell (ISBN 0-632-03224-3)
Tilley, C. 1994. A Phenomenology of Landscape: Places, Paths and Monuments. Berg Publishers (ISBN 1-85496-919-5)
Tooms, J.S., et al. 1965. Geochemical and geophysical mineral exploration experiments in Mounts Bay, Cornwall. Colston Research Soc. **17**, 363-391
Turner, R.E., Taylor, R.T., Goode, A.J.J., Owens, B. 1979. Palynological evidence for the age of the Mylor Slates, Mount Wellington, Cornwall. Proceedings of the Ussher Society **4**, 274-283
Vines, S.K. 2000. Simple Principle Components. Applied Statistics **49**, 441-451
Watson, J.S. 1996. Fast, simple method of powder pellet preparation for x-ray fluorescence analysis. X-Ray Spectrometry **25**, 173-174
Warr, L., Primer, T.J., Robinson, D. 1991. Variscan very low-grade metamorphism in south-west England: a diastathermal and thrust related origin. Journal of Metamorphic Geology **9**, 751-764
Warren, S. 1919. A stone axe factory at Graig Lwyd, Penmaenmawr. J.R.A.I **XLIX**, 342-365
Warren, S. 1922. The Neolithic stone axes of Graig Lwyd, Penmaenmawr. Archaeologia Cambrensis **77**, 1-35
Weber, K. 1984. Variscan events: early palaeozoic continental rift metamorphism and late Palaeozoic crustal shortening. In Hutton, D.H.W., Sanderson, D.J. Variscan tectonics of the North Atlantic Region. Geological Society special publication **14**, 3-22
Williams, B. 1990. The archaeology of Rathlin Island. Archaeology Ireland **4**, 47-51
Williams-Thorpe, O., Jones, M.C., Webb, P.C., Rigby, I.J. 2000. Magnetic Susceptibility thickness corrections for small artefacts and comments on the effects of 'background materials. Archaeometry **42**, 101-108
Williams-Thorpe, O., Potts, P.J., Webb, P.C. 1999a. Field Portable non-destructive analysis of lithic archaeological samples by x-ray fluorescence instrumentation using a mercury iodide detector: Comparison with wavelength-dispersive XRF and a case study in British Stone axe provenancing.. Journal of Archaeological Science **26**, 215 to 237
Williams-Thorpe, O., Aldiss, D., Rigby, I.J., Thorpe, R.S. 1999b. Geochemical provenancing of igneous glacial erratics from southern Britain and implications for prehistoric stone implement distributions. Geoarchaeology **14**, 209-246
Williams-Thorpe, O., Thorpe, R.S. 1993a. Magnetic Susceptibility used in non-destructive provenancing of Roman granite columns. Archaeometry **35-2**, 185-195
Williams-Thorpe, O., Thorpe, R.S. 1993b. Geochemistry and trade of eastern Mediterranean millstones from the Neolithic to Roman Periods. Journal of Archaeological Science **20**, 263-320
Williams-Thorpe, O., Jones, M.C, Tindle, A.G., Thorpe, R.S. 1996. Magnetic susceptibility variations at Mons Claudianus and in Roman Columns: A method of provenancing to within a single quarry. Archaeometry **38-1**, 15-41
Wilson, A.C., Taylor, R.T. 1976. Stratigraphy and sedimentation in West Cornwall. Transactions of Royal Geological Society of Cornwall **20**, 246-259
Yardley, B.W.D., MacKenzie, W.S., Guilford, C. 1990. Atlas of metamorphic rocks and their textures. Longman (ISBN 0-582-30166-1)
Zeigler, P.A. 1986. Geodynamic model for the Palaeozoic crustal consolidation of western and central Europe. Tectonophysics **126**, 303-328